

新 制
工
938
京大附図

Seismic Response and Seismic Design
of
Prestressed Concrete Building Structures

プレストレストコンクリート建築構造物の
地震応答と耐震設計

by

Minehiro Nishiyama

September, 1993

9959
b566

Seismic Response and Seismic Design
of
Prestressed Concrete Building Structures

by

Minehiro Nishiyama

September, 1993

Preface

The primary objectives of this study are to summarize current seismic design code provisions for prestressed concrete building structures, to explain the problems concerning the seismic design of such buildings and to present the fundamental methods to predict the behaviour of prestressed concrete sections, members and building frames.

Chapter 1 introduces the basic concept of prestressing.

The current seismic design procedure for prestressed concrete building structures in Japan is summarized in Chapter 2. This chapter also contains a comparison of the seismic design forces in the Japanese and New Zealand loadings codes. Problems connoted in the design procedure of prestressed concrete building structures will be discussed with some design examples.

In Chapter 3 moment-curvature characteristics of prestressed, partially prestressed and reinforced concrete member sections will be discussed in terms of yield curvature, ductility and ultimate available curvature. In addition, an analytical procedure for predicting moment-curvature characteristics of prestressed concrete member sections which incorporates stress-strain relationships of concrete, ordinary reinforcement and prestressing steel is described.

Prestress introduced into a beam and through the beam-column joint has been shown to improve the shear resistance of such joints. However, very little experimental work has been conducted. Reversed cyclic loading tests on prestressed concrete beam-column joint assemblages by the author will be reported in Chapter 4. Main parameters investigated are the locations of prestressing steel bar in the section and amount of prestressing force.

In Chapter 5 moment-curvature relationships of prestressed, partially prestressed and reinforced concrete sections are idealized on the basis of the idealization proposed by Thompson and Park and the experimental work described in Chapter 4.

Dynamic response analyses of single-degree-of-freedom prestressed concrete systems are discussed in Chapter 6. On the basis of the analytical results and substitute damping procedure proposed by Gulkan and Sozen a method for predicting displacement response of prestressed, partially prestressed and reinforced concrete will be presented.

No literature is presently available describing two-dimensional dynamic response analyses of prestressed concrete building frames although analyses on single- or multi-

degree-of-freedom systems have been carried out. In Chapter 7 two-dimensional dynamic response analyses conducted on prestressed and reinforced concrete model frames will be reported. The analytical results will be compared with the past research and the results of multi-degree-of-freedom shear systems.

In Chapter 8 a seismic design proposal by AIJ task-committee on the seismic design of prestressed concrete building structures is to be summarized. In this proposal a column sidesway (soft story) mechanism is incorporated as one of intended failure mechanism. This is because of difficulty of designing a prestressed concrete building for a beam sidesway failure mechanism. Some design examples which demonstrate this difficulty is shown. Reversed cyclic loading tests on high strength reinforced concrete columns will be reported to see if adequate ductility is secured.

Two attempts have been made in order to improve the seismic performance of precast prestressed concrete beam - column assemblages. Reversed cyclic loading tests on precast prestressed concrete beam - column joint assemblages conducted to confirm the effects of the above ideas will be described in Chapter 9.

Chapter 10 summarizes the conclusions of this study and suggests recommendations for future research.

As an appendix the response of unbonded prestressed concrete building frames will be discussed on the basis of both experimental and analytical work.

Acknowledgements

The research reported in this thesis was undertaken at the Department of Architectural Engineering, Kyoto University, under the overall guidance of Professor H. Muguruma.

I wish to sincerely thank Prof. H. Muguruma for his invaluable help and constant encouragement. Prof. F. Watanabe is thanked for the helpful advice and the fruitful discussions.

Thanks are also due to Dr. G. A. MacRae for his indispensable advice on the language. Without him I would not have had the imprudence to write the thesis in English.

Thanks are extended to Mr. T. Iwamoto for his assistance and advice in the experimental program. Mr. Y. Komatsu is thanked for his help in making test units and measuring devices.

I am also grateful for the help of the students. In particular, thanks are due to Mr. T. Nishizaki (now Takenaka Corp.), Mr. M. Ohira (now Takenaka Corp.), Mr. Y. Ohta (now Takenaka Corp.) and Mr. H. Oda (now West Japan Railway).

Thanks are also due to Prof. R. Park and aggressive Prof. T. Paulay for their invaluable advice and encouragement. I also wish to thank my fellow graduate students during my stay at Department of Civil Engineering, University of Canterbury in 1990, in particular Dr. P. Chen, Prof. F. Yanez, Dr. J. Restrepo, Mr. Li Bing, and Dr. A. Mori. Some computer program in this thesis were based on the work of Dr. Larry Dodd.

Finally, I wish to express my sincere gratitude to my wife, Fusako, and my parents for their constant encouragement, understanding and support over the years.

(Acknowledgements written in Japanese is attached at the end of this thesis.)

Contents

1	INTRODUCTION.....	1
1.1	Prestressed concrete	1
1.2	Seismic performance of prestressed concrete building structures	4
1.3	Aims of this research	6
2	CURRENT SEISMIC DESIGN PROCEDURE FOR PRESTRESSED CONCRETE BUILDINGS IN JAPAN	9
2.1	Introduction	9
2.2	Current seismic design procedure for prestressed concrete buildings in Japan	9
2.2.1	Code approaches	9
2.2.2	First phase design	11
2.2.3	Second phase design by strength design (Alternative 1)	11
2.2.4	Second phase design by capacity design (Alternative 2)	15
2.3	Comparison of seismic design loads in New Zealand and Japan	17
2.4	Comparison of prestressed concrete buildings with reinforced concrete buildings with regard to seismic design load	20
2.5	Conclusions	23
3	MOMENT - CURVATURE CHARACTERISTICS OF PRESTRESSED, PARTIALLY PRESTRESSED AND REINFORCED CONCRETE MEMBERS UNDER REVERSED CYCLIC LOADING	25
3.1	Introduction	25
3.2	Past research	26
3.3	Moment - curvature relationships of prestressed, partially prestressed and reinforced concrete beam sections	28
3.4	Theoretical study of strength and ductility of prestressed concrete members	37

3.4.1	Computer analysis program	37
3.4.2	Stress-strain models for concrete and reinforcing steels	38
3.4.2.1	Stress-strain model for confined concrete	38
3.4.2.2	Cyclic loading behaviour	41
3.4.3	Stress-strain model for reinforcing steel	45
3.4.3.1	Monotonic stress-strain behaviour	45
3.4.3.2	Cyclic Loading Behaviour	46
3.4.4	Stress-Strain Model for Prestressing Steels	48
3.4.4.1	Monotonic Stress-Strain Behaviour	48
3.4.4.2	Cyclic Loading Behaviour	49
3.5	Procedure of Moment-curvature Analyses	52
3.5.1	General assumptions	52
3.6	Conclusions	55

4 *HYSTERETIC RESTORING FORCE CHARACTERISTICS AND SHEAR RESISTANCE OF PRESTRESSED BEAM-COLUMN JOINT ASSEMBLIES*57

4.1	Introduction	57
4.2	Review of Previous Research and Code Provisions	59
4.2.1	Hysteretic Restoring Force Characteristics of Prestressed Concrete Beam-Column Assemblies	59
4.2.2	Shear Strength of Prestressed Concrete Beam-Column Joint Cores ..	63
4.2.3	Code Provisions on Seismic Design of Prestressed Concrete Beam-Column Joint Assemblies	72
4.3	Tests on Prestressed Concrete Beam-Exterior Column Assemblies with Various Locations of Prestressing Steel Tendons.....	74
4.3.1	Test Program	74
4.3.2	Details of beam-column joint core	79
4.3.3	Development Length for Series B Test Units	87
4.3.4	Loading.....	89
4.3.5	Measurements.....	90
4.3.6	General Behaviour of Test Units	91
4.3.7	Damage Sustained by Test Units	94
4.3.8	Details of Test Results	97
4.3.9	Series A (Units PC1, PC2 and RC1)	100
4.3.10	Series B (Units PC3, PC4 and RC2)	110
4.3.11	Tensile force in prestressing steel bars in Series A and B	116

4.3.12	Contribution of beam prestress to joint shear resistance	118
4.3.13	Influence of location of prestressing steel on joint shear resistance .	119
4.3.14	Comparison of experimental results with theoretical predictions	120
4.4	Test on Prestressed Concrete Beam-Exterior Column Joint Assemblies with Various Amount of Prestressing Force	123
4.4.1	General	123
4.4.2	Test Program	123
4.4.3	General Behaviour of Test Units	133
4.4.4	Details of Test Results	137
4.5	Re-examination of the Test Results in Thompson and Park's Research Work [4.6].....	148
4.6	Conclusions	152

5 ***MOMENT-CURVATURE IDEALIZATION OF PRESTRESSED, PARTIALLY PRESTRESSED AND REINFORCED CONCRETE SECTIONS..... 155***

5.1	Introduction	155
5.2	Review of Previous Research.....	155
5.3	Moment-curvature idealization proposed by Thompson and Park	157
5.3.1	Prestressed concrete idealization	157
5.3.2	Ramberg-Osgood idealization.....	159
5.3.3	Partially prestressed concrete idealization	161
5.4	An idealization of hysteresis loops of prestressed, partially prestressed and reinforced concrete proposed by the author	161
5.4.1	Modifications with the prestressed concrete idealization	163
5.4.2	Partially prestressed and reinforced concrete idealization	165
5.5	Comparison of experimental and idealized moment-curvature characteristics	167
5.6	Examples of idealized moment - curvature characteristics for prestressed, partially prestressed and reinforced concrete sections under reversed cyclic loading	174
5.7	Conclusions	183

6 DYNAMIC RESPONSE ANALYSIS OF SINGLE-DEGREE-OF-FREEDOM PRESTRESSED CONCRETE SYSTEMS 185

6.1	Introduction	185
6.2	Review of Previous Research	185
6.3	Inelastic Dynamic Response Analyses of Single-mass Shear Systems	187
6.3.1	Equation of dynamic equilibrium and the analytical procedure	187
6.3.2	Parameters investigated	189
6.3.3	Earthquake records	191
6.3.4	Response spectra of the idealized curves	191
6.3.5	Comparison between prestressed concrete and reinforced concrete with pinched hysteresis loops	209
6.4	Prediction of displacement response by substitute damping	218
6.4.1	Introduction	218
6.4.2	Substitute damping	219
6.4.3	Prediction of displacement response by substitute damping	222
6.4.4	Comparison of dynamic response between prestressed concrete and reinforced concrete systems	225
6.5	Conclusions	228

**7 DYNAMIC RESPONSE ANALYSIS OF PRESTRESSED CONCRETE BUILDING FRAMES ..
..... 231**

7.1	Introduction	231
7.2	Damping model	231
7.3	Non-linear beam model	232
7.4	Column moment - axial load interaction	236
7.5	Tracking a moment - curvature relationship	236
7.6	Structural layout and description of the buildings	237
7.7	Design of possible plastic hinge regions	237
7.8	Design of non-plastic hinge regions	239
7.9	Natural period of buildings	241
7.10	Moment - curvature idealization assigned to plastic hinge regions	242
7.11	Selected ground acceleration records	243
7.12	Calculation results of four- and eight-story frames	243
7.12.1	Results of four-story frames	243
7.12.2	Results of eight-story frames	251
7.13	Design of 16-story frames	257
7.13.1	Results of 16-story frames	257

7.14	Comparison of interstory drift responses among prestressed, partially prestressed and reinforced concrete frames	261
7.15	Comparison of dynamic responses between two-dimensional frame analyses and analyses using multi-mass shear system	263
7.16	Conclusions	270
8	<i>SEISMIC DESIGN OF PRESTRESSED CONCRETE BUILDING FRAMES</i>	273
8.1	Introduction	273
8.2	Seismic design method proposed by the AIJ task-committee on seismic design of prestressed concrete	274
8.2.1	Design category	274
8.2.2	Material strength used in structural design	276
8.2.3	Seismic design load	277
8.2.4	Structural analysis	280
8.2.5	Design of members	280
8.2.6	Design of the beam-column joint	287
8.2.7	Design Requirements for Walls in DWF System	288
8.3	Design example of prestressed concrete buildings	289
8.3.1	General description of model frame	289
8.3.2	Design of prestressed concrete beams	290
8.3.3	Calculation of secondary stress by prestressing	292
8.3.4	Design for seismic actions	293
8.3.5	Calculation of beam flexural strength	293
8.3.6	Calculation results	293
8.4	Ductility of high strength reinforced concrete columns with high strength transverse reinforcement	296
8.4.1	Introduction	296
8.4.2	Column test units and test procedures	297
8.4.3	Test results	300
8.4.4	Modification of previously proposed stress-strain model of confined concrete	305
8.5	Seismic design of building frames of limited ductility	313
8.6	Conclusions	316

**9 REVERSED CYCLIC LOADING TESTS ON
PRECAST PRESTRESSED CONCRETE BEAM-
EXTERNAL COLUMN JOINT ASSEMBLIES319**

9.1	Background	319
9.2	Test program	322
9.2.1	Description of test units	322
9.2.2	Joint induced shear force	329
9.2.3	Theoretical shear strength of joint cores	329
9.2.4	Details of steel in beam-column joint	331
9.2.5	Loading	331
9.2.6	Measurements	332
9.3	Test results	332
9.3.1	General behaviour of test units	332
9.3.2	Location of Prestressing tendons	332
9.3.3	Prestress introduced into the prestressing tendon at the center of the section	338
9.3.4	Grouted and ungrouted tendons	338
9.3.5	Tensile stress of tendons	339
9.4	Conclusions	343

10 MAJOR CONCLUSIONS AND RECOMMENDATIONS FOR FUTURE RESEACH.....345

10.1	Major conclusions	345
	Chapter 2	345
	Chapter 3	345
	Chapter 4	346
	Chapter 5	347
	Chapter 6	348
	Chapter 7	349
	Chapter 8	350
	Chapter 9	351
10.2	Recent trend of seismic design of prestressed concrete building structures	352
10.3	Recommendations for future research	353

Tables and Figures

Chapter 1

Table 1.1	Comparison of structural types (in case of six-story office building) .3
Fig.1.1	Typical measured lateral-load displacement hysteresis loops for subassemblages of post-tensioned prestressed concrete portal frame controlled by flexural plastic hinging [1.6]5

Chapter 2

Table 2.1	Coefficients F_e and F_s with regard to the eccentricity ratio R_e and stiffness ratio R_s , respectively15
Table 2.2	Member dimensions for four-story prestressed and reinforced concrete model frames22
Table 2.3	Effective member stiffnesses22
Fig.2.1	Flow diagram for the design procedure10
Fig.2.2	Design spectral coefficient, R_t13
Fig.2.3	Eccentricity ratio, R_e14
Fig.2.4	Stiffness ratio, R_s14
Fig.2.5	Equal energy concept and the reduction factor, D_s17
Fig.2.6(a)	Four-story prestressed concrete model frame21
Fig.2.6(b)	Four-story reinforced concrete model frame21

Chapter 3

Fig.3.1	Moment - curvature curves of reinforced, partially prestressed and prestressed concrete beam sections theoretically obtained29
Fig.3.2	Typical stress - strain relationship of prestressing steel31
Fig.3.3	Yield curvature by Harajli and Naaman [3.5]32
Fig.3.4	Yield curvature definition used in the University of Canterbury33
Fig.3.5	Yield curvature by Zahn [3.9]33
Fig.3.6	Influence of cyclic loading in the analysis [3.10]35
Fig.3.7	Stress distribution in the column section [3.10]35

Fig.3.8	Definition of ultimate curvature by Zahn [3.9]	36
Fig.3.9	Monotonic stress strain behaviour for unconfined and confined concrete	38
Fig.3.10	Confined strength determined from the confining stresses	41
Fig.3.11	Unloading path from the compression envelope curve	43
Fig.3.12	Assumed tension strength deterioration due to compressive loading	43
Fig.3.13	Stress - strain curves for reloading branch	44
Fig.3.14	Monotonic stress strain curve for ordinary-strength reinforcing steel	47
Fig.3.15	Cyclic loading behaviour for ordinary-strength reinforcing steel	47
Fig.3.16	Monotonic stress - strain relation assumed for prestressing steel	49
Fig.3.17	Load reversal in the inelastic range	51
Fig.3.18	Shifted envelope for load reversal behaviour	51
Fig.3.19	Typical stress - strain response	52

Chapter 4

Table 4.1	Theoretical shear strengths of the joint cores calculated using Eqs.4.1 and 4.2	66
Table 4.2	Specifications of the test units	77
Table 4.3	Ideal flexural strength of the beams and columns of each test unit ..	77
Table 4.4	Mechanical properties of concrete	78
Table 4.5	Mechanical properties of steel	78
Table 4.6	Theoretical internal forces in beams at flexural strength and maximum shear forces	80
Table 4.7	Maximum input joint shear force and joint shear strength.....	84
Table 4.8	Required total area of joint shear reinforcement	85
Table 4.9	Required total area of joint shear reinforcement according to NZS 3101:1982	86
Table 4.10	Flexural strengths obtained experimentally and theoretically	97
Table 4.11	Horizontal joint shear strength provided by prestressing steel.....	119
Table 4.12	Specifications of test units	127
Table 4.13	Mechanical properties of concrete	127
Table 4.14	Ideal flexural strength of the beams, theoretical internal forces in beams at flexural strength and maximum shear forces	128
Table 4.15	Mechanical properties of steel reinforcement	129
Table 4.16	Maximum input joint shear force and joint shear strengths	130
Table 4.17	Required total area of joint shear reinforcement	131
Table 4.18	Theoretical internal forces in beams at flexural strength and maximum shear forces	149
Table 4.19	Nominal shear strength in ACI 318-89 and joint shear strength proposed by Thompson and Park	149

Table 4.20	Ideal horizontal joint shear strength specified in NZS 3101:1982..151
Fig.4.1(a)	Precast prestressed concrete beam - column assembly test units (Units 1 and 2) by Blakeley and Park [4.1]59
Fig.4.1(b)	Precast prestressed concrete beam - column assembly test units (Units 3 and 4) by Blakeley and Park [4.1]60
Fig.4.2	Moment - displacement curve obtained from Unit 1 by Blakeley and Park [4.1]61
Fig.4.3	Moment - displacement curve obtained from Unit 2 by Blakeley and Park [4.1]62
Fig.4.4	Moment - displacement curve obtained from Unit 3 by Blakeley and Park [4.1]62
Fig.4.5	Moment - displacement curve obtained from Unit 4 by Blakeley and Park [4.1]63
Fig.4.6	Dimensions of beam-column test unit by Park and Thompson [4.6] 64
Fig.4.7	Beam and column cross sections with the steel details [4.6]64
Fig.4.8	External forces acting on the joint core [4.6]66
Fig.4.9(a)	Test results67
Fig.4.9(b)	Test results68
Fig.4.9(c)	Test results68
Fig.4.9(d)	Test results69
Fig.4.9(e)	Test results69
Fig.4.10(a)	Overall dimensions of the test units75
Fig.4.10(b)	Beam and column sections of the test units76
Fig.4.11	Beam internal forces and the column shear force acting on the joint core at the ideal flexural strength of the beam79
Fig.4.12	Design of beam - column joint according to NZS 3101:198281
Fig.4.13	Design of beam - column joint according to ACI 318-8982
Fig.4.14	Design of beam - column joint according to AIJ Guidelines83
Fig.4.15	Anchorage strength of a reinforcing bar related to the bearing strength on concrete by Fujii et al. [4.13]88
Fig.4.16	Loading setup90
Fig.4.17	Measuring apparatus90
Fig.4.18(a)	Vertical deflection at the end of the beam plotted against the corresponding load of the beam (PC1)91
Fig.4.18(b)	Vertical deflection at the end of the beam plotted against the corresponding load of the beam (PC2)92
Fig.4.18(c)	Vertical deflection at the end of the beam plotted against the corresponding load of the beam (PC3)92
Fig.4.18(d)	Vertical deflection at the end of the beam plotted against the corresponding load of the beam (PC4)93
Fig.4.18(e)	Vertical deflection at the end of the beam plotted against the corresponding load of the beam (RC1)93
Fig.4.18(f)	Vertical deflection at the end of the beam plotted against

	the corresponding load of the beam (RC2)	94
Fig.4.19(a)	Test units after testing (Series A).....	95
Fig.4.19(b)	Test units after testing (Series B).....	96
Fig.4.20	Equivalent viscous damping factor	98
Fig.4.21	Definition of equivalent viscous damping factor	99
Fig.4.22(a)	Stresses in the joint shear reinforcement measured at the peak of each loading run (PC1)	100
Fig.4.22(b)	Stresses in the joint shear reinforcement measured at the peak of each loading run (PC2)	101
Fig.4.22(c)	Stresses in the joint shear reinforcement measured at the peak of each loading run (RC1)	102
Fig.4.23	Components of deformation in the joint core.....	103
Fig.4.24(a)	Shear stress versus the measured shear distortion angle curve (PC1)	104
Fig.4.24(b)	Shear stress versus the measured shear distortion angle curve (PC2).....	105
Fig.4.24(c)	Shear stress versus the measured shear distortion angle curve (RC1)	105
Fig.4.25(a)	Contribution of each deformation component to the overall beam end deflection (PC1).....	106
Fig.4.25(b)	Contribution of each deformation component to the overall beam end deflection (PC2).....	107
Fig.4.25(c)	Contribution of each deformation component to the overall beam end deflection (PC3).....	107
Fig.4.25(d)	Contribution of each deformation component to the overall beam end deflection (PC4).....	108
Fig.4.25(e)	Contribution of each deformation component to the overall beam end deflection (RC1)	108
Fig.4.25(f)	Contribution of each deformation component to the overall beam end deflection (RC2)	109
Fig.4.26(a)	Stresses in the joint shear reinforcement measured at the peak of each loading run (PC3).....	110
Fig.4.26(b)	Stresses in the joint shear reinforcement measured at the peak of each loading run (PC4)	111
Fig.4.26(c)	Stresses in the joint shear reinforcement measured at the peak of each loading run (RC2)	112
Fig.4.26(d)	Stresses in the joint shear reinforcement measured at the peak of each loading run for all test units	113
Fig.4.27(a)	Shear stress versus the measured shear distortion angle curve (PC3)	114
Fig.4.27(b)	Shear stress versus the measured shear distortion angle curve (PC4)	114
Fig.4.27(c)	Shear stress versus the measured shear distortion angle curve (RC2).....	115

Fig.4.28(a)	Envelope curves of the tensile forces in the prestressing steel bars (PC1)	116
Fig.4.28(b)	Envelope curves of the tensile forces in the prestressing steel bars (PC2)	117
Fig.4.28(c)	Envelope curves of the tensile forces in the prestressing steel bars (PC3)	117
Fig.4.28(d)	Envelope curves of the tensile forces in the prestressing steel bars (PC4)	118
Fig.4.29	Moment - curvature characteristics compared	121
Fig.4.30(a)	Test units	125
Fig.4.30(b)	Test units	126
Fig.4.31	Beam internal forces and column shear acting on the joint	129
Fig.4.32	Loading setup and measuring devices	132
Fig.4.33(a)	Horizontal load - deflection relationships at the beam ends	134
Fig.4.33(b)	Horizontal load - deflection relationships at the beam ends	135
Fig.4.34	Test units after testing	136
Fig.4.35	Equivalent damping factor	138
Fig.4.36(a)	Moment at the column face - average curvature relationships measured in the beam plastic hinge regions	139
Fig.4.36(b)	Moment at the column face - average curvature relationships measured in the beam plastic hinge regions	140
Fig.4.37	Maximum shear distortion angles measured in the joint cores	141
Fig.4.38	Measured longitudinal strains at the center of gravity in the beam section	142
Fig.4.39(a)	Concrete strains measured at the extreme fibers of the beam section... ..	143
Fig.4.39(b)	Concrete strains measured at the extreme fibers of the beam section... ..	144
Fig.4.40	Tensile force measured in the transverse reinforcement in the joint cores	146
Fig.4.41	Joint shear strength according to AIJ Guidelines and proposed equation	147

Chapter 5

Table 5.1	Numerical values for the parameters for the prestressed concrete idealization	170
Table 5.2	Material and section properties	181
Table 5.3	Numerical values for the parameters for the idealization of the sections	182
Fig.5.1	Idealized moment - rotation hysteresis loops by Spencer [5.2]	156
Fig.5.2	PS model by Okamoto [5.3]	156

Fig.5.3	Restoring force characteristics model by Okada et al. [5.4]	156
Fig.5.4	Prestressed concrete idealization by Thompson and Park [5.1]	157
Fig.5.5	Reinforced concrete idealization by Thompson and Park [5.1]	160
Fig.5.6	Prestressed concrete idealization by Thompson and Park in large ductility region.....	162
Fig.5.7	Monotonic moment - curvature idealization curves up to the yield point or crushing point for prestressed and reinforced concrete sections	162
Fig.5.8(a)	Comparison between the idealizations by Thompson and Park, and by the author	164
Fig.5.8(b)	Comparison between the idealizations by Thompson and Park, and by the author	165
Fig.5.9	Idealized hysteresis loops for partially prestressed and reinforced concrete sections	166
Fig.5.10(a)	Comparison between idealized and experimentally obtained moment - curvature characteristics	168
Fig.5.10(b)	Comparison between idealized and experimentally obtained moment - curvature characteristics	169
Fig.5.11(a)-(f)	Comparison between the experimental and analytical moment - curvature curves up to the first yield point or crushing point	172
Fig.5.11(g)-(j)	Comparison between the experimental and analytical moment - curvature curves up to the first yield point or crushing point	173
Fig.5.12	Examples of idealized curves (different flexural cracking moments).....	175
Fig.5.13	Ratios of the areas surrounded by the idealized moment - curvature curves to those of the reinforced concrete idealization	176
Fig.5.14	Examples of idealized curves (same flexural cracking moment)....	177
Fig.5.15	Ratios of the areas surrounded by the idealized moment - curvature curves to those of the reinforced concrete idealization	178
Fig.5.16	Idealized moment - curvature curves for the sections under reversed cyclic loading	179
Fig.5.17	Prestressed, partially prestressed and reinforced concrete sections	180
Fig.5.18	Analytical moment - curvature curves subjected to monotonic loading	182

Chapter 6

Table 6.1	Range of parameters investigated.....	190
Table 6.2	Characteristics of earthquake wave records	191
Fig.6.1	Idealized structural system	188
Fig.6.2(a)	Displacement response spectra ($V_u/V_{cr}=2.0$, $K_e/K_y=2.0$ and El Centro NS (Original))	192
Fig.6.2(b)	Displacement response spectra	

	($V_u/V_{cr}=2.0$, $K_e/K_y=2.0$ and Miyagiken-oki NS (Original)).....	192
Fig.6.2(c)	Displacement response spectra ($V_u/V_{cr}=2.0$, $K_e/K_y=2.0$ and El Centro NS (50cm/s))	193
Fig.6.2(d)	Displacement response spectra ($V_u/V_{cr}=2.0$, $K_e/K_y=2.0$ and Miyagiken-oki NS (50cm/s))	193
Fig.6.2(e)	Velocity response spectra ($V_u/V_{cr}=2.0$, $K_e/K_y=2.0$ and El Centro NS (Original))	194
Fig.6.2(f)	Velocity response spectra ($V_u/V_{cr}=2.0$, $K_e/K_y=2.0$ and Miyagiken-oki NS (Original)).....	194
Fig.6.2(g)	Velocity response spectra ($V_u/V_{cr}=2.0$, $K_e/K_y=2.0$ and El Centro NS (50cm/s))	195
Fig.6.2(h)	Velocity response spectra ($V_u/V_{cr}=2.0$, $K_e/K_y=2.0$ and Miyagiken-oki NS (50cm/s))	195
Fig.6.2(i)	Acceleration response spectra ($V_u/V_{cr}=2.0$, $K_e/K_y=2.0$ and El Centro NS (Original))	196
Fig.6.2(j)	Acceleration response spectra ($V_u/V_{cr}=2.0$, $K_e/K_y=2.0$ and Miyagiken-oki NS (Original)).....	196
Fig.6.2(k)	Acceleration response spectra ($V_u/V_{cr}=2.0$, $K_e/K_y=2.0$ and El Centro NS (50cm/s))	197
Fig.6.2(l)	Acceleration response spectra ($V_u/V_{cr}= 2.0$, $K_e/K_y=2.0$ and Miyagiken-oki NS (50cm/s))	197
Fig.6.3(a)	Load - displacement relationships of SDOF systems.....	198
Fig.6.3(b)	Load - displacement relationships of SDOF systems.....	199
Fig.6.4(a)	$Q_y / Q_E - \mu$ (Prestressed concrete)	201
Fig.6.4(b)	$Q_y / Q_E - \mu$ (Partially prestressed concrete)	202
Fig.6.4(c)	$Q_y / Q_E - \mu$ (Reinforced concrete)	203
Fig.6.5	Shear force response of the system responding elastically	204
Fig.6.6(a)	Comparison of maximum displacement response	205
Fig.6.6(b)	Comparison of maximum displacement response	206
Fig.6.7(a)	Comparison of maximum displacement response	207
Fig.6.7(b)	Comparison of maximum displacement response	208
Fig.6.8	Load - displacement relationships of prestressed concrete system and reinforced concrete system with pinched hysteresis loops.....	209
Fig.6.9(a)	Displacement response spectra of reinforced concrete system with pinched hysteresis	212
Fig.6.9(b)	Velocity response spectra of reinforced concrete system with pinched hysteresis	213
Fig.6.9(c)	Acceleration response spectra of reinforced concrete system with pinched hysteresis	214
Fig.6.10	Comparison in displacement response between conventionally reinforced concrete and <i>PH</i> system	215
Fig.6.11	Comparison in displacement response between prestressed concrete and <i>PH</i> system	216

Fig.6.12	Comparison in displacement response between partially prestressed concrete and <i>PH</i> system	217
Fig.6.13	Substitute damping ratio	220
Fig.6.14	Substitute damping ratio by Gulkan and Sozen [6.9].....	220
Fig.6.15	Umemura spectra	224
Fig.6.16	Yield capacity - ductility ratio response relationships	226
Fig.6.17	Yield capacity - displacement response relationships	226

Chapter 7

Table 7.1	Natural period of four-, eight- and sixteen-story frames	241
Table 7.2	Characteristics of earthquake wave records	243
Table 7.3	Curvature ductility ratios of the plastic hinge regions of the beams and columns	249
Table 7.4	Curvature ductility ratios of the plastic hinge regions of the beams and columns of eight-story frame	255
Table 7.5	Curvature ductility ratios of the plastic hinge regions of the beams and columns of sixteen-story frame	260
Table 7.6	Maximum interstory drift responses of the frames	262
Fig.7.1	Beam model [7.1]	233
Fig.7.2	Beam plastic hinge model (small deflection theory) [7.1]	235
Fig.7.3	Column yield moment - axial load interaction model	236
Fig.7.4	Structural layout of the frames to be designed	238
Fig.7.5	Design moment of the members of a four-story building frame	240
Fig.7.6	Design moments and of each layer of an eight-story building frame	240
Fig.7.7	Moment - curvature idealization of beam plastic hinge region.....	242
Fig.7.8	Maximum interstory drift of four-story building frame	244
Fig.7.9	Story shear force - interstory drift relationship obtained from static inelastic analysis	245
Fig.7.10	Interstory drift ductilities	246
Fig.7.11 (a)	Moment - curvature curves in the plastic hinge of the second floor beams (El Centro NS)	247
Fig.7.11 (b)	Moment - curvature curves in the plastic hinge of the second floor beams (Tohoku Univ. NS)	247
Fig.7.11 (c)	Moment - curvature curves in the plastic hinge of the second floor beams (Hachinohe EW)	248
Fig.7.13	Maximum story shear force	250
Fig.7.14	Maximum interstory drift response of eight-story frame	251
Fig.7.15	Story shear force - interstory drift relationship obtained from static inelastic analysis	252
Fig.7.16	Maximum interstory ductilities	253

Fig.7.17 (a)	Moment - curvature curves in the plastic hinge of the second floor beams (El Centro NS)	253
Fig.7.17 (b)	Moment - curvature curves in the plastic hinge of the second floor beams (Tohoku Univ. NS).....	254
Fig.7.17 (c)	Moment - curvature curves in the plastic hinge of the second floor beams (Hachinohe EW)	254
Fig.7.19	Maximum story shear force	256
Fig.7.20	Maximum interstory drift of sixteen-story building frame	258
Fig.7.21	Maximum interstory drift ductilities	258
Fig.7.22	Story shear force - interstory drift relationship obtained from static inelastic analysis	259
Fig.7.23	Story shear force response of sixteen-story building frame	261
Fig.7.24(a)	Story shear force - interstory drift relationships obtained from incremental plastic analysis and idealized relationships (Four-story frame) .	263
Fig.7.24(b)	Story shear force - interstory drift relationships obtained from incremental plastic analysis and idealized relationships (Eight-story frame)	264
Fig.7.24(c)	Story shear force - interstory drift relationships obtained from incremental plastic analysis and idealized relationships (16-story frame)	264
Fig.7.25(a)	Comparison of maximum interstory drift between two-dimensional analysis and multi-mass shear system (Four-story frame)	266
Fig.7.25(b)	Comparison of maximum interstory drift between two-dimensional analysis and multi-mass shear system (Eight-story frame)	266
Fig.7.25(c)	Comparison of maximum interstory drift between two-dimensional analysis and multi-mass shear system (16-story frame).....	267
Fig.7.26(a)	Story shear force - interstory drift response of multi-mass shear system	268
Fig.7.26(b)	Story shear force - interstory drift response of two-dimensional frame analysis	269
Fig.7.27	Comparison of interstory responses of prestressed, partially prestressed and reinforced concrete frames (Two-dimensional analyses and multi-mass shear system analyses).....	270

Chapter 8

Table 8.1	Material strength for reinforcing steel	276
Table 8.2	Base shear coefficient for prestressed concrete structures	276
Table 8.3	Magnification factors	276
Table 8.4	Coefficients F_e and F_s with regard to the eccentricity ratio R_e and stiffness ratio R_s , respectively	279
Table 8.5	Maximum interstory drift angle	285
Table 8.6	Prestressing force, sectional area of prestressing steel and ordinary non-prestressed steel	291
Table 8.7	Mechanical properties of steel	297

Table 8.8	Mechanical properties of concrete	299
Table 8.9	Comparison of maximum experimentally measured flexural strengths and maximum calculated flexural strengths using ACI methods	303
Table 8.10	Maximum flexural strengths theoretically predicted.....	306
Fig.8.1	Design flow	275
Fig.8.2	Design spectral coefficient, R_f	278
Fig.8.3	Eccentricity ratio, R_e	278
Fig.8.4	Stiffness ratio, R_s	279
Fig.8.5	Shear force - interstory drift envelope model.....	282
Fig.8.6	Analytical results of maximum interstory drift angle	284
Fig.8.7	Model frame investigated	289
Fig.8.8	Tendon profile of beam.....	292
Fig.8.9(a)	Calculated M_{nyd} / M_{scd}	294
Fig.8.9(b)	Calculated M_{nyd} / M_{scd}	295
Fig.8.10	Test specimens	298
Fig.8.11	Loading setup and measuring devices	298
Fig.8.12(a)	Moment - displacement curves	301
Fig.8.12(b)	Moment - displacement curves	302
Fig.8.13	Definition of yield displacement	304
Fig.8.14(a)	Comparison of moment - curvature curves experimentally measured and theoretically predicted	308
Fig.8.14(b)	Comparison of moment - curvature curves experimentally measured and theoretically predicted	309
Fig.8.15	Stress - strain model on confined concrete.....	310
Fig.8.16	Comparison of analytical results under monotonic and cyclic loading	311
Fig.8.17	Distribution of concrete stress	312

Chapter 9

Table 9.1	Specifications of test units	322
Table 9.2	Age of the test units	324
Table 9.3	Mechanical properties of steel reinforcement	324
Table 9.4	Mechanical properties of prestressing steel.....	325
Table 9.5	Mechanical properties of concrete and grout mortar	327
Table 9.6	Ideal flexural strength of the beams, theoretical internal forces in beams at flexural strength and maximum shear forces	330
Table 9.7	Maximum input joint shear force and joint shear strengths	330
Table 9.8	Maximum load capacities experimentally and theoretically obtained	339

Fig.9.1	Procedure for improving seismic performance of precast prestressed concrete beam-column assemblages.....	321
Fig.9.2	Stress-strain relationship of grout mortar for the connection.....	323
Fig.9.3(a)	Test unit (PCX-1).....	325
Fig.9.3(b)	Test unit (PCX-2).....	326
Fig.9.3(c)	Test unit (PCX-3).....	326
Fig.9.4(a)	Stress-strain relationship of concrete for the test units PCX-1, PCX-3 and PCX-5	328
Fig.9.4(b)	Stress-strain relationship of concrete for the test units PCX-2, PCX-4 and PCX-6	328
Fig.9.5	Beam internal forces and column shear acting on the joint	329
Fig.9.6	Loading setup and measuring devices	331
Fig.9.7(a)	Horizontal load - deflection relationships at the beam ends	333
Fig.9.7(b)	Horizontal load - deflection relationships at the beam ends	334
Fig.9.7(c)	Horizontal load - deflection relationships at the beam ends	334
Fig.9.8(a)	Test units after testing	336
Fig.9.9(b)	Test units after testing	337
Fig.9.9(a)	Tendon force measured at the column side - deflection at the beam ends relationships	340
Fig.9.9(b)	Tendon force measured at the column side - deflection at the beam ends relationships	341
Fig.9.8(c)	Tendon force measured at the column side - deflection at the beam ends relationships	342

Publishment

1. M. Nishiyama, F. Watanabe and H. Muguruma, "Seismic Response of Prestressed, Partially Prestressed and Reinforced Concrete Buildings," Proceedings of Japan Concrete Institute, Vol.15 No.2, 1993, pp.1125-1130 (in Japanese).
2. M. Nishiyama, F. Watanabe and H. Muguruma, "Axial Loading Tests on High-Strength Concrete Prisms Confined by Ordinary and High-Strength Steel," Proceedings of the 3rd International Symposium on Utilization of High-Strength Concrete, Lillehammer Norway, 20-24 June 1993, pp.412-419.
3. F. Watanabe, M. Nishiyama and H. Muguruma, "Strength and Ductility of Ultra High Strength Concrete Column," Journal of Structural and Construction Engineering, AIJ, No.466, Apr., 1993, pp.99-106 (in Japanese).
4. M. Nishiyama, H. Kato, Y. Ohta and H. Muguruma, "Seismic Design of Prestressed Concrete Moment Resisting Frame in which Column Sidesway Mechanism Develops," Proceedings of the 3rd Symposium on Developments in Prestressed Concrete, 1992, pp.391-396 (in Japanese).
5. F. Watanabe, M. Nishiyama and H. Muguruma, "A consistent seismic design concept of prestressed concrete buildings," Proceedings of the 10th World Conference on Earthquake Engineering, 19-24 July 1992, Madrid Spain, pp.4383-4388.
6. H. Muguruma, M. Nishiyama, F. Watanabe and H. Tanaka, "Ductile Behaviour of High-strength Concrete Columns Confined by High-strength Transverse Reinforcement," Proceedings of ACI International Conference on Evaluation and Rehabilitation of Concrete Structures and Innovations in Design, SP-128 Vol.2, Hong Kong, December 1991, pp.877-891.
7. M. Nishiyama, F. Watanabe and H. Muguruma, "Seismic Performance of Prestressed Concrete Beam-Column Joint Assemblages," Proceedings of Pacific Conference on Earthquake Engineering, New Zealand, 20-23 November 1991, pp.217-228.
8. H. Muguruma, M. Nishiyama and F. Watanabe, "Ductility Evaluation of Reinforced Concrete Columns with Normal and High Strength Concrete," Proceedings of Pacific Conference on Earthquake Engineering, New Zealand, 20-23 November 1991, pp.159-170.

9. M. Nishiyama, F. Watanabe and H. Muguruma, "Cyclic Loading Tests on Prestressed Concrete Beam-External Column Joint Assemblies," *Journal of Structural and Construction Engineering*, AIJ, No.429, Nov., 1991, pp.31-40 (in Japanese).
10. M. Nishiyama, M. Ohira, F. Watanabe and H. Muguruma, "Improvement of Seismic Performance of Beam-Column Joint Assemblies by Prestressing Force," *Proceedings of JCI Symposium on Extensive Utilization of Prestressing Technology*, July 1991, pp.135-144.
11. M. Nishiyama, T. Fujimura, F. Watanabe and H. Muguruma, "Ductile Behaviours of Reinforced Concrete Columns with High Strength Concrete and Transverse Steel," *Proceedings of Japan Concrete Institute*, Vol.13, 1991, pp.409-414 (in Japanese).
12. M. Nishiyama, "Seismic Design of Prestressed Concrete Buildings," *Bulletin of the New Zealand National Society for Earthquake Engineering* Vol.23, No.4, Dec. 1990, pp.288-304.
13. M. Nishiyama, H. Muguruma and F. Watanabe, "Hysteretic Restoring Force Characteristics of Unbonded Prestressed Concrete Structure Under Earthquake Loads", *Bulletin of the New Zealand National Society for Earthquake Engineering* Vol.22, No.2, June 1989, pp.112-121.
14. M. Nishiyama, T. Nishizaki, H. Muguruma and F. Watanabe, "Seismic Design of Prestressed Concrete Beam-Exterior Column Joints", *Transactions of The Japan Concrete Institute* Vol.11, 1989, pp.439-446.
15. M. Nishiyama, H. Muguruma and F. Watanabe, "On the Unbonded Prestressed Concrete Members in Seismic Structures," *Proceedings of Ninth World Conference on Earthquake Engineering*, August 2-9, 1988, Tokyo-Kyoto, JAPAN(Vol.VIII), pp.743-748.
16. H. Muguruma, F. Watanabe and M. Nishiyama, "Curvature Ductility Design of Reinforced and Prestressed Concrete Members," *Proceedings of Ninth World Conference on Earthquake Engineering*, August 2-9, 1988, Tokyo-Kyoto, JAPAN(Vol.VIII), pp.617-622.
17. H. Muguruma, F. Watanabe and M. Nishiyama, "Development of Ductile Pretensioned High Strength Spun Concrete Piles and Ductility Design Criteria," *Proc. of The 31st Japan Congress on Materials Research* 1988, pp.103-109.
18. M. Nishiyama, H. Muguruma and F. Watanabe, "Hysteretic Restoring Force Characteristics of Unbonded Prestressed Concrete Framed Structure under Earth-

quake Load," Proc.of Pacific Concrete Conference,Auckland,New Zealand 8-11 Nov.1988, pp.101-112.

19. M. Nishiyama, H. Muguruma and F. Watanabe, "Improving the Flexural Ductility of Concrete Members by Lateral Confining of Concrete," JCI Colloquium on Ductility of Concrete Structures and its Evaluation, March 1988, pp.33-44 (in Japanese).
20. H. Muguruma, F. Watanabe and M. Nishiyama, "Behaviour of Unbonded Prestressed Concrete Beam in Rigid Frame," Transactions of the Japan Concrete Institute 1986, pp.259-266.

Chapter 1

INTRODUCTION

1.1 Prestressed concrete

The ACI building code [1.1] defines reinforced concrete and prestressed concrete for general use in the code as follows;

Reinforced concrete -

Concrete reinforced with no less than the minimum amount required by this code, prestressed or nonprestressed, and designed on the assumption that the two materials act together in resisting forces.

Prestressed concrete -

Reinforced concrete in which internal stresses have been introduced to reduce potential tensile stresses in concrete resulting from loads.

Prestressed concrete is a type of reinforced concrete in which the steel reinforcement has been tensioned against the concrete to improve its response to external loads in the aspect of both capacity and deformation. It should be discussed within the category of reinforced concrete.

Prestressed concrete was first introduced to Japanese engineers 41 years ago when pretensioned roof panels were constructed. Since many applications have been attempted and succeeded in the civil engineering field. However, in the building construction field a relatively small number of buildings have been erected. Some of these have attracted the attention of the structural engineering community because of their innovation and dynamism. Several reasons why prestressed concrete structures have not been very successful are that calculation and construction are complicated, they are a little more expensive than reinforced concrete structures, and only a small number of engineers have experience with it. However, prestressed concrete is just an extension of reinforced concrete. For structural engineers who understand reinforced concrete, prestressed concrete is also understandable. Design in prestressed concrete can result in much larger spans of beams without cracking (or with small crack widths), and smaller deflections than design in reinforced concrete. It also leads to more slender structures. Generally span-to-depth ratios of reinforced and prestressed concrete beams are approximately 10 and 20, respectively. Thus, prestressing can save 20~30 % of the concrete volume.

It was reported [1.2] that prestressing would increase the cost of a typical office building by only 2~4%. In this case the prestressed concrete building had twice as long beams as the reinforced concrete beams in one direction and in the orthogonal direction it has the same span length as the reinforced concrete building. Adoption of SRC (steel reinforced concrete) increases the cost by 20~30% compared with reinforced concrete. This example shows that the cost of a prestressed concrete building is not expensive enough to dissuade structural engineers from adopting prestressed concrete as a structural type because prestressed concrete has some advantages over reinforced concrete.

The advantages of prestressed concrete building structures are:

1. high durability due to the use of high-quality concrete
2. more slender members resulting in a lighter-weight building
3. larger space because of larger span beams
4. a reduced construction term and rationalization of construction by assembling precast prestressed elements in construction sites
5. no cracking is effective for offensive circumstances
6. less damage due to less energy absorbed in "pinched" hysteresis loops

The comparison of structural types is summarized in Table 1.1 using a six-story building as an example.

A prestressed concrete building usually consists of prestressed concrete beams and reinforced concrete columns and walls. In case of precast prestressed concrete buildings columns may be prestressed. According to the current concrete design codes in Japan ordinary prestressed concrete buildings lower than 31 m can be designed either by the ultimate strength design procedure or by the ultimate capacity design procedure. In the ultimate strength design procedure elastic analysis can be employed to obtain design stresses of the members while in the capacity design procedure plastic analysis is required to obtain an ultimate capacity of each layer. Since the ultimate strength design procedure is supposed to be easier than the ultimate capacity design procedure and non-iterative, most of structural designers prefer ultimate strength design to ultimate capacity design. However, is a building with only one prestressed concrete beam called a prestressed concrete building? This must be left to the structural designers' discretion.

The other problems will be discussed in this thesis on the basis of the author's research results. *Structural concrete* is usually divided into four categories: Class I (prestressed concrete), Class II (partially prestressed concrete), Class III (partially prestressed concrete or prestressed reinforced concrete) and Class IV (ordinary reinforced concrete).

Class I: Stress at the extreme tension fiber of the section is in compression under service load conditions. There is no possibility of cracking under service loads.

Table 1.1 Comparison of structural types (in case of six-story office building)

	Reinforced concrete	Partially prestressed concrete	Prestressed concrete	Precast prestressed concrete	Steel reinforced concrete	Steel
Standard span length	$l < 10\text{m}$	$10 < l < 15$	$12 < l < 20$	$12 < l < 20$	$10 < l < 18$	$l < 20$
Beam height	$l/10$	$l/10 \sim l/12$	$l/18 \sim l/20$	$l/15 \sim l/20$	$l/13 \sim l/15$	$l/13 \sim l/15$
Crack	Crack	Controls crack width	No crack	No crack	Crack	
Durability	Average	Good	Better	Best	Good	Becomes rusty
Fire resistance	Good	Good	Good	Good	Good	Needs to be covered with fire resistance material
Vibration problem	No problem	No problem	No problem	No problem	No problem	Prone
Labor needed at construction site	Much	Much	Much	Less	Much	Less
Term of construction	Average	Average	Average	Short	Long	Short
Cost	1	1.03	1.03~1.05	1.15	1.2~1.4	1

From "Design and construction manual of prestressed concrete" by Prestressed Concrete Contractors Association.

Class II: Stress at the extreme tension fiber of the section is in tension but not greater than the allowable tensile stress of concrete under service load condition.

Class III: Flexural cracking under service load condition is permitted. However, the crack width shall be less than the allowable values which is specified depending on the environmental condition or the designers' decision.

Class IV: Ordinary reinforced concrete.

In this thesis, however, three categories are adopted : fully prestressed concrete, partially prestressed concrete and reinforced concrete. Fully prestressed concrete corresponds to the above category Class I. Class II and III are included in partially prestressed concrete.

1.2 Seismic performance of prestressed concrete building structures

Even with the advantages described above it has been considered that the seismic performance of prestressed concrete is inferior to that of reinforced concrete because of its hysteretic characteristics and ductility. Hysteresis loops of prestressed concrete members are narrower than those of reinforced concrete members, which have less energy dissipation. Past research on prestressed concrete members have pointed out that the behavior of prestressed concrete is less ductile than that of reinforced concrete.

Chapter 21 of ACI 318-89 contains special requirements for the design and construction of a structure with reinforced concrete members. The design forces, related to earthquake motions, are determined on the basis of energy dissipation in the nonlinear range of response. Section 21.2.5 of this chapter specifies reinforcement in members resisting earthquake-induced forces. It requires that the ratio of the actual ultimate tensile stress to the actual tensile yield strength be not less than 1.25. This requirement is based on the assumption that the capacity of a structural member to develop inelastic rotation capacity is a function of the length of the yield region along the axis of the member. According to the experimental results [1.3] the larger the ratio of ultimate to yield moment, the larger the yield region. Prestressing steel does not have such a large ratio. For instance, according to ASTM [1.4], the ratio of the minimum tensile strength to the minimum yield strength for prestressing tendons is 1.17 for 0.5 and 0.6 in. stress-relieved strands, respectively. Therefore, prestressed concrete members are considered not to develop sufficient inelastic rotation for plastic hinging to spread over the whole structure. Besides that, precompressed concrete may fail in compression at an earlier stage of loading than reinforced concrete. However, past research [1.5] showed that high-uniform elongation prestressing steel and transverse confining steel can improve ductility of prestressed concrete members.

Park [1.6] pointed out that "prestressed concrete members have significantly narrower moment-curvature hysteresis loops as shown in Fig.1.1, and hence very much lower hysteretic energy dissipation, than reinforced concrete or structural steel members.

The maximum displacements reached by code-designed prestressed concrete single-degree-of-freedom systems have been found to be on average 30% greater than reinforced concrete systems of similar initial strength, initial stiffness and viscous damping, when responding to severe earthquakes [1.7]." However, Park also pointed out in the same reference [1.6]:

It is evident that in the past there has been excessive emphasis on the desirability of achieving in design structures which, when subjected to cyclic deformations in the inelastic range due to severe earthquake loading, display "fat" load-deformation hysteresis loops. It is now realized that some variation in hysteresis loop shape will not have a major influence on the inelastic dynamic response of earthquake excitation. That is, hysteresis loops showing some pinching or stiffness degradation will not lead to significantly larger inelastic displacements, providing that the structure has some damping of viscous type and is capable of some further damping by hysteretic energy dissipation.

Besides that, in the reference [1.8] Thompson stated that:

The effect of earthquake response spectra may be extremely significant. In practice a prestressed concrete frame will be more flexible than a reinforced concrete structure carrying the same gravity loads, due to its smaller section sizes, and hence the displacement ductility demands may be less than that of an equivalent reinforced concrete structure of the same strength. On this evidence the case for the use of greater seismic design loads for prestressed concrete than for reinforced concrete is debatable.

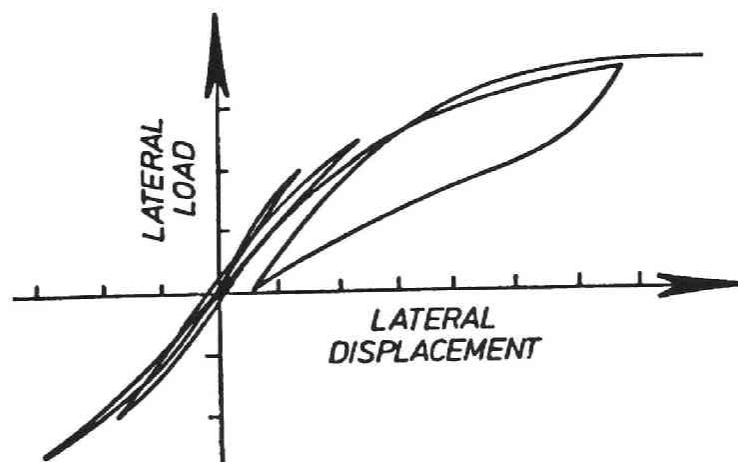


Fig.1.1 Typical measured lateral-load displacement hysteresis loops for subassemblages of a post-tensioned prestressed concrete portal frame controlled by flexural plastic hinging [1.6]

1.3 Aims of this research

The primary objective of this study is to extract the problems from the current seismic design code provisions for prestressed concrete building structures and to present the fundamental information so that the response of prestressed concrete sections, members and building frames can be predicted. On the basis of the above knowledge a tentative rational seismic design procedure will be discussed.

This research is consisted of nine chapters and an appendix:

The current seismic design procedure for prestressed concrete building structures in Japan is summarized in Chapter 2. The seismic design loads used in the Japanese and New Zealand loadings codes are compared and some aspects in the current seismic design procedures in New Zealand and Japan are discussed by comparison between the design methods for reinforced and prestressed concrete building structures.

In Chapter 3 moment-curvature characteristics of prestressed, partially prestressed and reinforced concrete member sections will be discussed in terms of yield curvature, ductility and ultimate available curvature. In addition, an analytical procedure for predicting moment-curvature characteristics of prestressed concrete member sections which incorporates stress-strain relationships of concrete, ordinary reinforcement and prestressing steel is described.

Reversed cyclic loading tests on prestressed concrete beam-column joint assemblages by the author will be reported in Chapter 4. These were conducted to examine the effect of prestress on the shear resistance of beam-column joints when the prestress was introduced into a beam through the joint. The main parameters investigated are the locations of prestressing steel bar in the section and amount of prestressing force introduced into the beam. The experimental results will be discussed in terms of hysteresis behavior of the assemblages and shear resistance of the joint core.

In Chapter 5 the moment-curvature relationships of prestressed, partially prestressed and reinforced concrete sections are idealized on the basis of the moment-curvature model proposed by Thompson and Park and the experimental work described in Chapter 4.

Dynamic response analyses of single-degree-of-freedom prestressed concrete systems are carried out in Chapter 6. On the basis of the analytical results and substitute damping procedure proposed by Gulkan and Sozen a method for predicting displacement response of prestressed, partially prestressed and reinforced concrete will be presented.

In Chapter 7 two-dimensional dynamic response analyses conducted on prestressed, partially prestressed and reinforced concrete model frames will be reported. The

analytical results will be compared with past research and the results of dynamic response analyses on a multi-degree-of-freedom shear system.

In Chapter 8 a seismic design proposal by AIJ task-committee on seismic design of prestressed concrete building structures is summarized. In this proposal a column sidesway (soft story) mechanism is incorporated as one of the intended failure mechanisms. This is because of difficulty of designing a prestressed concrete building in a beam sidesway failure mechanism. Some design examples are shown which demonstrate the problems of this approach. Reversed cyclic loading tests on high strength reinforced concrete columns will be reported to see if adequate ductility is secured even for high strength concrete columns with a concrete compressive strength of 130 MPa.

Two attempts have been made in order to improve the seismic performance of precast prestressed concrete beam - column assemblages. Reversed cyclic loading tests on precast prestressed concrete beam - column joint assemblages conducted to confirm the effects of the above ideas will be described in Chapter 9.

Chapter 10 summarizes the conclusions of this research and suggests recommendations for future research.

In addition, two papers written by the author are attached as an appendix in order to discuss the response of unbonded prestressed concrete both experimentally and analytically.

[References]

- 1.1 "Building Code Requirements for Reinforced Concrete (ACI 318-89) and Commentary - ACI 318R-89," American Concrete Institute, Detroit, 1989.
- 1.2 "Design manual for prestressed concrete buildings," Japan Prestressed Concrete Contractors Association, 1989.
- 1.3 ACI-ASCE Committee 352, "Recommendations for Design of Beam-Column Joints in Monolithic Reinforced Concrete Structures," (ACI 352R-76) (Reaffirmed 1981), American Concrete Institute, Detroit, 1976, 19pp.
- 1.4 American Society for Testing and Materials, "Specification for Uncoated 7-wire Stress-Relieved Steel Strand for Prestressed Concrete," ASTM A416-85, ASTM, Philadelphia, 1985.
- 1.5 H. Muguruma, F. Watanabe and M. Nishiyama, "Improving the Flexural Ductility of Pretensioned High Strength Spun Concrete Piles by Lateral Confining of Concrete," Proceedings of Pacific Conference on Earthquake Engineering, Wairakei, New Zealand, 1987, pp.385-396.
- 1.6 Park, "Evaluation of Ductility of Structures and Structural Assemblages from Laboratory Testing," Bulletin of the New Zealand National Society for Earth-

- quake Engineering, Vol.22, No.3, September 1989, pp.155-166.
- 1.7 Thompson, K.J. and Park, R : Seismic Response of Partially Prestressed Concrete, Journal of Structural Division, Proceedings of ASCE Aug.1980 ST8, pp.1755-1775.
 - 1.8 K. J. Thompson : Ductility of Concrete Frames under Seismic Loading, Ph. D. Thesis, University of Canterbury, New Zealand, 1975.

CURRENT SEISMIC DESIGN PROCEDURE FOR PRESTRESSED CONCRETE BUILDINGS IN JAPAN

2.1 Introduction

In this chapter, the current seismic design procedure for prestressed concrete buildings in Japan is summarized. This chapter contains comparison of seismic design loads between New Zealand and Japan, too because the current loadings code in New Zealand (NZS 4203:1984) [2.1] is the only code in the world that has a provision for prestressed concrete structures. Then, some aspects in the current seismic design procedure in New Zealand and Japan will be disclosed by comparing design methods for reinforced and prestressed concrete building structures.

2.2 Current seismic design procedure for prestressed concrete buildings in Japan

2.2.1 Code approaches

Since the Standard for Structural Design and Construction of Prestressed Concrete Structures [2.2] was issued by Architectural Institute of Japan (AIJ) in 1961, the structural design of prestressed concrete buildings has been based on the strength design method. The design of reinforced concrete buildings had been based on allowable stress design until a drastic revision was made in 1981. The current seismic design method for prestressed concrete buildings was also revised in 1981 by taking into account some innovation provisions of the revised design and loading code for reinforced concrete buildings.

The design procedure for prestressed concrete structures issued in 1961 and revised in 1981 is divided into some options with respect to the height of a building to be designed. For a building height equal to or less than 60 m, there are six options which a designer can consider. In this chapter, two typical options which can be applied to a building lower than or equal to 60m are described.

Figure 2.1 is a flow diagram of the design procedure, showing two alternatives. The structural design of both alternatives is divided into two phases. One is the first phase design based on the allowable stress design concept with linear elastic analysis. The

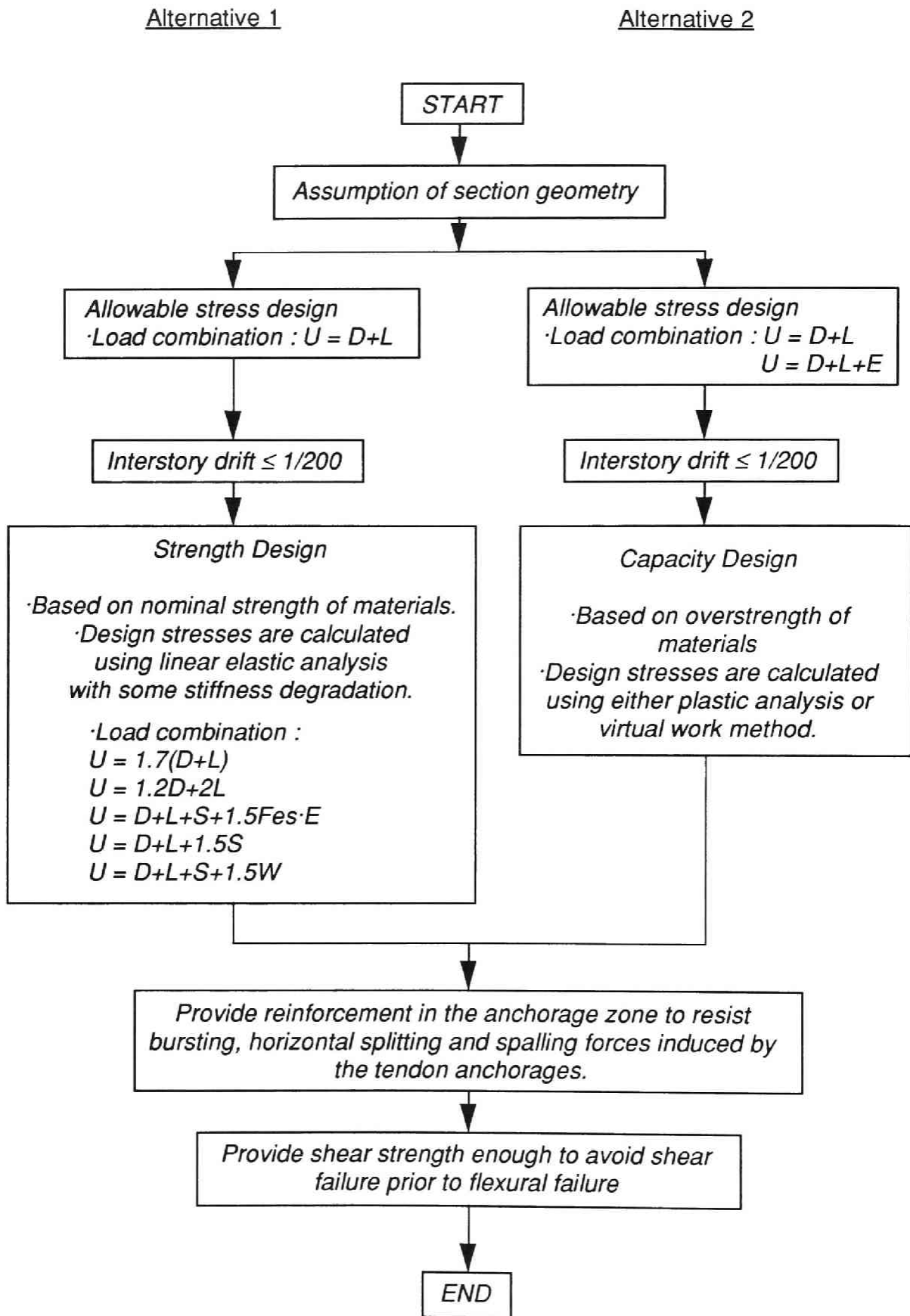


Fig.2.1 Flow diagram for the design procedure

other is the second phase design based on the strength design method with specified strengths of materials or capacity design based on overstrength of materials. The first phase design is for checking serviceability, and the second is for confirming that the building has a greater ultimate strength than is required by the design seismic load. Prestressing is primarily introduced to improve serviceability by reducing the crack widths and deflections of beams and slabs. However, excessive prestressing may result in unsatisfactory behaviour at service loads such as excessive camber. Therefore, the checking of serviceability is inevitable.

2.2.2 First phase design

In the first phase design using the alternative 1, the service load combination is $D + L$, where D and L denote the service dead and live load, respectively. The service snow load, S , may be added as well, if necessary. It is not required to consider earthquake at this stage because the second phase design will ensure sufficient strength. Members are designed either not to crack (fully prestressed concrete) or to meet the specified crack width limit (partially prestressed concrete) under this load combination. Deflections of members are expected to be within acceptable limits. Interstory drift calculated for the design earthquake load of $D + L + E$ by elastic analysis shall be smaller than or equal to $1/200$, where E denotes the seismic design load due to lateral shear force Q_i given by Eq.2.6. This limitation may be eased to $1/120$ where it is confirmed that non-structural elements may not be damaged so seriously.

When the alternative 2 is used, an allowable stress design is also required for the seismic load combination of $D + L + E$.

The second phase design is supposed to be carried out to confirm that a building designed according to the first phase design has an ultimate strength equal to or greater than the seismic design load based on possible severe earthquake motions. Practically, when designing relatively large buildings in which earthquake loading is dominant, structural designers first may conduct the second phase design and then confirm that the members meet the first phase design requirements.

2.3.3 Second phase design by strength design (Alternative 1)

This design method is applied to a building lower than or equal to 31 m. In the ultimate strength design procedure, the flexural and shear strengths of members are calculated using nominal strengths of materials. The design actions in the members under the factored design load are calculated using linear elastic analysis. The design loads, U , shall be not less than whichever of the following load combinations is applicable and gives the most critical effect:

$$U = 1.7(D + L) \quad (2.1)$$

$$U = 1.2D + 2L \quad (2.2)$$

$$U = D + L + (S) + 1.5F_{es} \cdot E \quad (\text{with earthquake}) \quad (2.3)$$

$$U = D + L + 1.5S \quad (\text{with snow}) \quad (2.4)$$

$$U = D + L + 1.5W \quad (\text{with wind}) \quad (2.5)$$

In Eq.2.3, E denotes design load due to lateral shear force Q_i , which is given by

$$Q_i = W_i \cdot C_i \quad (2.6)$$

where W_i = gravity load above the i -th story,

C_i = lateral seismic shear coefficient of the i -th story which is given by the following equation.

$$C_i = Z \cdot R_i \cdot A_i \cdot C_o \quad (2.7)$$

where Z = seismic hazard zoning coefficient and varies between 0.8 to 1.0,

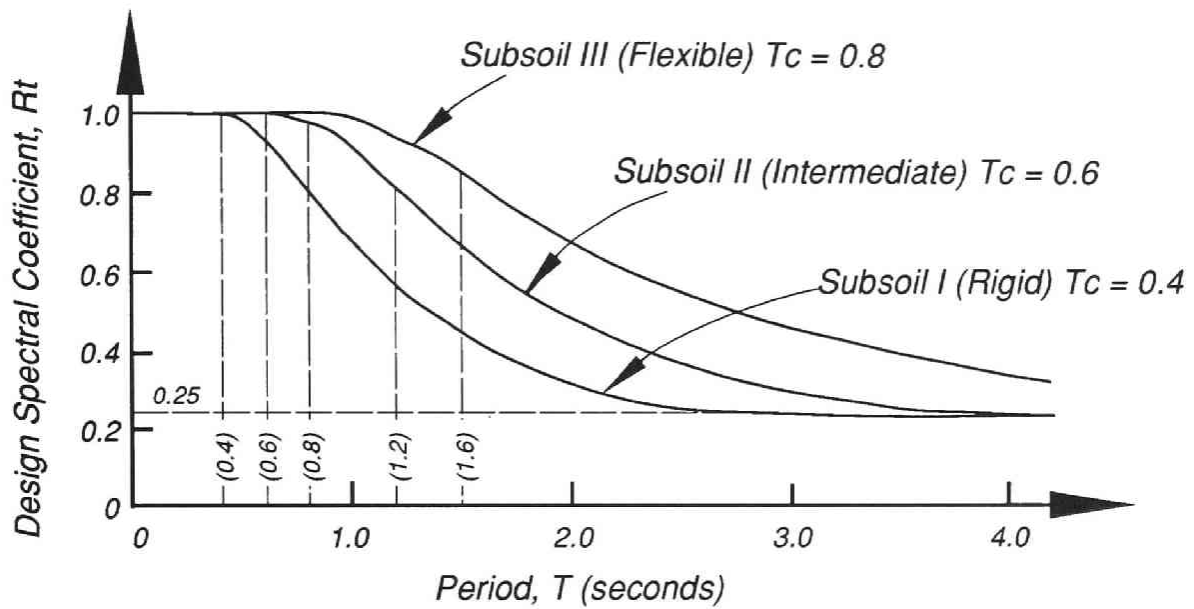
R_i = design spectral coefficient which depends on a subsoil profile and a natural period of vibration of a building, and R_i is given by Eq.2.8.

$$R_i = \left\{ \begin{array}{ll} 1 & T < T_c \\ 1 - 0.2(T/T_c - 1)^2 & T_c \leq T \leq 2T_c \\ 1.6T_c/T & 2T_c < T \end{array} \right\} \quad (2.8)$$

where T is a period of first mode of a building and T_c is a factor with respect to a subsoil profile. A longer natural period results in smaller R_i . R_i ranges between 1.0 to 0.25, and is expressed schematically in Fig.2.2. Also, A_i = the distribution factor of lateral shear forces along the height. A_i is given by Eq.2.9.

$$A_i = 1 + \left(\frac{1}{\sqrt{\alpha_i}} - \alpha_i \right) \frac{2T}{1 + 3T} \quad (2.9)$$

where α_i is the ratio of the reduced gravity load above the i -th layer to the total reduced gravity load above the level of imposed lateral ground restraint. Also, C_o is the basic seismic coefficient of 0.2, and corresponds to a ground acceleration of about 0.08 - 0.10g. Recently, it has become popular to express the intensity of an earthquake in terms of the velocity because the velocity is related directly to the energy. Thus, the above acceleration corresponds to a ground velocity of 25-30 cm/s.



$$R_t \begin{cases} 1 & (T < T_c) \\ 1 - 0.2(T/T_c - 1)^2 & (T_c \leq T \leq 2T_c) \\ 1.6T_c/T & (2T_c) \end{cases}$$

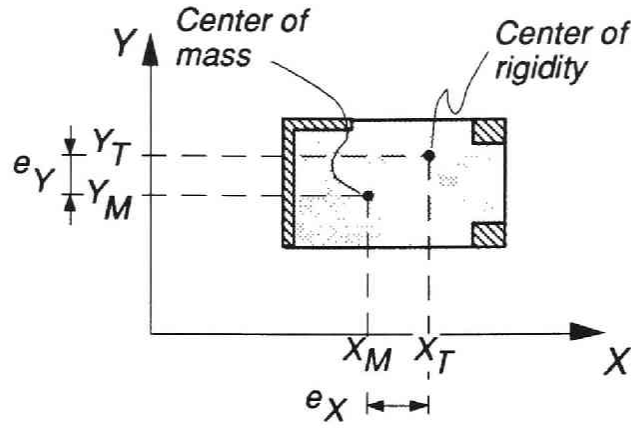
Fig.2.2 Design spectral coefficient, R_t

In Eq.2.3,

$$F_{es} = F_e \cdot F_s \quad (2.10)$$

where F_e is a coefficient that is related to the eccentricity ratio R_e in each story (see Fig.2.3) and ranges between 1.0 and 1.5. The arrangement of the seismic load resisting elements in a building should be as symmetrical as possible about the center of mass of the building in order to minimize the torsional response of the building during an earthquake. Also, F_s is a coefficient that is dependent on the stiffness ratio R_s in each story (see Fig.2.4) and ranges between 1.0 and 1.5. F_s is introduced because the existence of an extremely flexible story can lead to a dangerous concentration of damage into the story. Values for F_e and F_s with regard to R_e and R_s , respectively, are given in Table 2.1.

F_{es} from Eq.2.10 varies between 1.0 and 2.25. F_{es} was introduced to provide an extra strength in the case of buildings with an unsymmetrical arrangement of the seismic load resisting elements and/or with extremely flexible stories.



$$e_x = [X_M - X_T] \quad e_y = [Y_M - Y_T]$$

$$R_{ex} = \frac{e_x}{\sqrt{K_t / K_{hx}}} \quad R_{ey} = \frac{e_y}{\sqrt{K_t / K_{hy}}}$$

$$K_{hx} = \sum_i J_{xi} \quad K_{hy} = \sum_i J_{yi}$$

$$K_t = \sum_i J_{xi} \cdot y_i^2 + \sum_i J_{yi} \cdot x_i^2$$

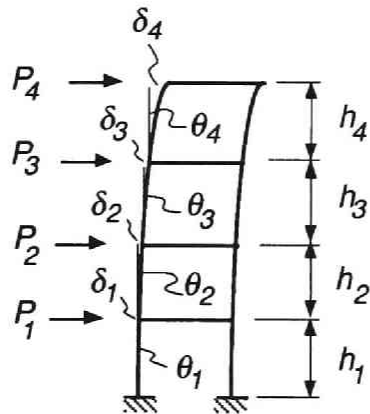
Note:

J_{xi}, J_{yi} : Lateral stiffnesses of vertical structural element i in X and Y directions, respectively.

x_i, y_i : Coordinates of i -th element measured from the center of torsion.

R_{ex}, R_{ey} : Eccentricity ratios in X and Y directions, respectively.

Fig.2.3 Eccentricity ratio, R_e



$$\theta_j = \frac{\delta_j}{h_j}$$

$$R_{sj} = \frac{1}{\theta_j} \cdot \frac{1}{n \left[\sum_{i=1}^n \frac{1}{\theta_i} \right]}$$

Note:

θ_j : Interstory drift of j -th story under seismic design load of the first phase design.

δ_j : Interstory displacement.

h_j : Story height.

R_{sj} : Stiffness ratio.

n : Number of stories.

Fig.2.4 Stiffness ratio, R_s

Table 2.1 Coefficients F_e and F_s with regard to the eccentricity ratio R_e and stiffness ratio R_s , respectively.

R_e	F_e	R_s	F_s
≤ 0.15	1.0	≥ 0.60	1.0
0.15 - 0.30	Linear interpolation	0.30 - 0.60	Linear interpolation
≥ 0.30	1.5	≤ 0.30	1.5

The code does not rely on the plastic deformation of prestressed concrete members. There is no provision on moment redistribution. Prestressed concrete members usually have higher flexural crack loads than reinforced concrete, and they recover to their original states and respond elastically even after they are loaded up to near their ultimate strengths. However, in practice it is unusual for a member section to contain prestressed steel without non-prestressed mild flexural steel except for precast prestressed concrete structures. A reasonable amount of non-prestressed mild steel in the member section results in hysteresis loops and energy dissipation characteristics which are similar to those obtained from reinforced concrete members. Besides, the ultimate state typical for prestressed concrete members due to compression failure in concrete followed by critical reduction in load carrying capacity can be avoided by appropriate confining of the concrete. A seismic design procedure which accounts for the ductility of members is given in a seismic design procedure proposed by the AIJ sub-committee on seismic design of prestressed concrete [2.3].

2.3.4 Second phase design by capacity design (Alternative 2)

The more recent seismic design procedure for reinforced concrete buildings was introduced in 1981, soon after the severe Miyagiken-oki earthquake in 1978. The design procedure is divided into two phases : one is the seismic design for moderate earthquakes and the other is for severe earthquakes. A moderate earthquake is defined as an earthquake which is assumed to happen a few times within the service life of buildings. Buildings are expected to respond to it in an elastic manner and not to be damaged. A severe earthquake is defined as a devastating earthquake which is assumed to possibly happen once in the service life of buildings. Buildings are expected not to collapse but possibly undergo some structural and non-structural damage.

After the 1981 Code came into force, prestressed concrete buildings could be designed according to either the previous standard for design and construction of prestressed concrete described or the new seismic design procedure issued in 1981. This is a reason why there are some options in the design of prestressed concrete buildings. A building higher than 31 m and lower than or equal to 60m shall be designed according to the more recent design method.

In Japan, the design procedure issued in 1981 is called capacity design, but this capacity design is different from the one described in NZS 3101:1982 [2.4]. In NZS 3101:1982, energy-dissipating elements of mechanisms are chosen and suitably detailed and other structural elements are provided with sufficient reserve strength capacity to ensure that the chosen energy-dissipating mechanisms are maintained at near their full strength throughout the deformations that may occur. However, in the design procedure in Japan issued in 1981, it is not necessary to consider favourable energy-dissipating mechanisms, although a ductile moment resisting frame is so designed as to avoid brittle failures such as shear failure. The building is required to have sufficient ultimate strength to resist severe seismic actions whatever the collapse mechanism may be.

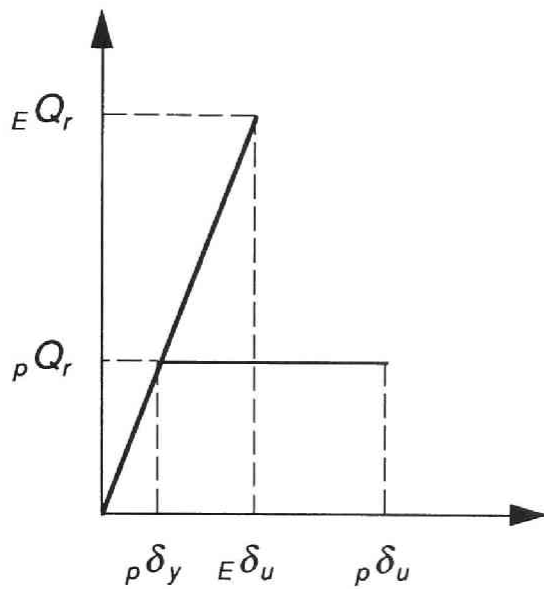
The lateral load resistance in each story is calculated using inelastic analysis or the virtual work method based on the overstrengths of materials. The building is required to have a lateral shear strength greater than the shear force at each story corresponding to the load combination of $U = D + L + 1.5F_{es} \cdot E'$, where, E' is due to seismic story shear Q_i' , which is given by

$$Q_i' = D_s \cdot W_i \cdot Z \cdot R_t \cdot A_i \cdot C_o \quad (2.11)$$

where C_o is the standard base shear coefficient and for the second phase design $C_o = 1.0$. This corresponds to a ground acceleration of 0.30 - 0.40 g and a velocity of approximately 50 cm/s. D_s is the reduction factor which depends on the type and the ductility of the structure. This factor is based on the equal energy concept in which the energy absorbed by a building which yields with elasto-plastic characteristics is assumed to be equal to that of a building which is strong enough to respond elastically. From Fig.2.5,

$$D_s = \frac{1}{\sqrt{2\mu - 1}} \quad (2.12)$$

where μ is the allowable displacement ductility factor in each story. D_s ranges from 0.3 for ductile frames to 0.55 for a building in which a large portion of lateral load is assigned to walls and braces. Other coefficients are the same as those described in the previous section.



Note:

$E Q_r, p Q_r$: Lateral inertia load responses in structures with elastic and elasto-plastic characteristics, respectively.

$E \delta_u, p \delta_u$: Maximum horizontal displacements.

$p \delta_y$: Horizontal displacement at first yield.

μ : Ductility ratio.

$$D_s = \frac{p Q_r}{E Q_r} = \frac{1}{\sqrt{2\mu - 1}}$$

$$\mu = \frac{p \delta_u}{p \delta_y}$$

Fig.2.5 Equal energy concept and the reduction factor, D_s

Comparing the seismic design load of the strength design method in the previous section with that of this alternative design method, it is found that they are identical in the case of prestressed concrete ductile frames. However, the strength design method is based on a linear elastic analysis and nominal material strengths, while the capacity design method is based on plastic analysis and material overstrengths.

In case a designer chooses this option, he has to conduct an allowable stress design for the load combination of $U = D + L + E$, where E is identical to the load used in Eq.2.3.

2.3 Comparison of seismic design load between New Zealand and Japan

It is said that the seismic design load specified in the Japanese code is much larger than that specified in NZS 4203:1984 [2.1], although the seismicity of both countries is supposed to be almost the same. The New Zealand code is based on the equal displacement concept in which the maximum horizontal deflection reached by a building which yields with elasto-plastic characteristics is assumed to be the same as that of a building which is strong enough to respond in the elastic range. The Japanese code is based on the equal energy concept in which the energy absorbed by a building which yields with elasto-plastic characteristics is assumed to be the same as that of a building which is strong enough to respond elastically. However, for buildings with a relatively long period of vibration, the Japanese code uses the equal displacement

concept. If available ductilities are expected to be the same, the yield force, Q_{yd} and Q_{ye} , required by the equal displacement and equal energy concepts, respectively, are given by the following equations.

$$Q_{yd} = Q_e / \mu \quad (2.13)$$

$$Q_{ye} = Q_e / \sqrt{2\mu - 1} \quad (2.14)$$

where, Q_e is the required strength of an elastically responding building. Therefore, $Q_{ye} \geq Q_{yd}$ for $\mu \geq 1$.

For example, consider a prestressed concrete ductile frame with a symmetrical arrangement of the seismic load resisting elements about the center of mass and without extremely flexible stories. Let the frame be built on a rigid subsoil in the most hazardous zone. The design loads U in NZS for the strength method with earthquake are given by the following load combinations.

$$U = 1.0D + 1.3L_R + E_N \quad (2.15)$$

$$U = 0.9D + E_N \quad (2.16)$$

The Japanese code gives the following load combination.

$$U = D + L + 1.5 \cdot F_{es} \cdot E \quad (2.17)$$

Here, $E_J = 1.5 \cdot F_{es} \cdot E$ is regarded as the seismic design load in the Japanese code, while in NZS, E_N is the seismic design load. The effects of seismic loads in relation to the total design loads are different in the two codes because the load factors for dead load and live load are different.

In NZS, the seismic design load is given by the total horizontal seismic force V , while in the Japanese code it is given by the shear force acting on each story. The distribution of the seismic load along the height of a building in NZS 4203:1984 is a triangular shape with a concentrated load at the top of the building. The Japanese code gives the A_i distribution described in the section on the second phase strength design. The Design Guideline for Earthquake Resistant Reinforced Concrete Buildings based on Ultimate Strength Concept published by AIJ in 1990 [2.5] have adopted the same distribution as NZS 4203:1984.

The total horizontal seismic force, V , in NZS 4203:1984, and the shear force acting on the first story, Q_1 , in the Japanese code are given by $C_d \cdot W_t$ and $C_1 \cdot W_1$, respectively.

Therefore, the seismic design coefficient C_d in NZS can be compared with the base shear coefficient C_1 of the Japanese code, if the total reduced gravity loads above the level of imposed lateral restraint W_l in NZS and W_1 in the Japanese code are assumed to be identical. C_d is given by the following equation:

$$C_d = C \cdot R \cdot S \cdot M = 0.8C \quad (2.18)$$

where, the risk factor R is assumed to be the smallest value, 1.0, because the Japanese code, which does not have a factor corresponding to the risk factor, is supposed to be at least satisfied and a designer can provide further load capacity to a building within the budget if he predicts its failure would lead to an unusually high level of loss. The structural type factor S is taken as 0.8 for a ductile frame and the structural material factor M is taken as 1.0 for a prestressed concrete building. The basic seismic coefficient C depends on the period of vibration of the building, the seismic zone and the subsoil.

C_1 is given by the following equation:

$$C_1 = 1.5 \cdot F_{es} \cdot Z \cdot R_t \cdot A_1 \cdot C_o = 0.3 \cdot R_t \quad (2.19)$$

where, F_{es} is taken as 1.0 for a building with a symmetrical arrangement of seismic load resisting elements about the center of mass and without extremely flexible stories, $Z = 1.0$ for the most hazardous zone, $A_1 = 1.0$ for the first story and $C_o = 0.2$. The design spectral coefficient R_t depends on the period of vibration of the building and the subsoil.

In NZS, the period T shall be established from properly substantiated data, or computation, or both. T may be calculated by the following Rayleigh formula:

$$T = 2\pi \sqrt{\frac{\sum (w_z \cdot d_x^2)}{g \sum (F_x \cdot d_x)}} \quad (2.20)$$

Therefore, T can be calculated from the real structural stiffness and mass. On the other hand, in the Japanese code, the period in seconds is calculated using the following equation for reinforced concrete buildings:

$$T = 0.02h \quad (2.21)$$

where, h is the height of the building in meters. Hence T depends on the height only, and this may lead to a much shorter period than the real period and a larger R_t , although R_t can be reduced by 25% if the period is established from properly substantiated data

or computation. This equation indicates that, for example, a 30m-high reinforced concrete building has the period of only 0.6 seconds.

For a comparison of seismic loads, it is assumed that the same periods T are obtained for a building designed to both codes. Then using $C = 0.15$ and $R_t = 1.0$ for buildings with a short period of vibration ($T \leq 0.4$ seconds) result in giving $C_d = 0.12$ and $C_1 = 0.3$, which means that Q_1 in the Japanese code is 2.5 times larger than V in NZS. For buildings with a long period ($T \geq 3.0$ seconds), $C = 0.075$ and $R_t = 0.25$ result in giving $C_d = 0.06$ and $C_1 = 0.075$, which means that Q_1 is 1.25 times larger than V . In the Japanese code, R_t can be reduced to 0.25 for longer periods than 2.56 seconds in case of rigid subsoil, while in NZS C for a longer period than 1.2 seconds can be reduced to half of the value for a short period.

2.4 Comparison of prestressed concrete building with reinforced concrete building with regard to seismic design load

In NZS 4203:1984, the structural material factor M for ductile prestressed concrete buildings is 25% larger than that for ductile reinforced concrete buildings. This 25% higher total horizontal seismic design load for prestressed concrete buildings is to allow for the larger response of prestressed concrete buildings than that of reinforced concrete buildings.

However, this provision does not result in a 25% larger seismic design load for prestressed concrete buildings than that for ordinary reinforced concrete unless the prestressed and ordinary reinforced concrete buildings have exactly the same structural configuration of frames and dimensions of members. Normally, prestressed concrete as a structural type can lead to longer spans. Hence prestressed concrete frames may be more flexible than ordinary reinforced concrete frames designed to sustain the same gravity load. Therefore, the natural period of vibration of prestressed concrete frames may be longer than that of reinforced concrete frames of the same height. That may result in smaller seismic design loads for prestressed concrete frames because in current seismic design codes, a smaller seismic design load can be applied to buildings with longer periods.

Consider a simple example involving two buildings. One is a four-story prestressed concrete building with beams of 21 m span, shown in Fig.2.6(a). The other is a four-story three-bay reinforced concrete building with beams of 7m span, shown in Fig.2,6(b). The latter has one-third span length of the former because it is not practical to build a reinforced concrete beam of 21 m length and a 7 m span is considered to be appropriate. These two frames are designed to sustain the same gravity loads and are supposed to be *equivalent* to each other. The member dimensions for these two buildings are summarized in Table 2.2. The overall depths of the prestressed and reinforced concrete beams are assumed to be 1/20 and 1/10 of span length, respec-

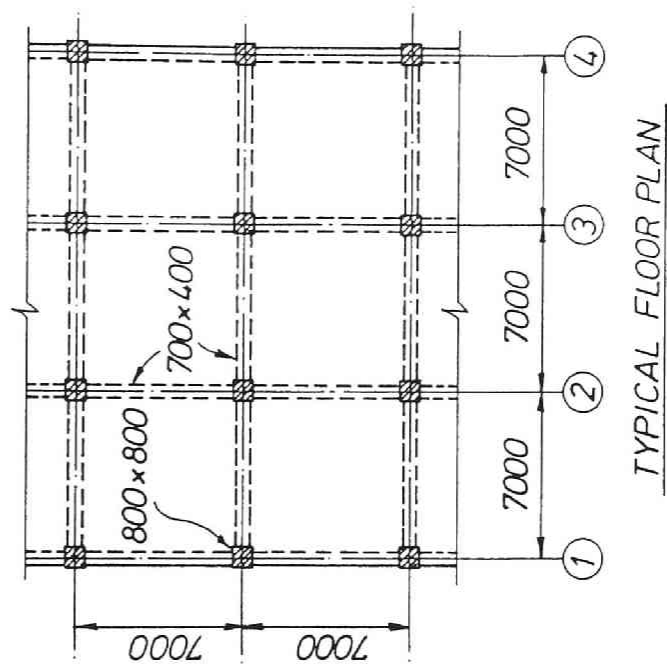
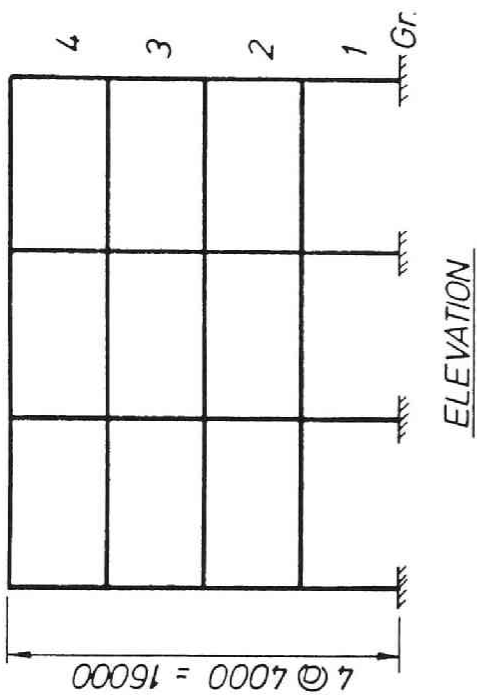


Fig.2.6(b) Four-story reinforced concrete model frame

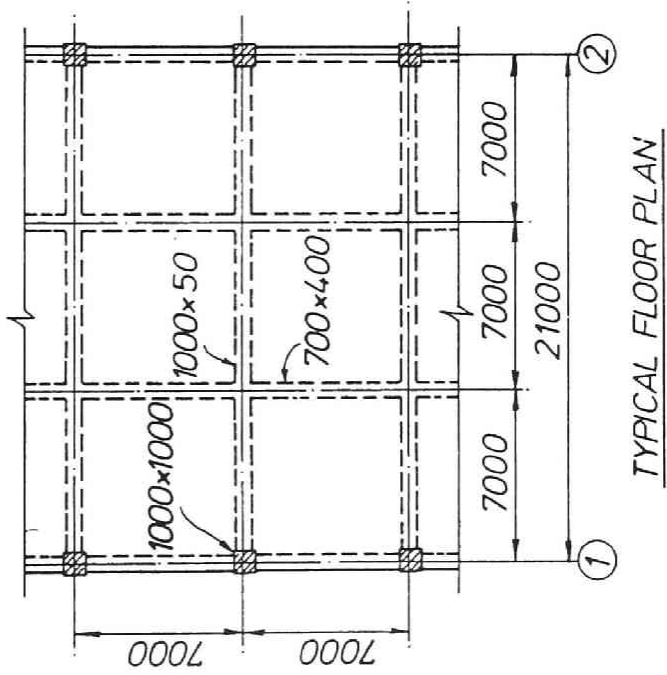
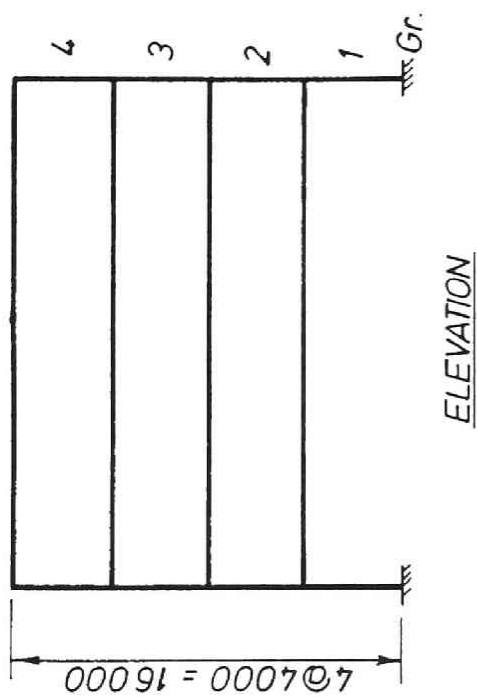


Fig.2.6(a) Four-story prestressed concrete model frame

tively. Columns of the prestressed concrete building have larger dimensions than those of the reinforced concrete building because they are subjected to larger actions due to both gravity load and horizontal load than those of the reinforced concrete building. The prestressed concrete beams have a larger modulus of elasticity because they are usually constructed of concrete with higher compressive strength. Here, the prestressed concrete beams are assumed to have concrete with a compressive strength of 30 MPa, while the reinforced concrete beams and columns are assumed to have a compressive strength of 20 MPa. The modulus of elasticity is calculated using $E_c = 4700\sqrt{f'_c}$. Total gravity load is assumed to be 9.8 kN/m² on each floor. The span length of the plane frame perpendicular to the frame considered is assumed to be 7 m. The effective member stiffnesses are assumed to be based on 50% of the area and moment of inertia of the gross section of the beams and 80% for the columns. Assumed stiffnesses are listed in Table 2.3.

Table 2.2 Member dimensions for four-story prestressed and reinforced concrete model frames

Members	Prestressed concrete frame (mm)	Reinforced concrete frame (mm)
Main beams	1000 x 500	700 x 400
Secondary beams	700 x 400	
Columns	1000 x 1000	800 x 800

Table 2.3 Effective member stiffnesses

Properties	Beams	Columns
Area	0.5A _g	0.8A _g
Moment of inertia	0.5I _g	0.8I _g

Natural periods of the first mode of these frames are 0.992 second for the reinforced concrete and 1.214 seconds for the prestressed concrete. These result in basic seismic coefficients of $C = 0.096$ for the reinforced concrete frame and $C = 0.075$ for the prestressed concrete, using Fig.2.7. Fig.2.7 is from Fig.3 of Chapter 3 of NZS 4203:1984. Products of these seismic coefficients C and the structural material factor M are 0.077 for the reinforced concrete frame and 0.075 for the prestressed concrete frame. Therefore, if they have the same total gravity load above the level of imposed lateral restraint, the seismic design load for the prestressed concrete frame is smaller than for the reinforced concrete frame even after structural material factor M is taken into account. However, it should be noted that a too flexible frame may not meet the interstory drift limitation of the design code. No allowance of this kind can be made in the Japanese code because the period depends on only the height of the frame.

Prestressed and reinforced concrete are not comparable. Each of them has its own field to be adopted. The comparison in this section is just an example to demonstrate how much larger design seismic load for a prestressed concrete building is required compared with that for an *equivalent* reinforced concrete building if it should exist. The word *equivalent* is vague : equivalent in cost, construction performance, structural performance, serviceability, structural configuration. Inherently prestressed and reinforced concrete should be treated as structural systems in a same category; structural concrete. Prestressed and reinforced concrete was compared in order to establish a design procedure or a design criterion of prestressed concrete buildings as an extension of that for reinforced concrete buildings.

2.5 Conclusions

The current seismic design procedure for prestressed concrete buildings in Japan was summarized. The design procedure is complicated because of the options which a designer may choose.

The following aspect of the design of prestressed concrete buildings were described and compared with those for reinforced concrete buildings: in NZS 4203:1984, the structural material factor M for prestressed concrete is 25% larger than that for reinforced concrete. However, this does not necessarily lead to 25% greater design seismic load. As shown in the section on the comparison of the seismic design loads, the design seismic load required for a prestressed concrete building may be smaller than that for an equivalent reinforced concrete building because of the longer period of vibration of the prestressed concrete building.

[References]

- 2.1 "Code of Practice for General Structural Design and Design Loadings for Buildings NZS 4203:1984", Standard association of New Zealand, 1984.
- 2.2 "The Standard for Structural Design and Construction of Prestressed Concrete

- Structures," Architectural Institute of Japan, 1987.
- 2.3 F. Watanabe, M. Nishiyama and H. Muguruma, A consistent seismic design method
 - 2.4 "Code of Practice for the Design of Concrete Structures NZS 3101 Part 1: 1982, and Commentary NZS 3101 Part 2:1982, Standards Association of New Zealand, 1982.
 - 2.5 "Design Guideline for Earthquake Resistant Reinforced Concrete Buildings Based on Ultimate Strength Concept," Architectural Institute of Japan, 1988.

MOMENT - CURVATURE CHARACTERISTICS OF PRESTRESSED, PARTIALLY PRESTRESSED AND REINFORCED CONCRETE MEMBERS UNDER REVERSED CYCLIC LOADING

3.1 Introduction

Nowadays higher strength structural materials are being used at construction sites. These materials enable smaller dimensions of members and make possible the design of taller reinforced concrete buildings. However, conventional reinforced concrete cannot make the most use of these higher strength materials because serviceability (for example, crack widths of beams and slabs under gravity load) can not be improved although the ultimate strength of members can be higher. In contrast, prestressed concrete can extract the full potential of those materials. Design in prestressed concrete can result in much longer spans of beams without cracking or with small crack widths, and smaller deflections than design in reinforced concrete.

Many prestressed concrete building structures have been erected. However, it must be recognized that past research on prestressed concrete is inferior in quality and quantity to that on reinforced concrete. Especially, there are a few systematic research on seismic performance of prestressed concrete buildings, which is indispensable to countries with high seismicity like Japan.

To carry out the seismic design of prestressed concrete buildings, prediction of their response to earthquakes is needed. To attain this target, research should go through the following four steps; 1) moment - curvature characteristics of member sections, 2) moment (or load) - rotation (or deflection) relationships of members, 3) shear force (or stress) - shear distortion angle characteristics of beam - column joint and 4) lateral load - interstory drift angle of each story of a building. As for the first and second steps it has been recognized that hysteresis loops of prestressed concrete members are significantly narrower than reinforced concrete, which leads to less energy dissipation. However, there is few research which relates parameters peculiar to prestressed concrete members (for example, the amount and location of prestressing steel, the average prestress, the amount of confining reinforcement, cover thickness and so on) with moment - curvature characteristics under reversed cyclic loading although several experimental and analytical research on flexural and shear behaviour of prestressed concrete members can be found in the past literature. One of the reasons is that there are much more parameters which define the behavior of prestressed

concrete members than reinforced concrete members. In addition, most of past research that tried to evaluate the ductility of prestressed concrete sections and/or members have dealt with moment - curvature or load - deflection relationships under monotonic loading or envelope curves which were obtained from the experimental results of test units under reversed cyclic loading. These provide an approximation for the overall behavior of such sections and/or members and therefore indicate the maximum possible ductility available. The effect of cyclic loading on the deformability of prestressed concrete members has not yet been clarified.

The final target of this study is not only prediction of seismic response of prestressed concrete building structures but also the establishment of a seismic design procedure for prestressed concrete. In this chapter, after reviewing previous research, comparison of moment - curvature characteristics of prestressed, partially prestressed and reinforced concrete member sections is reported. Then, an analytical procedure which incorporates stress - strain relationships of concrete, ordinary reinforcement and prestressing steel is described. The analytical procedure will be used in the later chapters to obtain moment - curvature curves theoretically.

3.2 Past research

Blakeley and Park [3.1] obtained theoretically the moment - curvature relationships of prestressed, partially prestressed and reinforced concrete beam sections on the basis of the stress - strain models under cyclic loading for concrete, non-prestressed mild steel and prestressing steel. They compared the theoretical results with the moment - curvature behaviour of the full-scale prestressed concrete beam - column assemblies subjected to high intensity cyclic loading. Since it was time-consuming to obtain the moment - curvature relationships by this theory, they presented an idealization of the cyclic loading moment - curvature characteristics of the members which accounted for stiffness degradation after crushing of the concrete in the member has occurred. This stiffness degradation followed by moment capacity reduction is typical for fully prestressed concrete sections. According to their conclusion the idealizations proposed to represent the cyclic loading of concrete and prestressing steel can be successfully used to determine the moment - curvature relationships of a prestressed concrete member under cyclic load. The theoretically obtained characteristics have been proved to agree well with experimentally derived curves in terms of stiffness degradation and energy dissipation.

Thompson and Park [3.2] conducted the tests on ten concrete beam - interior column frame assemblies subjected to static cyclic loading simulating the effect of severe earthquake loading. The frame members were near full-scale and contained a range of proportions of prestressing steel and non-prestressed steel. The behaviour of the frames emphasized the need for transverse steel in the plastic hinge zones of flexural members and in beam - column joint cores to ensure ductile behaviour and to avoid diagonal tension failure. The ductility of prestressed beams was enhanced by the

presence of non-prestressed reinforcing steel in the compression zones of members. A central prestressing tendon at mid-depth in the beam passing through the joint was shown to be effective in contributing to joint core shear strength. Thompson [3.3] obtained theoretically the moment - curvature relationships of prestressed, partially prestressed and reinforced concrete beam sections by the same analytical method that Blakeley and Park [3.1] employed. The theoretically obtained moment - curvature curves were compared with the test results. In addition, he investigated the influence of amount and location of prestressing steel, amount of transverse reinforcement and cover thickness on the ductility of prestressed and partially prestressed concrete beam sections.

The term “prestressed concrete” is somewhat ambiguous. Fully prestressed concrete and partially prestressed concrete can be generally involved in this category. Cohn and Bertlett [3.4] redefined partially prestressed concrete in terms of three variables related to the total amount of steel reinforcement, the proportion of total amount of high strength steel to the total amount of non-prestressed steel reinforcement, and the degree of prestressing. This definition enabled any structural concrete section design to be identified by a point in the three dimensional space of the chosen variables. Limit states for all types of structural concrete sections were also defined. The effects of the three primary variables above on the inelastic behaviour and ductility of partially prestressed concrete sections were investigated.

Prediction of the moment capacity of a prestressed concrete section is important for the design of the section. It can be realized by evaluating the tensile stress in the prestressing steel as accurately as possible. Harajli and Naaman [3.5] experimentally and analytically investigated the stress f_{ps} in the prestressing steel at ultimate moment capacity of partially prestressed concrete beams. They conducted an extensive parametric evaluation as well. It clarified the effects of various parameters such as the type of section, the reinforcing index, the partial prestressing ratio, concrete strength, prestressing and reinforcing steel grades and different amount of compression reinforcement on f_{ps} . Sensitivity of f_{ps} to the variation of certain parameters was also studied.

Two typical research were reported in Japan. Okada et al. [3.6] carried out the tests on 66 prestressed concrete beams with rectangular sections under reversed cyclic loading. The experimental variables involved were a shear span ratio, a tensile reinforcement index, a ratio of prestressing steel index to that for prestressing steel and non-prestressed steel, the amount and spacing of confining reinforcement and the location of prestressing steel. A restoring force model for prestressed concrete beams was proposed on the basis of the test results. The deformations at flexural yielding and the equivalent damping factors predicted by the proposed model showed considerably good agreement with those measured in the tests. In addition, an earthquake response analysis using the model for a reinforced concrete column was conducted. The analytical results agreed well with the pseudo-dynamic test results.

Okamoto [3.7] has tried to establish the seismic design procedure of prestressed concrete building structures on the basis of the extensive research results on ductility and load - deflection hysteresis characteristics of prestressed concrete members. He has proposed two models for load - deflection characteristics of prestressed concrete members called PS model and modified PS model. However, equivalent damping factors obtained by these models are not quantitatively related with prestressing steel ratios : parameters which can express the characteristics of constituent members in a prestressed concrete frame.

3.3 Moment - curvature relationships of prestressed, partially prestressed and reinforced concrete beam sections

Deformation at yielding and ductility ratio

Figure 3.1 indicates the moment - curvature curves of reinforced, partially prestressed and prestressed concrete beam sections theoretically predicted under monotonic loading. These beam sections have approximately the same flexural strength. The beam sections are also shown in Fig.3.1. The analytical method including the assumed stress - strain curves of the materials will be described in the later part of this chapter. By using the classification proposed by Cohn and Bertlett [3.4], the sections can be described by the three parameters as below;

Reinforced concrete section

$$\omega = 0.0$$

$$\gamma = 0.0$$

$$\kappa = 0.0$$

Partially prestressed concrete section

$$\omega = 0.163$$

$$\gamma = 0.543$$

$$\kappa = 0.6$$

Prestressed concrete section

$$\omega = 0.327$$

$$\gamma = 1.0$$

$$\kappa = 0.6$$

$$\text{where, } \omega = \frac{A_p f_{ps} + A_s f_y - A'_s f'_y}{b d f'_c} \quad (3.1)$$

$$\gamma = \frac{M_{pn}}{M_n} = \frac{A_p f_{ps}}{A_p f_{ps} + A_s f_y} \quad (3.2)$$

$$\kappa = \frac{M_d}{M} \quad (3.3)$$

ω = net reinforcement index

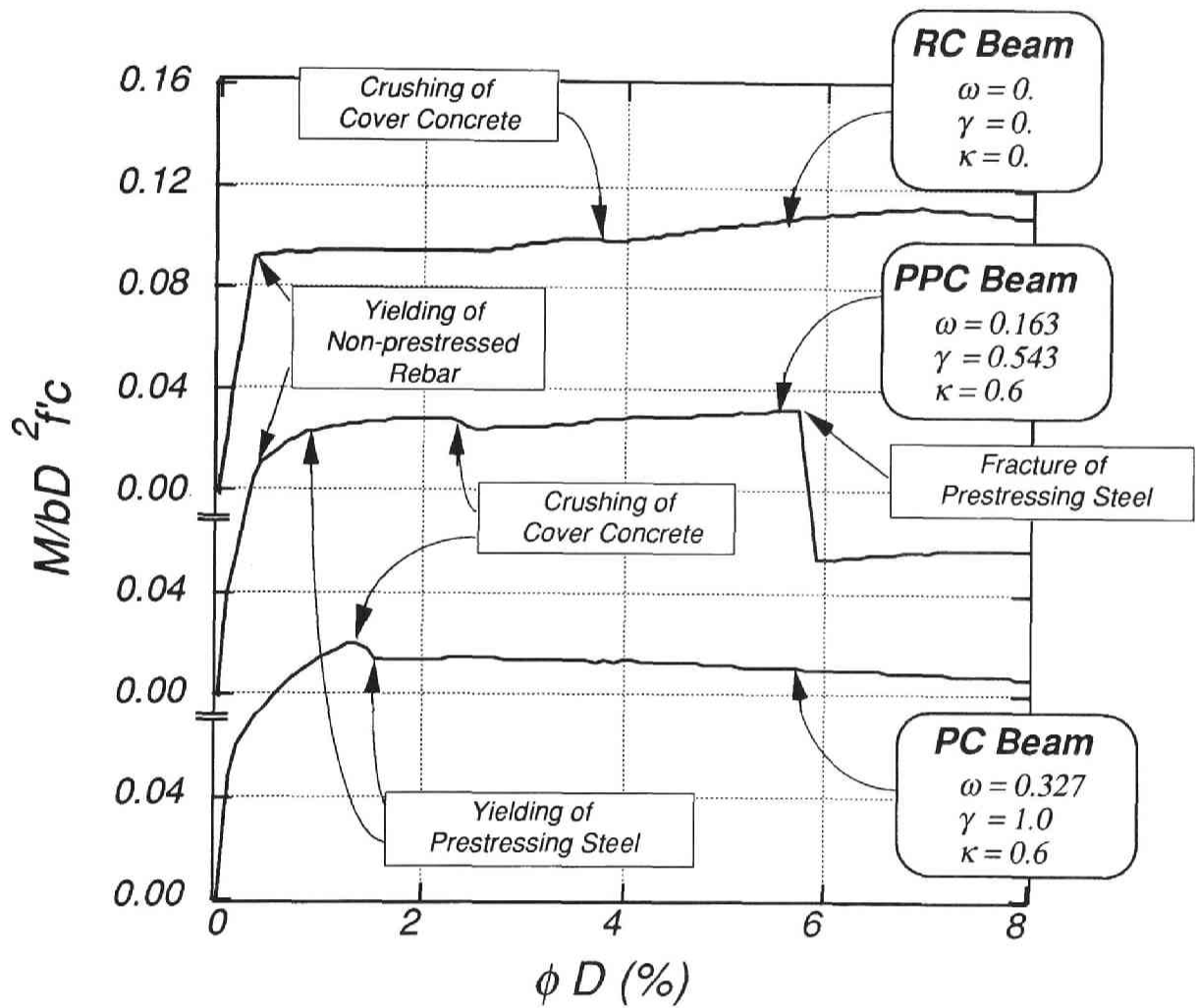


Fig.3.1 Moment - curvature curves of reinforced, partially prestressed and prestressed concrete beam sections theoretically obtained

γ = mixed reinforcement index
 κ = degree of prestressing
 A_p = sectional area of prestressing steel
 f_{ps} = stress in prestressing steel
 A_s = sectional area of tensile reinforcement
 f_y = yield stress of mild steel
 A'_s = sectional area of compressive reinforcement
 f'_y = yield stress of compressive reinforcement
 b = beam width
 d = effective depth taken to the centroid of the total tension force at yielding given by the following equation

$$d = \frac{A_p f_{ps} d_p + A_s f_y d_s}{A_p f_{ps} + A_s f_y} \quad (3.4)$$

f'_c = compressive strength of concrete
 M_{pn} = moment capacity contributed by prestressing steel
 M_n = nominal (ultimate) moment capacity
 M_d = decompression moment
 M = service moment

Comparison of these moment - curvature characteristics revealed the characteristics of each section.

1) The yield point on the moment-curvature curve of the reinforced concrete section can be clearly defined as the point where any longitudinal reinforcement reaches yield strain, which results in abrupt stiffness reduction. In the partially prestressed concrete section, the yield point can be defined although it is not so clear as the reinforced concrete section. However, in the prestressed concrete section successive gradual reduction in stiffness after cracking can be observed and this is followed by crushing or spalling of the unconfined cover concrete.

2) Crushing of the unconfined cover concrete occurs at the smallest curvature in the prestressed concrete section because of the larger compressive strain sustained than the other sections.

3) Points indicated as "Yielding of prestressing steel" are the points where strain of prestressing steel reached limit of proportionality on the stress - strain curve. The point of limit of proportionality is indicated as Point A in Fig.3.2. In the partially prestressed concrete section moment increased after yielding of prestressing steel occurred while gradual reduction in moment capacity was observed in the prestressed concrete section.

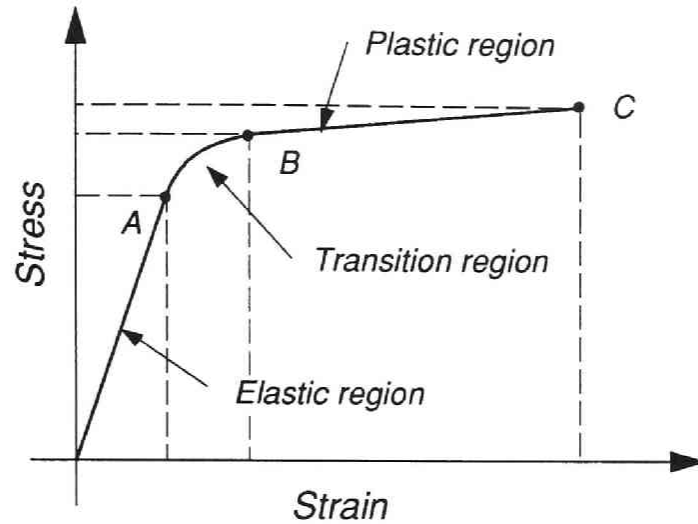


Fig.3.2 Typical stress - strain relationship of prestressing steel

4) A sudden large reduction in moment capacity occurred in the partially prestressed section due to fracture of prestressing steel : a strain at fracture was assumed to be 2%. This can be defined as an ultimate point of the partially prestressed concrete section. However in the prestressed concrete section a clear ultimate point can not be observed even in a large deformation of $\phi \cdot D = 8\%$.

Ductility ratio which is defined as the ratio of the ultimate curvature to the yield curvature is often used as a index of estimation of ductility or deformability. However, care must be exercised in interpreting what are meant by the term “yield curvature” and “ultimate curvature”. In case of a reinforced concrete section without axial load “yield curvature” means the curvature at first yield of longitudinal reinforcement in the section. In case of a prestressed concrete section it is disputable how to define the yield curvature : should it be referred to as the curvature at first yield of longitudinal reinforcement, at first yield of prestressing steel or any other points?

Okamoto specified [3.7] the term “yield curvature” as the curvature where stress in prestressing steel reaches its nominal yield stress. This is usually referred to as 0.2% off-set yield stress. However, it is difficult to apply this definition to any kind of prestressed concrete section including partially prestressed concrete section in a unified manner because crushing or spalling of the cover concrete which results in abrupt large reduction in capacity may occur before stress in prestressing steel reaches its nominal yield stress.

Harajli and Naaman [3.5] proposed a definition of yield curvature for partially prestressed beams based on the moment-curvature relationship of the section. The yield curvature was defined as the curvature corresponding to the intersection of two lines shown in Fig.3.3 : the first line is an extension of the initial linear portion of the

moment-curvature curve while the second line is an extension of the final portion of the curve to be assumed linear.

These two definitions are based on the assumption that yielding of a section should originate in yielding of prestressing steel. Cohn and Bartlett [3.4] assumed that the yield curvature corresponds to that of the ordinary reinforcing steel. However, this may be on the unsafe side especially when a small amount of reinforcing steel is provided in the section.

In the University of Canterbury in New Zealand the yield curvature defined as that calculated at moment M_{ACI} assuming the section has a constant flexural rigidity equal to that computed or experimentally obtained at $0.75M_{ACI}$ has been used (see Fig.3.4). M_{ACI} is the nominal moment of resistance calculated on the basis of the ACI code [3.8] approach. However, the flexural strength obtained has been found quite conservative for members carrying moderate to high levels of axial load. A recent study by Zahn [3.9] suggested new definitions for the yield curvature and ideal moment capacity to allow for the expected enhancement of flexural strength above the ACI method predictions. The definitions are illustrated in Fig.3.5 for a typical moment-curvature curve. The actual moment-curvature behaviour is idealized as elasto-plastic with the initial elastic portion passing through the point where first-yield occurs. The first-yield curvature ϕ_y are defined as that where either any longitudinal reinforcement reached yield strain or the extreme compression fiber concrete reached a strain of 0.002. This is the strain corresponding to the expected peak in the unconfined stress-strain curve. The yield curvature, not the first-yield curvature, is found by scaling the first-yield curvature ϕ_y by the ratio of the ideal moment capacity M_i to the first-yield moment M_y . The definition has been developed for a reinforced concrete column section.

The definitions above were arbitrary. Besides, a prestressed concrete section under

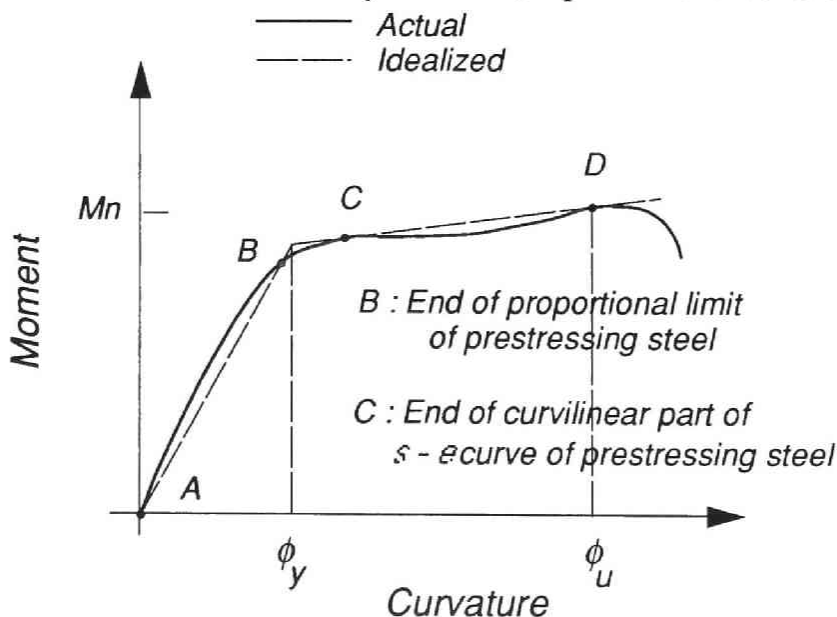


Fig.3.3 Yield curvature by Harajli and Naaman [3.5]

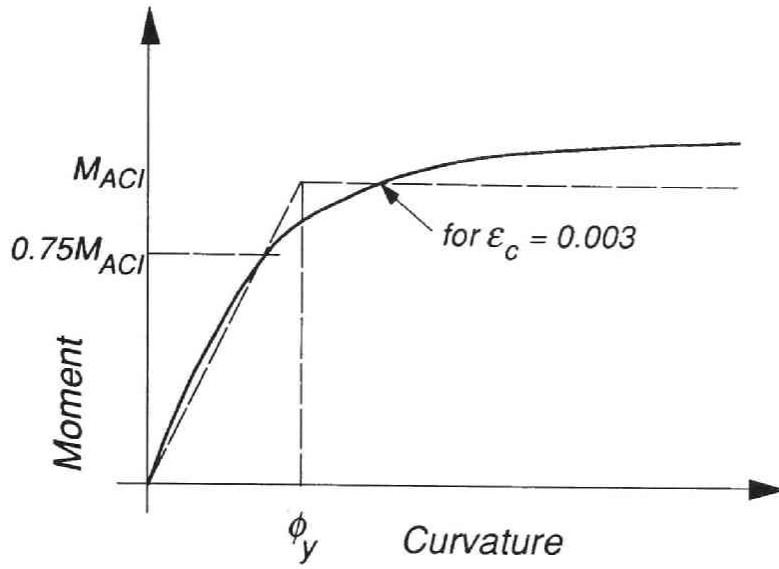


Fig.3.4 Yield curvature definition used in the University of Canterbury

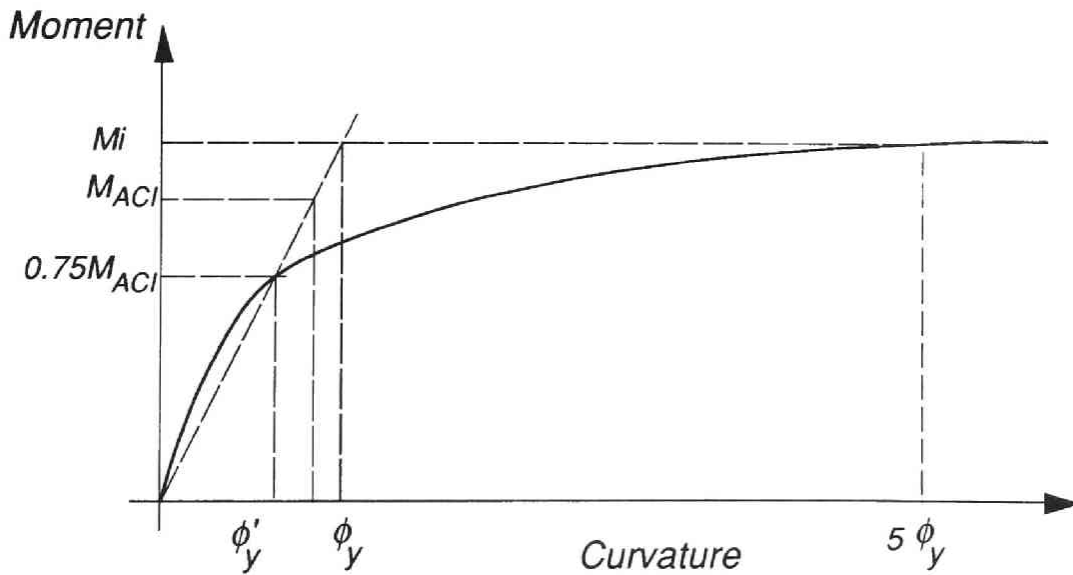


Fig.3.5 Yield curvature by Zahn [3.9]

reversed cyclic loading indicates narrower hysteresis loops with smaller residual deformation than a reinforced concrete section. Therefore, expressing ductility by a ductility ratio is not of great significance because ductility should be related to energy dissipation capability. In this study a ductility ratio is often indicated. This is defined as the ratio of a deformation to the yield deformation which is found when either of any longitudinal reinforcement reaches yield strain. However, a corresponding rotation angle or curvature itself is also referred to whenever ductility ratios are indicated.

Ultimate available curvature and influence of cyclic loading

A recent study on concrete flexural members by Suzuki et al. [3.10] suggested new definitions of the ultimate available curvature on the moment-curvature curve of the members. The ultimate available curvature was derived from a moment-curvature curve subjected to monotonic loading to failure. This is based on monotonic loading behaviour because it was aimed at an ultimate point which is of physical significance and can be easily calculated. Besides, a suitable amount of transverse reinforcement provided can prevent a large reduction in strength even under high-intensity cyclic loading into inelastic range. However, it has been observed in past research that the available ductility of a section depends much on the imposed curvature history. The ultimate curvature resulting from monotonic flexure is usually greater than that resulted from cyclic flexure with full reversals. Therefore, it is necessary to define a suitable standard curvature history to measure the available curvature ductility.

Subjected to high axial load, a column section may not sustain the axial load under cyclic loading although it can sustain the same level of axial load under monotonic loading. This is described in the reference [3.11] by means of analyzing a column section. The influence of cyclic loading in the analysis is expressed in Fig.3.6. The figure illustrates three moment-curvature curves of the column section of a test unit called CH-4 subjected to high axial load of $0.473 f'cAg$. All of them were obtained theoretically: (A) the moment-curvature curve under monotonic loading calculated using the modified Muguruma et al. model proposed in the reference [3.12], (B) the moment-curvature curve under cyclic loading using the same model used in (A), and (C) the moment-curvature curve under cyclic loading using the re-modified model assuming that a descending branch of the skeleton curve after peak-stress does not fall below the stress of $0.5 \sigma_{cm}$. σ_{cm} was the peak-stress. As shown in Fig.3.6, the reduction in strength under cyclic loading (Curve (B) or (C)) is much larger than that of monotonic loading (Curve (A)) in the post-peak region. The theoretical moment-curvature curve of cyclic loading (B) dropped suddenly at the smaller curvature than that of monotonic loading, and the large reduction in strength resulted in instability in the analysis. This is because the resultant compressive force in core concrete was not able to become large enough to sustain such a high axial load. The stress distribution in the column section in the analysis of reversed cyclic loading is different from that in the analysis of monotonic loading even if they are obtained at the same curvature. This is because stresses in concrete on reloading paths are smaller than those on the

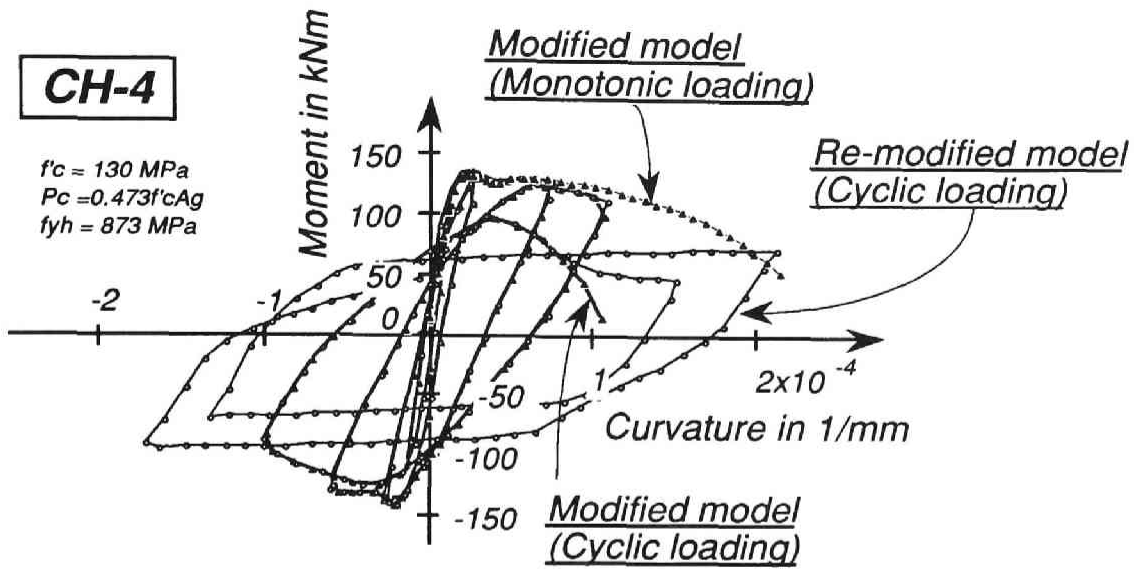


Fig.3.6 Influence of cyclic loading in the analysis [3.10]

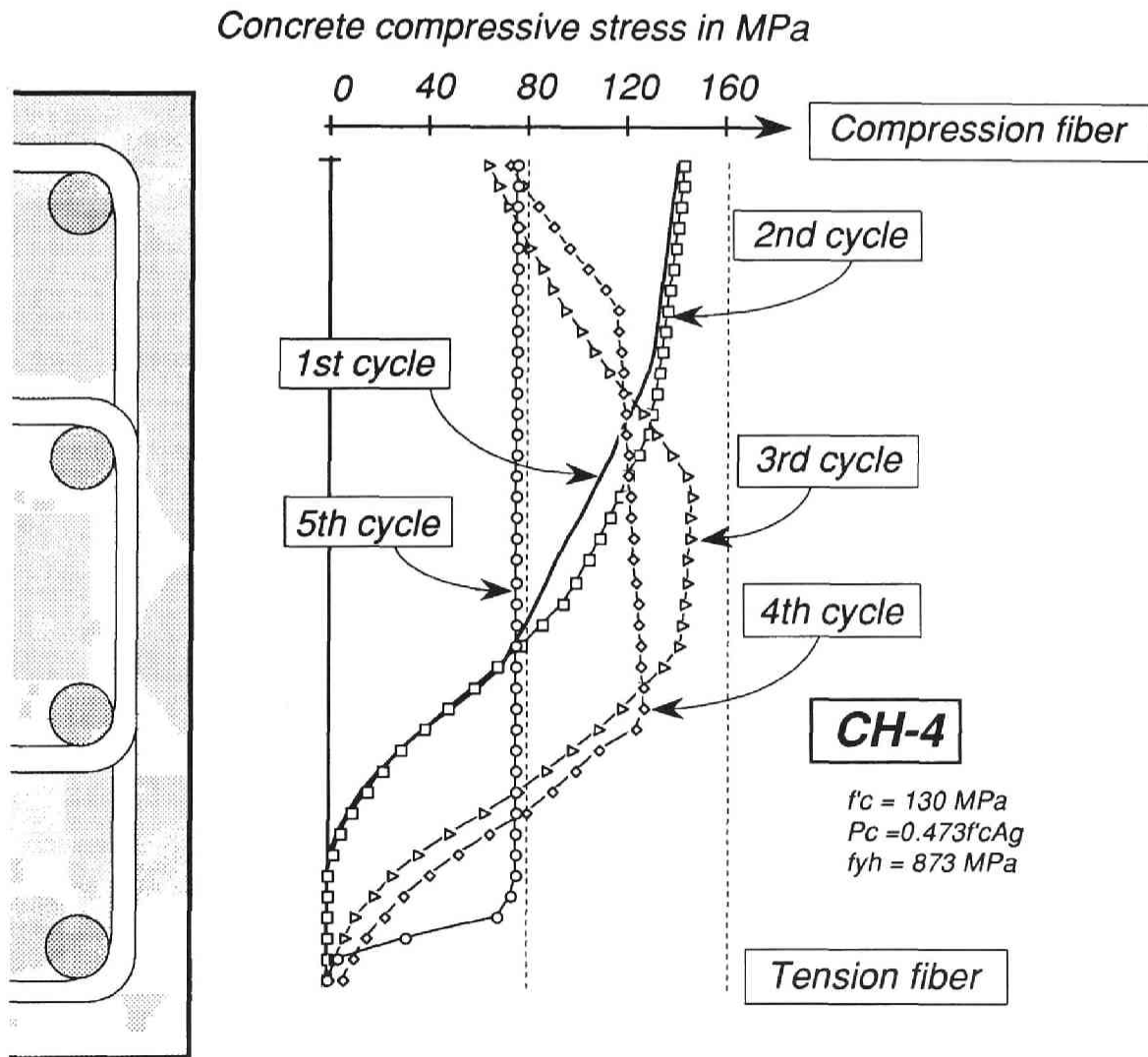


Fig.3.7 Stress distribution in the column section [3.10]

envelope curve at the same strains (Fig.3.7). Thus, the effect of cyclic loading should be taken into account.

Zahn [3.9] adopted a sequence of four identical cycles of imposed bending moment to curvatures of equal magnitude in both positive and negative directions as a standard by which the available curvature ductility factor of a column section is measured (Fig.3.8). The section is considered to have achieved its ultimate curvature when one or more of the following ultimate limit state conditions is reached.

- 1) The moment reached at either positive or negative curvature peak of the last cycle has reduced to $0.8M_i$, where M_i is the ideal flexural strength of the section.
- 2) The strain energy accumulated in the confining reinforcement at the end of the fourth cycle is equal to its strain energy absorption capacity and it fractures.
- 3) The longitudinal reinforcing steel fractures or buckles.

The peak curvature when one or more of the above conditions applies is defined as the available ultimate curvature. The available ultimate curvature has to be determined by

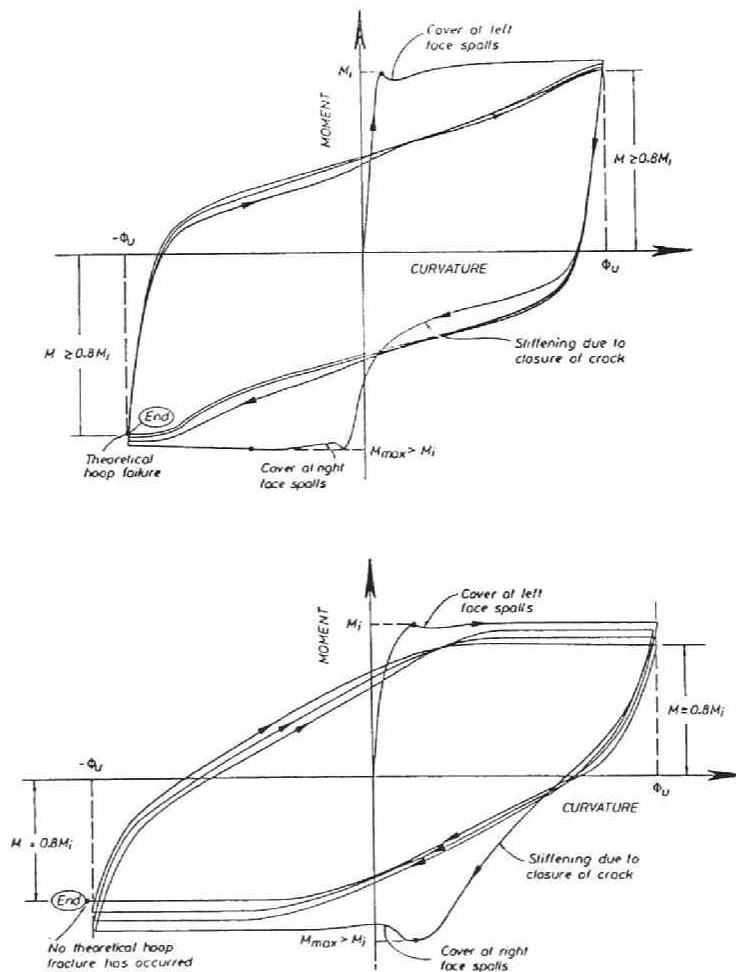


Fig.3.8 Definition of ultimate curvature by Zahn [3.9]

iteration. They adopted an energy balance approach proposed by Mander et al. [3.11] to predict the stage of hoop or spiral bar fracture. The approach reflects the principle that the lateral expansion of core concrete at large compression strains is passively resisted by confining reinforcement, which has to follow that expansion, thus absorbing strain energy. The increase in the strain energy capacity of compressed concrete due to confinement is equivalent to the strain energy stored by the confining reinforcement as it yields in tension. Hoop or spiral fracture occurs when the strain energy stored in the compressed concrete, plus the additional strain energy required to yield the longitudinal reinforcement in compression, is equal to the strain energy capacity of the confining reinforcement.

In the moment-curvature analysis by Zahn [3.9] the moment reduction to $0.8M_i$ is caused by the reduction in stress at the previous unloading strain, ϵ_{un} , which was incorporated in the stress-strain model of concrete to allow for the degradation effects due to cyclic loading : the stress in the reloading path at ϵ_{un} reaches $f_{new} = 0.92 f_{un} + 0.08 f_{ro}$, where f_{un} is the stress corresponding to ϵ_{un} , and f_{ro} is the stress from where reloading occurs (Fig.3.14). No other cause can be thought. Even if another few cycles are imposed, further reduction in moment capacity can not be observed. Therefore, a sequence of two identical cycles to curvatures of equal magnitude in both positive and negative directions is enough to specify the ultimate curvature.

3.4 Theoretical study of strength and ductility of prestressed concrete members

3.4.1 Computer analysis program

A computer program for determining the moment-curvature behaviour of arbitrarily shaped prestressed and reinforced concrete members was developed by the author on the basis of the research work conducted by Mander et al. [3.13]. A section analyzed is divided into some parallel strips which lie perpendicular to the direction of the applied load. These strips represent the material properties. The distribution of flexural strains is always assumed to be linear through the depth of the section: plane sections before bending remain plane after bending. Analysis proceeds by incrementing the curvature at the critical section in a series of small steps. The position of the neutral axis is obtained by iteration until equilibrium of the internal forces is achieved. After that the moment of resistance of the section is calculated. In this way the moment - curvature behaviour of the critical section is followed piecewise.

Reversed cyclic loading histories could be simulated by specifying the required maximum curvature at the peak of successive loading cycles and number of steps to reach the curvature. As shown in the later chapters of this thesis, cyclic moment curvature analyses described above can give approximate predictions of strength and stiffness degradation which might be observed from experimental results.

3.4.2 Stress-strain models for concrete and reinforcing steels

The stress-strain models for confined concrete used in this study was developed by Mander et al [3.13]. In their research work the model has been found to give good agreement with experimentally measured uniaxial stress-strain response [3.14]. The model is used to predict the stresses resulting from an arbitrary applied strain history. The monotonic loading curves for tension and compression envelop the behaviour predicted for cyclic loading.

3.4.2.1 Stress-strain model for confined concrete

Control parameters

Fig.3.9 shows the monotonic stress-strain behaviour for unconfined and confined concrete. It was necessary to input the following parameters to the computer program to control the stress-strain behaviour.

For unconfined concrete:

f'_c = unconfined compressive cylinder strength in MPa

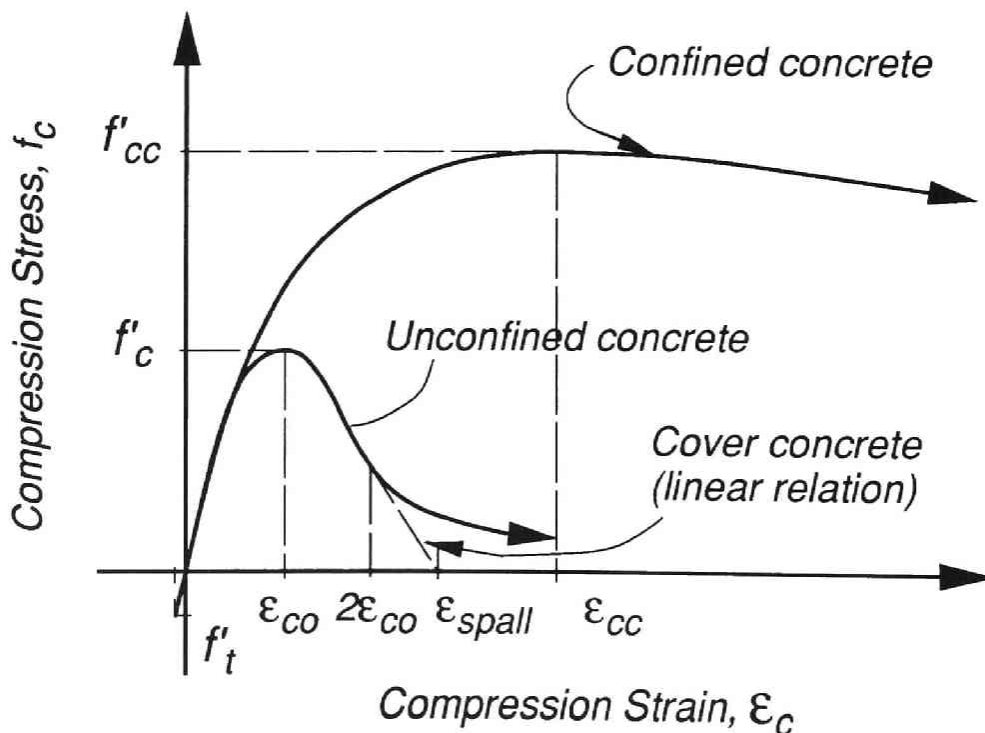


Fig.3.9 Monotonic stress - strain behaviour for unconfined and confined concrete

f'_t = concrete tensile strength, if not specified $f'_t = 0.6\sqrt{f'_c}$ in MPa

E_c = initial tangent modulus of elasticity, if not specified $E_c = 5000\sqrt{f'_c}$ in MPa

ϵ_{co} = strain at unconfined strength f'_c . $\epsilon_{co}=0.002$ is assumed for ordinary strength concrete

ϵ_{spall} = strain at which unconfined cover concrete spalls

For confined concrete:

f'_{cc} = peak strength of confined concrete

ϵ_{cc} = strain at confined strength f'_{cc}

ϵ_{cu} = ultimate strain sustainable

Monotonic loading behaviour

Monotonic compression loading:

The monotonic envelop stress-strain relation in compression for confined concrete is given by Eq.3.5.

$$f_c = f'_{cc} \frac{x^r}{r-1+x^r} \quad (3.5)$$

f_c = concrete stress

x = ϵ / ϵ_{cc}

ϵ = concrete strain

r = $E_c / (E_c - E_{sec})$

E_{sec} = secant modulus = f'_{cc} / ϵ_{cc}

For unconfined concrete the same equation is used but the parameters f'_{cc} and ϵ_{cc} are replaced by f'_c and ϵ_{co} . The falling branch of the stress-strain curve for the unconfined cover concrete for strain ϵ greater than $2\epsilon_{co}$ is taken as a straight line reducing to the strain - stress coordinate $(\epsilon_{spall}, 0)$, where ϵ_{spall} is the spalling strain. Thus, ϵ_{spall} should be greater than or equal to $2\epsilon_{co}$.

Monotonic tension loading:

The tension strength f'_t can be input. However, if the data are not available, f'_t suggested in the New Zealand Concrete Design Code NZS 3101 [3.15] can be used. According to NZS 3101:1982, f'_t can be derived from the unconfined cylinder

compressive strength f'_c by the expression in Eq.3.6.

$$f'_t = 0.6\sqrt{f'_c} \quad (f'_t \text{ and } f'_c \text{ in MPa}) \quad (3.6)$$

The stress-strain behaviour in tension is assumed to be elastic until the tensile strength f'_t is exceeded, as given by Eqs.3.7 and 3.8.

$$f_c = E_c \varepsilon \quad \text{for } \varepsilon < f'_t / E_c \quad (3.7)$$

$$f_c = 0.0 \quad \varepsilon \geq f'_t / E_c \quad (3.8)$$

As indicated in the above equations, the same initial tangent modulus of elasticity E_c is used for both compression and tension loading.

Determination of Confined Strength f'_{cc} :

The peak strength f'_{cc} of confined concrete in compression loading is dependent on the confining stresses f_{l1} and f_{l2} provided by transverse reinforcement in the two transverse directions. By using the confining stress ratios f_{l1} / f'_c and f_{l2} / f'_c , the confined strength ratio f'_{cc} / f'_c can be found from Fig.3.10. Fig.3.10 was based on an ultimate strength failure criterion for concrete under a general multiaxial state of stress.

Determination of Strain ε_{cc} at Confined Strength:

The strain ε_{cc} at the confined strength f'_{cc} can be obtained using Eq.3.9.

$$\varepsilon_{cc} = \varepsilon_{co} \{1 + R(f'_{cc} / f'_c - 1)\} \quad (3.9)$$

The parameter R has been found to be approximately constant by previous researchers but values between about 3 and 10 have been suggested. According to Mander's recommendations a constant value of $R = 5$ was used in this study. The strain ε_{co} corresponding to the unconfined strength f'_c was assumed to be equal to 0.002 for all concrete strength considered. This value of ε_{co} is commonly used for normal strength concrete. For high strength concrete larger values than 0.002 are usually assumed. Muguruma et al. [3.16] proposed the following equation on the basis of the experimental results in which cylinder compressive strength ranges 26.2 to 87.5 MPa.

$$\varepsilon_{co} = 0.0013(1 + f'_c / 98.6) \quad (3.10)$$

For instance, Eq.3.10 gives $\varepsilon_{co} = 0.169\%$ for concrete of 30MPa in compressive strength. Concrete compressive strength considered in this study is approximately 30

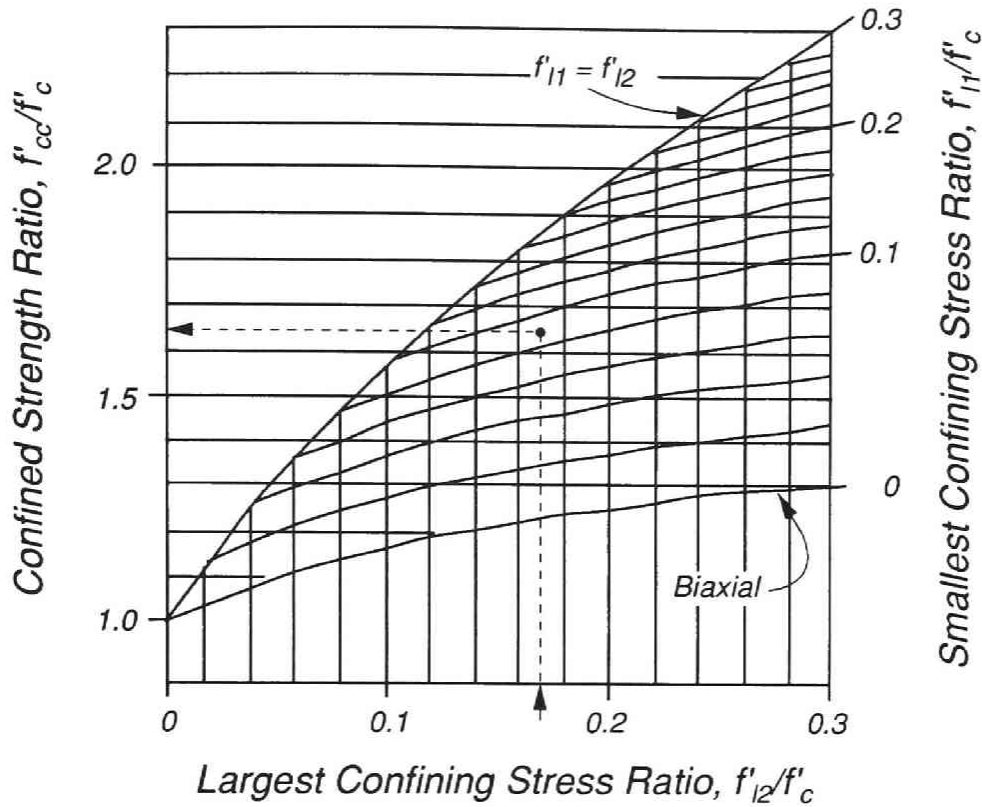


Fig.3.10 Confined strength determined from the confining stresses

to 40 MPa. Thus, ϵ_{co} of 0.002 can be used.

3.4.2.2 Cyclic Loading Behaviour

Initial loading is assumed to traverse along the envelope stress-strain curves. Different behaviour is assumed for unloading from either the compression or tension envelope curves.

Compression Unloading:

Behaviour on unloading from the compression envelop curve is shown diagrammatically in Fig.3.11. Unloading is assumed to take place from a strain stress coordinate (ϵ_{un}, f_{un}) . The tangent modulus at the start of unloading E_u is assumed to be given by Eq.3.11.

$$E_u = bcE_c \quad (3.11)$$

$$\text{where } b = f_{un} / f'_c \quad \text{but } b \geq 1 \quad (3.12)$$

$$c = (\epsilon_{cc} / \epsilon_{un})^{0.5} \quad \text{but } c \leq 1 \quad (3.13)$$

E_c = initial tangent modulus

The stress-strain relation is given by Eq.3.14.

$$f_c = f_{un} \left(1 - \frac{x^r}{r-1+x^r} \right) \quad (3.14)$$

$$\text{where } r = E_c / (E_c - E_{sec}) \quad (3.15)$$

$$E_{sec} = f_{un} / (\epsilon_{un} - \epsilon_{pl}) \quad (3.16)$$

$$\begin{aligned} \epsilon_{pl} &= \epsilon_{un} - (\epsilon_{un} + \epsilon_a) / (1 + E_c \epsilon_a / f_{un}) \\ &= \text{plastic strain} \end{aligned} \quad (3.17)$$

$$\begin{aligned} \epsilon_a &= a (\epsilon_{un} \epsilon_{cc})^{0.5} \\ &= \text{common strain} \end{aligned} \quad (3.18)$$

$$\begin{aligned} a &= \epsilon_{cc} / (\epsilon_{cc} + \epsilon_{un}) \text{ or } 0.09 \epsilon_{un} / \epsilon_{cc} \\ &\text{whichever is greater} \end{aligned} \quad (3.19)$$

$$x = (\epsilon - \epsilon_{un}) / (\epsilon_{pl} - \epsilon_{un}) \quad (3.10)$$

Tensile Unloading:

Tensile strength is assumed to deteriorate depending on the magnitude of previous compressive straining as shown in Fig.3.12. On unloading from compression the tensile strength is assumed to be given by Eq.3.20.

$$\begin{aligned} f_t &= f'_t \left(1 - \epsilon_{pl} / \epsilon_{cc} \right) && \text{for } \epsilon_{cc} > \epsilon_{pl} \\ &= \text{zero} && \text{for } \epsilon_{cc} < \epsilon_{pl} \end{aligned} \quad (3.20)$$

The stress-strain relation is given by Eq.3.21.

$$f_c = E_t (\epsilon - \epsilon_{pl}) \quad (3.21)$$

$$\text{where } E_t = f_t / \epsilon_t \quad (3.22)$$

$$\epsilon_t = f'_t / E_t \quad (3.23)$$

After the cracking strain has been exceeded, $\epsilon > (\epsilon_t - \epsilon_{pl})$, the tensile strength is assumed to be zero.

Reloading Behaviour:

Fig.3.13 illustrates situations where reloading may occur from either the compression unloading curve or the tension unloading curve after cracking. Reloading is assumed

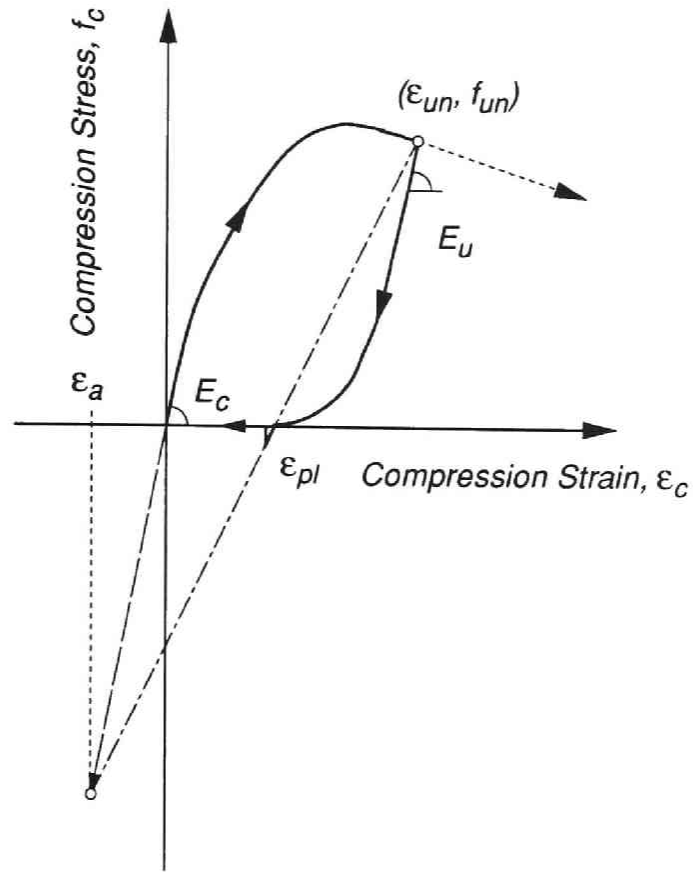


Fig.3.11 Unloading path from the compression envelope curve

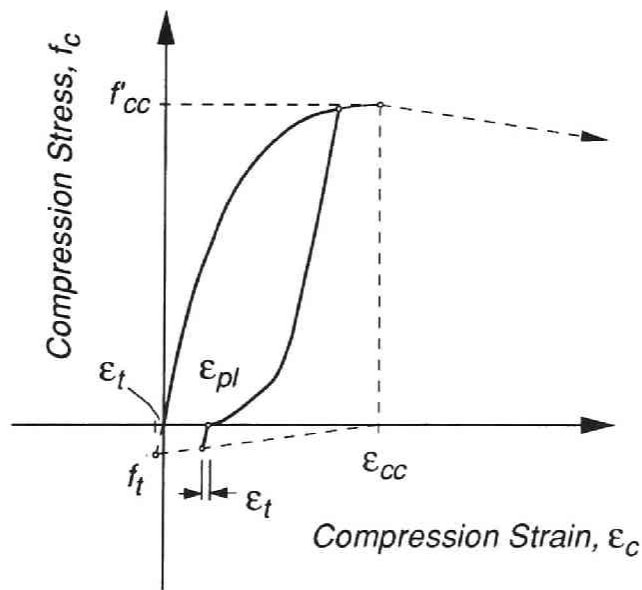


Fig.3.12 Assumed tension strength deterioration due to compressive loading

to occur from a strain - stress coordinate (ϵ_{ro}, f_{ro}) and the stress-strain relation is assumed to be linear as the previous compression loading curve is approached. The stress at the previous unloading strain ϵ_{un} is reduced from f_{un} to f_{new} , as given by Eq.3.23 to allow for degradation effects due to load cycling.

$$f_{new} = 0.92 f_{un} + 0.08 f_{ro} \quad (3.23)$$

The linear stress-strain relation is given by Eq.3.24.

$$f_c = f_{ro} + E_r (\epsilon - \epsilon_{ro}) \quad (3.24)$$

where $E_r = (f_{new} - f_{ro}) / (\epsilon_{un} - \epsilon_{ro})$ (3.25)

A cubic transition is then used to intersect the monotonic compression curve at a return coordinate (ϵ_{re}, f_{re}) where ϵ_{re} is given by Eq.3.26 and f_{re} is given by the expression for the monotonic compression curve in Eq.3.5. In Mander's idealization a parabolic curve was used.

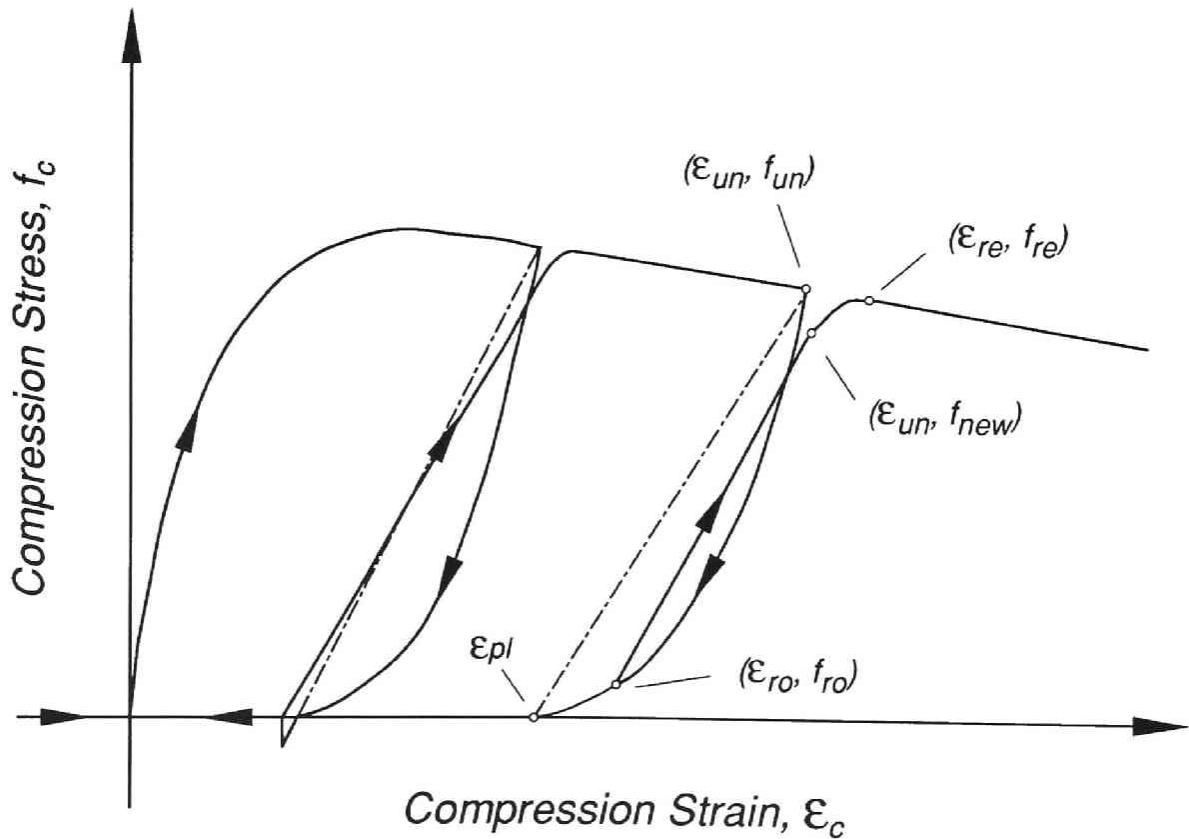


Fig.3.13 Stress - strain curves for reloading branch

$$\varepsilon_{re} = \varepsilon_{un} + (f_{un} - f_{new}) / \{E_r (2 + f'_{cc} / f'_c)\} \quad (3.26)$$

The cubic stress-strain relation is given by Eq.3.27.

$$f_c = f_{re} + E_{re}x + Ax^2 + Bx^3 \quad (3.27)$$

$$\text{where } x = \varepsilon - \varepsilon_{re} \quad (3.28)$$

$$A = \frac{3}{x_{un}^2} (f_{new} - f_{re}) - \frac{1}{x_{un}} (E_r - 2E_{re}) \quad (3.29)$$

$$B = \frac{-2}{x_{un}^3} (f_{new} - f_{re}) - \frac{1}{x_{un}^2} (E_{re} + E_r) \quad (3.30)$$

$$x_{un} = \varepsilon_{un} - \varepsilon_{re} \quad (3.31)$$

E_{re} is the tangent modulus at the return coordinate determined from the monotonic equation (Eq.3.5).

3.4.3 Stress-strain model for reinforcing steel

Stress-strain model for ordinary reinforcing steel proposed by Yokoo et al. [3.17] was incorporated in the analysis. However, some modifications were made.

3.4.3.1 Monotonic stress-strain behaviour

The assumed monotonic stress-strain behaviour for reinforcing steel is illustrated in Fig.3.14. The application of the model in the computer analysis program requires the following parameters governing the monotonic stress-strain behaviour to be input by the user for both tension and compression loading cases:

f_y = yield stress

E_s = elastic modulus

ε_{sh} = strain at commencement of strain hardening

The stress-strain relations are then given by Eqs. 3.32, 3.33 and 3.34 for loading on the initial elastic line, yield plateau, and on the strain hardened curve respectively.

$$f_s = E_s \varepsilon_s \quad \text{where } 0 < \varepsilon_s < \varepsilon_y \quad (3.32)$$

$$f_s = f_y \quad \text{where } \varepsilon_y < \varepsilon_s < \varepsilon_{sh} \quad (3.33)$$

$$E_s \varepsilon_s = f_s \left[1 + A^{-R} \left| \frac{f_s}{f_y} \right|^{R-1} \right] \quad \text{where } \varepsilon_s > \varepsilon_{sh} \quad (3.34)$$

where f_s = steel stress
 ε_s = steel strain
 ε_y = yield strain = f_y / E_s

The numerical values for A and R in this study are assumed to be 0.603 and 3.814, respectively. These parameters were derived from the tensile monotonic loading test results conducted by Fujimura [3.18].

3.4.3.2 Cyclic Loading Behaviour

On load reversal from a coordinate (ε_i, f_i) on the monotonic curve a softened curve is followed due to Bauschinger effects as illustrated in Fig.3.15. The monotonic or skeleton curve is shifted to a new coordinate origin at (ε_i, f_i) .

When reversal is from the yield plateau, the numerical values for A and R depend on an inelastic strain, ε_p , given by Eq.3.37.

$$A = 1.943 \varepsilon_p^{(-0.0749)} \quad (3.35)$$

$$R = 16.4 \varepsilon_p^{(-0.214)} \quad (3.36)$$

$$\text{where } \varepsilon_p = \left[\left(\varepsilon - \varepsilon_i \right) - \frac{f - f_i}{E_s} \right] / \varepsilon_y \quad (3.37)$$

After the total length of the yield plateau experienced reaches $|\varepsilon_{sh} - \varepsilon_y|$, the yield plateau does not reappear any longer.

Reversal may occur from a softened branch before merging with the skeleton curve has occurred. The reloading curve is expressed by the same equation as the previously reversed curve.

When reversal takes place from the strain hardened skeleton curve, the numerical values for A and R in tension and compression paths are given by the different equations.

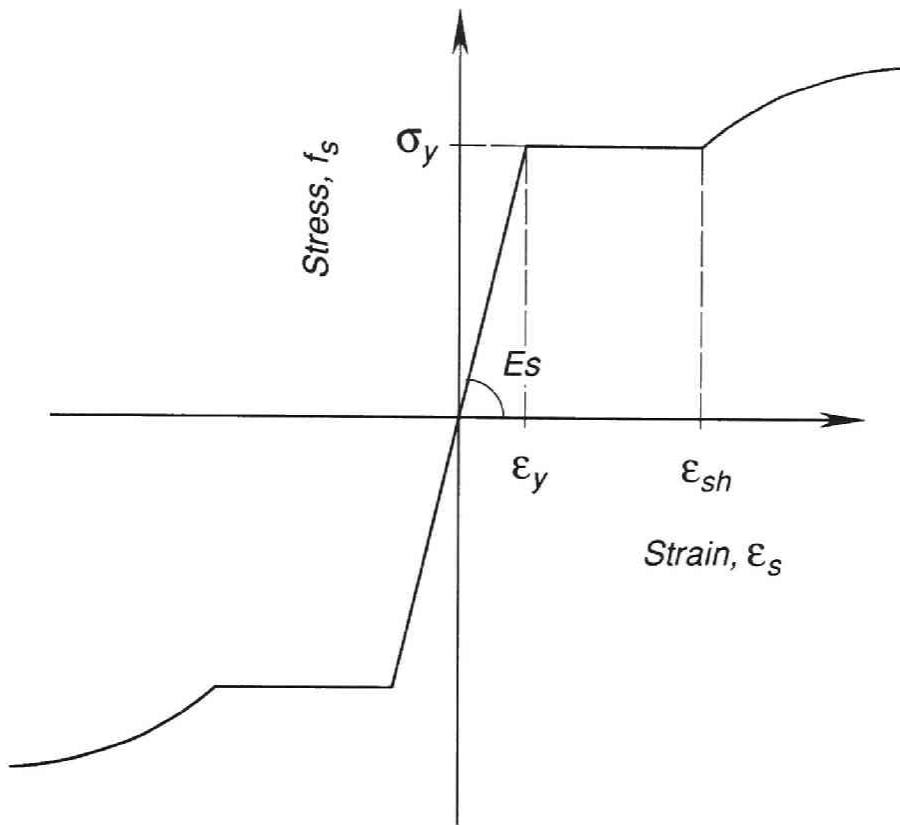


Fig.3.14 Monotonic stress - strain curve for ordinary-strength reinforcing steel

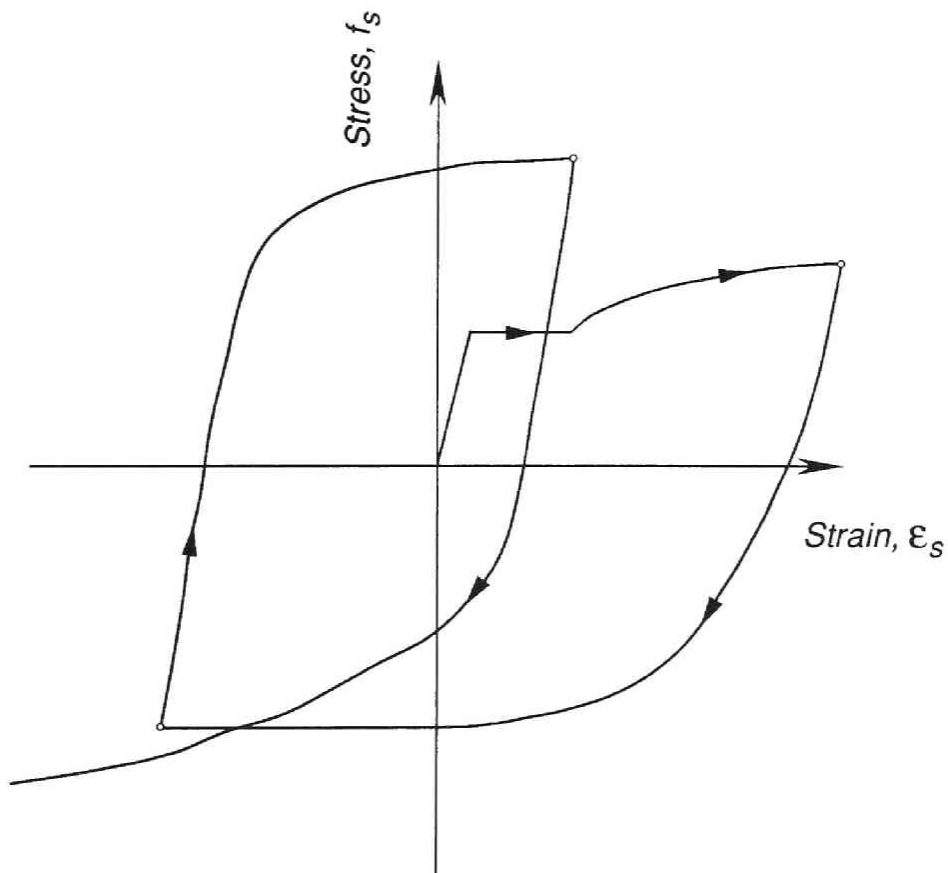


Fig.3.15 Cyclic loading behaviour for ordinary-strength reinforcing steel

For compression paths:

$$A = 0.548S_{mc} + 0.518 \quad (3.38)$$

$$R = 5.640S_{mc} - 3.929 \quad (3.39)$$

For tension paths:

$$A = 0.526S_{mt} + 0.681 \quad (3.40)$$

$$R = 4.156S_{mt} + 1.503 \quad (3.41)$$

where $S_{mc} = \max \left(\left| \frac{f_2 - f_1}{f_y} \right|, \left| \frac{f_3 - f_2}{f_y} \right|, \dots, \left| \frac{f_{k+1} - f_k}{f_y} \right| \right) \quad (k = 1, 2, \dots, i) \quad (3.42)$

$f_{k+1} - f_k =$ stress amplitude of k -th compression path

$$S_{mt} = \max \left(\left| \frac{f_2 - f_1}{f_y} \right|, \left| \frac{f_3 - f_2}{f_y} \right|, \dots, \left| \frac{f_{k+1} - f_k}{f_y} \right| \right) \quad (k = 1, 2, \dots, i) \quad (3.43)$$

$f_{k+1} - f_k =$ stress amplitude of k -th tension path

3.4.4 Stress-Strain Model for Prestressing Steels

The stress-strain model used for prestressing tendons was that proposed by Thompson [3.9].

3.4.4.1 Monotonic Stress-Strain Behaviour

A monotonic stress-strain relation is assumed to form an envelope for repeated loadings of the same sign and is illustrated in Fig.3.16. The curve is defined piece-wise as an initial linear portion, a hyperbolic curved portion, and an upper linear branch. The following input data is required to describe the monotonic stress-strain behaviour of the tendons:

$\epsilon_{pa} =$ strain at limit of proportionality

$\epsilon_{pb} =$ strain at beginning of upper linear branch

$\epsilon_{pu} =$ ultimate strain

$f_{pa} =$ stress corresponding to ϵ_{pa}

$f_{pb} =$ stress corresponding to ϵ_{pb}

$f_{pu} =$ ultimate stress at strain ϵ_{pu}

$f_{pi} =$ initial tendon stress after losses

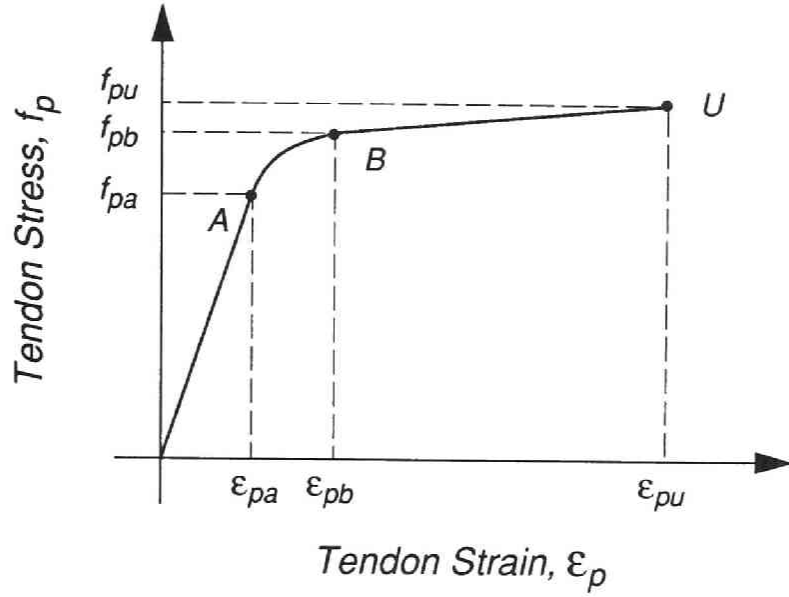


Fig.3.16 Monotonic stress - strain relation assumed for prestressing steel

The stress-strain relations corresponding to the monotonic loading curve in Fig.3.16 are defined piece-wise by Eqs.3.44 to 3.46.

$$f_p = \epsilon_p E_p \quad \text{for } \epsilon_p \leq \epsilon_{pa} \quad (3.44)$$

$$f_p = (f_{pb} \epsilon_{pb} - f_{pa} \epsilon_{pa}) / (\epsilon_{pb} - \epsilon_{pa}) + \epsilon_{pa} \epsilon_{pb} (f_{pa} - f_{pb}) / \epsilon_p (\epsilon_{pb} - \epsilon_{pa})$$

$$\text{for } \epsilon_{pa} < \epsilon_p \leq \epsilon_{pb} \quad (3.45)$$

$$f_p = f_{pb} + (f_{pu} - f_{pb}) (\epsilon_p - \epsilon_{pb}) / (\epsilon_{pu} - \epsilon_{pb})$$

$$\text{for } \epsilon_{pb} < \epsilon_p \leq \epsilon_{pu} \quad (3.46)$$

where ϵ_p = tendon strain

f_p = tendon stress

E_p = initial Young's modulus = f_{pa} / ϵ_{pa}

3.4.4.2 Cyclic Loading Behaviour

Load reversal in the elastic range will be governed by Eq.3.44. For load reversal in the inelastic range the stress-strain behaviour is illustrated in Fig.3.17. (ϵ_o, f_o) are the coordinates of the reversal point. Unloading will occur along a curve with initial slope ϕE_p , where ϕ is a modification factor to allow for softening effects which occur with

increasing levels of strain. The stress-strain relationship is obtained from Eq.3.47.

$$(\varepsilon_p - \varepsilon_o)\phi E_p = (f_p - f_o) \left[1 + \left\{ (f_p - f_o) / (f_{ch} - f_o) \right\}^{r-1} \right] \quad (3.47)$$

where $\phi = 58.27 \varepsilon_m^2 - 7.506 \varepsilon_m + 1.043$ but $\phi < 1.0$ (3.48)
 $\varepsilon_m =$ current value of maximum imposed strain

The stress-strain envelope for reversed loading is taken as the original monotonic envelope shifted along the strain axis as shown in Fig.3.18. The origin of the envelope is taken at coordinates $(\varepsilon_{zmx}, 0)$ for tensile loading and $(\varepsilon_{zmn}, 0)$ for compression loading. ε_{zmx} is the maximum tensile value of the residual strain ε_{zero} which would be the strain at zero stress (i.e., residual plastic strain) if the tendon unloaded with modulus equal to the initial Young's modulus. Similarly ε_{zmn} is the maximum compressive value of ε_{zero} .

The parameter f_{ch} , given by Eq.3.49, is a characteristic stress and r , given by Eq.3.50, is a Ramberg-Osgood exponent.

$$f_{ch} = \phi E_p U (\varepsilon_{pb} + \varepsilon_o - \varepsilon_{zmx} - f_{pb} / U - 2f_o / \phi E_p) / (\phi E_p - U) \quad (3.49)$$

$$r = 57.883 - 59116 \varepsilon_{pl} \quad \text{but } r > 20 \quad (3.50)$$

For compression unloading these parameters are found using Eqs.3.51 and 3.52.

$$f_{ch} = \phi E_p U (-\varepsilon_{pb} + \varepsilon_o - \varepsilon_{zmn} + f_{pb} / U - 2f_o / \phi E_p) / (\phi E_p - U) \quad (3.51)$$

$$r = 5.003 - 194.5 \varepsilon_{pl} \quad (3.52)$$

where $\varepsilon_{pl} =$ plastic strain on the previous cycle

$$U = (f_{pu} - f_{pb}) / (\varepsilon_{pu} - \varepsilon_{pb}) \quad (3.53)$$

Where the plastic strain in the previous cycle ε_{pl} is less than 0.001 for tensile loading or 0.0003 for compressive loading, the previous loading curve in that direction is followed once it is reached. Also, the tendon stress f_p cannot exceed the monotonic curve value (refer to Fig.3.18).

A typical example of stress-strain response for prestressing tendons obtained from the model is shown in Fig.3.19.

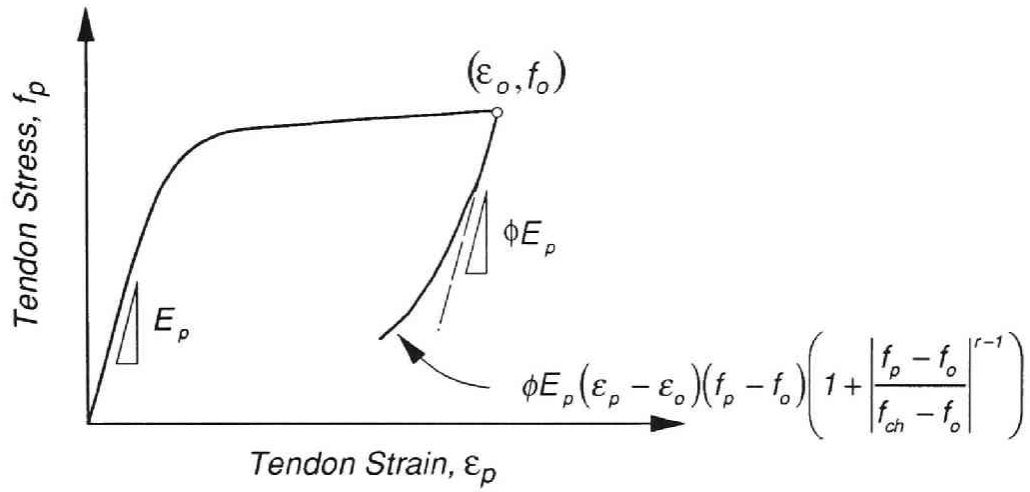


Fig.3.17 Load reversal in the inelastic range [3.19]

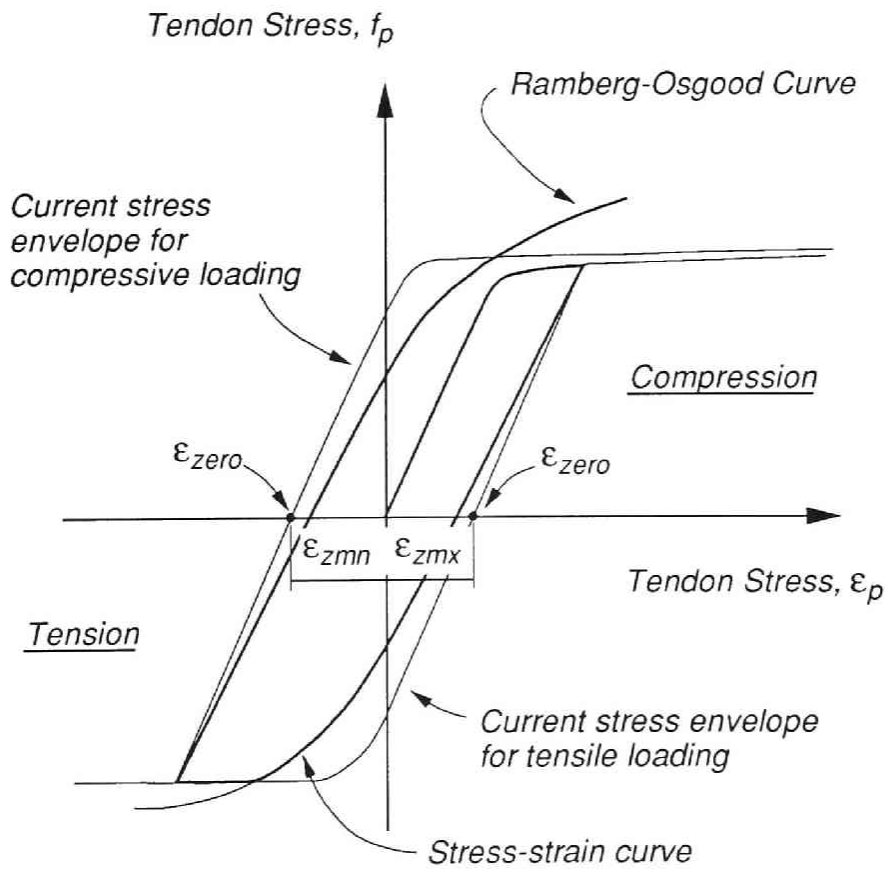


Fig.3.18 Shifted envelope for load reversal behaviour [3.19]

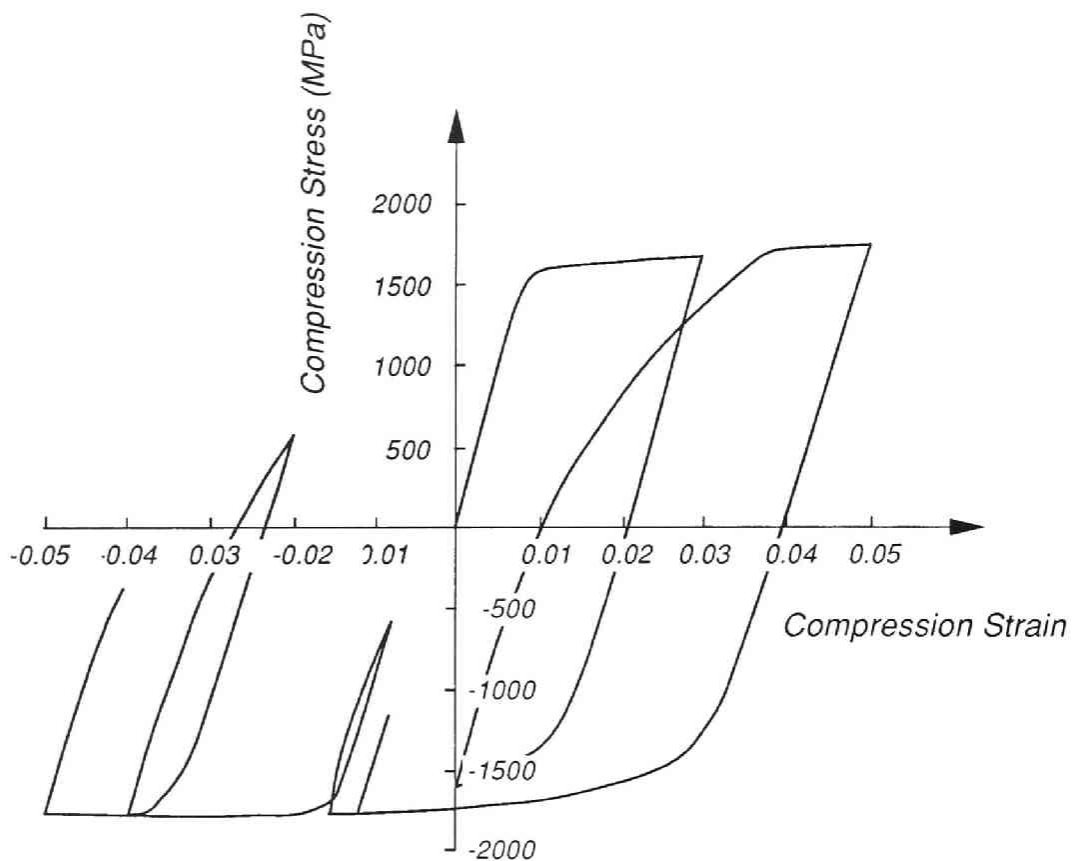


Fig.3.19 Typical stress strain response [3.19]

Since the numerical coefficients in Eq.3.48, 3.50 and 3.52 were quoted exactly as they appeared in Thompson's research work, the number of significant figures were not uniform in these coefficients.

3.5 Procedure of Moment-curvature Analyses [3.19]

3.5.1 General assumptions

The following assumptions were made in the moment-curvature analyses:

1. Plane sections remain plane after bending.
2. When the compressive strain exceeds the spalling strain (ϵ_{spall}), the cover concrete is considered to have spalled and thereafter sustain zero stress.
3. When the concrete stress exceeds the tensile strength, the concrete is assumed to crack and thereafter the tensile stress is ignored.
4. The effects of creep and shrinkage are ignored.
5. There is no bond slip between non-prestressed ordinary reinforcing steel and the core concrete.

For the purpose of analysis the cross section is divided into a number of discrete elements parallel to the neutral axis of bending. Similarly, the prestressing or non-prestressed longitudinal steel is divided into a number of levels. The strain distribution for the cross section is given by:

$$\varepsilon(y) = \varepsilon_o + \phi y \quad (3.53)$$

where ε_o = strain at the centroidal axis,

ϕ = section curvature,

y = distance from the reference axis corresponding to the centroidal axis of the beam section.

Hence for a given strain profile, the axial load, P , and the bending moment, M , can be calculated as follows;

$$P = \sum_{i=1}^{n_c} f_{ci} A_{ci} + \sum_{j=1}^{n_p} f_{pj} A_{pj} + \sum_{k=1}^{n_s} f_{sk} A_{sk} \quad (3.54)$$

$$M = \sum_{i=1}^{n_c} f_{ci} A_{ci} y_{ci} + \sum_{j=1}^{n_p} f_{pj} A_{pj} y_{pj} + \sum_{k=1}^{n_s} f_{sk} A_{sk} y_{sk} \quad (3.55)$$

where f_{ci} = stress in the i -th concrete layer (compression -ve),

f_{pj} = stress in the j -th prestressing steel level (compression -ve),

f_{sk} = stress in the k -th nonprestressed longitudinal steel level (compression -ve),

y_{ci} = distance from the center of the i -th concrete layer to the reference axis,

y_{pj} = distance from the center of the j -th prestressing steel level to the reference axis,

y_{sk} = distance from the center of the k -th nonprestressed longitudinal steel level to the reference axis.

Moment-curvature relationships are calculated for a prescribed external axial load, P_e , on the cross section. Force and strain compatibility which are expressed by Eqs. 3.53, 3.54 and 3.55, must be solved simultaneously. Incremental forces (ΔP and ΔM) are related to incremental deformations ($\Delta \phi$ and $\Delta \varepsilon_o$) by the instantaneous section stiffness:

$$\begin{bmatrix} \Delta M \\ \Delta P \end{bmatrix} = \begin{bmatrix} EI & EZ \\ EZ & EA \end{bmatrix} \begin{bmatrix} \Delta \phi \\ \Delta \varepsilon_o \end{bmatrix} \quad (3.56)$$

By numerically integrating the instantaneous values of Young's modulus across the section, the section stiffness coefficients are obtained as follows;

$$EA = \sum_{i=1}^{n_c} E_{ci} A_{ci} + \sum_{j=1}^{n_p} E_{pj} A_{pj} + \sum_{k=1}^{n_s} E_{sk} A_{sk} \quad (3.57)$$

$$EZ = \sum_{i=1}^{n_c} E_{ci} A_{ci} y_{ci} + \sum_{j=1}^{n_p} E_{pj} A_{pj} y_{pj} + \sum_{k=1}^{n_s} E_{sk} A_{sk} y_{sk} \quad (3.58)$$

$$e_y = EZ / EA \quad (3.59)$$

where EA = effective axial stiffness,
 EZ = first moment of area of stiffness,
 e_y = eccentricity from the neutral axis of the incremental section stiffness,
 E_{ci} = modulus of elasticity of concrete at i-th layer,
 E_{pj} = modulus of elasticity of prestressing steel at j-th level,
 E_{sk} = modulus of elasticity of nonprestressed longitudinal steel at k-th level.

Therefore the effective flexural stiffness, EI , about the neutral axis of the incremental section is defined as:

$$EI = \sum_{i=1}^{n_c} E_{ci} A_{ci} y_{ci}^2 + \sum_{j=1}^{n_p} E_{pj} A_{pj} y_{pj}^2 + \sum_{k=1}^{n_s} E_{sk} A_{sk} y_{sk}^2 - EA \cdot e_y^2 \quad (3.60)$$

To generate moment-curvature curves for a prescribed axial load, P_e , only the second row of the matrix from Eq.3.56 is used, thus;

$$\Delta P = EZ \cdot \Delta\phi + EA \cdot \Delta\varepsilon_o \quad (3.61)$$

where $\Delta P = P - P_e$ (3.62)

is the out-of-balance force and P is determined using Eq.3.54.

Successive curvature increments ($\Delta\phi$) are applied and the centroidal strain ($\Delta\varepsilon_o$) is determined using the following algorithm.

Step 1 : The curvature increment ($\Delta\phi$) is added to the value of the previous total curvature (ϕ_{n-1}) to give the new section curvature:

$$\phi_n = \phi_{n-1} + \Delta\phi \quad (3.63)$$

Step 2 : From the out-of-balance force and the curvature increment, if any, the change in the centroidal strain necessary to restore force equilibrium is calculated using Eq.3.64, which gives:

$$\Delta \varepsilon_o = \frac{\Delta P - EZ \cdot \Delta \phi}{EA} \quad (3.64)$$

This value is then added to the previous total centroidal strain ($\varepsilon_{o,n-1}$) to give the corrected centroidal strain:

$$\varepsilon_{o,n} = \varepsilon_{o,n-1} + \Delta \varepsilon_o \quad (3.65)$$

Step 3 : From the revised strain profile given by $\varepsilon(y)_n = \varepsilon_{o,n} + \phi_n y$, calculate the new axial load (P) and new moment (M) using Eqs.3.54 and 3.55, respectively.

Step 4 : Calculate the out-of-balance force (ΔP) using Eq.3.61. If the absolute value of ΔP exceeds a specified tolerance, then set $\Delta \phi$ to zero and the analysis returns to Step 2. Otherwise choose the next curvature increment ($\Delta \phi$) and return to Step 1.

3.6 Conclusions

1. Moment - curvature relationships of prestressed, partially prestressed and reinforced concrete beam sections were compared in terms of yield curvature, ultimate available curvature and ductility ratio as well as a whole shape of the curves.
2. The analytical procedure for obtaining moment - curvature relationships of prestressed, partially prestressed and reinforced concrete sections based on stress - strain relationships of constitutive materials was described. Analytical results will be shown in the later chapter of this thesis.

[References]

- 3.1 R.W.G.Blakeley and R.Park : Seismic Resistance of Prestressed Concrete Beam-Column Assemblies, ACI J. Sept. 1971 Title No.68-57, pp.677-692.
- 3.2 R.Park and K.J.Thompson : Cyclic Load Tests on Prestressed and Partially Prestressed Beam-Column Joints, PCI J. Sept.-Oct. 1977, pp.84-110.
- 3.3 K. J. Thompson : Ductility of Concrete Frames under Seismic Loading, Ph. D. Thesis, University of Canterbury, New Zealand, 1975.
- 3.4 M.Z.Cohn and B.Bartlett : Computer-Simulated Flexural Tests of Partially Prestressed Concrete Sections, J.SD,Proc.of ASCE Dec.1982 ST12, pp.2747-2765.
- 3.5 M.H.Harajli and A.E.Naaman : Evaluation of the Ultimate Steel Stress in Partially Prestressed Flexural Members, PCI J. Sept.-Oct. 1985, pp.54-81.

- 3.6 M. Okada, M. Hamahara, H. Suetsugu and J. Motooka : Elasto-plastic hysteretic behavior of prestressed concrete beams, Transactions of AIJ, No.410, 1990, pp.63-69.
- 3.7 Okamoto, S : Fundamental Study on Earthquake Resisting Behaviours of Prestressed Concrete Frame Structures, Chapter 6; Seismic Response of Prestressed Concrete Buildings, Ph. D Thesis, Kyoto University, Japan 1986.
- 3.8 Building Code Requirements for Reinforced Concrete (ACI318-89) and Commentary (ACI318R-89), 1989.
- 3.9 F. A. Zahn : The Ductility of Bridges, Ph. D. Thesis, University of Canterbury, 1985.
- 3.10 K. Suzuki, T. Nakatsuka and M. Awano : Ultimate Limit Index Points of Concrete Flexural Members -(Part 1) Mechanism of existence for ultimate limit index points proposed -, Journal of Structural and Construction Engineering (Transactions of AIJ), No.383, January 1988, pp.49-57.
- 3.11 H. Muguruma, M. Nishiyama, F. Watanabe and H. Tanaka : Ductile Behaviour of High-strength Concrete Columns Confined by High-strength Transverse Reinforcement, Proceedings of ACI International Conference on Evaluation and Rehabilitation of Concrete Structures and Innovations in Design, SP-128 Vol.2, Hong Kong, December 1991, pp.877-891.
- 3.12 H. Muguruma and F. Watanabe, Ductility Improvement of High Strength Concrete Column with Lateral Reinforcement, High Strength Concrete, Second International Symposium, ACI SP-121, 1990, pp.47-60.
- 3.13 J. B. Mander, M. J. N. Priestley and R. Park, Seismic Design of Bridge Piers, Research Report 84-2, Department of Civil Engineering, University of Canterbury, February 1984.
- 3.14 J. B. Mander, Seismic Design of Bridge Piers, Ph. D. Thesis, Department of Civil Engineering, University of Canterbury, 1983.
- 3.15 Code for Practice for the Design of Concrete Structures NZS 3101 Part 1: 1982, and Commentary NZS 3101 Part 2: 1982, Standard Association of New Zealand, 1982.
- 3.16 H. Muguruma, M. Nishiyama and F. Watanabe, Ductility Evaluation of Reinforced Concrete Columns with Normal and High Strength Concrete, Proceedings of Pacific Conference on Earthquake Engineering, New Zealand, 20-23 November 1991, pp.159-170.
- 3.17 Y.Yokoo, T.Nakamura, T.Komiyama and Y.Kawada, Non-Stationary Hysteretic Uniaxial Stress-Strain Relations of a Wide-Flange Steel, Transactions of Architectural Institute of Japan, No.259, September 1977, pp.53-66.
- 3.18 T. Fujimura, Behavior of High Strength Concrete Column, Master Thesis, Kyoto University, 1991.
- 3.19 D. Whittaker, Seismic Performance of Offshore Concrete Gravity Platforms, Ph. D. Thesis, University of Canterbury, New Zealand, October 1987.

HYSTERETIC RESTORING FORCE CHARACTERISTICS AND SHEAR RESISTANCE OF PRESTRESSED BEAM-COLUMN JOINT ASSEMBLIES

4.1 Introduction

Prestressed concrete members usually have higher moments at the commencement of flexural cracking than similar reinforced concrete members. Even after they are loaded up to near their ultimate strengths they recover to their original states and respond elastically unless fracture of the prestressing tendons or of the anchorages takes place. For this reason it has been said that, if their cracking, yielding and ultimate displacements and the corresponding moment capacities are the same, the displacement response of prestressed concrete frames to earthquake ground motions may be larger than that of reinforced concrete frames. However, the restoring force characteristics of a frame are not dominated only by those of the beams. The moment-rotation relationships of the potential plastic hinge regions of the columns may also have a large effect on the seismic performance of the frame as may the performance of the beam-column joints even though joint cores are generally assumed to have high rigidity in seismic response analyses.

Prestress introduced into a beam and through the joint has been shown to improve the shear resistance of beam-column joints. The following reasons can be given:

- (1) The joint core is compressed in the horizontal direction as well as in the vertical direction due to the axial force on the column. Hence the joint core is subjected to biaxial compression which leads to higher compressive strength than uniaxial compression.
- (2) Prestressing is considered to increase the diagonal compression strut action in the joint core because the prestress results in a larger neutral axis depth and restraint of the width of diagonal cracks.

Besides this, prestress can improve the hysteretic restoring force characteristics of beam-column joint assemblages because it helps to preserve the rigidity of the joint cores. Stiffness degradation in joints results in pinched hysteresis loops with reduced energy dissipation. However, too much prestress, as indicated in Chapter 3, results in less ductility in the beams. This problem of decreased ductility may be overcome by providing more confining reinforcement in the potential plastic hinge regions. Based on the above reasons, well designed prestressed concrete frames are superior to

reinforced concrete frames from the view point of energy dissipation. Very little research has been carried out to prove that it is possible to have improved performance with prestressed members.

In this chapter, after reviewing previous research and code provisions on the seismic design and seismic performance of prestressed concrete beam-column assemblages, their hysteretic restoring force characteristics and shear behaviour are discussed based on two series of tests conducted by the author.

4.2 Review of Previous Research and Code Provisions

4.2.1 Hysteretic Restoring Force Characteristics of Prestressed Concrete Beam-Column Assemblies

Few past research studies have been carried out on prestressed concrete beam-column assemblies while those on reinforced concrete beam-column assemblies are very numerous. Previous research on prestressed concrete beam-column assemblies can be divided into two categories: i) research on the hysteretic restoring force characteristics in order to carry out an inelastic dynamic response analysis of a prestressed concrete frame structure and ii) those on the shear strength of beam-column joints to conduct shear design of the joint core.

In the first category of research R.W.G.Blakeley and R.Park [4.1] conducted tests on four full size precast, prestressed concrete beam - column assemblies shown in Fig.4.1 under large displacement reversed cyclic loading. The columns were pretensioned. The beams were post-tensioned with cables passing through the column into an exterior anchor block. The cables were grouted.

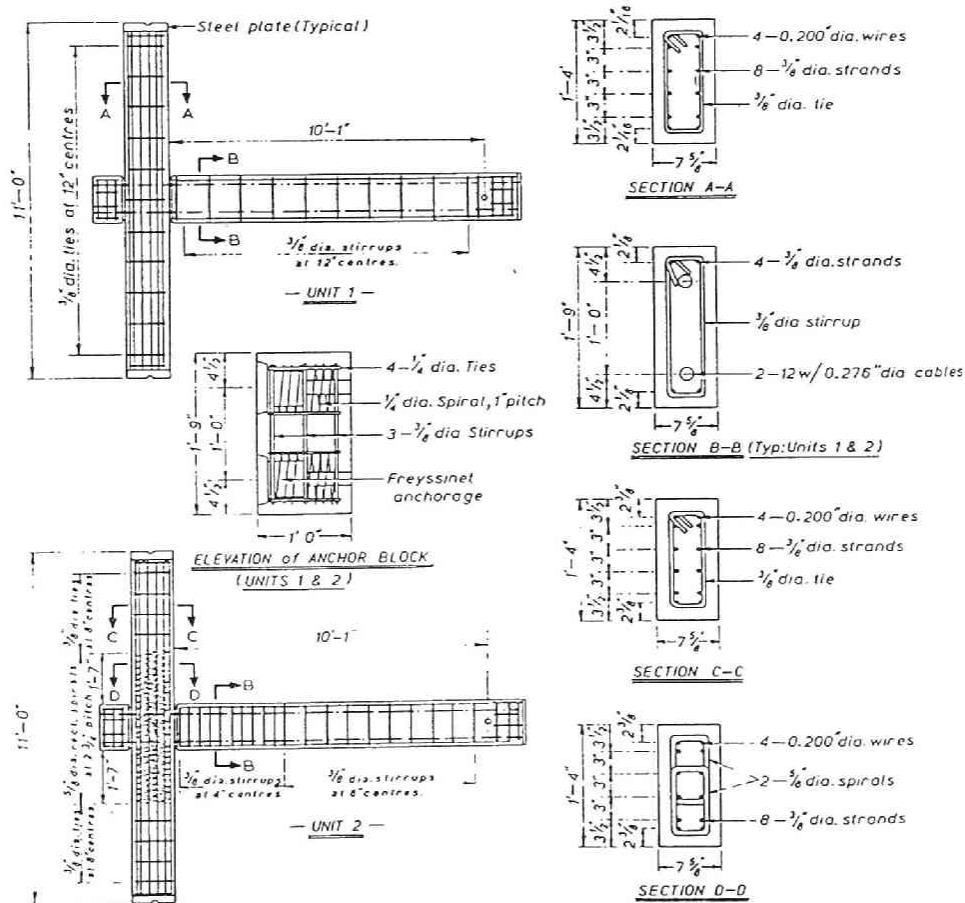


Fig.4.1(a) Precast prestressed concrete beam - column assembly test units (Units 1 and 2) by Blakeley and R. Park [4.1]

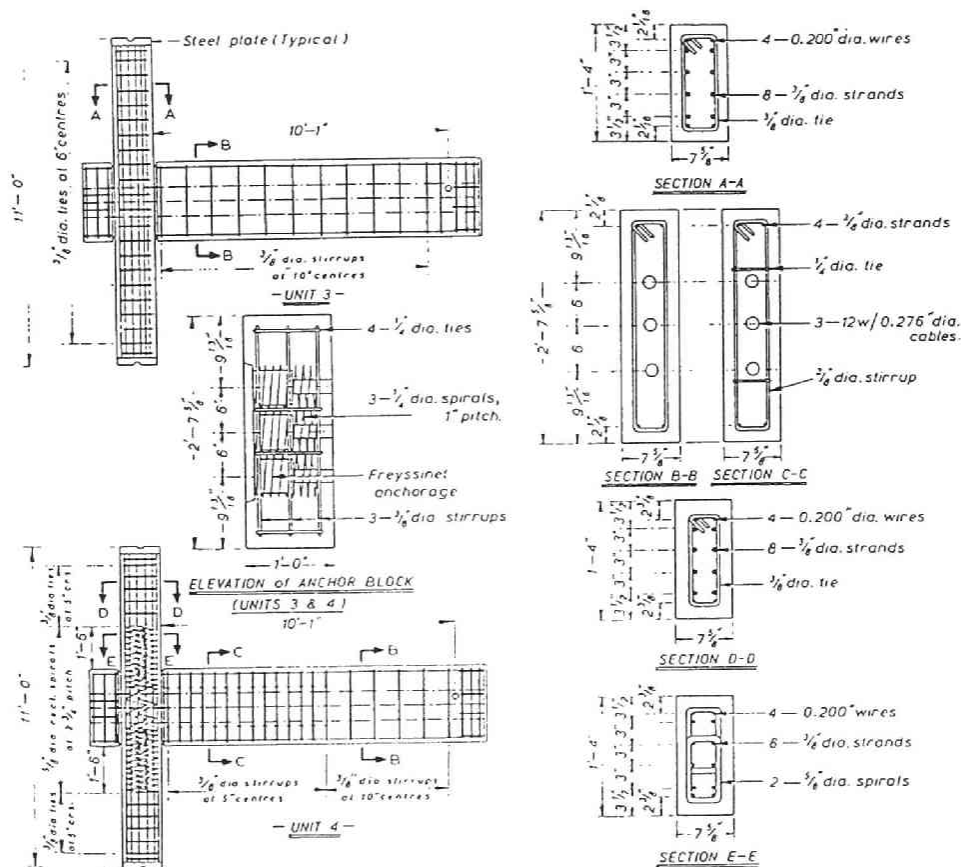


Fig.4.1(b) Precast prestressed concrete beam - column assembly test units (Units 3 and 4) by Blakeley and R. Park [4.1]

The test variables included the amount of transverse confining steel for ductility and the position of the plastic hinge in the members. Thus, their research was aimed at obtaining the hysteretic restoring force characteristics of prestressed concrete members or beam-column joint assemblages and comparing them with those of reinforced concrete. Shear behaviour of the joint cores was not of great concern.

Four test units, Unit 1, 2, 3 and 4 were constructed and tested. The mild steel stirrups and ties in Units 1 and 3 satisfied the shear requirements in the commonly used code for prestressed concrete : ACI 318-63 [4.2] (also ACI 318-71 [4.3]) and the British CP115 [4.4]. Units 2 and 4 also contained special transverse steel for confinement. When the paper was written, no recommendations for the amount of special transverse steel required in the beam - column joint cores for ductility was available for prestressed concrete. In Units 2 and 4, the shear reinforcement in the beams satisfied SEAOC 1968 [4.5].

The longitudinal non-prestressed mild steels in the beams were terminated at the column face. Moist pack mortar joints, 1 in. (25.4mm) thick, were formed between the columns and the beams.

Units 1 and 2 were designed to form plastic hinges in the beam at the joint, and for Units 3 and 4 plastic hinges were planned to be formed in the column immediately above or below the beam connection.

Figures 4.2-4.5 show the moment - rotation curves and moment - displacement curves. Conclusions reached from the tests are summarized below:

1. This series of tests showed that prestressed concrete framed structures can be capable of resisting moderate earthquakes without structural damage, and of withstanding severe earthquakes with some possible structural damage.
2. Energy dissipation is relatively small prior to the commencement of crushing of the concrete, but substantial once crushing has occurred.
3. Large post-elastic deformation capacity can be available in prestressed concrete members, even when the transverse reinforcement satisfies only reinforced concrete code requirements for shear.
4. Substantial stiffness degradation occurs when prestressed concrete members are subjected to high intensity cyclic loading.

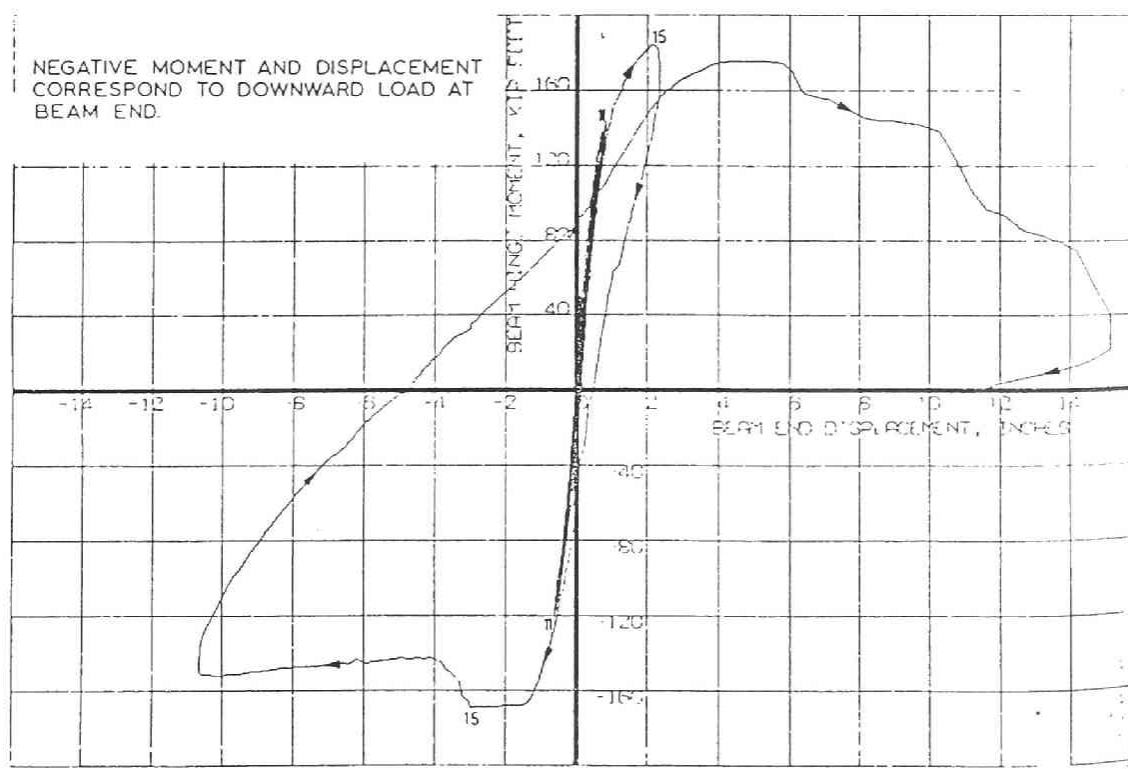


Fig.4.2 Moment - displacement curve obtained from Unit 1 by Blakeley and Park [4.1]

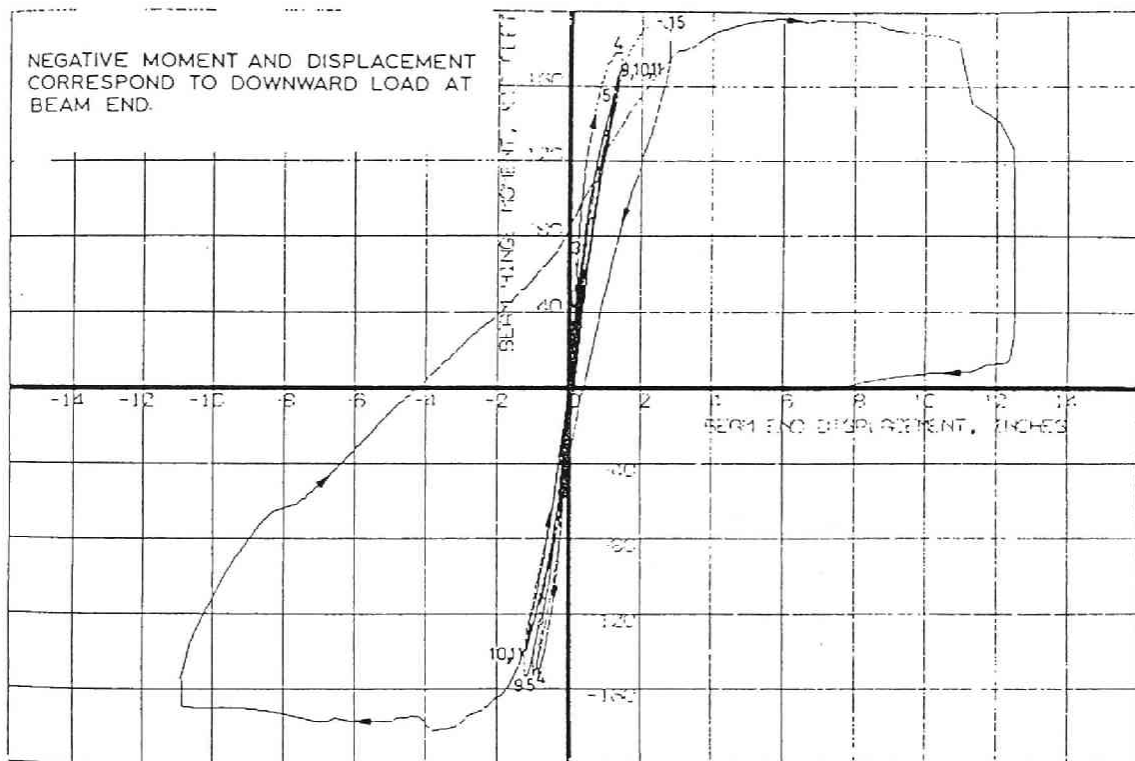


Fig.4.3 Moment - displacement curve obtained from Unit 2 by Blakeley and Park [4.1]

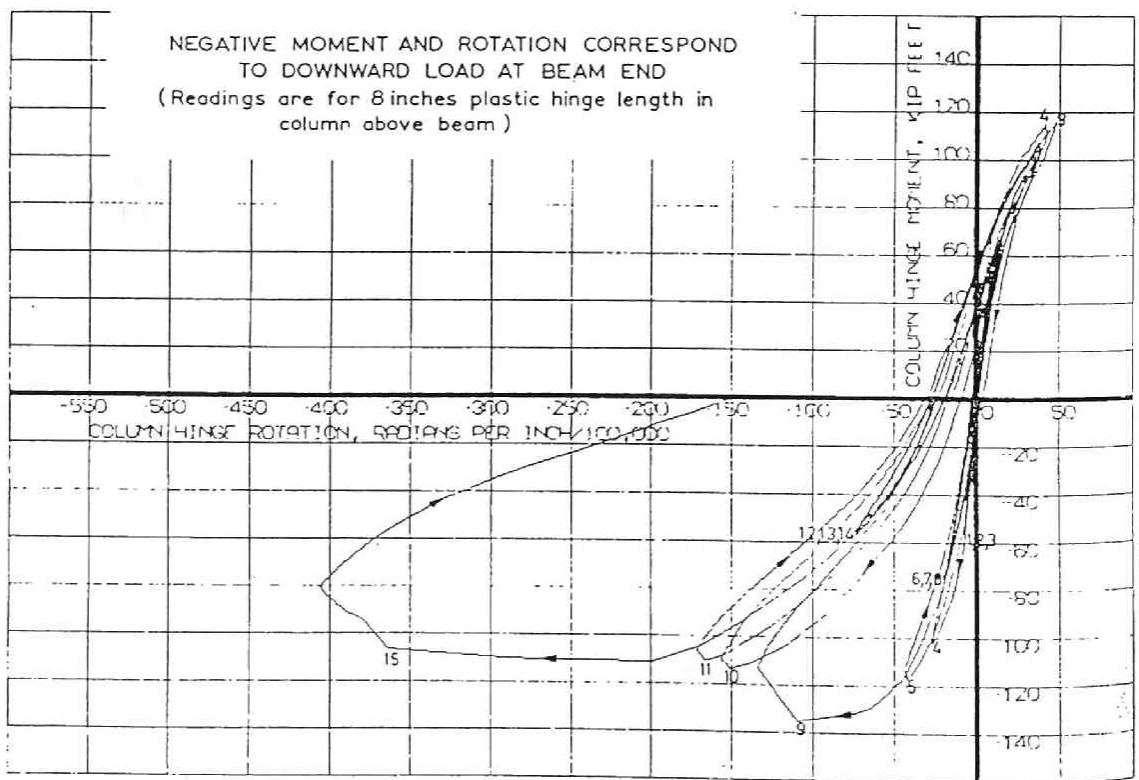


Fig.4.4 Moment - rotation curve obtained from Unit 3 by Blakeley and Park [4.1]

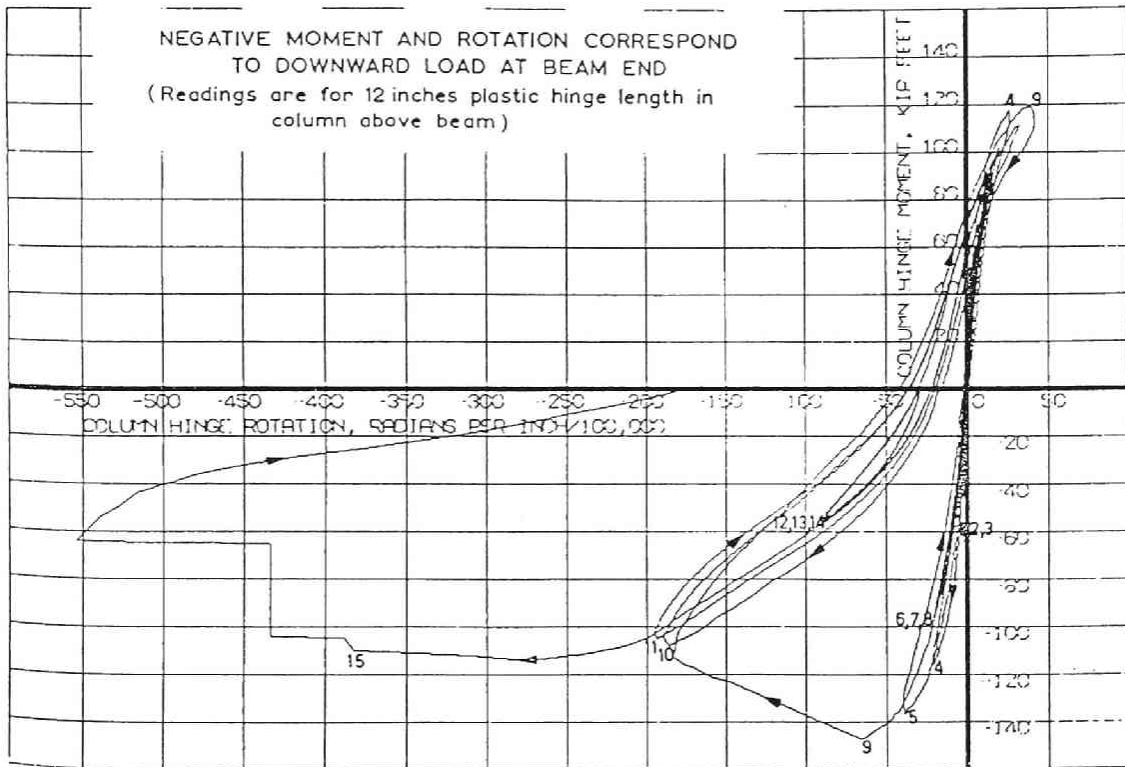


Fig.4.5 Moment - rotation curve obtained from Unit 4 by Blakeley and Park [4.1]

At the time of their tests there was little information on the behaviour of prestressed concrete structures under severe earthquake loading as well as on the behaviour of prestressed concrete members under high intensity cyclic loading. Therefore, until this research was published, the behaviour of prestressed concrete members under cyclic loading had been linked to a bilinear elastic system with much less energy dissipation and less ductility than reinforced concrete. However, their tests proved that substantial energy dissipation and large post-elastic deformations can be expected for prestressed concrete as well as reinforced concrete members, in spite of the moist mortar joints without longitudinal non-prestressed reinforcement.

4.2.2 Shear Strength of Prestressed Concrete Beam-Column Joint Cores

R. Park and K. J. Thompson [4.6] conducted the first tests which focused on the shear strength of prestressed concrete beam-column joint cores. The tests were carried out on ten concrete beam - interior column frame assemblies subjected to static reversed cyclic loading. The loading pattern selected simulating the effect of severe earthquake loading. The dimensions of a beam-column test unit are shown in Fig.4.6. From the beams of the ten beam test units, five were fully prestressed and contained nominal non-prestressed steel, four were partially prestressed, and one contained only non-prestressed reinforcement. The beam and column cross sections with the steel details are shown in Fig.4.7.

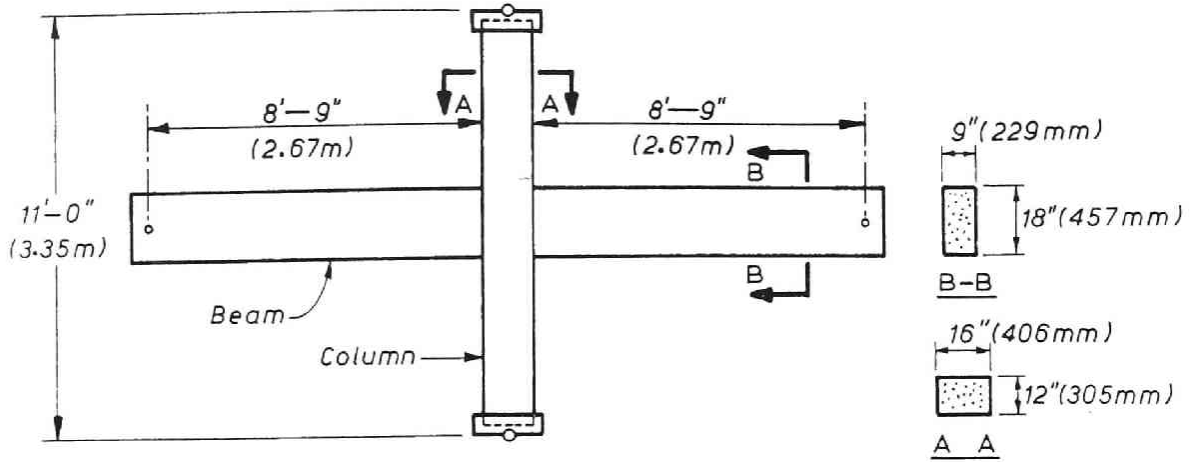


Fig.4.6 Dimensions of beam-column test unit by Park and Thompson [4.6]

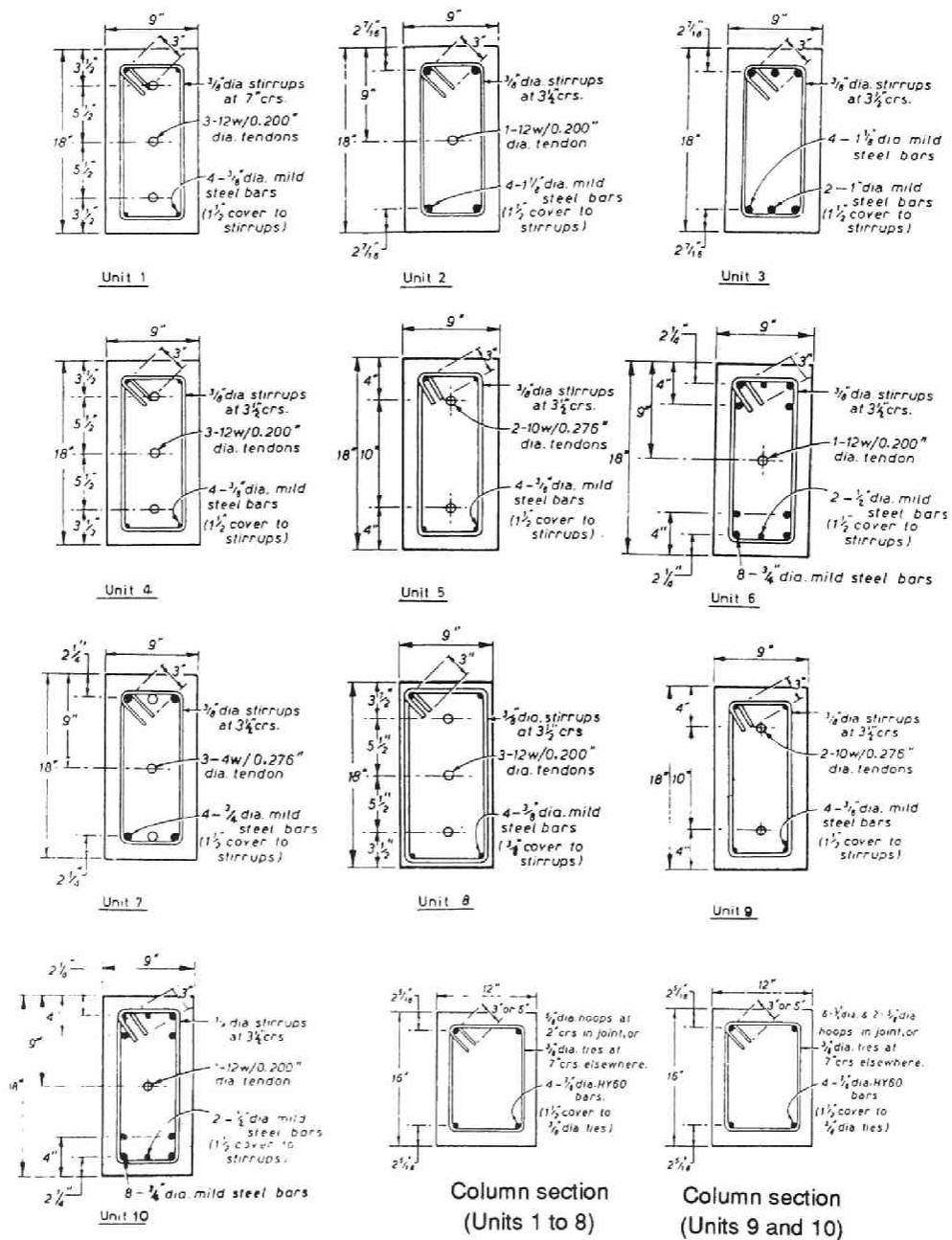


Fig.4.7 Beam and column cross sections with the steel details [4.6]

The transverse steel in each joint core consisted of eight rectangular column ties (hoops) which were placed around the longitudinal column bars between the top and bottom layers of longitudinal beam steel. The average spacing between the tie centers was 2 in. (51 mm) near the mid-depth of the joint core. In Units 1 to 8, the eight ties were formed from 5/8-in. (15.9 mm) diameter bar. In Units 9 and 10, the top and bottom ties were formed from 5/8-in. (15.9 mm) diameter bar and the six intermediate ties were formed from 3/4-in. (19.1 mm) diameter bar.

To calculate the theoretical shear strength V_u of the test units, they applied Eq.4.1 described in Appendix A of ACI 318-71 [4.3] to the column in the joint core region.

$$V_u = v_c b d + A_v f_y d / s \quad (4.1)$$

where, v_c = nominal shear stress carried by the concrete (psi)

b = column width (in.)

d = distance from extreme compression fiber to centroid of tension steel of column section (in.)

A_v = area of one layer of shear reinforcement (in.²)

f_y = yield strength of reinforcement (psi)

s = spacing between centers of layers of shear reinforcement (in.)

v_c was given by the following equation.

$$v_c = 2(1 + 0.0005 N_u / A_g) \sqrt{f'_c} \quad (4.2)$$

where N_u = column axial compressive load (lb)

A_g = gross area of column section (in²)

f'_c = compressive strength of concrete (psi)

The theoretical shear strengths of the joint cores calculated using Eq.4.1 and 4.2 are shown in Table 4.1.

The maximum horizontal shear force, V_{max} , occurs in the middle region of the beam depth between the neutral axis positions of the beam sections shown in Fig.4.8 and is given by Eq.4.3.

$$V_{max} = T_4 + T_1 + C_5 + C_c - T_3 - V_{col} \quad (4.3)$$

where, T_1, T_3 = tensile force in prestressing tendons (lb)

T_4 = tensile force in non-prestressed steel (lb)

C_5 = compressive force in non-prestressed steel (lb)

Table 4.1 Theoretical shear strengths of the joint cores calculated using Eqs.4.1 and 4.2

Unit	ACI318-71**		Proposed***	
	V_u (kips)	V_{max} / V_u	V_u (kips)	V_{max} / V_u
1	217	0.98	291	0.73
4	219	1.01	291	0.76
5*	220	1.13	249	1.00
8*	218	0.99	292	0.74
9*	288	0.84	327	0.74
7	220	0.89	272	0.72
2*	221	0.97	294	0.73
6*	220	0.99	290	0.75
10	293	0.71	371	0.56
3	220	0.94	249	0.83

Note:

- * Yielding of ties and softening of joint core eventually occurred during the inelastic loading cycles in the tests.
 - ** Shear carried by concrete was 12 to 18% of V_u .
 - *** Shear carried by concrete was 10 to 15% of V_u and by ties was 73 to 89% of V_u).
- V_u : Theoretical horizontal shear strength
 V_{max} : Theoretical maximum applied horizontal shear force

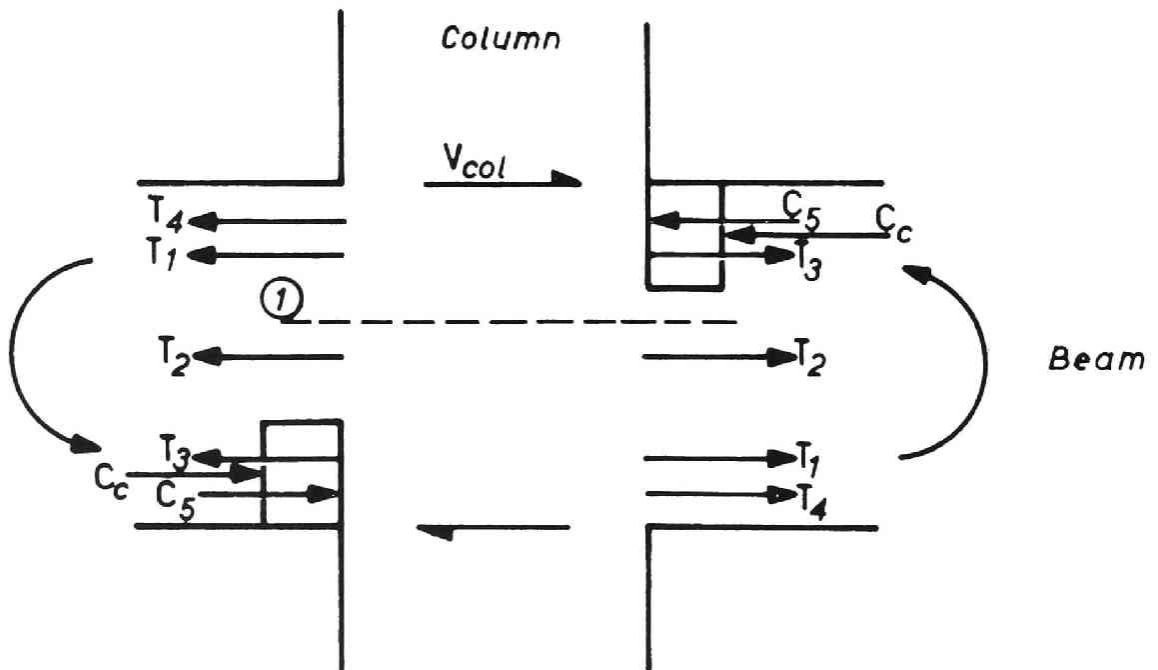


Fig.4.8 External forces acting on the joint core [4.6]

C_c = compressive force in concrete (lb)

V_{col} = shear force in column (lb)

The calculated ratio of the maximum theoretical horizontal shear force in the joint core V_{max} to the theoretical joint core horizontal shear strength V_u varies between 0.71 and 1.13. Only Unit 5 had a V_{max} / V_u value greater than 1.01. So, according to the ACI 318-71, all the joint cores were adequately reinforced for shear with the exception of Unit 5.

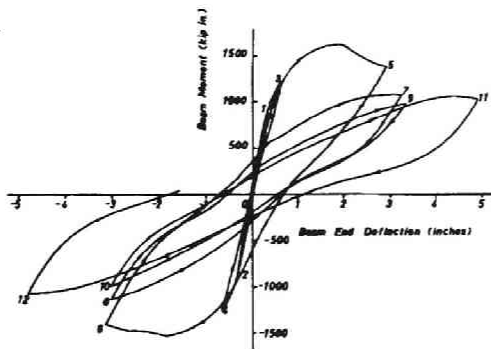
Test Results

Fig.4.9 shows the relationship of the measured beam moment at the column face versus the beam end deflection for all units. The results are summarized as follows;

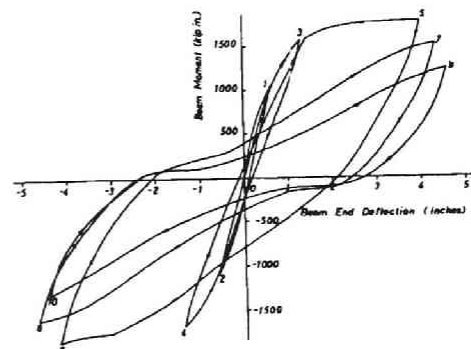
Units 1, 4, 5, 8 and 9 with fully prestressed beams

Unit 1 and 4: The degradation in the strength and stiffness was due mainly to the reduction in the sectional area of the beams when the cover concrete crushed. The compression steel in the beams was nominal. No serious damage was observed in the joint cores.

Unit 1

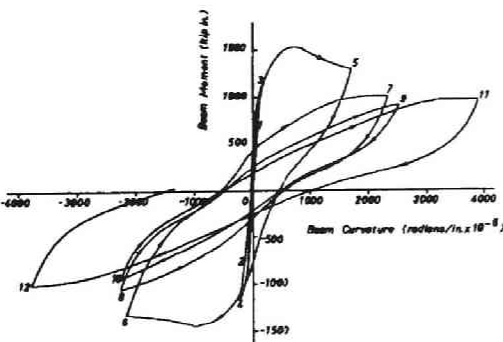


Unit 2

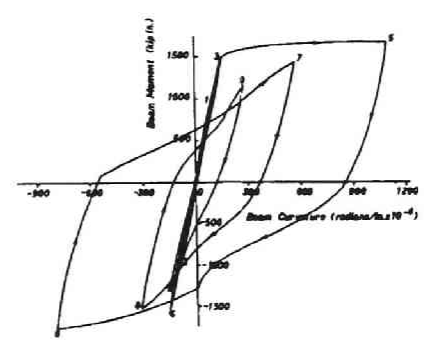


(a) Beam moment at column face versus left beam end deflection

Unit 1



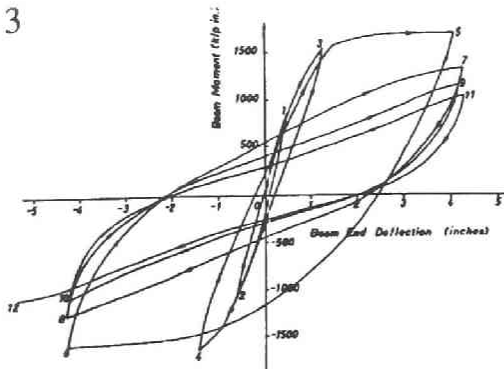
Unit 2



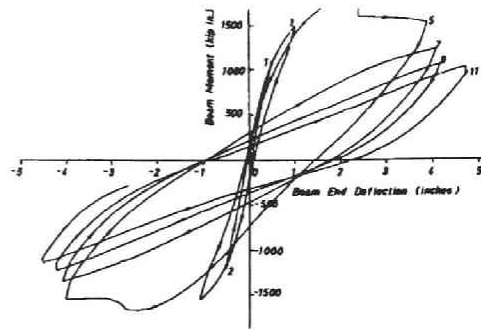
(b) Beam moment at 6 in from column face versus average curvature in left beam over 12 in gauge length adjacent to column face

Fig.4.9(a) Test results

Unit 3

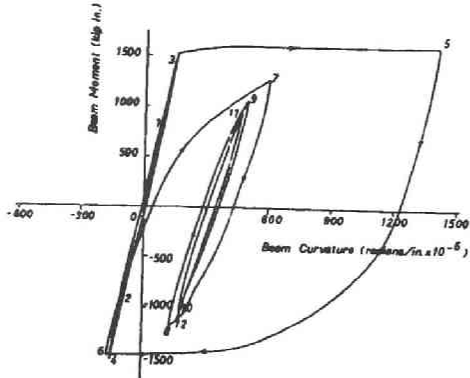


Unit 4

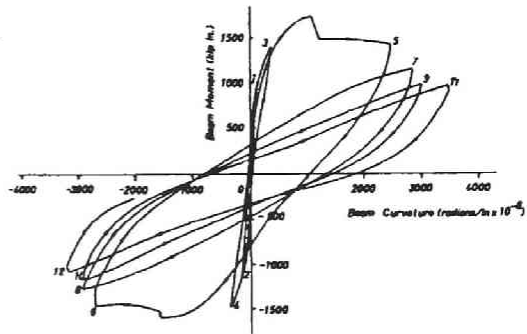


(a) Beam moment at column face versus left beam end deflection

Unit 3



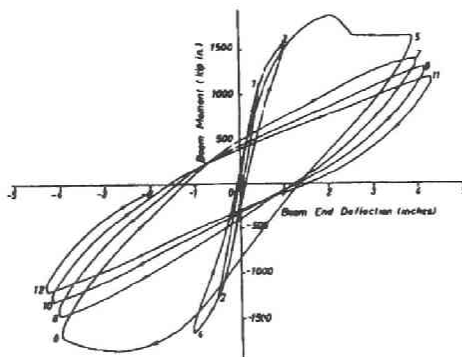
Unit 4



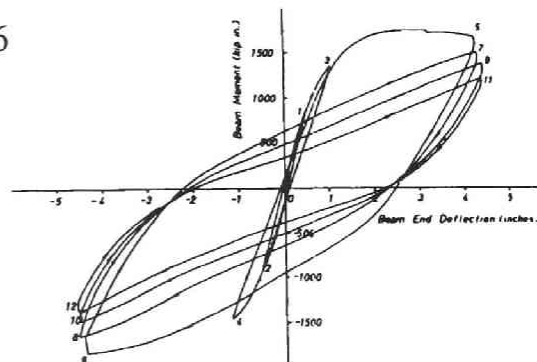
(b) Beam moment at 6 in from column face versus average curvature in left beam over 12 in gauge length adjacent to column face

Fig.4.9(b) Test results

Unit 5

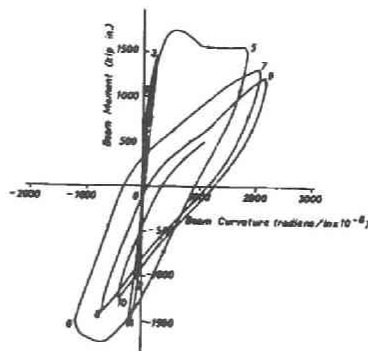


Unit 6

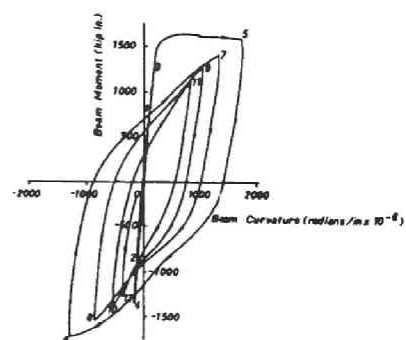


(a) Beam moment at column face versus left beam end deflection

Unit 5



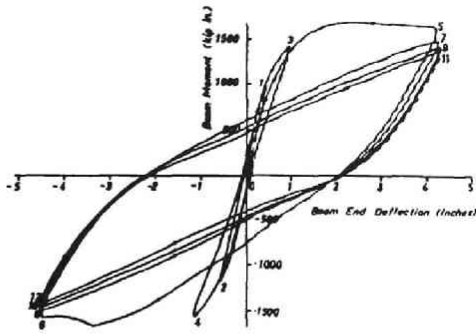
Unit 6



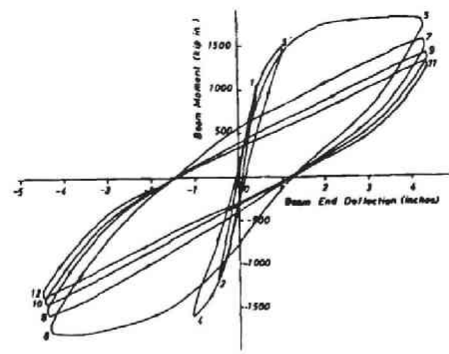
(b) Beam moment at 6 in from column face versus average curvature in left beam over 12 in gauge length adjacent to column face

Fig.4.9(c) Test results

Unit 7

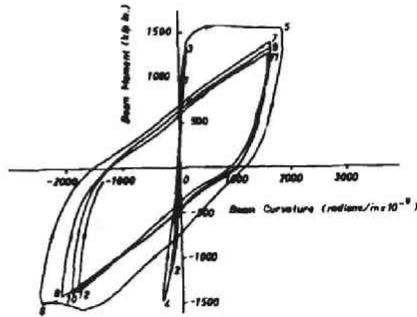


Unit 8

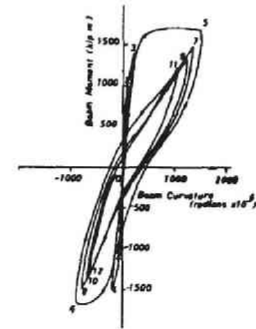


(a) Beam moment at column face versus left beam end deflection

Unit 7

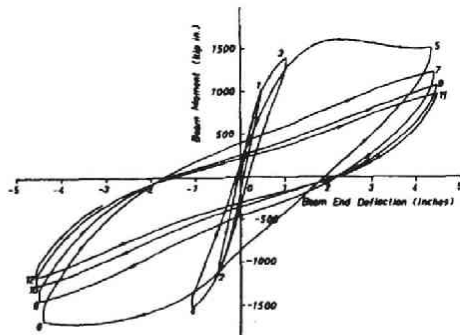


Unit 8

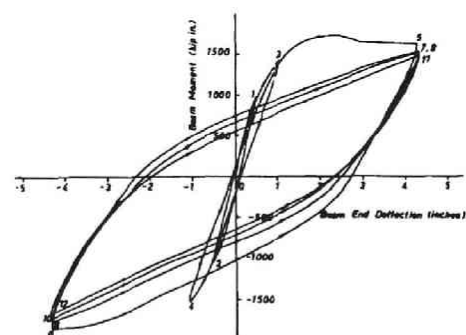


(b) Beam moment at 6 in from column face versus average curvature in left beam over 12 in gauge length adjacent to column face
Fig.4.9(d) Test results

Unit 9

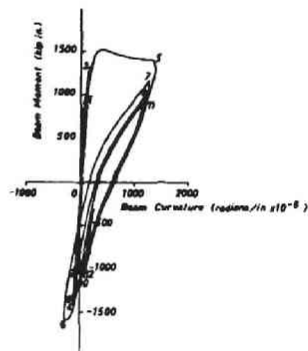


Unit 10

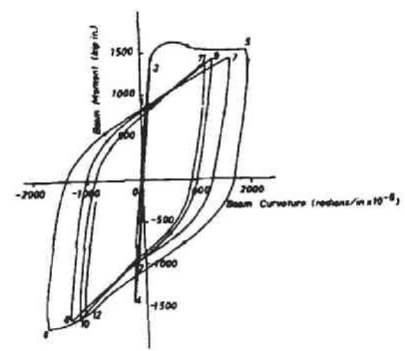


(a) Beam moment at column face versus left beam end deflection

Unit 9



Unit 10



(b) Beam moment at 6 in from column face versus average curvature in left beam over 12 in gauge length adjacent to column face
Fig.4.9(e) Test results

Unit 8: Although reduction in moment capacity due to concrete crushing was observed, it was less significant than in Unit 4 because of the larger area of confined core.

Unit 5, 8 and 9: The degradation of the strength and stiffness was due mainly to the gradual degradation of the joint cores. This deterioration of the joint cores was the result of repeated opening and closing of diagonal tension cracks in each direction and yielding of the ties in the joint core. Units 5 and 9 contained at least as much joint core shear reinforcement as Units 1 and 4, but lacked a prestressing tendon at the center of the beam depth. The joint cores were not effectively compressed by the prestressing force because of yielding of the prestressing tendons near the extreme tension and compression fiber.

The deterioration of the joint core of Unit 8, even though it had a central prestressing tendon through the joint core and the same joint core reinforcement as Units 1 and 4, occurred because of the high level of moment being maintained in the loading cycles in the inelastic range. An upper limit of applied total horizontal joint shear force across a joint should be specified.

Units 2, 6, 7 and 10 with partially prestressed beams

After the beam moment capacity had been reached and crushing of the concrete had commenced, the energy dissipation capacity of the members was greater than for the units with fully prestressed beams although significant degradation of stiffness, and in some cases strength, occurred.

The inelastic deformations concentrated mainly in the beam plastic hinges in Units 7 and 10 showing the beneficial effect of the non-prestressed longitudinal steel in the compression zones of the beam plastic hinges.

In the case of Units 2 and 6 the degradation of strength and stiffness was due mainly to deterioration of the joint cores. These units contained as much joint shear reinforcement and more non-prestressed longitudinal steel than Unit 7. The bond forces from the non-prestressed steel in these units caused the moment-deflection relationship to indicate a pinched hysteresis.

Unit 3 - ordinary reinforced beam

After the maximum moment had been reached in each direction, the subsequent reduction in stiffness and strength of the unit was due to damage concentrating in the joint core. The 25.4 and 28.6 mm diameter beam bars slipped through the joint core during the load cycles in the inelastic range. Joint core shear failure in this reinforced concrete unit was more extensive than in any of the other units.

Shear Strength of Beam-column Joint Core

Table 4.1 shows the ratio of the experimental maximum applied horizontal joint core shear force, calculated using Eq.4.3, to the theoretical horizontal shear strength, calculated by ACI 318-71 procedure given by Eqs. 4.1 and 4.2. ACI318-71 indicated that the joint cores were adequately reinforced for shear except for Unit 5. The test results revealed that only the joint core ties of Units 1,4,7 and 10 did not yield and softening of joint core did not occur during the tests.

The authors applied the draft New Zealand concrete design code at the time when the paper was published [4.7] to the test units. According to the draft code, the horizontal shear strength of the joint core, V_u , is given by Eq.(4.4).

$$V_u = V_c + 0.7P_{cs} + nA_v f_y \quad (4.4)$$

$$\text{where, } V_c = 3(1 + f'_c / 3630) \sqrt{\frac{N_u}{A_g} - \frac{f'_c}{10}} \quad (4.5)$$

P_{cs} = prestressing force in the prestressing steels located in the middle third of the beam depth (lb)

n = number of the shear reinforcement which crosses the corner-to-corner crack

A_v = sectional area of one layer of shear reinforcement (in.²)

f_y = yield strength of shear reinforcement (psi)

N_u = axial load on the column (lb)

A_g = gross sectional area of the column (in.²)

f'_c = compressive strength of concrete (psi)

V_c = horizontal shear force carried by the concrete shear resisting mechanism (lb). When $N_u / A_g < 0.1f'_c$, V_c is assumed to be zero.

Table 4.1 also shows the ratio of the theoretical maximum applied horizontal core shear force to the horizontal shear strength calculated by Eq.4.4. Design by the proposed New Zealand procedure resulted in less joint core reinforcement than the ACI procedure. The ratios in Table 4.1 indicates that all the test units would not fail in joint shear. The authors concluded that the main reason for this wrong prediction was that there was no vertical reinforcement capable of carrying shear present in the joint cores. The truss mechanism, one of the two typical shear resisting mechanisms, did not work effectively.

From their tests, two important aspects on shear behaviour of prestressed concrete beam-column joint cores can be pointed out;

- (1) Some prestressing tendons should be provided in the vicinity of the beam mid depth to improve the shear capacity of the joint cores.
- (2) Prestressing force in the prestressing steels located in the middle third of the beam depth will increase the shear resistance.

4.2.3 Code Provisions on Seismic Design of Prestressed Concrete Beam-Column Joint Assemblies

Among the current concrete design codes in the world, NZS 3101:1982 [4.8] is the only one known to have addressed the seismic design of prestressed concrete beam-column joints. Based on Park and Thompson's research [4.6], additional tests conducted by Y.S.Keong [4.9] and other research on reinforced concrete beam-column joint assemblages [4.10], NZS 3101:1982 [4.8] has specified the principles and requirements for prestressed concrete beam-column joints designed for seismic loading. The design procedure itself is an extension of that for reinforced concrete beam-column joints which includes the ideal horizontal joint shear strength provided by a concrete shear resisting mechanism, V_{ch} , due to the effective prestressing force expressed in Eq.4.6.

$$V_{ch} = 0.7P_{cs} \quad (4.6)$$

where P_{cs} = the force after all losses in the prestressing steel are taken into account.
This steel must be located within the central third of the beam depth.

Some supplementary requirements are specified in Section 13.5.5 " Joints in pre-stressed frames " of NZS 3101:1982 [4.8]. Some provisions considered to be of particular importance are:

- (1) Anchorage for post-tensioned tendons shall not be placed within beam-column joint cores in order to avoid tensile bursting stresses in a region already subjected to severe diagonal tension from beam and column forces.
- (2) Except as provided by 13.5.5.3 (the following item (3)) the beam prestressing tendons which pass through joint cores shall be placed at the face of the columns, so that at least one tendon is centered at not more than 150 mm from the beam top and at least one at not more than 150 mm from the beam bottom. Such an arrangement of tendons results in more ductile plastic hinge behaviour of beams under inelastic cyclic loading than when the tendons are all concentrated at the mid-depth in the beam. However, in addition to top and bottom tendons, it is very desirable to have at least one tendon located within the middle third of beam depth to help carry the joint core shear force.

- (3) When partially prestressed beams are designed in which the non-prestressed reinforcement provided at least 80 % of the design resisting moment for earthquake plus gravity load combinations, prestress may be provided by one or more tendons passing through the joint core and located within the middle third of the beam depth, at the face of the column, to minimize loss of effective prestress force under reversed inelastic cycling, and to improve the shear resistance of the joint core.

4.3 TESTS ON PRESTRESSED CONCRETE BEAM-EXTERIOR COLUMN ASSEMBLIES WITH VARIOUS LOCATIONS OF PRESTRESSING STEEL BARS

4.3.1 Test Program

Description of Test Units

Two series of test units, which represented the joint region at the exterior columns of one-way moment resisting frames with plastic hinging occurring in the beams at the column faces, were constructed and tested. Fig.4.10 shows the overall dimensions of the units tested. Both series of test units had a total column height of 1.9 m and a total beam length of 1.85 m measured from the column face. The column cross section was a 300 mm square. The beam had a 200x300 mm rectangular cross section. Each test unit was cast monolithically in a vertical position.

The main features of each unit were as follows:

Series A:

- PC1: Prestressing steel bars were located within the central third of the beam depth.
- PC2: Prestressing steel bars were located near the extreme fibre of the beam section.
- RC1: Reinforced concrete beam - exterior column joint with non-prestressed longitudinal beam bars welded to an anchorage plate on the outer side of the column.

Series B:

- PC3: Similar to PC1 except that both the non-prestressed longitudinal top and bottom beam bars were bent downwards into the joint core or the column core.
- PC4: Similar to PC2 except that both the non-prestressed longitudinal top and bottom beam bars were bent downwards into the joint core or the column core.
- RC2: Similar to RC1 except that both the non-prestressed longitudinal top and bottom beam bars were bent downwards into the joint core or the column core.

The main variable of the tests was the location of prestressing steel bars. Park and Thompson pointed out in their paper [4.6] that only prestressing steel located within the central third of the beam depth can be allowed for shear resistance of beam-column joint cores. NZS 3101:1982 [4.8] adopted their research results and specifies the contribution of prestressing force to shear resistance of joint cores as $V_{ch} = 0.7P_{cs}$. The prestressing steel provided in the vicinity of the extreme tension fiber of a beam section is predicted to yield and lose its prestressing force under high-intensity reversed cyclic loading. However, the occurrence of this phenomena depends on the ratio of prestress to the yield strength of a prestressing steel bar and the intensity of loading and deformation to be imposed on the test units.

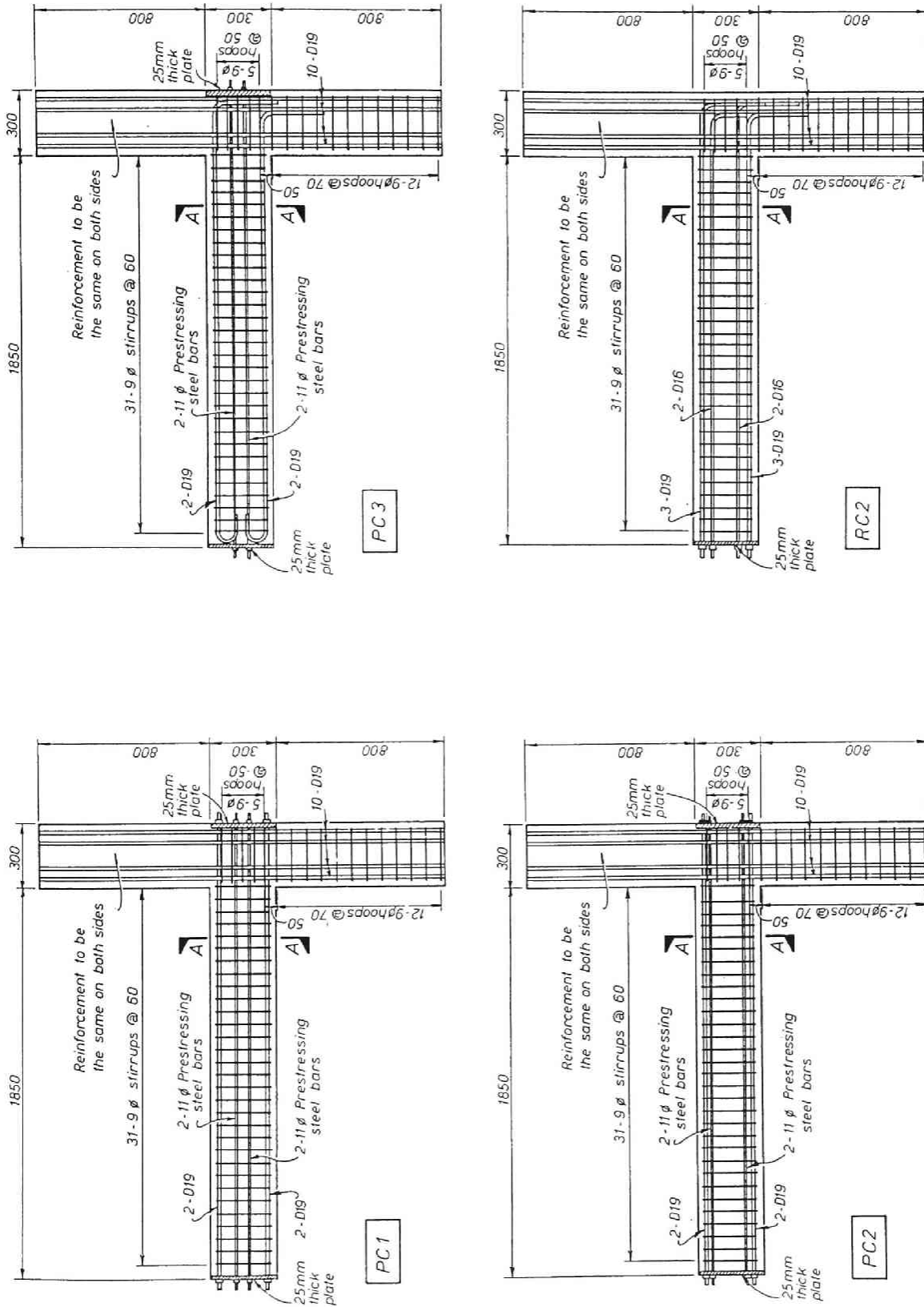


Fig.4.10(a) Overall dimensions of the test units

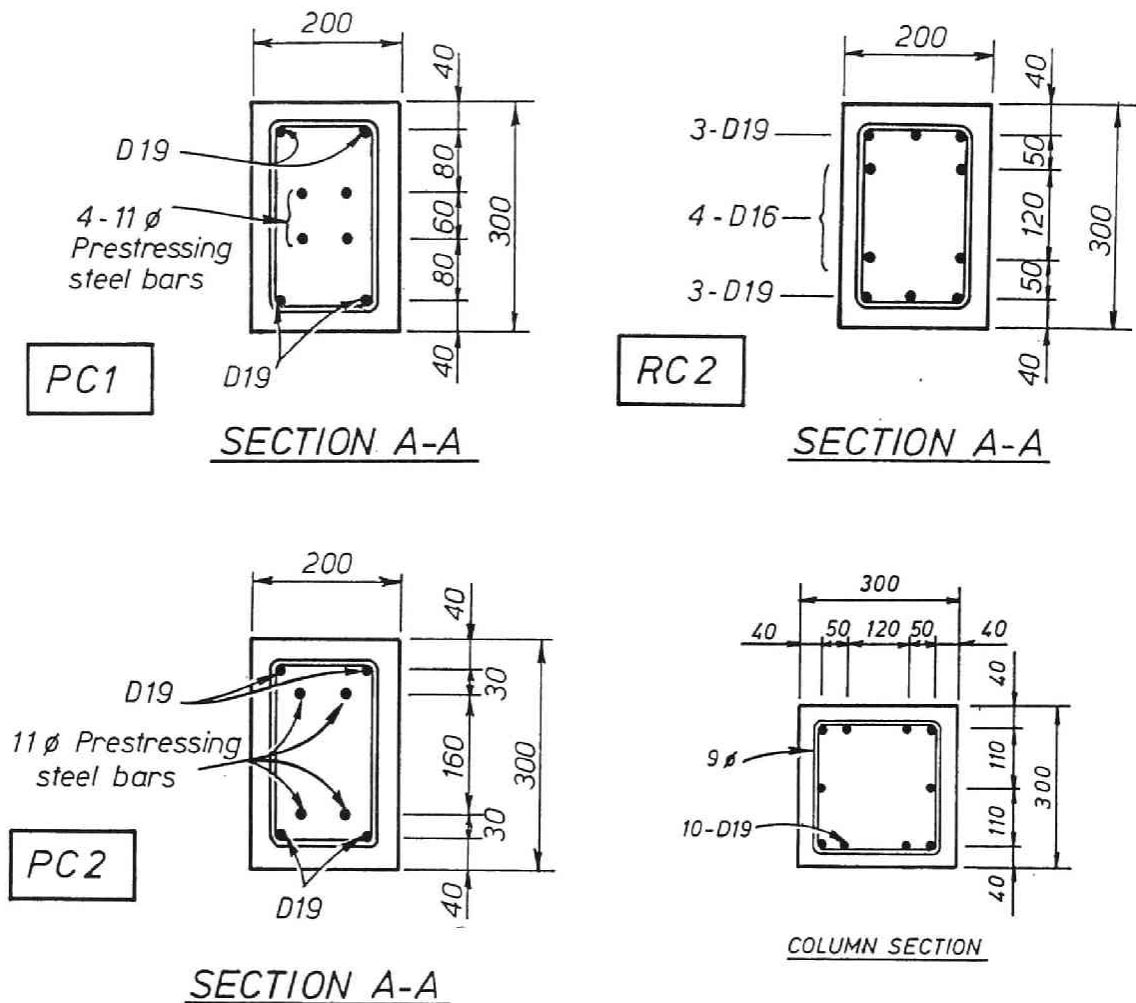


Fig.4.10(b) Beam and column sections of the test units

The objectives of these tests are;

- (1) to investigate how the location of prestressing steel in the beam section affects the shear behaviour of beam-column joint core,
- (2) to compare a prestressed concrete beam-column joint with the behaviour of a reinforced concrete joint in terms of load carrying capacity, ductility and energy dissipation, and
- (3) to get information to establish a design procedure for shear in prestressed concrete beam-column joints. Such a procedure has been found only in the New Zealand concrete design code NZS 3101:1982 [4.8].

The specification of the test units are summarized in Table 4.2. The longitudinal steel content for each unit was such that the flexural strength of the column section was

Table 4.2 Specifications of the test units

Specimen	f _c (MPa)	COLUMN			JOINT	BEAM		
		Longitudinal Rebar	P (kN)	P/(A _g f _c)		pw _j (%)	Longitudinal Rebar	e (e/D) (mm)
P C 1	41.2	10-D19	264.6	0.0714	0.960 (φ 9)	4-D19	30 (1/10)	276.8
P C 2	29.8		98.0	0.0364			80 (1/3.8)	283.9
P C 3			30 (1/10)	303.3				
P C 4			80 (1/3.8)	294.2				
R C 1			41.2	264.6		0.0714	6-D19,4-D16	
R C 2	29.8		98.0	0.0364				

f_c' : Compressive strength of concrete, P:Axial force on column, A_g:Gross area of column section,
 e : Eccentricity of prestressing steel bar measured from centroidal axis of beam section,
 D : Whole depth of beam, Pe :Effective prestress,
 Pw_j : Ash/(bc•jb) (Ash:Total cross-sectional area of horizontal reinforcement within joint core,
 bc:Width of column, jb:Distance between centroids of nonprestressed compression and
 tension rebars.)
 Measured yield strength of rebar : D19 ---> 426 MPa, D16 ---> 359 MPa, φ9 ---> 335 MPa.
 Specified yield strength (0.2% offset) : 1275 MPa, and
 Specified tensile strength of prestressing tendon : 1422 MPa.

greater than that of the beam section. The flexural strength of the column was at least 50% larger than that of the beam. Therefore, under severe cyclic loading plastic hinging was forced to occur in the beams adjacent to the column faces rather than in the column. Table 4.3 lists the ideal flexural strength of the beams of each test unit calculated using the ACI318-89 [4.11] equivalent rectangular stress block. This calculation is based on the measured material strengths and the capacity reduction factor φ was assumed to be unity. The beams of all six test units were designed to have approximately the same flexural strength.

Table 4.3 Ideal flexural strength of the beams and columns of each test unit

Unit	M _{uB} (kN)	M _{uC} (kN)	M _{uC} / M _{uB}
PC1	103.2	157.8	1.53
PC2	105.3	157.8	1.50
PC3	98.2	139.2	1.42
PC4	101.5	139.2	1.37
RC1	113.9	157.8	1.39
RC2	110.4	139.2	1.26

Each series of tests consisted of three units: two units with a prestressed concrete beam and one with an ordinary reinforced concrete beam. The first series, called Series A, contained Units PC1, PC2 and RC1 whose non-prestressed longitudinal beam bars were welded to an anchorage plate on the outer side of the column to ensure the anchorage detailing of beam bars should not affect the behaviour of joints. The second series, called Series B, consisted of Units PC3, PC4 and RC2 whose non-prestressed longitudinal top and bottom beam bars were bent downwards into the joint core or the column core. The latter is an anchorage detail which is common practice in Japan, although the Design Guidelines for Earthquake Resistant Reinforced Concrete Buildings based on Ultimate Strength Concept [4.12] published in 1988 recommend that top bars should be bent downwards and bottom bars be bent upwards into the column core.

As described later, the test units of the first series with higher axial load on the columns had an extremely good performance with respect to capacity and ductility. Therefore, in the second series the test units were designed to have a larger possibility of a joint shear failure with a lower axial load on the columns and the anchorage detailing of the beam bars than the test units of the first series.

The mix design for the concrete used for the test units was:

25 mm aggregate	994 kg/m ³
Sand	762 kg/m ³
Portland Cement	393 kg/m ³
Water	173 litre/m ³

Water/Cement ratio = 0.44

The mechanical properties of the materials and other details are included in Tables 4.4

Table 4.4 Mechanical properties of concrete

Specimen	Compressive strength f'c (MPa)	Strain at f'c (%)	Initial Modulus of elasticity (10 ⁴ MPa)
PC1 PC2 RC1	41.2	0.22	3.70
PC3 PC4 RC2	29.8	0.22	3.00

Table 4.5 Mechanical properties of steel

	Yield strength (MPa)	Yield strain (%)	Modulus of Elasticity (10 ⁵ MPa)
D19	425	0.23	1.85
D16	359	0.20	1.82
φ 9	335	0.18	1.87

and 4.5.

The prestressing steel bars were post-tensioned to approximately 70 percent of their ultimate strength at transfer and grouted. The concrete compressive prestress in the beams of each unit at transfer, P_e , as measured by load cells at the ends of the tendons, is listed in Table 4.2.

4.3.2 Details of beam-column joint core

Joint induced shear force

Fig.4.11 shows the beam internal forces and the column shear force acting on the joint core at the ideal flexural strength of the beam. The maximum horizontal shear force V_{jh} occurs in the middle region of beam depth just below the neutral axis position of the beam section. V_{jh} is given by the following equation:

$$V_{jh} = T_1 + T_2 + P_1 + P_2 - V_{col} \quad (4.7)$$

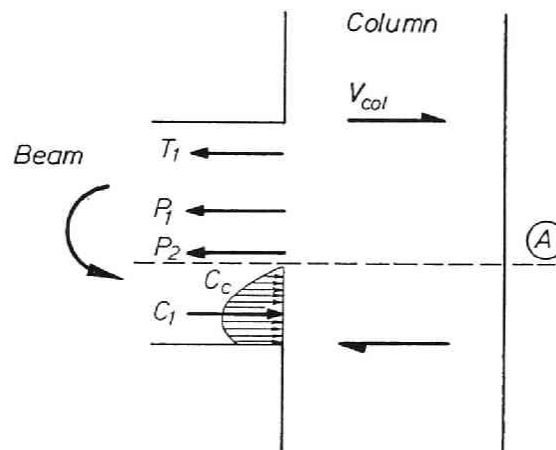


Fig.4.11 Beam internal forces and the column shear force acting on the joint core at the ideal flexural strength of the beam

Table 4.6 shows the neutral axis depth, the beam internal forces and ideal flexural strength calculated using the ACI318-89 equivalent rectangular stress block.

In a practical design, prestressing steel bars are usually located centrally between the top and bottom non-prestressed longitudinal reinforcement in a beam section. This results in a smaller effective depth of prestressing steel bars than that of non-prestressed tensile reinforcement. Designed to have approximately the same flexural strength that the reinforced concrete beam section, the prestressed concrete beam section sustains the greater horizontal shear force than the reinforced concrete section.

Table 4.6 Theoretical internal forces in beams at flexural strength and maximum shear forces

Unit	C (mm)	C1 (kN)	Cc (kN)	P1 (kN)	P2 (kN)	T1 (kN)	Vcol (kN)	Vjh (kN)	VNZS (kN)
PC1	82.1	195.2	469.9	191.6	231.6	241.2	86.2	578.9	867.6
PC2	93.5	233.9	411.1	173.4	230.4	241.2	82.4	562.6	867.6
PC3	75.1	178.0	430.1	130.5	236.4	241.2	87.9	520.2	736.8
PC4	85.4	217.2	375.2	116.2	235.0	241.2	85.2	507.2	736.8
RC1	68.9	223.0	362.2			585.2	82.8	502.4	867.6
RC2	74.5	246.3	314.6			560.9	80.3	480.6	736.8

Note:

C : Neutral axis depth

Cc : Resultant compression force in concrete

C1 : Compression force in non-prestressed bottom reinforcement

P1, P2 : Tensile force in prestressing steel bar

T1 : Tensile force in non-prestressed top reinforcement

Vcol : Shear force in column

Vjh : Theoretical maximum applied horizontal shear force

VNZS : $1.5\sqrt{f'_c} \cdot A_j$ (NZS 3101:1982),

where f'_c : Compression strength of concrete (MPa) and A_j : Specified cross-sectional area of the joint (mm²)

* All values were calculated using measured material properties.

Theoretical shear strength of joint cores

(i) Requirement for the maximum induced joint shear specified in NZS 3101:1982

NZS 3101:1982 requires in section 9.5.3.2 that the nominal horizontal shear force in the joint in either principal direction, V_{jh} , shall not exceed the force specified below.

$$1.5\sqrt{f'_c} b_j h_c \text{ (kN)} \quad (4.8)$$

The effective joint width, b_j , shall be taken as (refer to Fig.4.12)

(a) when $b_c > b_w$

either $b_j = b_c$

or $b_j = b_c + 0.5h_c$, whichever is the smaller.

(b) when $b_c < b_w$

either $b_j = b_w$

or $b_j = b_c + 0.5h_c$, whichever is the smaller.

where, f'_c = concrete compressive strength (MPa)
 b_c = overall width of column (mm)
 b_w = web width of beam (mm)
 h_c = overall depth of column in the direction of the horizontal shear to be considered (mm).

All test units satisfied this requirement.

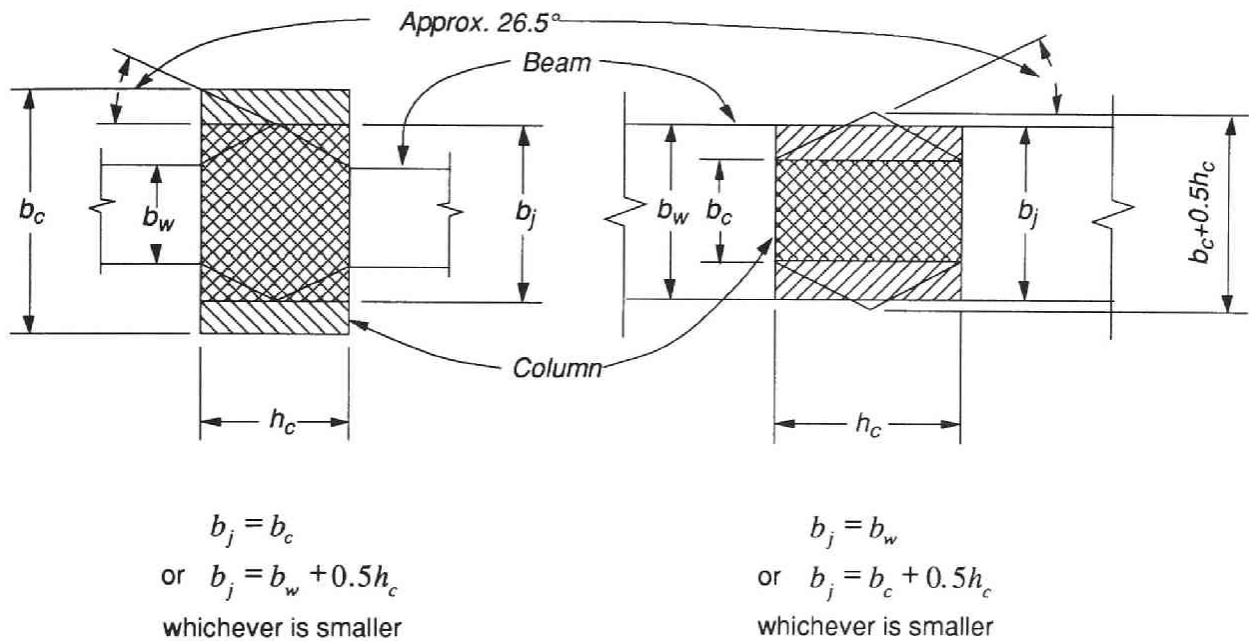


Fig.4.12 Design of beam - column joint according to NZS 3101:1982

(ii) Joint shear strength according to ACI318-89 [4.11]

The nominal shear strength of the external joint without orthogonal beams shall not be taken greater than the force specified below for normal weight aggregate concrete.

$$12\sqrt{f'_c}A_j \text{ (lb.) } (f'_c \text{ in psi}) \quad (4.9)$$

$$\text{or } 1.0\sqrt{f'_c}A_j \text{ (N) } (f'_c \text{ in MPa}) \quad (4.10)$$

where, A_j = effective cross-sectional area within a joint (mm^2), shown in Fig.4.13, in a plane parallel to plane of reinforcement generating shear in the joint. The joint depth shall be the overall depth of the column. Where a beam frames into a support of larger width, the effective width of the joint shall not exceed the smaller of:

- (a) beam width plus the joint depth
- (b) twice the smaller perpendicular distance from the longitudinal axis of the beam to the column side.

The joint shear forces in Units PC1, PC2, RC1 and RC2 satisfied the requirement. Since the design assumptions are based on the experimental results that indicated that the joint shear strength was not sensitive to joint shear reinforcement, the joint shear strength is related to f'_c only. The calculated joint shear strengths of Units PC3 and PC4 were less than the induced shear force.

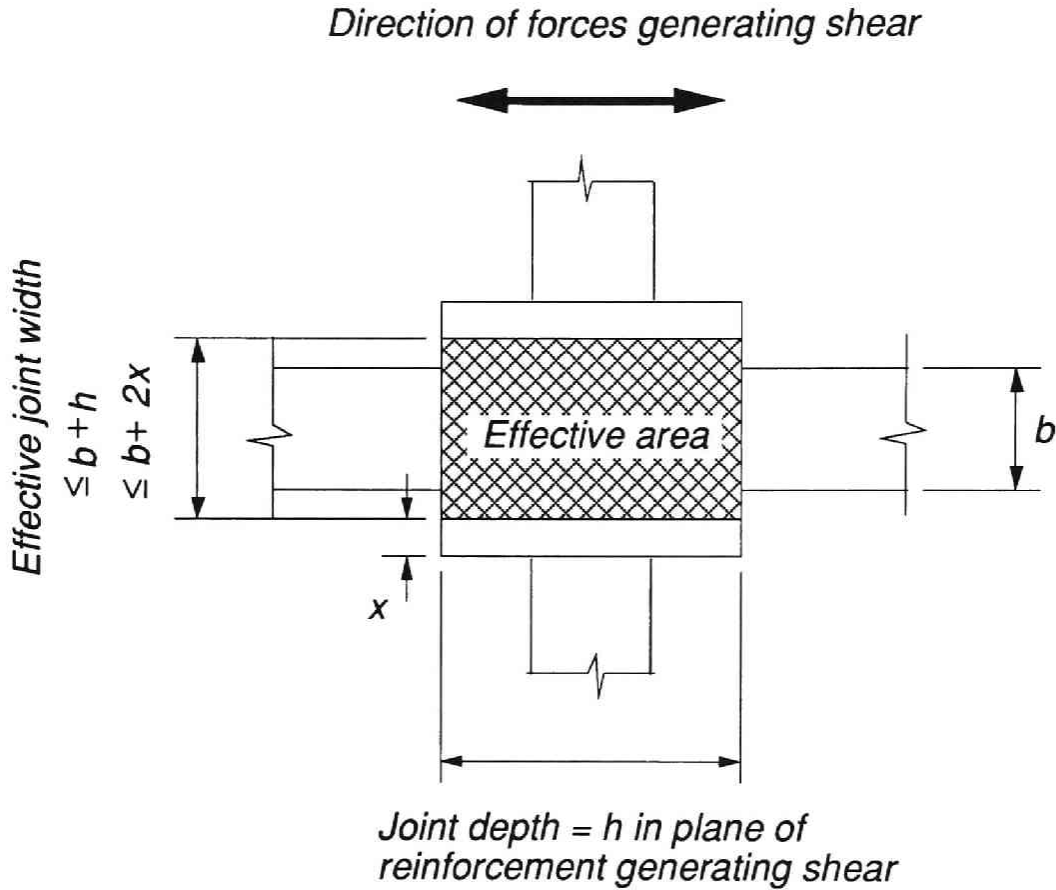


Fig.4.13 Design of beam - column joint according to ACI 318-89

(iii) Joint shear strength according to AIJ “Design Guidelines for Earthquake Resistant Reinforced Concrete Buildings Based on Ultimate Strength Concept” [4.12]

The nominal shear strength, V_{ju} , of the exterior joint without orthogonal beams shall not be taken to be greater than the force specified below.

$$V_{ju} = 0.18\sigma_B b_j D_j \quad (4.11)$$

where, σ_B = compressive strength of concrete

b_j = effective width of the joint specified below.

$$b_j = b_b + b_{a1} + b_{a2} \quad (4.12)$$

b_b = beam width

either $b_{ai} = b_i / 2$

or $b_{ai} = D / 4$, whichever is the smaller.

b_i is the smaller perpendicular distance from the longitudinal axis of the beam to the column side, shown in Fig.4.14.

D = overall depth of the column.

D_j = overall depth of the column,

or the development length for the longitudinal beam bar with a standard 90-deg hook.

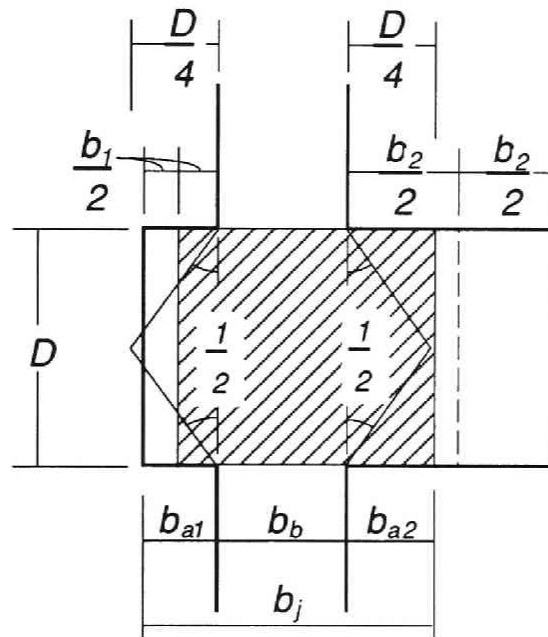


Fig.4.14 Design of beam - column joint according to AIJ Guidelines

The V_{ju} values in Table 4.7 were calculated assuming D_j = overall depth of the column. The design assumptions of this guideline are the same as ACI318-89. According to the calculation results, the AIJ guideline indicated that Units PC1, PC3, PC4 and RC2, which consisted of concrete with lower compressive strength, had higher possibility of joint shear failure than the other test units.

Transverse reinforcement in joint core

The transverse steel in each joint core consisted of five rectangular column hoops which were placed around the longitudinal column bars between the top and bottom layers of longitudinal beam steel. The average spacing between the tie centers was 40 mm. The five ties were formed from 9 mm diameter round bar.

The measured steel properties are given in Table 4.5.

Table 4.7 Maximum input joint shear force and joint shear strength

Unit	VNZS (kN)	VACI (kN)	VAIJ (kN)
PC1	867.6	578.4	556.2
PC2	867.6	578.4	556.2
PC3	736.8	491.2	402.3
PC4	736.8	491.2	402.3
RC1	867.6	578.4	556.2
RC2	736.8	491.2	402.3

Note:

$$V_{NZS} : 1.5\sqrt{f'_c} \cdot A_j \text{ (NZS 3101:1982)}$$

$$V_{ACI} : 1.0\sqrt{f'_c} \cdot A_j \text{ (ACI 318-89)}$$

$$V_{AIJ} : 0.18f'_c \cdot A_j \text{ (AIJ Guidelines)}$$

where f'_c : compressive strength
of concrete (MPa) and A_j : specified
cross-sectional area of the joint (mm²)

(i) ACI318-89 (21.4.4)

To ensure adequate confinement of the joint and to provide lateral support to the reinforcement, ACI318-89 requires that the total cross-sectional area of rectangular hoop reinforcement be at least

$$A_{sh} = 0.30sh'' \frac{f'_c}{f_{yh}} \left(\frac{A_g}{A_{ch}} - 1 \right) \quad (4.13)$$

but not less than

$$A_{sh} = 0.09sh'' \frac{f'_c}{f_{yh}} \quad (4.14)$$

where, A_g = gross area of section

A_{ch} = area of core bound by rectilinear ties

A_{sh} = total area of rectilinear transverse steel at section, including hoops and cross ties

f'_c = compressive strength of concrete cylinder

f_{yh} = yield stress of transverse steel

h'' = cross-sectional dimension of core

s = spacing of ties

Table 4.8 summarizes the transverse reinforcement, A_{sh} , required by ACI 318-89. For units PC1, PC2 and RC1, A_{sh} is required to be larger than 166 mm^2 . The total area of reinforcement provided was 128 mm^2 , which was less than the requirement. For units PC3, PC4 and RC2, A_{sh} is required to be larger than 120 mm^2 , which was less than provided in their joints.

Table 4.8 Required total area of joint shear reinforcement

Unit	Ash.prov (mm^2)	Ash.NZS (mm^2)	Ash.ACI (mm^2)	Ash.AIJ (mm^2)
PC1	640.0	131.6	850.4	234.2
PC2	640.0	690.1	850.4	227.6
PC3	640.0	919.1	615.1	290.9
PC4	640.0	1514.0	615.1	283.7
RC1	640.0	616.4	850.4	197.5
RC2	640.0	1434.6	615.1	268.8

Note:

- Ash.prov : Total area of horizontal joint shear reinforcement provided in the joint
- Ash.NZS : Total area of horizontal joint shear reinforcement required by NZS3101:1982
- Ash.ACI : Total area of horizontal joint shear reinforcement required by ACI318-89
- Ash.AIJ : Total area of horizontal joint shear reinforcement required by
AIJ "Design Guidelines for Earthquake Resistant Reinforced Concrete Buildings
Based on Ultimate Strength Concept"

(ii) NZS 3101:1982

When beams are prestressed through the joint, $0.7P_{cs}$ can be considered to be a fraction of ideal horizontal joint shear strength, V_{ch} , provided by concrete shear resisting mechanism in NZS 3101:1982. P_{cs} is the force after all losses in the prestressing steel that is located within the central third of the beam depth. This provision cannot be applied to Units PC2 and PC4, because the prestressing bars were near the extreme fibers of the beam section. Another V_{ch} , a fraction of horizontal joint shear strength provided by concrete shear resisting mechanism due to axial load on the column [Eq.9-9 of NZS], was considered to be zero because the average compression stress on the gross concrete area of the column was less than $0.1f'_c$. However, for external joints where the beam flexural steel is anchored outside the column core in a stub satisfying Section 5.5.2 of NZS, some V_{ch} [Eq.9-11] can be taken into account even if the average column compression stress is less than $0.1f'_c$. This can be applied to units PC1 and PC2 whose non-prestressed beam bars were welded to the anchorage plates on the outer side of the columns. These are summarized in Table 4.9. The corresponding horizontal design shear forces resisted by the joint shear reinforcement, V_{sh} , are calculated and listed in the same table. Dividing these forces by the measured yield

strength of joint shear reinforcement, f_{yh} , gives the total area of horizontal joint shear reinforcement, A_{jh} , as listed in the table. The total area provided in each unit was 640 mm². This is sufficient for PC1 but insufficient for the rest. The provided reinforcements range between 42 % and 485 % of the joint shear reinforcement required in the joints. If V_{ch} [Eq.9-11] is not allowed, transverse reinforcement is insufficient for all test units as listed in Table 4.9.

Table 4.9 Required total area of joint shear reinforcement according to NZS 3101:1982

Unit	V_{ch} (Eq.9-10) (kN)	V_{ch} (Eq.9-11) (kN)	V_{sh} = $V_{jh} - V_{ch}$ (kN)	$A_{jh.req}$ = V_{sh}/f_y (mm ²)	$A_{jh.prov}$ (mm ²)
PC1	193.8	0.589 V_{jh}	44.1	132	640.0(485%)*
PC2	0.0	0.589 V_{jh}	231.2	690	(93%)
PC3	212.3		307.9	919	(70%)
PC4	0.0		507.2	1514	(42%)

Note:

V_{ch} (Eq.9-10) :Horizontal shear force to be resisted by the prestressing force, 0.7 P_{cs} in §9.5.4.2(b) (Eq.9-10) (P_{cs} is the force after all losses in the prestressing steel.)

V_{ch} (Eq.9-11) :Horizontal joint shear strength provided by concrete shear resisting mechanism only, as specified in §9.5.4.2(c) (Eq.9-11)

V_{sh} :Horizontal joint shear strength provided by horizontal joint shear reinforcement

$A_{jh.req}$:Total area of horizontal joint shear reinforcement required in NZS 3101:1982

$A_{jh.prov}$:Total area of horizontal joint shear reinforcement provided

f_y :Measured yield stress of joint shear reinforcement (MPa)

* $A_{jh.prov}/A_{jh.req}$ ratio

(iii) AIJ “Design Guideline for Earthquake Resistant Reinforced Concrete Buildings Based on Ultimate Strength Concept”

AIJ Guidelines require that the total cross-sectional area of joint shear reinforcement be at least

$$A_{sh} = 0.003V_{jh} / V_{ju} bs \quad (4.15)$$

but not less than $0.002 bs$,

where, A_{sh} = total area of a set of joint shear reinforcement in spacing s

V_{jh} = theoretical shear force induced in the joint

V_{ju} = theoretical shear strength prescribed by Eq.4.11

b = joint width

s = spacing of hoops

The required transverse reinforcement for each test unit is listed in Table 4.8. Since V_{jh} was greater than V_{ju} for units PC1, PC3, PC4 and RC2, it is no use indicating the total cross-sectional area of joint shear reinforcement required by the guidelines. For units PC2 and RC1, the required total cross-sectional area of joint shear reinforcement was less than provided in the joint.

4.3.3 Development Length for Series B Test Units

According to ACI318-89 special provisions for seismic design, the development length l_{dh} for a bar with a standard 90-deg hook in normal weight-aggregate concrete shall not be less than $8d_b$, 6in.(152.4mm), and the length required by Eq.4.16.

$$l_{dh} = f_y d_b / 65 \sqrt{f'_c} \quad (f_y \text{ and } f'_c \text{ in psi, and } d_b \text{ and } l_{dh} \text{ in inch.})$$

or $l_{dh} = f_y d_b / 5.395 \sqrt{f'_c} \quad (f_y \text{ and } f'_c \text{ in MPa, and } d_b \text{ and } l_{dh} \text{ in mm.})$
(4.16)

The required development length was 275mm, which was 6mm longer than the development length used for the test units in Series B.

Fujii et al. [4.13] proposed a method for evaluating the anchorage strength of a reinforcing bar based on the bearing strength on concrete at the inside of a 90-deg hook from the test results of reinforced concrete beam - external column joint assemblies as shown in Fig.4.15. The bearing strength was given by the following equation.

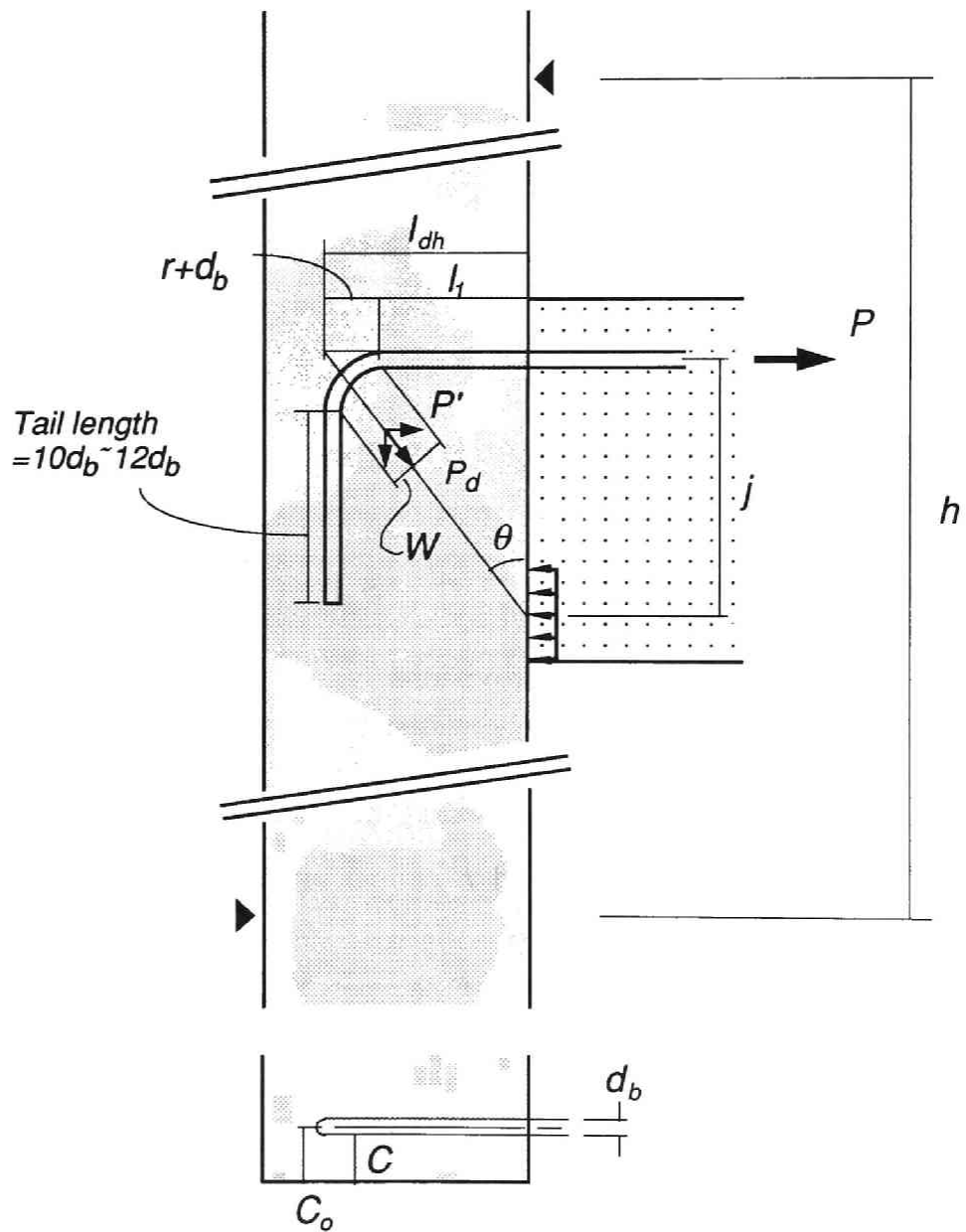


Fig.4.15 Anchorage strength of a reinforcing bar related to the bearing strength on concrete by Fujii et al. [4.13]

$$P = wd_b f_{bear} \sin \theta \cdot h / (h - j) \quad (\text{kg}) \quad (4.17)$$

where, $w = \beta \sqrt{2} r \cos(\pi / 4 - \theta)$

$$\theta = \tan^{-1}(l_{dh} / j)$$

$$l_{dh} = l_1 + r + d_b$$

$$\beta = (r / 3d_b) - 0.84$$

$$f_{bear} = \alpha \gamma \sqrt{\sigma_B}$$

$$\alpha = 16.1 C_o / d_b$$

$$\gamma = 1 + 30 A_s / (l_1 s)$$

d_b = diameter of longitudinal reinforcing bar (cm)

r = radius of bend (cm)

l_1 = development length measured from column face to the beginning of the bend (cm)

s = spacing of hoops (cm)

C_o = thickness of cover concrete measured from the center of longitudinal reinforcement (cm)

h = distance between the contraflexure points of the column (cm)

σ_B = compressive strength of concrete (kg/cm²)

A_s = sectional area of transverse reinforcement provided in the joint core (cm²)

j = internal lever arm of the beam section (cm)

The bearing strength calculated based on Eq.4.17 was approximately the same as the yield tensile force in the longitudinal reinforcement.

4.3.4 Loading

The unit was loaded as shown schematically in Fig.4.16 by vertical axial load on the column and by a vertical load on the end of the beam representing shear induced by seismic loading. The ends of the column were held on the same vertical line during the test and the applied beam load induced reactive shears at the ends of the column. By reversing the direction of the vertical beam load, the effect of earthquake loading was simulated.

The axial loads applied to the columns during the tests were 264.6 kN for Units PC1, PC2 and RC1, and 98.0 kN for Units PC3, PC4 and RC2, which corresponded to $0.071 f'_c A_g$ and $0.036 f'_c A_g$, respectively, where f'_c and A_g denote the compressive strength of concrete and the gross sectional area of the column.

The first loading cycle was up to the first yield displacement, and was followed by a

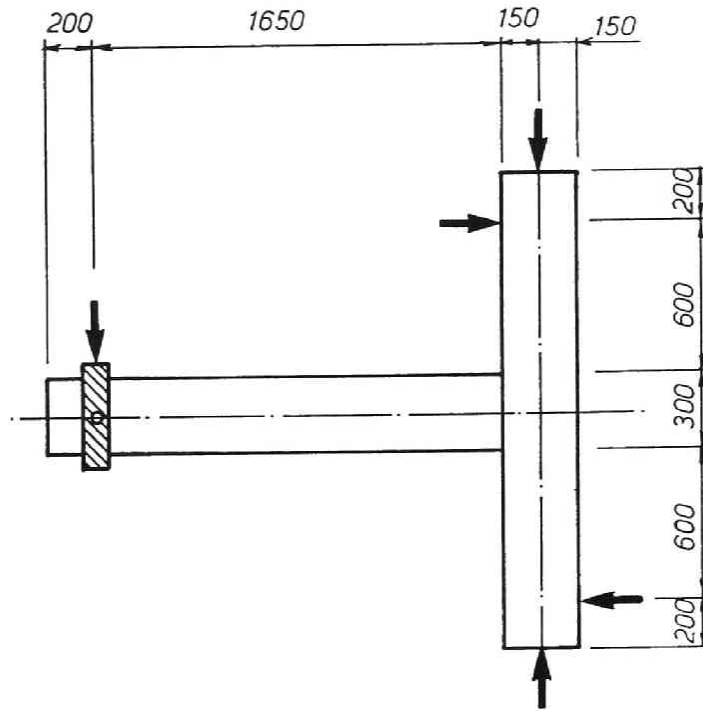


Fig.4.16 Loading setup

series of deflection controlled cycles in the inelastic range comprising two full cycles to each of the displacement ductility factors of ± 2 , ± 3 , and higher. The “first yield” displacement at the end of the beam was found when the strain reading of the outermost non-prestressed longitudinal reinforcement exceeded its yield strain.

4.3.5 Measurements

Beam end deflection was measured by a linear displacement transducer which was attached to the measuring apparatus fixed to the ends of the column as shown in

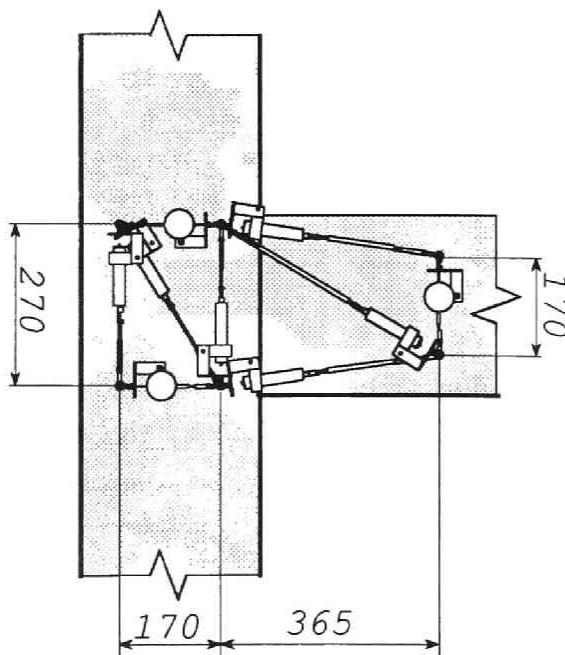


Fig.4.17 Measuring apparatus

Fig.4.17. Thus, the deflection included the deformation of the beam, joint and column. Curvatures and shear deformations of the beam in the potential plastic hinge regions and the shear distortion of the joint core were measured and calculated from the readings of the linear displacement transducers attached to the units shown in Fig.4.17.

4.3.6 General Behaviour of Test Units

Figure 4.18 shows the vertical deflection at the end of the beam plotted against the corresponding load of the beam for each unit. All test units except RC2 was able to be loaded to well beyond the beam rotation angle of 1/15 with little reduction in moment capacity. In unit RC2, after the maximum moment had been reached in each direction, the subsequent reduction in stiffness and strength was due to damage concentrating in the joint core.

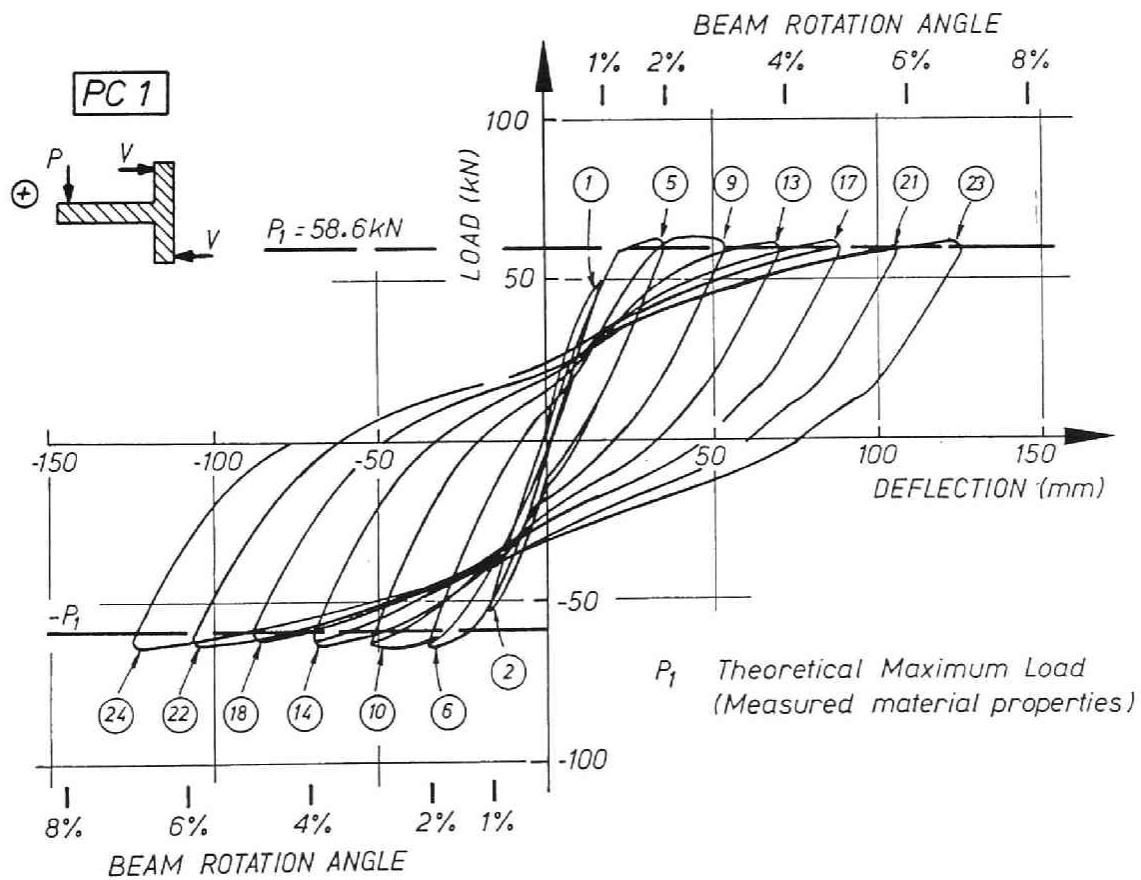


Fig.4.18(a) Vertical deflection at the end of the beam plotted against the corresponding load of the beam (PC1)

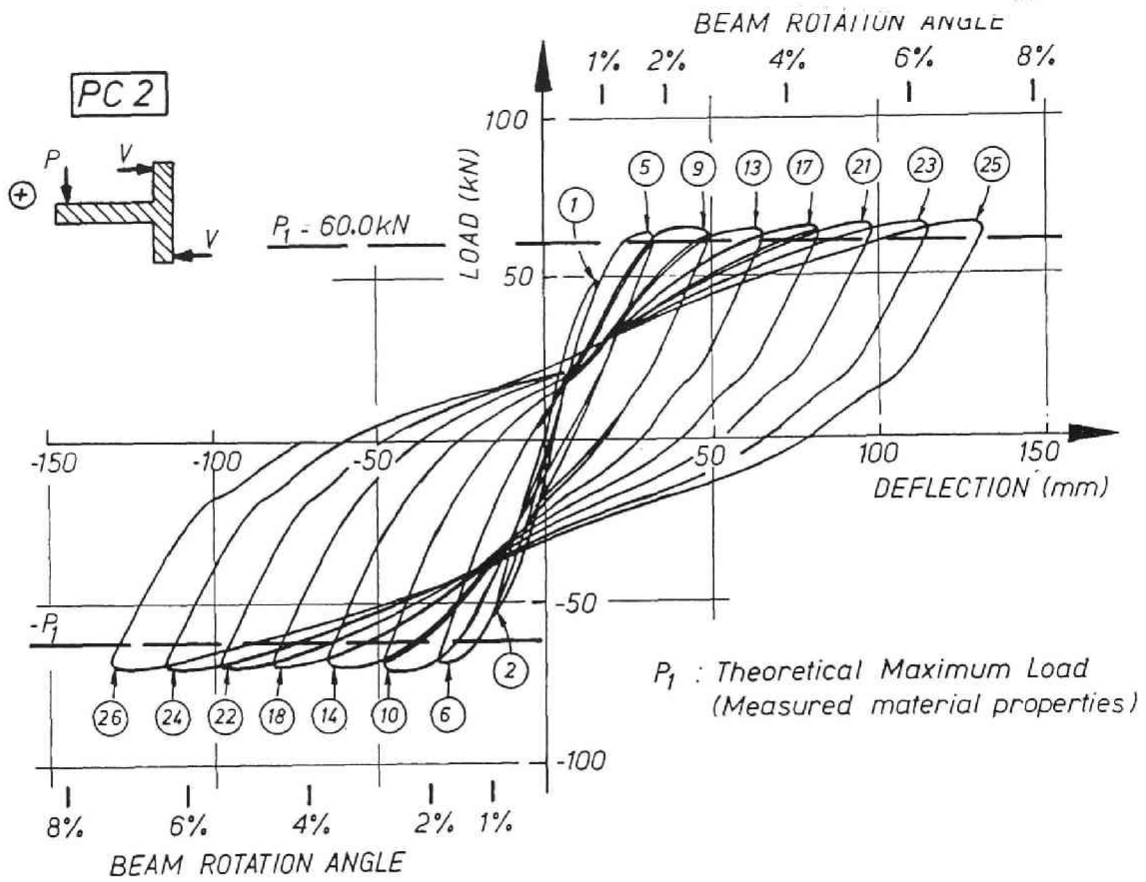


Fig.4.18(b) Vertical deflection at the end of the beam plotted against the corresponding load of the beam (PC2)

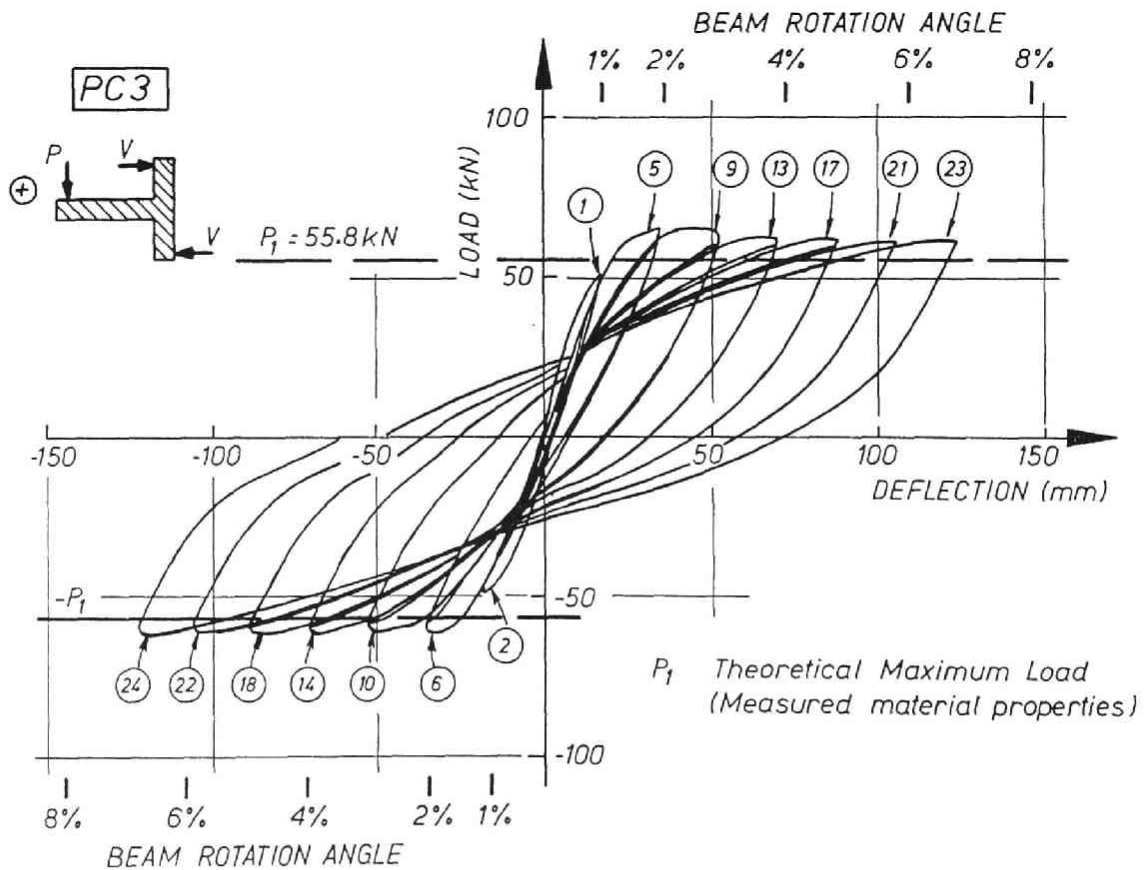


Fig.4.18(c) Vertical deflection at the end of the beam plotted against the corresponding load of the beam (PC3)

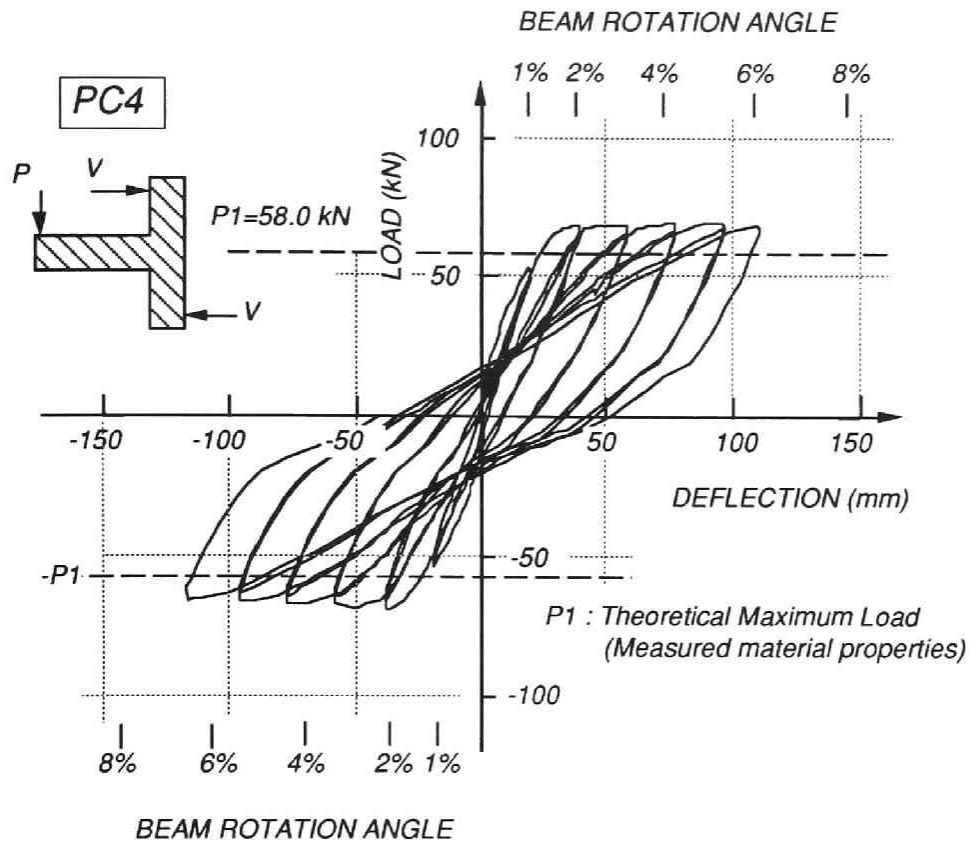


Fig.4.18(d) Vertical deflection at the end of the beam plotted against the corresponding load of the beam (PC4)

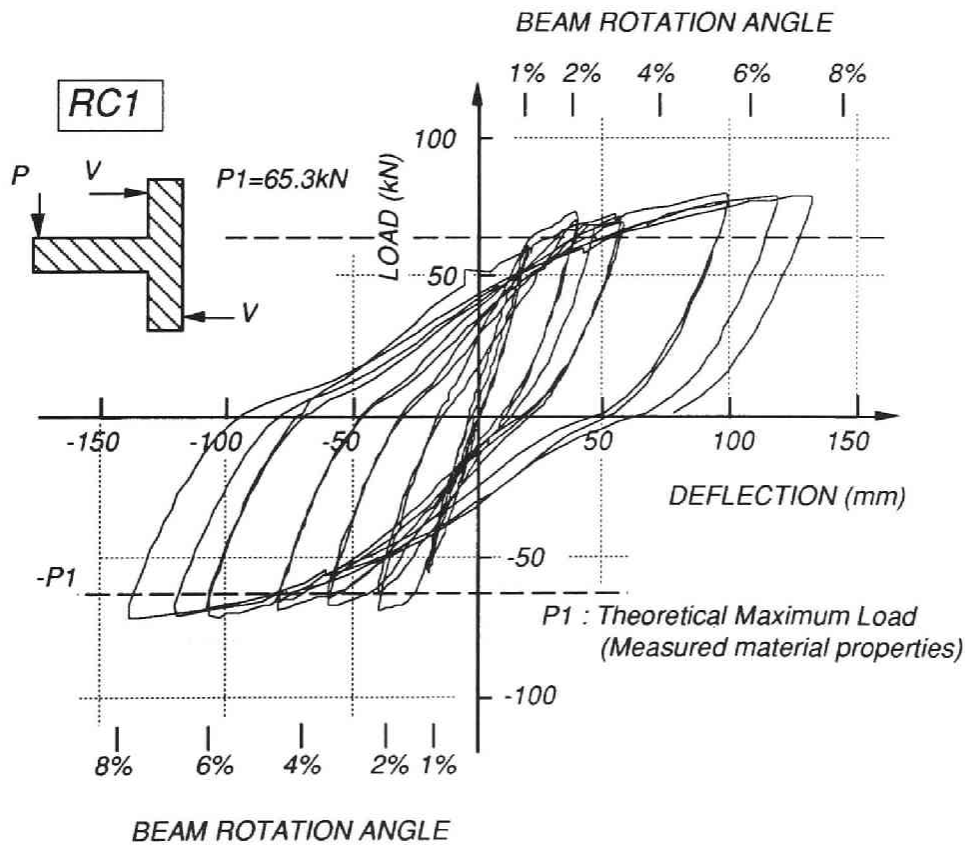


Fig.4.18(e) Vertical deflection at the end of the beam plotted against the corresponding load of the beam (RC1)

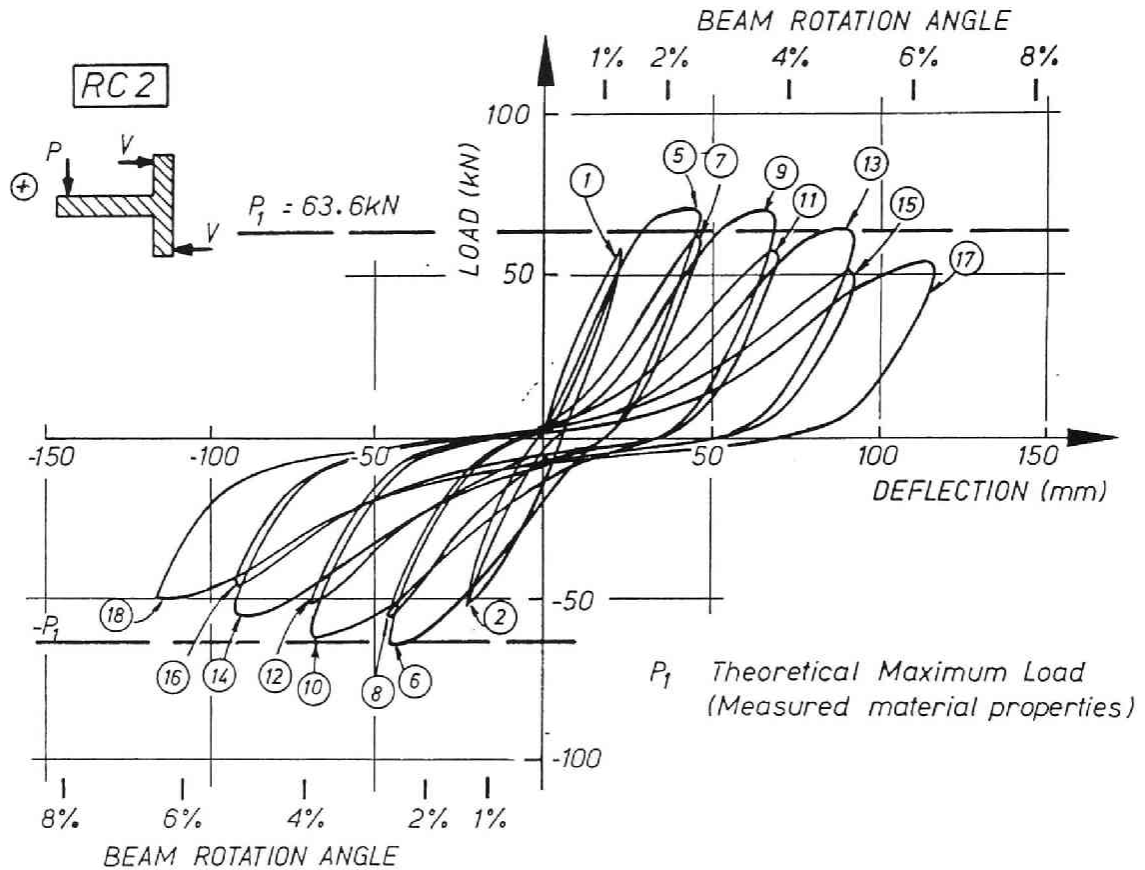


Fig.4.18(f) Vertical deflection at the end of the beam plotted against the corresponding load of the beam (RC2)

4.3.7 Damage Sustained by Test Units

Figure 4.19 shows the test units after testing. In the prestressed concrete test units the damage concentrated in the beam plastic hinge region while in the reinforced concrete units more visible cracks in the beam-column joint core were observed without serious damage in the beam plastic hinge region. In RC2, cover concrete on the side of the joint core spalled off with cracks running along the beam longitudinal reinforcement embedded and anchored in the joint core.

Comparison of Units PC2 and PC4 having the prestressing steel near the extreme fibers with Units PC1 and PC3 having the prestressing steel in the mid-depth of the beam section revealed that there were more visible cracks in the former than in the latter. This is due to smaller resultant total prestressing force on the beam section. Prestressing steel in the tension side of the beam section is likely to yield while the prestress in the compression side loses most of its prestress when it is located near the extreme compression fiber. This will be discussed later.

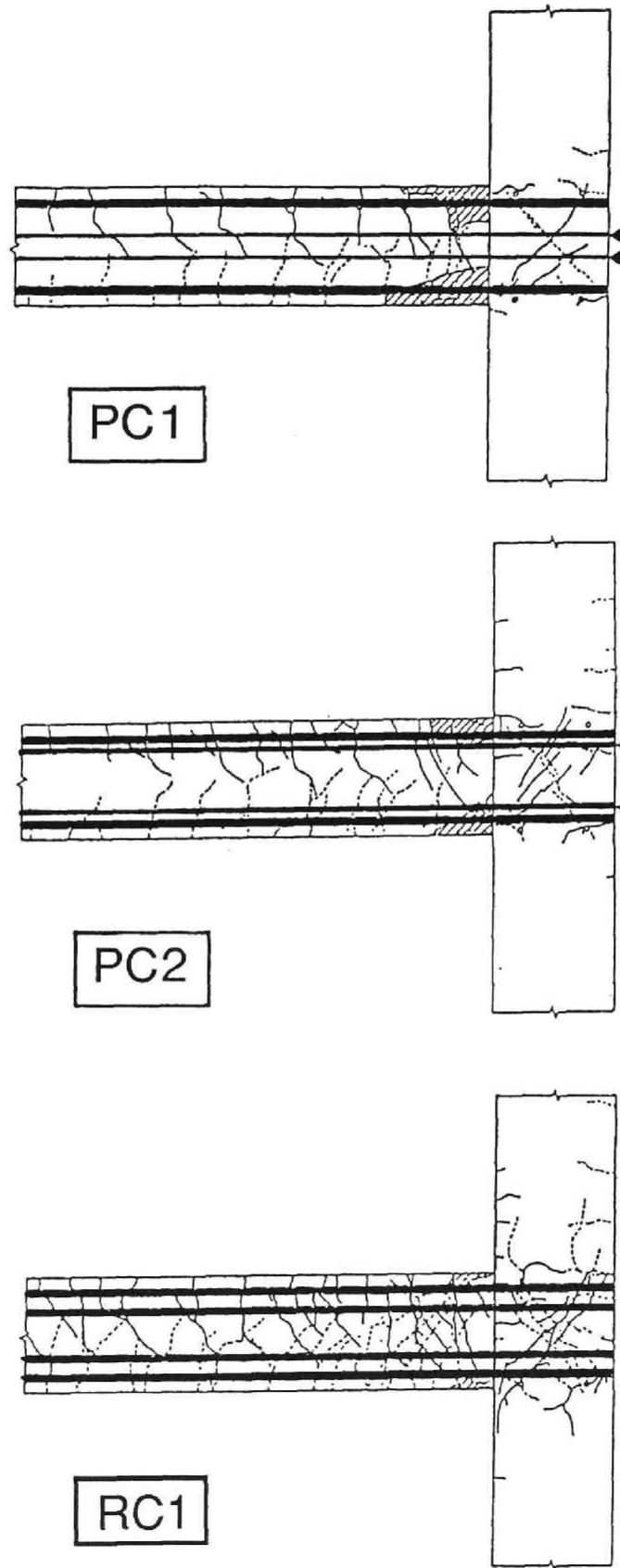


Fig.4.19(a) Test units after testing (Series A)

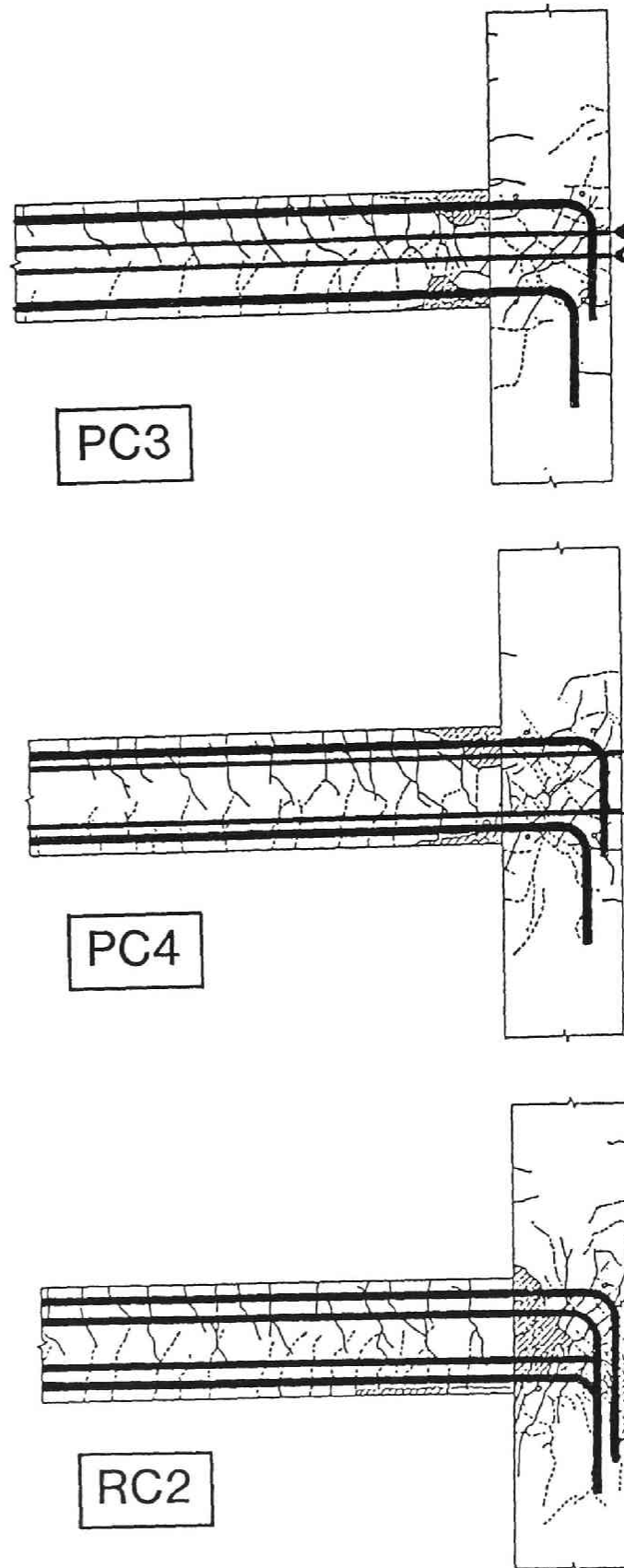


Fig.4.19(b) Test units after testing (Series B)

4.3.8 Details of Test Results

Flexural Strength

Table 4.10 summarizes beam flexural strengths obtained experimentally and theoretically. The theoretical values were calculated using the ACI equivalent concrete stress block with the measured material strengths of concrete and ordinary reinforcement, and with the nominal yield strength of prestressing steel bars. The tensile forces in the prestressing steel were calculated based on the assumption that plane sections before bending remain plane after bending and perfect bond between concrete and prestressing steel. The stress-strain curves for prestressing steel and non-prestressed ordinary reinforcement were simplified by idealizing them as two straight lines representing elastic perfectly plastic approximation. The capacity reduction factor was assumed to be unity. The flexural strengths theoretically obtained were the flexural moment when the concrete strain at the extreme fiber of the beam section attained 0.3%. In all test units with the exception of PC3 bottom prestressing steel bars reached their yield strengths in the calculation.

Table 4.10 Flexural strengths obtained experimentally and theoretically

Unit	My (kNm)	Mu (kNm)	Mcal (kNm)
PC1	84.8	108.7	103.2
PC2	84.8	118.1	105.3
PC3	84.8	108.4	98.2
PC4	88.4	115.0	101.5
RC1	91.1	129.2	113.9
RC2	96.8	116.9	110.4

Note:

My : Moment capacity at yielding obtained experimentally

Mu : Maximum moment capacity obtained experimentally

Mcal : Maximum moment capacity obtained theoretically

The theoretical ultimate flexural strengths calculated using the ACI318-89 methods were between 0.88 and 1.03 of the maximum load capacities measured. The ideal strengths calculated using the ACI methods are considered to give acceptable lower bounds. The overstrength was due to the maximum load occurring at an extreme fiber concrete compression strain greater than 0.3 % used in the calculation, to the extra confinement given to the beam concrete by the adjacent column, and to the overstrength of prestressing steel bars larger than specified. The ultimate strain employed in the calculation is of great importance for moment capacity because prestressing steel in conventional beam section with prestressing steel having smaller effective depth than non-prestressed reinforcement is predicted to remain elastic at the extreme compres-

sion fiber strain of 0.3% and larger strain results in proportional increment of stress in prestressing steel and moment capacity.

Energy dissipation

Past research [4.14] has shown that less energy dissipation occurs in prestressed concrete than in reinforced concrete members. In the tests, narrower hysteresis loops of the prestressed concrete test units than those of reinforced concrete units can be observed as shown in Fig.4.18. Equivalent viscous damping factor of the first loading cycle to each specified displacement was plotted against ductility ratio $\mu = \delta / \delta_y$ in Fig.4.20. δ_y was defined as the displacement at the end of the beam when the strain reading of the outermost non-prestressed longitudinal reinforcement first exceeded its yield strain. The equivalent viscous damping factor h_{eq} was calculated by the following equation from Ref.[4.15].

$$h_{eq} = \frac{1}{4\pi} \frac{\Delta W}{W_e} \quad (4.18)$$

where,

ΔW = area surrounded by one cycle of hysteresis loop

W_e = equivalent potential energy represented by a triangular region

in Fig.4.21. $W_e = \frac{1}{2} k_e a^2$

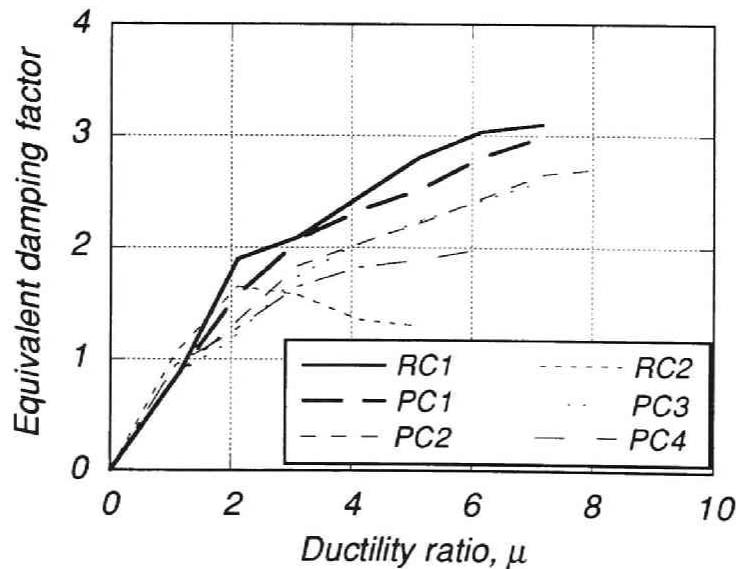


Fig.4.20 Equivalent viscous damping factor

Unit RC1 had the largest equivalent damping factor at any stage of loading. Until the ductility ratio of 4, which corresponds to the beam rotation angle of approximately 4%, the prestressed concrete test units showed as large equivalent damping as the reinforced concrete units. Beyond that deformation the equivalent damping of Unit RC1 increased steeper than the prestressed concrete units and at ductility ratio of 6 it was 27% larger than the prestressed concrete units.

However, from the viewpoint of Japan's seismic design a constituent member is expected to sustain a rotation angle of at least 1/50. Thus, the beam rotation angle of 4% attained in the tests was more than expected and within the range of that deformation expected in the seismic design energy dissipation of prestressed concrete was comparable to that of reinforced concrete.

This is mainly due to non-prestressed longitudinal reinforcement provided. The ratio of the moment of the non-prestressed steel taken about the centroid of the concrete compression block at the ultimate moment capacity of the section to the ultimate capacity ranged between 0.45 and 0.48 for the prestressed concrete units.

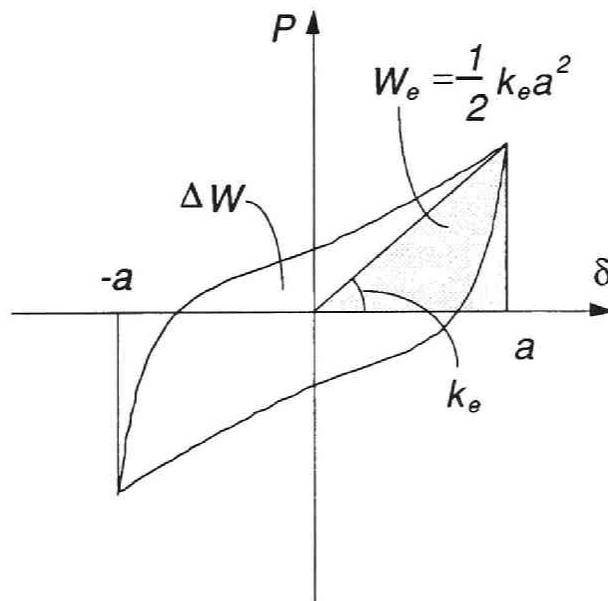
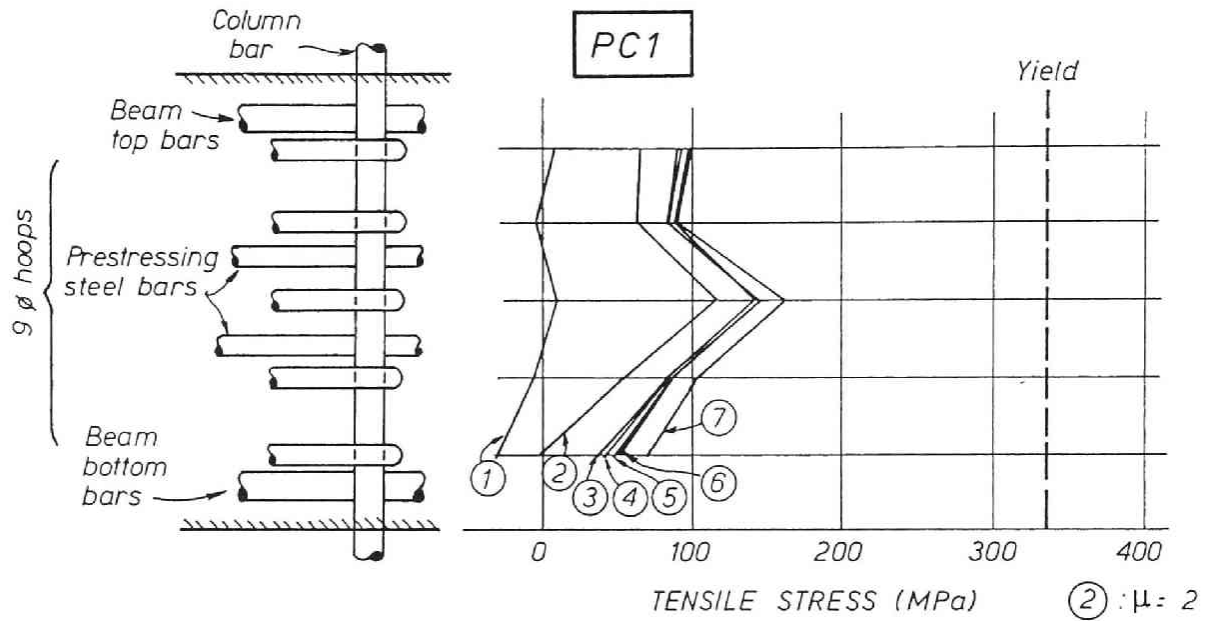


Fig.4.21 Definition of equivalent viscous damping factor

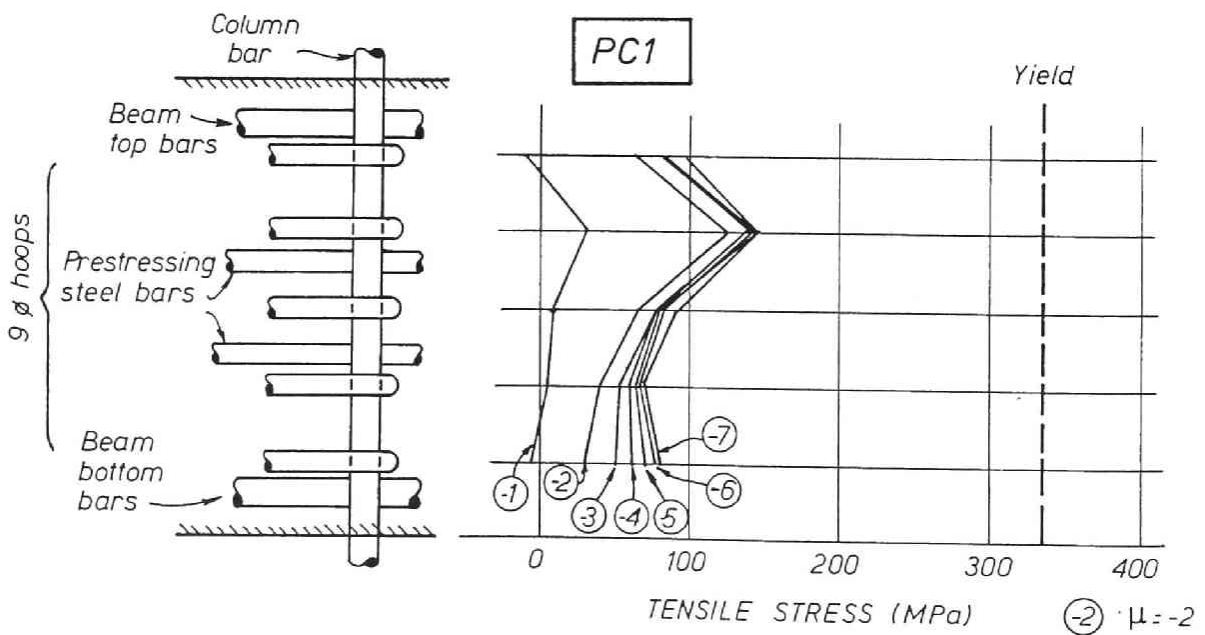
4.3.9 Series A (Units PC1, PC2 and RC1)

Effect of prestressing force on shear behaviour of joint

The performance of these units was good with little reduction in the load capacities and little pinching. Their satisfactory behaviour was due to the rather higher strength concrete and the almost perfect anchorage of non-prestressed ordinary reinforcement.



(a) Bar Stresses at Positive Ductilities



(b) Bar Stresses at Negative Ductilities

Fig.4.22(a) Stresses in the joint shear reinforcement measured at the peak of each loading run (PC1)

However, a closer observation of the joint behaviour indicates the difference among these units. Fig.4.22 shows the stresses in the joint shear reinforcement measured at the peak of each loading run. From these figures, the joint shear reinforcement in unit RC1 yielded while those in units PC1 and PC2 remained elastic. Unit RC1 yielded at stresses of half and two-thirds of the yield stress developed in the joint shear reinforcements of unit PC1 and PC2, respectively.

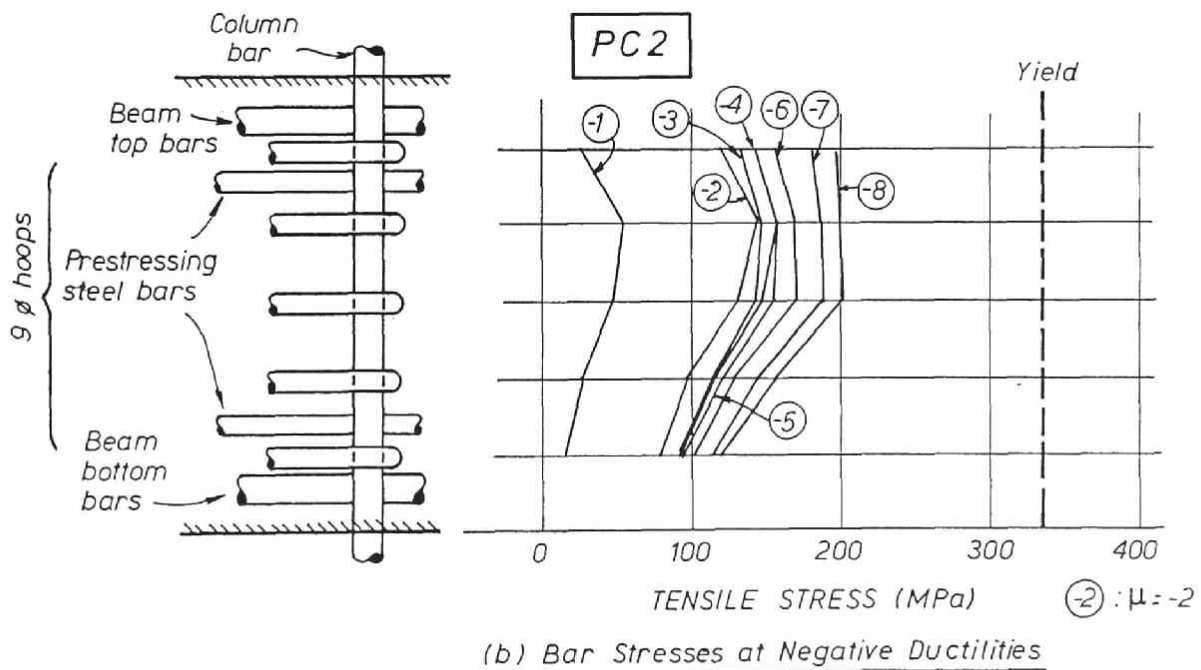
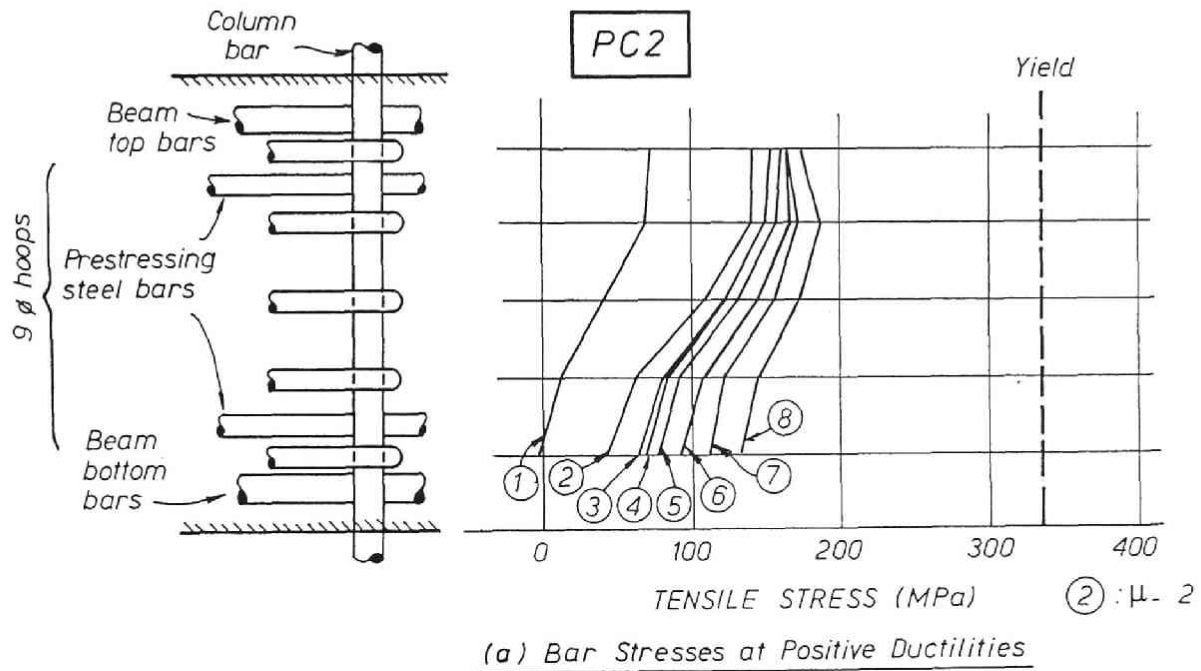


Fig.4.22(b) Stresses in the joint shear reinforcement measured at the peak of each loading run (PC2)

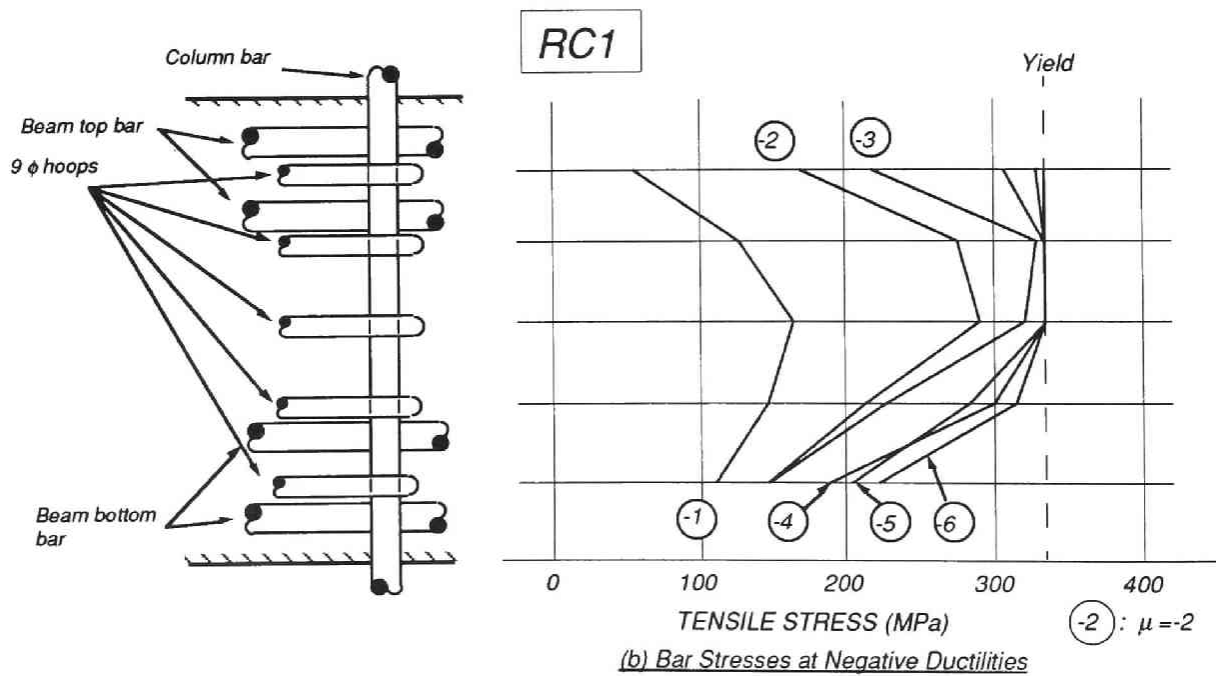
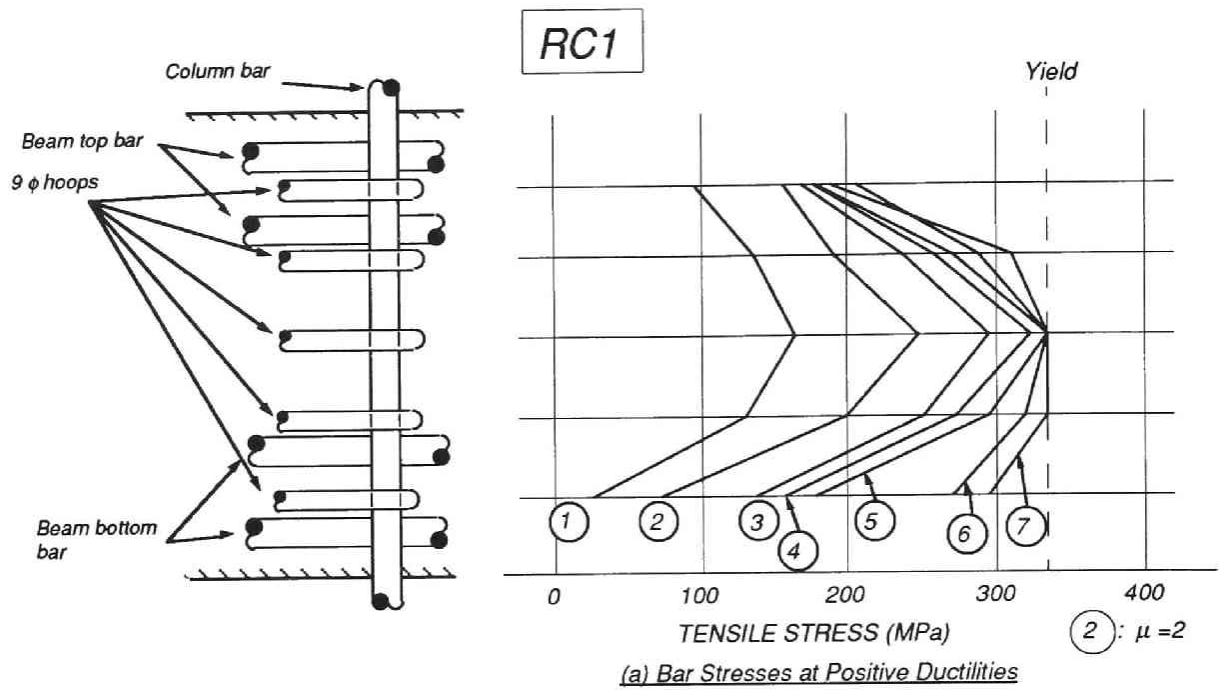


Fig.4.22(c) Stresses in the joint shear reinforcement measured at the peak of each loading run (RC1)

As described in the previous section, flexural and shear deformation of the beam potential plastic hinge region and shear deformation of the joint core were measured during reversed cyclic loading. The flexural curvature and shear distortion angle in the beam potential plastic hinge region and joint core region were calculated from the relative displacements of the rods embedded as shown in Fig.4.17. Fig. 4.23 indicates the components of deformation in the joint core. The measured relative displacements were also shown in Fig. 4.20 and denoted as $\delta_1 \sim \delta_5$. These displacements can be expressed by the following equations.

$$\begin{aligned}
 \delta_1 &= -(L_1 \cdot L_2) \cdot \phi_2 / 2 + L_2 \cdot \varepsilon_2 \\
 \delta_2 &= -(L_1 \cdot L_2) \cdot \phi_1 / 2 + L_1 \cdot \varepsilon_1 \\
 \delta_3 &= (L_1 \cdot L_2) \cdot \phi_2 / 2 + L_2 \cdot \varepsilon_2 \\
 \delta_4 &= (L_1 \cdot L_2) \cdot \phi_1 / 2 + L_1 \cdot \varepsilon_1 \\
 \delta_5 &= L_1 \cdot \varepsilon_1 \cdot \sin \alpha + L_2 \cdot \varepsilon_2 \cdot \cos \alpha + L_2 \cdot \gamma \cdot \sin \alpha \\
 \alpha &= \tan^{-1}(L_1 / L_2)
 \end{aligned}
 \tag{4.19}$$

- where, ϕ_1, ϕ_2 = flexural curvatures
 $\varepsilon_1, \varepsilon_2$ = longitudinal strain
 γ = shear distortion angle
 L_1 = vertical length between the top and bottom measuring rods
 L_2 = horizontal distance between the measuring rods

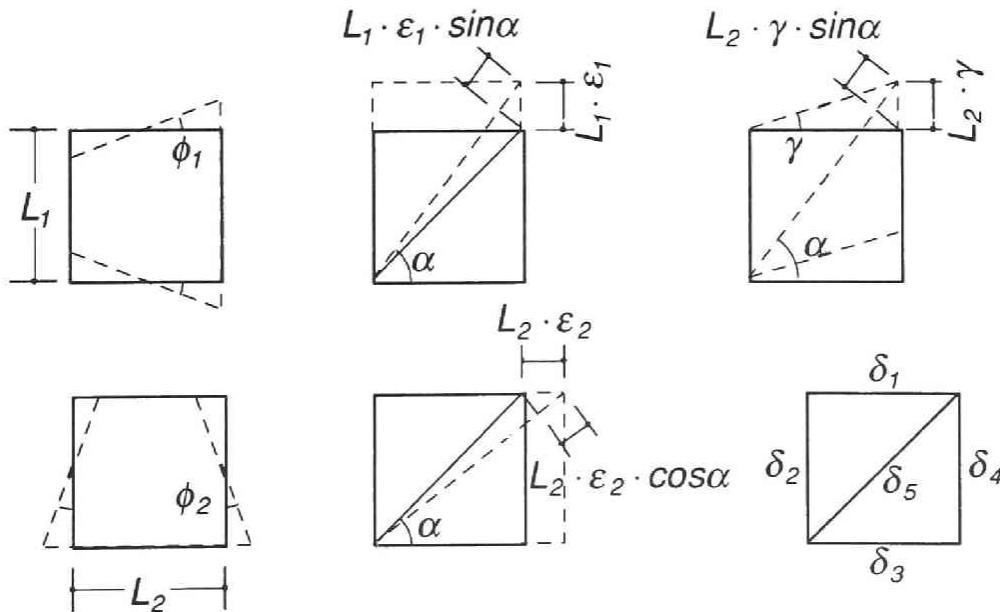


Fig.4.23 Components of deformation in the joint core

Equation 4.19 can be solved in respect of ϕ_1 , ϕ_2 , ε_1 , ε_2 and γ .

$$\begin{aligned}\phi_1 &= (\delta_4 - \delta_2) / (L_1 \cdot L_2) \\ \phi_2 &= (\delta_3 - \delta_1) / (L_1 \cdot L_2) \\ \varepsilon_1 &= (\delta_4 + \delta_2) / (2 \cdot L_1) \\ \varepsilon_2 &= (\delta_3 + \delta_1) / (2 \cdot L_2) \\ \gamma &= \{ \delta_5 - (\delta_2 + \delta_4) \sin(\alpha / 2) - (\delta_1 + \delta_3) \cos(\alpha / 2) \} / (L_2 \cdot \sin \alpha)\end{aligned}\tag{4.20}$$

Figure 4.24 shows the shear stress versus the measured shear distortion angle curves. It is shown from these figures that the joint shear deformation was confined by the prestressing force.

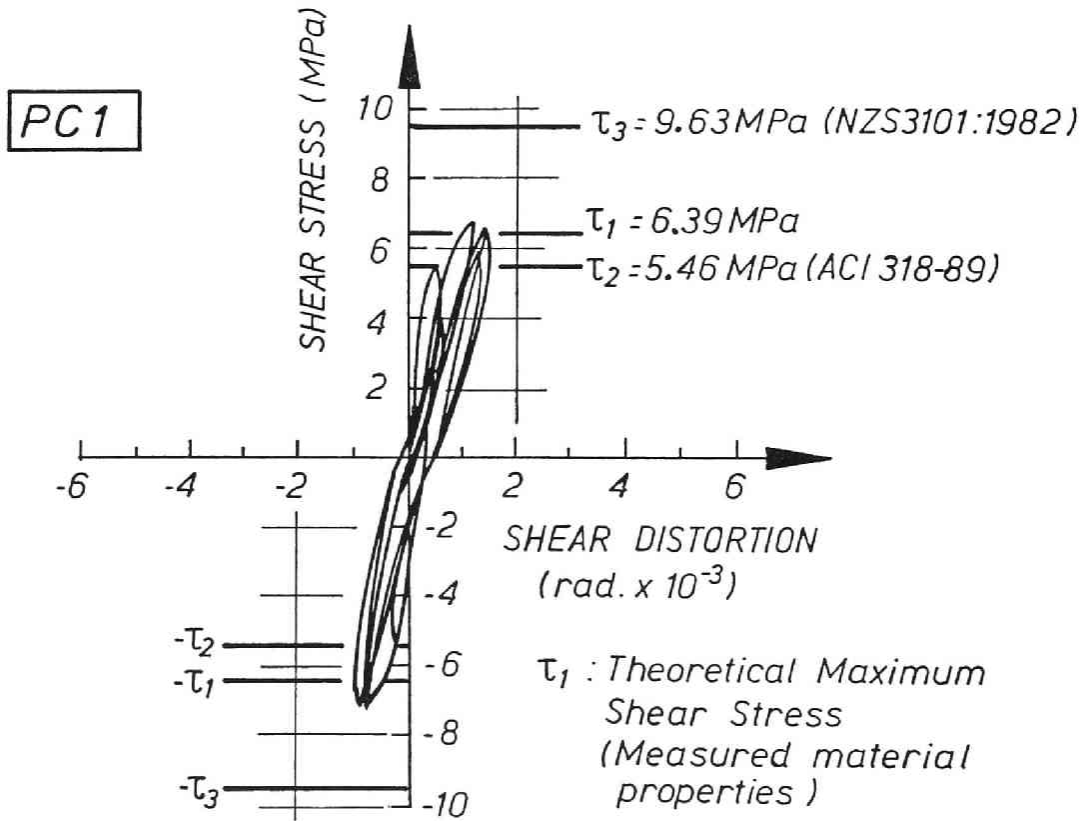


Fig.4.24(a) Shear stress versus the measured shear distortion angle curve (PC1)

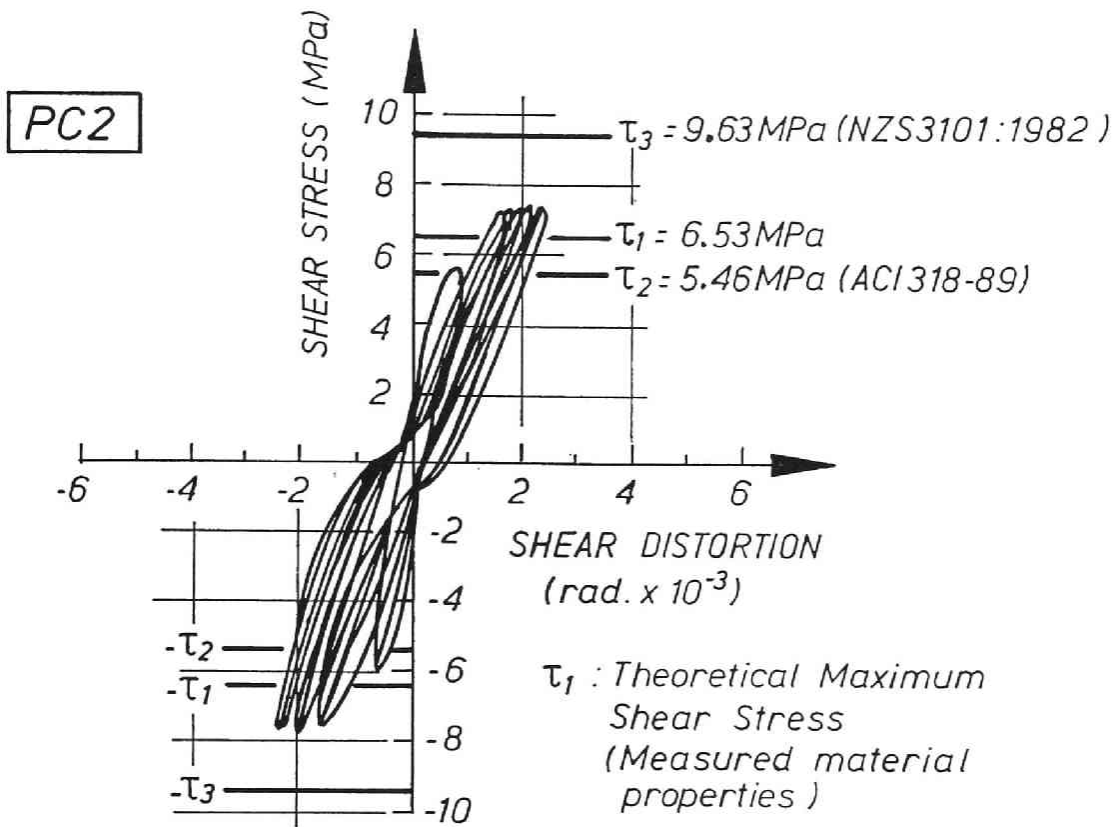


Fig.4.24(b) Shear stress versus the measured shear distortion angle curve (PC2)

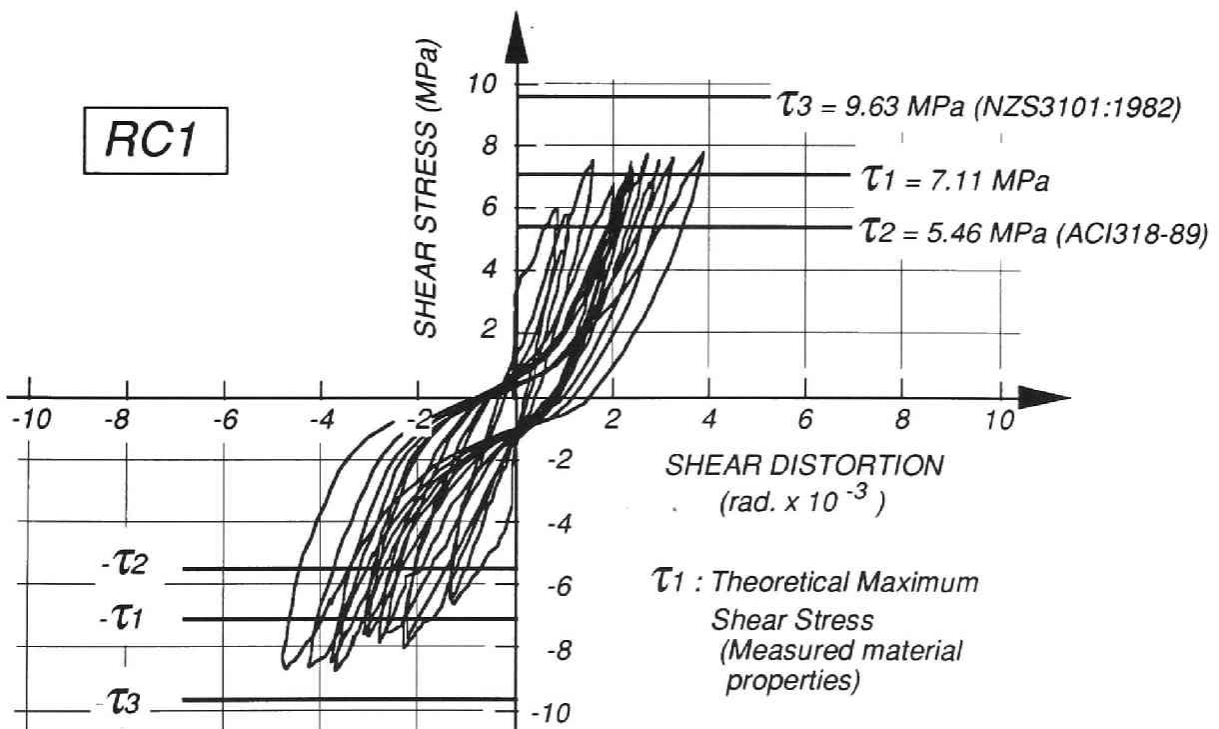
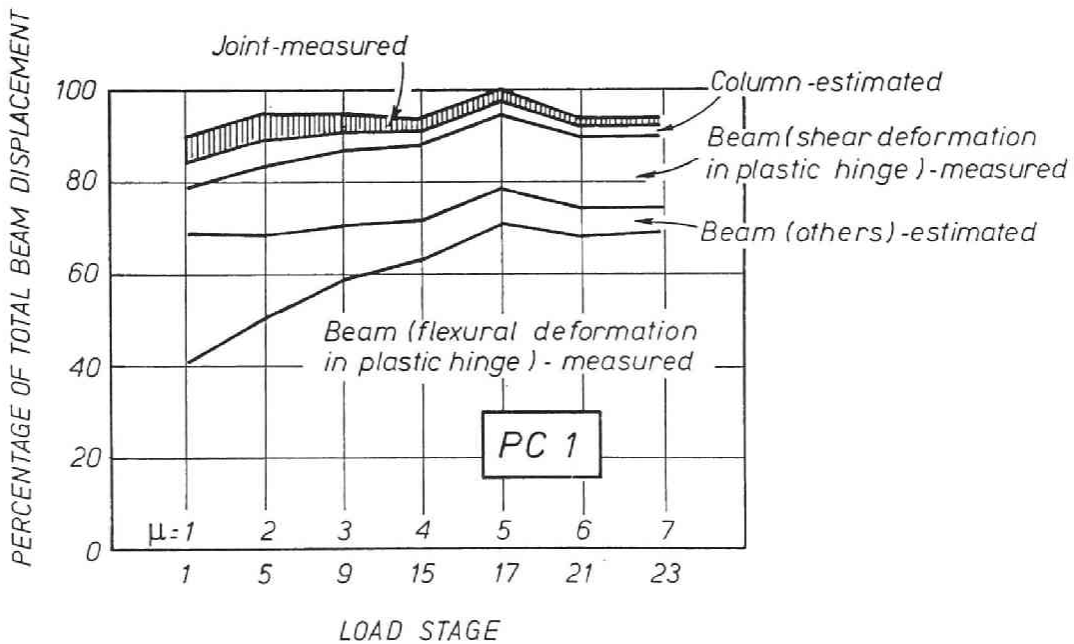


Fig.4.24(c) Shear stress versus the measured shear distortion angle curve (RC1)

The beam end displacement consisted of the following five components;

- 1) flexural deformation in the beam plastic hinge region,
- 2) flexural deformation in the beam outside the plastic hinge region,
- 3) shear deformation in the beam plastic hinge region,
- 4) flexural deformation of the column and
- 5) shear distortion of the beam-column joint core.

Shear deformation of the beam outside the hinge region and of the column were considered to be so small that they were neglected. The components 2) and 4) were estimated by the method described in the appendix A. The remainder were calculated using the strains obtained above. The contributions of these deformations to the overall beam end deflection are shown in Fig.4.25. The component of the contribution of joint shear deformation of RC1 was slightly larger than that of PC1 or PC2. It is noted that the ratios of the shear deformation of the beam to the overall deflection of RC1 was larger than those of PC1 and PC2. Prestressing force suppressed not only the joint shear deformation but the shear deformation of the beam.



(a) At Positive Ductilities

Fig.4.25(a) Contribution of each deformation component to the overall beam end deflection (PC1)

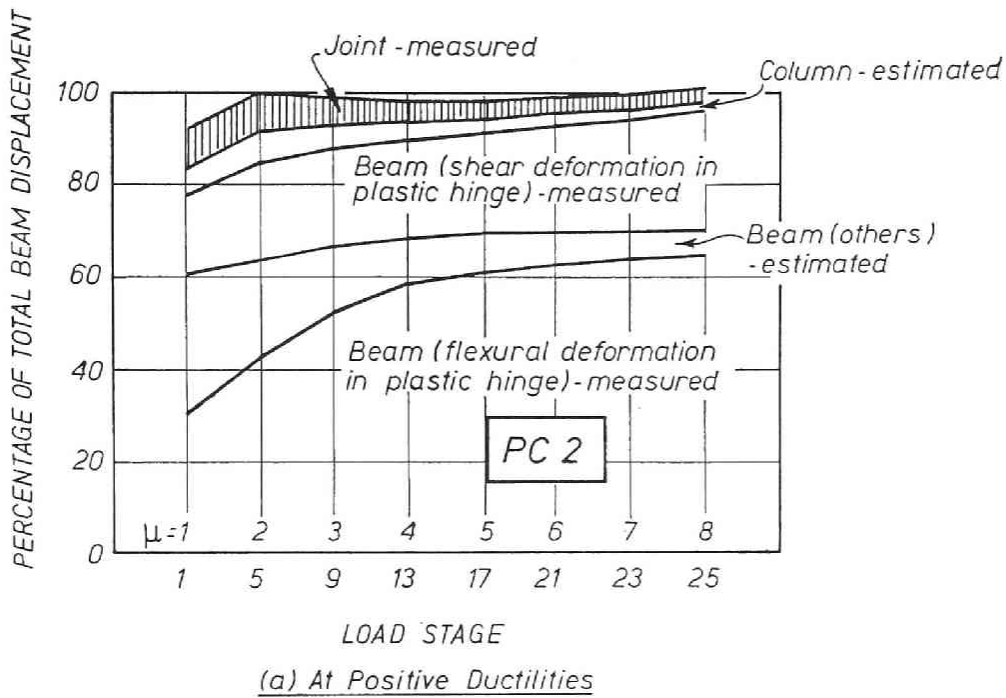


Fig.4.25(b) Contribution of each deformation component to the overall beam end deflection (PC2)

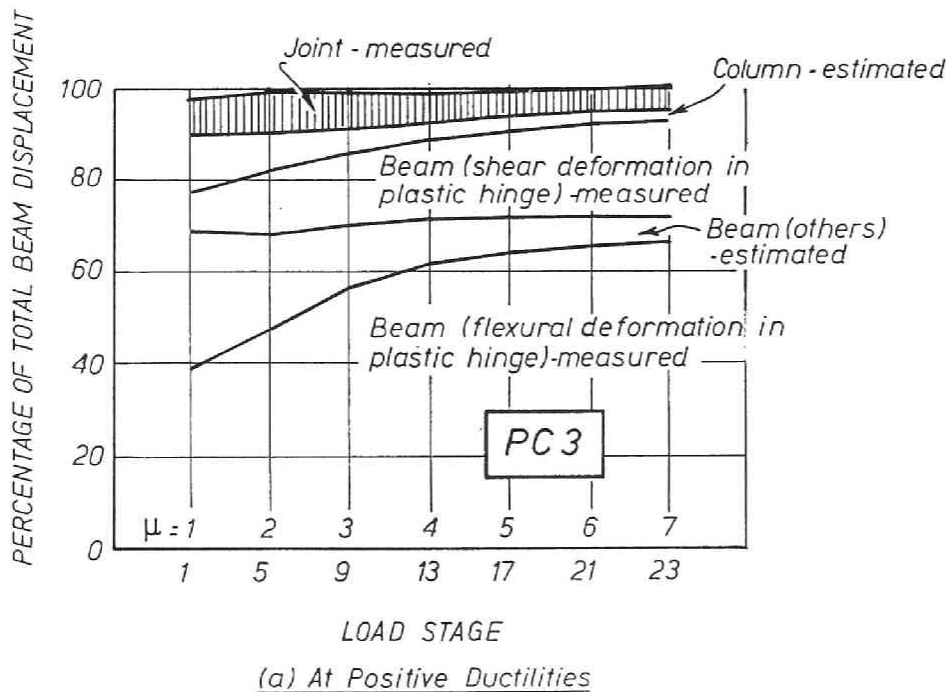
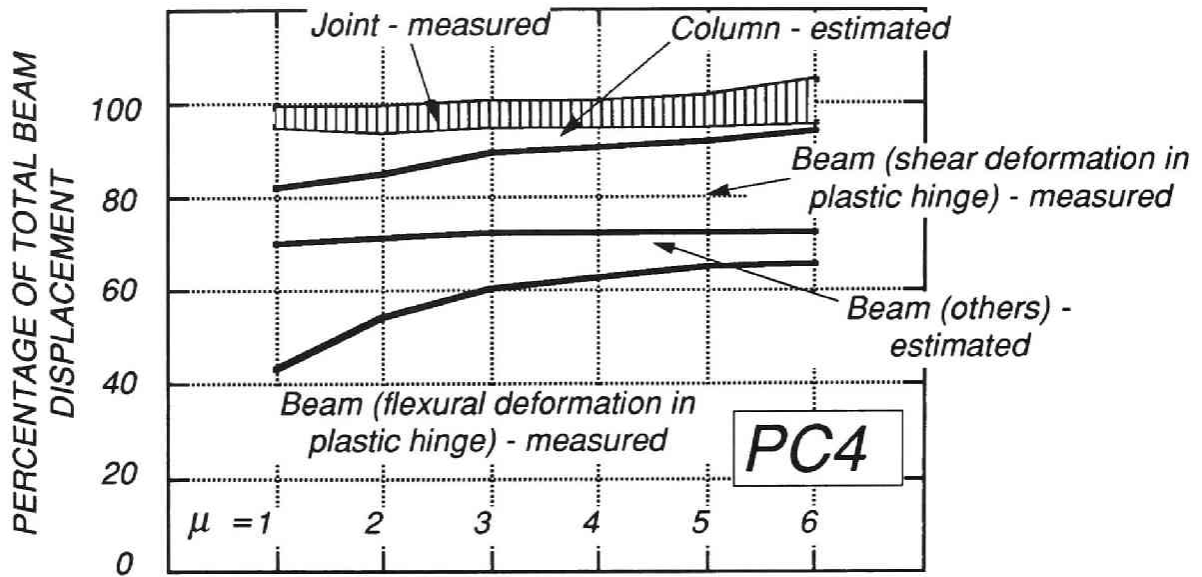
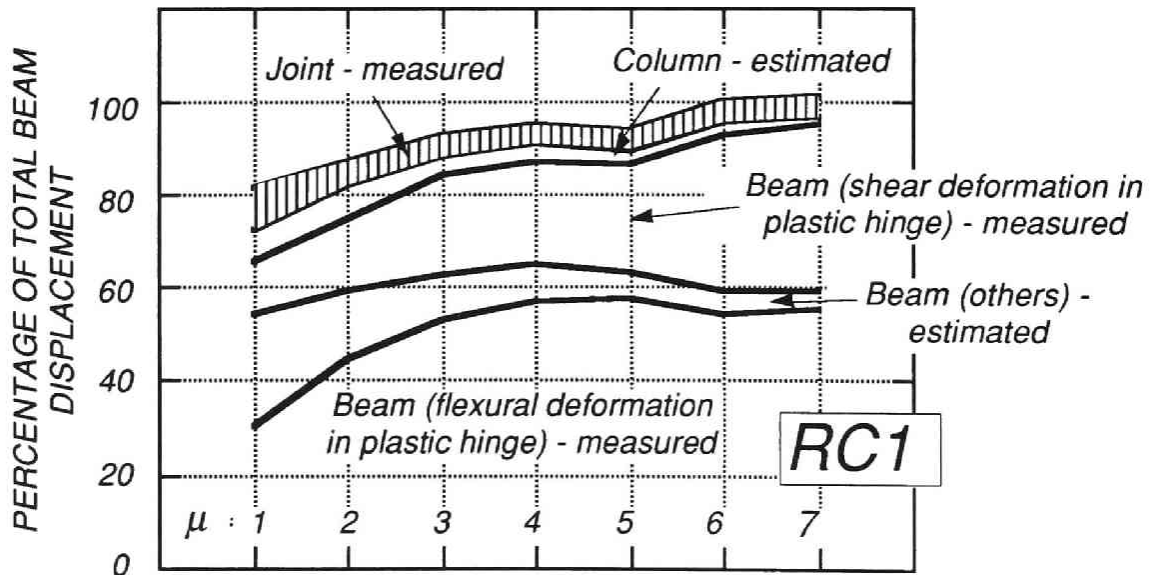


Fig.4.25(c) Contribution of each deformation component to the overall beam end deflection (PC3)



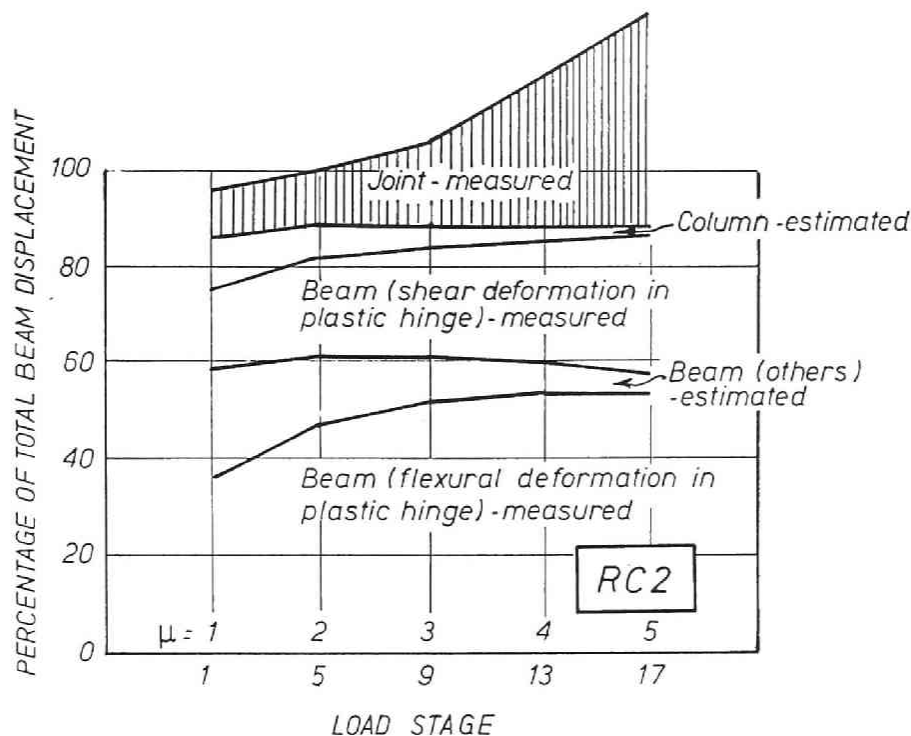
(a) At Positive Ductilities

Fig.4.25(d) Contribution of each deformation component to the overall beam end deflection (PC4)



(a) At Positive Ductilities

Fig.4.25(e) Contribution of each deformation component to the overall beam end deflection (RC1)



(a) At Positive Ductilities

Fig.4.25(f) Contribution of each deformation component to the overall beam end deflection (RC2)

Location of prestressing steel bars

The load-deflection curves show little difference between PC1 and PC2. The stresses developed in the joint shear reinforcement of PC1 with the prestressing steel bars at the central third of the beam depth were slightly smaller than those of PC2 whose beam had the prestressing steel bars near the extreme fibers of the section. The same matter can be pointed out about the contributions of joint shear distortion to the beam end deflection and the measured shear distortion angle curves of these two units. Therefore, prestressing steel near the extreme fibers improved the joint shear resistance as well as the one at the central third of the beam depth even in post-elastic range.

The provision in NZS 3101:1982 that only the prestressing steel located within the central third of the beam depth is effective on the joint shear resistance, may be extreme. Its effect depends on the ratio of effective stress in prestressing steel to yield strength and therefore on how much permanent set strains are sustained under high intensity loading. Further examination of the contribution of the prestressing force and the joint shear reinforcement to the shear resistance of the joints will be described together with the results of the Series B tests described in the later part of this chapter.

4.3.10 Series B (Units PC3, PC4 and RC2)

Effect of Prestressing Force on Shear Behaviour of Joint

The difference in the performance among these three units was clearer than the former three units due to the rather lower strength concrete and the inadequate anchorage details of the beam longitudinal reinforcement; both the top and bottom bars were bent downwards into the joint core or the column core. The performance of PC3 and PC4 were good with little reduction in the load carrying capacities and little pinching as

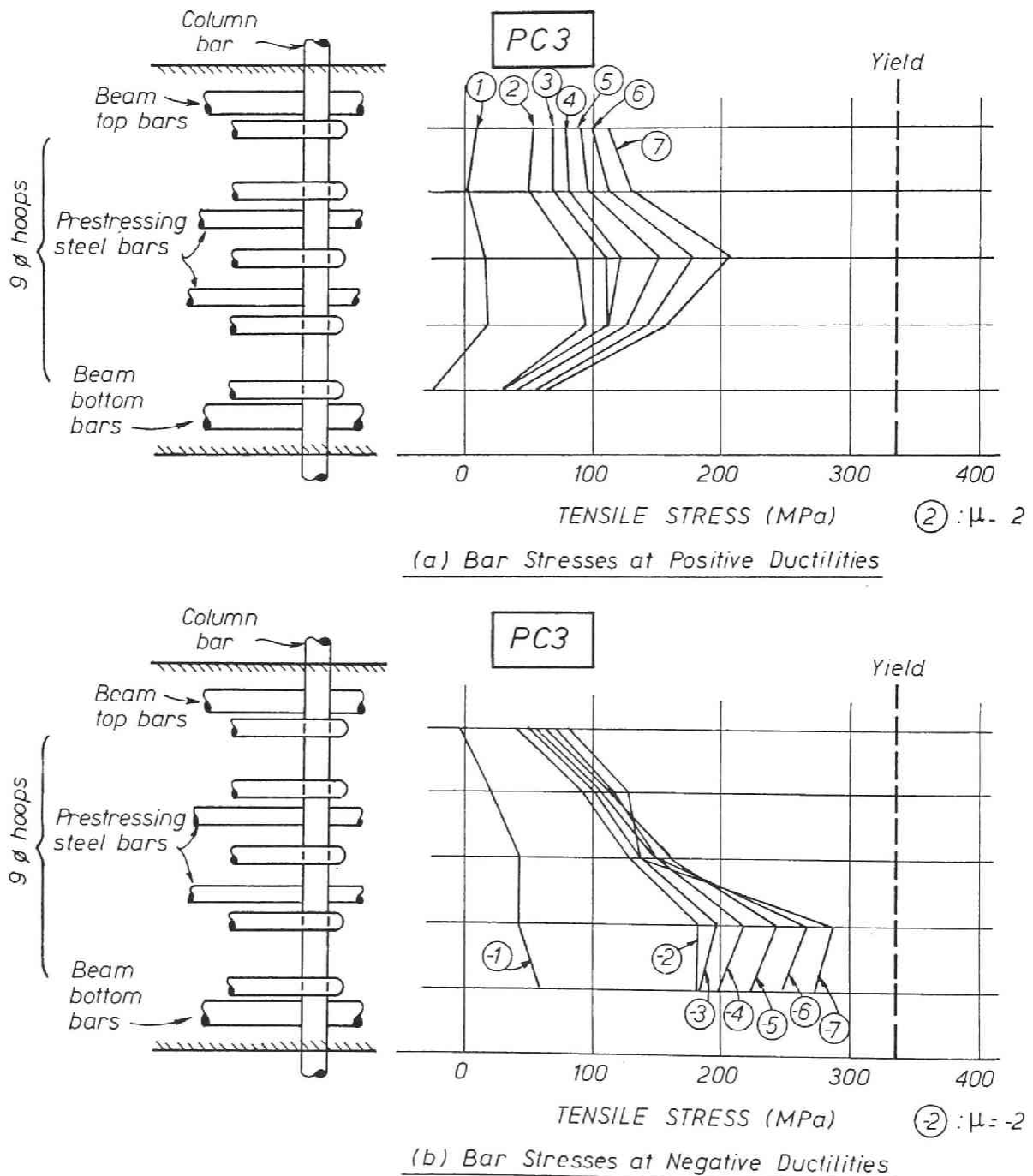


Fig.4.26(a) Stresses in the joint shear reinforcement measured at the peak of each loading run (PC3)

shown in Fig.4.18. Contrarily, in unit RC2 some pinching and capacity reduction of the load-deflection loops was noticeable even in the loading cycles of lower ductility values. Fig.4.26 shows the stresses in the joint shear reinforcement measured at the peak of each loading run. Most of the shear reinforcement in RC2 yielded in the loading cycles of smaller deformation, while those stresses of PC3 and PC4 were below the joint yield stress. The shear stress versus the measured shear distortion angle curves of these units shown in Fig.4.27 indicates the effect of prestressing force on shear behaviour of the joint. The maximum shear distortion measured in Unit RC2 was eight times that in Units PC3 and PC4.

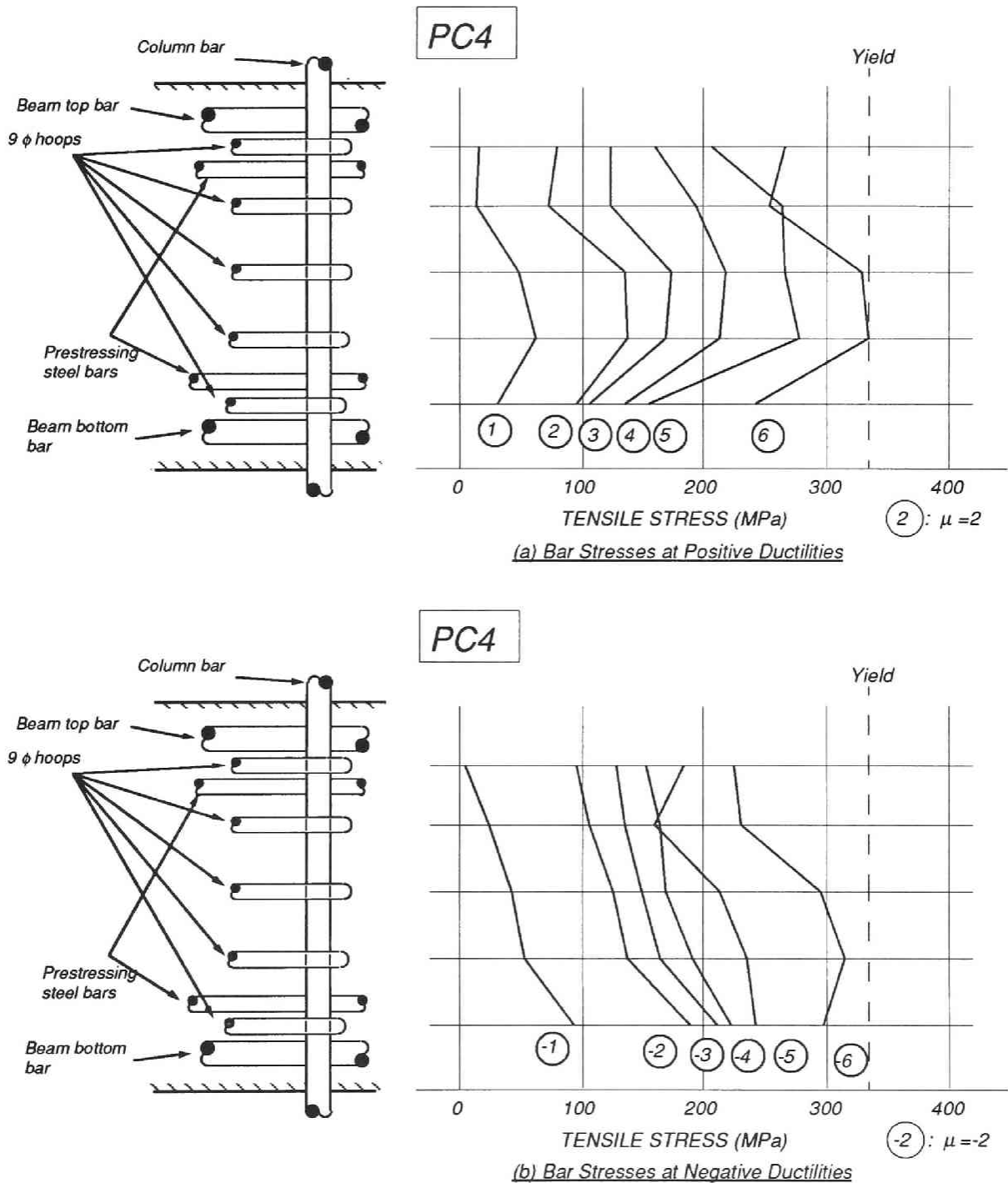


Fig.4.26(b) Stresses in the joint shear reinforcement measured at the peak of each loading run (PC4)

Comparison of the load-deflection and shear stress-shear distortion curves for these units gives a good indication of where the inelastic deformation was concentrated. The contribution of the joint shear deformation to overall deflection shows that RC2 failed in joint shear. This disclosed that the prestressing force in the beam had a great effect on the performance of the beam-column joint. In other words, the prestressing force prevented the joint from failing in shear and improved the behavior of the beam-column joint assembly.

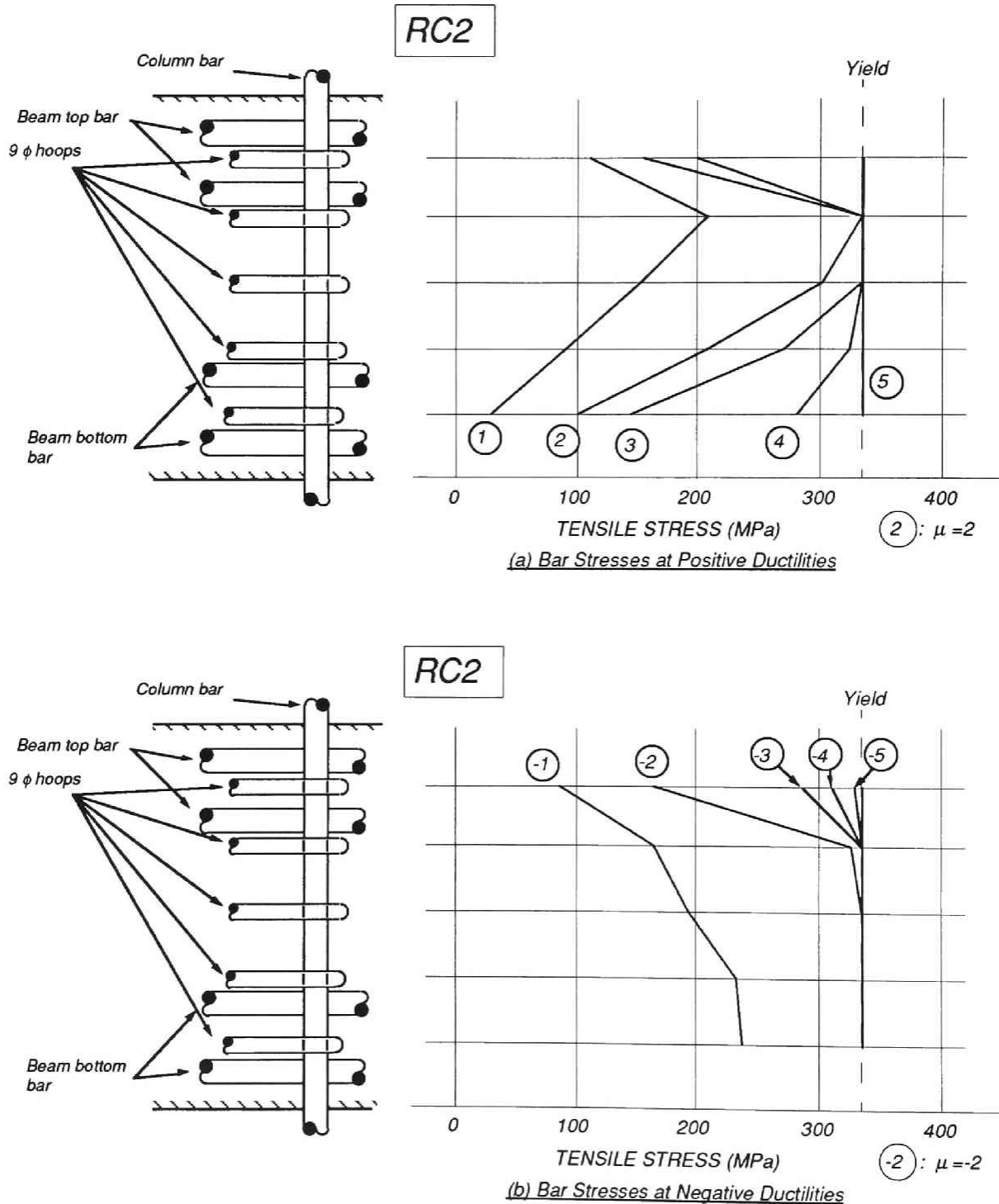


Fig.4.26(c) Stresses in the joint shear reinforcement measured at the peak of each loading run (RC2)

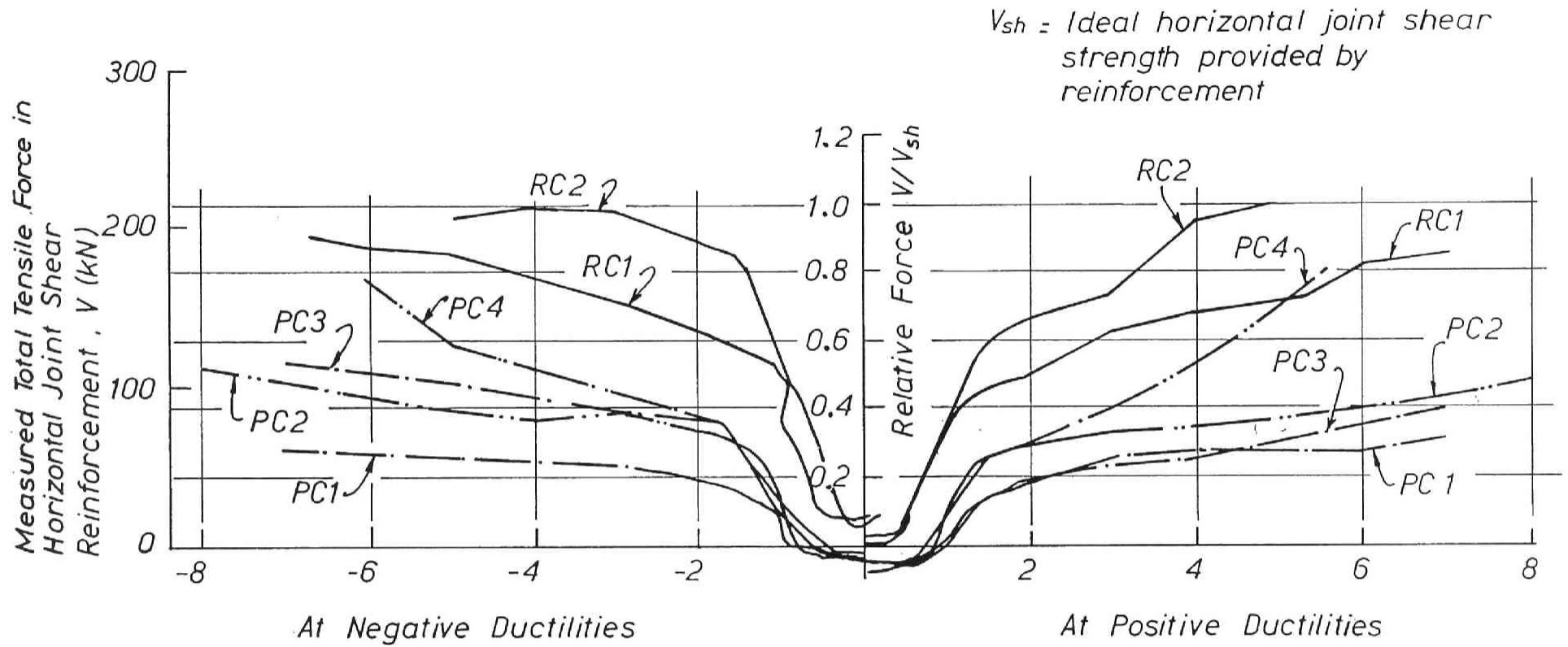


Fig.4.26(d) Stresses in the joint shear reinforcement measured at the peak of each loading run for all test units

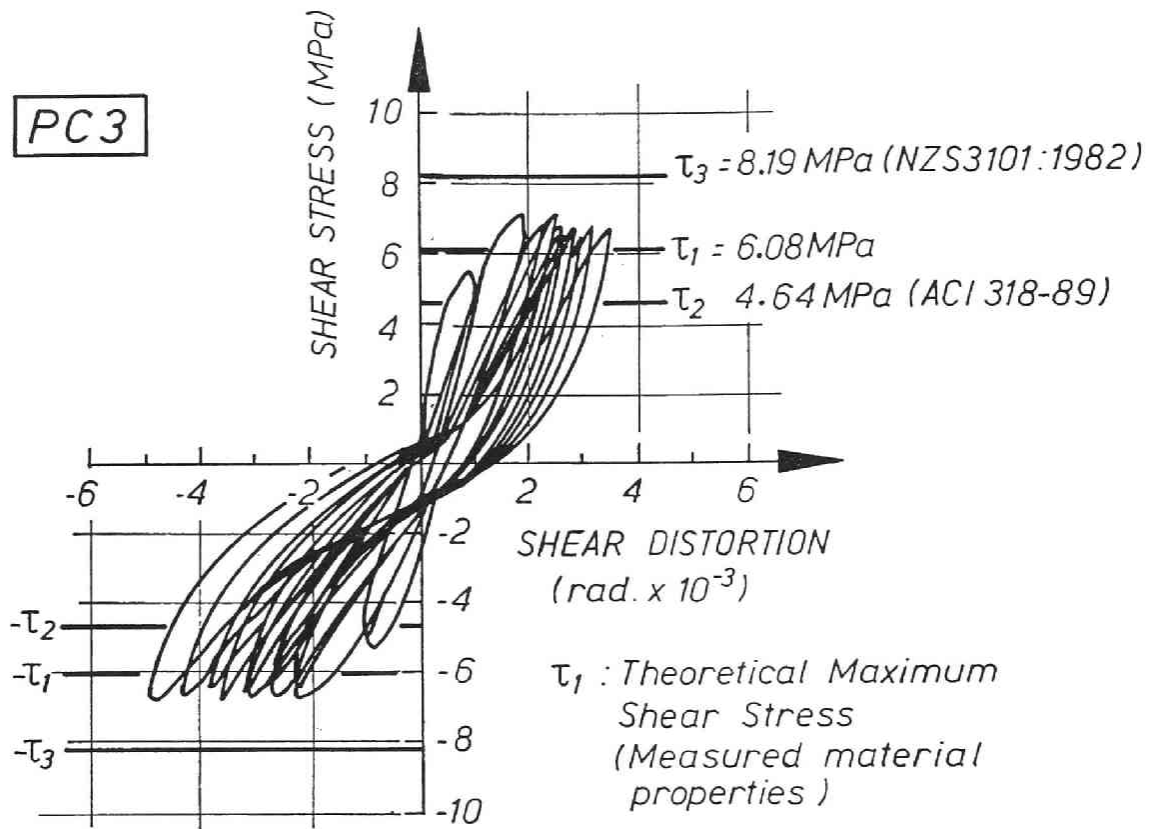


Fig.4.27(a) Shear stress versus the measured shear distortion angle curve (PC3)

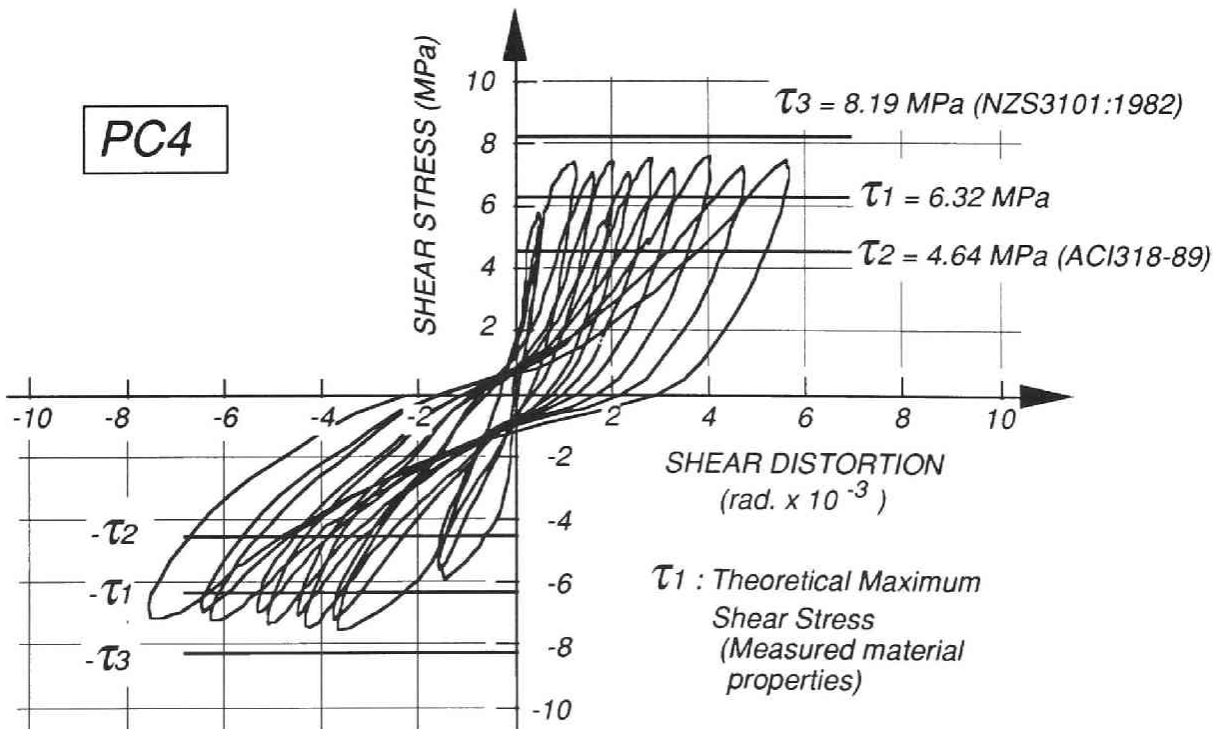


Fig.4.27(b) Shear stress versus the measured shear distortion angle curve (PC4)

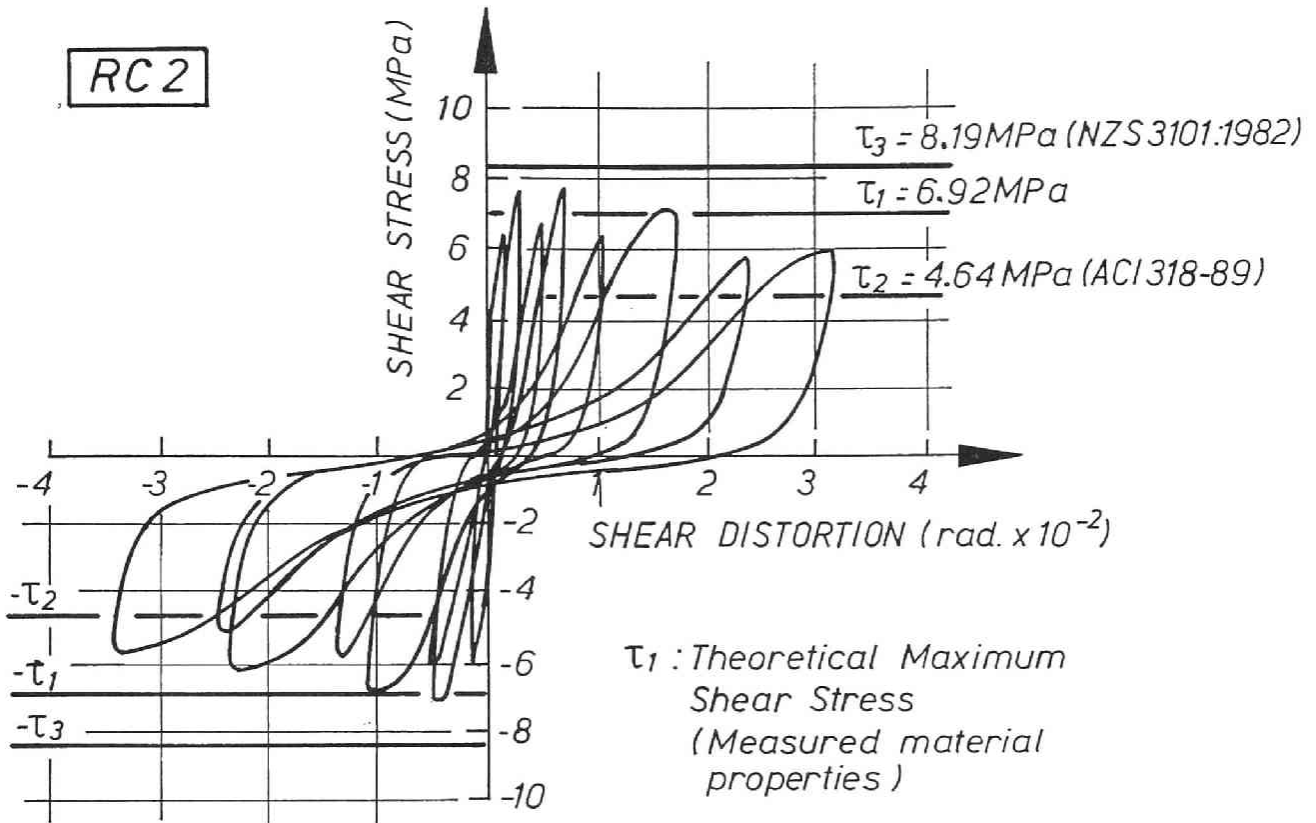


Fig.4.27(c) Shear stress versus the measured shear distortion angle curve (RC2)

Location of Prestressing Steel Bars

The location of prestressing steel influenced on the joint performance as shown in Figs. 4.22, 4.24, 4.26 and 4.27; comparison of joint shear stress - shear distortion relationships and of stress developed in joint shear reinforcement between Units PC1 and PC2, and between Units PC3 and PC4. The stresses developed in the joint reinforcement of Unit PC4, which has the prestressing steels near the extreme fibers of the section, were at most 1.5 times those of unit PC3 with the prestressing steels in the central third of the beam depth. The shear distortion angle of the last loading run of unit PC4 was approximately twice that of unit PC3, although they were much smaller than that of unit RC2. However, as indicated in Series B the difference between PC3 and PC4 was so small and the overall performances were approximately the same that the prestressing force in the steel near the extreme fibers of the section can be taken into consideration when designing the beam-column joint. The provision of NZS 3101:1982 that only the prestressing steel located within the central third of the beam depth can be accounted for joint shear strength should be reconsidered.

4.3.11 Tensile force in prestressing steel bars in Series A and B

Figure 4.28 shows the envelope curves of the tensile forces in the prestressing steel bars at the peak of each loading run measured by load-cells at both ends of the tendons. Because of the bond between concrete and bars, they did not represent the maximum tensile forces developed in the prestressing steels or the tensile forces which occurred at the beam critical section. However, they can be assumed to give a good estimation of the maximum tensile forces, because the bond deterioration between concrete and prestressing steel bars is likely to occur even during the early stage of inelastic load excursion, as observed in the past research [4.16].

In Units PC2 and PC4 with the prestressing steel bars near the extreme fibers of the section, the bars in the tension side of the beam section almost yielded while the tensile force in the bars in the compression side lost most of their introduced prestressing forces in the loading cycles of higher ductility values as shown in Fig.4.28. In Units PC1 and PC3 with the bars at the central third of the beam section, the tensile forces did not fluctuate so widely as Units PC2 and PC4. The stresses in the bars in the tension side of the beam section appeared to almost reach their yield strengths at the critical section of the beam. The total prestressing forces on the beam section of Units PC1 and PC3 were slightly larger than those of Units PC2 and PC4. The reason is that the yield strengths in the bars located in the tension side of the beam section were nearly developed in all units, that is, they had reached the uppermost limit, while the introduced prestressing forces of the bars in the compression side were almost lost in Units PC2 and PC4.

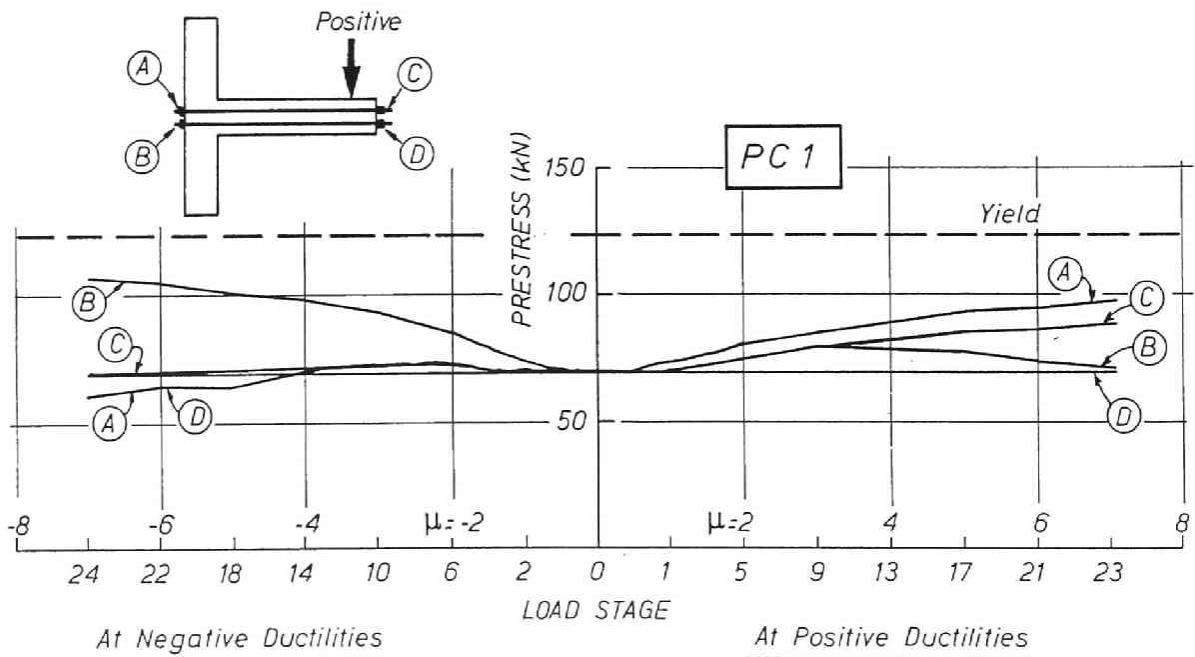


Fig.4.28(a) Envelope curves of the tensile forces in the prestressing steel bars (PC1)

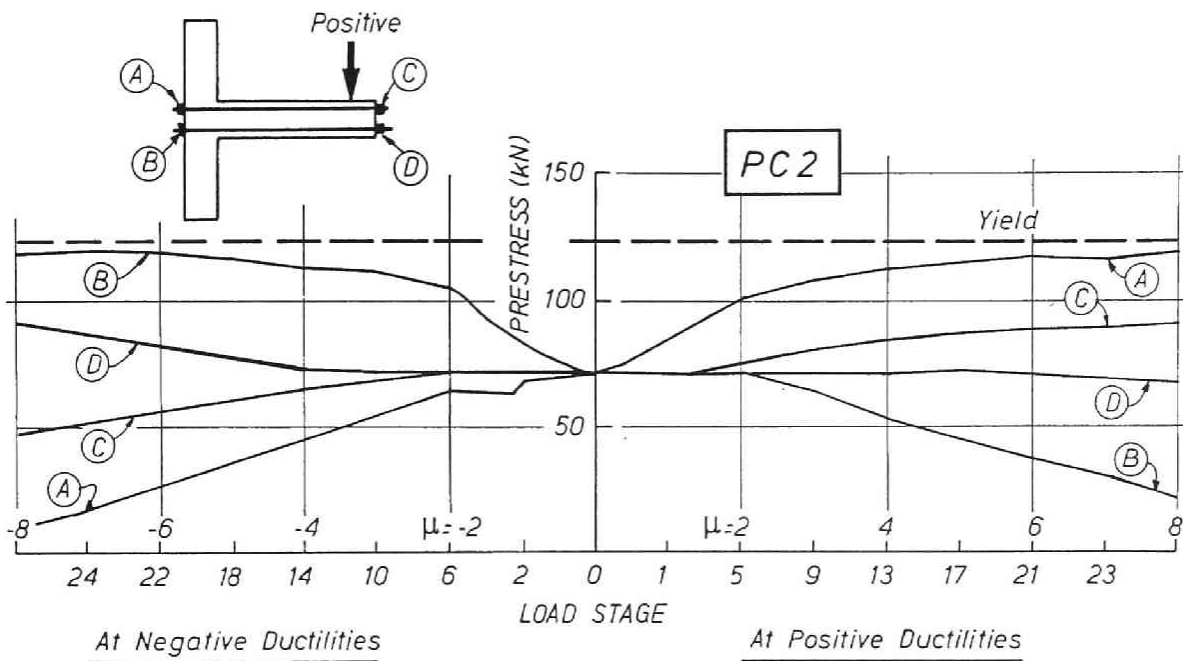


Fig.4.28(b) Envelope curves of the tensile forces in the prestressing steel bars (PC2)

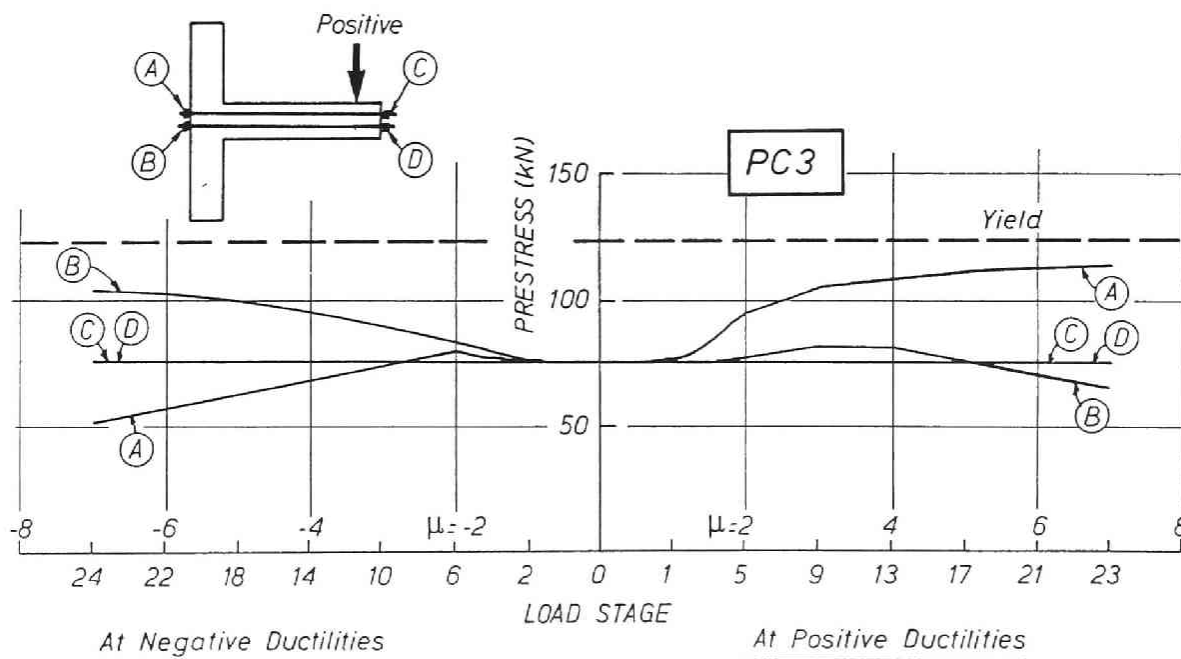


Fig.4.28(c) Envelope curves of the tensile forces in the prestressing steel bars (PC3)

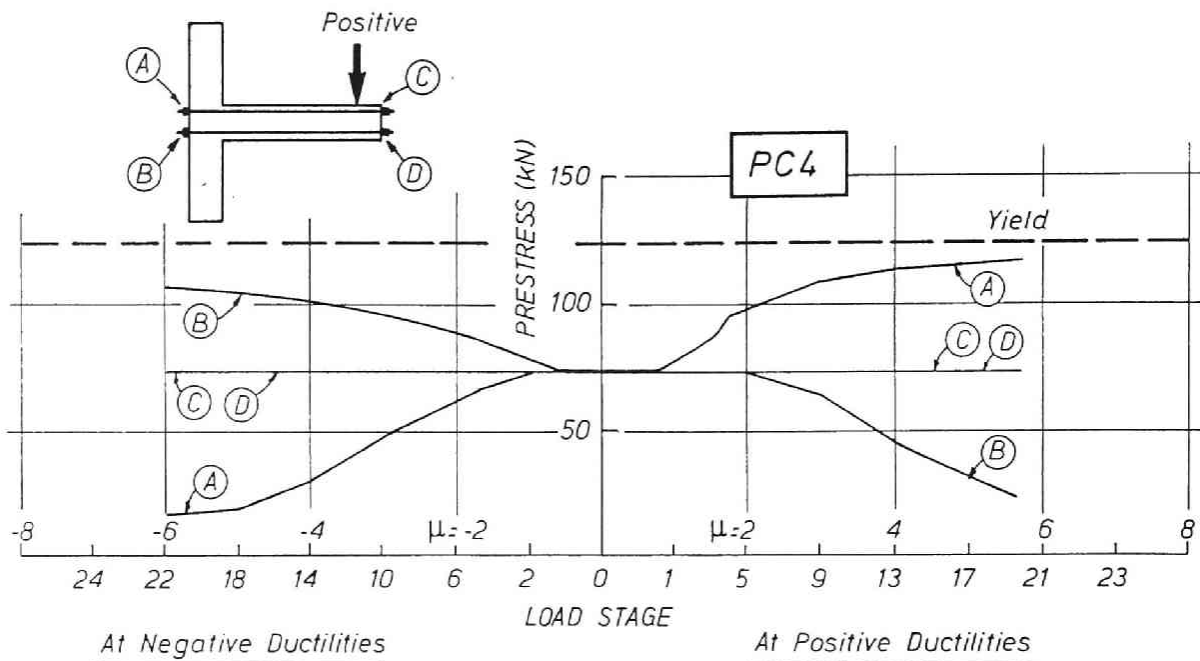


Fig.4.28(d) Envelope curves of the tensile forces in the prestressing steel bars (PC4)

4.3.12 Contribution of beam prestress to joint shear resistance

According to NZS 3101:1982, the contribution of the prestress to the shear resistance of the joint is specified to be $0.7P_{cs}$. In units PC1 and PC3, 193.8kN and 212.3 kN can be reduced from the total horizontal shear force induced in the joint. The required total area of horizontal joint shear reinforcement are listed in Table 4.9. These are between 42% and 485% of the horizontal joint shear reinforcement provided in the test units. It was only unit RC2 that failed in shear in the joint while the other units were loaded well into the inelastic region with little reduction in the load carrying capacity. They displayed “fat” load-deflection hysteresis loops. PC4 with only 42% of the required NZS 3101:1982 joint reinforcement showed good performance. Table 4.11 lists the tensile forces, $V_{sh.meas}$, in the joint reinforcement measured at the peak of each loading run with the ductility factor of 4, which corresponded to the beam rotation angle of approximately 1/25. Even in unit PC4, only 70% of the yield force in the joint reinforcement developed.

V_{cp} is the horizontal joint shear strength provided by prestressing force. This is estimated by the following equation.

$$V_{cp} = V_{jh} - V_{sh.meas} - V_{ch} \text{ [Eq.9-11]} \quad (4.21)$$

Table 4.11 Horizontal joint shear strength provided by prestressing steel

Unit	V sh.meas (kN)	V _{cp} (kN)	V _{cp} /P _e
PC1	85.4	152.5	0.55
PC2	106.9	124.3	0.44
PC3	113.4	406.8	1.34
PC4	150.8	356.4	1.21

Note:

- V_{sh.meas} : Total tensile force measured in horizontal shear reinforcement
- V_{cp} : Horizontal joint shear strength provided by prestressing steel bar
- P_e : Total effective prestressing force

The last term applies only to the units of Series A. The ratio of V_{cp} to total effective prestressing force, P_e , ranges between 0.44 and 1.34 as listed in Table 4.11. For the units whose non-prestressed beam bars were welded to the anchorage plates on the outer side of the column, V_{cp} was smaller than specified in NZS 3101. For the units whose non-prestressed beam bars were bent downwards into the joint core or the column core, which is common practice in Japan, V_{cp} was much larger than that. Without the contribution of V_{ch} [Eq.9-11 in NZS], V_{cp} for the units of Series A increased by at least 224%, and V_{cp} / P_e also increased to 1.78 for PC1 and 1.61 for PC2. It is conservative that the contribution of V_{ch} [Eq.9-11 in NZS] be assumed to be zero. Both kinds of joints seem to have a much larger value of V_{cp} than that predicted by NZS 3101.

Past research on reinforced concrete beam - column joints have shown that it is difficult to measure the tensile force in joint reinforcement which is used only for the shear resistance, because the pressure of the joint core concrete against the sides of the reinforcement tends to bend the sides outwards. Therefore, these values in the table are not supposed to indicate the exact contribution of the prestressing force. However, the provision in NZS 3101:1982 seems to be overly conservative.

4.3.13 Influence of location of prestressing steel on joint shear resistance

The test results indicated that there was little influence of the location of prestressing steel on the joint shear resistance. This result was different from that of Park and Thompson [4.6] who concluded that the location of the prestressing steel had a large influence on the joint shear strength. The ratio of the effective stress to the yield strength in the prestressing steel was found to be of great importance in assessing the joint shear strength. In the units of Park and Thompson [4.6] it varied between 74% and 83% while in the units tested by the author it was approximately 60%. The larger

margin between the effective and yield stress leads to the later occurrence of yielding of prestressing steel. According to the current design code for prestressed concrete structures in Japan [4.17], allowable stress to be introduced into prestressing steel is specified to be $0.8f_{py}$ or $0.7f_{pu}$, whichever is smaller. f_{py} and f_{pu} denote the yield strength and tensile strength of prestressing steel, respectively. Considering loss of prestress due to creep and shrinkage of concrete, relaxation of steel stress and so on, stress in the prestressing steel results in approximately $0.6f_{py}$. Therefore, in the design of prestressed concrete members prestressing steel outside the central third of the section should be accounted for in the assessment of the shear strength of the joint core.

4.3.14 Comparison of the experimental results with theoretical predictions

In the following sections, a comparison of the experimental results for the test units and theoretical predictions is made. This includes the moment-curvature hysteresis loops, the load-displacement hysteresis loops, the maximum plastic rotation and curvature, and the available curvature ductility factor. The cyclic moment curvature theory described in Chapter 3 was used to make the comparisons.

Figs. 4.29(a) to (f) show the moment-curvature characteristics compared. The experimental curvature is the average of that measured over 365 mm gauge length, which consisted of the beam potential plastic hinge region of 300 mm from the column face and part of the joint region of 65 mm from the column face. The moment is that at the column face. In all cases the cover concrete was assumed to have spalled at strains greater than 0.007. Buckling of the non-prestressed reinforcement was not considered.

For all units except for RC2, the experimental curves can be well followed by the predicted theoretical curves with respect to the moment capacities and the general shape of the loops. For Unit RC2, which failed in joint core shear, those curves showed quite different characteristics. The experimental curve showed large pinching and reduction in load capacity which was caused by the deterioration of bond.

The significant difference between the experimental and theoretical curves is that the hysteresis loops obtained from the experiments in large inelastic deformation are narrower than those theoretically predicted. This may be because of the stress-strain relationship assumed for the reinforcing steel in the analyses. Not including buckling of longitudinal reinforcement into the analyses may also play an important role. Generally, loop shape of moment-curvature curves is likely to be similar to the stress-strain curve of longitudinal reinforcement. This part of hysteresis loops are largely affected by the shape of the stress-strain relationship of the longitudinal reinforcement.

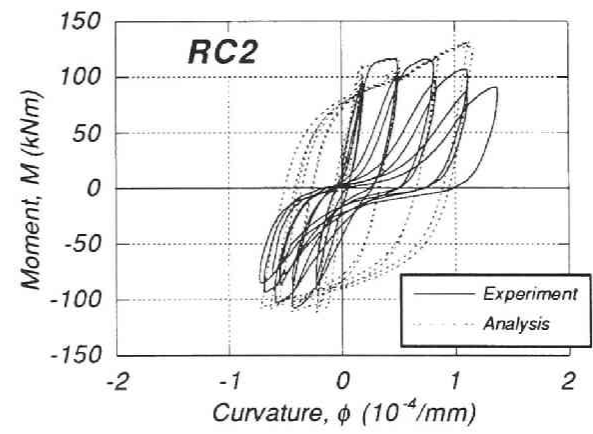
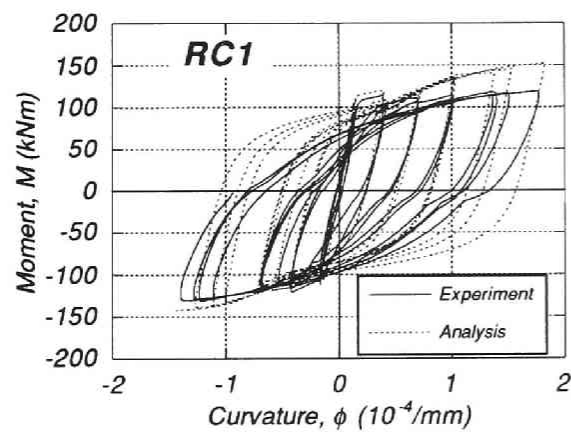
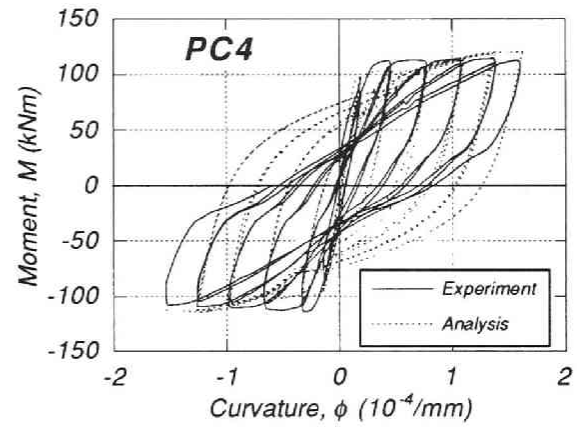
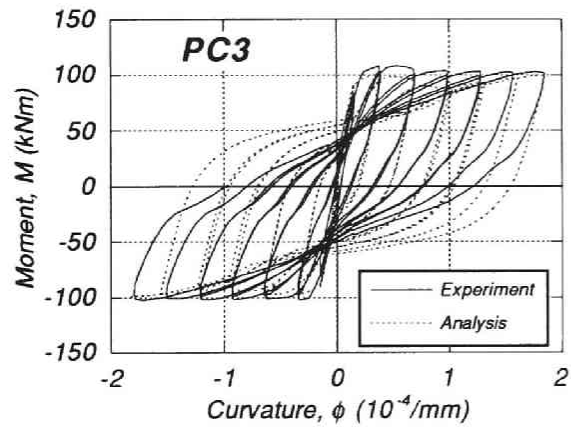
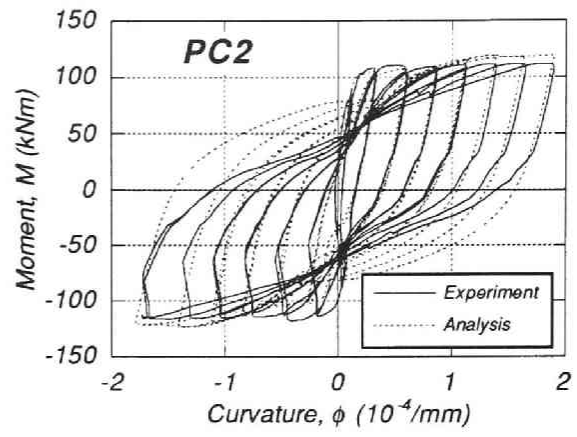
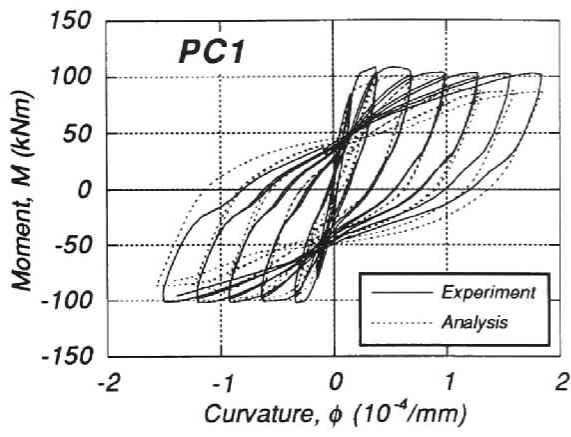


Fig.4.29 Moment - curvature characteristics compared

4.4 Test on Prestressed Concrete Beam-Exterior Column Joint Assemblies with Various Amount of Prestressing Force

4.4.1 General

Based on the test results described in 4.3 the following three items require further discussion.

1. It has been pointed out in past research [4.14] that reinforced concrete members are superior to prestressed concrete with respect to energy dissipation and deformability. However, this conclusion was obtained from the tests on prestressed concrete beams [4.14]. In case of a beam-column subassembly, its behaviour is considered to be largely dominated by the performance of the jointing part. Thus, hysteresis loops of a prestressed concrete beam-column subassembly might be better than those of a reinforced concrete because prestress introduced into the beam can improve the shear behaviour of the beam-column joint core.
2. Larger prestress has more beneficial effect on the shear behaviour of a beam-column joint core. However, it also results in crushing and spalling of the unconfined cover concrete and buckling of non-prestressed compression reinforcement of the beam in the earlier stage of the loading. Besides, larger prestress results in larger compressive strain of concrete and it may lead to the deterioration of the concrete due to reversed cyclic loading.
3. In the tests reported in Chapter 4.3 the same amount of prestressing force was assigned to all test units. The effect of the intensity of prestressing force on shear behaviour of a joint core has not yet been clarified.

The objective of these tests is to investigate the load - deformation characteristics and shear behaviour of prestressed concrete beam - exterior column joint assemblies with various amount of prestress.

4.4.2 Test Program

Description of Test Units

Three prestressed concrete beam - external column joint assemblages and one reinforced concrete beam - column joint assemblage were constructed. Those beams had prestressing forces of 0.06, 0.12, 0.18 and 0.0 $f'_c A_g$, respectively. f'_c and A_g denote concrete compressive strength and gross sectional area of beam, respectively. The term 'prestress level' is defined as the ratio of prestressing force introduced into the beam to $f'_c A_g$. The upper limit of a prestress level assigned to the test unit was 0.18

because of the following reasons; According to Standard for Structural Design and Construction of Prestressed Concrete Structures published by Architectural Institute of Japan (AIJ) [4.17], the permissible concrete compressive stress to be introduced into a member under service loads is specified to be $1/3 \cdot f'_c$. Assuming that a member is subjected to concentric compressive load by prestressing force which results in the permissible stress, this prestressing force corresponds to a prestress level of approximately 0.3. In a practical member, prestress is introduced to counteract or reduce the moment caused by vertical loads. Thus, the member is so designed to have a compressive stress less than $1/3 \cdot f'_c$ at the extreme compression fiber and tensile stress less than the permissible tensile stress specified in the Standard at the extreme tension fiber. In case of partially prestressed concrete, tensile stress greater than the permissible tensile stress is sometimes allowed to control crack width. The average compressive stress, if divided by f'_c it is equivalent to a prestress level, comes to around $1/6 \cdot f'_c$. Moreover, based on the test results described in Chapter 4.3 and the preliminary calculations of the moment capacities of the beams, a test unit with a prestress level of 0.2 was predicted to fail in beam flexure rather than in joint shear.

Fig.4.30 shows the overall dimensions of the four units tested. The dimensions are identical to the test units described in Chapter 4.3. The test units had a total column height of 1.9m and a total beam length of 1.85m measured from the column face. The column cross section was a 300mm square. The beam had a 200x300mm rectangular cross section. The specifications of each test unit are summarized in Table 4.12.

The mix design for the concrete used for the test units was :

25 mm aggregate	985 kg/m ³
Sand	829 kg/m ³
Portland Cement	325 kg/m ³
Water	172 litre/m ³

Water/Cement ratio = 0.53

The compressive cylinder strength had reached $f'_c = 34.4$ MPa for Unit RCB-1 and $f'_c = 31.8$ MPa for the other units at the stage of testing, that is, at the age of 30 days. The mechanical properties of concrete are summarized in Table 4.13. All units were cast vertically, compacted using vibrators, and were damp cured in the laboratory.

Prestress was introduced into the beams 14 days after concrete casting. The prestressing steel bars were post-tensioned and grouted. The W/C of the grout mortar was 40%.

Prestressing steel is usually draped with the location of their resultant force not

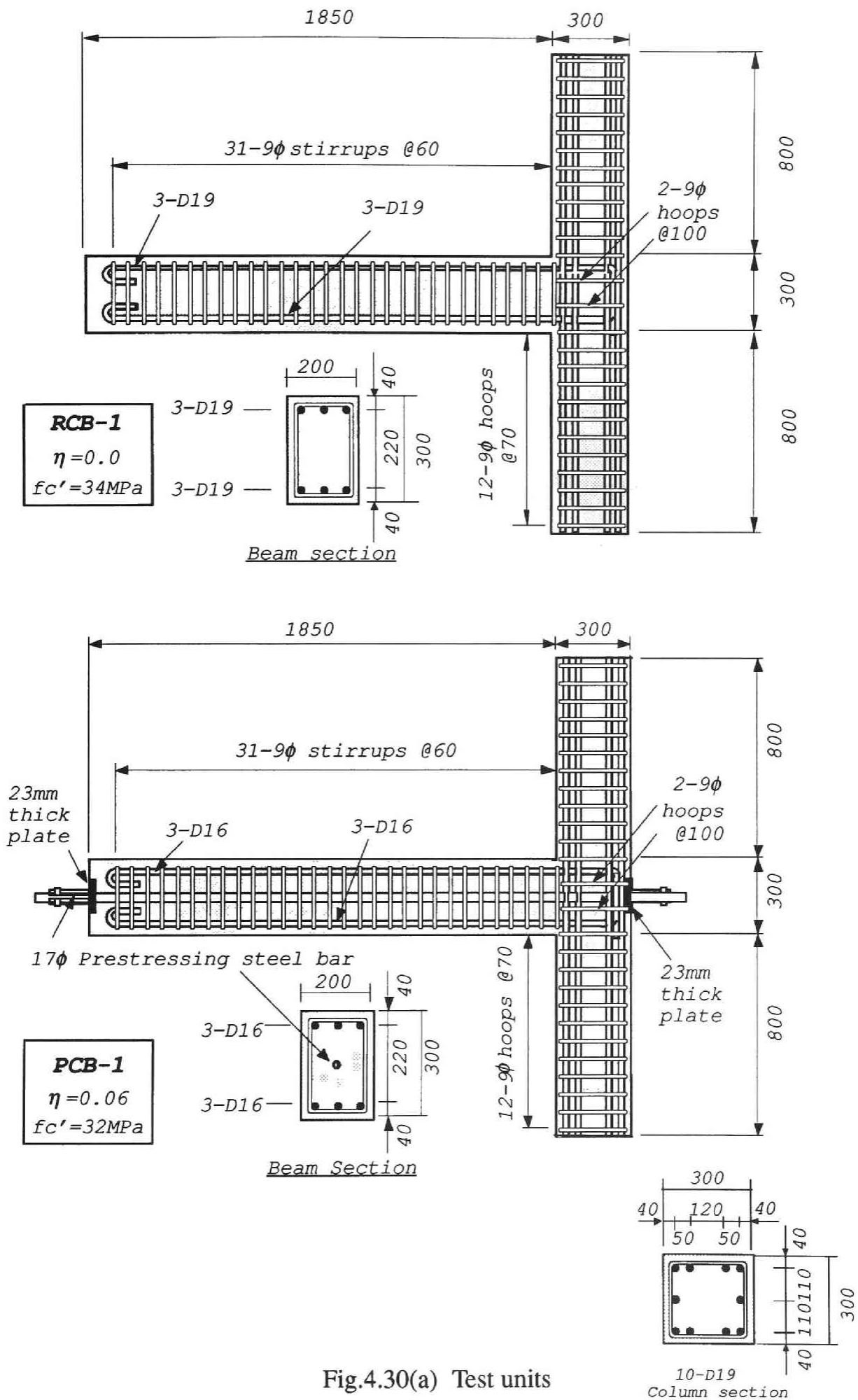


Fig.4.30(a) Test units

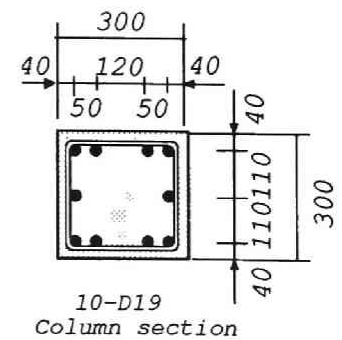
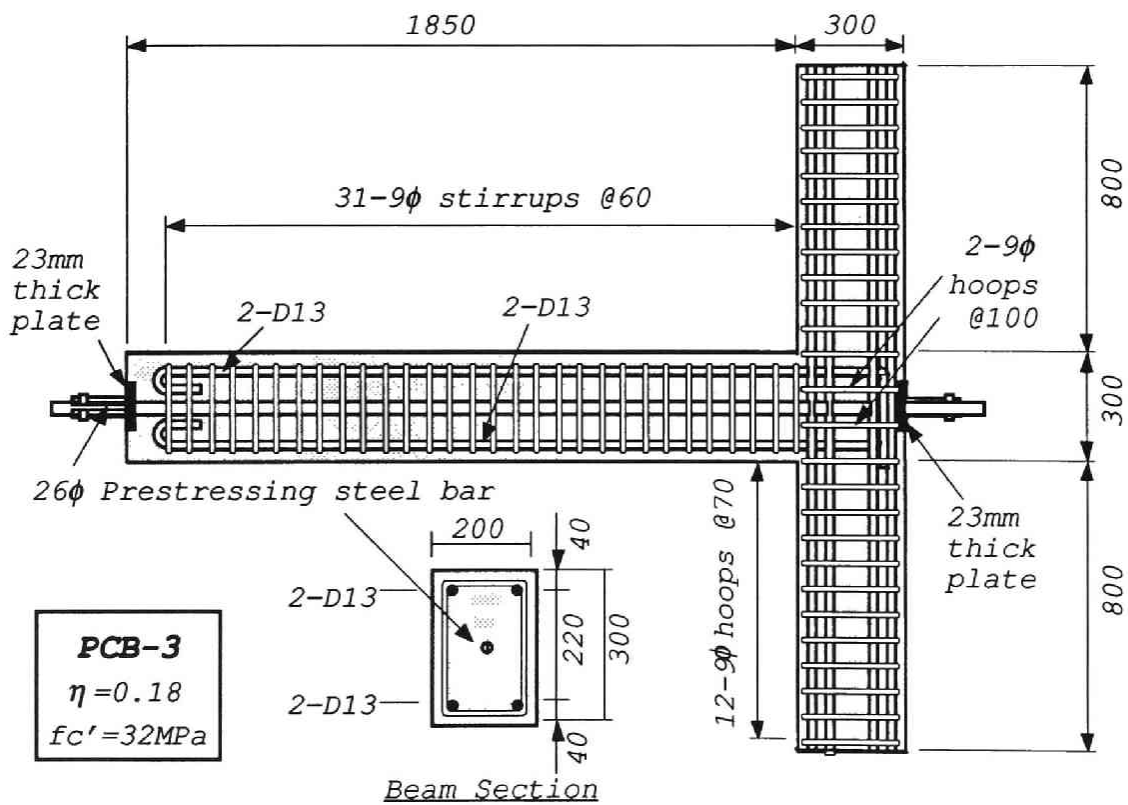
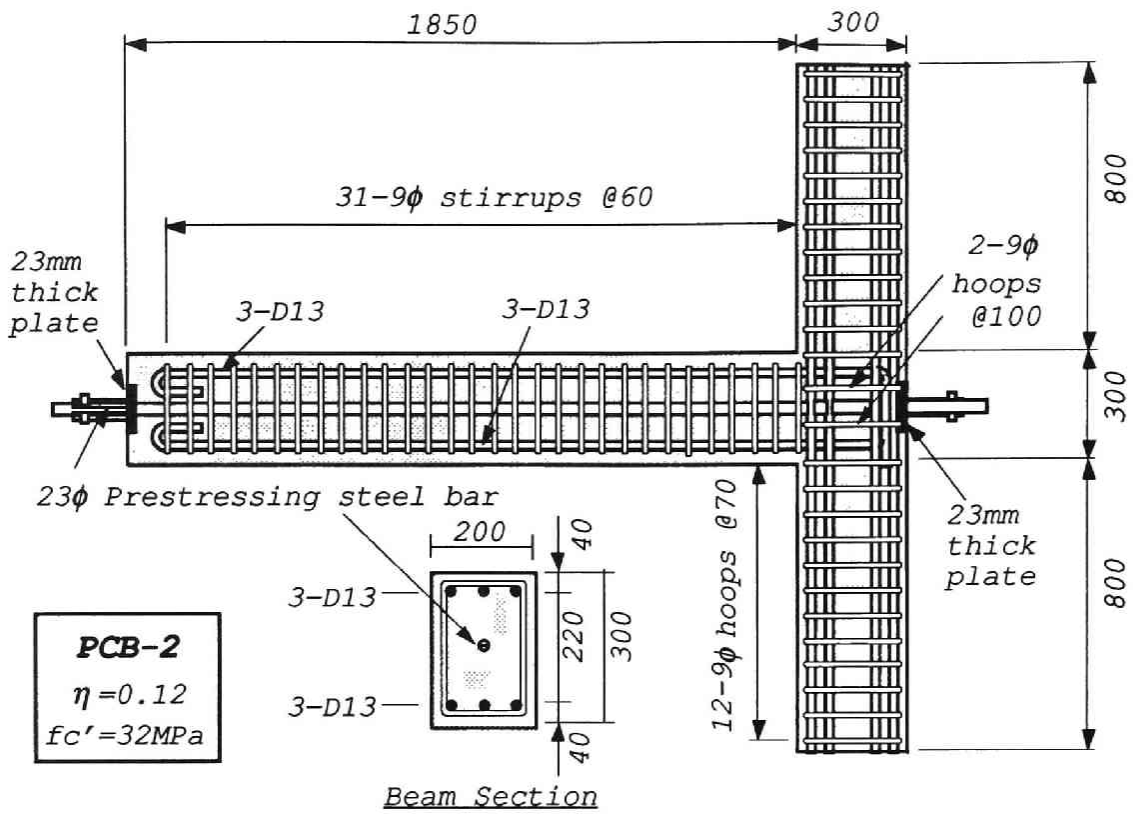



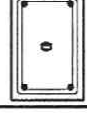


Fig.4.30(b) Test units

Table 4.12 Specifications of test units

UNIT	Compressive Strength of Concrete f'_c (MPa)	Prestressing Steel bar	Effective Prestressing force P_e (kN)	$P_e / A_b f'_c$	Beam Section
RCB - 1	34.4	-	-	0	 3 - D19 3 - D19
PCB - 1	31.8	$\phi 17$ SBPR95/120	123.6	0.06	 3 - D16 3 - D16
PCB - 2	31.8	$\phi 23$ SBPR95/120	234.7	0.12	 3 - D13 3 - D13
PCB - 3	31.8	$\phi 26$ SBPR110/125	360.3	0.18	 2 - D13 2 - D13

Note:

A_b : Gross sectional area of beam

0.2% offset yield stress of prestressing steel bar:

$\phi 17$ --- 1167 MPa, $\phi 23$ --- 1157 MPa, $\phi 26$ --- 1216 MPa

Table 4.13 Mechanical properties of concrete

Unit	Compressive strength f'_c (MPa)	Strain at f'_c (%)	Initial Modulus of elasticity (10^4 MPa)
RCB-1	34.4	0.14	3.83
PCB-1	31.8	0.12	3.83
PCB-2			
PCB-3			

coincident with the centroid of a member section. However, the prestressing steel bar of the test units was placed at the center of the section because the main objective of the experiments was to investigate the fundamental seismic performance of pre-stressed concrete beam - column joint assemblies.

Table 4.14 lists the ideal flexural strength of the beam of each test unit calculated using the ACI318-89 [4.11] equivalent rectangular stress block based on the measured material strengths with the capacity reduction factor ϕ of unity. The beams of all four test units were designed to have approximately the same flexural strength.

The longitudinal steel content was such that for each unit the flexural strength of the column section was greater than that of the beam section. Plastic hinging was expected to occur in the beams at the column faces.

Table 4.14 Ideal flexural strength of the beams, theoretical internal forces in beams at flexural strength and maximum shear forces

Unit	n (mm)	C _c (kN)	C _s (kN)	P _s (kN)	T _s (kN)	M _{cal} (kNm)	V _{col} (kN)	V _{jh} (kN)
RCB-1	48.0	222.9	88.8	0.0	311.7	73.2	48.8	262.9
PCB-1	71.8	319.4	163.4	264.9	217.9	80.5	53.7	429.2
PCB-2	93.0	413.8	134.2	396.4	151.6	77.8	51.8	496.2
PCB-3	111.0	494.0	100.4	493.3	101.1	73.8	49.2	545.2

Note:

- n : Neutral axis depth
- C_c : Resultant compressive force in concrete
- C_s : Compression force in non-prestressed compression rebar
- P_s : Tensile force in prestressing steel bar
- T_s : Tensile force in non-prestressed tensile rebar
- M_{cal} : Theoretical maximum moment calculated using the equivalent stress block specified in ACI318-89
- V_{col} : Shear force in column
- V_{jh} : Theoretical maximum applied horizontal shear force

The mechanical properties of steel reinforcement are summarized in Table 4.15.

Table 4.15 Mechanical properties of steel reinforcement

	f_y (MPa)	ϵ_y (%)	f_u (MPa)	E_s (10^5 MPa)
D19	362	0.23	563	1.57
D16	365	0.22	521	1.67
D13	398	0.21	554	1.87
$\phi 9$	316	0.16	427	2.00

Note:

f_y : yield strength, ϵ_y : yield strain

f_u : Tensile strength, E_s : modulus of Elasticity

Joint induced shear force

Figure 4.31 shows the beam internal forces and the column shear force acting on the joint core when the ideal flexural strength of the beam develops. The maximum horizontal shear force V_{jh} occurs in the middle region of beam depth just below the neutral axis position of the beam section. V_{jh} is given by the following equation:

$$V_{jh} = T + P - V_{col} \quad (4.23)$$

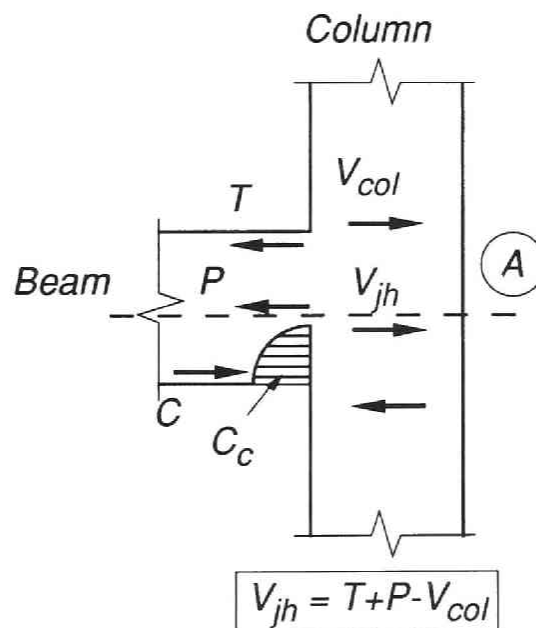


Fig.4.31 Beam internal forces and column shear acting on the joint

T , P and V_{col} denote tensile force developed in non-prestressed reinforcement, tensile force in prestressing steel bar and column shear force. Table 4.14 shows the neutral axis depth, the beam internal forces, the ideal flexural strength calculated using the ACI318-89 [4.11] equivalent rectangular stress block as well as V_{jh} for each test unit.

Theoretical shear strength of joint cores

Table 4.16 summarizes the requirement for the maximum induced joint shear specified in NZS 3101:1982 [4.8], joint shear strengths according to ACI318-89 [4.11] and to “Design Guidelines for Earthquake Resistant Reinforced Concrete Buildings Based on Ultimate Strength Concept” published by AIJ (hereafter referred to as AIJ Guidelines) [4.12]. Prestressing steel bars are usually placed between the top and bottom non-prestressed longitudinal reinforcement in a beam section. This results in a smaller effective depth of prestressed sections than that of non-prestressed sections. Considering prestressed and reinforced concrete beam - column joints with identical dimensions whose beams are designed to have approximately the same flexural strength, the tensile force to be developed in the prestressing steel is larger than that in non-prestressed reinforcement, and the former have greater horizontal shear force in the joint core than the latter.

Table 4.16 Maximum input joint shear force and joint shear strengths

Unit	V_{NZS} (kN)	V_{ACI} (kN)	V_{AIJ} (kN)
RCB-1	791.8	525.8	356.0
PCB-1	761.3	505.5	329.1
PCB-2	761.3	505.5	329.1
PCB-3	761.3	505.5	329.1

Note:

$$V_{NZS} : 1.50\sqrt{f'_c} \cdot A_j \text{ (NZS 3101:1982)}$$

$$V_{ACI} : 1.00\sqrt{f'_c} \cdot A_j \text{ (ACI 318-89)}$$

$$V_{AIJ} : 0.18 \cdot f'_c \cdot A_j \text{ (AIJ Guideline)}$$

where f'_c : compressive strength of concrete (MPa) and A_j : specified cross-sectional area of the joint (mm^2)

Details of steel in beam-column joint

The transverse reinforcement in the joint core of Unit RCB-1 was designed to satisfy the AIJ Guideline requirement [4.12]. The amount of transverse steel of the other test units was identical to that of RCB-1. The transverse steel in each joint core consisted of two rectangular column hoops which were placed around the longitudinal column bars between the top and bottom layers of longitudinal beam steel. The average spacing between the tie centers was 100 mm. The two ties were formed from 9 mm diameter round bar with a yield strength of 316 MPa.

Transverse shear reinforcement required in the joint core, based on the provisions of ACI 318-89 [4.11], NZS 3101:1982 [4.8] and AIJ Guidelines [4.12], are listed in Table 4.17. The amount of shear reinforcement provided in the joint core of all test units did not meet the amount required by ACI 318-89 [4.11] and NZS 3101:1982 [4.8]. Even after considering the effect of prestressing force on the joint core shear, NZS 3101:1982 [4.8] still requires much more reinforcement than the other codes. The NZS 3101:1982 [4.8] requirements for joint core reinforcement are generally considered to be excessive. AIJ Guidelines [4.12] require more steel in Unit PCB-2 and PCB-3 than provided.

The method for evaluating the anchorage strength of a reinforcing bar related to the bearing strength on concrete inside the 90-deg hook proposed by Fujii et al. [4.13] from both monotonic and cyclic loading tests on beam-column joint assemblages indicated that the anchorage strength of the beam longitudinal reinforcement of the test units was at least twice its yield tensile force. The 90-deg hook was followed by the tail longer than $12d_b$. d_b denotes the diameter of longitudinal reinforcement.

Table 4.17 Required total area of joint shear reinforcement

Unit	Ash.prov (mm ²)	Ash.NZS (mm ²)	Ash.ACI (mm ²)	Ash.AIJ (mm ²)
RCB-1	256	832	602	132
PCB-1	256	1084	556	234
PCB-2	256	1050	556	270
PCB-3	256	927	556	300

Note:

Ash.prov : Total area of horizontal joint shear reinforcement provided in the joint

Ash.NZS : Total area of horizontal joint shear reinforcement required by NZS3101:1982

Ash.ACI : Total area of horizontal joint shear reinforcement required by ACI318-89

Ash.AIJ : Total area of horizontal joint shear reinforcement required by AIJ Guideline

Loading

The unit was rotated by 90 degrees and set in the loading rig as shown in Fig.4.32. A horizontal load was applied at the end of the beam representing shear induced by seismic loading. The ends of the column were held on the same horizontal line between the pin and roller supports during the test and the applied beam load induced reactive shears at the ends of the column. By reversing the direction of the horizontal beam load, the effect of earthquake loading was simulated.

The first loading cycle was up to the first yield displacement, and this was followed by a series of deflection controlled cycles in the inelastic range comprising two full cycles to each of the displacement ductility factors of ± 2 , ± 3 , and higher. The "first yield" displacement measured at the end of the beam was found when the strain reading of the outermost non-prestressed longitudinal reinforcement exceeded its yield strain and the sudden change of stiffness in the applied horizontal load - beam end deflection curve was observed.

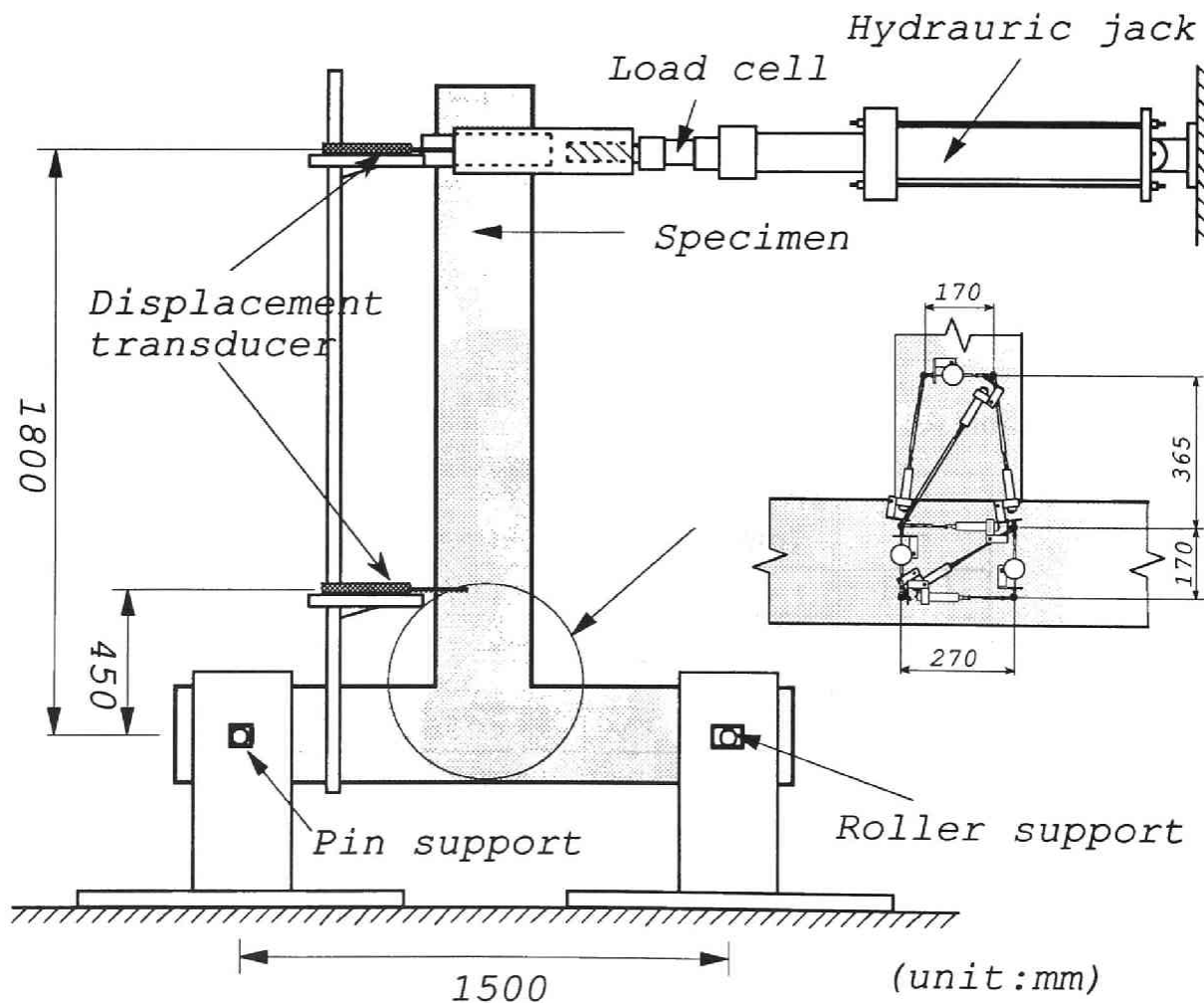


Fig.4.32 Loading setup and measuring devices

Measurements

Beam end deflection was measured by a linear displacement transducer which was attached to the pole fixed to the mid-height of the column as shown in Fig.4.32. The deflection was consisted of the deformation of the beam, joint and column of half-height. It did not include the column deformation between the pin support and the place to which the measuring pole was fixed. No visible crack could be found in this part of the column and the deformation of this part was considered to be small enough to be disregarded. Curvature and shear deformation of the beam in the potential plastic hinge region and shear distortion of the joint core were measured and calculated from the readings of the linear displacement transducers attached to the units as shown in Fig.4.32 by the calculation method described in Chapter 4.3.

Strain gauges were attached to the beam longitudinal reinforcement at the beginning of 90 degree hook, at the column face and at the center of these points. They were also attached to the joint transverse reinforcement on both sides of the column.

4.4.3 General Behaviour of Test Units

Figs.4.33(a)-(d) show the horizontal deflection at the end of the beam plotted against the corresponding load of the beam for each unit. In unit RCB-1, after the maximum moment had been reached at the ductility factor of 2 (beam rotation angle of approximately 3%) in each direction, a reduction in stiffness and strength with pinched hysteresis was observed. This is mainly because of the bond deterioration of beam longitudinal reinforcement in the joint, which followed the yield penetration of longitudinal bars. Unit PCB-1 with a prestress level of 0.06 was able to be loaded to beyond a beam rotation angle of 1/15 with little reduction in stiffness and strength. The load - deflection hysteresis loops indicated that larger energy dissipation could be expected in PCB-1 than in Unit RCB-1. The performance of the test unit PCB-2 with a prestressing force of $0.12 f'_c A_g$ was much better than that of the reinforced concrete joint assemblage but a little worse than that of the assemblage with a prestressing force of $0.06 f'_c A_g$. Crushing and spalling of the cover concrete followed by a small reduction in strength was observed. Buckling of the beam longitudinal bars followed by little reduction in moment capacity was observed at a beam rotation angle of approximately 6%. In PCB-3 with the largest prestress level of 0.18, the cover concrete of the beam spalled off, which led to a small reduction in strength. Buckling of the beam longitudinal reinforcement resulted in a slight reduction of strength, which was larger than that in PCB-2. Buckling of reinforcement did not result in such a large reduction in strength because moment capacity carried by non-prestressed reinforcement was rather small.

It should be noted in Unit PCB-3 that the reduction in strength between the first and second loading cycles to the same displacement became significant as the reversed

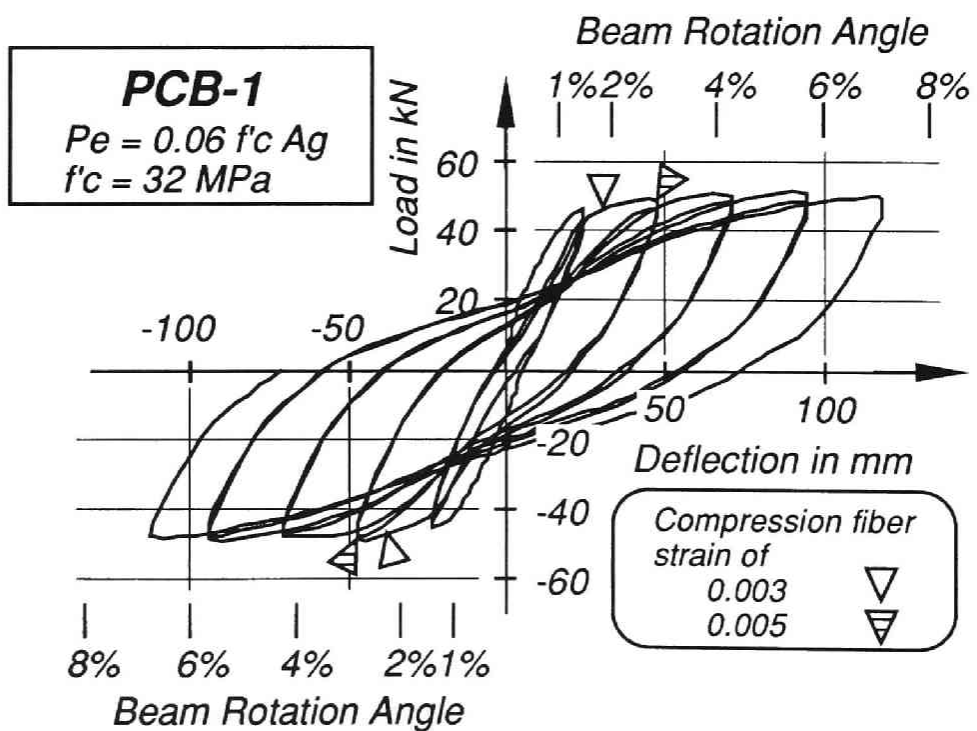
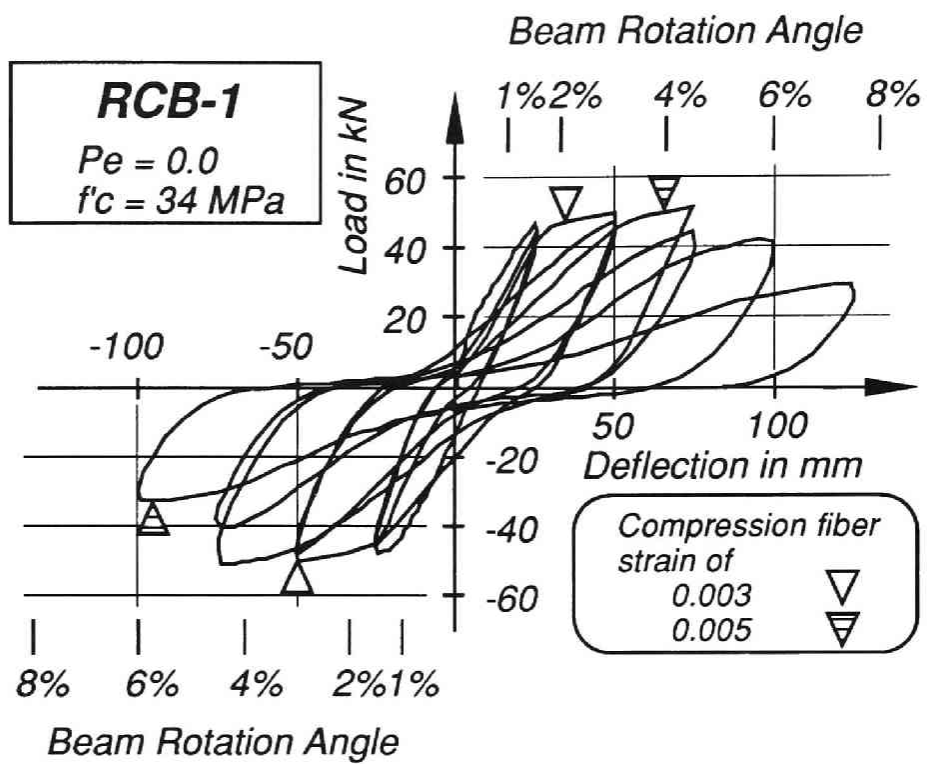


Fig.4.33(a) Horizontal load - deflection relationships at the beam ends

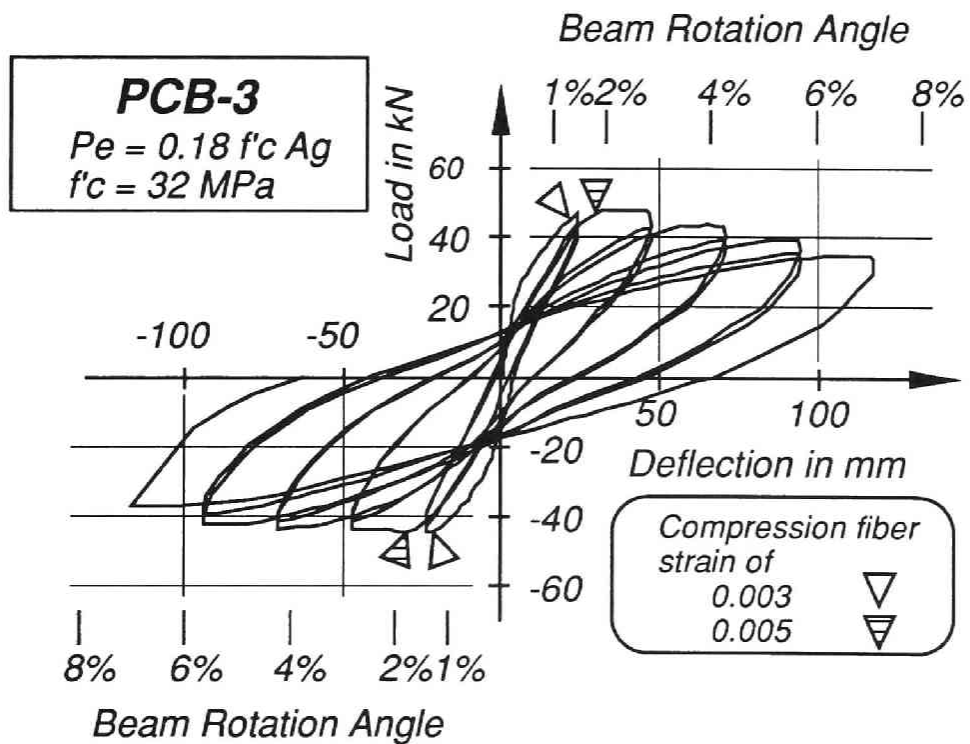
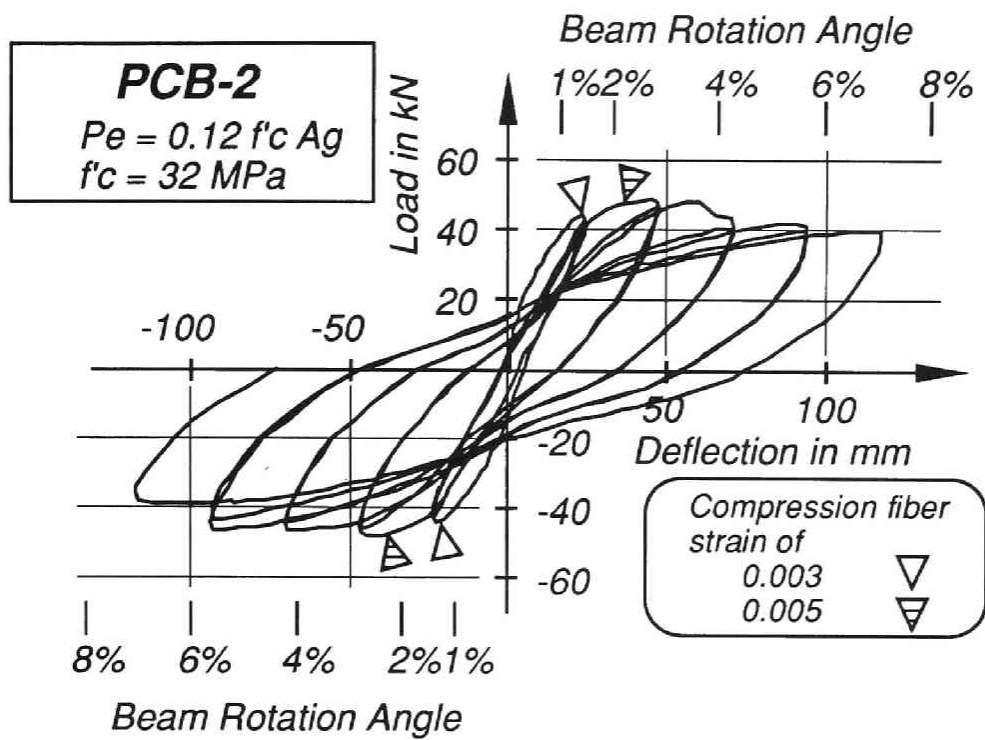


Fig.4.33(b) Horizontal load - deflection relationships at the beam ends

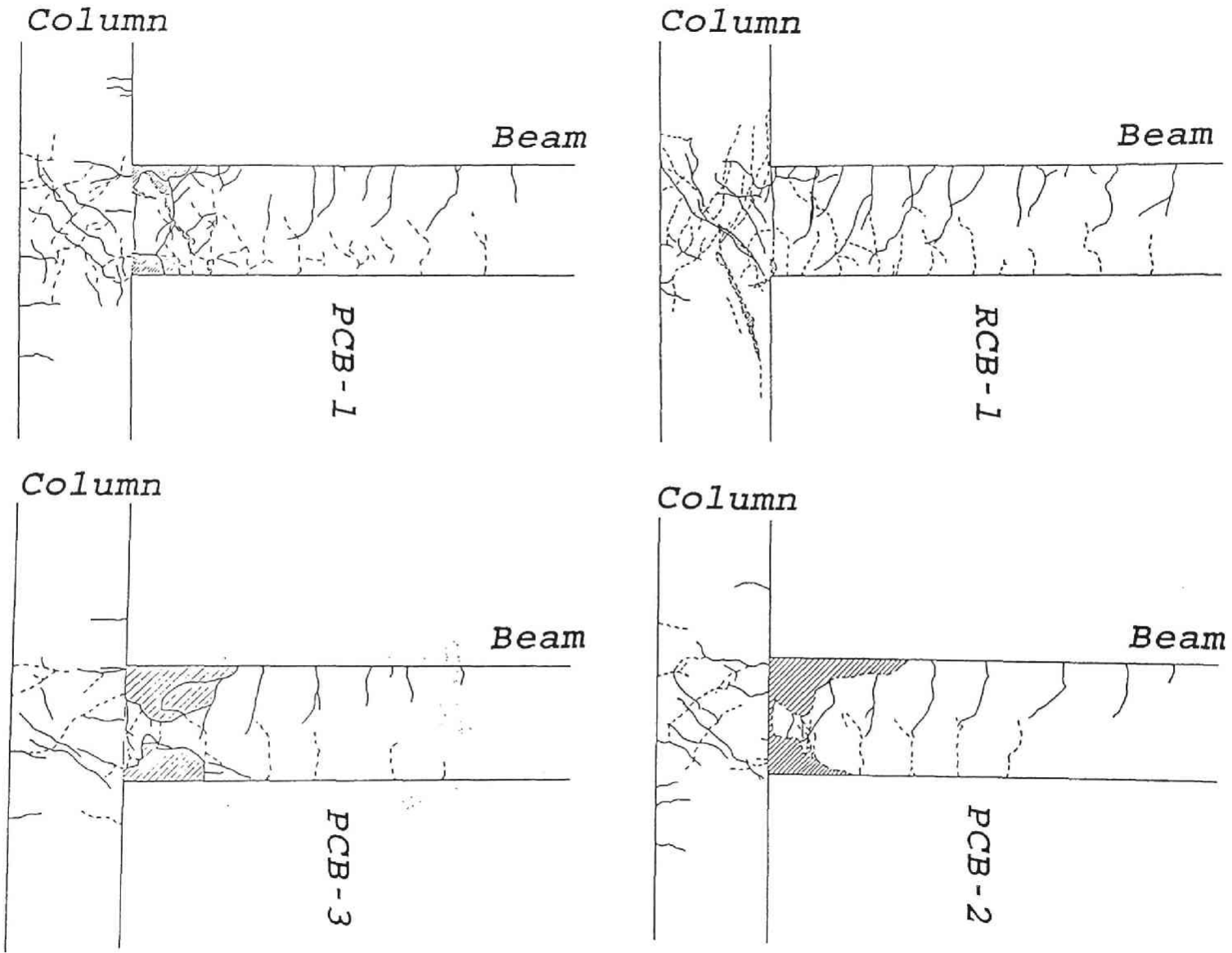


Fig.4.34 Test units after testing

cyclic loading progressed. This is because the concrete in compressive region of the section of the test units with a large prestress was subjected to larger compressive stress than that of the reinforced concrete test unit or the prestressed concrete unit with a small or moderate prestressing force at the same deflections. The points on the load - deflection curves where concrete compressive strains at extreme compression fiber first reached 0.3 and 0.5% are indicated in Fig.4.33. The strains included the initial strain due to introduction of prestress. As the prestress introduced into the beam section increased, the deflection where these strains were first reached decreased.

Figs.4.34(a)-(d) show the test units after testing. In Unit RCB-1, the joint shear cracks run from corner to corner of the joint core. It was observed in the prestressed concrete units that the cracks in the joint core extended from the anchorage region of prestressing steel to the compression regions of the beam critical section. This indicates that the concrete compression strut originated in the anchor of prestressing steel.

4.4.4 Details of Test Results

Hysteretic Restoring Force Characteristics

Equivalent viscous damping

Fig.4.35 shows equivalent viscous damping of the first loading cycle to each specified displacement plotted against the ductility factors. Until the ductility factor of 2 (beam rotation angle of approximately 1/30), the equivalent viscous damping for RCB-1 was the largest but the difference was not significant. As the loading cycle progressed, the equivalent viscous damping in RCB-1 decreased to less than that at the ductility factor of 2 while in the other test units the equivalent viscous damping increased proportionally with the ductility factor. This is easily predicted by the shape of load - deflection hysteresis loops shown in Fig.4.33. Past research has shown less energy dissipation of prestressed concrete members than reinforced concrete. However, in the case of beam - column joints the experimental results revealed that this is disputable.

The ductility factor attained four (beam rotation angle of approximately 4%) when the difference of equivalent viscous damping between the reinforced concrete test unit and the prestressed concrete test units became significant. In practical moment resisting frames such a large deformation is not expected to be reached. However, closer and more careful observation disclosed that in RCB-1 reduction in moment capacity due to cyclic loading was more noticeable than in the prestressed concrete test units. In these tests, two full cycles to each displacement ductility factor were imposed. If more cycles had been imposed on the units, further reduction in capacity and stiffness might have been observed in Unit RCB-1.

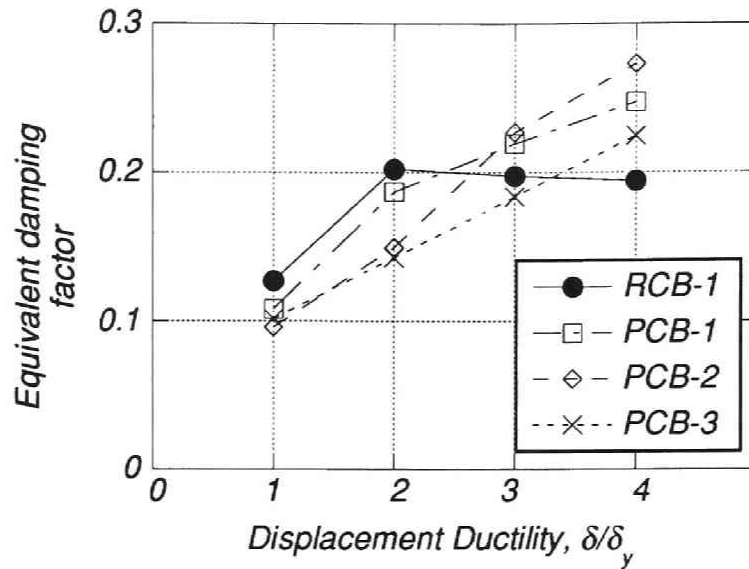


Fig.4.35 Equivalent damping factor

Deformation in beam plastic hinge region and joint core

Figures 4.36(a)-(d) show moment - curvature relationship in beam potential plastic hinge region of each test unit. The experimental curvature is the average of that measured over 365 mm gauge length, which consisted of the beam potential plastic hinge region of 300 mm from the column face and part of the joint region of 65 mm from the column face. The moment is that at the column face. Therefore, the curvature measured is supposed to include additional deformation due to yield penetration of beam longitudinal bars in the joint core region. Comparison of the moment - deflection and moment - curvature curves for each unit gives a good indication of where the inelastic deformation was concentrated. In all cases the major inelastic contribution to beam end deflection came from the deformation at the plastic hinge region in the beam close to the column face.

Figures 4.36(a)-(d) also show moment - curvature curves derived by the cyclic moment curvature theory described in Chapter 3 to make the comparisons. In all cases the cover concrete was assumed to have spalled off at strains greater than 0.007. Buckling of the non-prestressed reinforcement was not considered. It is noteworthy that the difference between the experimental and theoretically predicted curves are of great significance in RCB-1, while in the prestressed concrete units the experimental curves can be well followed by the predicted theoretical curves with respect to the moment capacities and the general shape of the hysteresis loops. It has been recognized that the shape of moment - curvature hysteresis loops in the cross section of reinforced concrete members are largely affected by the shape of stress - strain curves of longitudinal reinforcing steel. However, the experimental curve of RCB-1 showed large pinching and reduction in load carrying capacity which was caused by the

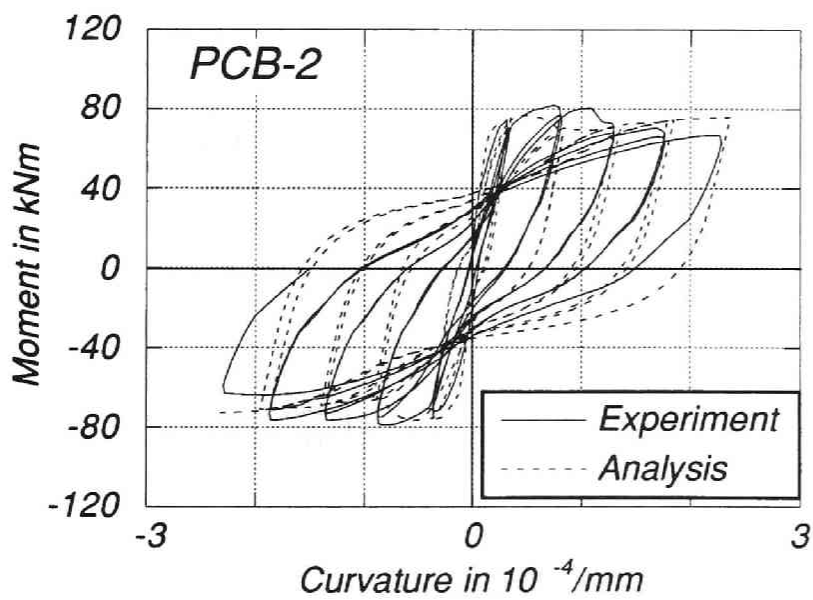
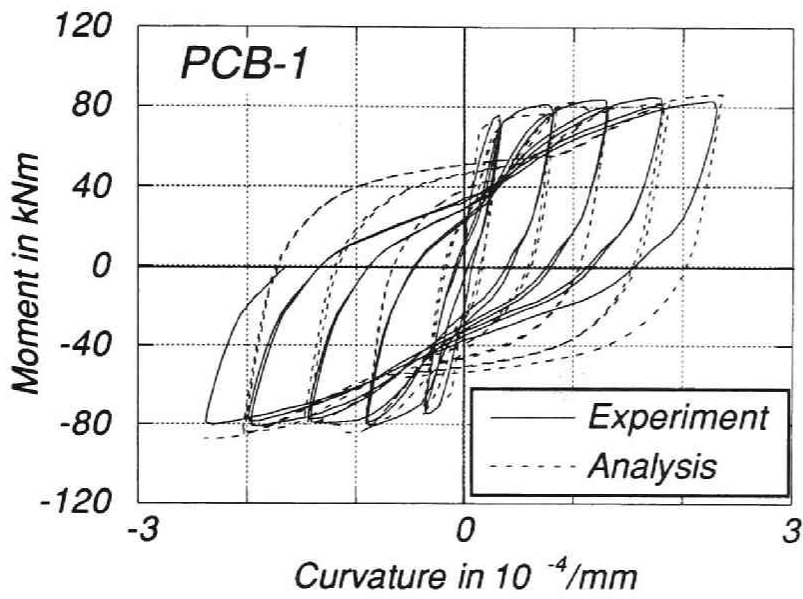


Fig.4.36(a) Moment at the column face - average curvature relationships measured in the beam plastic hinge regions

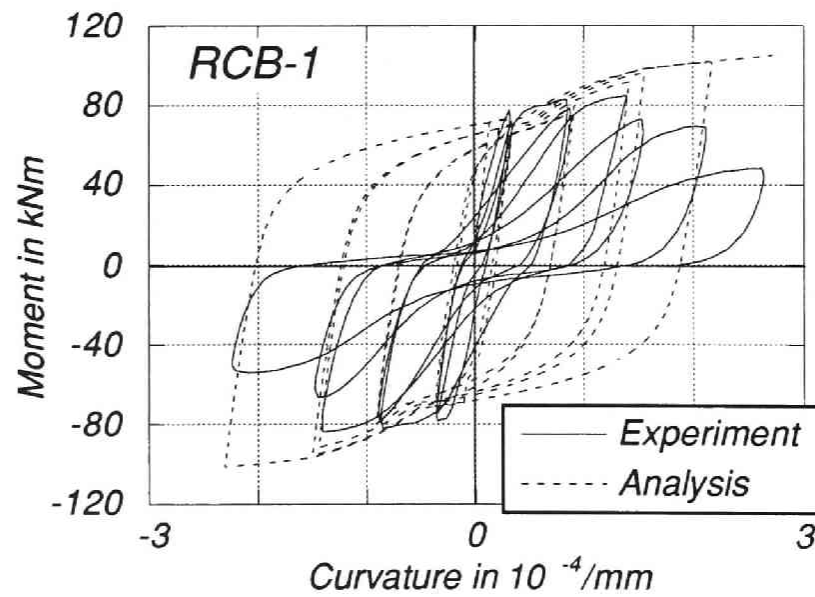
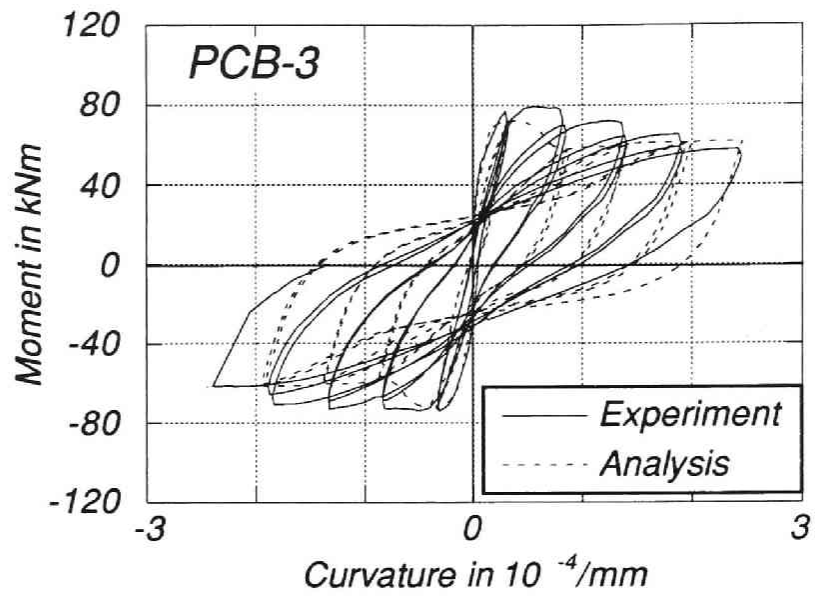


Fig.4.36(b) Moment at the column face - average curvature relationships measured in the beam plastic hinge regions

deterioration of bond, causing slip between concrete and beam longitudinal reinforcement in the joint core. Even in the prestressed concrete test units the deterioration of bond to be followed by yield penetration of beam longitudinal reinforcement is unavoidable, but it was much less significant than that in RCB-1. The basic assumption which was made when deriving the cyclic moment curvature theory for reinforced and prestressed concrete sections described in Chapter 3 appears to be more justified in the prestressed concrete test units than in the reinforced concrete test unit. The assumption is that plane sections before bending remain plane after bending, which implies that the longitudinal strain in the concrete and the steel at the various points across a section is proportional to the distance from the neutral axis. This assumption cannot be applied to the longitudinal reinforcing steel which slips relative to the surrounding concrete.

The maximum shear distortion angles measured in the joint cores at the maximum deflection in the first loading cycle to each specified displacement are plotted in Fig.4.37 against prestress levels assigned to the test units. As the prestress level increased, the maximum shear distortion angles decreased drastically. The maximum shear distortion angle in the final loading run of RCB-1 was more than twice as large as that of PCB-1. In Units PCB-2 and PCB-3 with twice and three times larger prestress levels than in Unit PCB-1, respectively the maximum shear distortion angles did not proportionally reduce to half and one-third of that Unit PCB-1. A prestressing force as small as $0.06 f'_c A_g$ resulted in much smaller shear distortion angles of the joint core than in the reinforced concrete joint. However, prestressing forces larger than $0.12 f'_c A_g$ did not result in much smaller shear distortion angle or in stiffer joint cores than prestressed concrete units with a prestressing force of $0.06 f'_c A_g$.

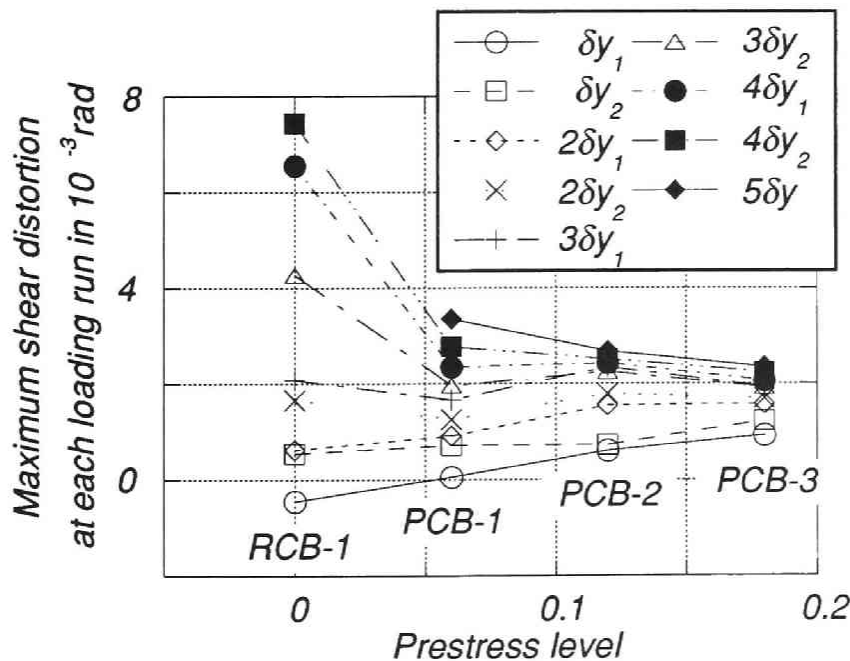


Fig.4.37 Maximum shear distortion angles measured in the joint cores

As described, the yield penetration of beam longitudinal reinforcement into the joint core as well as the bond deterioration followed by the formation of full depth cracks at the critical section of the beam were supposed to be the main reasons of the pinched hysteresis loops of RCB-1. This is confirmed by Fig.4.38. The figure indicates longitudinal strains at the center of gravity in the beam section measured within the plastic hinge region when the load - deflection hysteresis loops crossed the horizontal axis. These strains correspond to the residual longitudinal strains in the first loading run to each positive ductility factor. The light prestressing force of $0.06f'_c A_g$ confined the beam elongation much more effectively than in the reinforced concrete test unit. The concrete strains measured at the extreme fibers of the beam section in each test unit plotted against the measured deflection of the beam are shown in Figs.4.39(a)-(d). In RCB-1 the strains at the extreme fibers of the section were in tension during almost all loading cycles. If the tensile strains in the concrete were assumed to be negligible, then this shows that full depth cracks had developed. Contrarily, in the prestressed concrete test units some compressive region in the beam section always existed during the loading cycles although full depth cracks were observed in the vicinity of the beam deflection of zero in Unit PCB-1 with the smallest amount of prestressing force.

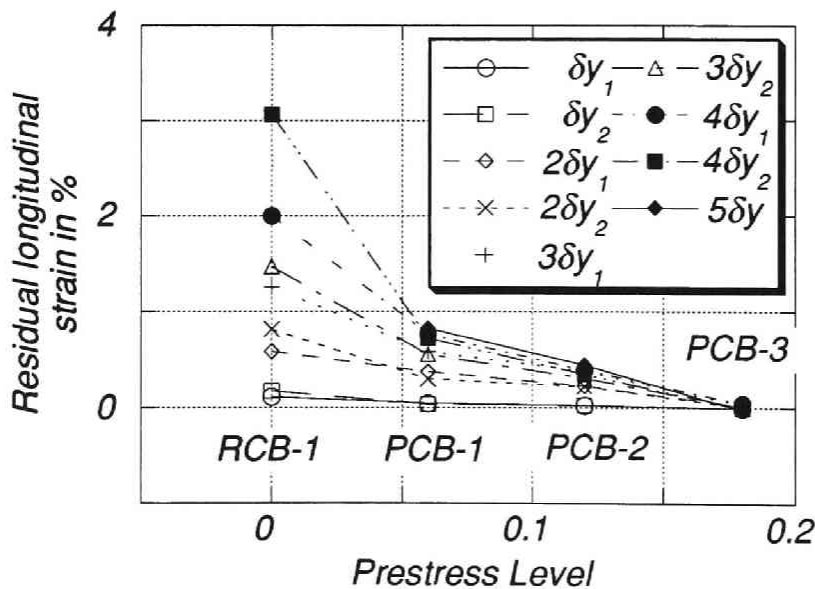


Fig.4.38 Measured longitudinal strains at the center of gravity in the beam section

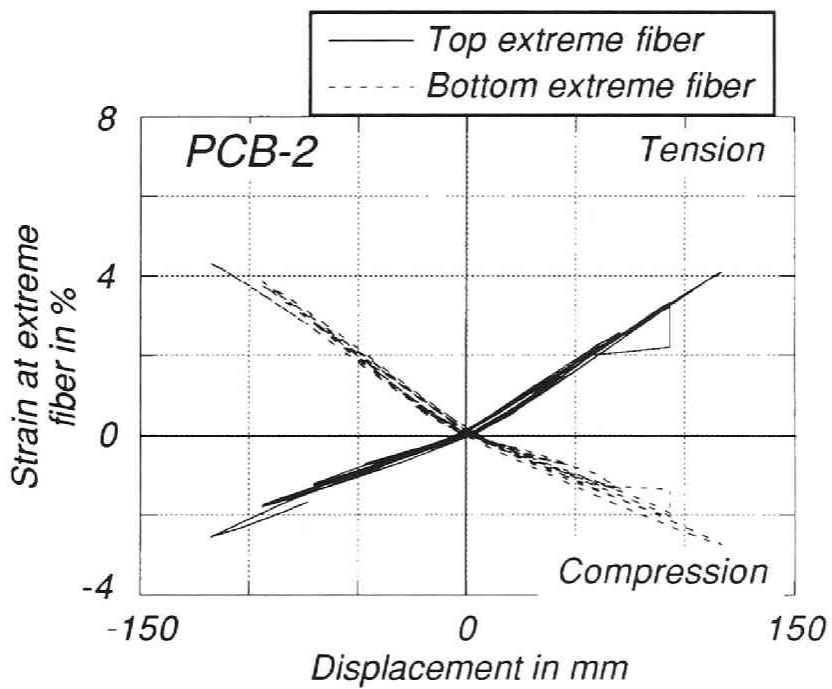
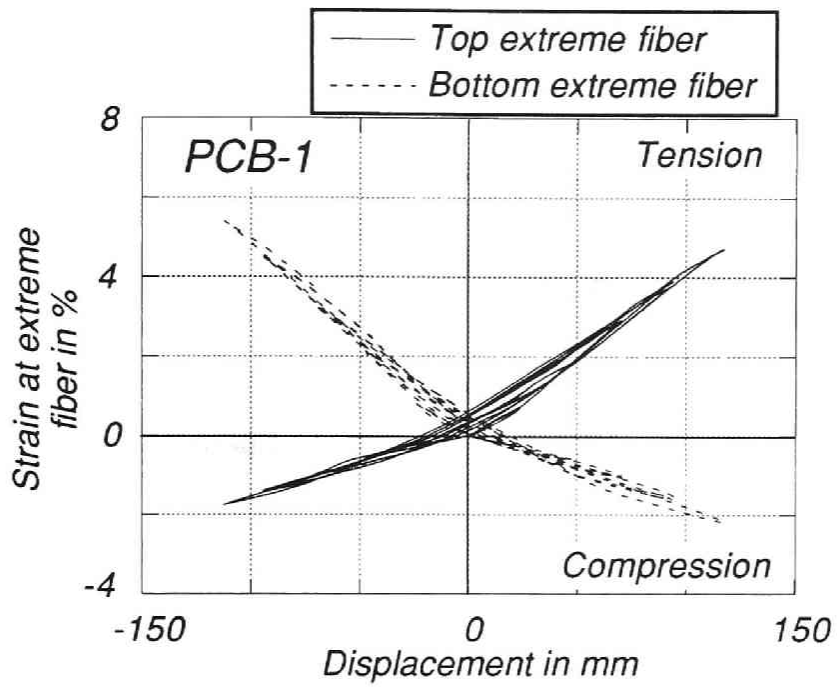


Fig.4.39(a) Concrete strains measured at the extreme fibers of the beam section

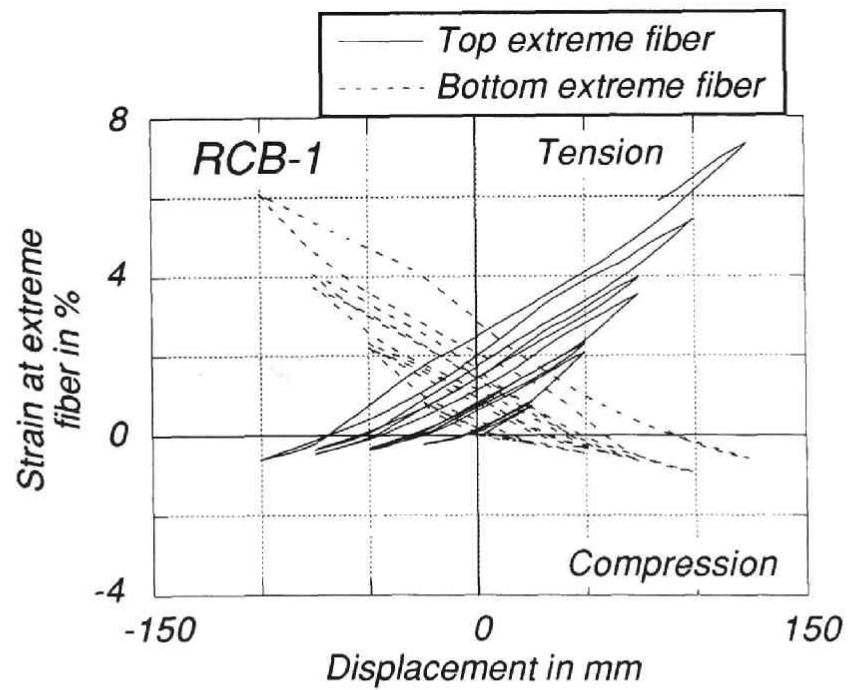
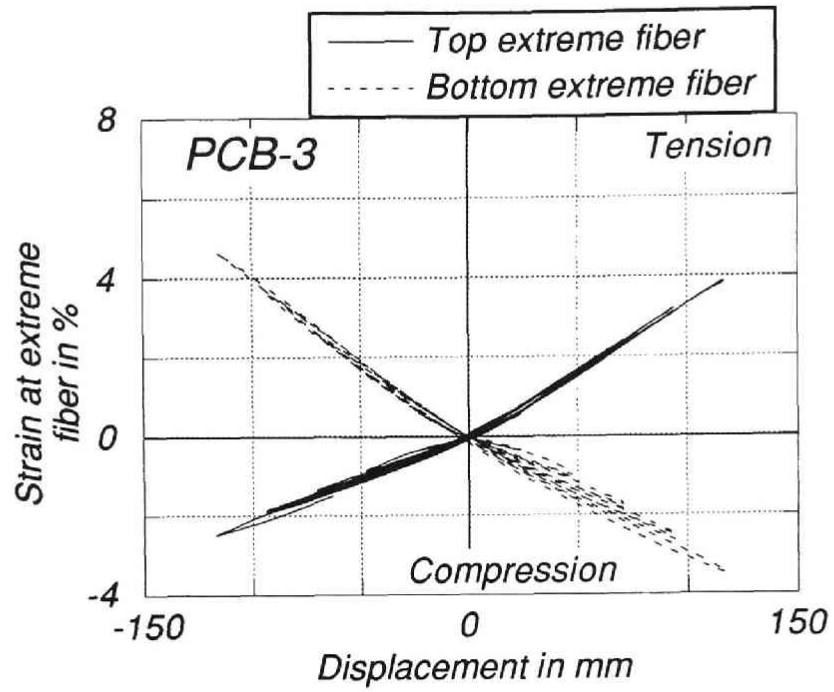


Fig.4.39(b) Concrete strains measured at the extreme fibers of the beam section

As described above, it is difficult to predict correctly the behaviour of a reinforced concrete beam - column joint assembly based on experimental and analytical results of beam specimens because the behaviour was largely affected by the joint core. It is impossible to completely impede beam longitudinal reinforcement from coming out of the joint core and to prevent full depth cracks from developing in a reinforced concrete beam - column joint assembly. Especially, it is unavoidable when the amount of beam top reinforcement is much greater than that of bottom reinforcement. Contrarily, the behaviour of the prestressed concrete beam - column joint assembly can be predicted without considering the shear deformation and/or the bond deterioration of beam longitudinal reinforcement, because the joint core keeps almost its elastic stiffness and the beam is not predominantly affected by the shear behaviour of the joint core due to prestressing force.

What is described above greatly influences seismic response analysis of a frame. In order to predict seismic responses of reinforced concrete frames as precisely as possible, the shear behaviour of beam - column joints need to be idealized and involved in the analysis. Besides, it is necessary to consider beam longitudinal reinforcement coming out of the beam - column joint core in the idealization of the behaviour of beam plastic hinge regions. However, the assumption of rigid beam - column joint core can be justified in the prestressed concrete beam - column joint assemblies. Moment - curvature hysteresis loops in beam plastic hinge regions can be idealized based on the analyses assuming that plane sections before bending remain plane after bending. Thus, the past research which has indicated larger responses of prestressed concrete frame structures than those of reinforced concrete should be reexamined.

Shear Behaviour of Joint core

The experiments reported in Chapter 4.3 have revealed that NZS 3101:1982 [4.8] underestimates the beneficial effect of prestressing force to joint shear resistance. However, a quantitative conclusion could not be reached because of measured tensile forces in the transverse reinforcement dispersing in a wide range and disputable estimation of joint shear force resisted by concrete.

Figure 4.40 shows the maximum total tensile force in the transverse reinforcement measured in the first loading run to each positive ductility ratio plotted against prestress levels. It is clear that larger prestressing force resulted in smaller tensile force in the transverse reinforcement.

The ratios of total tensile force in the prestressed concrete units to that in the reinforced concrete test unit measured at ductility factor of 3 are 0.603, 0.429 and 0.301 for PCB-1, PCB-2 and PCB-3, respectively. These values are almost as large as the ratios of moment capacity carried by non-prestressed reinforcing steel to the total moment capacity resisted by non-prestressed and prestressed reinforcement. Paulay et al. [4.18] have proposed that shear force induced in the joint core is resisted by two

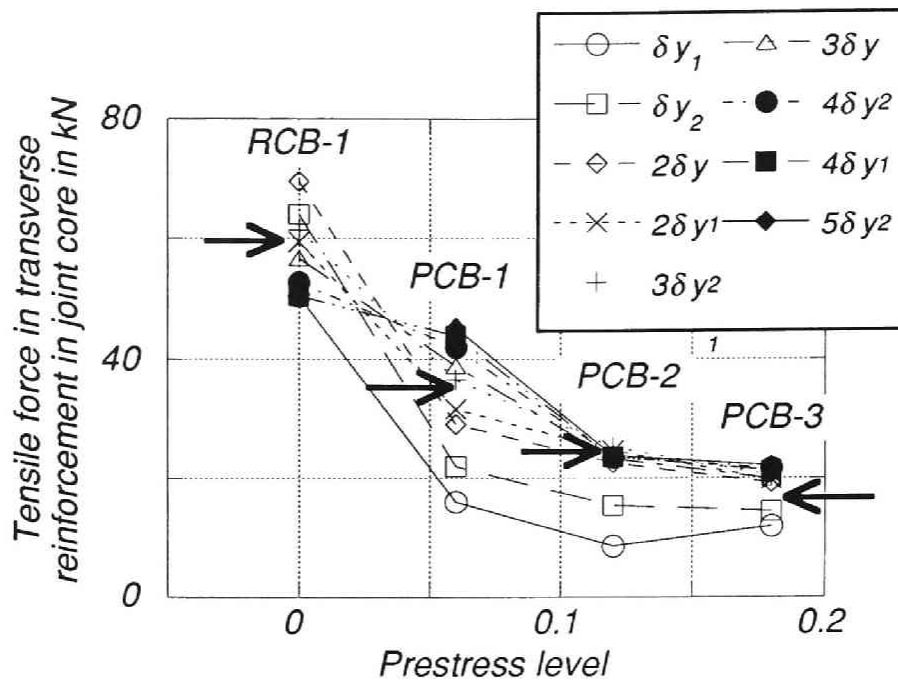


Fig.4.40 Tensile force measured in the transverse reinforcement in the joint cores

representative mechanisms : a truss mechanism consisted of transverse reinforcement and forces in longitudinal reinforcement of beams and columns transferred by bond action, and a strut mechanism consisted of concrete strut. In case of the prestressed concrete test units, shear force induced by longitudinal beam reinforcement is assumed to be attributed to the truss mechanism while the shear force transferred by the prestressing steel bar into the joint core is assumed to be assigned to the strut mechanism. This is because of poor bond between the prestressing steel and the surrounding concrete. In addition, about the same extent of bond deterioration of the beam longitudinal reinforcement was assumed in all test units. The total tensile force measured in the transverse reinforcement of RCB-1 was approximately 60 kN. Therefore, predicted tensile forces in PCB-1, PCB-2 and PCB-3 are 36.2 kN, 25.7 kN and 18.1 kN, respectively. They are indicated by arrows in Fig.4.40. The predicted values agree well with the measured values although in PCB-1 the measured values are scattered depending on the ductilities.

The design methods for beam - column joints prescribed in NZS 3101:1982 [4.8] are fundamentally based on the assumption that the induced shear force in the joint core is assigned to both concrete and transverse reinforcement in the joint core. On the contrary, the design assumptions of ACI 318-89 [4.11] and AIJ Guidelines [4.12] are based on the experimental results that indicated that the joint shear strength was not sensitive to joint shear reinforcement. The shear strength of the beam - column joint is assumed to be defined by compression failure of concrete diagonal strut. Applying the design equation specified in AIJ Guidelines [4.12] to the beam - column joints of the test units, the shear strength of each unit is indicated by the solid line in Fig.4.41.

As described in the previous chapter, when prestressed and reinforced concrete beams have the same moment capacity at the column face in beam - column joint assemblies, the horizontal shear force induced in the joint of a prestressed concrete assembly is greater than that of a reinforced concrete assembly. Thus, shear forces induced in the prestressed concrete test units are larger than those obtained by the AIJ methods. Nevertheless, as shown in the experimental results the larger prestressing force resulted in smaller shear distortion in the joint core and in fewer visible cracks.

To consider these beneficial effect of prestressing force, the joint shear strength V_{ju} is assumed to be given by the following equation based on the similar assumption to NZS 3101:1982 [4.8] that part of the shear force is attributed to the effective prestressing force.

$$V_{ju} = 0.18 f'_c b_j D_j + \alpha \cdot P_e \tag{4.20}$$

where, f'_c = compressive strength of concrete (indicated by σ_B in AIJ Guidelines [4.12])

b_j = effective depth of joint

D_j = column height or horizontal projected length of longitudinal reinforcement with a standard 90 degree hook.

α = coefficient of efficiency of prestressing force on shear strength of beam - column joint.

P_e = effective prestressing force

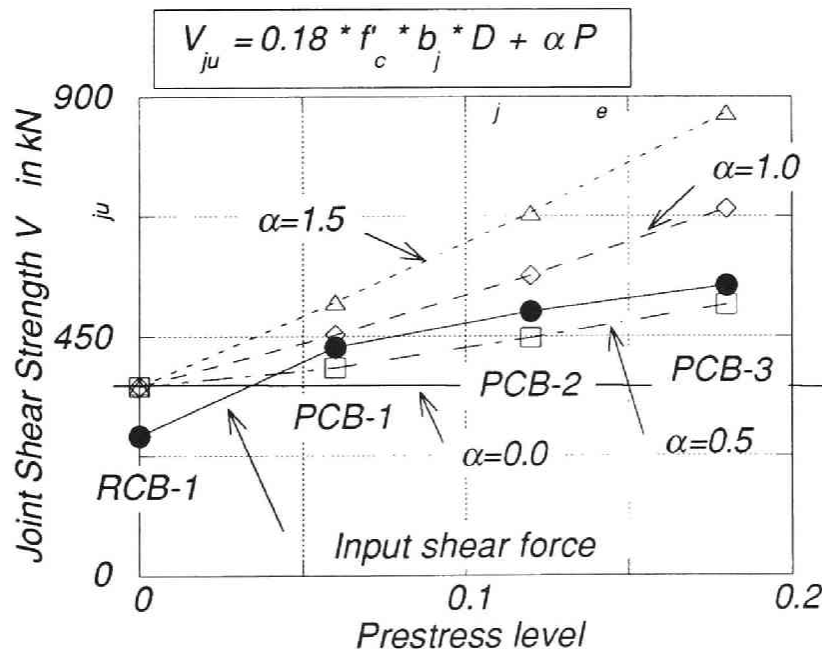


Fig.4.41 Joint shear strength according to AIJ Guidelines and proposed equation

Judging from the experimental results reported here, $\alpha = 1.0$ could be adopted, which leads to increment of shear strength by P_e . However, there is no available data obtained from the experiments in which prestressed concrete beam - column joint assembly test units failed in joint shear. Thus, we have to wait for a future research to define the upper limit of shear strength.

4.5 Re-examination of the Test Results in Thompson and Park's Research Work [4.6]

On the basis of their test results NZS 3101:1982 [4.8] specifies the contribution of the beam prestress to the joint shear strength. The test units [4.6] were designed according to the shear design method of a member in ACI318-71 [4.3], because ACI318-71 [4.3] did not have any provision for the design of beam-column joints. It is of great interest to re-examine the test results with respect to the current seismic design code provisions and knowledge which has been obtained since it was published.

Table 4.18 shows the neutral axis depth, the beam internal forces, ideal flexural strength calculated using the ACI methods. The total horizontal shear forces V_{jh} across the joints are listed in Table 4.19. According to ACI318-89 [4.11], the nominal shear strength of the joint with beams on two opposite faces shall be less than $1.25\sqrt{f'_c}A_j$ (f'_c in MPa and A_j in mm^2). It is given in Table 4.19 for each unit, assuming the strength reduction factor of 1.0. They are 93 to 125% of the shear strength obtained by the ACI Code [4.11]. The maximum value of 125% corresponds to Unit 9. However, the test units with $V_{jh} / V_{u.ACI}$ less than unity did not always fail in beam flexure. These values with one exception met the requirement of $1.5\sqrt{f'_c}A_j$ given in NZS 3101:1982 [4.8]. The joint shear force V_{jh} of Unit 9 was larger than the limitation prescribed in NZS 3101 [4.8].

The transverse reinforcement provided in the joint core met the requirement of ACI 318-89 [4.11] as listed in Table 4.19. The ratio of the total cross-sectional area of transverse reinforcement provided in the joint core to that required by ACI 318-89 [4.11] ranges between 1.22 and 1.57.

In accordance with NZS 3101:1982 [4.8], the ideal horizontal joint shear strength provided by concrete shear resisting mechanism, V_{ch} , only is given by the following equation, when the minimum average compression stress on the gross concrete area of the column above the joint exceeds $0.1f'_c / C_j$.

$$V_{ch} = \frac{2}{3} \sqrt{\frac{C_j P_e}{A_g} - \frac{f'_c}{10}} b_j h_c \quad (4.22)$$

Table 4.18 Theoretical internal forces in beams at flexural strength and maximum shear forces

Unit	c (mm)	T1 (kN)	T2 (kN)	T3 (kN)	T4 (kN)	C5 (kN)	Cc (kN)	Mb (kNm)
1	163.3	335.1	307.9	186.5	40.1	40.1	829.5	168.9
2	81.5	-	350.7		368.9	253.2	466.4	195.5
3	70.6	-	-		526.0	129.1	396.9	188.9
4	161.5	344.9	324.4	200.7	46.7	45.4	871.8	179.4
5	164.3	575.4		334.2	46.3	46.3	909.1	195.9
6	94.2	-	355.6		374.7	201.6	528.7	193.0
7	101.6	230.1	216.7	123.7	160.6	162.9	568.3	180.9
8	160.5	338.6	310.6	188.7	47.6	47.2	838.4	177.5
9	175.3	555.4		318.6	49.0	47.2	875.8	184.1
10	92.2		335.5		360.5	150.0	546.9	187.2

Note:

- c : Neutral axis depth
 T1, T2 and T3 : Tensile forces in prestressing tendons 1, 2 and 3
 T4 : Tensile force in nonprestressed steel
 C5 : Compressive force in nonprestressed steel
 Cc : Compressive force in concrete
 Mb : Theoretical flexural strength of beam

Table 4.19 Nominal shear strength in ACI 318-89 and joint shear strength proposed by Thompson and Park

Unit	V_{jh} (kN)	$V_{u,ACI}$ (kN)	$V_{jh} / V_{u,ACI}$	A_{prov} (mm ²)	A_{ACI} (mm ²)	A_{prov} / A_{ACI}
1	943.4	874.2	1.079	397.1	263.7	1.506
2*	952.3	954.2	0.998	397.1	314.1	1.264
3*	921.2	944.1	0.976	397.1	307.5	1.291
4	983.5	913.1	1.077	397.1	287.7	1.380
5*	1108.1	930.0	1.192	397.1	298.4	1.331
6*	970.1	940.3	1.032	397.1	305.0	1.302
7	872.2	937.7	0.930	397.1	303.4	1.309
8*	961.2	890.5	1.079	397.1	273.6	1.451
9*	1081.4	864.6	1.251	573.0	364.5	1.572
10	930.1	981.4	0.948	573.0	469.6	1.220

Note:

* Eventually failed in joint core shear in the tests during inelastic loading cycles

V_{jh} : Theoretical maximum horizontal shear force applied to joint core

$V_{u,ACI}$: Joint shear strength specified in ACI318-89 = $1.25\sqrt{f'_c} \cdot A_j$

A_{prov} : Total area of joint shear reinforcement provided

A_{ACI} : Total area of joint reinforcement required by ACI318-89

where, $C_j = \frac{V_{jh}}{V_{jx} + V_{jz}}$

V_{jx} = total horizontal joint shear force in x direction

V_{jz} = total horizontal joint shear force in z direction

P_e = design axial load in compression with given eccentricity due to gravity and seismic loading acting on the member during an earthquake

A_g = gross area of section

b_j = effective width of joint

h_c = overall depth of column in the direction of the horizontal shear to be considered

V_{ch} of each unit was calculated and listed in Table 4.20 with the ideal horizontal joint shear strength provided by horizontal joint shear reinforcement, V_{sh} .

The shear strength of joint cores are expressed as $V_{ch} + V_{sh}$ without accounting for prestressing force. Compared with V_{jh} , the values, $V_{ch} + V_{sh}$ are larger than V_{jh} . In Unit 9, the shear reinforcement in the joint core itself was theoretically capable of carrying 121% of the maximum shear force induced in the joint without the assistance of a concrete shear resisting mechanism. Without the assistance of prestressing force, all test units are considered to have little possibility of joint shear failure. However, Units 2, 3, 5, 6, 8 and 9 were reported to have failed in joint shear.

The beneficial effect of axial load on columns and shear reinforcement in the joint core would be overestimated in NZS 3101:1982 [4.8]. The provisions in ACI 318-89 [4.11], according to which several test units are considered to have high possibility of joint shear failure because of high shear forces introduced into the joint cores, may give a better suggestion of design of beam-column joint. As described before, the design assumptions of ACI 318-89 [4.11] are based on the experimental results that indicated that the joint shear strength was not sensitive to joint shear reinforcement. Referring to the experimental results, it can be concluded that the design assumptions of ACI 318-89 [4.11] can be justified.

Table 4.20 Ideal horizontal joint shear strength specified in NZS 3101:1982

Unit	V_{jh} (kN)	V_{ch} (kN)	V_{sh} (kN)	$V_{ch} + V_{sh}$ (kN)	$V_{jh} / (V_{ch} + V_{sh})$
1	943.4	181.8	943.4	1125.2	0.838
2*	952.3	170.0	943.4	1113.4	0.855
3*	921.2	171.6	943.4	1115.0	0.826
4	983.5	176.3	943.4	1119.7	0.878
5*	1108.1	173.8	943.4	1117.2	0.992
6*	970.1	172.2	943.4	1115.6	0.870
7	872.2	172.6	943.4	1116.0	0.782
8*	961.2	179.6	943.4	1123.0	0.856
9*	1081.4	183.1	1312.8	1495.9	0.723
10	930.1	165.5	1312.8	1478.3	0.629

Note:

* Eventually failed in joint core shear in the tests during inelastic loading cycles

V_{jh} : Theoretical maximum horizontal shear force applied to joint core

V_{ch} : Ideal horizontal joint shear strength provided by concrete shear resisting mechanism

V_{sh} : Ideal horizontal joint shear strength provided by horizontal joint shear reinforcement

4.6 Conclusions

On the basis of the test results described in Chapter 4.3 the following conclusions are derived.

1. It has been pointed out by past research that reinforced concrete members are superior to prestressed concrete with respect to energy dissipation and deformability. However, this conclusion was obtained from the tests on prestressed concrete beams. In case of a beam-column subassembly, its behaviour may be largely dominated by the performance of the jointing part. Thus, hysteresis loops of a prestressed concrete beam-column subassembly might be better than those of a reinforced concrete because prestress introduced into the beam can improve the shear behaviour of the beam-column joint core.
2. Larger prestress has more beneficial effect on the shear behaviour of a beam-column joint core. However, it also results in crushing and spalling of the unconfined cover concrete and buckling of non-prestressed compression reinforcement of the beam in the earlier stage of the loading. Besides, larger prestress results in larger compressive strain of concrete and it may lead to the deterioration of the concrete due to reversed cyclic loading.

The following conclusions can be derived from the test results reported above on the prestressed and reinforced concrete beam - column joint assemblies which had the same dimensions, moment capacities of the beams and anchorage detailing of beam longitudinal reinforcement.

1. The hysteresis loops obtained from the test results of the reinforced concrete test unit indicates reduction in capacity and pinching due to bond deterioration of beam longitudinal reinforcement followed by pulling out of reinforcement. Conversely, the prestressed concrete test units showed much better hysteresis loops even in the large ductilities. However, larger prestressing force resulted in spalling and crushing of cover concrete and buckling of beam longitudinal reinforcement.
2. Until the ductility factor of 2 (beam rotation angle of approximately $1/30$), the equivalent viscous damping for all test units were almost the same. Past research has pointed out that there is less energy dissipation of prestressed concrete than reinforced concrete members. However, including beam - column joints the experimental results revealed this is disputable when prestressing force is not excessive. As the loading cycles progressed, the equivalent viscous damping in RCB-1 decreased to less than that of the ductility factor of 2 while in the

prestressed concrete test units the equivalent viscous damping increased proportionally with the ductility factor.

3. Small amount of prestressing force caused a much smaller shear distortion angle and a much stiffer joint core than in the reinforced concrete joint. However, a prestressing force larger than $0.12 f'_c A_g$ resulted in a small shear distortion angle and stiff joint core as the prestressed concrete unit with a prestressing force of $0.06 f'_c A_g$.
4. In order to predict the seismic response of reinforced concrete frames as closely as possible, the shear behaviour of beam - column joints needs to be idealized and incorporated in the analysis. Besides, it is necessary to consider beam longitudinal reinforcement coming out of the beam - column joint core in the idealization of the behaviour of beam plastic hinge regions. However, the assumption of rigid beam - column joint core can be justified in the prestressed concrete beam - column joint assemblies. Moment - curvature hysteresis loops in beam plastic hinge regions can be idealized based on the analyses assuming that plane sections before bending remain plane after bending. Thus, from the view point above, the past research which indicated larger responses of prestressed concrete frame structures than those of reinforced concrete should be re-examined.
5. The ratio of the total tensile force in the prestressed concrete units to that in the reinforced concrete test units measured at a ductility factor of 3 was almost as large as the ratio of moment capacity carried by non-prestressed reinforcing steel to the total moment capacity resisted by non-prestressed and prestressed reinforcement.
6. To consider the beneficial effect of prestressing force on beam - column joint cores, their shear strength V_{ju} should be increased as the prestress level increases based on the assumption of NZS 3101:1982 [4.8] that part of shear force is attributed to the effective prestressing force.

Anchorage placed in beam - column joint core are common practice in Japan while the prestressing steel in the test units were anchored to the anchorage plate on the outer side of the column. NZS 3101:1982 [4.8] prohibited anchorages kept in beam - column joint cores. More research on this matter should be carried out.

[References]

- 4.1 R.W.G.Blakeley and R.Park : Seismic Resistance of Prestressed Concrete Beam-Column Assemblies, ACI J. Sept. 1971 Title No.68-57, pp.677-692.
- 4.2 Building Code Requirements for Reinforced Concrete (ACI318-63), American

- Concrete Institute, 1963.
- 4.3 Building Code Requirements for Reinforced Concrete (ACI318-71), American Concrete Institute, 1971.
 - 4.4 CP115
 - 4.5 SEAOC 1968
 - 4.6 R. Park and K. J. Thompson : Cyclic Load Tests on Prestressed and Partially Prestressed Beam-Column Joints, PCI J. Sept.-Oct. 1977, pp.84-110.
 - 4.7 General Structural Design and Design Loadings for Buildings DZ4203:1986, Standard Association of New Zealand.
 - 4.8 Code of Practice for the Design of Concrete Structures NZS 3101 Part 1 : 1982, and Commentary NZS 3101 Part 2 : 1982, Standard Association of New Zealand.
 - 4.9 Y. S. Keong : Prestressed Concrete Beam-Column Joints, Research Report 78/2, Feb. 1978.
 - 4.11 Building Code Requirements for Reinforced Concrete (ACI318-89) and Commentary (ACI318R-89), 1989.
 - 4.12 Design Guideline for Earthquake Resistant Reinforced Concrete Buildings Based on Ultimate Strength Concept, Architectural Institute of Japan, 1988.
 - 4.13 Fujii, S., Goto, S., Morita, S. and Kondo, G. : The Behavior of 90 deg. Bent Bar Anchorage in Exterior Beam - Column Joint, Part 2 : Evaluation of Anchorage Capacity, Preprints of AIJ Annual Meeting in Hokuriku, 1983, pp.1823-1824.
 - 4.14 R. A. Spencer : Stiffness and Damping of Nine Cyclically Loaded Prestressed Concrete, Journal of PCI, June 1969, pp.39-52.
 - 4.15 A. Shibata : Saishin Taishin Kouzou Kaiseki, Morikita Syuppan.
 - 4.16 Muguruma et al. : Bond Deterioration in Prestressed Concrete Beam-Column Joints, Preprints of AIJ Annual Meeting in Tohoku, 1982, pp.2213-2214.
 - 4.17 Standard for Structural Design and Construction of Prestressed Concrete Structures, Architectural Institute of Japan, 1988.
 - 4.18 T. Paulay, R. Park and M. J. N. Priestley : Reinforced Concrete Beam - Column Joints Under Seismic Actions, ACI Journal, Nov. 1978, pp.585-593.

MOMENT-CURVATURE IDEALIZATION OF PRESTRESSED, PARTIALLY PRESTRESSED AND REINFORCED CONCRETE SECTIONS

5.1 Introduction

It is commonly thought that prestressed concrete members have been considered to have narrower hysteresis loops which results in less energy dissipation than reinforced concrete loops. On the basis of the experimental results, some researchers have attempted to idealize moment-curvature or load-deflection hysteresis loops of prestressed concrete members. Dynamic response analyses which involved those idealizations have been carried out in the past and indicated a larger seismic displacement response in prestressed concrete systems than in reinforced concrete systems.

In this chapter, after reviewing previous research on the idealization of hysteresis loops of prestressed and partially prestressed concrete members, a new idealization of prestressed and partially prestressed concrete members is proposed by the author. This is based on the idealization proposed by Thompson and Park [5.1] and the experimental results reported in Chapter 4. Some examples of idealized moment-curvature characteristics for prestressed, partially prestressed and reinforced concrete sections under reversed cyclic loading are presented.

5.2 Review of Previous Research

R.A. Spencer [5.2] conducted cyclic loading tests on nine prestressed concrete members. On the basis of the test results of moment-rotation characteristics obtained he idealized moment-rotation hysteresis loops as shown in Fig.5.1. The loops were quite narrow with little energy dissipation. This is because the members tested contained prestressing steel only without non-prestressed mild steel.

Okamoto [5.3] proposed a load-deflection or moment-rotation idealization of prestressed, partially prestressed and reinforced concrete members on the basis of the extensive research work on prestressed and partially prestressed concrete beams and prestressed concrete frames. Hysteresis loops in the model, called the PS model, which is shown in Fig.5.2 were determined so as to give the same equivalent damping factor as the experimental hysteresis loops.

Okada et al. [5.4] proposed a restoring force characteristics model which can be applied for prestressed, partially prestressed and reinforced concrete beams on the

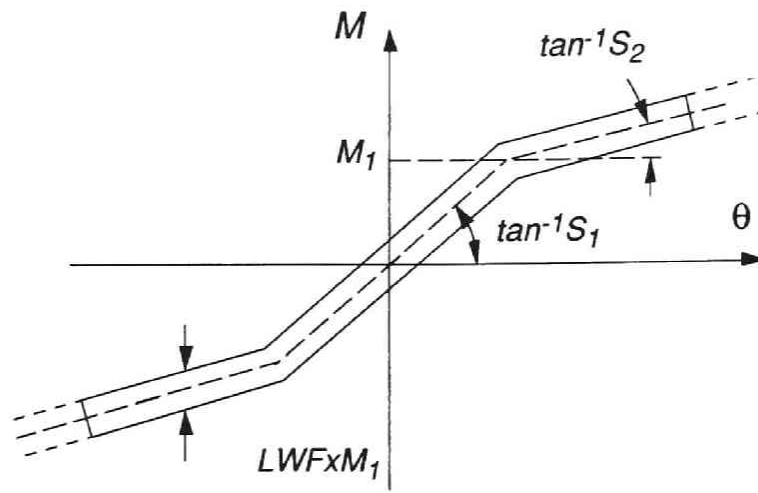


Fig.5.1 Idealized moment - rotation hysteresis loops by Spencer [5.2]

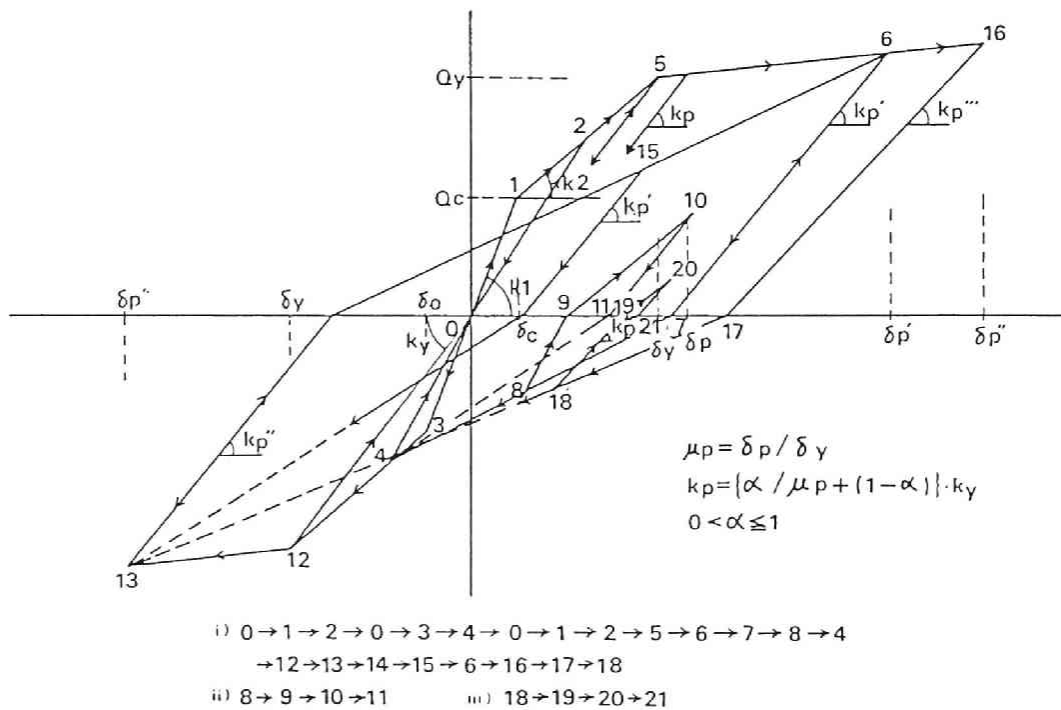


Fig.5.2 PS model by Okamoto [5.3]

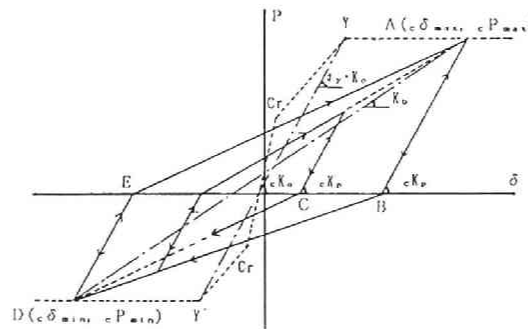


Fig.5.3 Restoring force characteristics model by Okada et al. [5.4]

basis of the test results of 66 prestressed concrete rectangular beams subjected to reversed cyclic loading. The test parameters included a shear span ratio, a tensile reinforcement index, a ratio of tensile reinforcement index for prestressing steel and for non-prestressed reinforcement, an amount and a spacing of confining reinforcement and a location of prestressing steel. The idealization is illustrated in Fig.5.3.

5.3 Moment-curvature idealization proposed by Thompson and Park

Thompson and Park developed an idealization for the moment-curvature characteristics of partially prestressed concrete members (ranging between fully prestressed and reinforced concrete members) under reversed cyclic loading by combining the responses of the prestressed concrete idealization presented by Blakeley [5.5] with some modifications and the Ramberg-Osgood idealization. They used a procedure similar to that suggested by Iwan [5.6].

5.3.1 Prestressed concrete idealization

The prestressed concrete model consists of three stages as shown in Fig.5.4. Stage 1 includes cycles in the post-cracking range but before crushing of the concrete commences. Stage 2 is reached when crushing has occurred in either direction of loading only, and Stage 3 is reached when crushing has occurred in both loading directions. Thompson as well as Blakeley noted that an abrupt change in stiffness followed by some capacity reduction resulted from crushing of the unconfined cover concrete because nonprestressed reinforcement was not provided with the prestressed concrete section considered. As shown in the test results in Chapter 4, large prestress resulted in crushing of unconfined cover concrete followed by load capacity reduction.

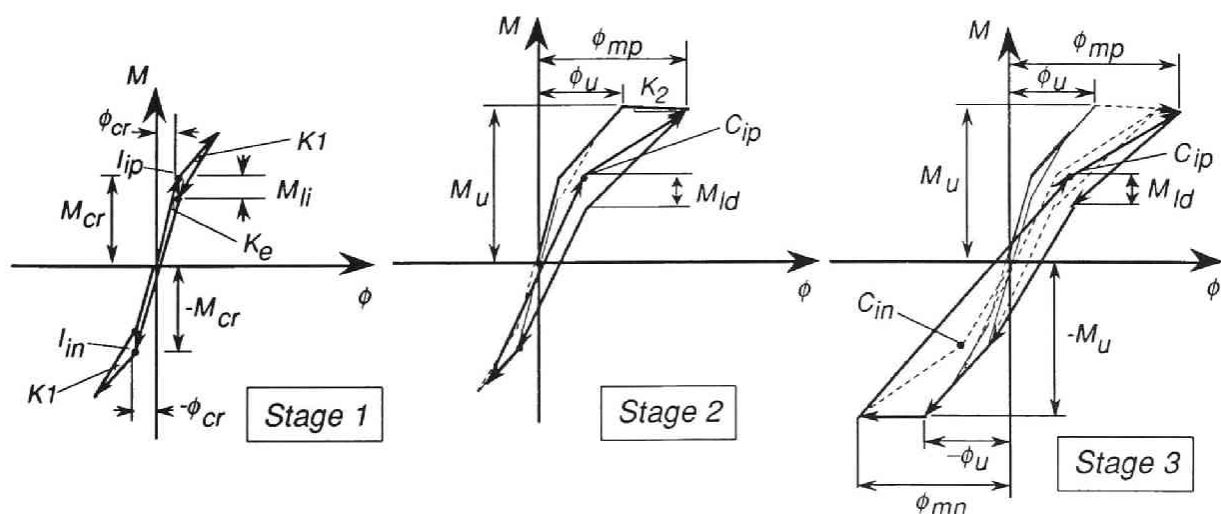


Fig.5.4 Prestressed concrete idealization by Thompson and Park [5.1]

The basic parameters which describe the idealized prestressed concrete envelope curve are: the elastic stiffness k_e , the maximum moment capacity M_u , the ratio γ_1 of the post-cracking stiffness k_1 to k_e , the ratio γ_2 of the post-crushing stiffness k_2 to k_e , and the ratio γ_{1f} of M_u to the cracking moment M_{cr} .

(a) Stage 1

For initial loading in Stage 1, the moment-curvature curve is followed with the stiffness $k_e = M_{cr} / \phi_{cr}$ to the initial positive inelastic point I_{ip} with coordinates (ϕ_{cr}, M_{cr}) . For loading beyond this point the curve is followed with stiffness k_1 . On unloading, the curve is followed from the unloading point to a point with coordinates $(\phi_{cr}, (M_{cr} - M_{li}))$, where M_{li} is the initial loop width moment value. This point together with the initial negative inelastic point I_{in} , $(-\phi_{cr}, -M_{cr})$, defines the stiffness for the remainder of the unloading and the commencement of negative loading. From I_{in} , further loading or unloading follows the same sequence described for positive loading.

(b) Stage 2

Once the maximum moment $+M_u$ or $-M_u$ has been reached in one loading direction only, at the crushing curvature ϕ_u the curve continues with stiffness k_2 . On unloading the value of M_{li} is replaced with M_{ld} , the degraded loop depth moment value. I_{ip} is replaced by C_{ip} , the current positive inelastic point, the coordinates of which are dependant on the maximum positive curvature, ϕ_{mp} .

(c) Stage 3

After curvatures greater than ϕ_u have been sustained in both directions, both I_{in} and I_{ip} are replaced by C_{in} and C_{ip} respectively, and M_{li} is replaced by M_{ld} .

(d) Numerical values of parameters

Thompson pointed out in his thesis [5.7] that use of a constant value of M_{ld} / M_u proposed by Blakeley [5.5] resulted in an over-estimation of the energy dissipation capacity of prestressed concrete members when subjected to small amplitude deformations after large curvatures had been imposed in both directions. Thompson proposed $M_{ld} / M_u = 0.4 \phi_r / \phi_m$ in order to describe the hysteresis loop widths, where ϕ_r is the value of curvature from which unloading commences, ϕ_m is the maximum positive curvature for unloading from a positive curvature, and ϕ_m is the absolute value of the maximum negative curvature for unloading from a negative curvature.

During Stages 2 and 3 the coordinates of $C_{ip}(\phi, M)$ are given by;

$$M = 0.5M_u \quad (5.1)$$

for $\phi_u < \phi_{mp} < 10\phi_u$,

$$\phi = \phi_{mp} \left(0.23 + 0.05 \frac{\phi_{mp}}{\phi_u} \right) \quad (5.2)$$

for $\phi_{mp} > 10\phi_u$

$$\phi = 0.7\phi_{mp} \quad (5.3)$$

where ϕ_u is the curvature at the maximum strength M_u , and ϕ_{mp} is the maximum positive curvature. Similarly the coordinates of C_{in} are found from Eq.5.1 and from the substitution of $|\phi_{mn}|$ for ϕ_{mp} in Eq.5.2 or 5.3.

5.3.2 Ramberg-Osgood idealization

The Ramberg-Osgood idealization for reinforced concrete proposed by Thompson is shown in Fig.5.5. The expression used to describe the idealization is

$$(\phi - \phi_o)E = (M - M_o) \left(1 - \left(\frac{M - M_o}{M_{ch} - M_o} \right)^{r-1} \right) \quad (5.4)$$

where, ϕ and M are the curvature and moment on the moment-curvature curve, E is the initial elastic stiffness of the section, ϕ_o and M_o are the values of ϕ and M at the beginning of the Ramberg-Osgood curve, M_{ch} is the characteristic moment, and r is the Ramberg-Osgood parameter.

The expression found for the characteristic moment M_{ch} is

$$M_{ch} = M_u (1 - 0.05\mu_c) \quad (5.5)$$

but M_{ch} is not less than $0.5M_u$, where M_u is the ultimate moment of the section and μ_c is the maximum imposed curvature ductility factor defined by

$$\mu_c = \phi_m / \phi_y \quad (5.6)$$

where ϕ_m is the maximum imposed curvature and ϕ_y is the yield curvature. However

in the Ramberg-Osgood system a distinct yield curvature does not exist, but the effective yield point can be defined as

$$\phi_y = M_u / E \quad (5.7)$$

This definition of yield point is then the same as for the elasto-plastic system. The chosen value of the Ramberg-Osgood parameter r is 20 before maximum moment is reached; subsequent to the maximum moment being reached in either loading direction the value of r is taken as 5.

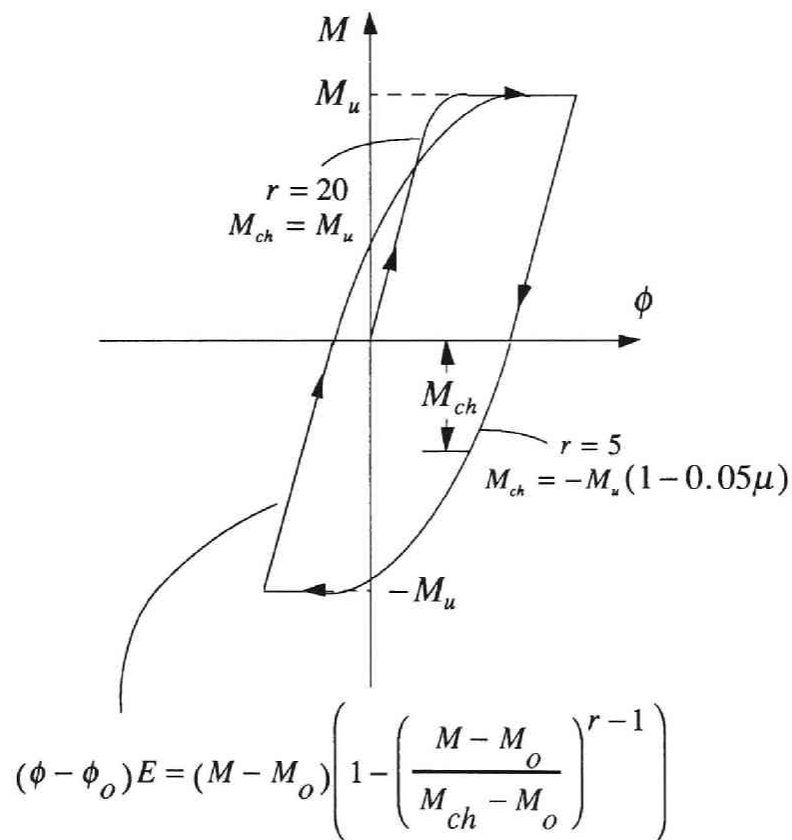


Fig.5.5 Reinforced concrete idealization by Thompson and Park [5.1]

5.3.3 Partially prestressed concrete idealization

An idealization for the moment-curvature characteristics of partially prestressed concrete members (which range between fully prestressed and reinforced concrete members) under cyclic loading was obtained by combining the response of the prestressed concrete system $M_p(\phi)$ with the response of the Ramberg-Osgood system $M_r(\phi)$ such that at a curvature ϕ the total moment sustained by the system $M(\phi)$ is

$$M(\phi) = \alpha M_r(\phi) + \beta M_p(\phi) \quad (5.8)$$

where, $\alpha = M_{ru} / M_u$

$$\beta = M_{pu} / M_u$$

$$\alpha + \beta = 1$$

M_u is the ultimate moment capacity of the partially prestressed section, M_{ru} is the moment of the non-prestressed steel taken about the centroid of the concrete compression block at the ultimate moment capacity of the section, and M_{pu} is the moment of the prestressed steel taken about the centroid of the concrete compression block at the ultimate moment capacity of the section.

5.4 An idealization of hysteresis loops of prestressed, partially prestressed and reinforced concrete proposed by the author

The idealization proposed by Thompson and Park is quite useful because it can cover the whole range of concrete members from fully prestressed members to reinforced concrete members depending on the contribution of prestressing steel to the ultimate moment capacity of the member section. However, it has two defects;

- (1) In the large ductility range, their prestressed concrete model indicates a somewhat pinched hysteresis, which is quite different from typical hysteresis loops for prestressed concrete sections as shown in Fig.5.6. This is because the moment of $C_{ip}(\phi, M)$ is considered to be so small that a loading path is bent upward at this point, which results in showing similar hysteresis loops to those of a reinforced concrete beam-column assemblage controlled by bond slip of longitudinal beam bars through the joint core.
- (2) Flexural cracking cannot be explicitly defined in their reinforced concrete model because it is described by a Ramberg-Osgood function. Fig.5.7 illustrates the moment-curvature idealization curves up to the yield point or crushing point for prestressed and reinforced concrete sections which have the same elastic stiffnesses and yielding or crushing moments. It has been observed in past research that

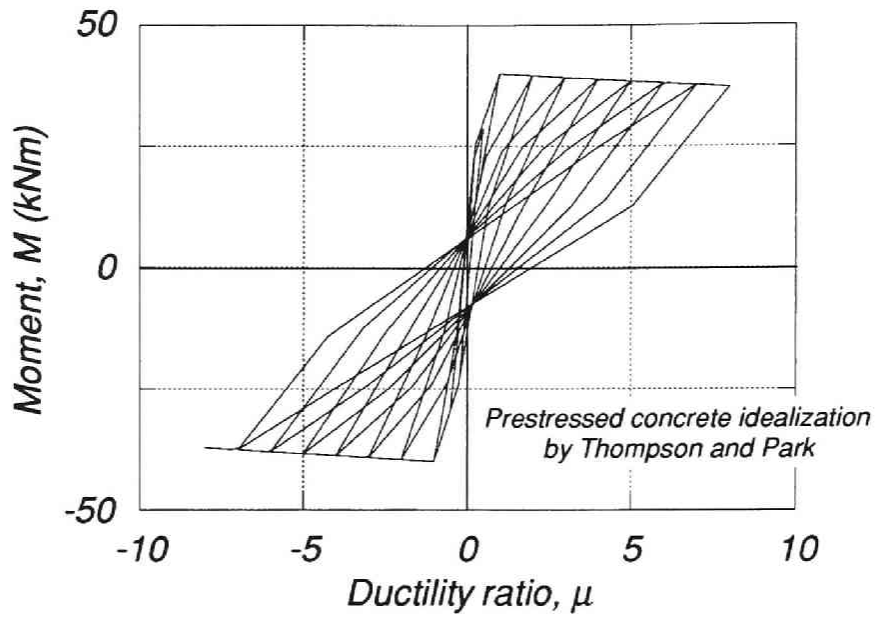


Fig.5.6 Prestressed concrete idealization by Thompson and Park in large ductility region

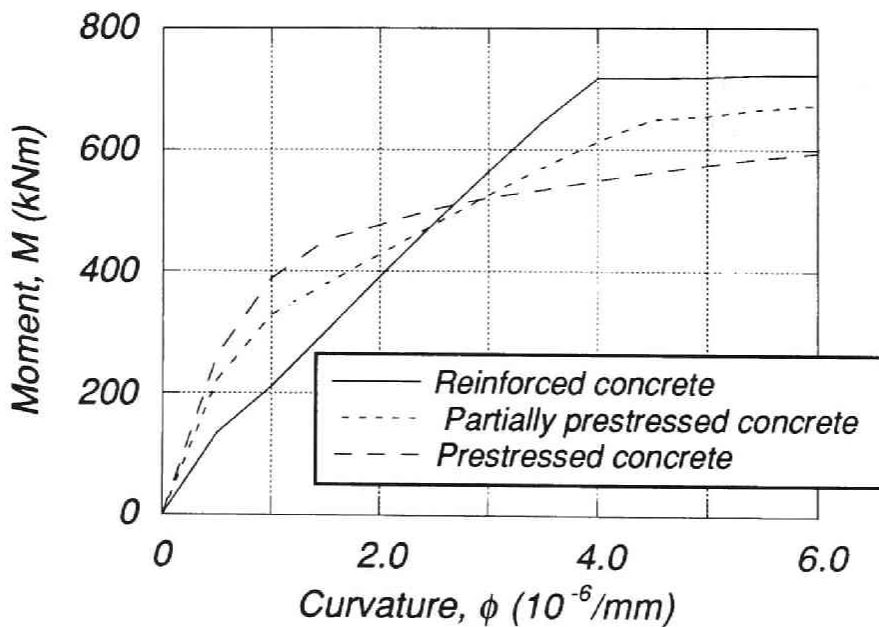


Fig.5.7 Monotonic moment - curvature idealization curves up to the yield point or crushing point for prestressed and reinforced concrete sections

prestressed concrete sections usually have higher moments at the commencement of flexural cracking than reinforced concrete and their post-cracking stiffnesses are lower than those of reinforced concrete if they have approximately the same flexural strengths. This observation differs from their idealizations.

In this study, the prestressed concrete idealization proposed by Thompson and Park is utilized with some modifications made by the author based on the test results reported in Chapter 4. An idealization for reinforced concrete is proposed by the author based on the similar curves as the prestressed concrete idealization. The variation from prestressed concrete sections to reinforced concrete sections including partially prestressed concrete is expressed by α and β , the same parameters described above.

5.4.1 Modifications with the prestressed concrete idealization

Some modifications with the prestressed concrete idealization proposed by Thompson and Park were made by the author. In their idealization a negative stiffness for the envelope curve was assumed after curvatures greater than ϕ_u have been sustained in either direction. The negative slope resulted from the capacity reduction due to crushing and spalling of the unconfined cover concrete. However, it depends on the intensity of prestressing force introduced into the beam, the cover thickness, the amount of transverse reinforcement and so on. A larger amount of prestressing force usually causes a larger reduction in moment capacity in the earlier stage of loading. The stiffness k_2 for the envelope curve beyond the crushing curvature ϕ_u was assumed to be a linear function of a prestress level η which was defined as the ratio of prestressing force to $f'_c A_g$ on the basis of the comparison with the experimental results.

$$k_2 = (-0.04 \eta + 0.004)k_e \quad (5.9)$$

where, $\eta = P_e / (f'_c A_g)$

P_e = effective prestressing force

f'_c = compressive strength of concrete

A_g = gross sectional area of member

The idealization for a prestressed concrete section made by Thompson and Park was found to indicate pinched hysteresis loops, which are typical for reinforced concrete members controlled by bond deterioration in the region of large deformation. This contradicts the test results obtained in past research. This is because the moment of the point C_{ip} which was given by Eq.5.1 is considered too small when large curvatures are imposed on the section. Therefore, the coordinates of $C_{ip}(\phi, M)$ were determined as follows,

$$M = 0.8M_u \quad (5.10)$$

for $\phi_u < \phi_{mp} < 10\phi_u$,

$$\phi = \phi_{mp} \left(0.3 + 0.05 \frac{\phi_{mp}}{\phi_u} \right) \quad (5.11)$$

for $\phi_{mp} > 10\phi_u$

$$\phi = 0.8\phi_{mp} \quad (5.12)$$

The loop widths described by $M_{ld} / M_u = 0.4\phi_r / \phi_m$ were found to be so large for prestressed concrete members that the expression was modified to $M_{ld} / M_u = 0.3\phi_r / \phi_m$. Fig.5.8 shows the comparison between the idealization by Thompson and Park and the hysteresis loops modified by the author.

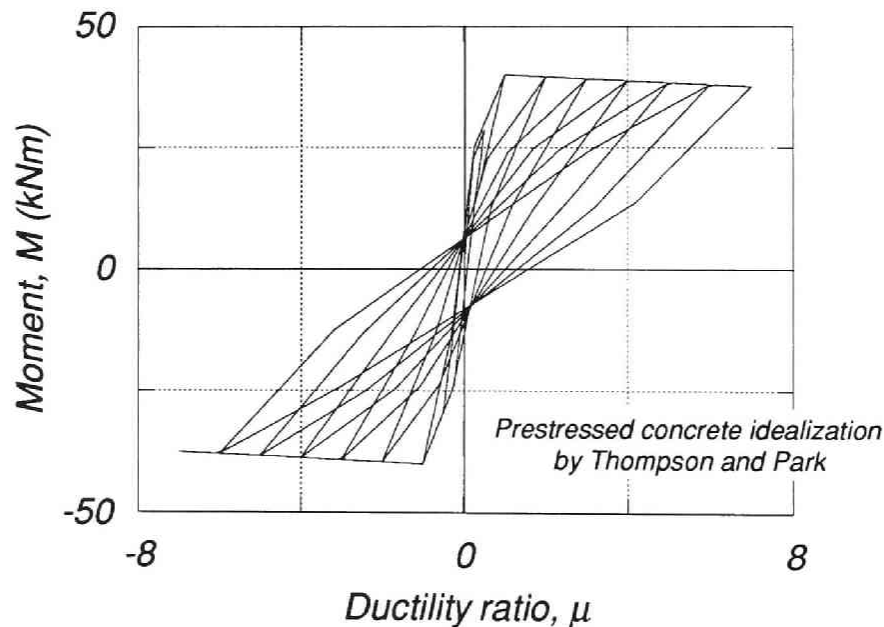


Fig.5.8(a) Comparison between the idealizations by Thompson and Park, and by the author

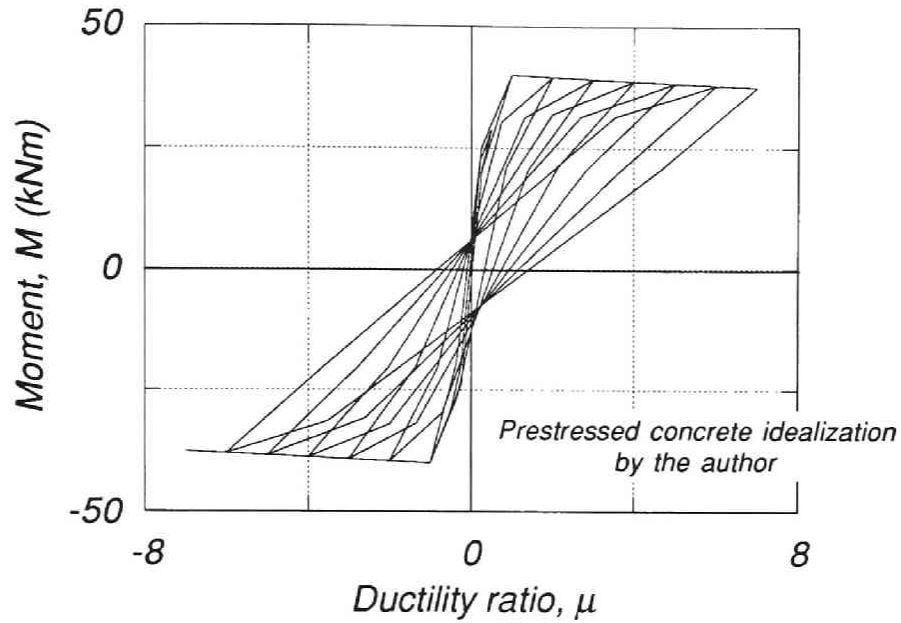


Fig.5.8(b) Comparison between the idealizations by Thompson and Park, and by the author

5.4.2 Partially prestressed and reinforced concrete idealization

The prestressed, partially prestressed and reinforced concrete idealizations are expressed by the same functions, in which the loop widths M_{li} and M_{ld} at the coordinate of I_{ip} , I_{in} , C_{ip} and C_{in} vary depending on the parameter α .

$$M_{li} / M_{cr} = (0.2 + 0.8\sqrt{\alpha})\phi_r / \phi_m \quad (5.13)$$

$$M_{ld} / M_u = (0.3 + 0.6\sqrt{\alpha})\phi_r / \phi_m \quad (5.14)$$

ϕ_r and ϕ_m are the curvature at unloading from the envelope curve and the current value of the maximum imposed curvature, respectively. Fig.5.9 illustrates the idealized hysteresis loops for a partially prestressed concrete section and a reinforced concrete section. The reinforced concrete idealization is similar to a degrading trilinear model which has been applied to reinforced concrete sections in past research.

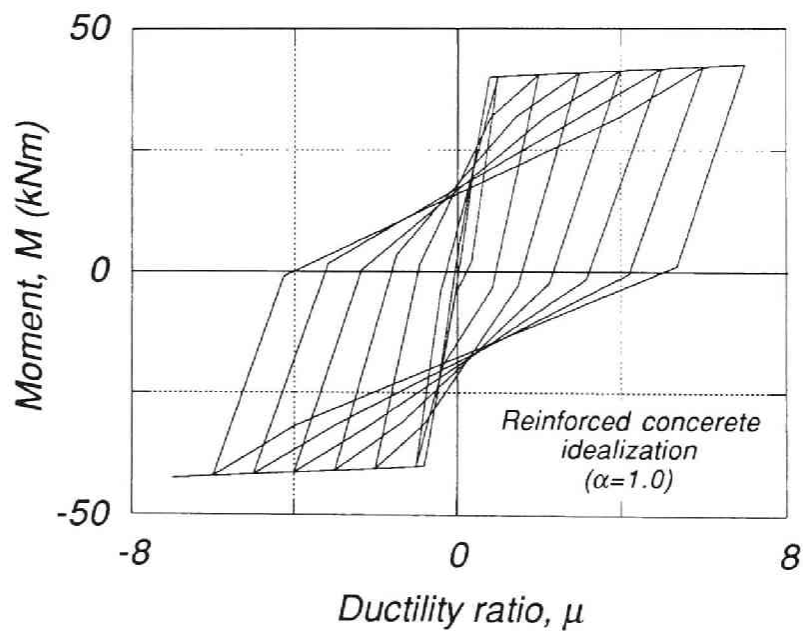
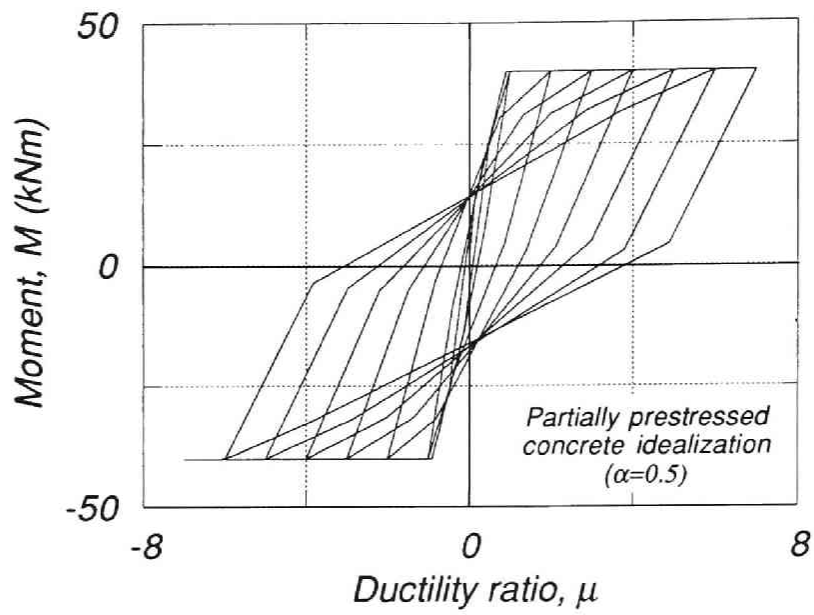


Fig.5.9 Idealized hysteresis loops for partially prestressed and reinforced concrete sections

5.5 Comparison of experimental and idealized moment-curvature characteristics

The experimental moment-curvature curves for the beams of ten units presented in Chapter 4 were used to test the idealized moment-curvature characteristics reported in this Chapter. Figs.5.10(a) to (j) show the compared moment - curvature characteristics. The experimental curvature was the average of that measured over a 365 mm gauge length, which consisted of the beam potential plastic hinge region of 300 mm from the column face and part of the joint region of 65 mm from the column face. The moment was that at the column face. The basic parameters for the prestressed concrete idealization (the elastic stiffness k_e , the maximum moment capacity M_u , the ratio γ_1 of the post-cracking stiffness k_1 to k_e , and the ratio γ_{1f} of M_u to the cracking moment M_{cr}) were obtained from the analytical moment - curvature curves under monotonic loading to failure as described in Chapter 3. They are given for each test unit in Table 5.1. Thompson gave constant values to γ_{1f} and γ_1 through all his test units. However, the idealization was developed in order to be adopted for moment-curvature hysteresis loops in potential plastic hinge regions of a building frame. Besides, the moment-curvature curves of a section under monotonic loading can be analyzed easily by an analytical procedure. Therefore, those parameters were determined from the moment-curvature curve for each beam section subjected to monotonic loading.

Figs.5.11(a) to (j) compare the experimental and analytical moment - curvature curves of the first cycle of loading up to the first yield point or crushing point. The elastic stiffnesses of the analytical curves agreed well with the experimental results. However, the post-cracking stiffnesses of the analytical curves were greater than the experimental results for all test units. Yielding which was defined as the first yielding of non-prestressed longitudinal reinforcement was observed in the analytical curves at the earlier stage of loading than in the experimental curves. Cracking or yielding was followed by the noticeable and abrupt change of stiffness in the analytical curves. In the experimental curves the gradual change of stiffness which resulted from cracking or yielding was observed. The difference between the experimental and analytical curves were more significant in the reinforced concrete test units than in the prestressed concrete.

The factors α and β for partially prestressed units were calculated from the stresses developed in the non-prestressed longitudinal reinforcement and the prestressing steel bars when the concrete strain at the extreme compression fiber of the section reached 0.3% using the ACI methods. However, the maximum moment attained in the idealized curves were obtained from the analytical moment - curvature curves when subjected to monotonic loading because the moment capacity calculated using the ACI methods was found to be too conservative. The moment capacity obtained analytically was conservative as shown in the figures although in the reinforced concrete test units

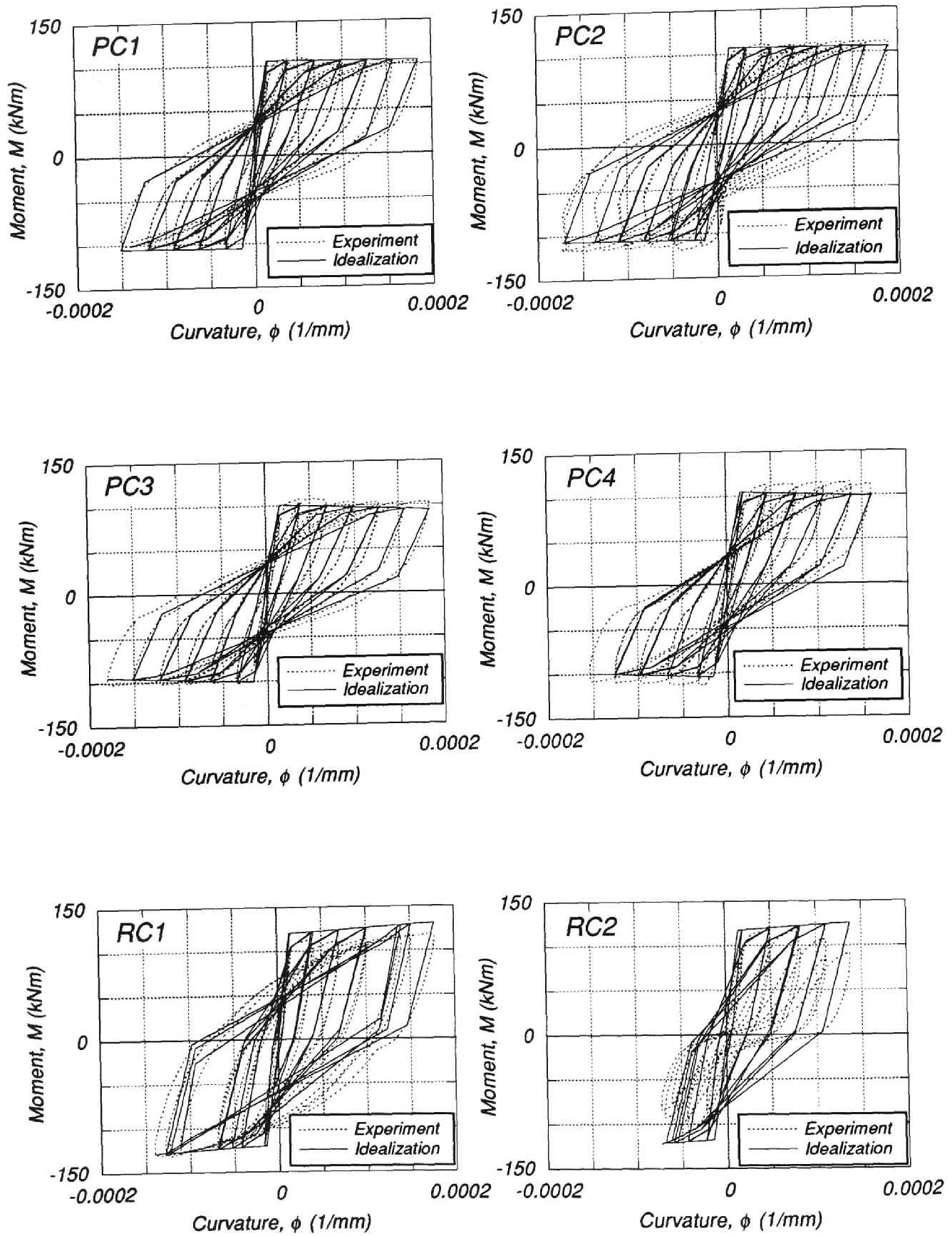


Fig.5.10(a) Comparison between idealized and experimentally obtained moment - curvature characteristics

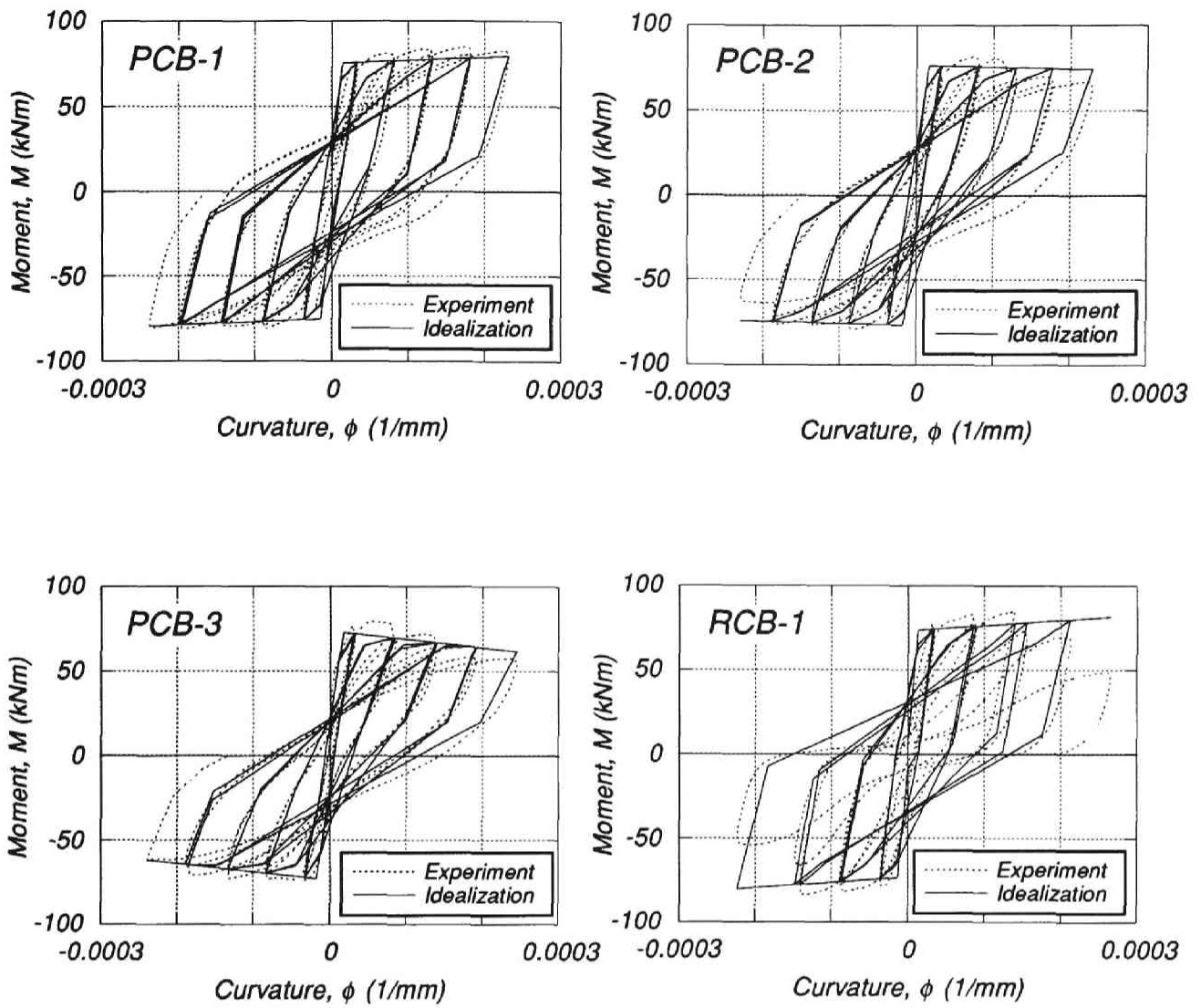


Fig.5.10(b) Comparison between idealized and experimentally obtained moment - curvature characteristics

Table 5.1 Numerical values for the parameters for the prestressed concrete idealization

Unit	k_e	M_u	γ_1	γ_{1f}	α	β	k_2
PC1	1.64	105.9	0.326	3.04	0.525	0.475	-0.0004
PC2	1.68	107.6	0.342	3.00	0.517	0.483	-0.0004
PC3	1.45	101.2	0.333	3.04	0.547	0.453	-0.0028
PC4	1.57	104.6	0.332	3.28	0.531	0.469	-0.0024
RC1	1.65	120.3	0.479	7.29	1.0	0.0	0.004
RC2	1.64	117.7	0.454	8.78	1.0	0.0	0.004
PCB-1	1.19	75.26	0.362	3.69	0.603	0.397	0.0016
PCB-2	1.42	76.6	0.246	3.03	0.436	0.564	-0.0008
PCB-3	1.56	72.88	0.176	2.48	0.308	0.692	-0.0032
RCB-1	0.776	73.61	0.691	7.17	1.0	0.0	0.004

Note:

k_e : Elastic stiffness ($10^7 \text{ kN} \cdot \text{mm}^2$)

M_u : Maximum moment capacity ($\text{kN} \cdot \text{m}$)

γ_1 : Ratio of post-cracking stiffness k_1 to k_e

γ_{1f} : Ratio of M_u to the cracking moment M_{cr}

α : Ratio of the moment of the nonprestressed steel taken about the centroid of the concrete compression block at the ultimate moment capacity to the ultimate moment capacity of the section

β : Ratio of the moment of the prestressed steel taken about the centroid of the concrete compression block at the ultimate moment capacity to the ultimate moment capacity of the section

k_2 : Ratio of stiffness for the envelop curve beyond the crushing or yielding curvature to the elastic stiffness

the analytical results were greater than the experimental ones.

The idealized moment - curvature characteristics coincide quite well with the experimental results except for the reinforced concrete test units RC2 and RCB1. The moment - curvature characteristics of these test units indicated that pinched hysteresis loops with capacity reduction became remarkable as the loading progressed. This, as investigated in Chapter 4, was due to the additional deformation caused by yield penetration of the longitudinal beam bars followed by full depth cracks in the beam plastic hinges.

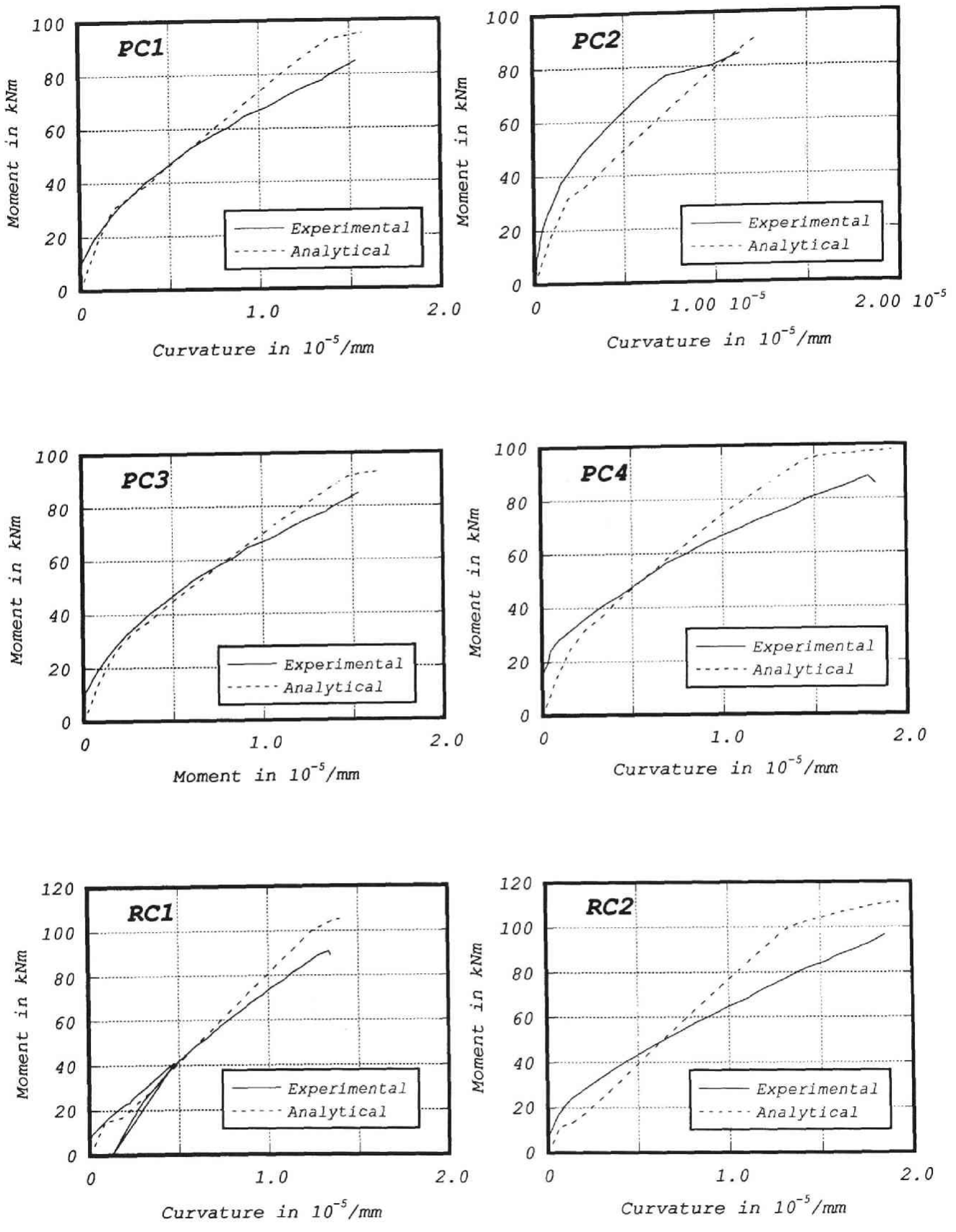


Fig.5.11(a)-(f) Comparison between the experimental and analytical moment - curvature curves up to the first yield point or crushing point

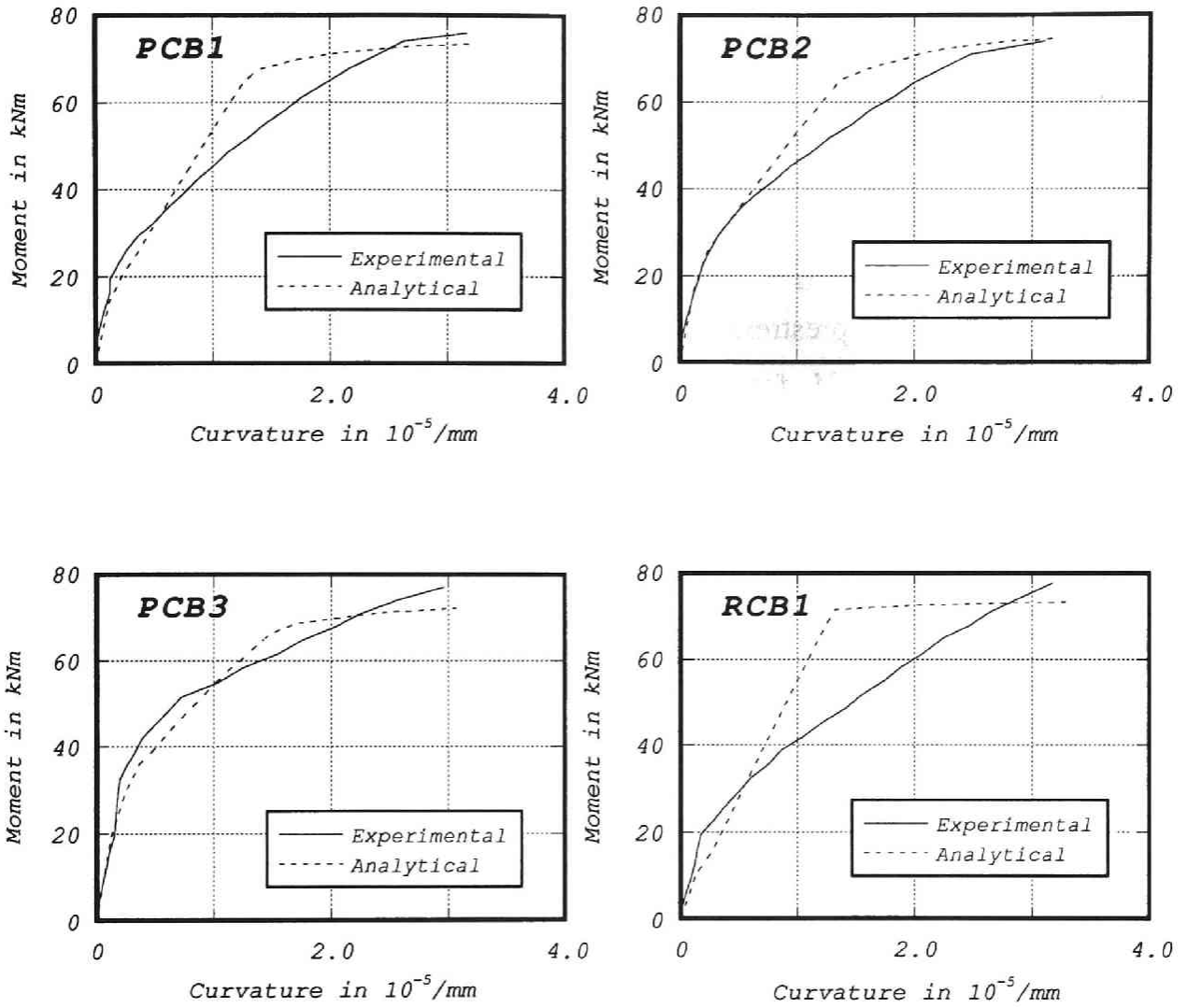


Fig.5.11(g)-(j) Comparison between the experimental and analytical moment - curvature curves up to the first yield point or crushing point

5.6 Examples of idealized moment - curvature characteristics for prestressed, partially prestressed and reinforced concrete sections under reversed cyclic loading

Figs.5.12(a) to (e) show a comparison of idealized moment - curvature curves for five fully prestressed, partially prestressed and reinforced concrete sections under reversed cyclic loading. The sections have the same initial stiffness k_e and moment capacity M_u . The (α, β) which is assigned to the sections are (0, 1), (0.25, 0.75), (0.5, 0.5), (0.75, 0.25) and (1, 0), which correspond to a fully prestressed concrete section through to a reinforced concrete section. The cracking moment of each section is assumed to be $0.625M_u$ for the fully prestressed concrete section with $(\alpha, \beta)=(0, 1)$, $0.5M_u$ for $(\alpha, \beta)=(0.25, 0.75)$, $0.375M_u$ for $(\alpha, \beta)=(0.5, 0.5)$, $0.25M_u$ for $(\alpha, \beta)=(0.75, 0.25)$ and $0.125M_u$ the reinforced concrete section with $(\alpha, \beta)=(1, 0)$. This reflects the fact that prestressed concrete sections usually have higher moments at the commencement of flexural cracking than reinforced concrete sections. The post-yielding stiffnesses for the sections are calculated according to the prestress levels which are assigned to them; 0.20 for the fully prestressed concrete section with $(\alpha, \beta)=(0, 1)$, 0.15 for $(\alpha, \beta)=(0.25, 0.75)$, 0.10 for $(\alpha, \beta)=(0.5, 0.5)$, 0.05 for $(\alpha, \beta)=(0.75, 0.25)$ and 0.0 for the reinforced concrete section with $(\alpha, \beta)=(1, 0)$.

The first loading cycle is up to the yield curvature which is four times the flexural cracking curvature. This is followed by a series of curvature controlled cycles to each of the curvature ductility factors of ± 2 , ± 3 and higher.

The ratios of the areas surrounded by the idealized moment-curvature curves shown in Fig.5.12 to those of the reinforced concrete idealization are plotted against curvature ductility factors in Fig.5.13. Before yielding, they are greater than unity. This is because there were larger flexural cracking moments than in the reinforced concrete section. The case in which the same flexural cracking moment is assumed for all through the sections will be referenced later. For ductility factors greater than unity each ratio is almost constant regardless of the ductility factors. The ratios are approximately 0.5 for the fully prestressed concrete section and 0.85 in average for the partially prestressed concrete section with $(\alpha, \beta)=(0.5, 0.5)$.

Figs.5.14(a) to (e) show a comparison of idealized moment - curvature curves which, this time, have the same flexural cracking moment. A similar figure to Fig.5.13 is drawn for the moment-curvature curves plotted in Fig.5.15 in respect to the idealized moment - curvature curves in Fig.5.14. The ratios are smaller than unity at any ductility factor.

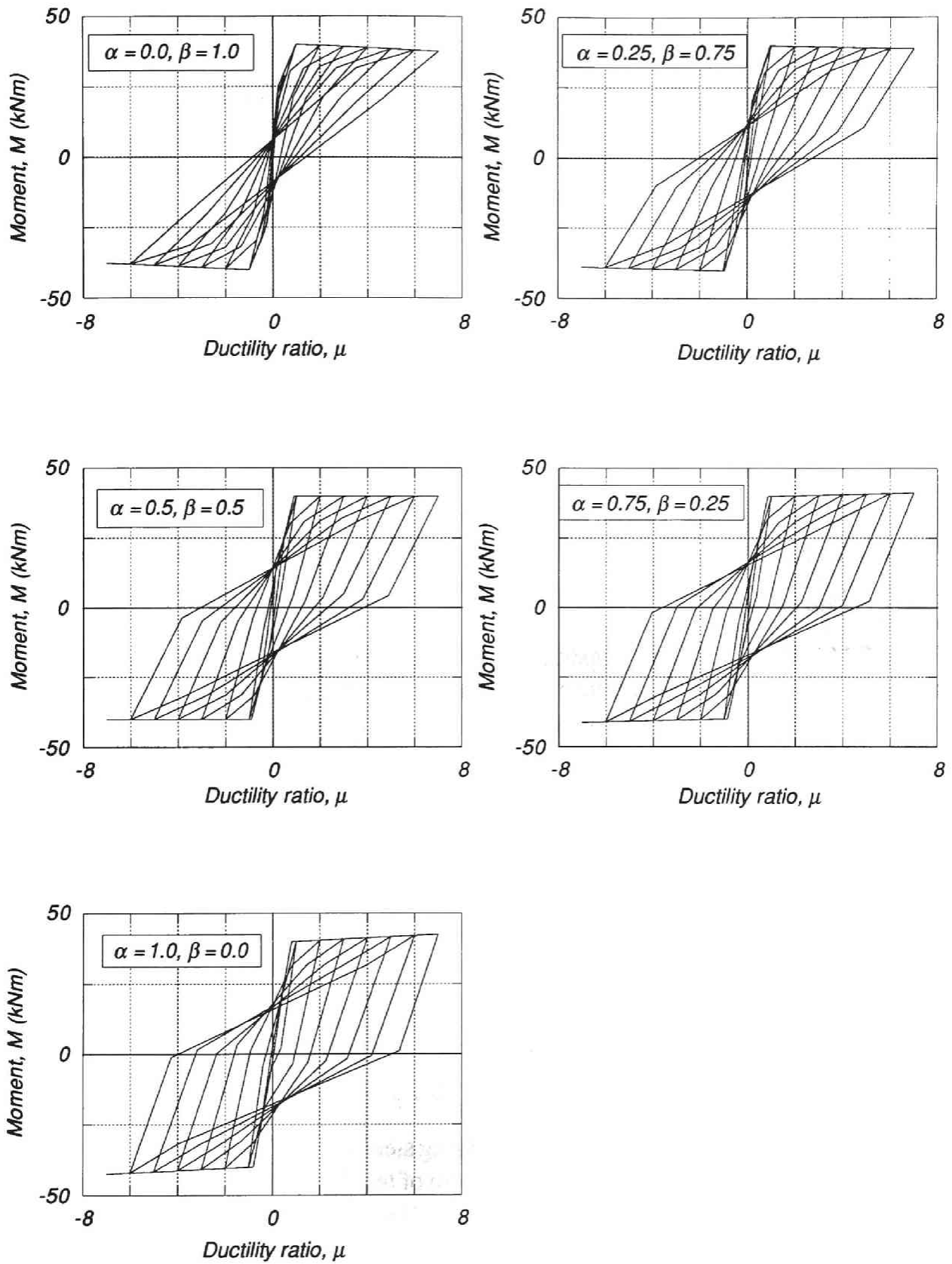


Fig.5.12 Examples of idealized curves (different flexural cracking moments)

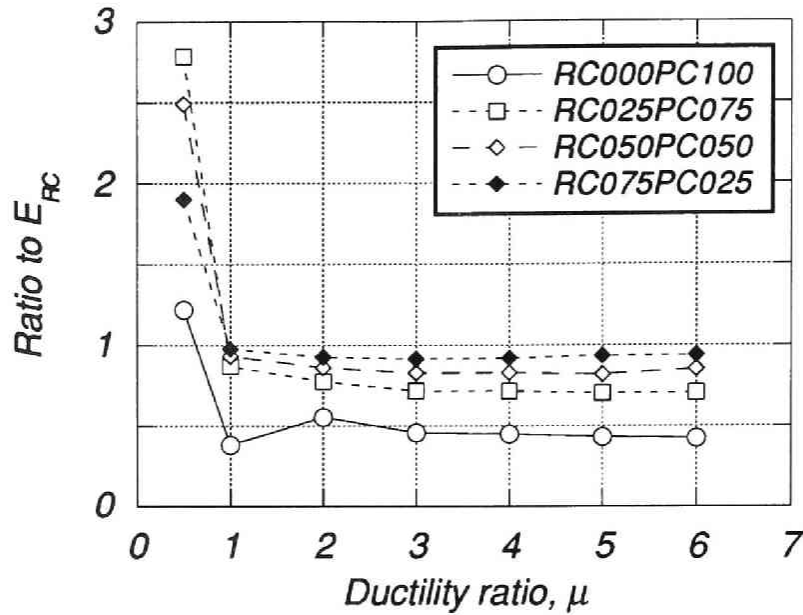


Fig.5.13 Ratios of the areas surrounded by the idealized moment - curvature curves to those of the reinforced concrete idealization

Figs.5.16(a) to (c) show a comparison of idealized moment - curvature curves for five prestressed, partially prestressed and reinforced concrete sections under reversed cyclic loading. Each section has the same overall dimensions and material properties. The sections are shown in Fig.5.17. The material and section properties are listed in Table 5.2. The fully prestressed and partially prestressed sections each contain one prestressing steel bar at the center. The amounts of top and bottom ordinary reinforcement are the same. By adjusting the sectional areas of non-prestressed longitudinal reinforcement and prestressing steel bar, they were so designed as to have approximately the same flexural strength. However, the initial stiffness k_e , the cracking moment M_{cr} and the post-cracking stiffness k_1 for each section were different. They were obtained from the analytical moment - curvature curves subjected to monotonic loading. They are summarized in Table 5.3.

The prestressing force for each section was $0.6f_{py}A_p$, where f_{py} and A_p are the yield strength and cross sectional area of prestressing steel, respectively. The prestress levels of all sections, which were defined as the ratio of tensile stress in the prestressing steel under service load condition to the yield strength, f_{py} , were the same. Therefore, a larger amount of prestressing steel resulted in a larger prestressing force on the section.

In case of designing a prestressed concrete member, prestress to be introduced into the member is determined from the design stress under the service load condition. The prestress level described above is usually determined by the allowable stress to be

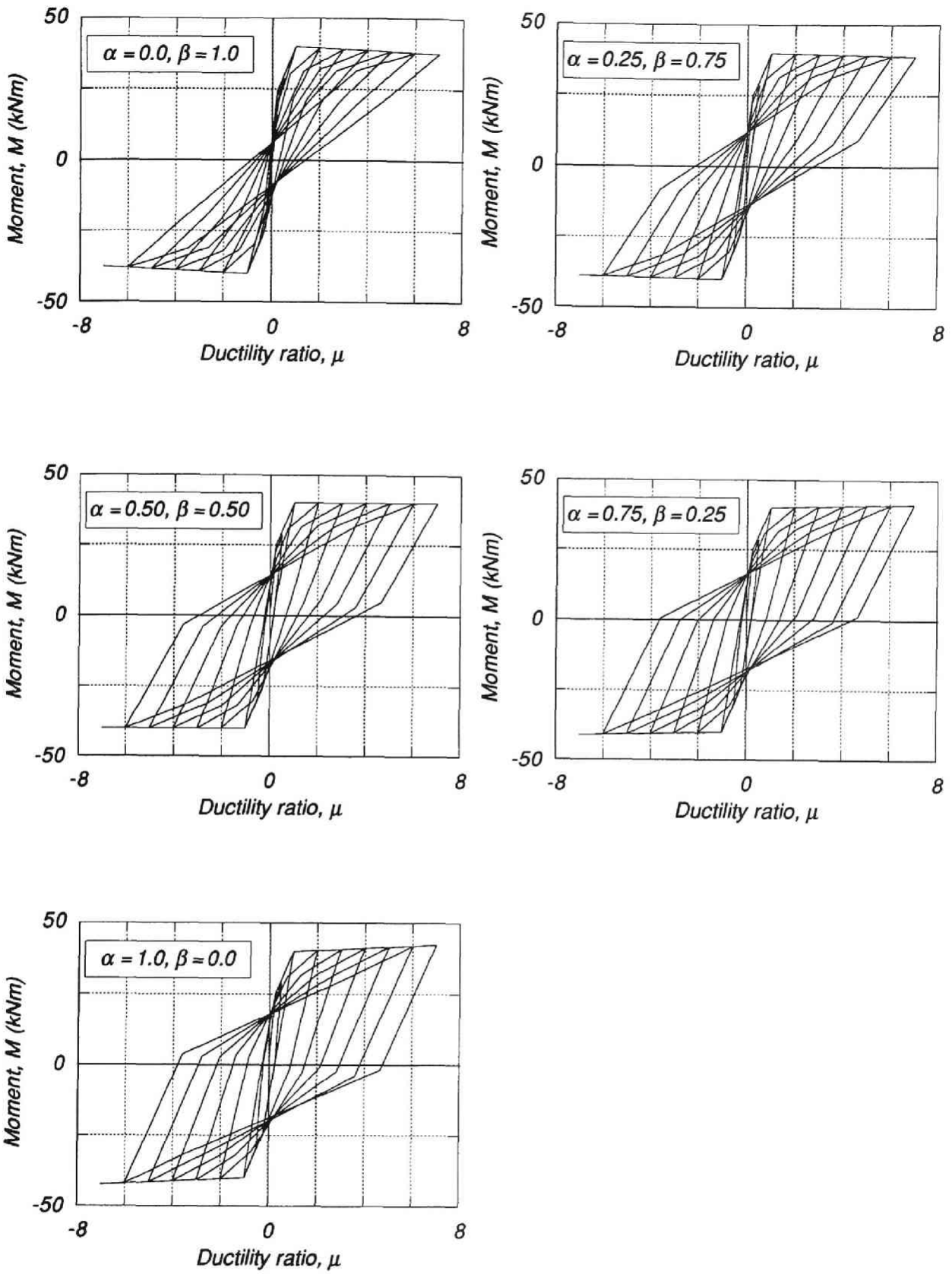


Fig.5.14 Examples of idealized curves (same flexural cracking moment)

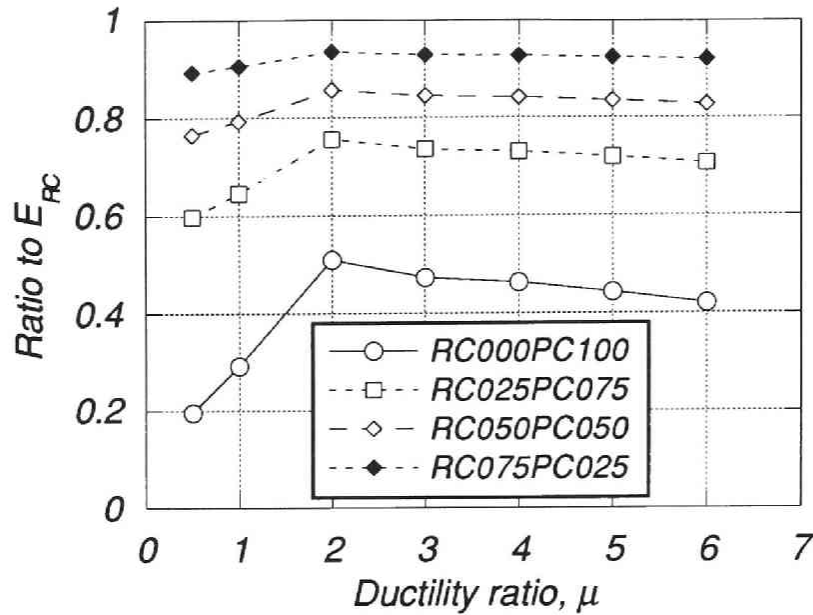


Fig.5.15 Ratios of the areas surrounded by the idealized moment - curvature curves to those of the reinforced concrete idealization

introduced into the prestressing steel which is specified in the design codes. Lower prestress levels may result in larger amount of prestressing steel and in larger reserved strength for the ultimate load condition. This is an uneconomic design of members, although, as shown in Chapter 4, a lower prestress level which resulted in larger reserve stresses before the yield of the prestressing steel had a beneficial effect on the shear behaviour of beam-column joint.

Fig.5.18 illustrates the analytical results of moment - curvature curves for the sections of interest under monotonic loading. They attained approximately the same flexural strength but the shape of the curves are quite different. As varying from reinforced concrete to fully prestressed concrete, the section has the larger elastic stiffness, the smaller post-cracked stiffness and the larger flexural cracking moment. In the reinforced concrete section, the yield point which resulted from the yielding of tensile reinforcement can be pointed out because an abrupt change of stiffness appeared in the curve. In the prestressed concrete section, the gradual change of stiffness after flexural cracking was observed and the strength reduction after the maximum moment was attained was more significant as the section varied from a partially prestressed concrete section to a fully prestressed concrete section. This was due to crushing of the cover concrete.

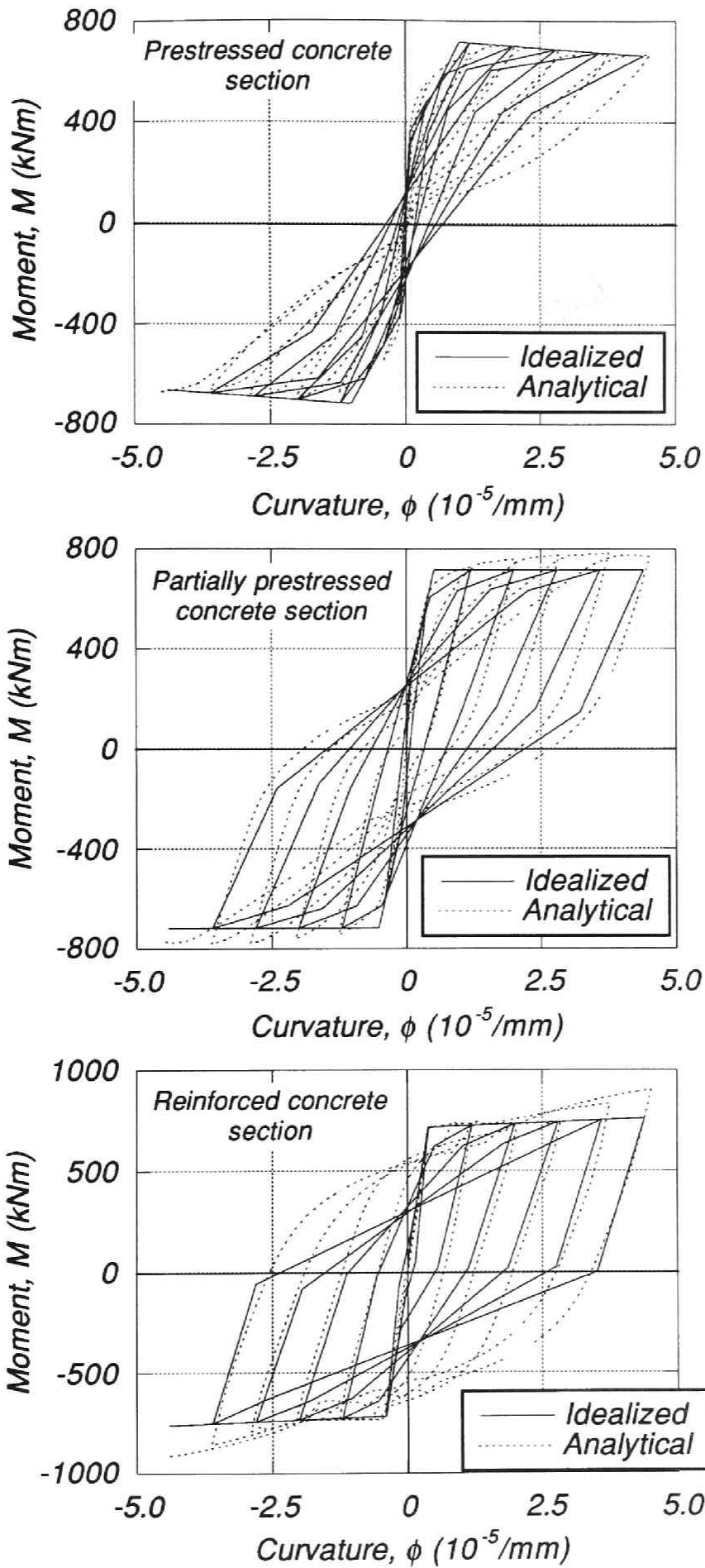


Fig.5.16 Idealized moment - curvature curves for the sections under reversed cyclic loading

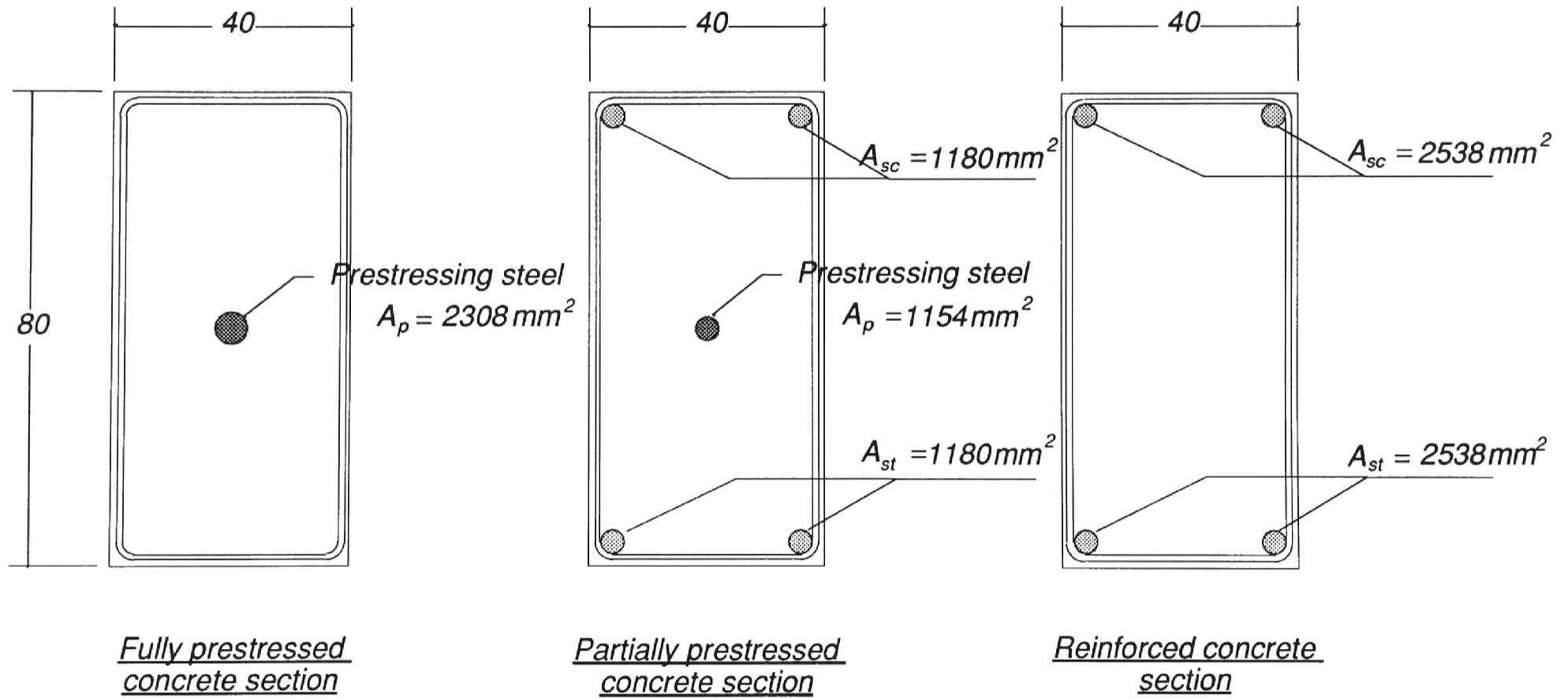


Fig.5.17 Prestressed, partially prestressed and reinforced concrete sections

Table 5.2 Material and section properties

Unconfined Concrete

Compression Strength (MPa)	-30.0
Tension Strength (MPa)	3.00
Youngs Modulus (MPa)	27386.
Strain At Peak Stress (MPa)	-0.0020
Spalling Strain	-0.0070
Tensile Strain	0.0001

Longitudinal Steel

	Compression	Tension
Yield Stress (MPa)	400.0	400.0
Ultimate Stress (MPa)	0.0	0.0
Youngs Modulus (MPa)	205947.	205947.
Strain-hardening Modulus (MPa)	0.	0.
Yield Strain	-0.0019	0.0019
Strain-hardening Strain	-0.0153	0.0153

Prestressing Steel

Tensile Elastic Limit Strain	0.0050
Compressive Elastic Limit Strain	-0.0035
Upper Branch Initial Strain	0.0130
Buckling Strain	-0.0115
Tensile Ultimate Strain	0.0500
Compressive Ultimate Strain	-0.0500
Tensile Elastic Limit Stress (MPa)	980.7
Compressive Elastic Limit Stress (MPa)	-680.7
Upper Branch Initial Stress (MPa)	1200.0
Ultimate Stress (MPa)	1500.0
Buckling Stress (MPa)	-900.0
Tendon Stress After Transfer (MPa)	600.0
0.2% Offset Yield Stress (MPa)	1103.4

Volumetric Ratio of Transverse Reinforcement

Volumetric Transverse Steel Content (X-direction)	=	0.0086
Volumetric Transverse Steel Content (Y-direction)	=	0.0142

Fully prestressed concrete section

Axial Prestress Force	=	-1920. kN
Prestress Force Ratio	=	$0.20 f'_c A_g$

Partially prestressed concrete section

Axial Prestress Force	=	-960. kN
Prestress Force Ratio	=	$0.10 f'_c A_g$

Table 5.3 Numerical values for the parameters for the idealization of the sections

Unit	k_e	M_u	γ_1	γ_{1f}	α	β	k_2
PC	3.878	717.	0.094	1.85	0.0	1.0	-0.004
PPC	3.277	717.	0.284	2.19	0.5	0.5	0.0
RC	2.692	717.	0.633	5.33	1.0	0.0	0.004

Note:

k_e : Elastic stiffness ($10^7 \text{ kN} \cdot \text{mm}^2$)

M_u : Maximum moment capacity ($\text{kN} \cdot \text{m}$)

γ_1 : Ratio of post-cracking stiffness k_1 to k_e

γ_{1f} : Ratio of M_u to the cracking moment M_{cr}

α : Ratio of the moment of the nonprestressed steel taken about the centroid of the concrete compression block at the ultimate moment capacity to the ultimate moment capacity of the section

β : Ratio of the moment of the prestressed steel taken about the centroid of the concrete compression block at the ultimate moment capacity to the ultimate moment capacity of the section

k_2 : Ratio of stiffness for the envelope curve beyond the crushing or yielding curvature to the elastic stiffness

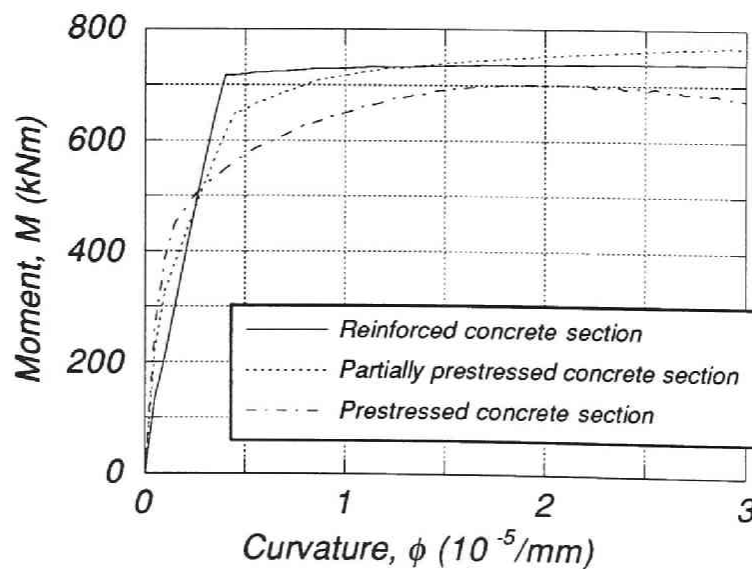


Fig.5.18 Analytical moment - curvature curves subjected to monotonic loading

5.7 Conclusions

On the basis of the above analytical study, the following conclusions are reached with regard to the idealization of prestressed, partially prestressed and reinforced concrete moment - curvature relationships:

1. By modifying the idealization suggested by Thompson and Park [5.1], the idealization of prestressed, partially prestressed and reinforced concrete moment - curvature relationships was proposed by the author on the basis of the experimental work and the analytical work. The idealization curves can be applied from fully prestressed concrete to reinforced concrete members.
2. The idealization was compared with the experimental results described in Chapter 4. It turned out that the moment - curvature curves obtained experimentally can be well predicted by the idealization. However, all the test units consisted of partially prestressed concrete beams. The idealization should undergo many trials because only a few experimental results of partially prestressed concrete beam - column joint assemblages available were used to calibrate it.
3. Some examples of idealized moment - curvature characteristics for fully prestressed, partially prestressed and reinforced concrete sections under reversed cyclic loading were given for some ranges of the parameters (α, β).

[References]

- 5.1 Thompson, K.J. and Park, R : Seismic Response of Partially Prestressed Concrete, Journal of Structural Division, Proceedings of ASCE Aug.1980 ST8, pp.1755-1775.
- 5.2 R.A.Spencer : Stiffness and Damping of Nine Cyclically Loaded Prestressed Concrete, PCI J. June 1969 pp.39-52.
- 5.3 Okamoto, S : Fundamental Study on Earthquake Resisting Behaviours of Prestressed Concrete Frame Structures, Chapter 6; Seismic Response of Prestressed Concrete Buildings, Ph. D Thesis, Kyoto University, Japan 1986, pp.250-281.
- 5.4 M. Okada, M. Hamahara, H. Suetsugu and J. Motooka : Elasto-plastic hysteretic behavior of prestressed concrete beams, Transactions of AIJ, No.410, 1990, pp.63-69.
- 5.5 R.W.G.Blakeley and R.Park : Prestressed Concrete Sections with Cyclic Flexure, J. of SD, Proc. of ASCE Aug.1973 ST8, pp.1717-1742.
- 5.6 W. D. Iwan : A Model for the Dynamic Analysis of Deteriorating Structures, Fifth World Conference on Earthquake Engineering, Rome, 1973, Paper 222, Session 5B.
- 5.7 K. J. Thompson : Ductility of Concrete Frames under Seismic Loading, Ph. D. Thesis, University of Canterbury, New Zealand, 1975.

DYNAMIC RESPONSE ANALYSIS OF SINGLE-DEGREE-OF-FREEDOM PRESTRESSED CONCRETE SYSTEMS

6.1 Introduction

Past research on prestressed concrete have shown larger response of prestressed concrete building structures than reinforced concrete building structures. This is because the hysteresis loops of prestressed concrete members have less energy dissipation than those of reinforced concrete members. Some researchers have conducted dynamic response analyses on prestressed and reinforced concrete systems and compared their responses. The first dynamic response analyses on prestressed concrete systems were reported by Thompson and Park [6.1]. They idealized moment-curvature hysteresis loops of prestressed concrete sections on the basis of the experimental results of prestressed, partially prestressed and reinforced concrete beam-column joint assemblies and the analytical work. The idealized hysteresis loops were involved in the dynamic response analysis program as a load-displacement relationship of a single-degree-of-freedom system. The conclusion they obtained from the analysis was 30% in average larger response of the prestressed concrete systems than that of the reinforced concrete systems with the same initial period of vibration.

In this chapter, after reviewing previous research on dynamic response analyses of prestressed concrete systems, the analytical results obtained from the dynamic response analyses conducted by the author will be presented. Then, a method to predict response of prestressed concrete systems are to be proposed. The analyses to be reported in this chapter involve those for single-degree-of-freedom systems. Analyses of multi-mass shear systems and two-dimensional systems will be described in the later chapters.

6.2 Review of Previous Research

As described in Chapter 5, Thompson and Park have conducted an extensive experimental and analytical research work on moment-curvature relationships of prestressed, partially prestressed and reinforced concrete member sections. Dynamic response analyses of single-degree-of-freedom systems to El Centro 1940 N-S earthquake and two artificial waves were carried out using the idealized moment-curvature hysteresis loops as load-displacement characteristics of the systems. The maximum displacements of prestressed, partially prestressed and reinforced concrete systems under severe earthquake motions generally increase with increasing pre-

stressed component. They derived 30% in average larger response of prestressed concrete systems than reinforced concrete systems.

However, the ratio of maximum displacements between the two systems significantly varied from the average value of 1.3. In some cases the displacement response of more highly prestressed systems is less than that of the reinforced concrete system of the same initial period. Their idealization for reinforced concrete members consists of a Ramberg-Osgood function with no definite stiffness reduction due to cracking. The period of vibration in the prestressed concrete system gets longer after cracking and this may result in the increased displacement response than that of the reinforced concrete system. However, it greatly depends on the characteristics of the earthquake record involved in the analysis. Thus, it turned out that the effect of earthquake response spectra might be more significant than that of the difference of hysteresis loops. They concluded that the load-displacement characteristics did not affect the ductility demand as much as the intensity of the earthquake excitation and the initial period of vibration.

Okamoto [6.2] has reached the similar conclusion by means of carrying out dynamic response analyses of multi-mass shear systems. He derived the following equation for predicting the maximum displacement response on the basis of the analytical results on the prestressed, partially prestressed and reinforced concrete systems and the linear elastic system with the same initial period of vibration.

$$\frac{Q_y}{Q_E} = \frac{(2\mu - 1)^{0.125\alpha}}{\sqrt{2\mu - 1}} \quad (6.1)$$

where, Q_y = yield capacity
 Q_E = capacity response of the linear elastic system
 μ = ductility ratio
 α = coefficient which allows for the degree of prestressing

He proposed another idealization for prestressed concrete systems called 'Modified PS Model' in which the idealized hysteresis loops before yielding has been so improved as to reflect real load-displacement curves better. The dynamic response analyses for multi-mass shear systems which involved this model suggested another expression.

$$\frac{Q_y}{Q_E} = \frac{(2\mu - 1)^{0.15(\alpha')^2}}{\sqrt{2\mu - 1}} \quad (6.2)$$

where, α' = coefficient to allow for the degree of prestressing in 'Modified PS Model'.

The restoring force characteristics applied to the single- or multi-mass shear systems in the above research were based on the moment - curvature or load - member rotation relationships measured in potential plastic hinge regions of the beam test units and the beams in beam - column joint assembly test units. However, Okamoto conducted pseudo-dynamic loading tests on one-bay two-story frames which consisted of prestressed concrete beams and reinforced concrete columns. The frames were idealized as a twin-mass shear system whose shear force-interstory drift relationship was assumed to follow modified PS model. The analytical results agreed well with the experimental results. However, the test units underwent a displacement of small ductility ratios ($\mu \approx 1.15 \sim 2.35$) while the coefficient α' to allow for the degree of prestressing in the model was determined as an average value in the ductility range up to 6.

6.3 Inelastic Dynamic Response Analyses of Single-mass Shear Systems

In this section, the idealized curves proposed in Chapter 5 are used as the load-displacement idealization except that the ordinates are load V and displacement x . Response spectra of the idealized curves to an earthquake excitation for various ranges of yield capacity, period of vibration, and so on are calculated to investigate the fundamental characteristics of the idealization. However, the author wants to emphasize that the purpose of this calculation is to examine the justification of the idealization because the idealized curves are not considered to express directly the load-deflection relationships of a structure or a layer of a building itself : they were derived based on the moment-curvature curves obtained experimentally. Although load-displacement hysteresis loops of a prestressed concrete member is considered to be similar to the idealization, the response of a building is largely affected by the load-deflection response of reinforced concrete constituent elements such as columns and walls. A comparison between the idealizations for a prestressed concrete and a reinforced concrete system which will be described in the later part of this section should be referred to as an extreme case of these systems.

6.3.1 Equation of dynamic equilibrium and the analytical procedure

Structural systems used in this analysis are idealized as shown in Fig.6.1. This consists of rigid girders of mass M , weightless columns with total lateral stiffness k and fraction of critical damping c .

Generally for a non-linear system at time t the equation of dynamic equilibrium is expressed as

$$M\ddot{y}_t + C\dot{y}_t + Q(y_t) = -M\ddot{y}_o \quad (6.3)$$

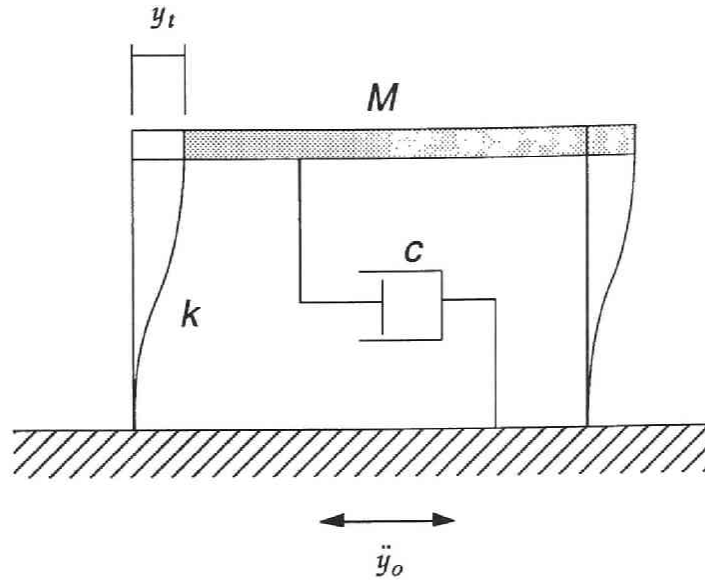


Fig.6.1 Idealized structural system

- where, M = mass of the system
 C = damping of the system
 $Q(y_t)$ = lateral resistance of the system
 \ddot{y}_t = acceleration of the system
 \dot{y}_t = velocity of the system
 y_t = displacement of the system
 \ddot{y}_o = ground acceleration

Eq.6.3 is rewritten in an incremental form as follows,

$$M \cdot \Delta \ddot{y}_t + C \cdot \Delta \dot{y}_t + \Delta Q(y_t) = -M \cdot \Delta \ddot{y}_o \quad (6.4)$$

The analytical method employed in this study is the impulse acceleration method [6.3]. An acceleration at time t_n is assumed to be introduced as impulses of $\dot{y}_n \Delta t / 2$ just before and after the time t_n . Δt is a time interval, i.e. $\Delta t = t_n - t_{n-1} = t_{n+1} - t_n$. Since the velocity in this time interval is assumed to be constant like a step function, the displacement varies linearly in this interval. Assuming that the average velocities in the intervals of $t_{n-1} \sim t_n$ and $t_n \sim t_{n+1}$ are $\dot{y}_{n-1/2}$ and $\dot{y}_{n+1/2}$, respectively, we can get the following equations.

$$\dot{y}_{n+1/2} - \dot{y}_{n-1/2} = \ddot{y}_n \Delta t \quad (6.5)$$

$$\dot{y}_{n-1/2} = \frac{y_n - y_{n-1}}{\Delta t} \quad (6.6)$$

$$\dot{y}_{n+1/2} = \frac{y_{n+1} - y_n}{\Delta t} \quad (6.7)$$

Therefore, the displacement at time t_{n+1} is derived from the values y_n , y_{n-1} , \ddot{y}_n and Δt which are known quantities.

$$y_{n+1} = 2y_n - y_{n-1} + \ddot{y}_n \Delta t^2 \quad (6.8)$$

In the case of a non-linear analysis, \ddot{y}_n is derived from the following two equations.

$$\dot{y}_n = \dot{y}_{n-\frac{1}{2}} + \frac{1}{2} \ddot{y}_n \Delta t = \frac{y_n - y_{n-1}}{\Delta t} + \frac{1}{2} \ddot{y}_n \Delta t \quad (6.9)$$

$$\ddot{y}_n = -\frac{C}{M} \dot{y}_n - \frac{Q(y_n)}{M} - \ddot{y}_{0n} \quad (6.10)$$

Thus, y_{n+1} is given as an inductive form.

$$y_{n+1} = \frac{1}{1 + \frac{1}{2} \frac{C}{M} \Delta t} \left\{ 2y_n - y_{n-1} + \frac{1}{2} \frac{C}{M} \Delta t \cdot y_{n-1} - \frac{Q(y_n)}{M} \Delta t^2 - \ddot{y}_{0n} \Delta t^2 \right\} \quad (6.11)$$

It should be noted that this method does not use a tangential stiffness but a lateral resistance $Q(y_n)$ itself. From Eqs.6.9 and 6.8 the following two equations are derived.

$$\dot{y}_n = \frac{1}{2\Delta t} (y_{n+1} - y_{n-1}) = \frac{1}{\Delta t} \left(\frac{y_{n+1} + y_n}{2} - \frac{y_n + y_{n-1}}{2} \right) \quad (6.12)$$

$$\ddot{y}_n = \frac{1}{\Delta t^2} (y_{n+1} - 2y_n + y_{n-1}) = \frac{1}{\Delta t} \left(\frac{y_{n+1} - y_n}{\Delta t} - \frac{y_n - y_{n-1}}{\Delta t} \right) \quad (6.13)$$

Thus, the velocity \dot{y}_n and the acceleration \ddot{y}_n are expressed as central differences.

The values of the first step of an analysis cannot be calculated by the impulse acceleration method because it requires the values of the first and second previous steps. In this study they are calculated using the average acceleration method. When both the displacement and velocity at time 0 are assumed to be null, the displacement in the first step is expressed as follows,

$$y_1 = - \left\{ (\ddot{y}_0)_1 + (\ddot{y}_0)_0 \right\} \Delta t^2 \left/ \left(4 + \frac{2c}{M} \Delta t + \frac{k}{M} \Delta t^2 \right) \right. \quad (6.14)$$

6.3.2 Parameters investigated

A full range of parameters which has a significant influence on the inelastic response spectra of the idealized curves is examined. In this study the lateral load strength at yielding of the system V_u is expressed as a portion of the weight of the structure W . The

ratio is denoted as β_u .

$$\beta_u = \frac{V_u}{W} \quad (6.15)$$

Once a period of vibration of the system, T_e is given, the stiffness of the system, K_e is obtained by the following equation.

$$K_e = \frac{4\pi^2}{T_e^2} M \quad (6.16)$$

For a system with unit mass,

$$K_e = \frac{4\pi^2}{T_e^2} \quad (6.17)$$

The period of vibration based on the elastic stiffness varies between 0.1 and 3.0 seconds. The range of β_u investigated is between 0.2 and 1.4. The elastic response is also involved in the analyses. The ratio of the cracking load to the lateral load at yielding β_{cr} ranges between 1/2 and 1/3. The ratio of the elastic stiffness to the secant stiffness at yielding K_e / K_y ranges between 2 and 4. A set of the parameters (α, β) which determines the main characteristics of the idealized hysteresis loops is (0, 1), (0.5, 0.5) and (1, 0). These are considered to correspond to fully prestressed, partially prestressed and reinforced concrete idealizations, respectively. The post-yielding stiffnesses are -0.004, 0 and 0.004 as a portion of the elastic stiffness for fully prestressed, partially prestressed and reinforced concrete systems, respectively. The damping of the system, C , is given as $C = 2h\omega$. The assumed damping factor was $h = 5\%$. The range of the parameters considered is summarized in Table 6.1.

Table 6.1 Range of parameters investigated

	Description	Range Investigated
$\beta_u = V_u / W$	Lateral load strength as a portion of the weight of system	0.2 to 1.4
$\beta_{cr} = V_{cr} / V_u$	Ratio of cracking load to lateral load strength	1/2 and 1/3
T_e	Period of vibration	0.1 to 3.0
K_e / K_y	Ratio of elastic stiffness to secant stiffness at yielding	2 and 4
(α, β)	Parameters for prestressed concrete idealization	(0,1), (0.5, 0.5) and (1, 0)
Earthquake records		El Centro NS 1940 and Miyagiken-oki NS 1974
Intensity of Earthquake records		Original and 50cm/s

6.3.3 Earthquake records

The two typical digitalized earthquake records are included in the analyses; the El Centro 1940 North-South Component and the earthquake motion recorded at the first floor of the building at Tohoku University during the Miyagiken-oki earthquake in 1974. Only the first 10 seconds of the earthquake records were used because the maximum acceleration and velocity are observed within the first 10 seconds of the records which are considered to give the largest effects. The time interval used in the analyses was 0.02 seconds. The characteristics of the digitalized earthquake records used in the analyses are summarized in Table 6.2.

Table 6.2 Characteristics of earthquake wave records

Earthquake records	El Centro NS 1940	Miyagiken-oki 1974
Maximum acceleration (cm/s ²)	341.7	258.2
Maximum velocity (cm/s)	33.4	36.2
Maximum displacement (cm)	10.9	14.5

6.3.4 Response spectra of the idealized curves

General results

Displacement, velocity and acceleration response spectra calculated for each system and earthquake record are illustrated in Fig.6.2. Typical load-displacement relationships of fully prestressed, partially prestressed and reinforced concrete are shown in Fig.6.3.

In Fig.6.4, the ratios of yield capacities of the systems of interest to the shear response capacity of the system responding elastically, Q_y / Q_E are plotted against ductility ratios, μ . The ductility ratio μ is defined as the ratio of the maximum displacement, δ_m to the yield displacement, δ_y . The two equations below also appear in the diagrams.

$$\frac{Q_y}{Q_E} = \frac{1}{\sqrt{2\mu - 1}} \quad (6.18)$$

$$\frac{Q_y}{Q_E} = \frac{1}{\mu} \quad (6.19)$$

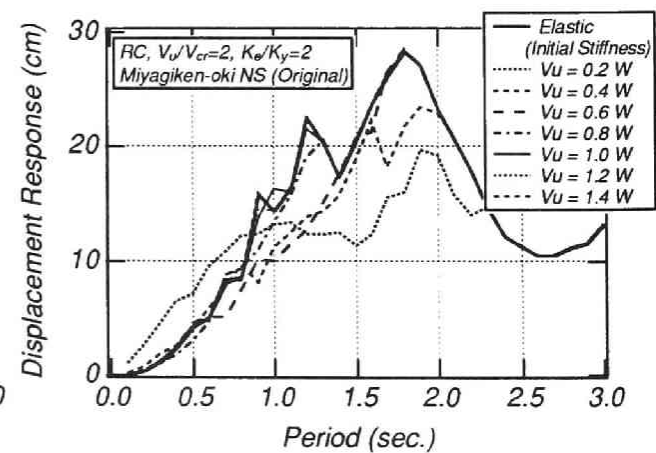
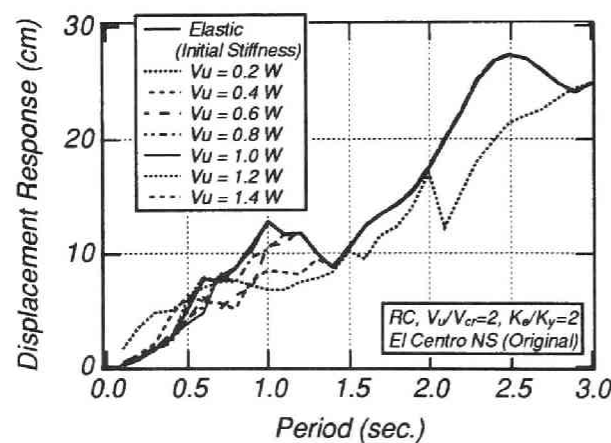
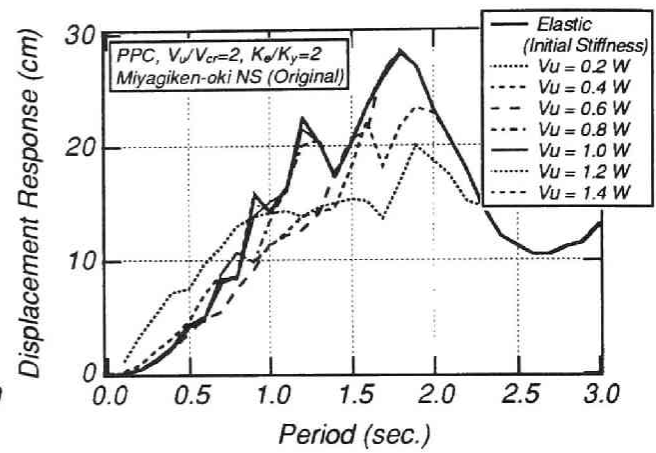
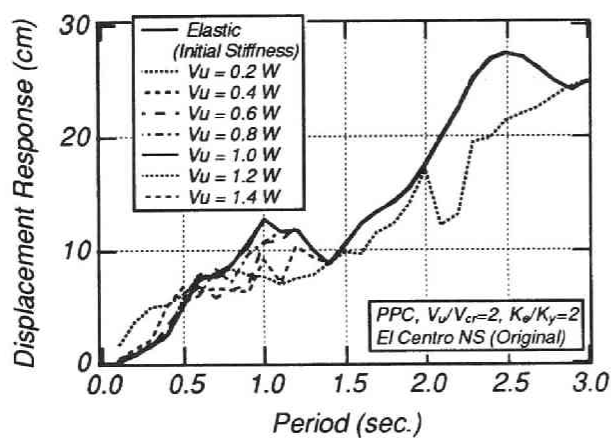
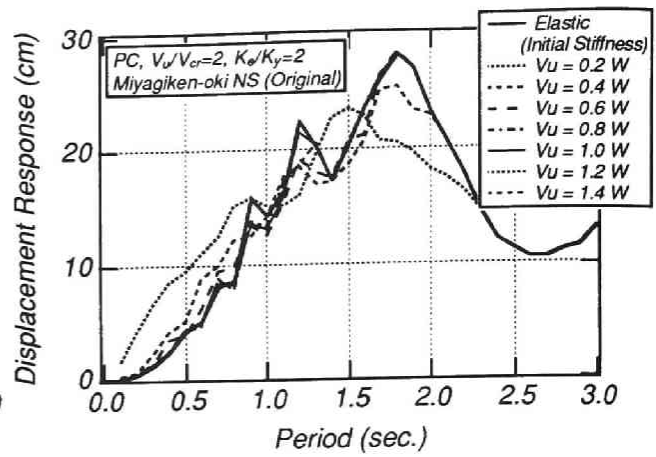
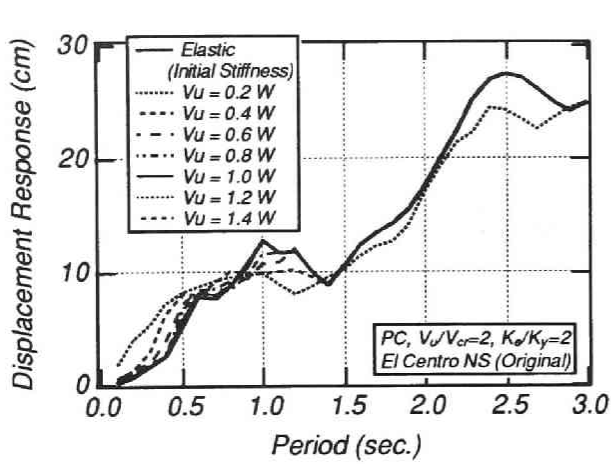


Fig.6.2(a) Displacement response spectra ($V_u/V_{cr}=2.0$, $K_\theta/K_y=2.0$ and El Centro NS (Original))

Fig.6.2(b) Displacement response spectra ($V_u/V_{cr}=2.0$, $K_\theta/K_y=2.0$ and Miyagiken-oki NS (Original))

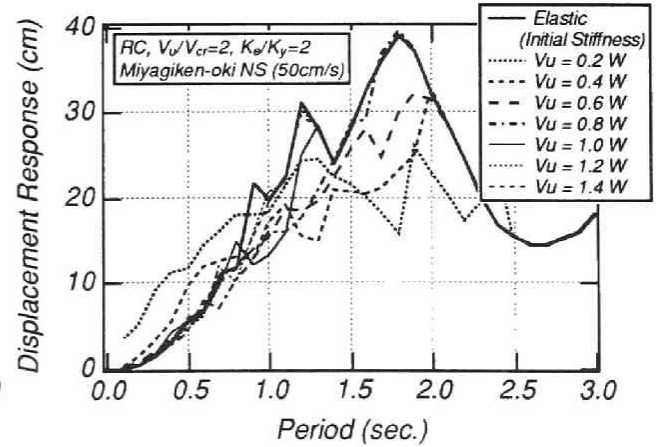
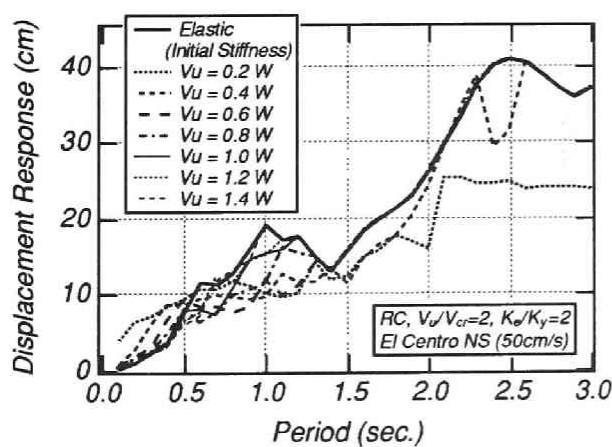
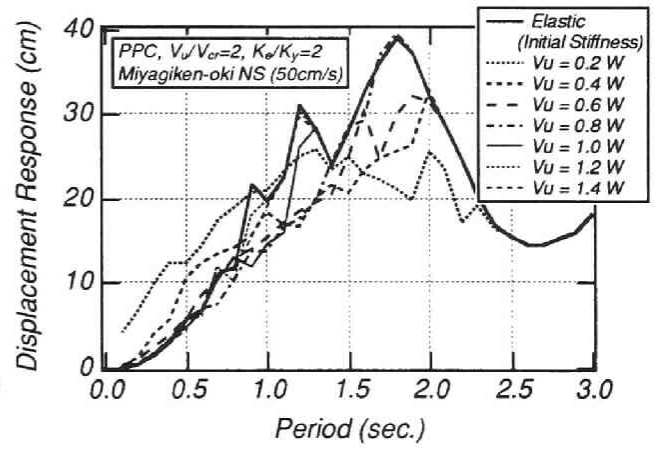
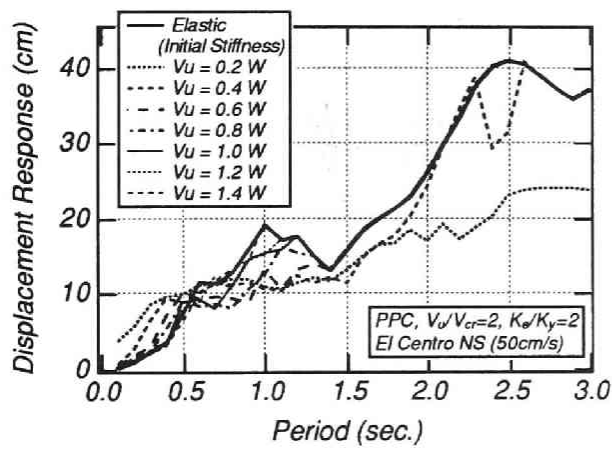
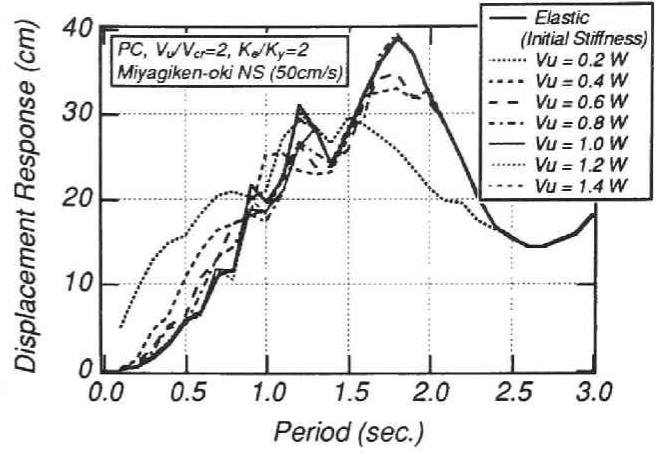
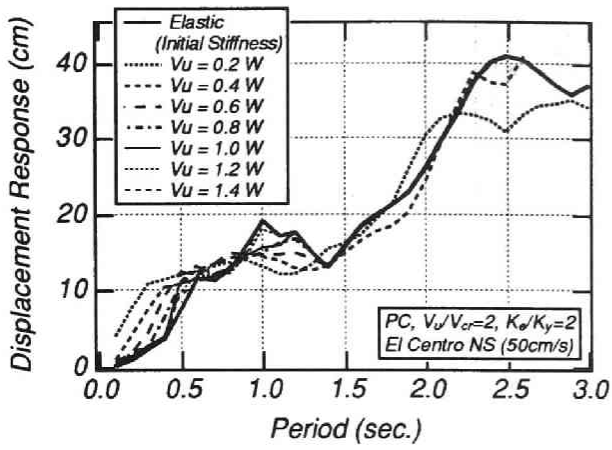


Fig.6.2(c) Displacement response spectra ($V_u/V_{cr}=2.0$, $K_e/K_y=2.0$ and El Centro NS (50cm/s))

Fig.6.2(d) Displacement response spectra ($V_u/V_{cr}=2.0$, $K_e/K_y=2.0$ and Miyagiken-oki NS (50cm/s))

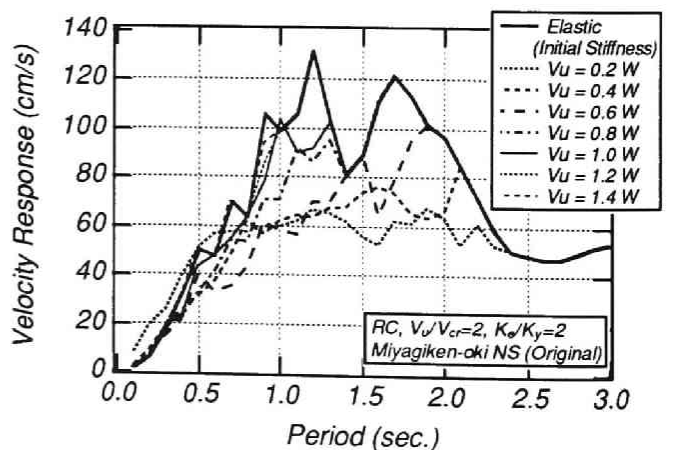
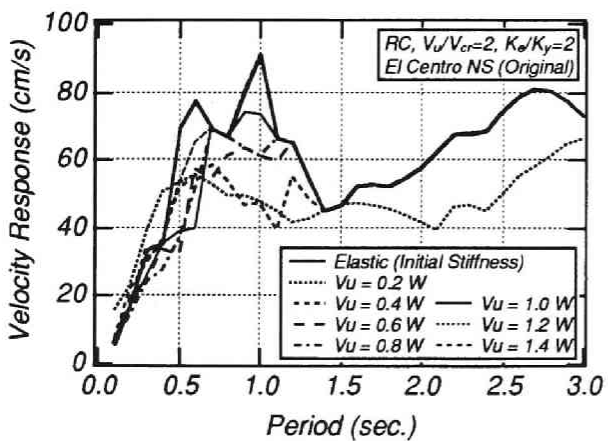
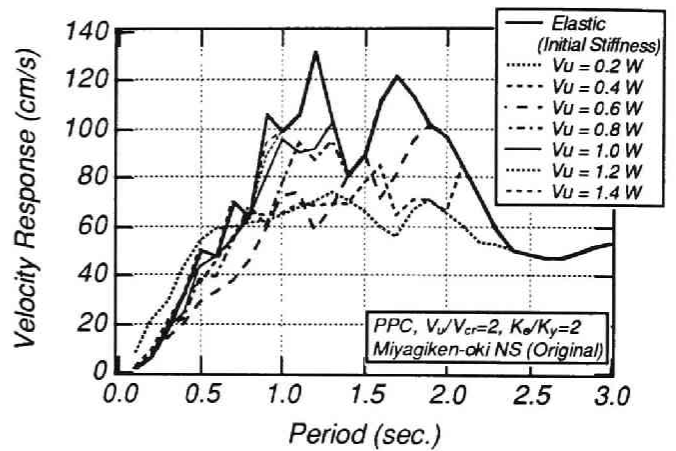
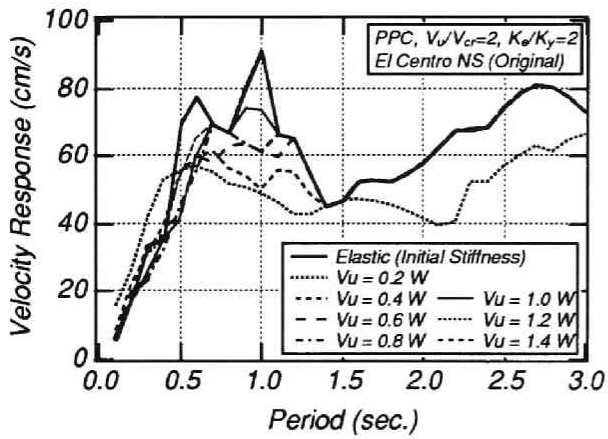
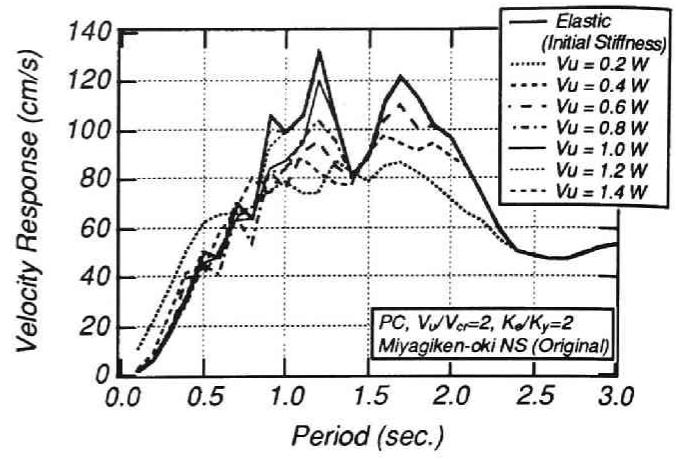
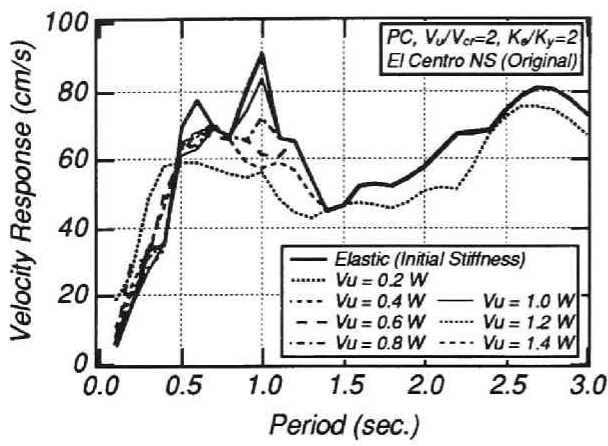


Fig.6.2(e) Velocity response spectra ($V_u/V_{cr}=2.0$, $K_e/K_y=2.0$ and El Centro NS (Original))

Fig.6.2(f) Velocity response spectra ($V_u/V_{cr}=2.0$, $K_e/K_y=2.0$ and Miyagiken-oki NS (Original))

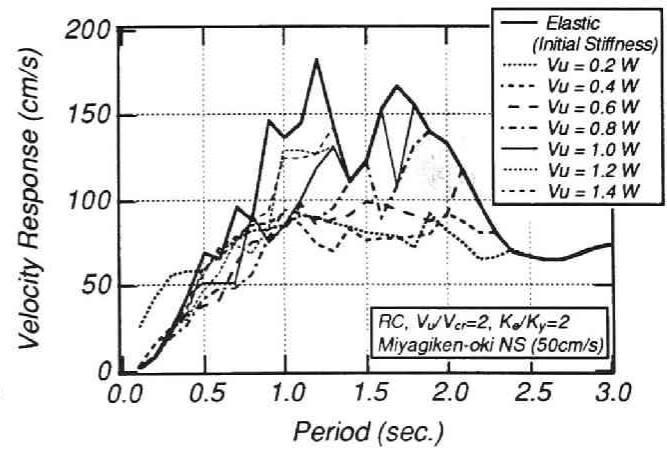
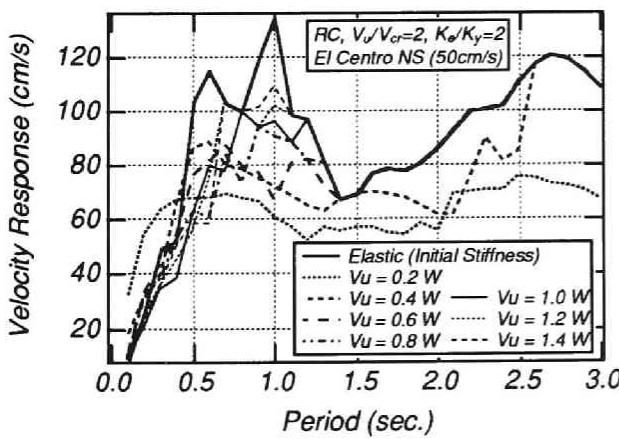
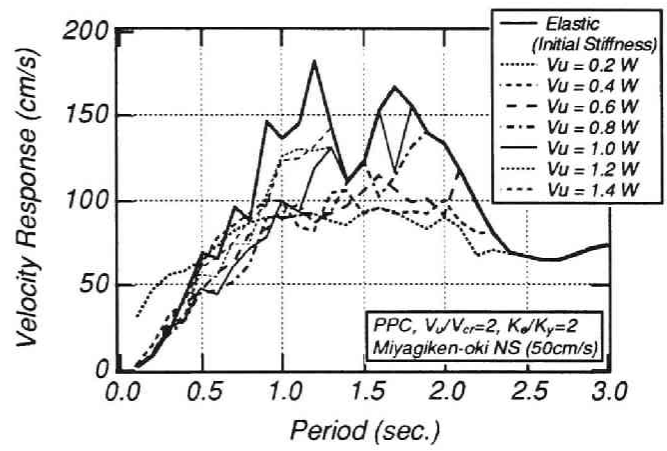
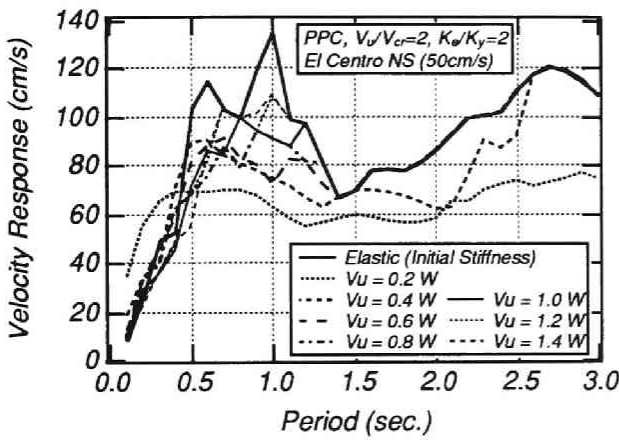
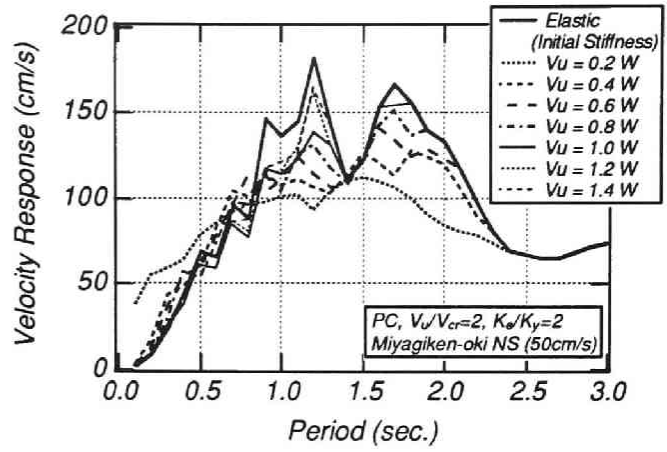
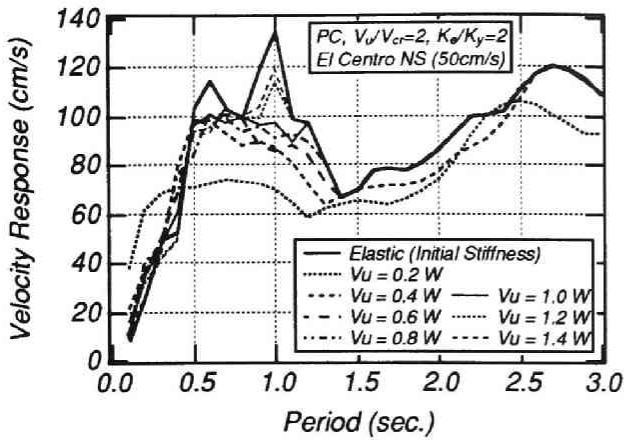


Fig.6.2(g) Velocity response spectra ($V_u/V_{cr}=2.0$, $K_e/K_y=2.0$ and El Centro NS (50cm/s))

Fig.6.2(h) Velocity response spectra ($V_u/V_{cr}=2.0$, $K_e/K_y=2.0$ and Miyagiken-oki NS (50cm/s))

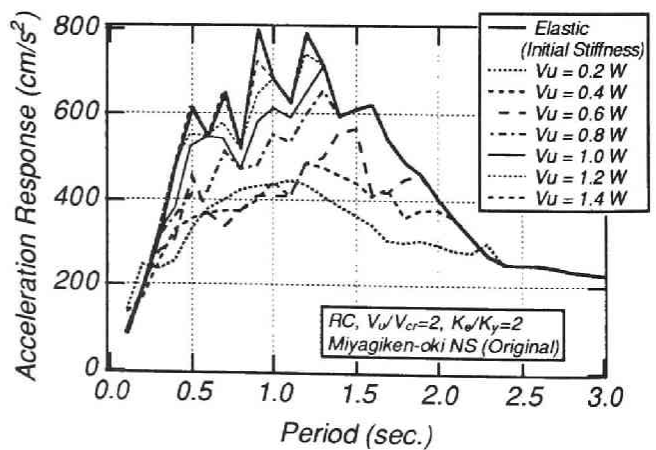
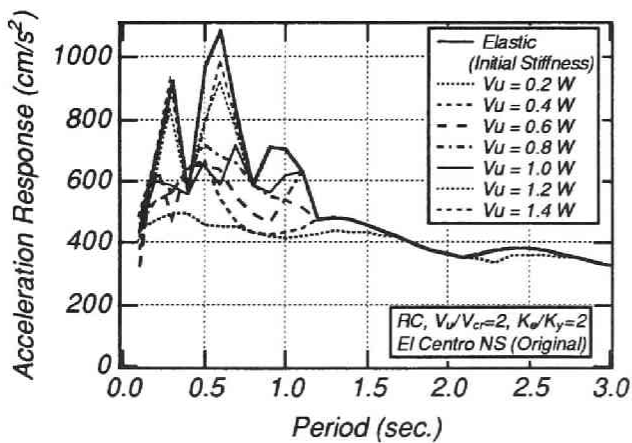
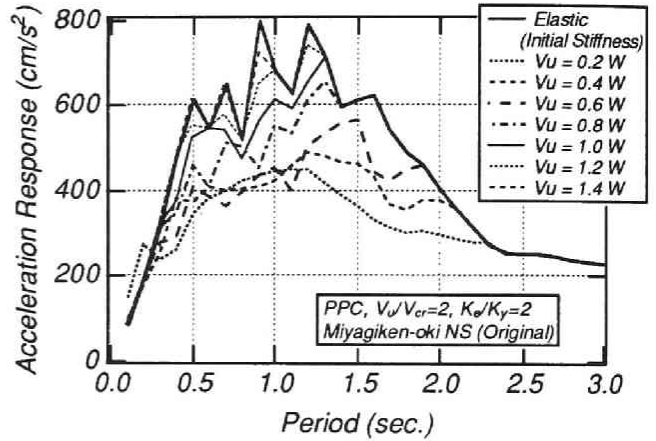
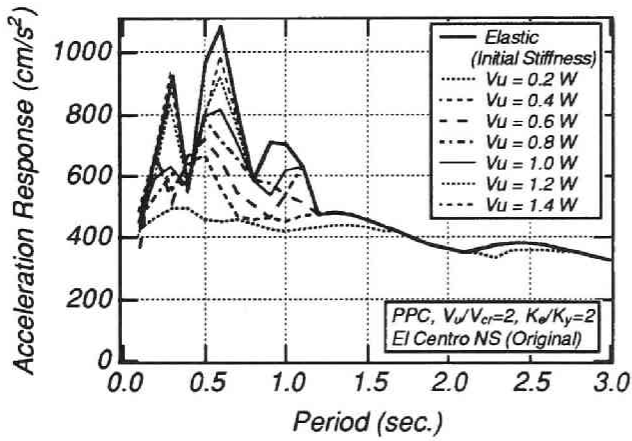
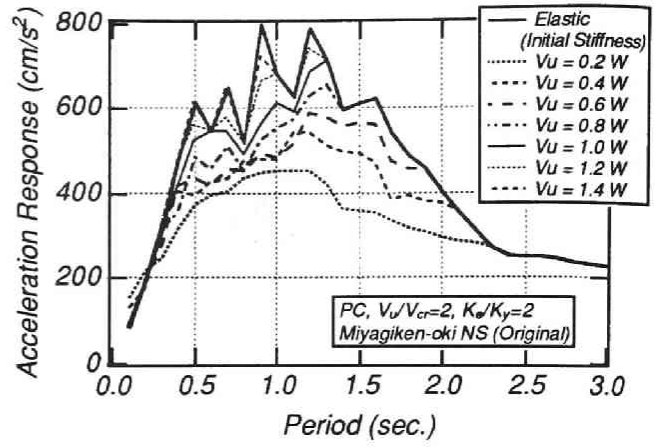
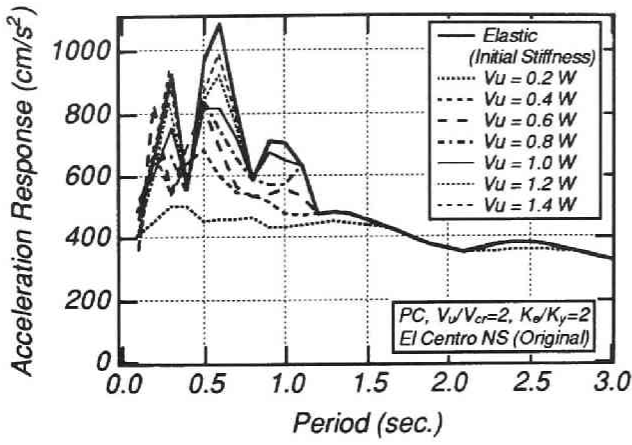


Fig.6.2(i) Acceleration response spectra ($V_u/V_{cr}=2.0$, $K_\theta/K_y=2.0$ and El Centro NS (Original))

Fig.6.2(j) Acceleration response spectra ($V_u/V_{cr}=2.0$, $K_\theta/K_y=2.0$ and Miyagiken-oki NS (Original))

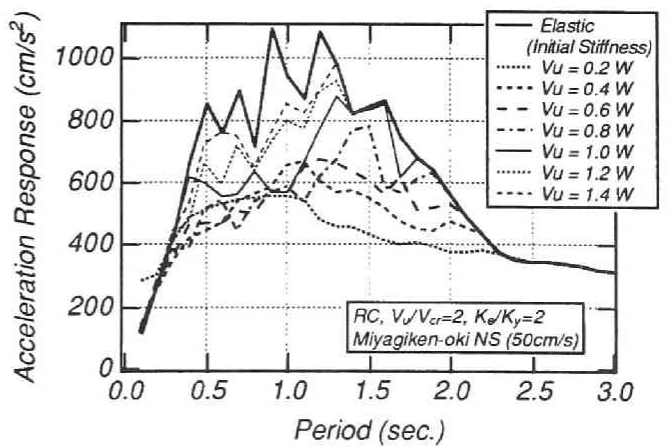
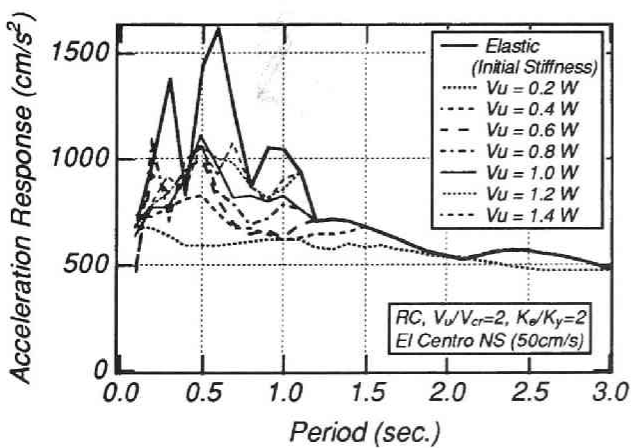
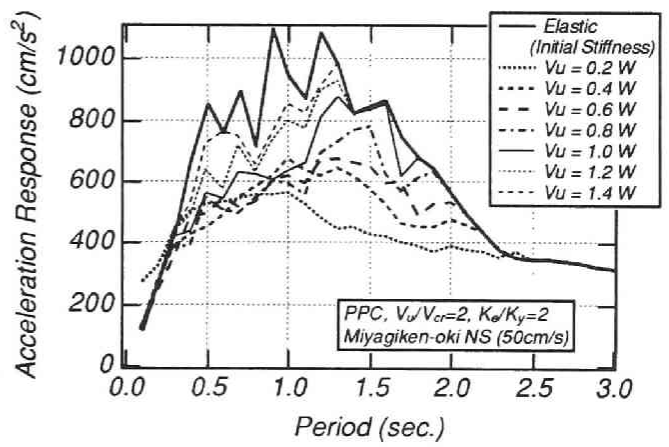
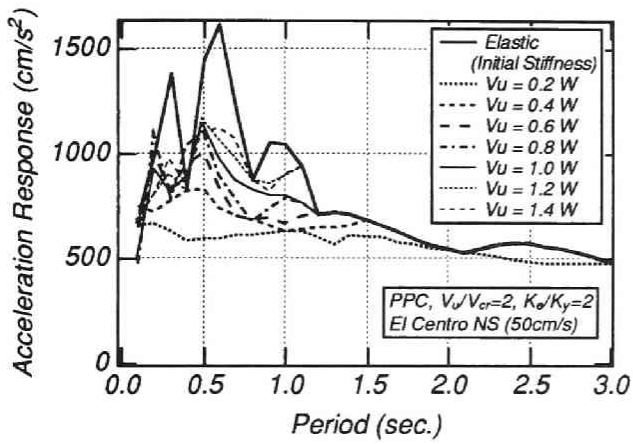
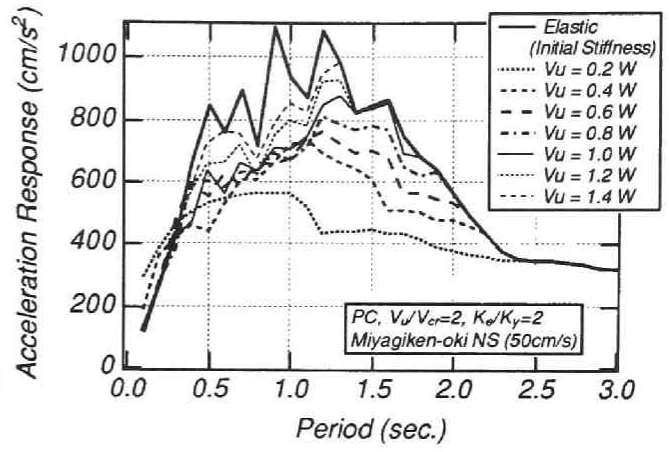
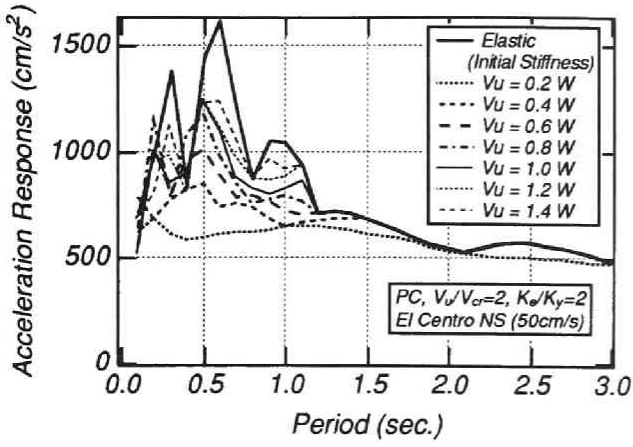


Fig.6.2(k) Acceleration response spectra ($V_u/V_{cr}=2.0$, $K_e/K_y=2.0$ and El Centro NS (50cm/s))

Fig.6.2(l) Acceleration response spectra ($V_u/V_{cr}=2.0$, $K_e/K_y=2.0$ and Miyagiken-oki NS (50cm/s))

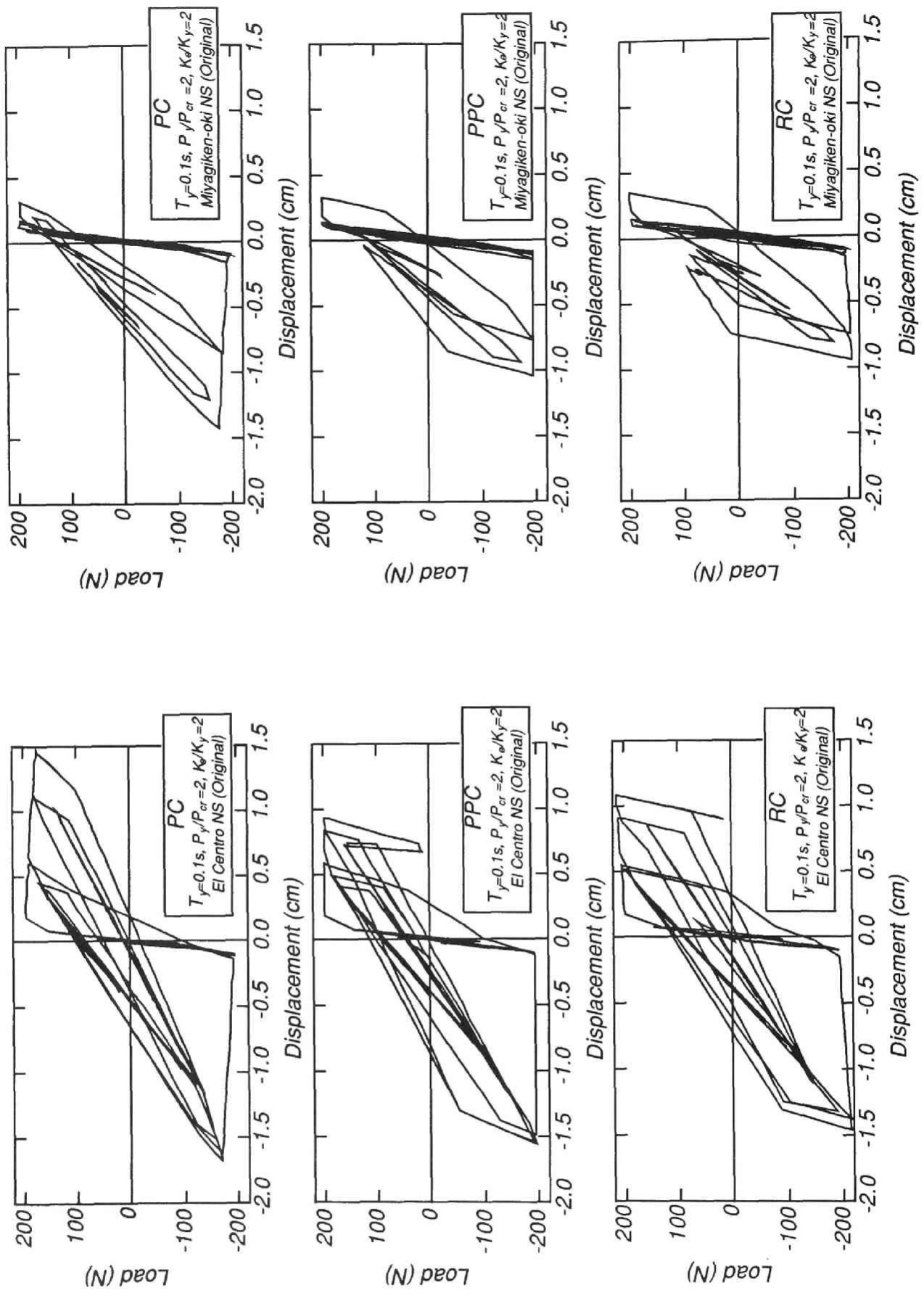


Fig.6.3(a) Load - displacement relationships of SDOF systems

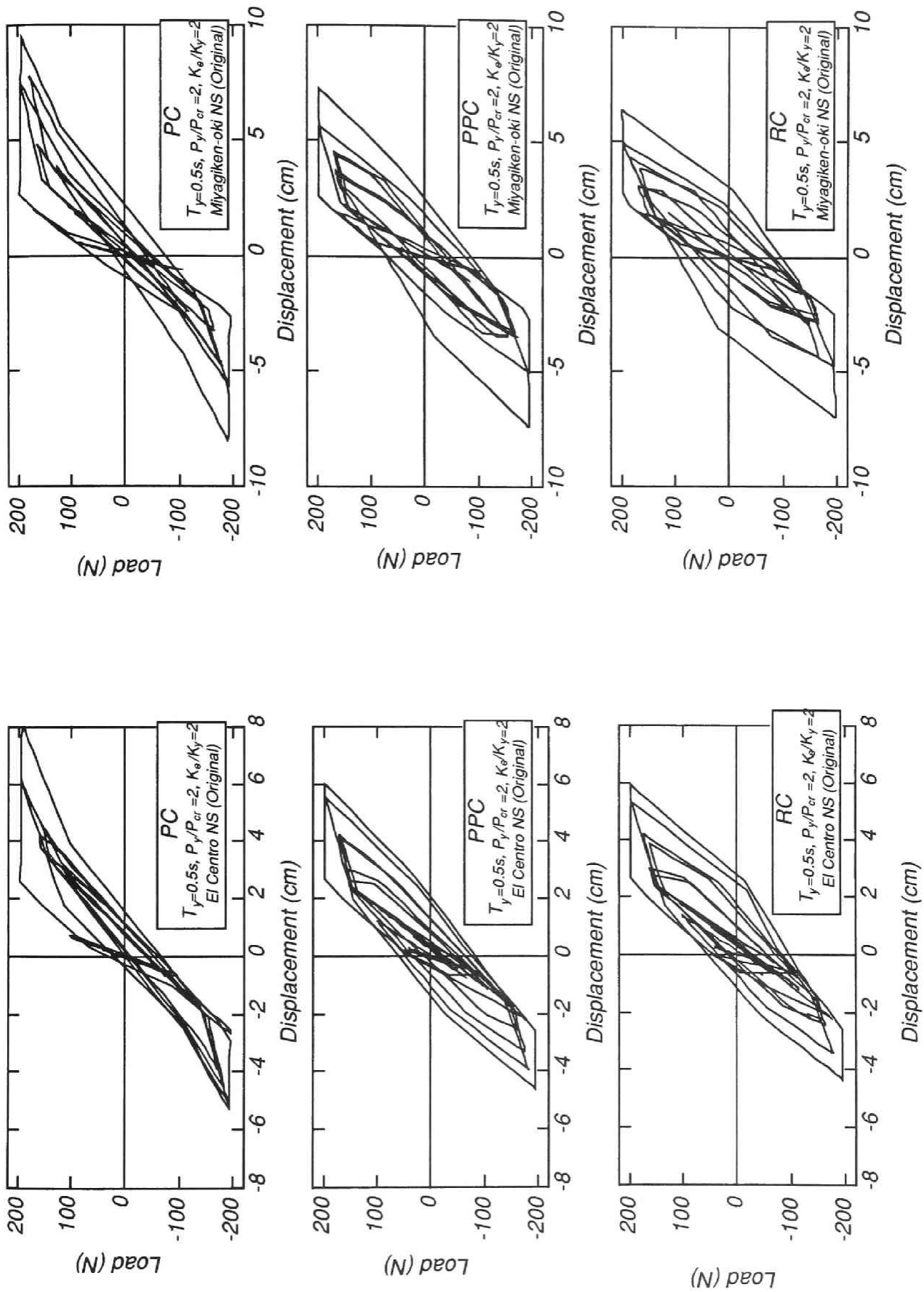


Fig.6.3(b) Load - displacement relationships of SDOF systems

Eq.6.18 is based on the equal energy concept in which the energy absorbed by a building which yields with elasto-plastic characteristics is assumed to be equal to that of a building which is strong enough to respond elastically. Strictly speaking, however, it is only an impulse input that physically concludes that Eq.6.18 is derived by the equal energy concept. Eq.6.19 is considered to indicate the equal displacement concept in which the maximum horizontal deflection reached by a building which yields with elasto-plastic characteristics is assumed to be the same as that of a building which is strong enough to respond in the elastic range. The markers above the line of Eq.6.19 suggest that the maximum responses of the systems cannot be predicted conservatively by the equal displacement concept. Similarly, the markers above the curve of Eq.6.18 indicate that the equal energy concept gave an unsafe prediction. In the case of the response against the El Centro earthquake wave few markers are observed above the Eq.6.18. However, as for the Miyagiken-oki earthquake several markers are located high above the curve in the large ductility region. These are the responses of the system with short period of vibration of 0.1 or 0.2 seconds.

Ishimaru [6.3] conducted dynamic response analyses on the bilinear elasto-plastic systems for three earthquake records with different characteristics. In the case of the systems with a frequency of 5.0 Hz using the Miyagiken-oki earthquake the responses fell into the region above the curve of Eq.6.18. As for the El Centro earthquake, the responses fell into the region below the curve of Eq.6.18 even for the system with the same frequency of 5.0 Hz. Eq.6.18 does not always give a conservative prediction for a maximum response displacement.

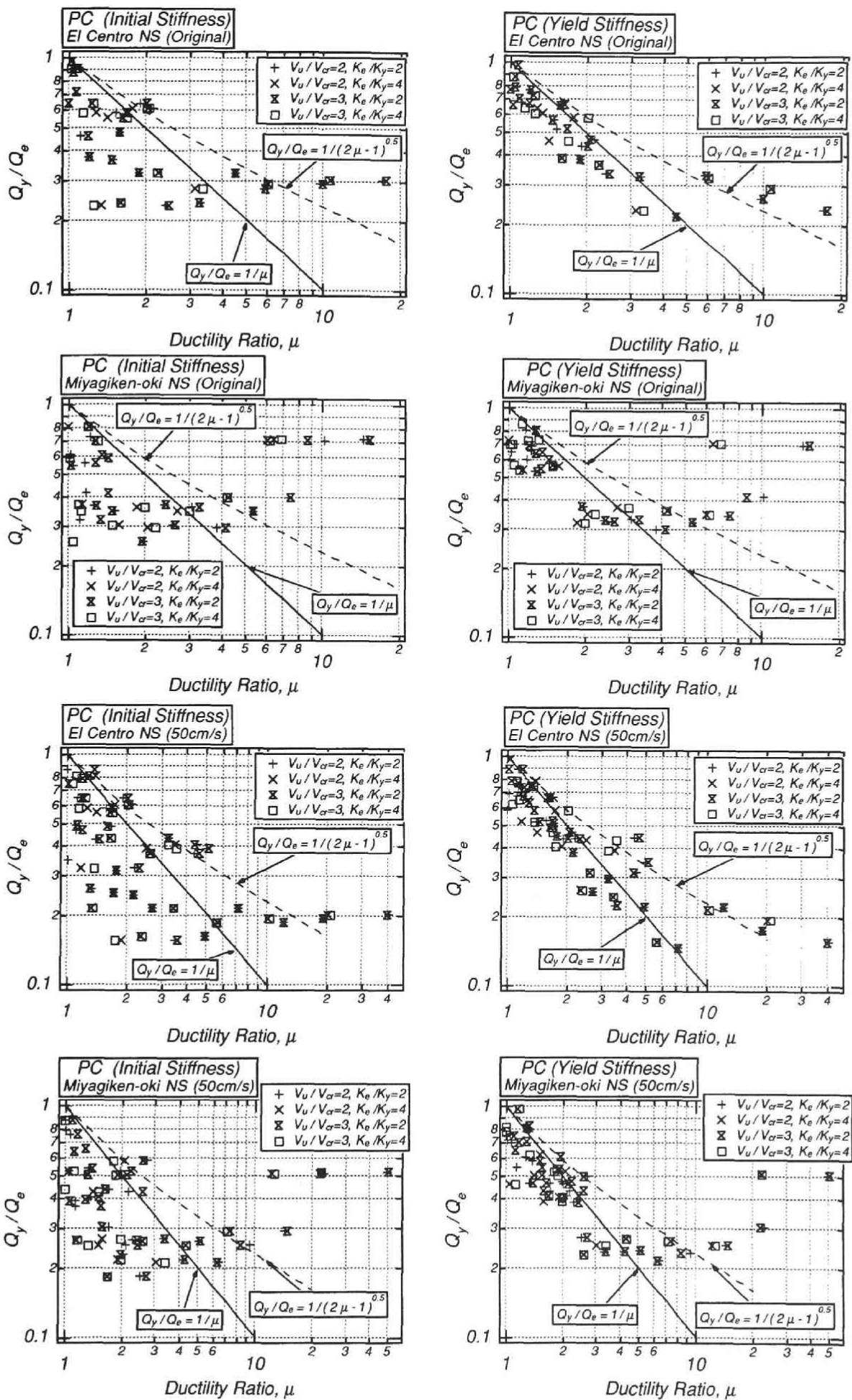


Fig.6.4(a) $Q_y/Q_e - \mu$ (Prestressed concrete)

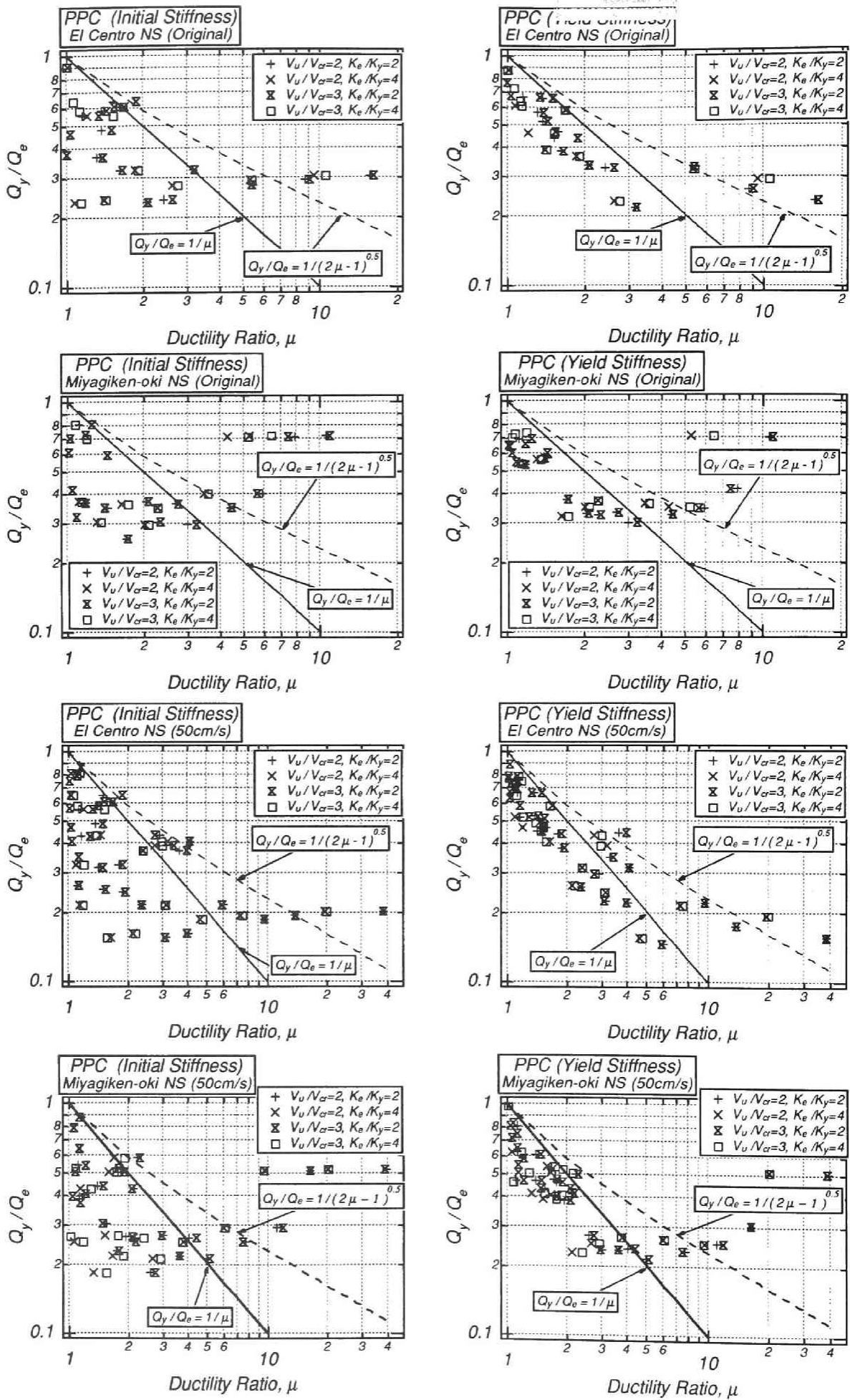


Fig.6.4(b) $Q_y/Q_E - \mu$ (Partially prestressed concrete)

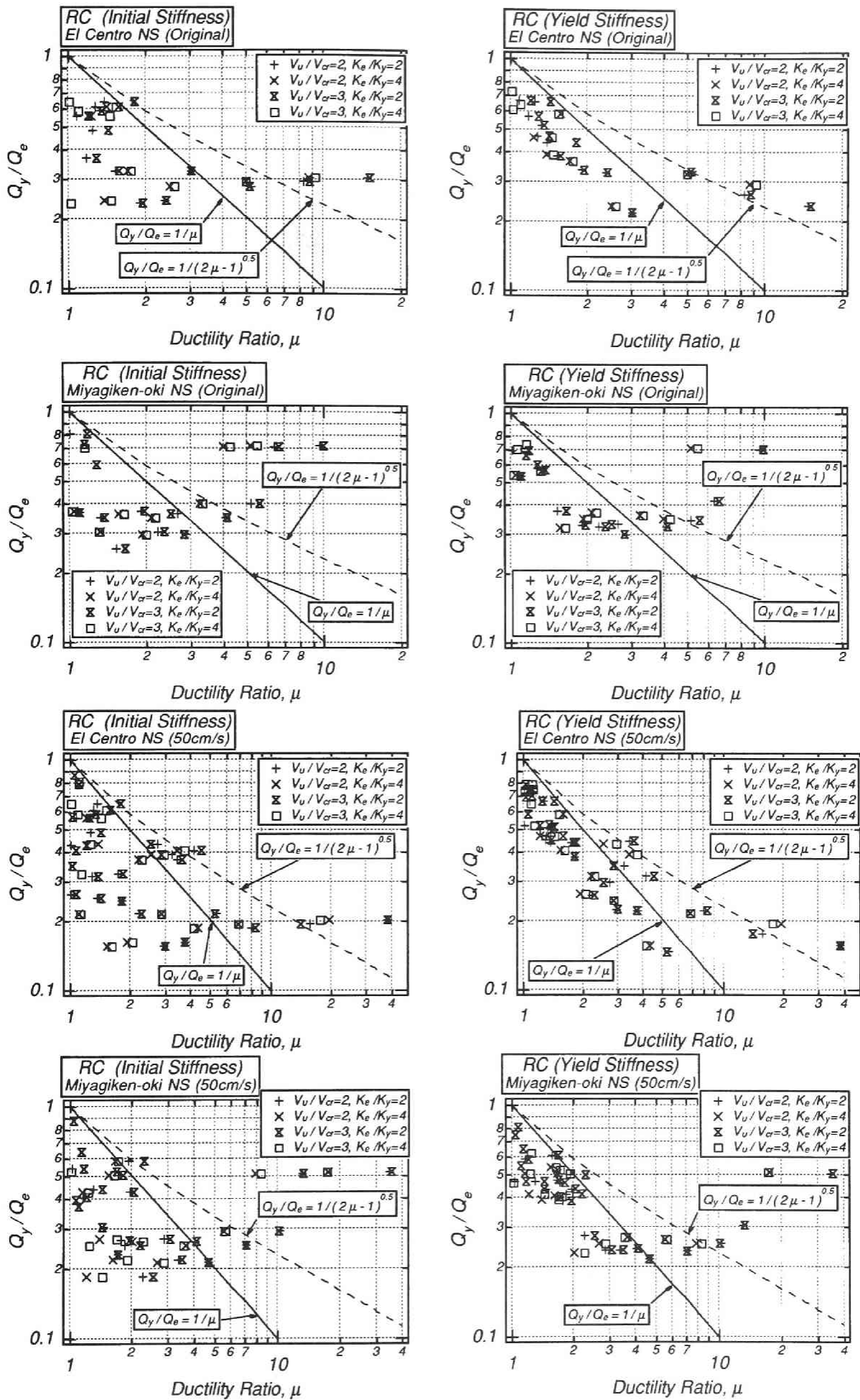


Fig.6.4(c) $Q_y/Q_E - \mu$ (Reinforced concrete)

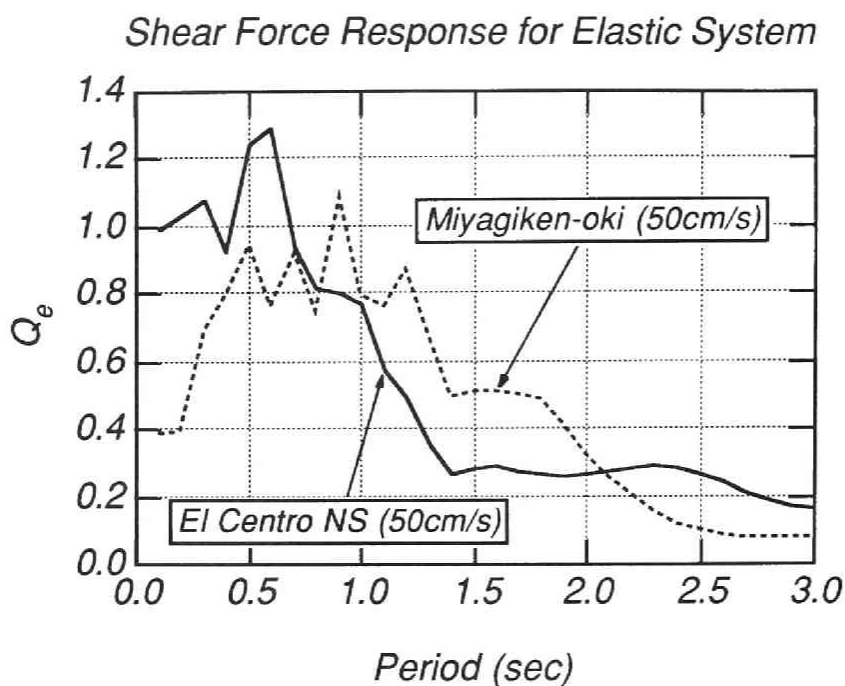


Fig.6.5 Shear force response of the system responding elastically

Figure 6.5 illustrates the shear force responses for the system responding elastically. It should be noted that much smaller response for the Miyagiken-oki earthquake than for the El Centro earthquake is observed for the period of 0.1 and 0.2 seconds. The displacement responses for these two earthquakes are almost the same. This is the reason why the responses above the curve of Eq.6.18 appear in Fig.6.4. The difference between the elastic responses of the earthquakes may be due to the characteristics of the waves.

Okamoto suggested Eq.6.2 in his doctoral thesis [6.2] on the basis of the dynamic response analysis using ‘Modified PS model’. In this study, however, it is difficult to derive a definite conclusion because the responses are significantly depending on the earthquake waves. As far as the El Centro NS component is concerned, Eq.6.18 gives a relatively good approximation for the maximum responses of the systems. In addition, for the systems with smaller Q_y / Q_E ratio Q_E should be estimated on the basis of the yield stiffnesses. In the case of the initial stiffnesses, there are some markers whose deviations from Eq.6.18 are quite large.

Comparison between prestressed and reinforced concrete

Figure 6.6 shows the ratios of the maximum displacement responses of the prestressed concrete systems to those of the corresponding reinforced concrete systems. The similar ratios of the partially prestressed concrete systems are plotted against period of vibration of the systems in Fig.6.7. The value in the parentheses following the yield

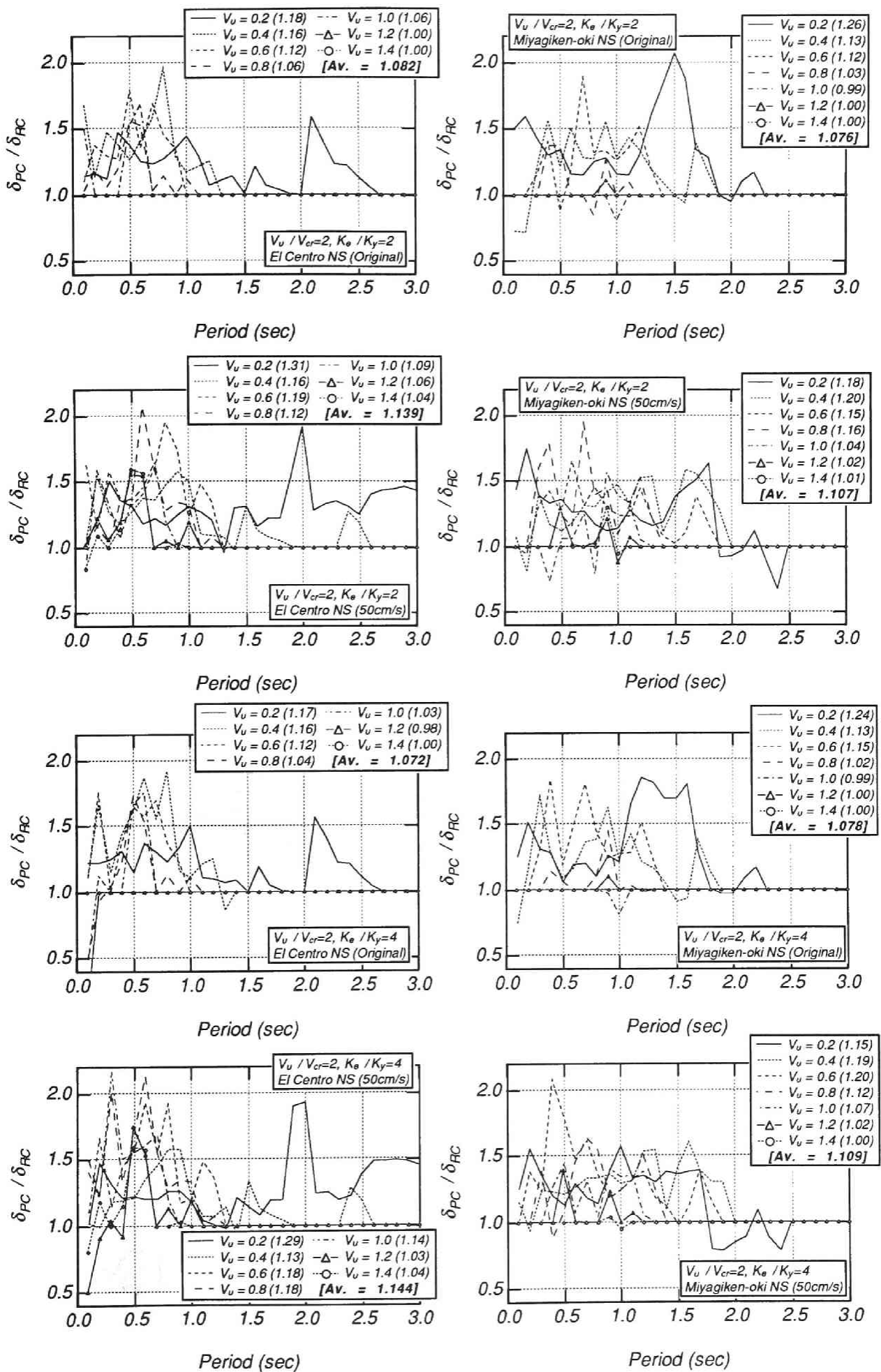


Fig.6.6(a) Comparison of maximum displacement response

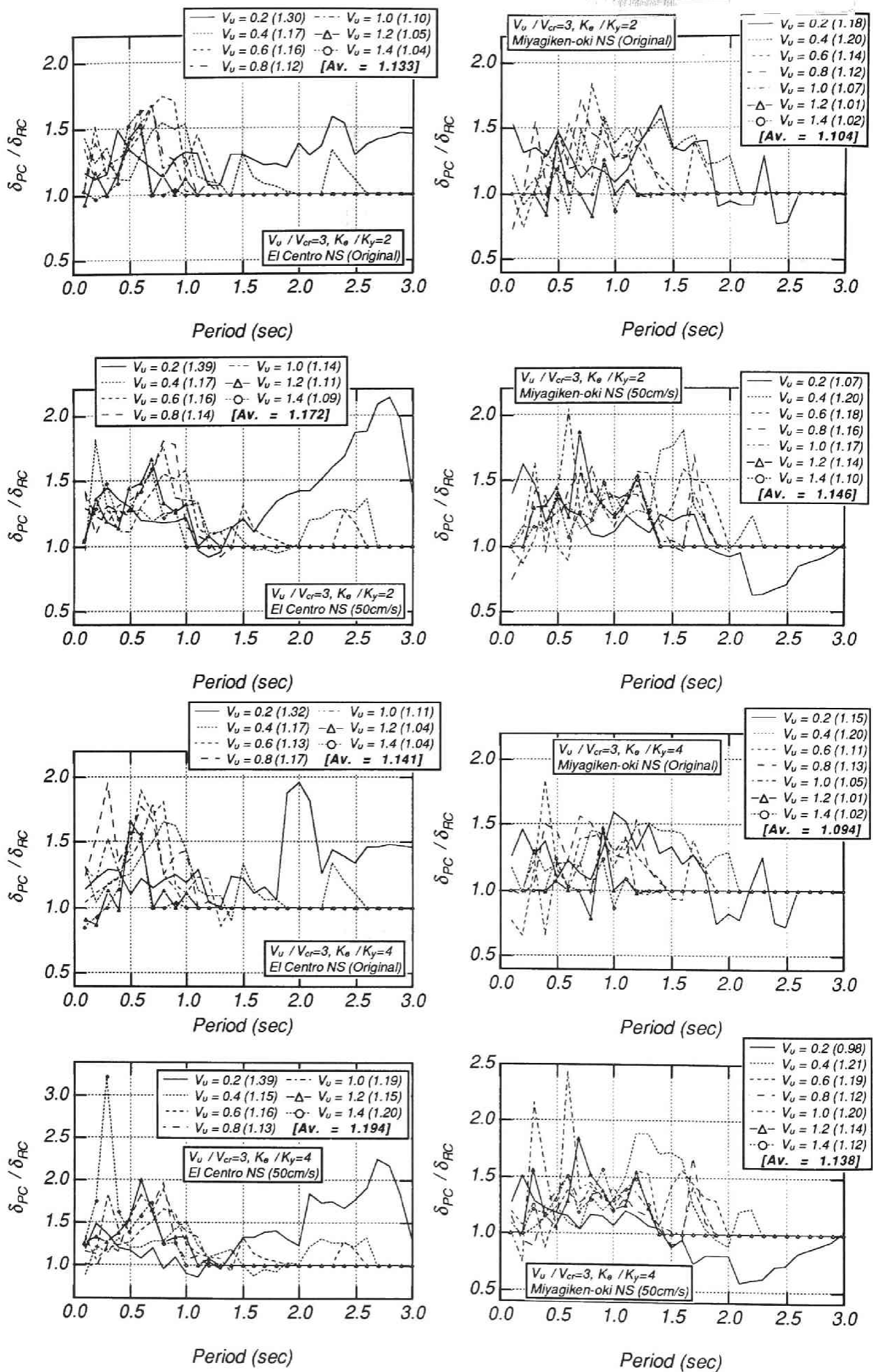


Fig.6.6(b) Comparison of maximum displacement response

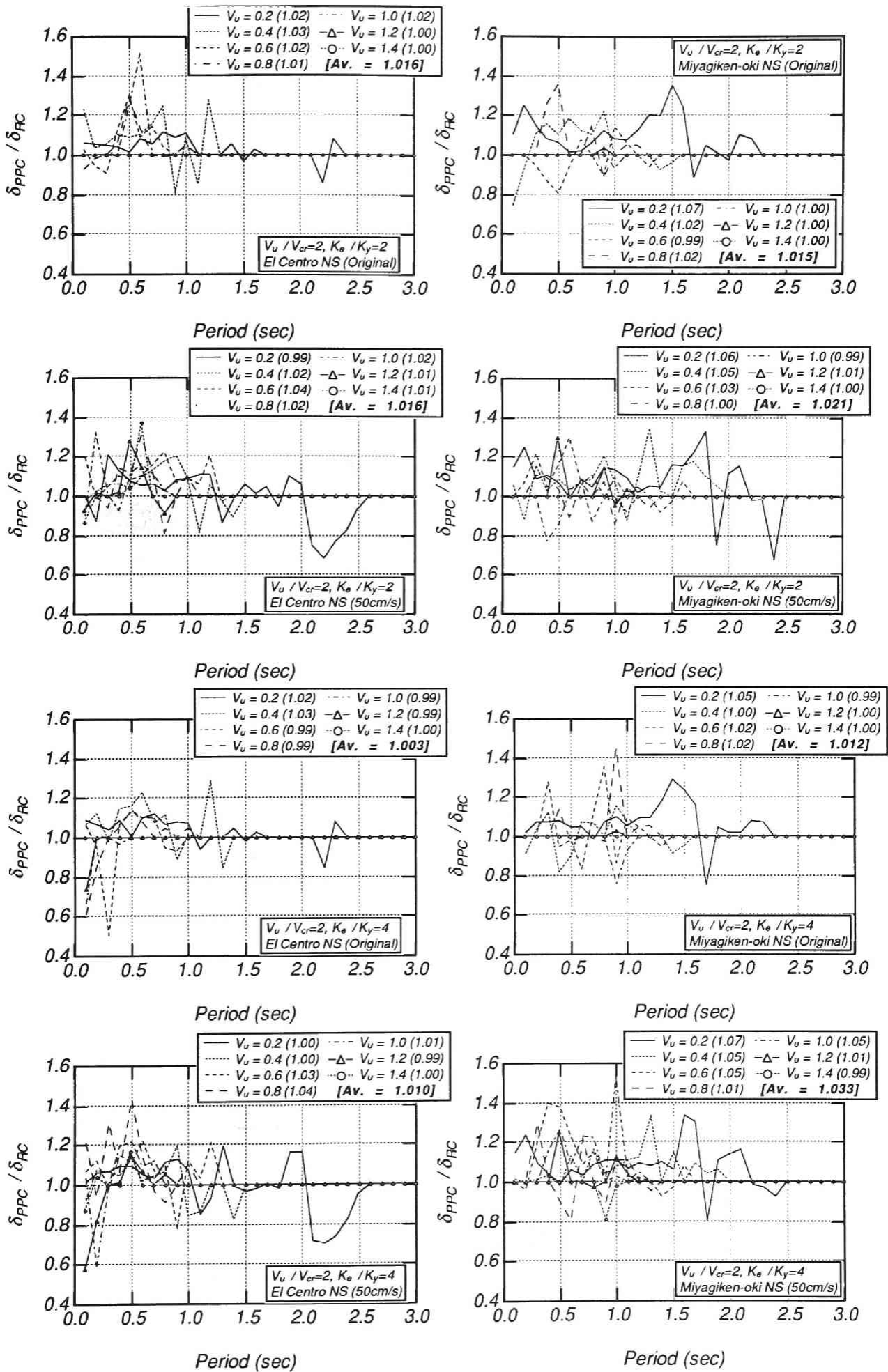


Fig.6.7(a) Comparison of maximum displacement response

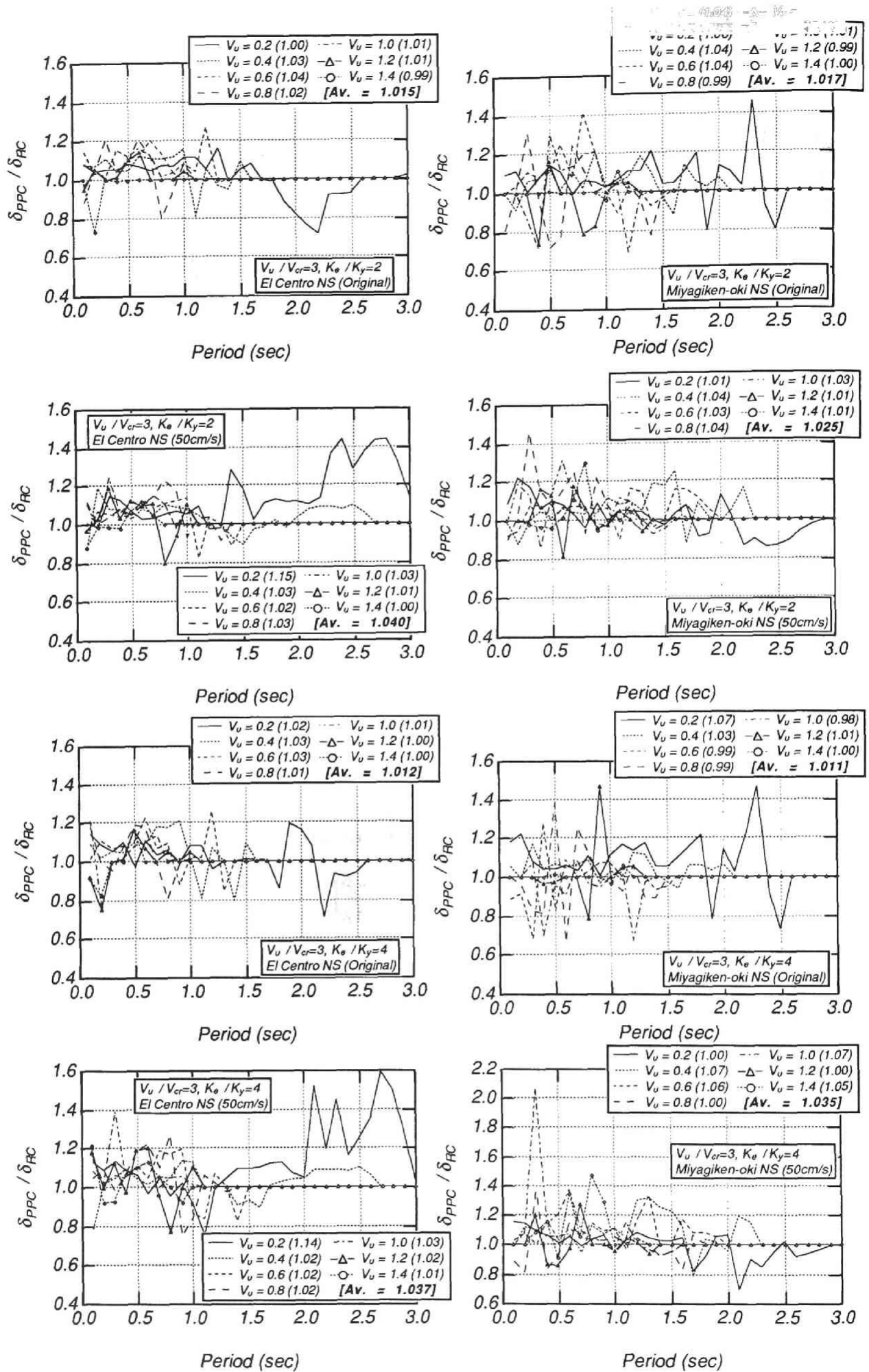


Fig.6.7(b) Comparison of maximum displacement response

capacity in the legend indicates the average of the ratio for each yield capacity of the systems. The average values over the period range of 0.1 to 3.0 seconds might not be of importance: if a larger period range was included in the analyses the average values would become smaller. The average values for the prestressed concrete systems range between 0.98 and 1.39 with the maximum value of 3.23 and the minimum of 0.29. For partially prestressed concrete systems those range 0.98 and 1.15 with the maximum value of 2.06 and the minimum value of 0.51. Generally, the ratios are larger in the period shorter than approximately 0.5 seconds. This corresponds to the displacement response spectra given in Fig.6.2.

If the structural damage can be estimated by the maximum displacement response, the damage of prestressed concrete systems is predicted to be 1.39 in average times that of reinforced concrete systems. Past research has indicated that the load capacity of a system may be increased by 20% if the displacement response should be reduced by 20%. NZS 4203:1984 [6.4] is based on the analytical results conducted by Thompson [6.1] and on this criteria, although the design seismic load - displacement response relationship is not linear.

6.3.5 Comparison between prestressed concrete and reinforced concrete with pinched hysteresis loops

As described in Chapter 4, hysteresis loops of a reinforced concrete beam - column joint assemblage are not always better than those of a prestressed concrete beam - column joint assemblage. Load - displacement hysteretic behaviour controlled by slip of longitudinal beam bars through the joint core due to bond deterioration indicates degradation of strength and stiffness and pinched hysteresis loops with reduced energy dissipation. However, the effect of pinching of the hysteresis loops on the response was found to be of little significance by Kitayama et al [6.5]. They concluded that some bond deterioration of beam bars within a beam - column joint may be acceptable.

Park [6.6] is pointing out on the basis of past research that some variation in hysteresis loop shape will not have a major influence on the inelastic dynamic response of

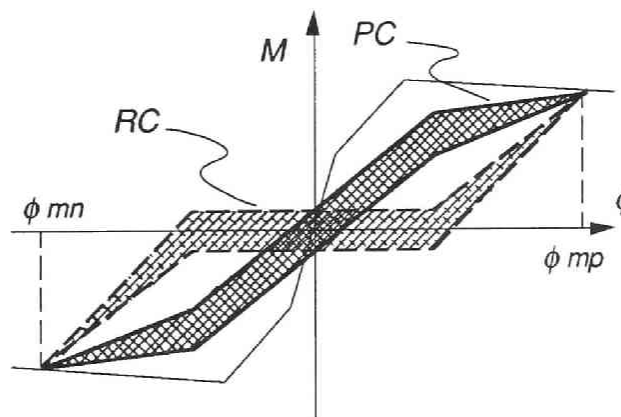


Fig.6.8 Load - displacement relationships of prestressed concrete system and reinforced concrete system with pinched hysteresis loops

structures when subjected to severe earthquake excitation. Thus, hysteresis loops showing some pinching or stiffness degradation will not lead to significantly larger inelastic displacements if the structure has some damping of viscous type and is capable of some further damping by hysteretic energy dissipation. Based on the dynamic response analyses, Thompson [6.7] reached the similar conclusion that the load - displacement characteristics do not affect the ductility demand as much as the intensity of the earthquake excitation and the initial period of vibration.

It is of great interest that responses of a prestressed concrete system are compared with those of a reinforced concrete system whose load - displacement hysteretic behaviour is controlled by slip of longitudinal beam bars, that is, indicates pinched hysteresis loops. Those two systems are assumed to dissipate the same amount of hysteretic energy when they are in steady state at a same amplitude. Fig.6.8 shows the load - displacement relationships of those two systems at the maximum displacement of δ_{mp} . The hysteresis loops for prestressed concrete systems proposed in Chapter 5 were used for load - displacement hysteretic behaviour of the prestressed concrete system. For the reinforced concrete system with pinched hysteresis loops, the hysteresis loops for reinforced concrete systems proposed in Chapter 5 were employed with some modification in post-elastic range. The coordinates of $C_{ip}(\phi, M)$ are given as follows,

$$M = 0.15M_u \quad (6.21)$$

for $\phi_u < \phi_{mp} < 10\phi_u$,

$$\phi = \phi_{mp} \left(0.3 + 0.05 \frac{\phi_{mp}}{\phi_u} \right) \quad (6.22)$$

for $\phi_{mp} > 10\phi_u$

$$\phi = 0.8\phi_{mp} \quad (6.23)$$

The loop width denoted by M_{ld} is assumed to be $0.3M_u$. The tangential stiffness of the hysteresis loops in the region between C_{ip} and C_{in} is kept zero once the system undergoes the yield displacement. Up to yielding, the hysteresis loops assigned to the pinched system are exactly the same ones for the reinforced concrete system proposed in Chapter 5.

Figure 6.9 indicates the displacement response spectra of the reinforced concrete systems with pinched hysteresis (hereafter referred to as *PH* system). The parameters assigned for the analyses are the same ones that were used in the previous analyses described in the preceding section. Fig.6.10 shows the ratios of the displacement responses of the reinforced concrete systems described in the preceding section to those of the *PH* systems. In addition, the ratios of the displacement responses of the

prestressed and partially prestressed concrete systems to those of the *PH* systems are plotted against period of vibration in Fig.6.11 and 12. Fig.6.10 indicates that the ratios in the range of the shorter period of vibration than 1.0 sec. are large. In the long period range, they are unity. In the small displacement range up to yielding, the responses of the reinforced concrete system and the *PH* system are the same because the hysteresis loops are identical. However, beyond the yield displacement, the load - displacement characteristics have an effect on the displacement response.

The average values of the ratios of displacement responses for the prestressed concrete system range between 1.09 and 1.14. They are slightly smaller than those in the comparison between the prestressed concrete system and the reinforced concrete system. The average values for the partially prestressed concrete are approximately unity.

As long as the parameters and the earthquake records used in the analyses are concerned, a system whose load - displacement behaviour is that of a fully prestressed concrete was found to respond on average approximately 10% in average larger than a system with pinched hysteresis loops of the same amount of hysteretic energy dissipated.

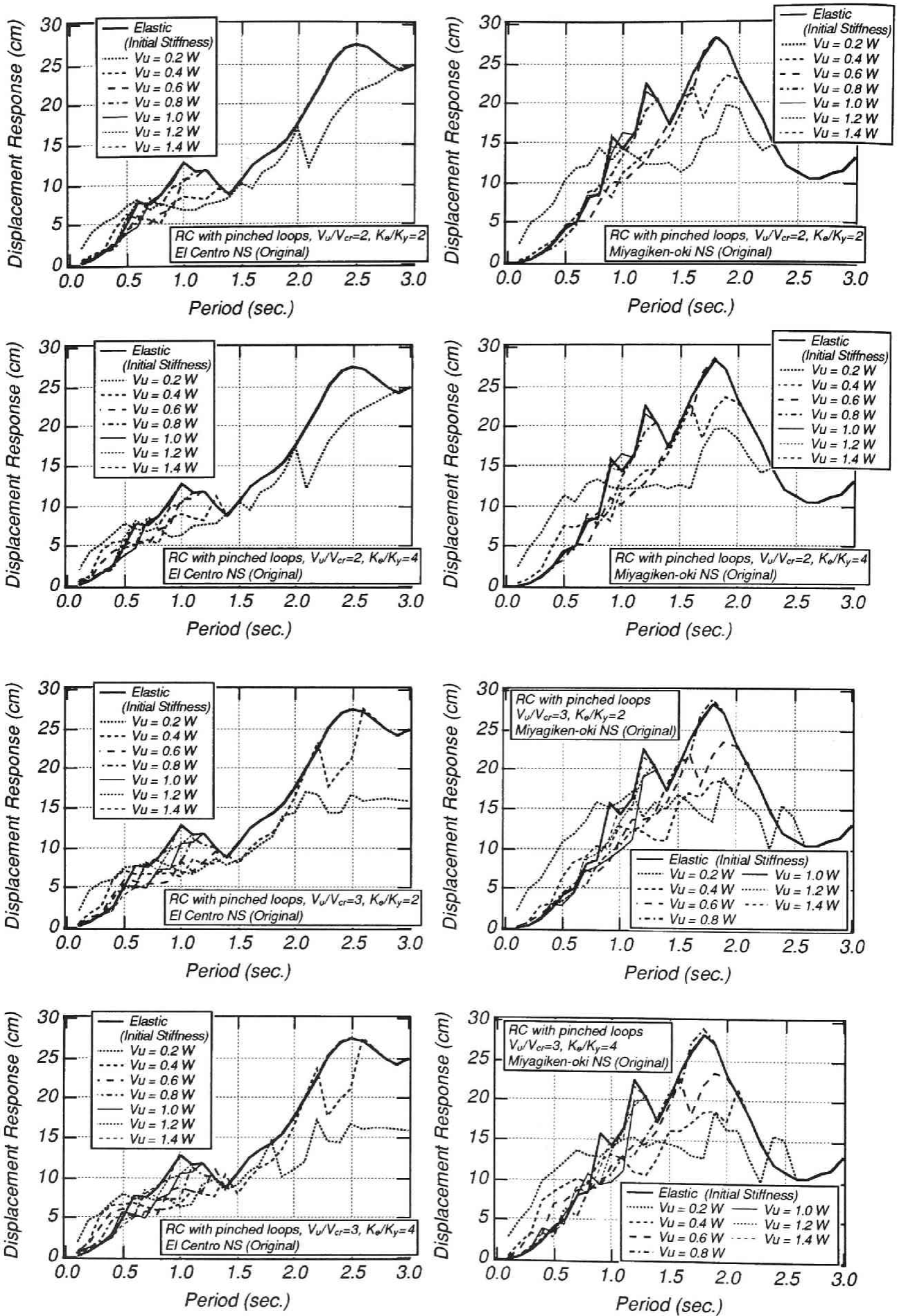


Fig.6.9(a) Displacement response spectra of reinforced concrete system with pinched hysteresis

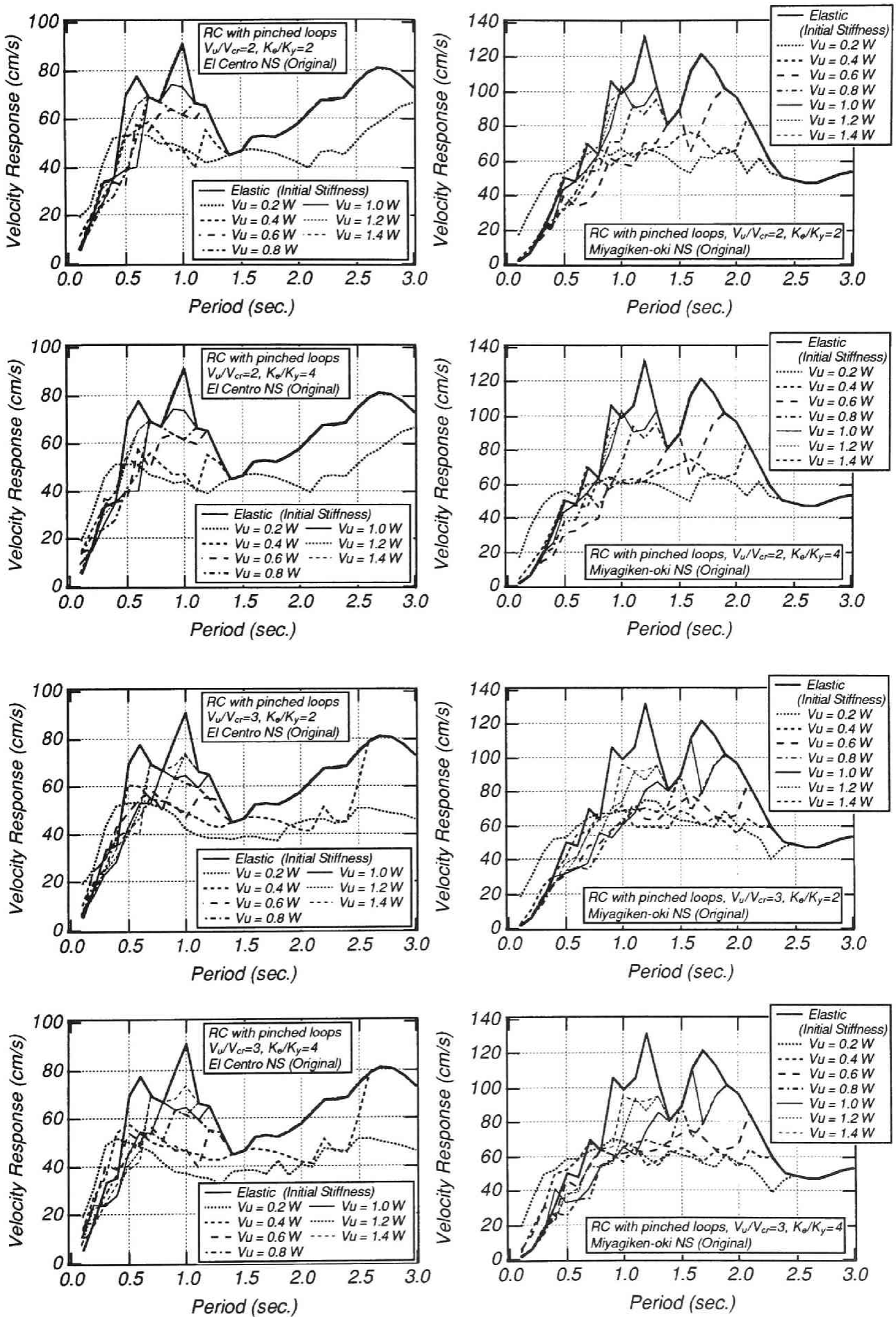


Fig.6.9(b) Velocity response spectra of reinforced concrete system with pinched hysteresis

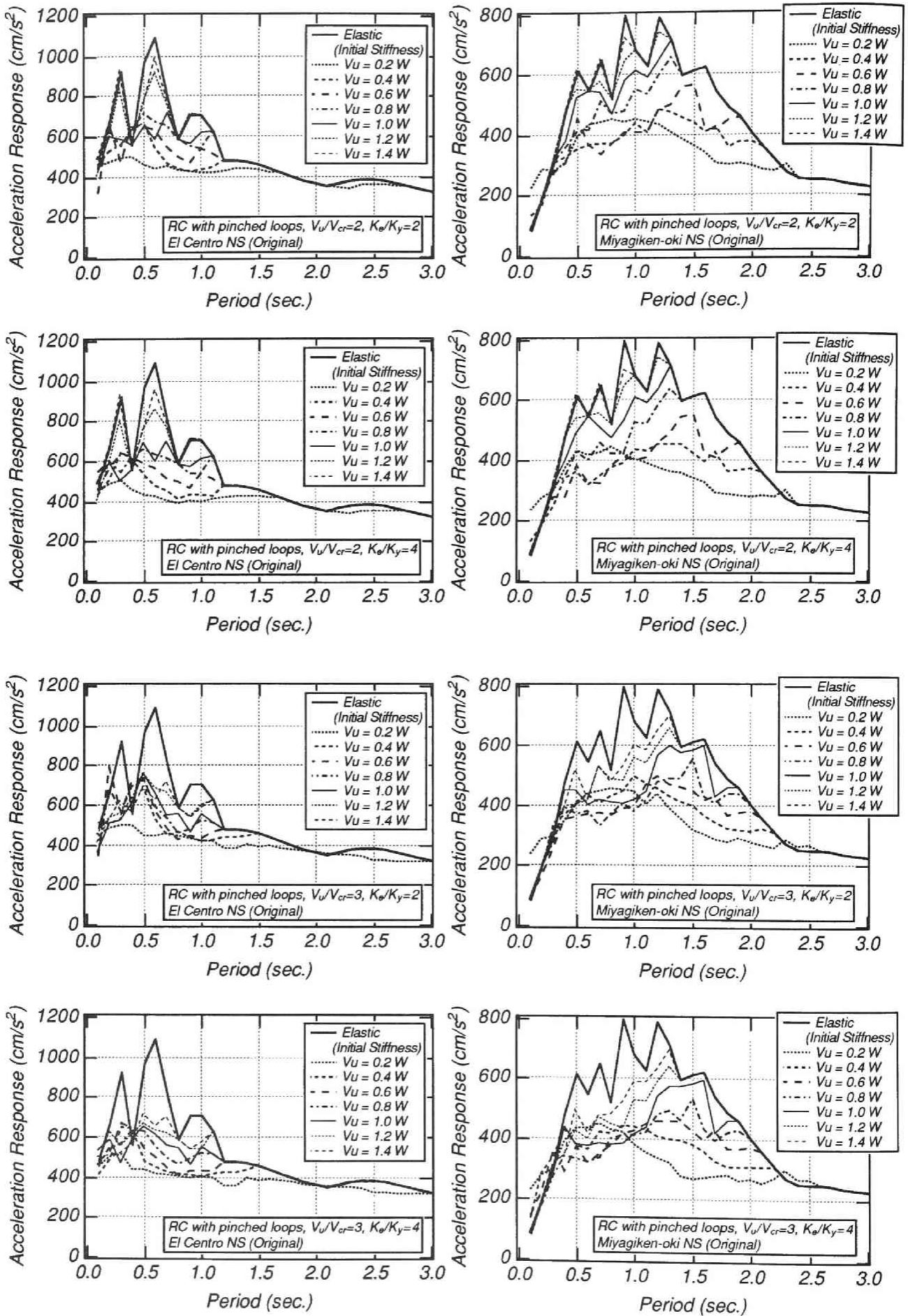


Fig.6.9(c) Acceleration response spectra of reinforced concrete system with pinched hysteresis

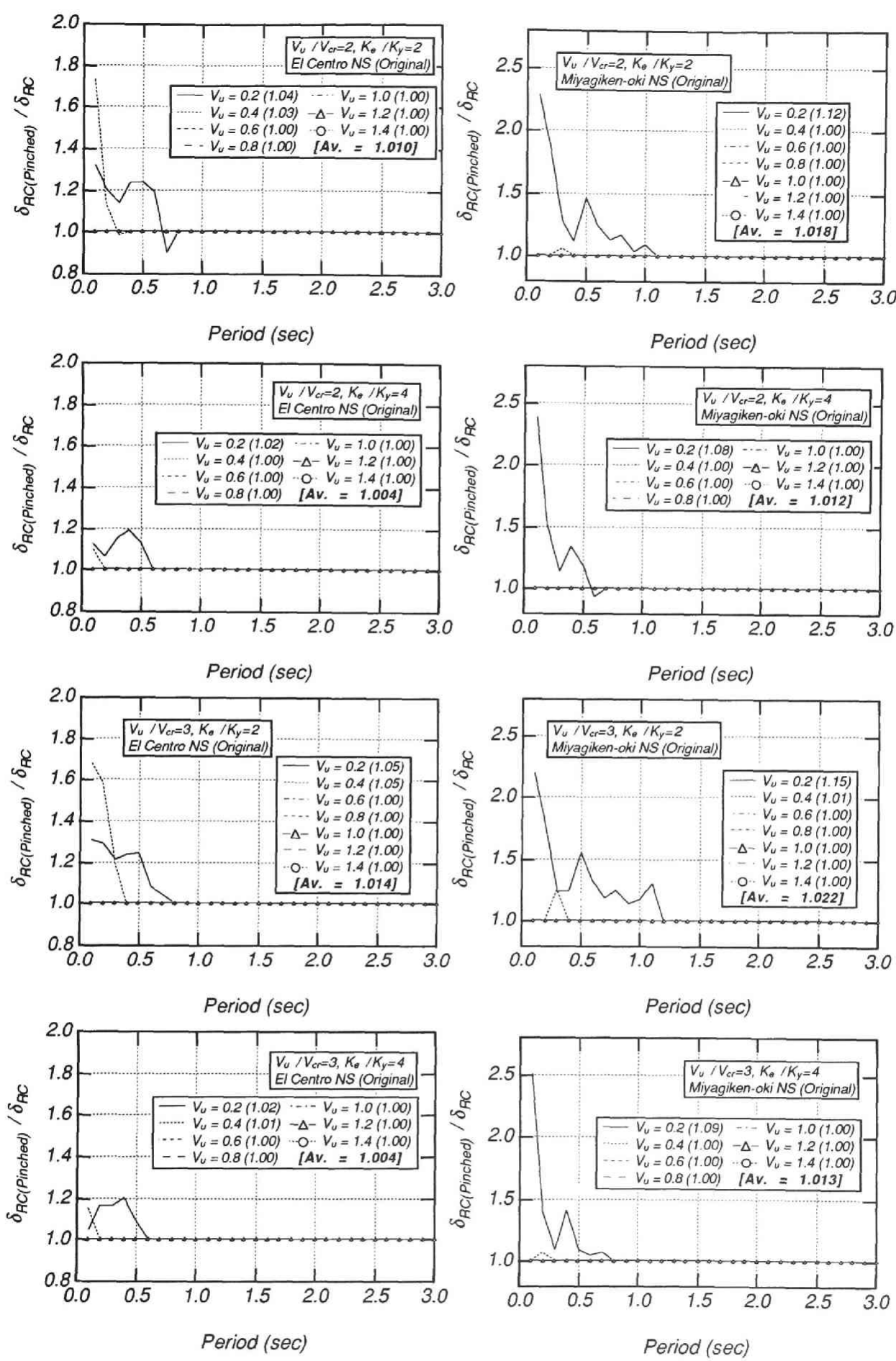


Fig.6.10 Comparison in displacement response between conventionally reinforced concrete and PH system

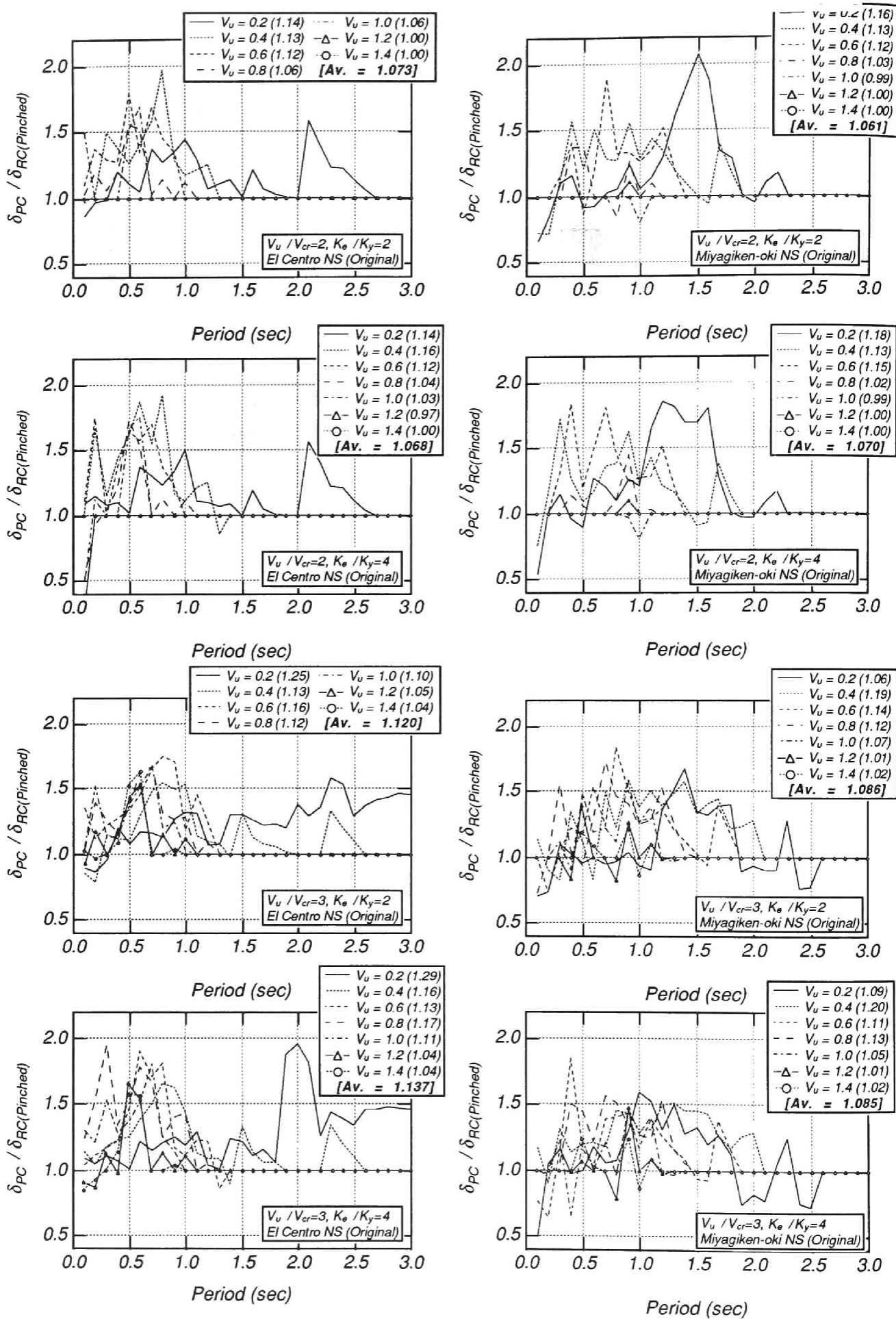


Fig.6.11 Comparison in displacement response between prestressed concrete and PH system

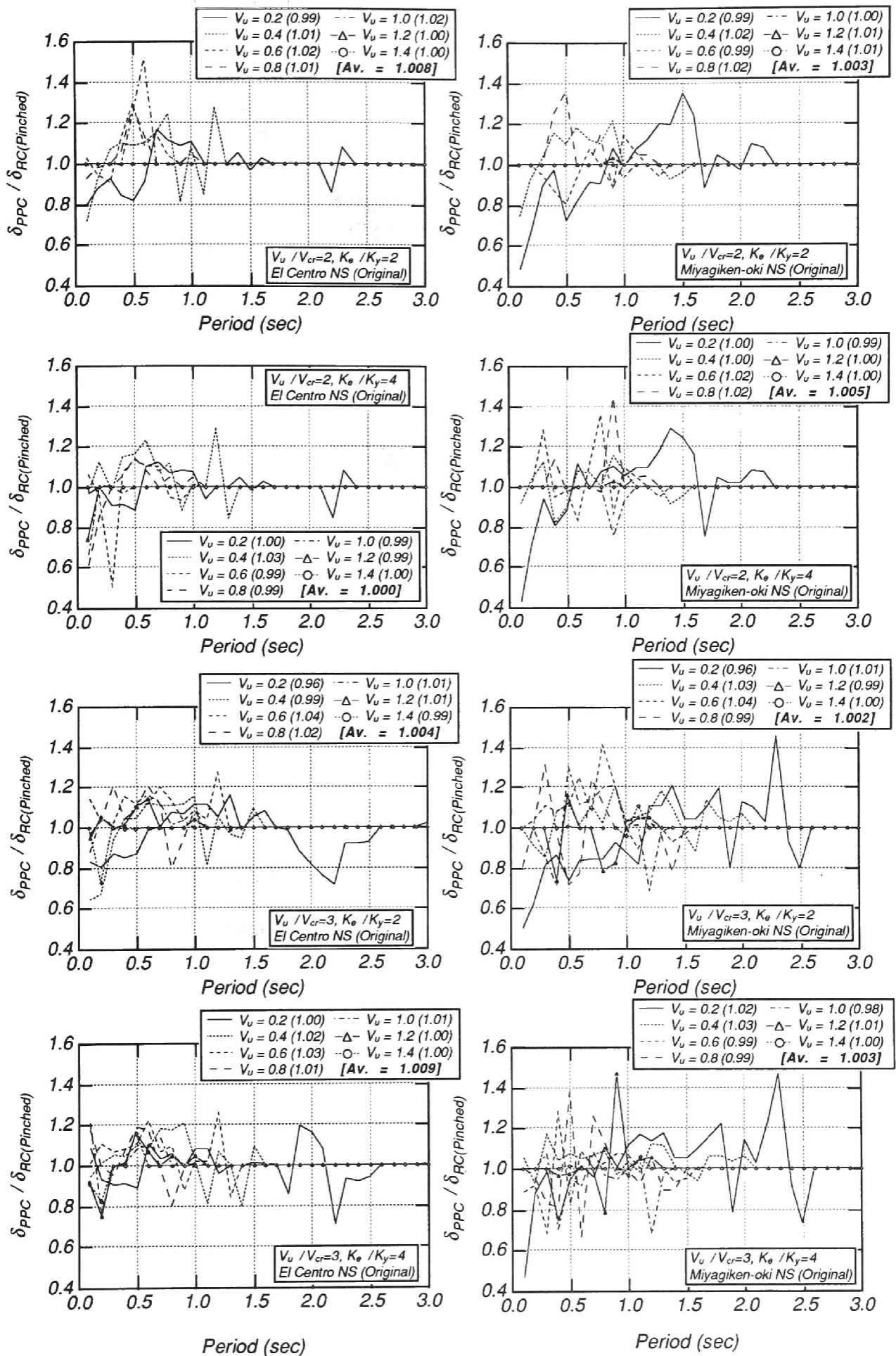


Fig.6.12 Comparison in displacement response between partially prestressed concrete and PH system

6.4 Prediction of displacement response by substitute damping

6.4.1 Introduction

Past research has been trying to represent a non-linear hysteresis loop by a vibrating linear system. Jacobsen suggested in his paper [6.8] that a particular hysteresis loop may be approximately interpreted by a vibrating linear system with equivalent viscous damping.

Gulkan and Sozen [6.9] calculated an average value of the substitute damping ratio, β_s , on the basis of the test results on one-story one-bay frames. β_s was obtained using the following equation.

$$\beta_s \left[2m\omega_0 \int_0^T \dot{x}^2 dt \right] = -m \int_0^T \ddot{y}\dot{x} dt \quad (6.24)$$

where, m = mass

\ddot{y} = base acceleration

\dot{x} = mass relative velocity

$2m\omega_0$ = critical damping coefficient for a single-degree-of-freedom oscillator

Equation 6.24 implies that energy input from horizontal uniaxial base motion which is represented by the right-hand term is entirely dissipated by an imaginary viscous damper associated with horizontal velocity of mass carried by the frame. The critical damping coefficient for a single-degree-of-freedom oscillator, $2m\omega_0$, was introduced to express the substitute damping coefficient as a ratio of the critical damping.

Using the concept of reduced stiffness and substitute damping, they proposed a procedure by which effects of inelastic response for reinforced concrete structures can be estimated on the basis of linear response. The reinforced concrete structures can be idealized as single-degree-of-freedom systems. The procedure can be used to obtain design base shear and maximum displacement to be reached during an earthquake.

Past research on dynamic response of prestressed concrete have discussed a magnification factor of dynamic response of prestressed concrete system to that of conventionally reinforced concrete system. However, it was based on rather scattered calculation results. In this study as well, ratios of displacement response of single-degree-of-freedom systems with prestressed concrete type hysteresis loops to those with reinforced concrete type ones scatter in the wide range depending on the earthquake records used and the natural frequency of the systems.

In this section, a method for predicting displacement response of prestressed concrete systems using the similar concept as Gulkan and Sozen proposed is introduced on the

basis of the calculation results in the former section and an additional analysis. The method is further extended to obtain design base shear.

6.4.2 Substitute damping

The substitute damping was calculated using the base acceleration, mass relative velocity time history response and Eq.6.24. Fig.6.13 indicates the calculated substitute damping plotted against ductility ratio, μ , which is defined as a ratio of maximum absolute displacement to yield displacement. The substitute damping was obtained from the calculation results of the section 6.3.4 of this chapter and the additional analysis: the skeleton curve was assumed to be bilinear, i.e., $\beta_{cr} = 1.0$ and $K_e = K_y$. The two earthquake wave records were used : El Centro 1940 NS Component and the earthquake motion recorded at the first floor of the building at Tohoku University during the Miyagiken-oki earthquake in 1974. The natural period of vibration investigated ranged between 0.1 and 3.0 seconds. The coefficient of viscous damping was assumed to be 0.05. Including the additional analysis, the parameters investigated are $\beta_{cr} = 1.0, 2.0$ and 3.0 , $T_e / T_y = 1.0, 2.0$ and 4.0 . T_y is a natural period of vibration based on the secant stiffness at yield displacement. T_e = a natural period of vibration based on the elastic stiffness. The ratio of yield capacity to the weight of a structure, which is denoted as β_u ranged 0.2 to 1.4. The plotted data in Fig.6.13 are from the results in which the maximum absolute displacement exceeded the yield displacement.

Gulkan and Sozen [6.9] suggested the substitute damping ratio, β_s , would vary with attained ductility, μ , as ratio of area *EBC* to area *ABF* indicated in Fig.6.14. Therefore, the following relationship can be obtained.

$$\beta_s \propto (1 - 1/\sqrt{\mu}) \quad (6.25)$$

They also suggested that if β_s is assumed to have a threshold value of 0.02 at $\mu = 1.0$, Eq.6.25 is expressed as,

$$\beta_s = \{1 + 10(1 - 1/\sqrt{\mu})\} / 50 \quad (6.26)$$

In this study, however, the best-fit linear equations in the range of $\mu = 1\sim 5$ for the plotted data are listed below and shown in Fig.6.13 by a solid line for prestressed concrete systems and by a dotted line for reinforced concrete systems.

For reinforced concrete with $\beta_{cr} = 1.0$ and $T_e / T_y = 1.0$,

$$\beta_s = 0.07606(\mu - 1) + 0.09132 \quad (6.27)$$

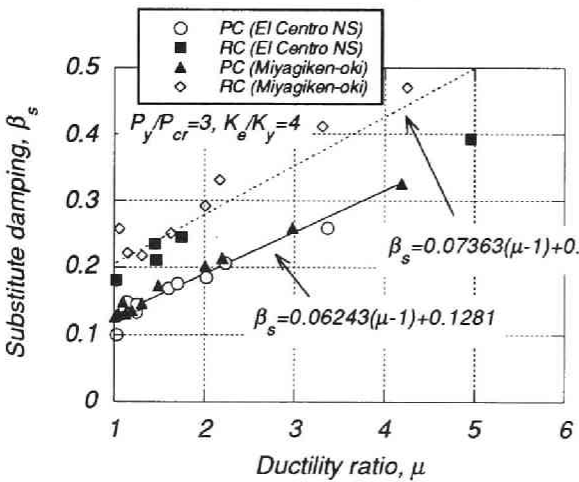
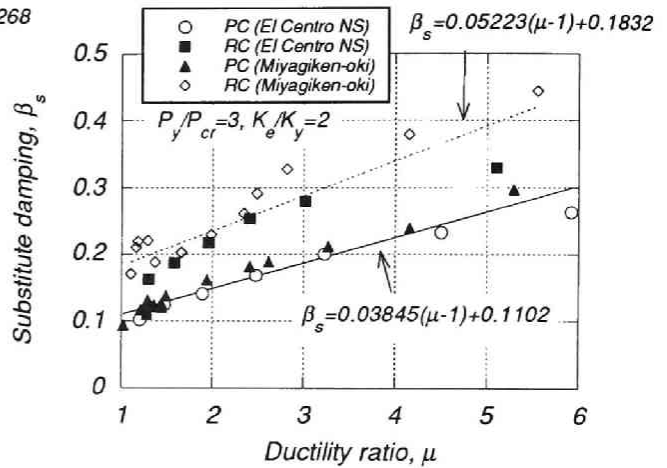
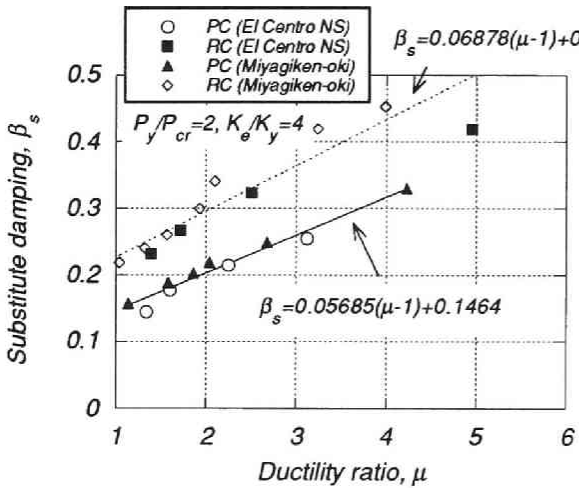
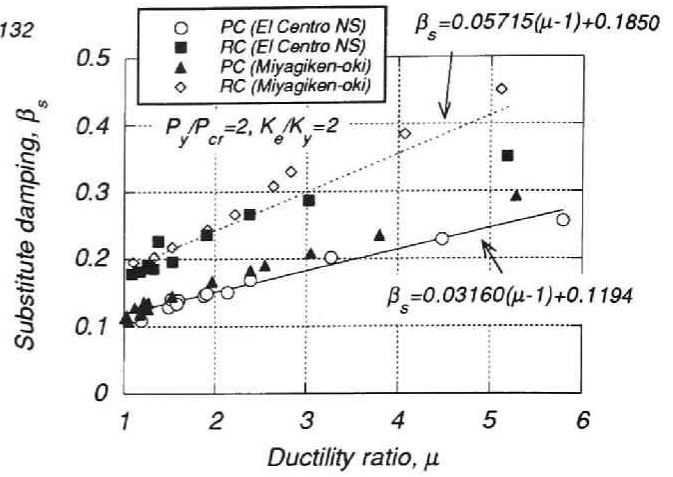
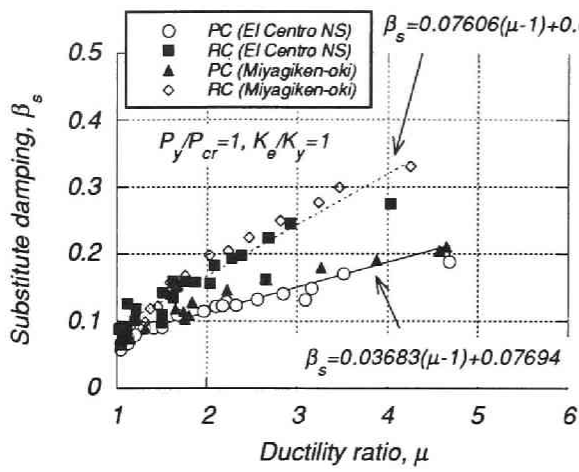
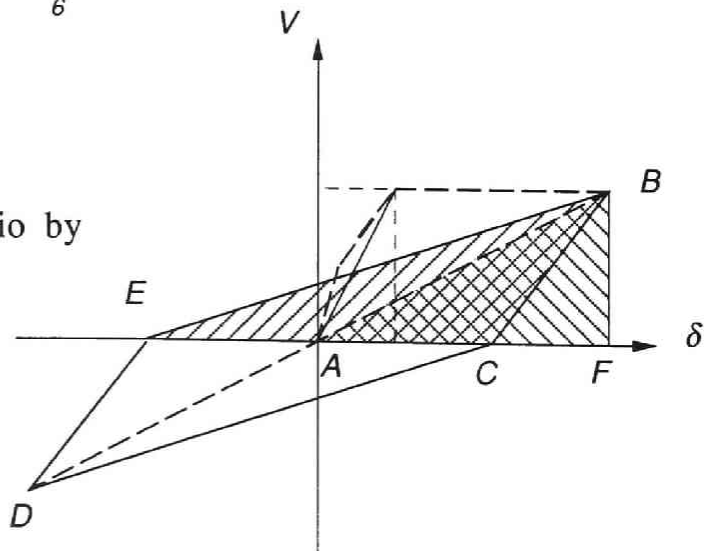


Fig.6.13 Substitute damping ratio

Fig.6.14 Substitute damping ratio by Gulkan and Sozen [6.9]



For prestressed concrete with $\beta_{cr} = 1.0$ and $T_e / T_y = 1.0$,

$$\beta_s = 0.03683(\mu - 1) + 0.07694 \quad (6.28)$$

For reinforced concrete with $\beta_{cr} = 2.0$ and $T_e / T_y = 2.0$,

$$\beta_s = 0.05715(\mu - 1) + 0.1850 \quad (6.29)$$

For prestressed concrete with $\beta_{cr} = 2.0$ and $T_e / T_y = 2.0$,

$$\beta_s = 0.03583(\mu - 1) + 0.1185 \quad (6.30)$$

The substitute damping for the other combinations of parameters are summarized in Table 6.2.

Iwan [6.10] proposed the following empirical relationship between an effective period shift T_{eq} / T_e and a ductility ratio μ on the basis of the calculation results of single-degree-of-freedom systems with hysteretic restoring force characteristics associated with linear, simple hysteretic and degrading hysteretic behaviour.

$$T_{eq} / T_e = 1 + 0.121(\mu - 1)^n \quad : n = 0.939 \quad (6.31)$$

To streamline the discussion, n is assumed to be unity. Within the range of $\mu = 1 \sim 5$, the difference between $n = 0.939$ and $n = 1.0$ is as much as 3%.

When calculating the substitute damping, $\sqrt{\mu} \cdot T_e$ was used as an equivalent period of vibration. The substitute damping must be modified by the factor given by the following equation based on the effective period shift suggested by Iwan.

$$\gamma = [1 + 0.121(\mu - 1)] / \sqrt{\mu} \quad (6.32)$$

The substitute dampings given by Eqs.6.27 to 6.30 were then modified as follows.

For reinforced concrete with $\beta_{cr} = 1.0$ and $T_e / T_y = 1.0$,

$$\beta_s = 0.07606(\mu - 1) \frac{[1 + 0.121(\mu - 1)]}{\sqrt{\mu}} + 0.09132 \quad (6.33)$$

For prestressed concrete with $\beta_{cr} = 1.0$ and $T_e / T_y = 1.0$,

$$\beta_s = 0.03683(\mu - 1) \frac{[1 + 0.121(\mu - 1)]}{\sqrt{\mu}} + 0.07694 \quad (6.34)$$

For reinforced concrete with $\beta_{cr} = 2.0$ and $T_e / T_y = 2.0$,

$$\beta_s = 0.05715(\mu - 1) \frac{[1 + 0.121(\mu - 1)]}{\sqrt{\mu}} + 0.1850 \quad (6.35)$$

For prestressed concrete with $\beta_{cr} = 2.0$ and $T_e / T_y = 2.0$,

$$\beta_s = 0.03583(\mu - 1) \frac{[1 + 0.121(\mu - 1)]}{\sqrt{\mu}} + 0.1185 \quad (6.36)$$

Response spectra are usually given in respect to a particular damping ratio. The response spectra for dampings other than this particular damping are assumed to be given using the following equations [6.11].

For $h \geq 0.05$

$$\frac{S(h_{eq})}{S(0.05)} = \frac{2.25}{1.75 + 10h_{eq}} \quad \text{but } (0.1s \leq T_{eq} \leq 2.5s) \quad (6.37)$$

$$\frac{S(h_{eq})}{S(0.05)} = 1 - \left(1 - \frac{2.25}{1.75 + 10h_{eq}}\right) \left(\frac{1 - \log T_{eq}}{0.60}\right) \quad \text{but } (2.5s \leq T_{eq} \leq 10.0s) \quad (6.38)$$

For $h \leq 0.05$

$$\frac{S(h_{eq})}{S(0.05)} = \frac{1.5}{1 + 10h_{eq}} \quad \text{but } (0.1s \leq T_{eq}) \quad (6.39)$$

6.4.3 Prediction of displacement response by substitute damping

A procedure based on linear response can be used to predict maximum displacement response and to evaluate design base shear. The procedure involves the following

steps.

1. Assume an admissible value of μ .
2. Calculate an effective period T_{eq} by using the assumed value of μ and Eq.6.31 (n is assumed to be unity).
3. Calculate β_s corresponding to the assumed value of μ by using Eqs.6.33 to 6.36.
4. Obtain maximum displacement by entering spectral response diagram with the effective period of T_{eq} and a damping ratio equal to β_s determined in Step 3. If the spectral response diagram is given in terms of the damping ratio other than β_s , Eqs.6.37 to 6.39 are used for extrapolation.
5. If the difference between a ductility factor which is obtained from the maximum displacement and the yield displacement, and the assumed value of μ becomes within a tolerable limit, the maximum displacement and the base shear are considered to give a good approximation. If the error is not in the tolerance, return to Step 1 with a new assumed value of μ .

Example

Consider a single-degree-of-freedom structure with prestressed concrete type hysteresis loops. A period of 1.0 second is assumed on the basis of the secant stiffness at yield displacement. When a mass of the structure M is 1.0 kg, the secant stiffness at yield displacement K_y is $39.478 \text{ kg} \cdot \text{cm} / \text{s}^2 / \text{cm}$. If the yield capacity of the structure is assumed to be $Q_y = 0.2M \cdot g$, the yield displacement is given by $Q_y / K_y = 4.965 \text{ cm}$, where g is acceleration of gravity. The skeleton curve of the system is assumed to be an elasto-perfectly plastic type : $\beta_{cr} = 1.0$ and $T_y / T_e = 1.0$.

If μ is assumed to be 4 the period is modified to 1.363 seconds. Eq.6.33 gives a substitute damping ratio of 0.152. For a particular ground motion, a displacement response of cm can be obtained by entering a spectral displacement response, for instance an average response spectrum by Umemura shown in Fig.6.15. The displacement, velocity and acceleration response spectra are given as follows.

$$S_D(\text{cm}) = \begin{cases} 90T^2 k_G & T \leq 0.5s \\ 45T k_G & 0.5 \leq T \leq 3 \\ 135 k_G & T > 3 \end{cases} \quad (6.40)$$

$$S_V (cm / s) = \begin{cases} 566Tk_G & T \leq 0.5s \\ 283k_G & 0.5 \leq T \leq 3 \\ 849k_G / T & T > 3 \end{cases} \quad (6.41)$$

$$S_A (cm / s^2) = \begin{cases} 3.6 \cdot g \cdot k_G & T \leq 0.5s \\ 1.8 \cdot g \cdot k_G / T & 0.5 \leq T \leq 3 \\ 5.4 \cdot g \cdot k_G / T^2 & T > 3 \end{cases} \quad (6.42)$$

where, $g = 980 \text{ cm} / \text{s}^2$ and $k_G =$ ratio of maximum ground acceleration to acceleration of gravity. Assuming the maximum ground acceleration of $319 \text{ cm} / \text{s}^2$, which is the maximum acceleration record of El Centro 1940 NS Component, the displacement response of 19.97 cm is obtained. Since Umemura spectra is considered to be given for an oscillator with a damping ratio of 0.05, the response should be transferred to a displacement response with the substitute damping of 0.152 by using Eq.6.38. This results in the displacement response of 13.73 cm, which corresponds to the ductility factor of 2.765. The difference between the assumed value and the result is significant. Then, return to Step 1 with a new assumption of $\mu = 2.765$.

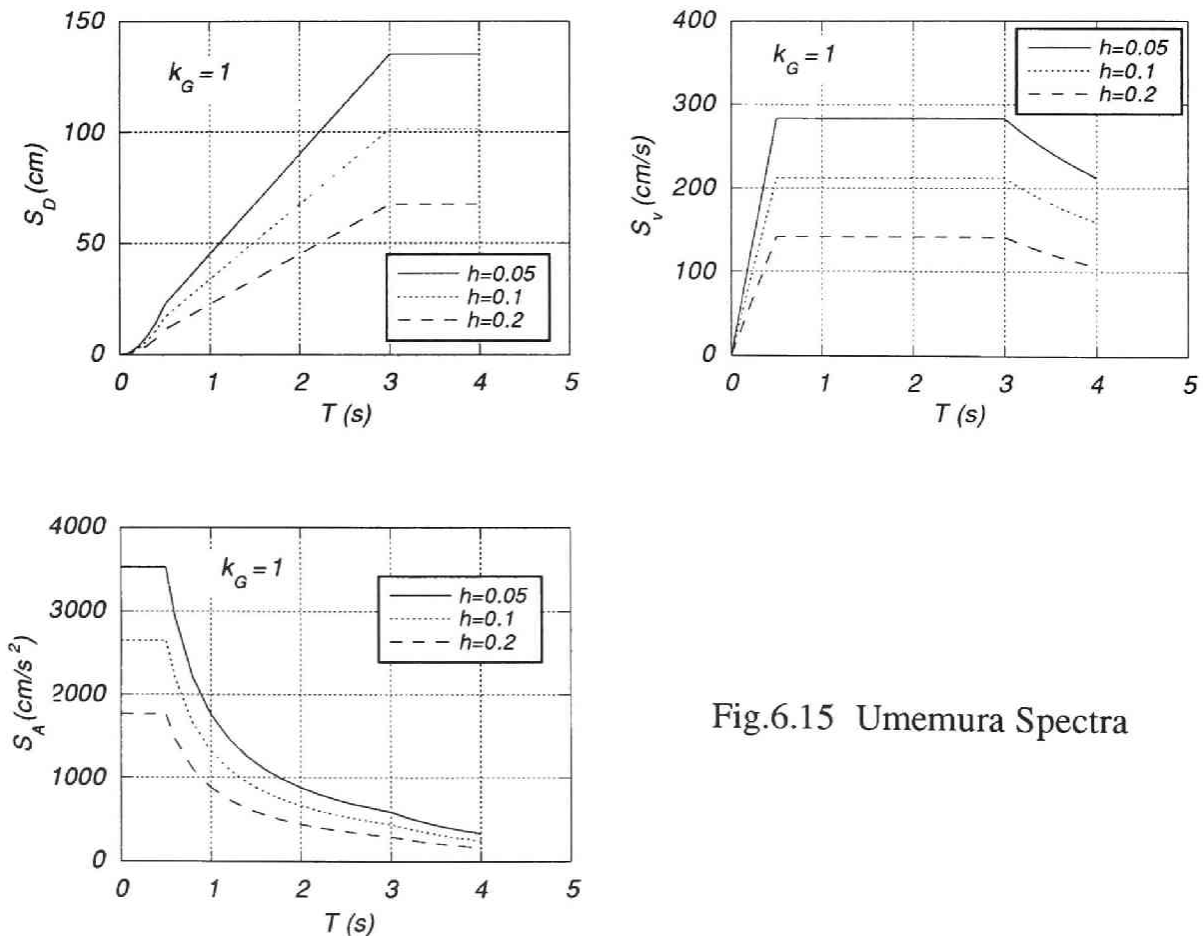


Fig.6.15 Umemura Spectra

$\mu = 2.765$ results in the effective period of 1.214 seconds and the substitute damping of 0.124. The displacement response obtained is 13.36 cm corresponding to the ductility ratio of 2.69. The difference is still large. Return to Step 1 with a new assumption of $\mu = 2.69$. This results in the effective period of 1.20 seconds, the substitute damping of 0.123 and the displacement response of 13.34 cm corresponding to the ductility ratio of 2.69.

The result of the time-history analysis for El Centro 1940 NS Component whose spectra are similar to Umemura spectra gives the maximum displacement of 10.43 cm. The rather favorable comparison between the “exact” and approximate value of the maximum displacement suggests that the substitute damping method may be used successfully in the region covered by the exact analyses.

6.4.4 Comparison of dynamic response between prestressed concrete and reinforced concrete systems

When comparing dynamic response of prestressed concrete systems with that of reinforced concrete system, a clear conclusion cannot be derived because of considerable scatter in the calculation results. Use of substitute damping gives a structural designer a good indication of how large displacement can be reached in a prestressed concrete system during an earthquake motion.

In the case of designing a prestressed concrete building frame it is of great importance to know how large the maximum displacement is reached during an earthquake comparing with a reinforced concrete building frame. There are two cases concerned : (1) the same yield capacities are given to both prestressed and reinforced concrete systems or (2) the same maximum displacement is predicted to be reached in both systems.

(1) the same yield capacity

The procedure described in the preceding example is followed to obtain the maximum displacement response of a reinforced concrete structure with the same yield capacity and secant stiffness at yielding as that of a prestressed concrete structure.

For instance, Fig.6.16 shows the ductility ratio response of prestressed and reinforced concrete systems to Umemura spectra of $k_G = 0.3255$. Their period at yielding is 1.0 second. Smaller yield capacity results in a larger ductility ratio as past research has pointed out. The difference between the responses of the prestressed and reinforced concrete systems becomes larger as their yield capacities decrease.

However, the situation is changed when their responses are expressed by the maximum displacements. Fig.6.17 illustrates the maximum displacement response of these systems by a solid line for the prestressed concrete system and by a dotted line for the

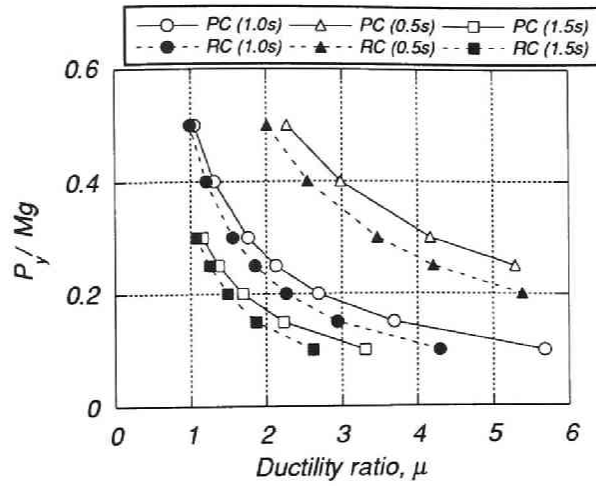


Fig.6.16 Yield capacity - ductility ratio response relationships

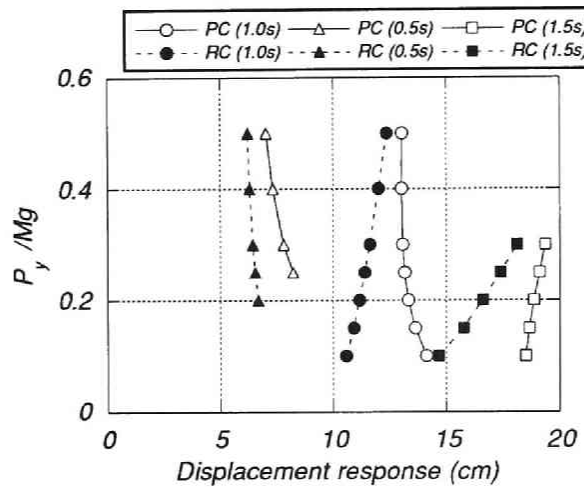


Fig.6.17 Yield capacity - displacement response relationships

reinforced concrete system. For the prestressed concrete system the maximum displacement response slightly decreases as the yield capacity increases. For the reinforced concrete system, however, the maximum displacement response rather increases as the yield capacity increases. These curves show that even if the yield capacity of the prestressed concrete system increases to some degree in order to reduce the maximum displacement response, it never reduces to as much a displacement response as the reinforced concrete system unless they respond in an elastic manner.

NZS 4203 : 1984 specifies 25% larger seismic design load for a prestressed concrete structure than an equivalent reinforced concrete structure. However, the fact described above reveals that additional yield capacity alone cannot lead to a reduced displacement response as much as the equivalent reinforced concrete structure. It is not so useful to increase yield capacity in order to reduce the maximum displacement response.

(2) the same displacement

This case is much more complicated and much more interesting than the former. There are two ways for the two systems to reach the same displacement. One is to boost up the yield capacity of the prestressed concrete system. The maximum displacement of the reinforced concrete system can be obtained by the same procedure described above. If the prestressed concrete system has the same secant stiffness that the reinforced concrete system, an assumed yield capacity gives a yield displacement from which the ductility ratio can be calculated. From this ductility ratio displacement response of prestressed concrete system is obtained. If the displacement response and the above maximum displacement response are the same, the assumed yield capacity is considered to give the same displacement response that the reinforced concrete system. However, as described above, it is difficult to have the same displacements in both systems when the yield capacity alone of the prestressed concrete system increases.

The other is to increase the secant stiffness at yielding of the prestressed concrete system. In this case the yield capacity of the prestressed concrete system is assumed to be equal to that of the reinforced concrete system. The secant stiffness at yielding of the prestressed concrete system should be increased so that the corresponding yield displacement decreased. From the yield displacement the same procedure in the former case is trailed until as large displacement response as the maximum displacement of the reinforced concrete system is obtained. However, it should be noted that the maximum ductility ratio is increased as the secant stiffness decreases.

Example

Consider a single-degree-of-freedom structure with reinforced concrete type hysteresis loops of the same characteristics that the preceding example. If the first trial starts with $\mu = 4$ which modifies the period to 1.363 seconds, Eq.6.33 gives a substitute damping ratio of 0.247. From Umemura displacement spectra the displacement response can be predicted 10.65 cm. This corresponds to the ductility factor of 2.15.

The second trial : $\mu = 2.15$ and $\beta_s = 0.159$. The predicted response is 11.23 cm, which corresponds to $\mu = 2.26$.

The third trial : $\mu = 2.26$ and $\beta_s = 0.165$. The predicted response is 11.18 cm, which corresponds to $\mu = 2.25$.

The prestressed concrete system with the same yield capacity should have a larger secant stiffness at yielding than the reinforced concrete system. If the period at yielding of the structure is assumed to be $T_y = 0.75$ second, the yield displacement is given by $Q_y / K_y = 2.793\text{cm}$. The maximum displacement obtained is 10.89 cm, which is approximately the same displacement that obtained above in the reinforced concrete

system. The ductility ratio attained 3.90, which is 73% larger than that of the reinforced concrete system.

6.5 Conclusions

From the above analytical study, the following conclusions are reached with regard to dynamic response of prestressed, partially prestressed and reinforced concrete single-degree-of-freedom systems:

1. The idealized curves proposed in Chapter 5 were used as the load-displacement idealization. Response spectra of the idealized curves to earthquake excitations for various ranges of yield capacity, period of vibration, and so on were calculated to investigate the fundamental characteristics of the idealization. However, these calculations were conducted in order to examine the characteristics of the idealization curves because the idealized curves are not considered to express directly the load-deflection relationships of a structure or a layer of a building itself : They were derived based on the moment-curvature curves obtained experimentally. The response of a building is largely affected by the load-deflection response of reinforced concrete constituent elements such as columns and walls. A comparison between the idealizations for a prestressed concrete and a reinforced concrete system which will be described in the later part of this section should be referred to as the extreme case of these systems.
2. Comparison of displacement responses between prestressed, partially prestressed and reinforced concrete systems showed that the average ratios of the maximum displacement responses of the prestressed concrete systems to those of the corresponding reinforced concrete systems ranged between 0.98 and 1.39 with the maximum value of 3.23. For partially prestressed concrete systems those ranged 0.98 and 1.15 with the maximum value of 2.06. Generally, the ratios are larger in the period shorter than approximately 0.5 seconds.
3. Responses of prestressed concrete systems were compared with those of corresponding reinforced concrete systems whose load - displacement hysteretic behaviour was controlled by slip of longitudinal beam bars, that is, indicated pinched hysteresis loops. The average values of the ratios of the maximum displacement response of the prestressed concrete systems to that of the reinforced concrete systems with pinched hysteresis loops ranged between 1.09 and 1.14. They are slightly smaller than those in the comparison between the prestressed and the reinforced concrete systems. The average values for the partially prestressed concrete are approximately unity.
4. Substitute damping was introduced and calibrated from the results of the time-history analyses in order to predict dynamic responses of prestressed, partially

prestressed and reinforced concrete systems. The substitute damping was proved to give a good approximation of responses of those systems.

5. Some examples using the substitute damping revealed that increasing the strength of some types of structures may increase the maximum displacement.

[References]

- 6.1 Thompson, K.J. and Park, R : Seismic Response of Partially Prestressed Concrete, Journal of Structural Division, Proceedings of ASCE Aug.1980 ST8, pp.1755-1775.
- 6.2 Okamoto, S. : Fundamental Study on Earthquake Resisting Behaviours of Prestressed Concrete Frame Structures, Chapter 6; Seismic Response of Prestressed Concrete Buildings, Ph. D Thesis, Kyoto University, Japan 1986, pp.250-281.
- 6.3 Ishimaru, T. : Dynamic Response of Structure 19 (7.5 Characteristics of Elasto-Plastic Behavior of B, D and S-type hysteresis loops), Kenchiku Gijyutsu No.377, January 1983, pp.155-167.
- 6.4 Code of Practice for General Structural Design and Design Loadings for Buildings NZS 4203 : 1984, Standard Association of New Zealand.
- 6.5 Kitayama, K., Otani, S. and Aoyama, H., Earthquake Resistant Design Criteria for Reinforced Concrete Interior Beam-Column Joints, Proceedings of Pacific Conference on Earthquake Engineering, Vol.1, Wairakei, 1987, pp.315-326.
- 6.6 Park, R., Evaluation of Ductility of Structures and Structural Assemblages from Laboratory Testing, Bulletin of the New Zealand National Society for Earthquake Engineering, Vol.22, No.3, September 1989, pp.155-166.
- 6.7 Thompson, K. J., Ductility of Concrete Frames under Seismic Loading, A Thesis for the Degree of Doctor of Philosophy in Civil Engineering at the University of Canterbury, 1975.
- 6.8 Jacobsen, L. S., Damping in Composite Structures, Proceedings of Second World Conference on Earthquake Engineering, Tokyo, 1960, pp.1029-1044.
- 6.9 Gulkan, P. and Sozen, M. A., Inelastic Response of Reinforced Concrete Structures to Earthquake Motions, ACI Journal, December 1974, pp.604-610.
- 6.10 Iwan, W. D., Estimating Inelastic Response Spectra from Elastic Spectra, Earthquake Engineering and Structural Dynamics, Vol.8, No.4, 1980, pp.375-388.
- 6.11 Inoue, Y. et al., A Proposal for Seismic Design Procedure of Apartment Houses Including Soil-Structure Interaction Effect, Proceedings of Ninth World Conference on Earthquake Engineering, August 2-9, 1988, Tokyo-Kyoto, JAPAN (Vol.VIII), pp.365-370.

DYNAMIC RESPONSE ANALYSIS OF PRESTRESSED CONCRETE BUILDING FRAMES

7.1 Introduction

Dynamic response characteristic of prestressed concrete single-degree-of-freedom systems was reported in Chapter 6 as they were compared with that of equivalent reinforced concrete systems. Similar analytical investigations have been carried out elsewhere in the past. However, two-dimensional analysis has not yet been conducted on prestressed concrete building frames. This kind of analysis is of great importance especially in order to develop a seismic design procedure for prestressed concrete building frames. Dynamic response analysis using a single- or multi-mass shear systems can save time and expense if story restoring force characteristics of a building frame are available. However, the restoring force characteristic in each story depends strongly on the ratio of the stiffness of the prestressed concrete beams to that of the reinforced concrete columns, and the combination of their flexural capacities. Moreover, the restoring force characteristic of a prestressed concrete beam itself fluctuates widely with the amount of prestressing force and the ratio of the amount of nonprestressed longitudinal reinforcement to that of prestressing steel bars. The displacement response of prestressed concrete derived by analysis using a single- or multi-mass shear system appears to be overestimated, although it may be the upper limit.

On the basis of the research work by Sharpe [7.1], the author has developed a computer program for two-dimensional dynamic response analysis which incorporates the moment-curvature idealization of prestressed concrete sections proposed in Chapter 5. In this chapter, after the outline of the analytical procedure, dynamic response analyses will be reported on model frames designed in prestressed and reinforced concrete.

Building frames to be treated in this chapter are the frames which consist of beams, columns and their assemblages. Structural walls are not taken into account.

7.2 Damping model

To model the material and velocity damping present in a dynamically excited frame, a general damping system was proposed by Caughey [7.2] to give damping forces proportional to both the mass and stiffness of the frame.

$$[C] = [M] \cdot \left\{ \sum_{j=0}^{N-1} a_j \cdot ([M]^{-1}[K])^j \right\} \quad (7.1)$$

Rayleigh damping, the first two terms of Eq.7.1, was used in this research. The damping matrix $[C]$ was defined by the following equation.

$$[C] = \alpha[M] + \beta[K] \quad (7.2)$$

$$\alpha = \frac{2\omega_1\omega_2(\omega_2\lambda_1 - \omega_1\lambda_2)}{\omega_1^2 - \omega_2^2} \quad (7.3)$$

$$\beta = \frac{2(\omega_1\lambda_1 - \omega_2\lambda_2)}{\omega_1^2 - \omega_2^2} \quad (7.4)$$

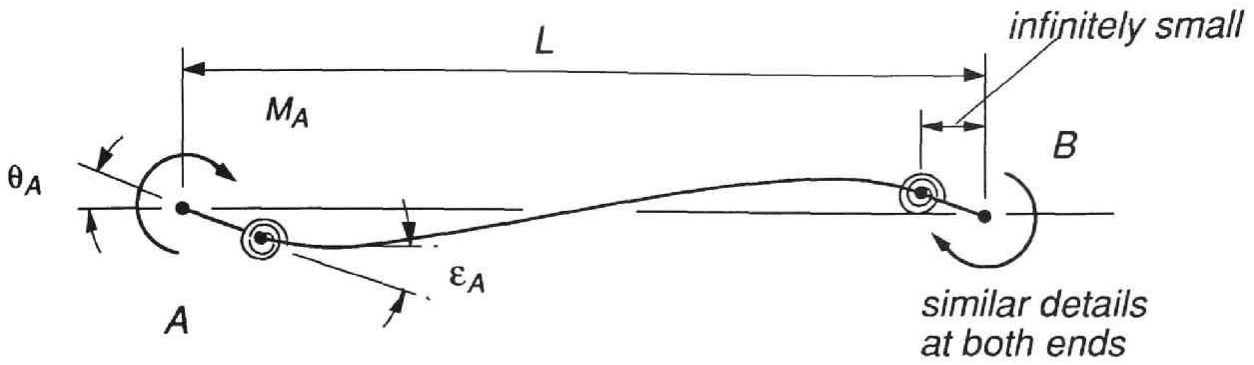
where ω_1 and ω_2 are the first and second natural circular frequencies, and λ_1 and λ_2 are the respective fractions of critical damping applicable to modes with these frequencies. In this thesis, both λ_1 and λ_2 are assumed to be 5%.

7.3 Non-linear beam model

Sharpe [7.1] employed Giberson's one-component model of non-linear beam [7.3]. A schematic diagram of the beam model is illustrated in Fig.7.1. It is a one-dimensional prismatic beam with spring hinges incorporated at infinitesimal distances from either end. By varying the rotational spring stiffness of the independent hinges, the full range of situations can be idealized: from the beam with a pinned end to the beam being linearly elastic along its entire length. Therefore, the full spectrum of possibilities can be covered. The spring rate of each of the hinges is expressed as a fraction of the elastic bending stiffness of the beam, $4EI / L$ (E , Young's modulus; I , moment of inertia; L , length).

Since the critical sections may occur at the interface of the members rather than at the intersection of their center-lines, a modification is made to the transformation matrix which relates the coordinates of the member to those of the entire system. Small rigid end-blocks at either or both of its ends are introduced on the basis of small deflection theory. This transformation is also shown in Fig.7.1.

The theoretical discontinuity in rotational deformation, which occurs at the critical sections in the beam-model, is assumed to extend over an infinitely small length. The rotation of the hinge at this point can only be related to the curvature at the same point in the real structure if the hinge is considered to have some finite length. This plastic hinge length varies with the amount of curvature, the type of material, section dimensions, shear span ratio and so on. However, if a constant value for this length is



spring-hinge rotational stiffness = $4EI \frac{f_s}{L}$
E : Young's Modulus
I : Moment of Inertia

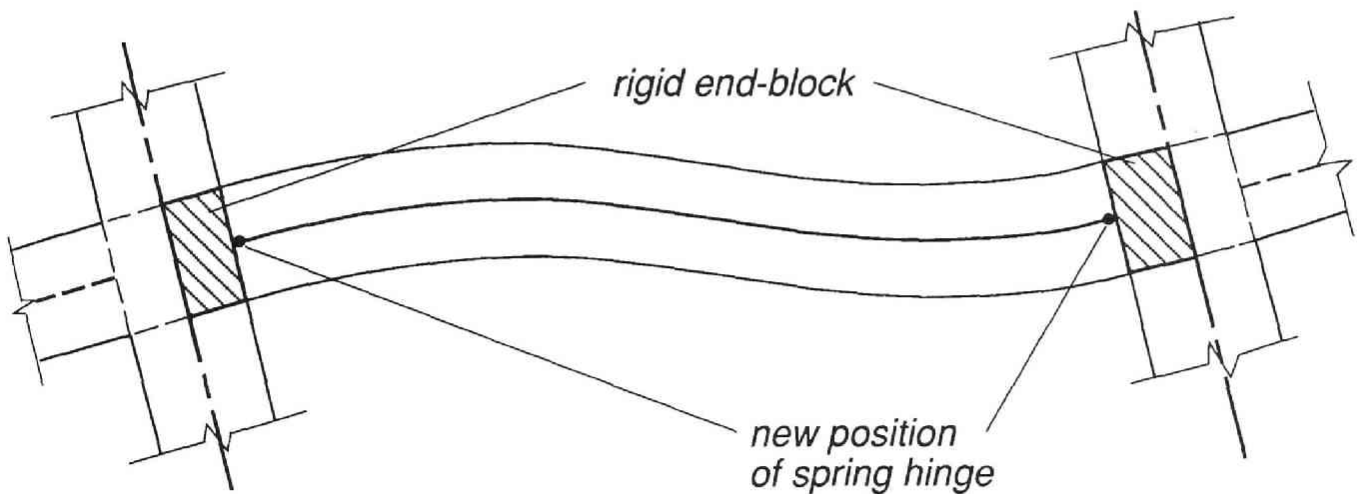
Case 1: Hinges A and B both non-linear.

$$\begin{Bmatrix} \Delta M_A \\ \Delta M_B \end{Bmatrix} = \frac{4EI/L}{1 + \frac{4}{3}(f_A + f_B + f_A \cdot f_B)} \begin{bmatrix} f_A \left(1 + \frac{4}{3} f_B\right) & \frac{2}{3} f_A \cdot f_B \\ \frac{2}{3} f_A \cdot f_B & f_B \left(1 + \frac{4}{3} f_A\right) \end{bmatrix} \begin{Bmatrix} \Delta \theta_A \\ \Delta \theta_B \end{Bmatrix}$$

Case 2: Hinges A non-linear, B linear.

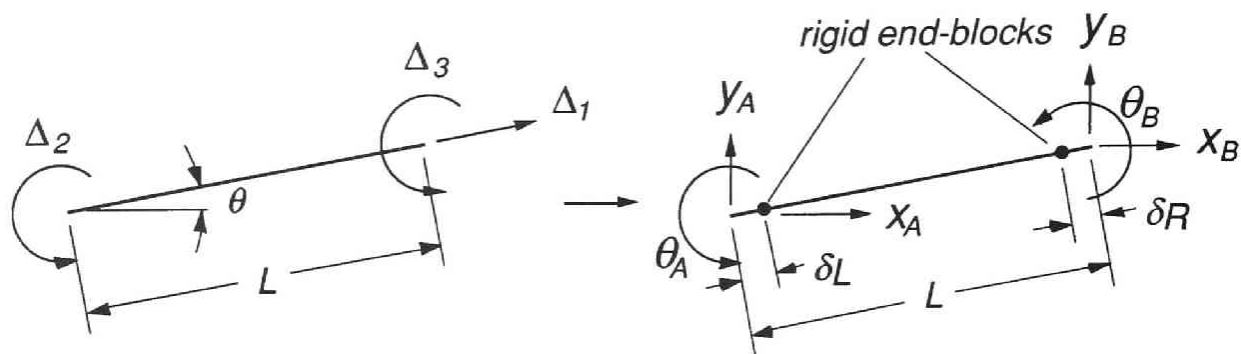
$$\begin{Bmatrix} \Delta M_A \\ \Delta M_B \end{Bmatrix} = \frac{4EI/L}{1 + f_A} \begin{bmatrix} f_A & \frac{1}{2} f_A \\ \frac{1}{2} f_A & \frac{3}{4} + f_A \end{bmatrix} \begin{Bmatrix} \Delta \theta_A \\ \Delta \theta_B \end{Bmatrix}$$

a) Giberson's one-component non-linear beam model



b) Beam model modified to incorporate rigid end-blocks which shift the position of the critical sections inwards.

Fig.7.1 Beam model [7.1] (to be continued to the next page)



c) The transformation from system- to member-coordinates

Fig.7.1 Beam model [7.1]

assumed, a relationship between the moment and the equivalent curvature at an equivalent plastic hinge region can be derived on the basis of small deflection theory and the beam-model's hinge rotation. Using the notation of Fig.7.2 and assuming the bending moment over the length of the hinge to be constant at that value, the finite plastic hinge is first considered to consist of two discontinuous parts, A-B and B-C. For each of these halves,

$$\frac{H}{2} = r\theta_1 \quad (7.5)$$

$$M = \frac{EI}{r} \quad (7.6)$$

For the equivalent continuous hinge A-C, in which constant curvature is assumed,

$$H = \rho\theta_2 \quad (7.7)$$

By the definition of Giberson's beam model

$$M = \frac{4EI}{L} f\varepsilon \quad (7.8)$$

where ε is the angle of rotation of the infinitely small spring hinge. By the geometry of the model,

$$2\theta_1 + \varepsilon = \theta_2 \quad (7.9)$$

Thus, by using Eq.7.5 and Eq.7.6, the following relationship can be derived.

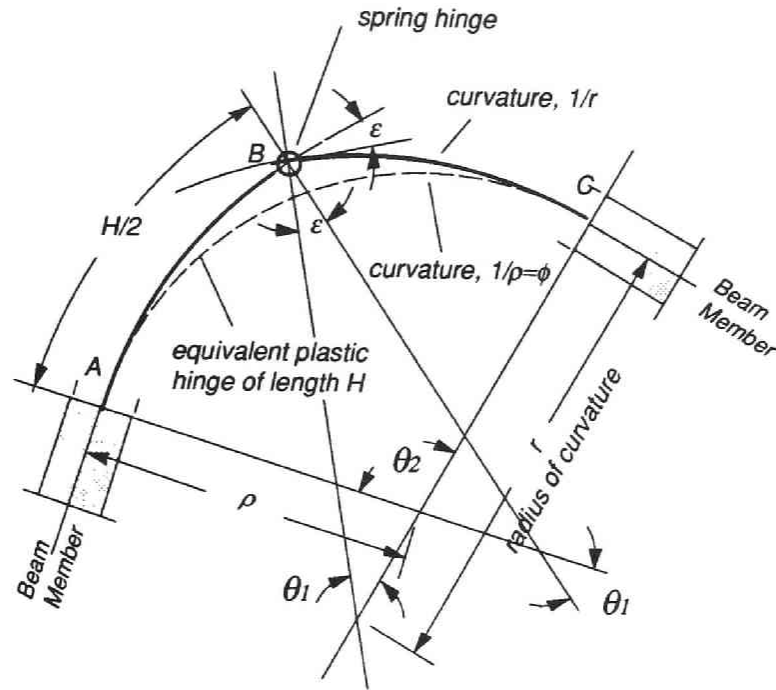


Fig.7.2 Beam plastic hinge model (small deflection theory) [7.1]

$$M = EI \frac{2\theta_1}{H} \quad (7.10)$$

$$= EI \frac{(\theta_2 - \varepsilon)}{H} \quad (7.11)$$

$$= EI \frac{1}{H} \left(\frac{H}{\rho} - \frac{ML}{4EI} \right) \quad (7.12)$$

$$= EI \frac{1}{1 + \frac{L}{4Hf}} \phi \quad (7.13)$$

where ϕ is the curvature of the equivalent plastic hinge region ($\phi = \frac{1}{\rho}$). The curvature of the plastic hinge can be expressed as the following incremental form.

$$\frac{dM}{d\phi} = EI \frac{1}{1 + \frac{L}{4Hf}} \quad (7.14)$$

It should be noted that this expression relies on the adoption of small deflection theory. This is consistent with similar assumptions made in the analysis of structural frames. Obviously, the selection of an unrealistically large plastic hinge length will invalidate the use of the above expression.

7.4 Column moment - axial load interaction

Figure 7.3 describes the interaction model chosen for this study. The interaction curve is modeled by a series of straight lines. For a typical reinforced concrete column, this series of lines are characterized by the following four points; pure axial tension, pure bending with no axial load, balanced yield and pure axial compression. More data regarding the region between the point representing balanced yield and that representing pure bending with no axial load can be accommodated if more accurate representation is needed.

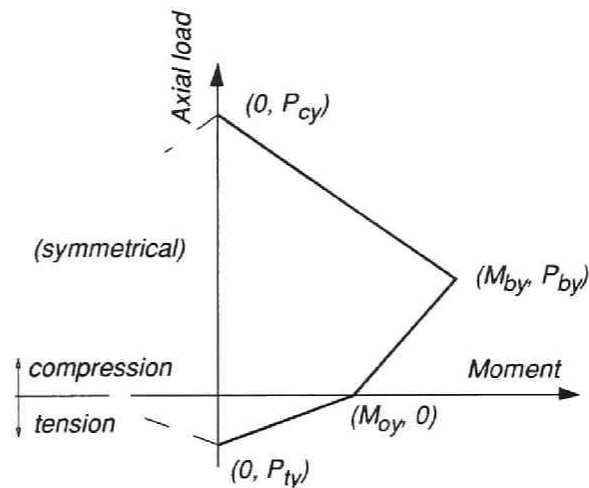


Fig.7.3 Column yield moment - axial load interaction model

7.5 Tracking a moment - curvature relationship

When the variation in moment, with respect to curvature, is large, there is an often unavoidable over- or underestimation of the moment at a particular curvature, which is inherent in the procedure when a change of stiffness is incurred. This arises from the necessary assumption of linear behavior for the duration of each constant length time-step.

There are four ways of getting around the problem of moment overshoot.

1. The excessive or deficit moment is reset to the value which correctly corresponds to the current curvature.
2. The moment in error is not reset and the analysis proceeds using the erroneous value as an initial condition for the following time-step.
3. The moment to which directed by the moment - curvature relationship for the current curvature is limited, and the difference between these two values as a constant excessive load is applied on the appropriate node for the duration of the next time-step.
4. An iterative procedure over any time-step in which any moment overshoot.

In this research the moment overshoot was counteracted by reinvesting it on the following (constant length) time-step.

7.6 Structural layout and description of the buildings

The buildings analyzed were designed in accordance with the requirements for BDF System specified in the seismic design procedure proposed by the AIJ task-committee on seismic design of prestressed concrete buildings and in part the AIJ Guidelines [7.4] were used. A building to be designed in BDF (Beam sidesway ductile frame) is required to fail in beam sidesway mechanism. The design procedure itself employs the capacity design method. The detail of this design procedure will be described in Chapter 8. The component of horizontal earthquake loading perpendicular to the plane of the frames considered was assumed to be resisted by structural wall or some other structural systems. The effect of vertical component of earthquake loading on the response of the buildings was neglected although it may be of significance for a building with long-span beams. Torsional moments and P- Δ effects were not considered in the design.

For simplification the design moment due to earthquake loading only was considered. The design moments due to dead and live loads and the secondary moment due to prestressing were not taken into account.

A uniformly distributed dead and live load of 9.8 kPa was assumed. A concrete compressive strength of 30 MPa was assumed in both beams and columns. Young's modulus of concrete was assumed to be 3.33×10^4 MPa. Equivalent plastic hinge length equal to whole depths of members was assumed.

There are two research work on plastic hinge length of prestressed concrete members. Park et al. [7.5] obtained an equivalent plastic hinge length of approximately half a whole depth of prestressed concrete beams from their test results. Okamoto [7.6] suggested equivalent plastic hinge length of

$$l_{eq} / D = 0.06 \cdot Z / D + 0.7 \quad (7.15)$$

where Z : shear span length, D : whole depth of the section. This can be applied to a member whose rotation angle at the either end is greater than 1/100 radian. Okamoto examined Park et al's experimental results by his expression and found that his equation can be applied to the prestressed concrete beams tested by Park et al. on the basis of the distribution of curvature along the beam length.

Structural layout of the frame to be designed is shown in Fig.7.4.

7.7 Design of possible plastic hinge regions

Beam ends, top of the top layer columns and bottom of the first layer columns were designed as possible plastic hinge regions. The design moments for these plastic hinge regions were determined by a linear analysis of the frame. The elastic analysis was

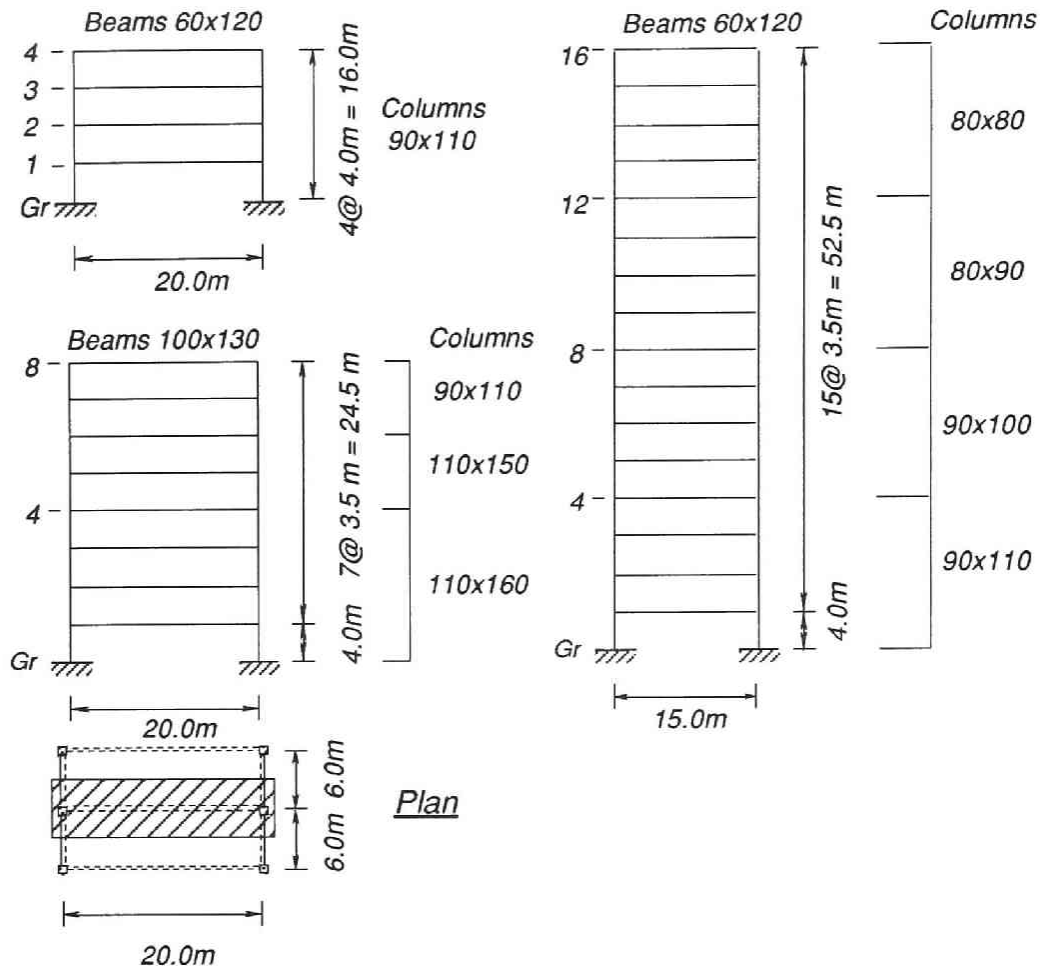


Fig.7.4 Structural layout of the frames to be designed

carried out on the assumption that stiffness of beams with plastic hinges at both ends and columns with a plastic hinge at either end were reduced to 50% and 70% of elastic stiffness, respectively. Members without plastic hinges were assumed to maintain elastic stiffness under design seismic load. Member sections were proportioned so that interstory drift of every layer was less than 1/300 radian in order to meet the requirement of AIJ Guidelines. Strictly speaking it is not a requirement. The Guidelines say that interstory drift of every layer of a building under design seismic load should be equal to or less than 1/200. However, the Commentary says stiffness reduction due to cracking should be accounted. In the case of preliminary calculation the following assumptions are considered to give a conservative displacement.

- 1) Elastic stiffness for the members without plastic hinge
- 2) Half an elastic stiffness for the beam members with plastic hinges at both ends
- 3) 70% elastic stiffness for the column members with plastic hinge at either end
- 4) Apply interstory drift limitation of 1/300

In designing four- and eight-story frames the above criteria were adopted.

However, for 16-story frame an impractically large column size was required to meet the above regulations. An alternative criteria was applied to the frame : stiffness

reduction was not considered and the interstory drift of every layer under design seismic lateral load was less than 1/200 radian. This is the design criteria described in the current design code for prestressed concrete structures in Japan. Design and analytical results of the 16-story frame will be described after analytical results of four- and eight-story frames are examined.

The average acceleration method ($\beta = 1/4$) was employed in the analysis. A_i distribution was employed as a distribution of design layer shear force along the height of the building.

7.8 Design of non-plastic hinge regions

To give columns a high degree of protection against premature yielding due to dynamic effects particularly from the higher modes of vibration of the building, the dynamic magnification factor was introduced. According to AIJ Guidelines this is given by the following equations.

$$\omega_{ci} = 1.0 + (\Delta\omega_i / \phi_0) \cdot (\beta_{chi} / \beta_{ci}) \quad (7.15)$$

$$\omega_{wi} = 1.0 + (\Delta\omega_i / \phi_0) \cdot (\beta_{whi} / \beta_{wi}) \quad (7.16)$$

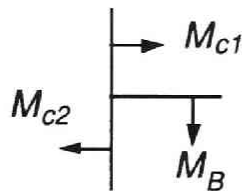
$$\begin{aligned} \Delta\omega_i &= 0.25 && (i = 1) \\ &= 0.20 && (2 \leq i \leq n/2) \\ &= 0.20 + 0.10(i - n/2) && (i > n/2) \end{aligned} \quad (7.17)$$

where ω_{ci}, ω_{wi} = dynamic magnification factors for column and wall in i -th layer
 ϕ_0 = $C_{10} / 0.25$
 C_{10} = base shear coefficient of a designed building
 β_{ci}, β_{wi} = ratio of story shear force attributed to column or wall to entire story shear force under fundamental period of vibration
 β_{chi}, β_{whi} = ratio of story shear force attributed to column or wall to entire story shear force under higher mode of vibration

Besides consideration of higher mode of vibration, for columns of two-way frames the effects of concurrent earthquake attack along both principal axes of the building should be considered. This was incorporated by adding 0.1 to the dynamic magnification factor according to AIJ Guidelines. For the four-story frame considered, ω_{ci} of each layer is given as follows.

$$\begin{aligned}
 \omega_{c4} &= 1.43 \\
 \omega_{c3} &= 1.35 \\
 \omega_{c2} &= 1.27 \\
 \omega_{c1} &= 1.31
 \end{aligned}
 \tag{7.18}$$

Therefore, design moments for the members are given in Fig.7.5. For the eight-story model frame, design moments of the members and ω_{ci} of each layer is given in Fig.7.6.



(Unit : kNm)

865.3	865.4
	100.9
1647.4	1075.1
	827.1
1062.3	1208.3
	1980.6
388.1	1053.5
	2599.0

Fig.7.5 Design moments of the members of a four-story building frame

(Unit : kNm)

1011.1	1011.1	$\omega_{c8} = 1.6$
	217.2	
2766.1	1629.7	$\omega_{c7} = 1.52$
	550.5	
3286.6	2217.1	$\omega_{c6} = 1.43$
	821.5	
3182.2	2443.1	$\omega_{c5} = 1.35$
	1488.5	
2576.8	2609.7	$\omega_{c4} = 1.27$
	2444.9	
1557.3	2626.2	$\omega_{c3} = 1.27$
	3979.6	
198.5	2429.6	$\omega_{c2} = 1.27$
	6231.7	
3455.2	1891.1	$\omega_{c1} = 1.31$
	6901.7	

Fig.7.6 Design moments and ω_{ci} of each layer of an eight-story building frame

Design axial loads on columns induced by an earthquake are derived on the assumption that ultimate flexural strength should develop at all potential plastic hinge regions of the beams above the specified layer at once. The following equation was used to design column longitudinal reinforcement.

$$M_u = 0.8a_t\sigma_y D + 0.5N \cdot D \left(1 - \frac{N}{bDf'_c} \right) \quad (7.19)$$

where M_u = ultimate flexural strength (design moment), a_t = sectional area of longitudinal reinforcement, σ_y = yield strength of reinforcement, N = design axial load, D = whole depth of column and f'_c = compressive strength of concrete. The sectional area of longitudinal reinforcement required for the columns was determined by Eq.7.19 for the minimum axial load. However, in some cases the amount of reinforcement was so small that it did not meet the requirement of minimum reinforcement specified in the AIJ code : 0.8% of gross sectional area of column. In this study all column sections contains longitudinal reinforcement whose sectional area is at least 0.8% of gross sectional area of the column. The moment-axial load interaction curve was calculated for each column section using the sectional area of the longitudinal reinforcement obtained above.

7.9 Natural period of buildings

The natural period calculated on the basis of the same stiffnesses of the member sections assumed in the linear analysis is given in Table 7.1.

Table 7.1 Natural period of four-, eight- and sixteen-story frames

Period (sec.)	4-story	8-story	16-story
1st	0.488	0.575	1.433
2nd	0.127	0.166	0.467
3rd	0.054	0.082	0.260

7.10 Moment - curvature idealization assigned to plastic hinge regions

The moment - curvature relationship assigned to plastic hinge regions of columns was bi-linear. Since stiffness degradation due to cracking can not be allowed in the idealization, the first segment up to yielding has a stiffness of 70% of the elastic stiffness of the gross section of the columns with plastic hinge at either end. The stiffness beyond yield point is assumed to be 1% of the stiffness of the first segment.

The moment - curvature relationship assigned to plastic hinge regions of the beams was the idealization proposed in Chapter 5. It is shown in Fig.7.7. The ratio of yielding moment to cracking moment was 2. The ratio of secant stiffness at yielding to elastic stiffness was assumed to be 4.

Prestressed concrete members and reinforced concrete members have quite different moment-curvature characteristics as described in Chapter 2. Thus, the moment-curvature relationship assigned to plastic hinge regions should reflect the difference and be based on a practical cross section provided with reinforcement. However, a reinforced concrete beam of 20m length is not practical: This was just for a comparative study. Besides, a region of large deflection is of interest in this research work and the moment-curvature characteristics up to yielding was considered not to affect the response of the frame significantly.

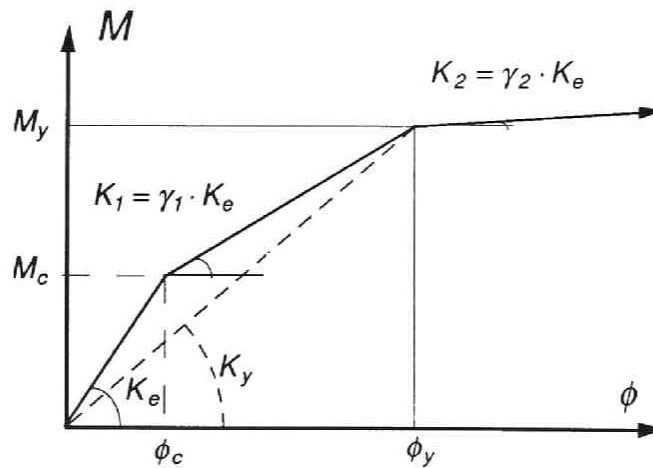


Fig.7.7 Moment - curvature idealization of beam plastic hinge region

7.11 Selected ground acceleration records

The three typical digitalized earthquake records were included in the analyses; The El Centro 1940 North-South Component, the earthquake motion recorded at Hachinohe harbor during the 1968 Tokachi-oki earthquake and the motion record at the first floor of the building at Tohoku University during the Miyagiken-oki earthquake in 1974. The first 16 seconds of the earthquake records were used because the maximum acceleration and velocity are observed within the first 16 seconds of the records which are considered to give the largest effects. The time interval used in the analyses was 0.005 seconds. To investigate the behavior of the frames during severe earthquakes the digitalized earthquake records were amplified so that the maximum velocity of each earthquake record was 50 cm/s. The maximum acceleration, velocity and displacement of the earthquake wave records used are summarized in Table 7.2.

Fig.7.2 Characteristics of earthquake wave records

Earthquake records	El Centro NS 1940	Miyagiken- oki 1974	Hachinohe EW 1968
Maximum acceleration (cm/s ²)	341.7	258.2	182.9
Maximum velocity (cm/s)	33.4	36.2	35.7
Maximum displacement (cm)	10.9	14.5	

7.12 Calculation results of four- and eight-story frames

The response of the four-story and eight-story frames were analyzed. The envelopes of the extreme structural deformations and member actions are presented in terms of (1) interstory drifts, (2) beam and column bending moments, shear forces and plastic rotations, (3) the development of plastic hinge formation during the earthquakes, and (4) shear force induced in each story.

7.12.1 Results of four-story frames

Interstory drift

Maximum interstory drift of each layer is plotted in Fig.7.8. Generally speaking the building with prestressed concrete beams exhibits the largest interstory drift among the three frames. The interstory drift responses of the reinforced concrete frame were the smallest among three types of frames.

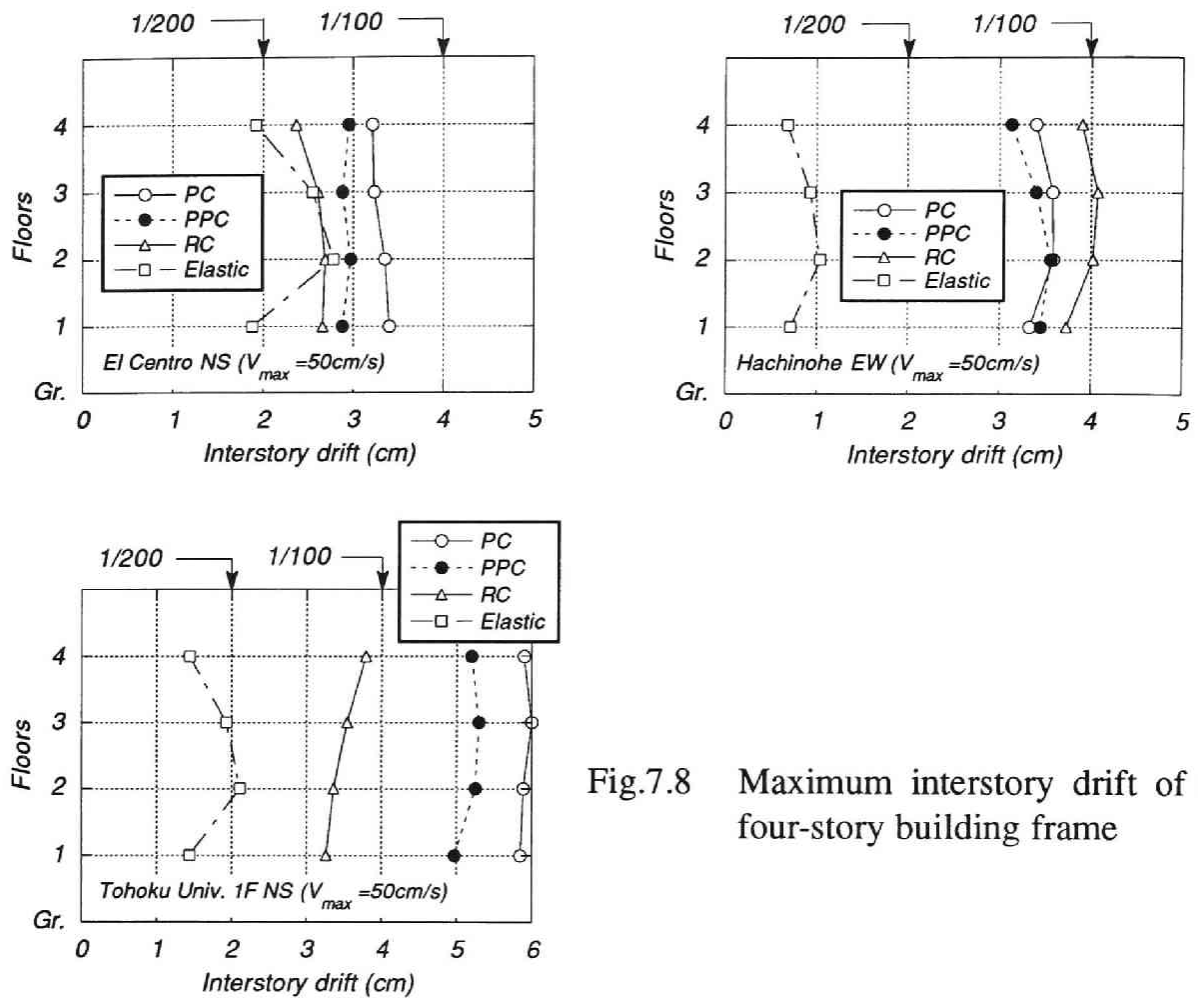


Fig.7.8 Maximum interstory drift of a four-story building frame

The ratio of the response of prestressed concrete building to that of the reinforced concrete building ranged between 0.87 and 1.58. The interstory drifts along the height of the building were almost the same because the intended failure mechanism was a beam sidesway mechanism.

In the analyses of SDOF systems described in Chapter 6 the ratios of the responses of the prestressed concrete systems with a various range of natural period and yield strength to those of the reinforced concrete systems scattered. In the analyses of the frames they were plotted in a relatively small range.

Comparison of the response results with the results obtained in Chapter 6 reveals that the ratios of the responses of the prestressed concrete systems to those of the reinforced concrete systems were larger in the analyses of the SDOF systems than in the two-dimensional analyses of the frame structures. This is because of the influence of the

column plastic hinge regions. Since the frames were so designed as to fail in a beam sidesway mechanism, this must be an extreme case in which the prestressed concrete beam plastic hinge regions strongly influenced the responses of the frames.

The story shear and interstory drift relationship of each frame obtained from the static inelastic analyses is plotted in Fig.7.9. The open circles in the figure indicate that the failure mechanism has formed ; plastic hinging occurred in the bottom of the first story columns, top of the top story columns and beam ends. Fig.7.10 shows the ductility ratios of the maximum interstory drift which are defined as the ratios of the maximum interstory drifts observed during the dynamic response analyses to the interstory drifts obtained from the static inelastic analyses when the failure mechanism formed. They were 3.59 to 11.9 for the prestressed concrete frames, 3.20 to 10.1 for the partially prestressed concrete and 2.90 to 7.57 for the reinforced concrete.

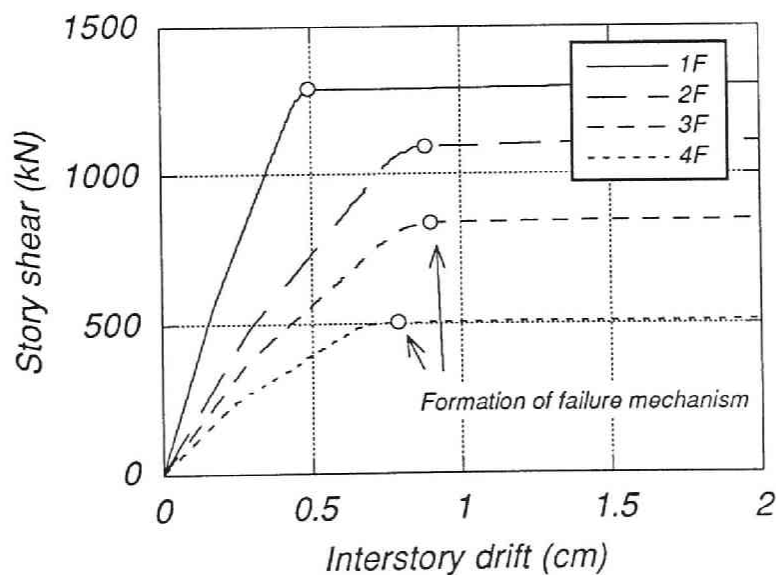


Fig.7.9 Story shear force - interstory drift relationship obtained from static inelastic analysis

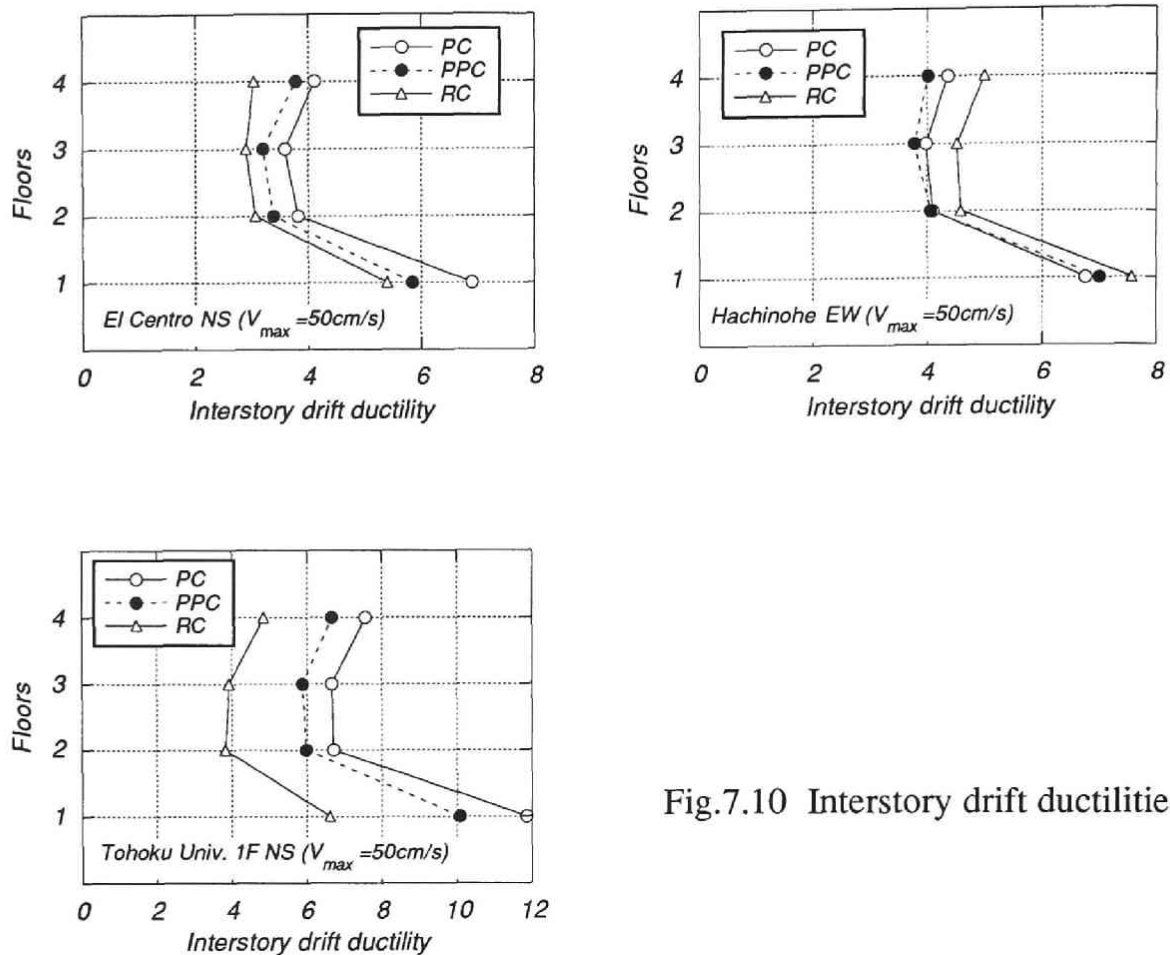


Fig.7.10 Interstory drift ductilities

Moment-curvature relationships of members

Moment-curvature relationships observed in the second floor beams during the dynamic response analyses are plotted in Fig.7.11. The curvature ductility ratios of the plastic hinge regions of the beams and columns are summarized in Table 7.3. The maximum rotation angles attained during the analyses are also included as the values in the brackets.

The ductility ratios of the 1st-story columns listed in the table are the ratios of the attained maximum curvature to the yield curvature with no axial load on the column.

The maximum rotation angle to be reached during a strong earthquake motion is expected to be less than 1/50 for beams and 1/67 for columns according to the AIJ Guidelines. The strong earthquake motion is usually defined as an earthquake wave whose maximum velocity is 50 cm/s. Therefore, although the responses of the prestressed concrete frames were larger than those of the reinforced concrete frames with the same design base shear, the deformations are considered to be within the tolerance. The important thing is the limitation of design interstory drift which can prevent a frame from undergoing an excessive deformation.

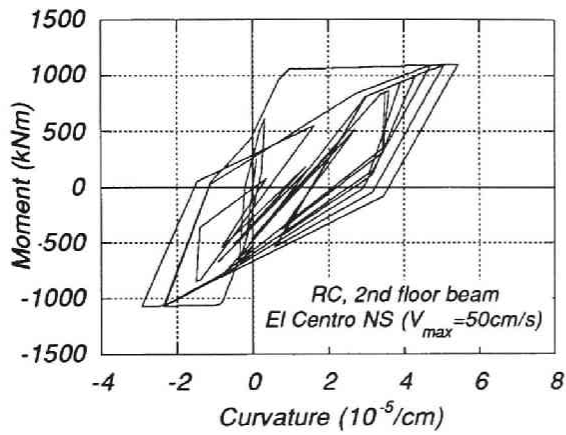
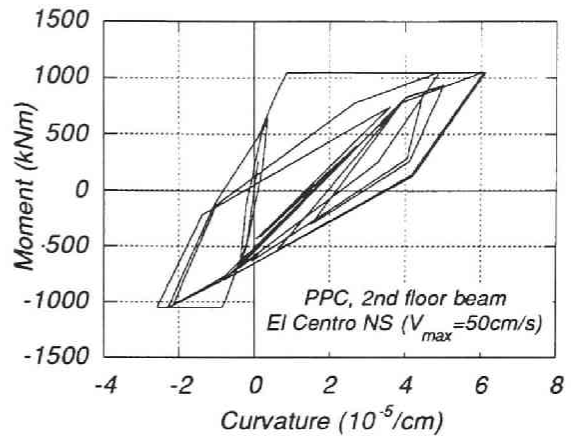
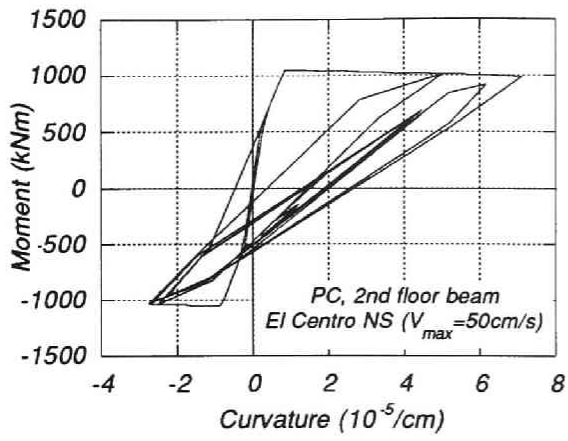


Fig.7.11 (a) Moment - curvature curves in the plastic hinge of the second floor beams (El Centro NS)

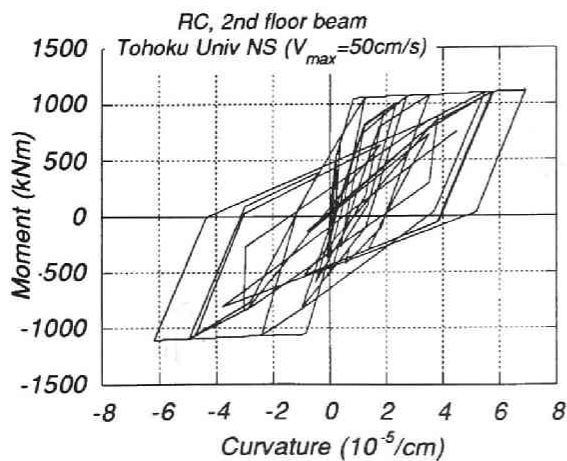
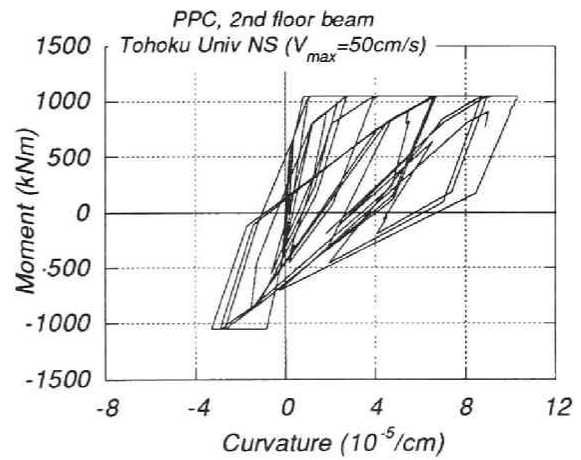
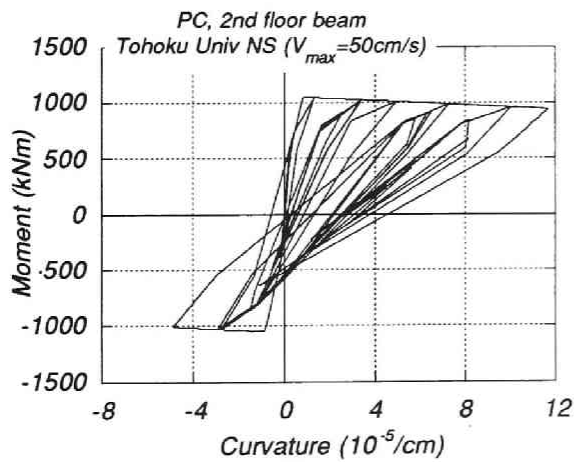


Fig.7.11 (b) Moment - curvature curves in the plastic hinge of the second floor beams (Tohoku Univ. NS)

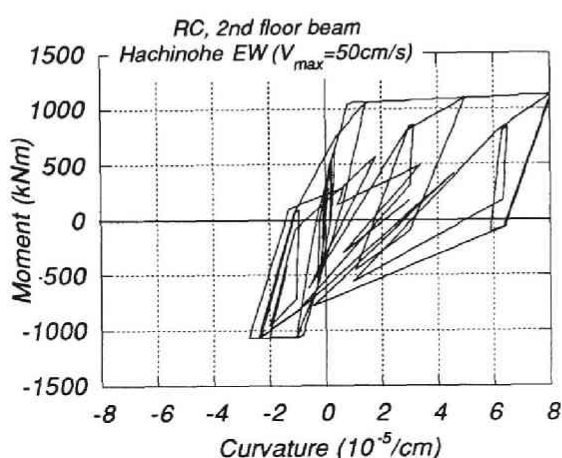
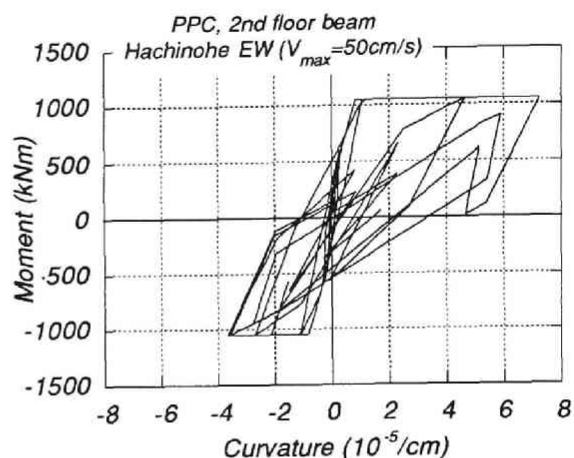
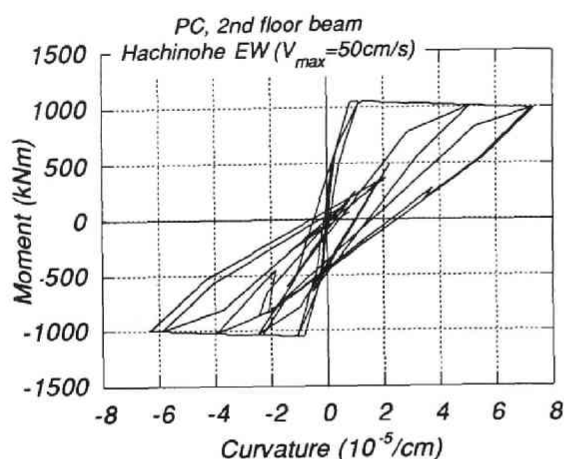


Fig.7.11 (c) Moment - curvature curves in the plastic hinge of the second floor beams (Hachinohe EW)

Plastic hinge formation

In all cases, the plastic hinges developed at the bottom end of the first story columns, at the top end of the fourth story columns and beam ends as intended in the design.

Story shear force

Figure 7.13 shows the maximum story shear forces attained during the earthquake excitations. The design story shear is also shown in the figure. In the case of design in beam sidesway mechanism a triangular distribution of design story shear seems suitable. The maximum story shears observed in the reinforced concrete frames were slightly larger than those of the prestressed concrete frames although interstory drifts of the prestressed concrete frames larger than those of the reinforced concrete frames were observed.

Table 7.3 Curvature ductility ratios of the plastic hinge regions of the beams and columns

El Centro NS	PC	PPC	RC
Roof beam	9.58 (1/128)	8.87 (1/138)	8.06 (1/152)
4th floor beam	7.97 (1/123)	7.16 (1/137)	6.10 (1/162)
3rd floor beam	7.02 (1/125)	6.29 (1/139)	5.71 (1/153)
2nd floor beam	8.75 (1/115)	7.53 (1/133)	6.90 (1/146)
Bottom of 1st-story column	3.91 (1/129)	3.20 (1/157)	2.98 (1/169)

Hachinohe EW	PC	PPC	RC
Roof beam	10.00 (1/122)	8.98 (1/136)	11.52 (1/106)
4th floor beam	8.57 (1/115)	7.95 (1/124)	9.71 (1/101)
3rd floor beam	7.84 (1/112)	7.64 (1/115)	8.83 (1/99)
2nd floor beam	8.96 (1/112)	9.03 (1/111)	9.94 (1/101)
Bottom of 1st-story column	3.74 (1/137)	3.87 (1/130)	4.18 (1/120)

Tohoku Univ. NS	PC	PPC	RC
Roof beam	17.69 (1/69)	15.47 (1/79)	11.10 (1/110)
4th floor beam	14.71 (1/67)	12.80 (1/77)	9.43 (1/104)
3rd floor beam	12.91 (1/68)	11.56 (1/76)	7.54 (1/116)
2nd floor beam	14.55 (1/69)	12.85 (1/78)	8.58 (1/117)
Bottom of 1st-story column	7.21 (1/71)	5.78 (1/87)	3.72 (1/135)

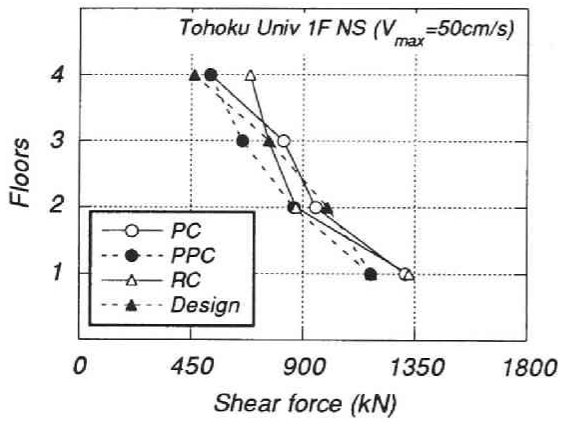
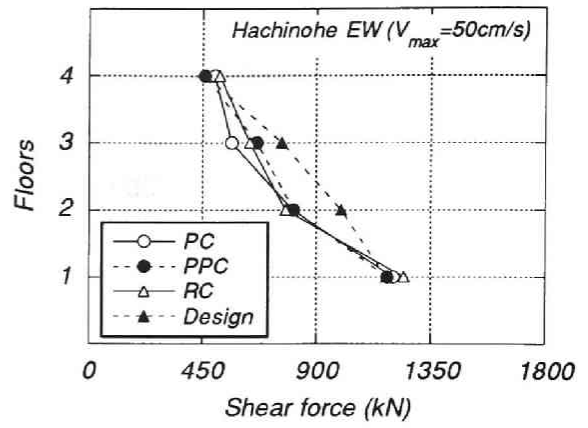
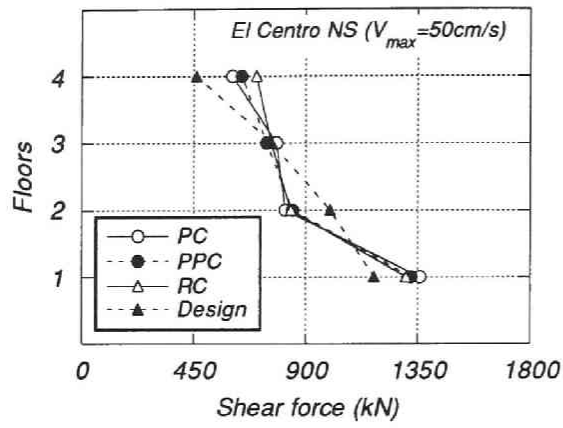


Fig.7.13 Maximum story shear force

7.12.2 Results of eight-story frames

Interstory drift

Maximum interstory drifts of each layer of the eight-story frames are plotted in Fig.7.14. In the case of El Centro earthquake record, the response of the prestressed concrete frame was the largest in every story among the three structural systems. The interstory drift responses of the partially prestressed and reinforced concrete frames were almost the same. The maximum interstory drift of the prestressed concrete frame during the earthquake motion was 9% larger than that of the reinforced concrete frame. However, in the case of Hachinohe wave the reinforced concrete frame exhibited the largest response and the prestressed concrete frame the smallest. The maximum interstory drift of the reinforced concrete frame was 35% larger than that of the prestressed concrete frame. The interstory drift responses of those frames were around 1/200 of the story height although the maximum velocity of the earthquake records were amplified to 50cm/s, which corresponds to a severe earthquake whose average return period is higher than the intended service life of building to be designed. For the earthquake wave recorded at Tohoku University, the maximum interstory drift of the partially prestressed concrete frame was the largest and exceeded 1/100 of the story height in the fifth and sixth stories. That of the prestressed concrete frame reached 1/100 of the story height in the top story. The ratio of the maximum interstory drift of the prestressed concrete frame to that of the reinforced concrete frame was 1.11. As for the partially prestressed concrete frame, the ratio reached 1.27.

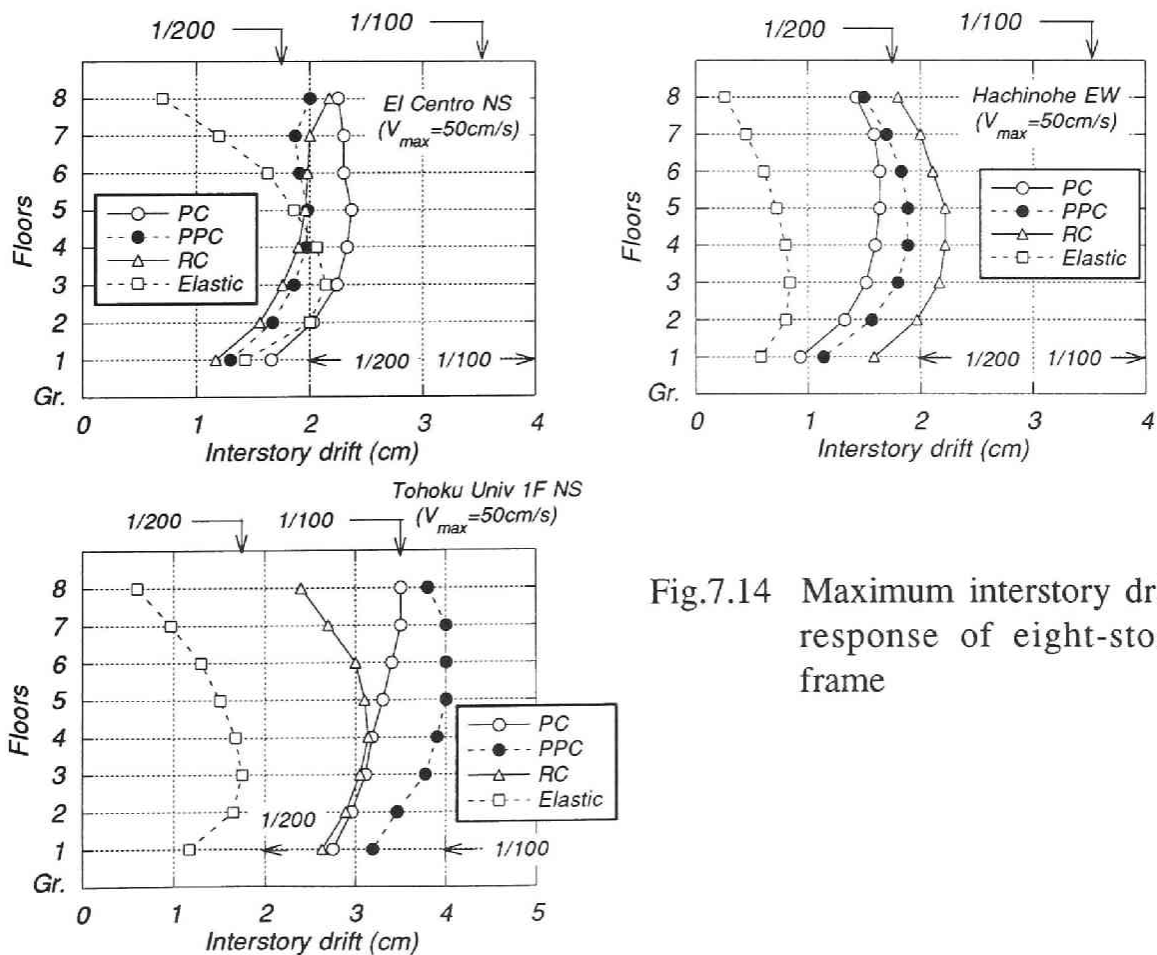


Fig.7.14 Maximum interstory drift response of eight-story frame

The above results shows that the responses of a building to an earthquake wave can not be determined only by the type of hysteresis loops assigned to possible plastic hinge regions. The characteristics of an earthquake record has the large influence on the responses of a building frame.

The story shear and interstory drift relationship of each frame obtained from the static inelastic analyses are plotted in Fig.7.15. The open circles in the figure indicate that the failure mechanism has formed ; plastic hinging occurred in the bottom of the first story columns, top of the top story columns and beam ends. Fig.7.16 shows the ductility ratios of the maximum interstory drift which are defined as the ratios of the maximum interstory drifts observed during the dynamic response analyses to the interstory drifts obtained from the static inelastic analyses when the failure mechanism formed. They were 1.76 to 8.97 for the prestressed concrete frames, 2.09 to 9.74 for the partially prestressed concrete and 2.07 to 6.15 for the reinforced concrete.

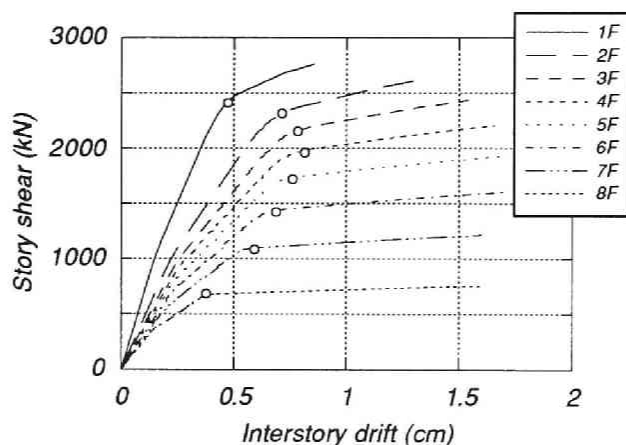


Fig.7.15 Story shear force - interstory drift relationship obtained from static inelastic analysis

Moment-curvature relationships of members

Moment-curvature relationships observed in the second floor beams during the dynamic response analyses are plotted in Fig.7.17. The curvature ductility ratios of the plastic hinge regions of the beams and columns are summarized in Table 7.3. The maximum rotation angles attained during the analyses are also included as the values in the brackets.

The ductility ratios of the 1st-story columns listed in the tables are the ratios of the maximum curvature attained to the yield curvature when the column has no axial load on it.

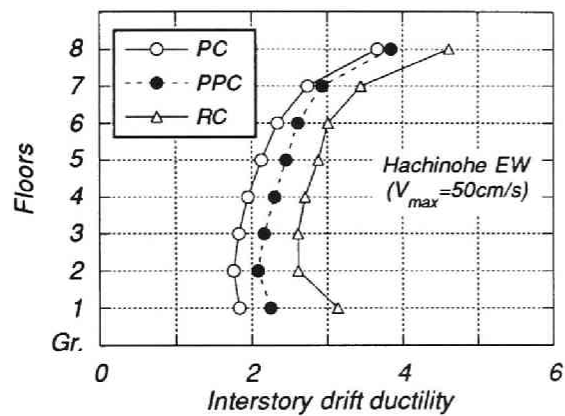
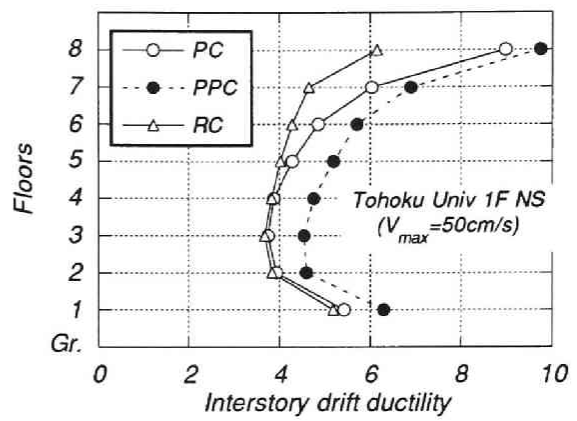
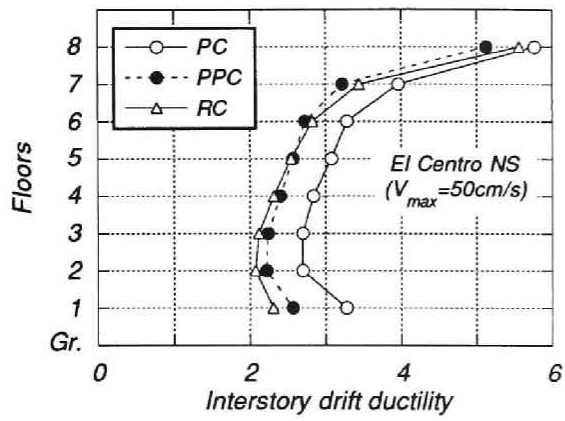


Fig.7.16 Maximum interstory ductilities

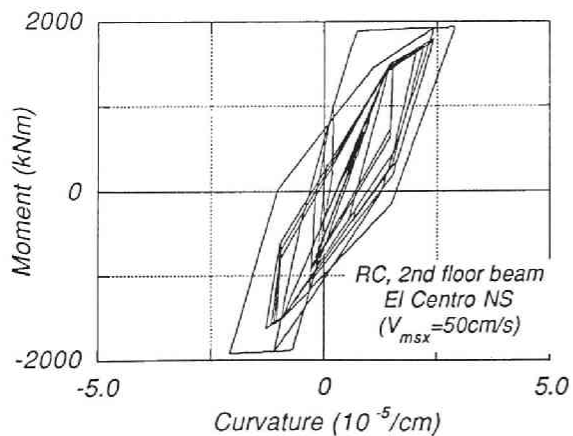
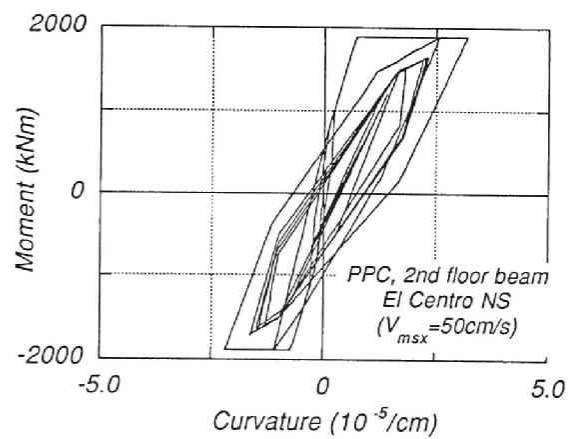
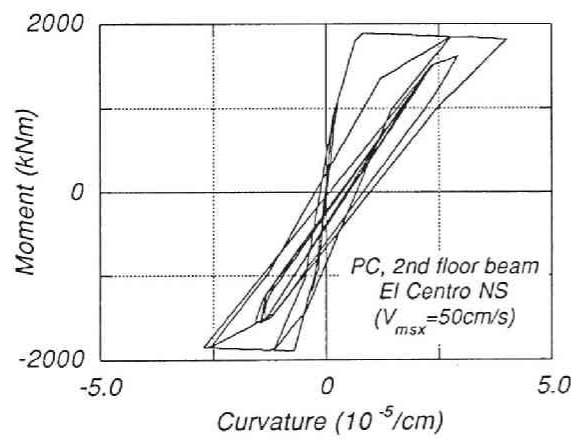


Fig.7.17 (a) Moment - curvature curves in the plastic hinge of the second floor beams (El Centro NS)

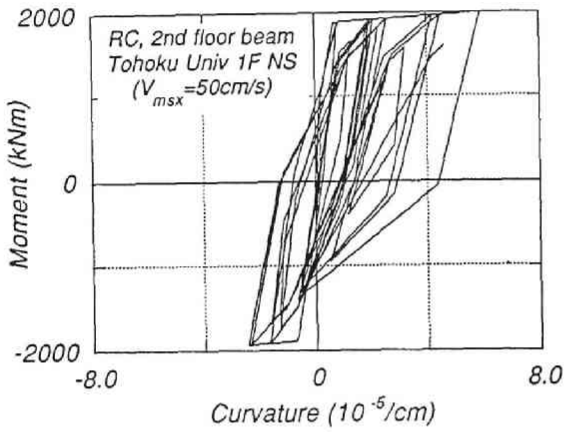
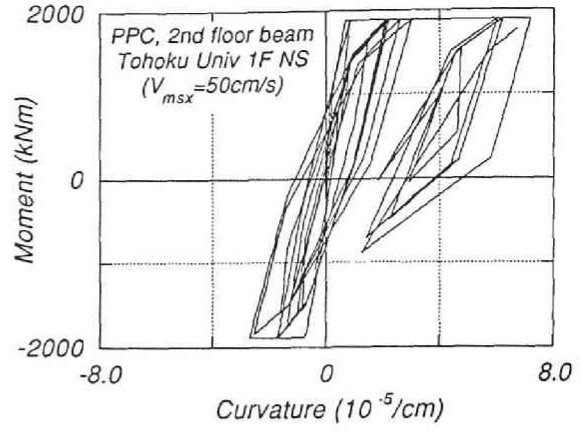
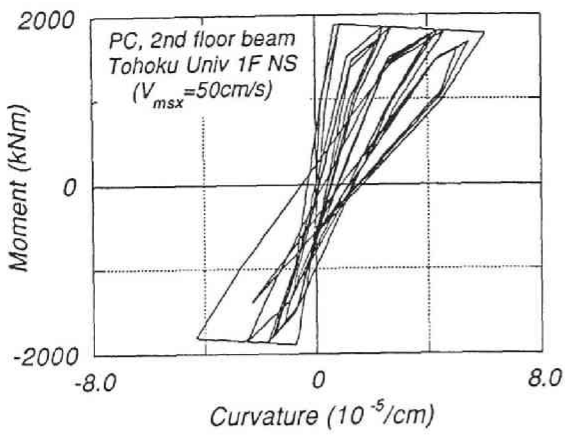


Fig.7.17 (b) Moment - curvature curves in the plastic hinge of the second floor beams (Tohoku Univ. NS))

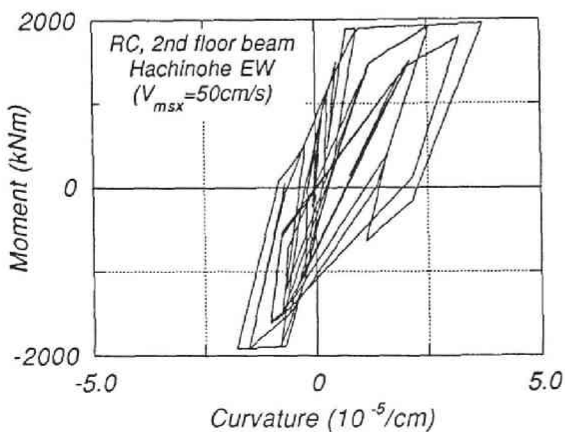
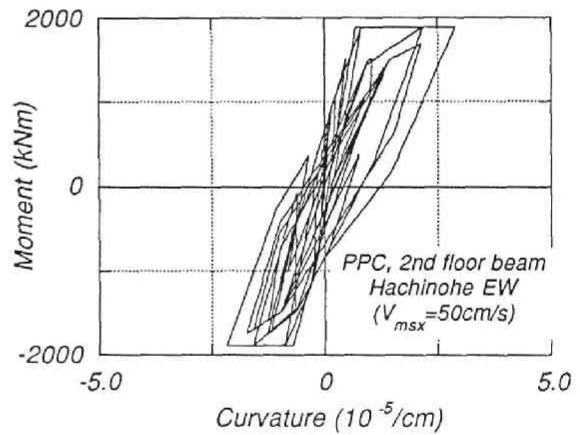
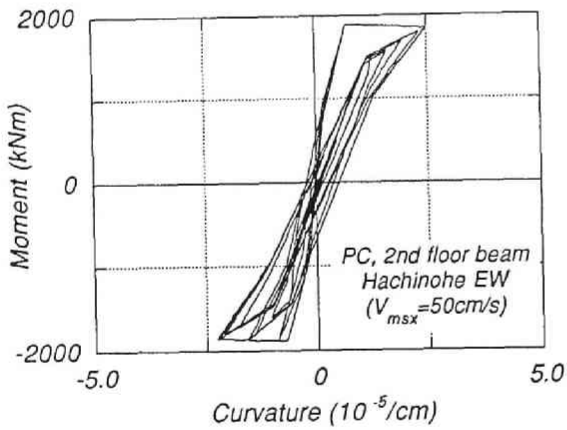


Fig.7.17 (c) Moment - curvature curves in the plastic hinge of the second floor beams (Hachinohe EW)

Table 7.4 Curvature ductility ratios of the plastic hinge regions of the beams and columns of eight-story frame

El CentroNS	PC	PPC	RC	TohokuUniv. NS	PC	PPC	RC	HachinoheEW	PC	PPC	RC
Roof beam	13.26 (1/154)	11.92 (1/172)	12.51 (1/164)	Roof beam	20.4 (1/101)	22.1 (1/93)	13.8 (1/148)	Roof beam	7.35 (1/279)	7.32 (1/280)	9.85 (1/208)
8th floor beam	7.93 (1/160)	6.61 (1/192)	7.20 (1/176)	8th floor beam	12.9 (1/98)	14.1 (1/90)	8.80 (1/144)	8th floor beam	4.86 (1/262)	5.04 (1/252)	6.23 (1/204)
7th floor beam	5.81 (1/161)	4.56 (1/205)	4.76 (1/196)	7th floor beam	8.84 (1/106)	10.7 (1/88)	7.56 (1/124)	7th floor beam	3.84 (1/243)	4.42 (1/211)	5.13 (1/182)
6th floor beam	5.26 (1/161)	4.33 (1/196)	4.33 (1/196)	6th floor beam	7.73 (1/110)	9.61 (1/88)	7.07 (1/120)	6th floor beam	3.49 (1/243)	4.19 (1/202)	4.88 (1/174)
5th floor beam	5.05 (1/157)	4.22 (1/188)	4.03 (1/197)	5th floor beam	6.94 (1/114)	8.83 (1/90)	6.88 (1/115)	5th floor beam	3.25 (1/244)	3.95 (1/201)	4.73 (1/168)
4th floor beam	4.90 (1/161)	4.01 (1/197)	3.68 (1/214)	4th floor beam	6.77 (1/117)	8.58 (1/92)	6.78 (1/116)	4th floor beam	3.14 (1/251)	3.95 (1/200)	4.71 (1/167)
3rd floor beam	5.08 (1/168)	3.98 (1/214)	3.64 (1/234)	3rd floor beam	7.10 (1/120)	8.86 (1/96)	7.16 (1/119)	3rd floor beam	3.15 (1/271)	3.85 (1/221)	4.82 (1/177)
2nd floor beam	5.72 (1/191)	4.55 (1/240)	4.13 (1/265)	2nd floor beam	8.62 (1/127)	10.3 (1/107)	8.44 (1/130)	2nd floor beam	3.56 (1/308)	4.13 (1/265)	5.34 (1/205)
Bottom of 1st-story column	2.09 (1/234)	1.66 (1/295)	1.51 (1/324)	Bottom of 1st-story column	3.43 (1/143)	3.97 (1/123)	3.31 (1/148)	Bottom of 1st-story column	1.25 (1/392)	1.47 (1/333)	2.03 (1/241)

As described in the preceding section the maximum rotation angle to be reached during a strong earthquake motion is expected to be less than 1/50 for beams and 1/67 for columns according to the AIJ Guidelines. Therefore, although the responses of the prestressed concrete frames were larger than those of the reinforced concrete frames when the design base shears were the same, the deformations are considered to be within the expectation.

Plastic hinge formation

In all cases, the plastic hinges developed at the bottom end of the first story columns, at the top end of the fourth story columns and beam ends as intended in the design.

Story shear force

Figure 7.18 shows the maximum story shear forces attained during the earthquake excitations along with the design story shear. The maximum responses of story shear were larger than the design story shear. The shape of the story shear force distribution was similar to that of the design shear force distribution. *Ai*-distribution of design shear force can be applied to the design of this eight-story frame.

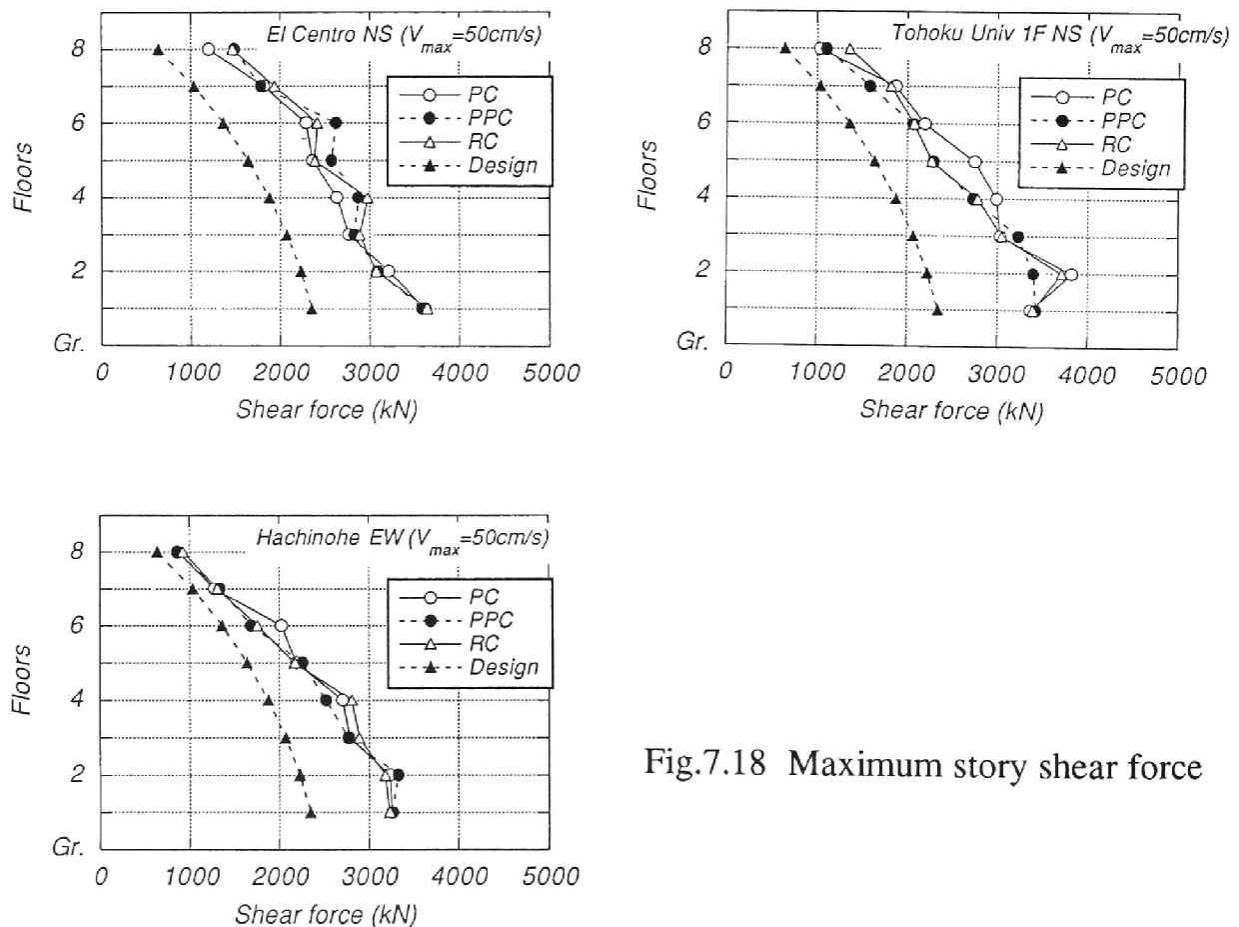


Fig.7.18 Maximum story shear force

7.13 Design of 16-story frames

The criteria adopted when designing 16-story frames were different from those for the four- and eight-story frames. As seen in the dimensions of the columns of the eight-story frame, as long as 20m spans resulted in huge cross-sections of the columns. It is considered not practical to design a taller frame than eight-story frame by the same criteria that used for the previous two kinds of frames. In the design of the former model frames stiffness reduction due to cracking was taken into account and the interstory drift angle of each story was within $1/300$ radian. These criteria for deformation are too strict for prestressed concrete frames which usually consist of long span beams. According to the current seismic design code for prestressed concrete frames the criteria for deformation is that the interstory drift angle of each story should be within $1/200$ radian assuming the whole cross section are effective for flexure. The author decided to adopt the design criteria conforming with the current seismic design code when designing 16-story frames and they are also designed to fail in a beam sidesway mechanism.

The reason why the author did not adopt the design criteria described in the current seismic design code for prestressed concrete structures is that the criteria is considered outdated and does not incorporate the capacity design concept.

A design trial of a 16-story frame with 20m span under the above deformation criteria revealed that impractically large column sections were still required. Therefore, a 16-story model frame with 15m span was chosen although the length of the span was $3/4$ of the beam length of the former two kinds of model frames.

In the analyses of the former two frames, the stiffness of the first story columns up to yielding was assumed to reduce to 70% of the elastic stiffness because cracking was taken into consider. However, in the analyses of the 16-story frame, such allowance was not made. Natural periods of the 16-story frame are shown in Table 7.1.

7.13.1 Results of 16-story frames

Interstory drift

Maximum interstory drift and maximum interstory drift ductility of each layer for each earthquake wave are plotted in Fig.7.19 and Fig.7.20, respectively. As the interstory drift response increased, the difference between the responses of the prestressed concrete and reinforced concrete frames became significant. The responses of the prestressed concrete frame were 72 to 155% those of the reinforced concrete frame at each floor level. The responses of the partially prestressed concrete frame were 39 to 147% those of the reinforced concrete frame.

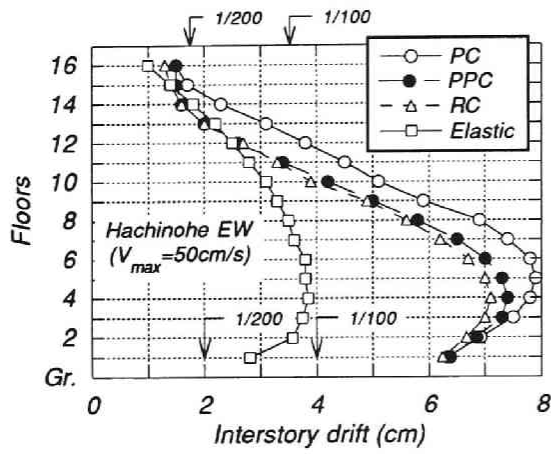
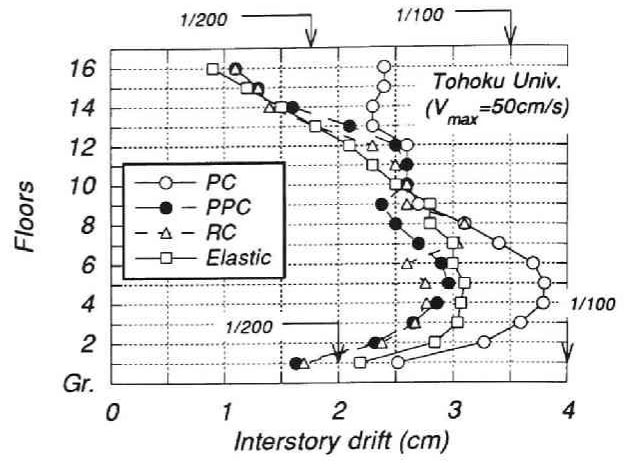
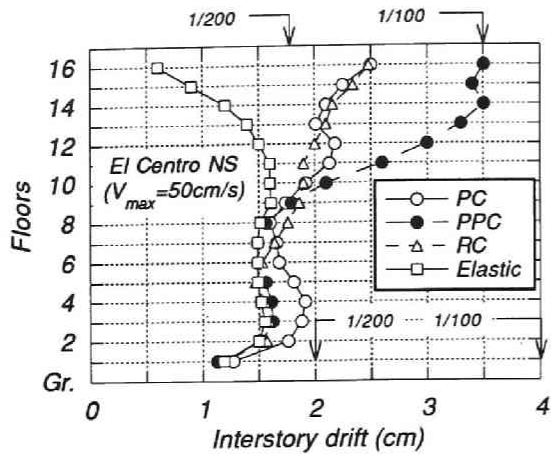


Fig.7.19 Maximum interstory drift of sixteen-story building frame

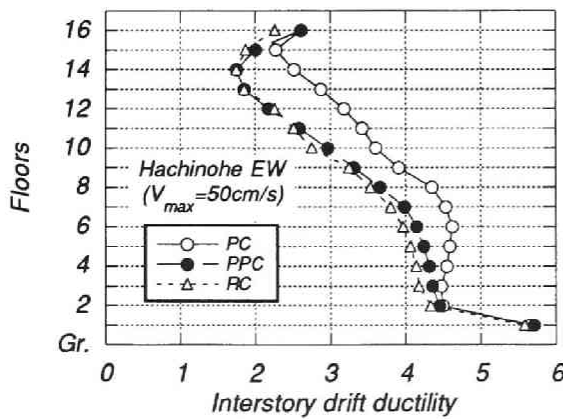
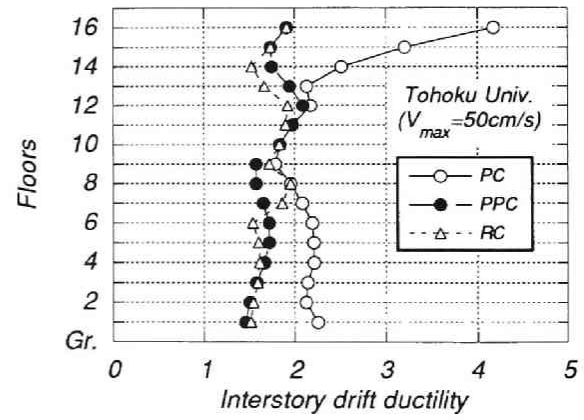
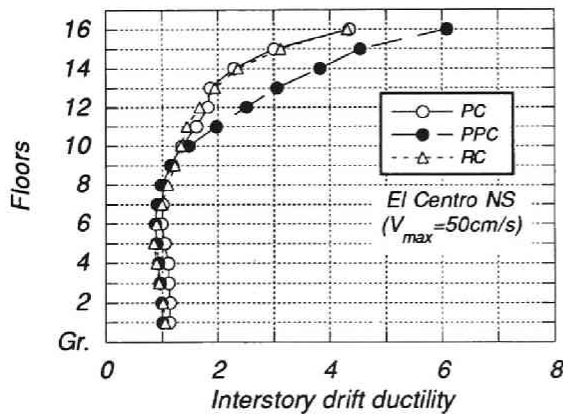


Fig.7.20 Maximum interstory drift ductilities

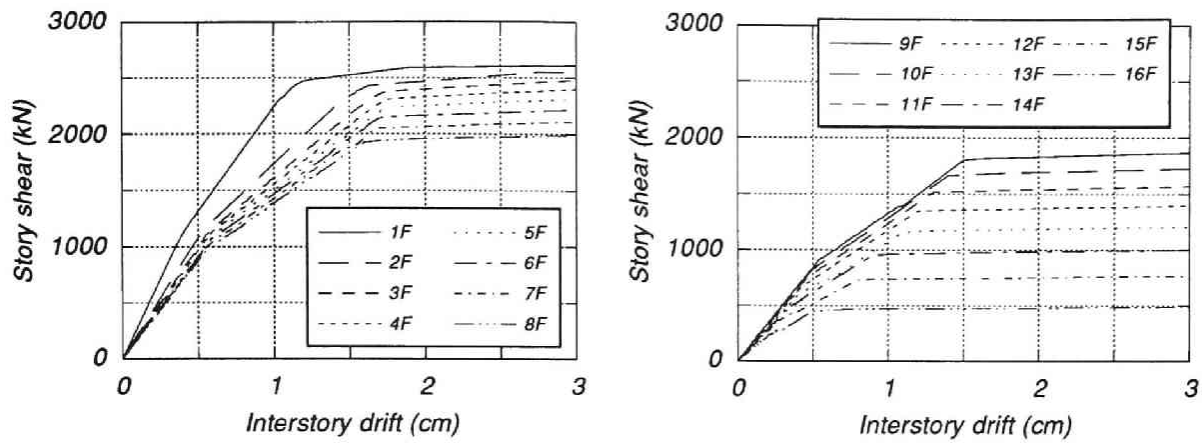


Fig.7.21 Story shear force - interstory drift relationship obtained from static inelastic analysis

Plastic hinge formation

In the frames analyzed using the El Centro NS wave, plastic hinges formed in all the beam ends. No plastic deformation was observed in the columns. Hachinohe EW wave caused plastic hinges in all the beams, in the bottom of the first story columns and in the several column ends in the mid-height floors. In the analysis using the earthquake wave recorded at Tohoku University, plastic hinges formed in all the beam ends and in the bottom of the first story columns, although they did not occur at the same time. The frames analyzed in this study were designed as to fail in a beam sidesway mechanism, but plastic hinges were observed in the several columns other than the columns which were expected to have a plastic hinge. This did not occur in the four- and eight-story frames. It is appeared that higher-mode vibration had an influence on the formation of plastic hinges in the columns in the midheight of the frames.

Story shear force

Being different from the other two frames, the sixteen-story frame exhibited less story shear force response than the design story shear force in most of the stories.

Table 7.5 Curvature ductility ratios of the plastic hinge regions of the beams and columns

El Centro NS	PC	PPC	RC
Roof beam	15.34 (1/138)	21.40 (1/99)	15.40 (1/137)
16th floor beam	7.76 (1/144)	10.67 (1/104)	7.62 (1/146)
15th floor beam	4.11 (1/191)	7.41 (1/106)	4.85 (1/162)
14th floor beam	2.99 (1/207)	5.93 (1/105)	3.27 (1/190)
13th floor beam	2.76 (1/188)	4.07 (1/128)	2.29 (1/227)
12th floor beam	2.44 (1/188)	3.48 (1/132)	1.90 (1/242)
11th floor beam	1.95 (1/213)	2.16 (1/192)	1.77 (1/234)
10th floor beam	1.43 (1/265)	1.58 (1/240)	1.48 (1/256)
9th floor beam	1.10 (1/319)	1.08 (1/327)	1.29 (1/272)
8th floor beam	1.03 (1/321)	0.93 (1/360)	1.17 (1/284)
7th floor beam	1.04 (1/306)	0.87 (1/362)	0.94 (1/335)
6th floor beam	1.02 (1/299)	0.86 (1/352)	0.86 (1/353)
5th floor beam	1.20 (1/247)	0.92 (1/322)	0.86 (1/343)
4th floor beam	1.19 (1/248)	0.95 (1/311)	0.90 (1/326)
3rd floor beam	1.23 (1/250)	0.98 (1/317)	0.99 (1/313)
2nd floor beam	1.44 (1/266)	1.16 (1/330)	1.26 (1/304)

Hachinohe EW	PC	PPC	RC
Roof beam	7.78 (1/272)	7.83 (1/270)	6.08 (1/348)
16th floor beam	4.24 (1/263)	3.83 (1/291)	3.43 (1/325)
15th floor beam	3.57 (1/219)	2.58 (1/304)	2.60 (1/301)
14th floor beam	4.05 (1/153)	2.33 (1/266)	2.41 (1/258)
13th floor beam	4.77 (1/109)	2.87 (1/181)	2.93 (1/178)
12th floor beam	5.06 (1/91)	3.38 (1/136)	3.41 (1/135)
11th floor beam	5.36 (1/77)	4.04 (1/103)	3.87 (1/107)
10th floor beam	5.62 (1/68)	4.55 (1/83)	4.21 (1/90)
9th floor beam	6.37 (1/55)	5.22 (1/67)	5.07 (1/69)
8th floor beam	6.68 (1/50)	5.64 (1/59)	5.40 (1/62)
7th floor beam	6.82 (1/46)	5.97 (1/53)	5.64 (1/56)
6th floor beam	6.76 (1/45)	6.14 (1/50)	5.80 (1/52)
5th floor beam	6.57 (1/45)	6.17 (1/48)	5.83 (1/51)
4th floor beam	6.38 (1/46)	6.14 (1/48)	5.86 (1/50)
3rd floor beam	6.37 (1/48)	6.27 (1/49)	6.01 (1/51)
2nd floor beam	7.26 (1/53)	7.18 (1/53)	6.94 (1/55)

Tohoku Univ. NS	PC	PPC	RC
Roof beam	13.82 (1/153)	4.80 (1/440)	5.28 (1/401)
16th floor beam	7.13 (1/156)	2.72 (1/409)	3.18 (1/350)
15th floor beam	4.72 (1/166)	2.30 (1/341)	2.19 (1/358)
14th floor beam	3.32 (1/187)	2.54 (1/244)	1.99 (1/312)
13th floor beam	3.25 (1/160)	2.71 (1/192)	2.49 (1/209)
12th floor beam	3.00 (1/153)	2.80 (1/164)	2.64 (1/174)
11th floor beam	2.67 (1/155)	2.57 (1/161)	2.49 (1/167)
10th floor beam	2.40 (1/159)	2.09 (1/182)	2.17 (1/175)
9th floor beam	2.49 (1/141)	1.95 (1/181)	2.31 (1/152)
8th floor beam	2.67 (1/124)	2.03 (1/164)	3.32 (1/100)
7th floor beam	2.83 (1/112)	2.09 (1/151)	1.88 (1/169)
6th floor beam	2.93 (1/104)	2.13 (1/143)	1.92 (1/158)
5th floor beam	2.88 (1/103)	2.07 (1/143)	1.90 (1/155)
4th floor beam	2.78 (1/106)	1.94 (1/152)	1.92 (1/153)
3rd floor beam	2.74 (1/113)	1.80 (1/172)	1.86 (1/166)
2nd floor beam	3.00 (1/128)	1.88 (1/204)	1.98 (1/194)

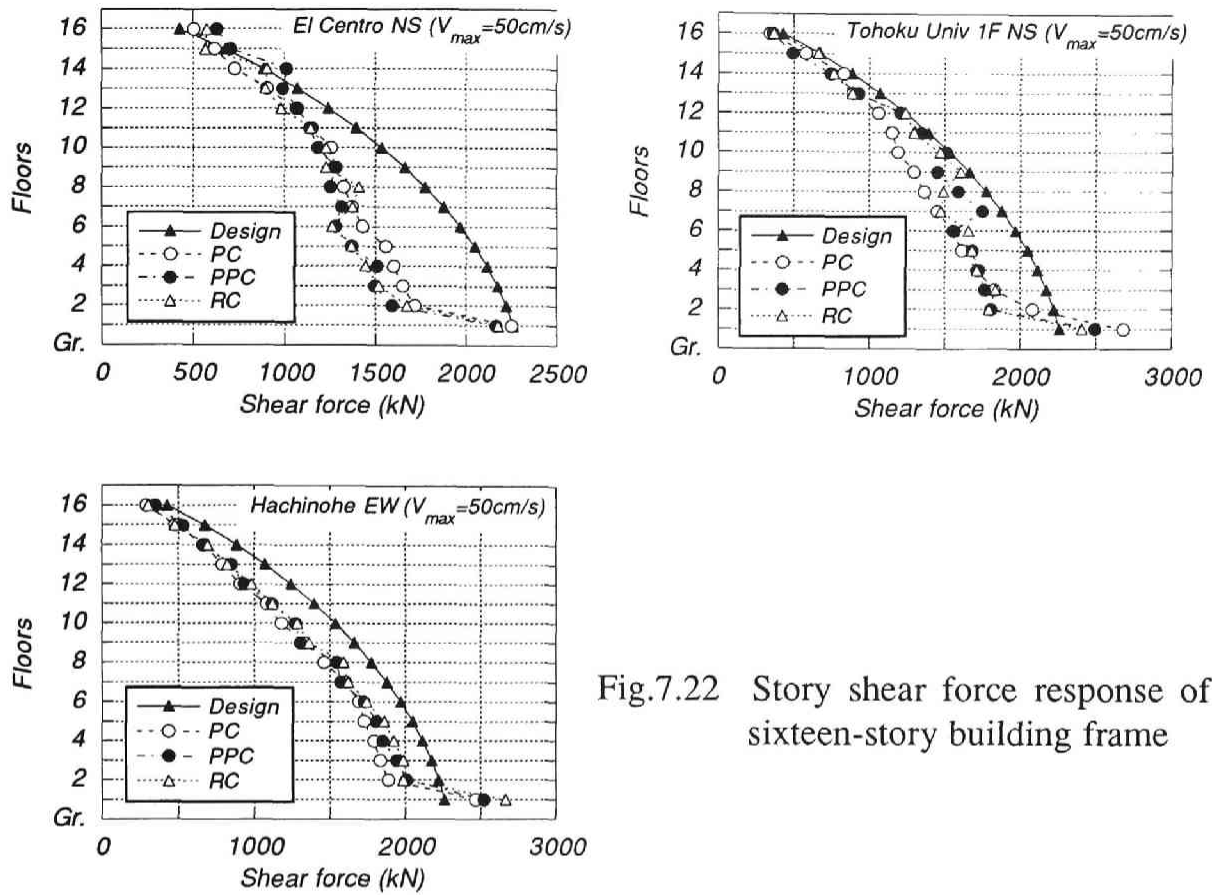


Fig.7.22 Story shear force response of sixteen-story building frame

7.14 Comparison of interstory drift responses among prestressed, partially prestressed and reinforced concrete frames

Table 7.5 summarizes the maximum interstory drift responses of the frames analyzed in this study. Note that all of them were not observed in the same level of floor. The values in the brackets () are the ratios of the maximum interstory drift responses of the prestressed and partially prestressed concrete frames to those of the reinforced concrete frames on whichever floor the responses should be observed.

Their responses are not so different compared with the analytical results obtained from the single-degree-of-freedom systems. The averages of the ratios through all the cases for the prestressed and partially prestressed concrete frames are 1.11 and 1.09, respectively. They are still rather small compared with the results of the SDOF systems. As much difference as these ratios is not of great significance : several factors which have greater influence on dynamic response results rather than hysteresis loop models assigned to the members.

As far as the interstory drift responses derived from the analyses carried out in this research were concerned, the interstory drift responses of the prestressed concrete frames were not always larger than those of the reinforced concrete frames. Besides,

Table 7.6 Maximum interstory drift responses of the frames

4-st. frame	Interstory drift responses (cm)		
	PC	PPC	RC
EI NS	3.40 [1F] (1.26)	2.97 [2F] (1.10)	2.69 [2F] (1.00)
Ha EW	3.59 [2F] (0.88)	3.56 [2F] (0.87)	4.07 [3F] (1.00)
Tu NS	6.00 [3F] (1.58)	5.30 [3F] (1.40)	3.79 [4F] (1.00)
8-st. frame	PC	PPC	RC
EI NS	2.37 [5F] (1.09)	2.00 [8F] (0.92)	2.17 [8F] (1.00)
Ha EW	1.64 [5 and 6F] (0.74)	1.89 [4 and 5F] (0.85)	2.22 [4 and 5F] (1.00)
Tu NS	3.50 [7 and 8F] (1.11)	4.00 [5, 6 and 7F] (1.27)	3.14 [4F] (1.00)
16-st. frame	PC	PPC	RC
EI NS	2.50 [16F] (1.01)	3.50 [14 and 16F] (1.41)	2.48 [16F] (1.00)
Ha EW	7.90 [5F] (1.11)	7.40 [4F] (1.04)	7.10 [4F] (1.00)
Tu NS	3.80 [5F] (1.23)	2.96 [5F] (0.95)	3.10 [8F] (1.00)

Note :

1. The brackets [] indicate the story (or stories) where the maximum interstory drift response was observed.
2. The values in the brackets () are the ratios of the interstory drift responses of PC and RC frames to those of RC frames.

it is reported by Ohta [7.7] that the effect of increasing the design horizontal load for the prestressed concrete frames was not enough to reduce their responses.

The seismic design concept which requires prestressed concrete frames to be designed against a larger seismic load than reinforced concrete frames, as specified in NZS 4203:1984, needs to be reconsidered. In addition, as shown in Chapter 4 the hysteresis loops of prestressed concrete members are not always inferior to those of reinforced concrete members. The seismic performance of prestressed concrete members is much better than that of reinforced concrete members in terms of energy dissipation for reinforced concrete frames in which the restoring force characteristics are dominated by bond deterioration between concrete and longitudinal reinforcement in the joints and the plastic hinge regions.

7.15 Comparison of dynamic responses between two-dimensional frame analyses and analyses using multi-mass shear system

Past research on the dynamic response of prestressed concrete buildings has been carried out using single- or multi-mass shear systems. The analyses described in the preceding sections of this chapter are the first two-dimensional analyses in which force - deformation relationships of the members of prestressed and partially prestressed concrete building frames are idealized on the basis of moment - curvature relationships of the members. Analyses using a multi-mass shear system are often carried out in practice to predict the responses of a frame. These analyses are useful to save time and expense. However, it is difficult to model the shear force - interstory drift relation in each layer, especially in prestressed and partially prestressed concrete building frames. In order to use analyses with a multi-mass shear system successfully, it is important to know how different the results using multi-mass shear systems are from the two-dimensional frame analysis results.

The envelope curve of shear force and interstory drift relationship of each layer was idealized from the static analyses results of the frame. The idealized envelope curve consisted of three lines characterized by the slope of the segment representing post-yield region and three points; the origin, the cracking and the yielding point. Fig.7.23 shows the calculated results of story shear force - interstory drift relationships obtained from an incremental plastic analysis and the idealized relationships.

The hysteresis loops assigned to each layer are those proposed in Chapter 5 except that the ordinates are story shear force Q_i and interstory drift x_i . It seems strange because the idealized hysteresis loops are based on moment - curvature curves measured in beam plastic hinge regions. However, depending on the ratio of prestressing steel to ordinary reinforcement and other factors a prestressed or partially prestressed concrete

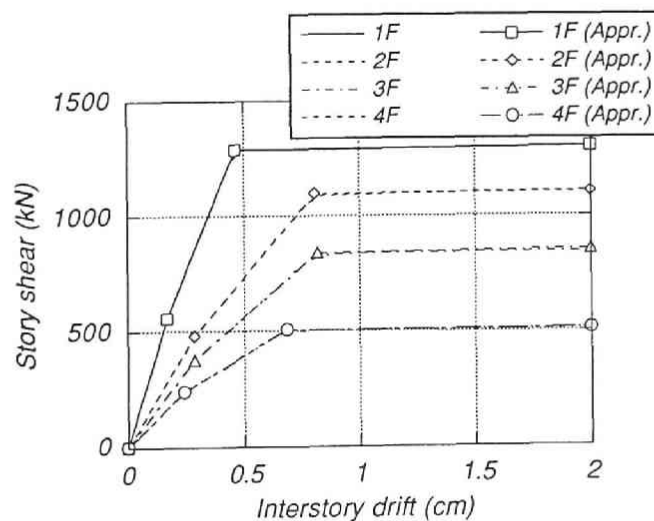


Fig.7.23(a) Story shear force - interstory drift relationships obtained from incremental plastic analysis and idealized relationships (Four-story frame).

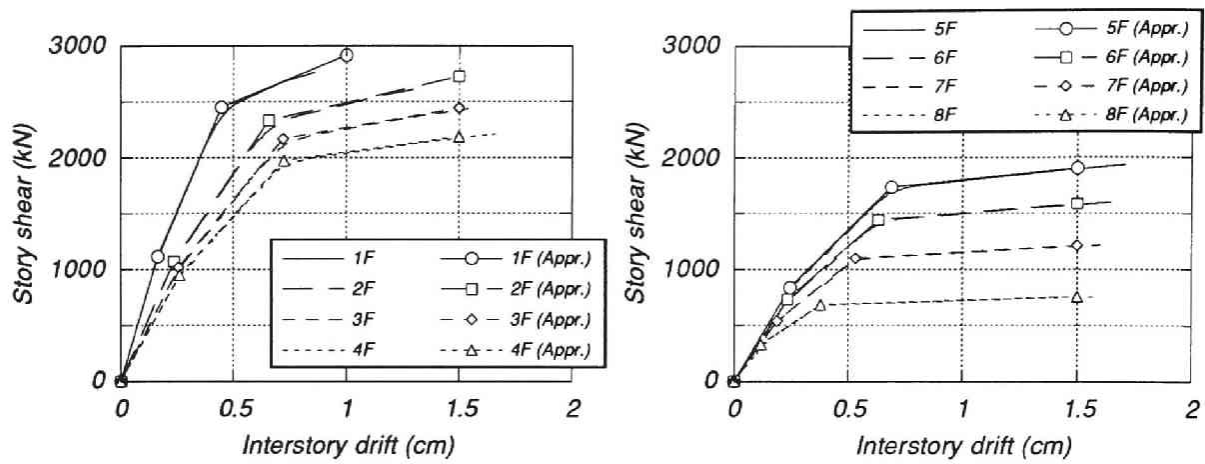


Fig.7.23(b) Story shear force - interstory drift relationships obtained from incremental plastic analysis and idealized relationships (Eight-story frame).

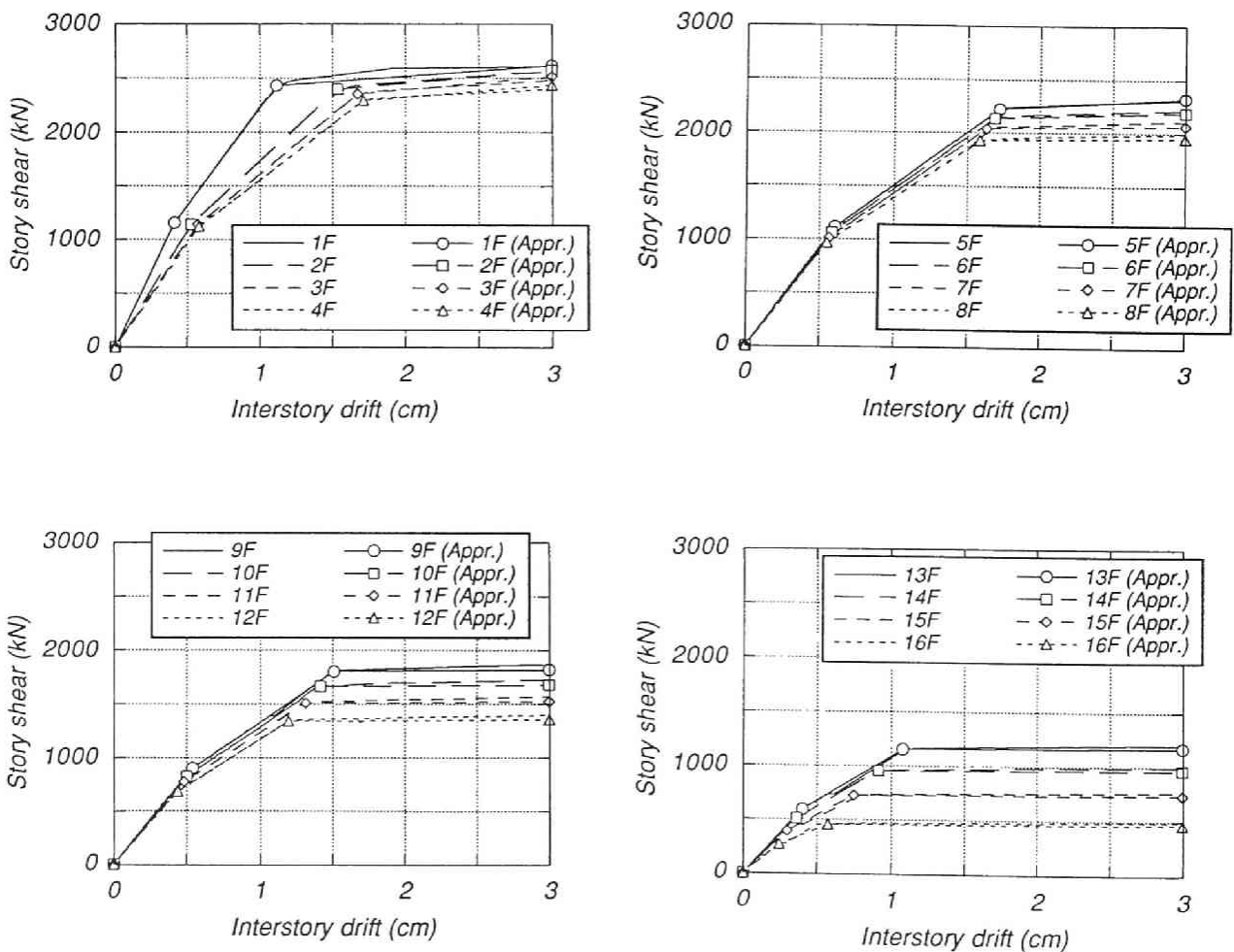


Fig.7.23(c) Story shear force - interstory drift relationships obtained from incremental plastic analysis and idealized relationships (16-story frame).

frame is considered to show the hysteretic behaviour between the two extremities of a fully prestressed and reinforced concrete idealization.

The impulse acceleration method described in Chapter 6 for single-degree-of-freedom systems was extended to apply to a multi-mass shear system and was used. Parameters needed for the analyses and models such as the formulation of damping, are the same were used in the two-dimensional frame analyses in this chapter.

Figure 7.24 compares the analytical results for each earthquake wave. The analytical results of multi-mass shear systems showed concentration of interstory drift response into one or more stories. In two-dimensional analyses a sudden change of the interstory drift responses along the height of the buildings can not be observed.

Four-story building: In the two-dimensional frame analyses, interstory drift responses in all stories were almost the same whichever earthquake wave was used. This reflects the fact that column hinging did not occur except for the bottom of the first-story columns and the top of the top story columns. However, in the multi-mass shear system, concentration of deformation into a particular story was observed. The maximum interstory drift in case of the earthquake wave Tohoku Univ NS reached $1/52$ radian in the first story while $1/284$ in the fourth story.

Eight-story building: Concentration of interstory drift is not so significant as in the four-story building. The distributions of the maximum interstory drifts of the two analytical results are quite different. In the two-dimensional analyses, almost a uniform distribution was observed. However, in the multi-mass shear system analyses the maximum interstory drifts in the mid-stories are significantly larger than in the bottom and top stories. The interstory drift responses at the top floor are the least in all the floors.

Sixteen-story building: In Hachinohe EW earthquake wave the significant concentration of interstory drift was observed in the seventh floor for all structural types considered. The distribution of the interstory drifts of the multi-mass shear systems was more similar to that of the two-dimensional analyses than in the case of the four- and eight-story frames.

Yu et al. [7.5] compared interstory drift response of a six-story reinforced concrete frame obtained from two-dimensional frame analyses and analyses in which the frame was idealized as a multi-mass shear system. They derived the same conclusion as described above; concentration of interstory drift response into a particular story was observed in multi-mass shear system. However, increment of a slope in the post-yield region resulted in more similar interstory drift response of the multi-mass shear system to that of two-dimensional frame analyses. Hysteresis loops assigned to each layer proved to have a large influence on the dynamic response and they should be determined carefully.

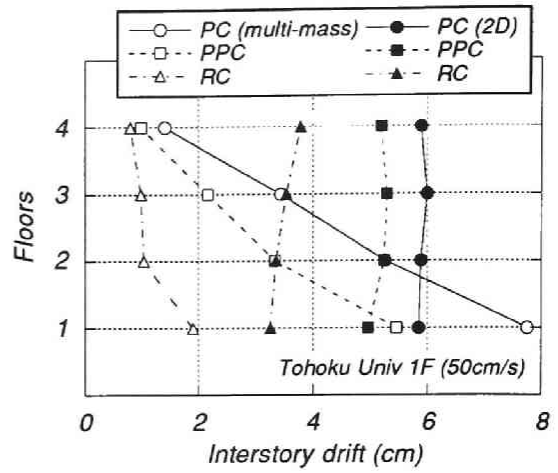
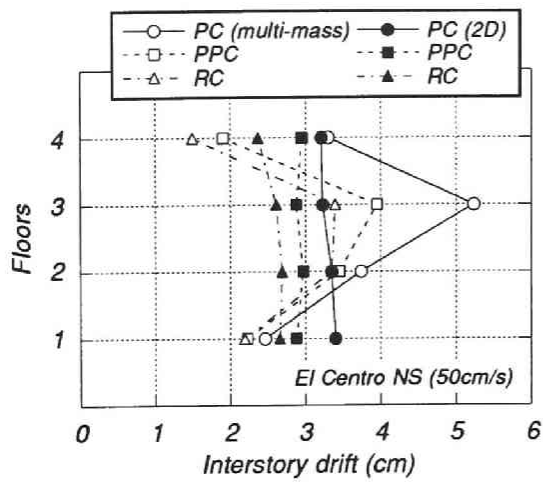


Fig.7.24(a) Comparison of maximum interstory drift between two-dimensional analysis and multi-mass shear system (Four-story frame)

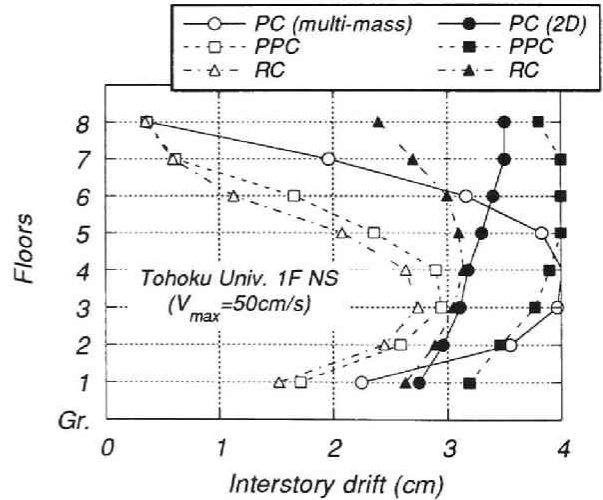
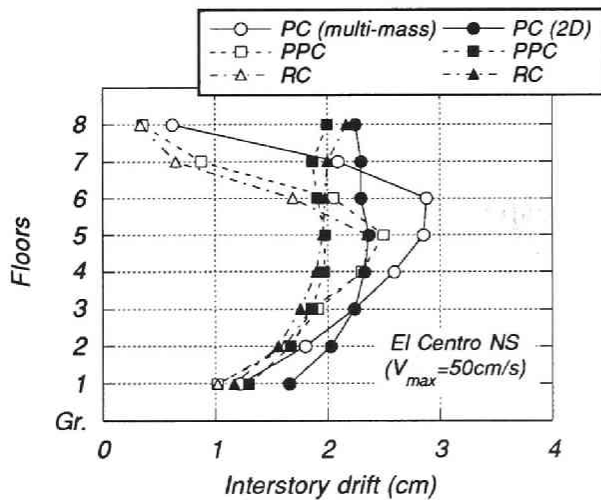
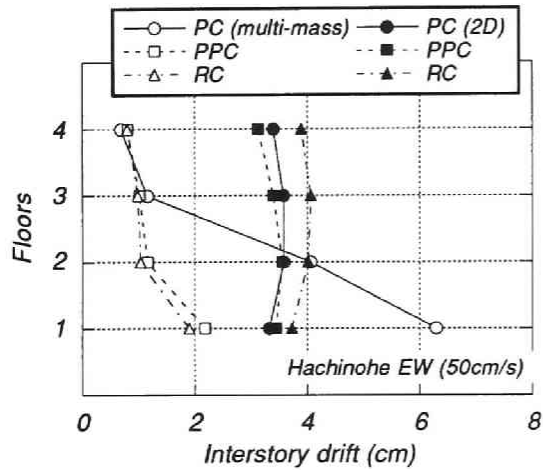
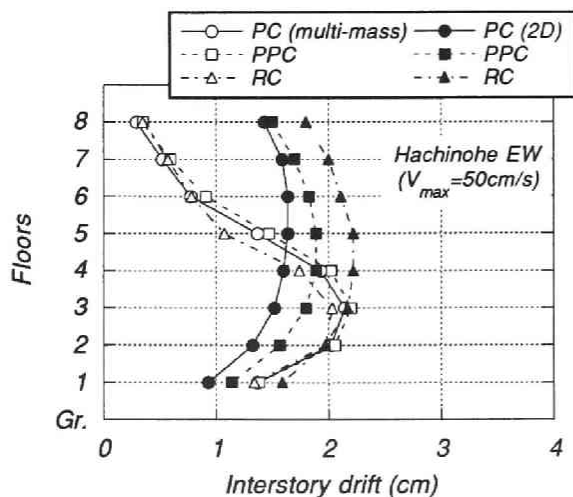


Fig.7.24(b) Comparison of maximum interstory drift between two-dimensional analysis and multi-mass shear system (Eight-story frame)



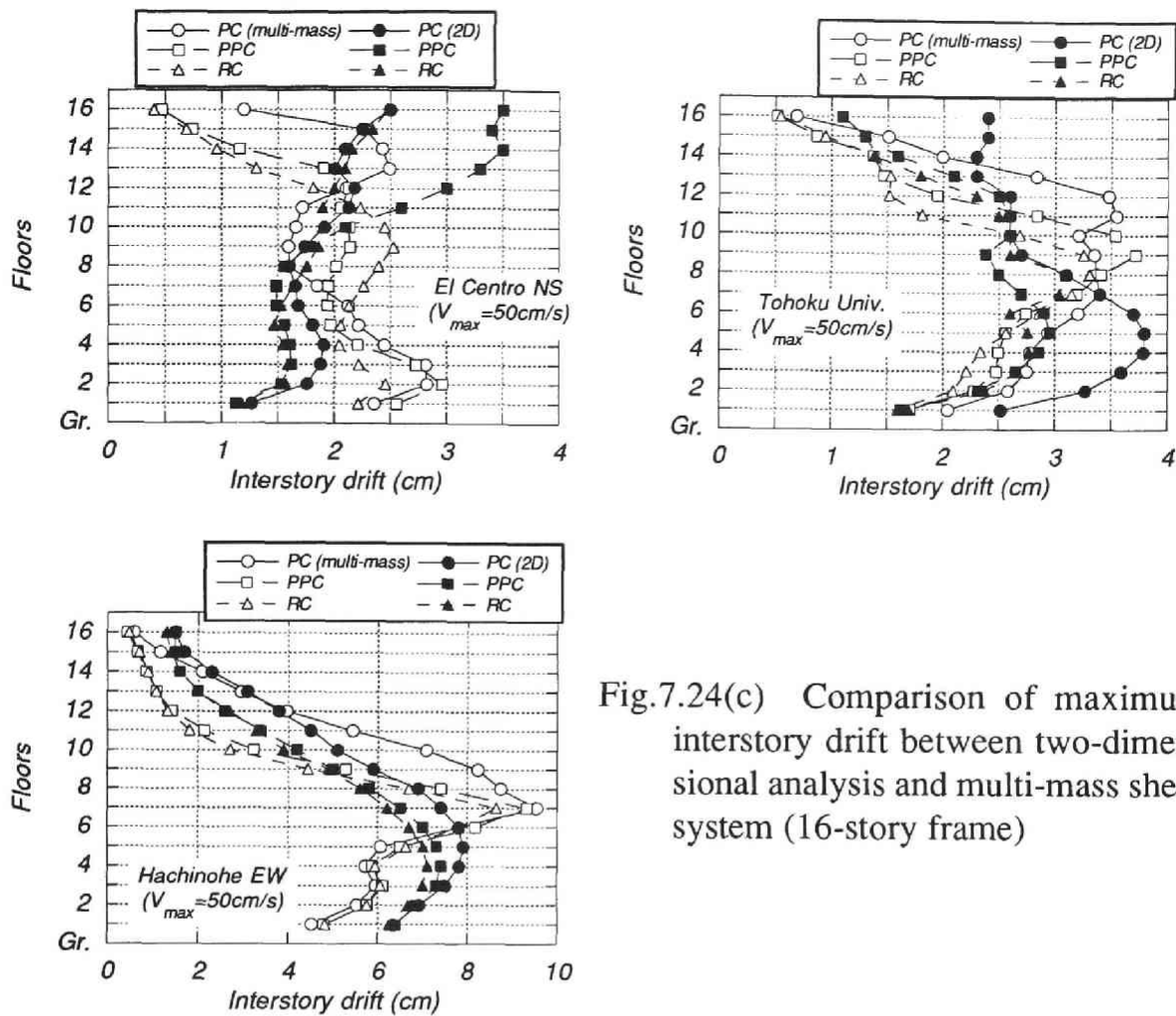


Fig.7.24(c) Comparison of maximum interstory drift between two-dimensional analysis and multi-mass shear system (16-story frame)

Fig.7.25 shows story shear force - interstory drift relation response of each layer of the eight-story model frame from the El Centro NS earthquake wave. One obtained from two-dimensional frame analysis was calculated using bending moment response of the columns. The curves are more like those of bi-linear hysteresis loops than those of prestressed concrete hysteresis loops. This result revealed that the assignment of prestressed concrete type hysteresis loops to each layer of a prestressed concrete frame which consists of prestressed concrete beams and reinforced concrete columns was not justified. Two-dimensional frame analysis should be conducted or a conversion factor between these two analyses should be introduced.

Comparison of the responses of prestressed concrete frames and reinforced concrete frames is illustrated in Fig.7.26. The ratios of the responses of the prestressed and partially prestressed concrete frames to those of the reinforced concrete frames are plotted against each earthquake wave. These figures exhibit that the analyses of multi-mass shear systems tend to overestimate the response of prestressed concrete frames compared with the two-dimensional analyses, especially in lower two building frames. For the 16-story frame the ratio of these two analytical methods are almost the same. As shown before, the distribution of interstory drifts of the two analytical methods are also similar. Therefore, dynamic response of prestressed concrete building frames is

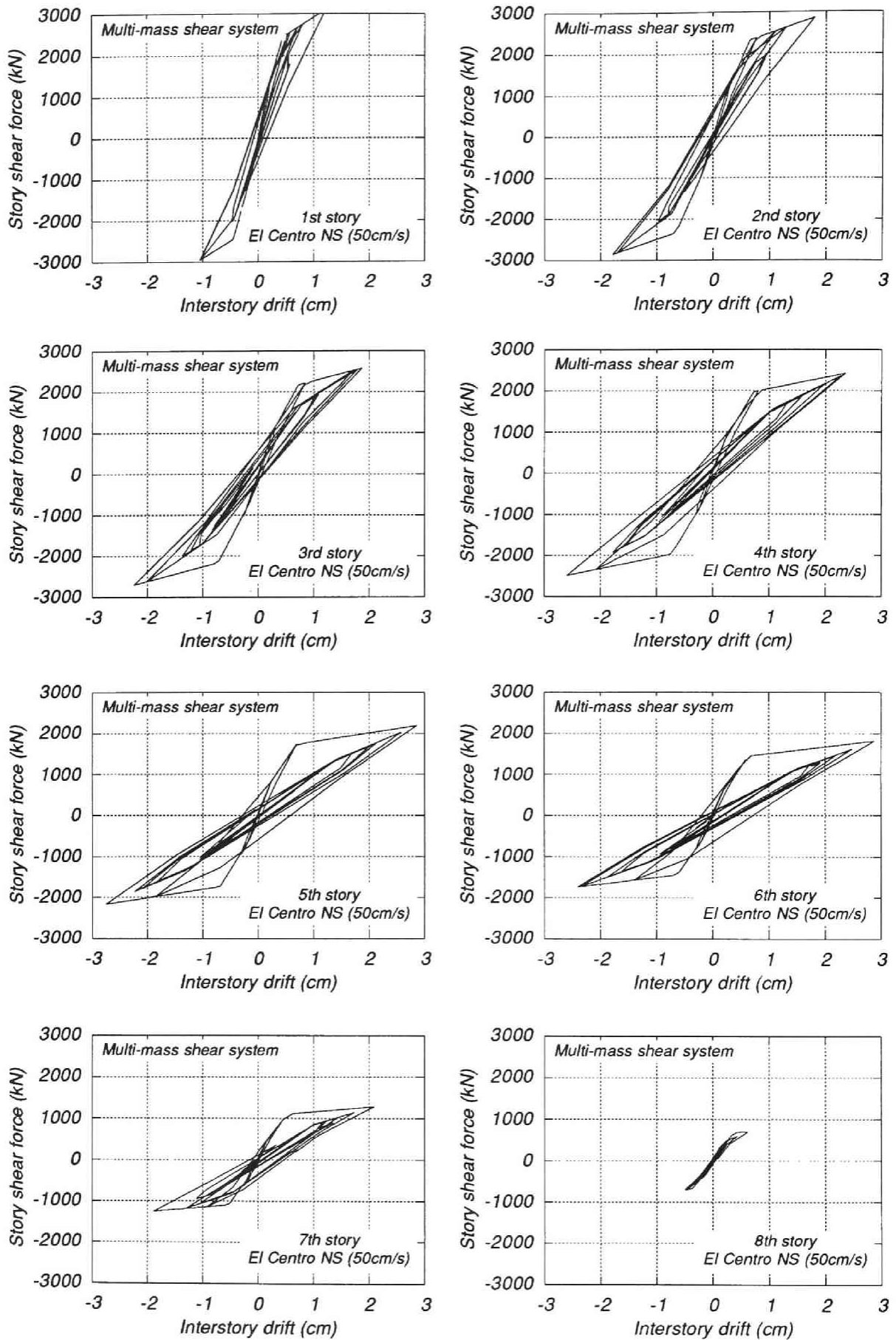


Fig.7.25(a) Story shear force - interstory drift response of multi-mass shear system

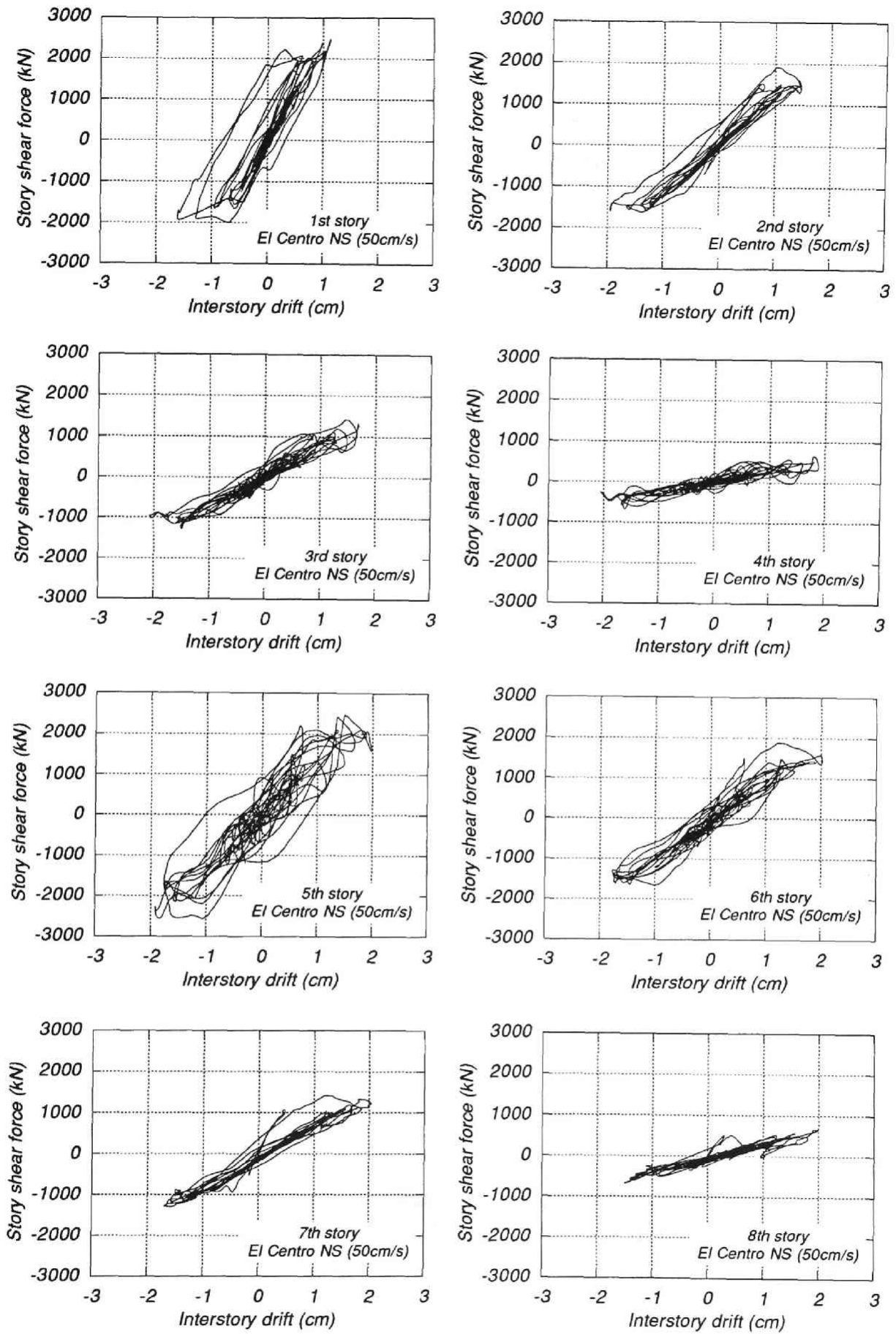


Fig.7.25(b) Story shear force - interstory drift response of two-dimensional frame analysis

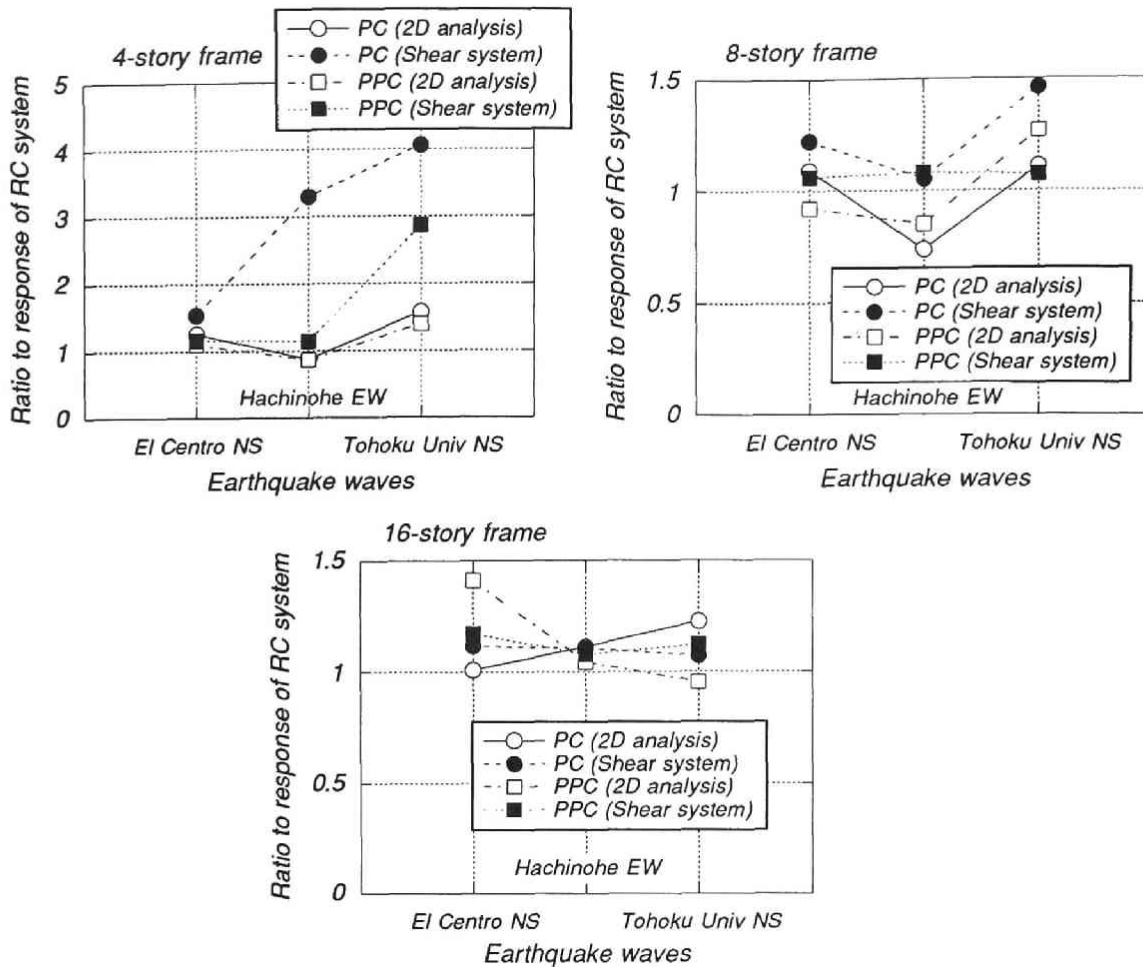


Fig.7.26 Comparison of interstory responses of prestressed, partially prestressed and reinforced concrete frames (Two-dimensional analyses and multi-mass shear system analyses)

not as large as past research has pointed out when compared with reinforced concrete frames.

7.16 Conclusions

From the above analytical study, the following conclusions have been reached with regard to dynamic response of prestressed, partially prestressed and reinforced concrete building frames:

1. Two dimensional dynamic analyses on the prestressed, partially prestressed and reinforced concrete building frames were carried out. Three typical earthquake wave records were used as their maximum velocities were amplified to 50cm/s. Four-, eight- and sixteen-story model frames were designed according to the AIJ Guidelines and the current seismic design method for prestressed concrete building structures. The frames were intended to fail with a beam-sidesway mechanism.

2. Comparison of the responses of the above model frames revealed that the responses of the prestressed concrete buildings were not always the largest. The interstory drift responses depended on the characteristics of the earthquake waves, too. Past research has pointed out larger response of prestressed concrete frames than that of reinforced concrete frames. Seismic design load for prestressed concrete frames specified in NZS 4203 : 1984 should be 25% larger than that for equivalent reinforced concrete frames. However, a difference large enough to give a motivation to assign a larger seismic design load for prestressed concrete frames was not observed. A remained reason to design a prestressed concrete building using a higher seismic design load is less ductile behaviour of prestressed concrete members than reinforced concrete members.
3. Comparison of the responses between the two-dimensional frame analyses and the analyses using a multi-mass shear system revealed that the ratio of the responses of the prestressed and partially prestressed concrete frames to those of the reinforced concrete frames were overestimated in the analyses of multi-mass shear systems compared with two-dimensional frame analyses. Story shear force - interstory drift responses using these analytical methods indicated that assignment of prestressed concrete type hysteresis loops to each layer of a prestressed concrete frame which consists of prestressed concrete beams and reinforced concrete columns is not suitable. Two-dimensional frame analysis should be conducted on prestressed concrete building frames.
4. Considering the test results on the beam-column joint assemblies described in Chapter 4, the current seismic design concept that prestressed concrete frames should be designed against larger seismic design load than reinforced concrete frames, as specified in NZS 4203:1984, needs reconsideration. An improved seismic design concept for prestressed concrete building frames will be discussed in the next chapter.

[References]

- 7.1 Sharpe, R. D. : The Seismic Response of Inelastic Structures, Ph. D Thesis, Department of Civil Engineering, University of Canterbury, New Zealand, November 1974.
- 7.2 Caughey, T. K. and M. E. J. O'Kelly : Classical Normal Modes in Damped Linear Dynamic Systems, Journal of Applied Mechanics, ASME, Vol.32, No.3, Sept. 1958, pp.361-364.
- 7.3 Giberson, M. F. : Two Nonlinear Beams with Definition of Ductility, Proceedings of ASCE, Vol.95, No.ST2, 1969.
- 7.4 Ohta, Y. : Seismic Response and Seismic Design of Prestressed Concrete Building Frame, Master Thesis, Department of Architectural Engineering, Kyoto University, Japan, March 1992.
- 7.5 Yu Xin et al. : Comparison of Response Analysis of R.C. Frame Represented by

Shear Model and Frame Model, Summaries of Technical Papers of Annual Meeting of AIJ, 1992, pp.403-404.

SEISMIC DESIGN OF PRESTRESSED CONCRETE BUILDING FRAMES

8.1 Introduction

The ductility-based structural design method (capacity design of ductile structures) was developed for reinforced concrete structures by Park and Paulay [8.1] and it has been adopted in New Zealand Design Codes [8.2, 8.3]. In Japan, the Design Guidelines [8.4] based on the similar philosophy were proposed by AIJ (Architectural Institute of Japan) Sub-committee for Seismic Design of Reinforced Concrete.

The seismic design methods in these codes and guidelines aim at a building surviving against a severe earthquake by energy absorption of plastic deformation at intended hinge regions. Beam yielding sidesway mechanism has been usually recommended as the most favorable collapse mechanism. The columns of a building are so designed as to have enough strength to assure the beam hinging mechanism and to generally remain in the elastic range during a strong earthquake motion. Plastic hinges are expected to form at the base of the first layer columns and the upper critical part of the top layer columns as well as in the exterior columns subjected to high tensile forces due to overturning moment. Flexural overstrength at beam plastic hinges, two-way frame actions and dynamic effects on column moments or forces are taken into account to estimate the probable maximum column moments or forces to be induced during an earthquake.

The design method which aims at the beam sidesway mechanism would be applicable even to prestressed concrete buildings. However, the direct application of the beam sidesway mechanism to the design of relatively low rise prestressed concrete buildings with fully prestressed concrete long-span beams would be impractical and uneconomical. Prestressing tendons are usually provided to cancel or reduce flexural moments due to dead and live loads. That results in much more strength of the beams than required for the actions due to design seismic loads.

On the basis of the trials of seismic design for prestressed concrete buildings the AIJ Task-committee on seismic design of prestressed concrete has reached the conclusion that a design procedure to assure a beam hinging mechanism is not always reasonable. The committee has proposed a seismic design method for prestressed concrete building structures, in which a column sidesway system is allowed. For a building which is predicted to collapse in a column sidesway mechanism, the structural safety under seismic load is assured by increasing the lateral seismic design force and by giving the smooth distribution of story shear strength and rigidity over the building height [8.5].

The seismic design procedure is distinguished by the fact that it accommodates not only prestressed concrete buildings but also reinforced concrete buildings. Uniform design code provisions have been recently proposed [8.1, 8.2]. However, they are intended to deal with structural members rather than the structure itself.

In this chapter, the seismic design method for prestressed concrete buildings which has been proposed by the AIJ Sub-committee for Seismic Design of Prestressed Concrete is introduced. As described above, column hinging mechanism is incorporated as a design category. Then, some calculation results show how difficult it is to design a prestressed concrete building in which beam sidesway mechanism is expected to develop. Since it is difficult to ensure ductile behavior in the plastic hinge regions of the columns under high axial load, especially for high strength reinforced concrete columns, so test results on high strength reinforced concrete columns confined by high strength transverse reinforcement will be reported. The test results are also used to improve a stress-strain idealization for high strength concrete proposed in past research.

8.2 Seismic design method proposed by the AIJ task-committee on seismic design of prestressed concrete

8.2.1 Design category

Figure 8.1 illustrates the design flow of seismic design procedure of prestressed concrete buildings proposed by the AIJ task-committee. Four design categories are considered. Each category is based on the intended structural system of a building to be designed.

- a) *BDF* System (Beam-sidesway Ductile Frame Structures) : beam hinging sidesway mechanism is intended and should be assured.
- b) *GDF* System (General Ductile Frame Structures): beam hinging sidesway mechanism is not necessarily assured. The column sidesway mechanism is assumed as a probable collapse mechanism. Any kind of collapse mechanism is possible unless it is brittle. Column critical sections should be designed as potential plastic hinge regions.
- c) *DWF* System (Ductile Wall Frame Structures): collapse mechanism should be initiated by either the flexural yielding at the bottom of walls or the rotational yielding at wall foundations.
- d) *SRS* System (Strength Resisting Structures): elastic response is expected even during a severe earthquake. Plastic deformation is not relied on.

It is assumed that the allowable maximum interstory drift during a strong motion earthquake for *BDF*, *GDF* and *DWF* systems is approximately 0.01 rad. The corresponding member rotation angle of beams and columns is assumed to be 0.02 rad. Thus, plastic hinge regions are required to achieve the rotation of 0.02 rad. without

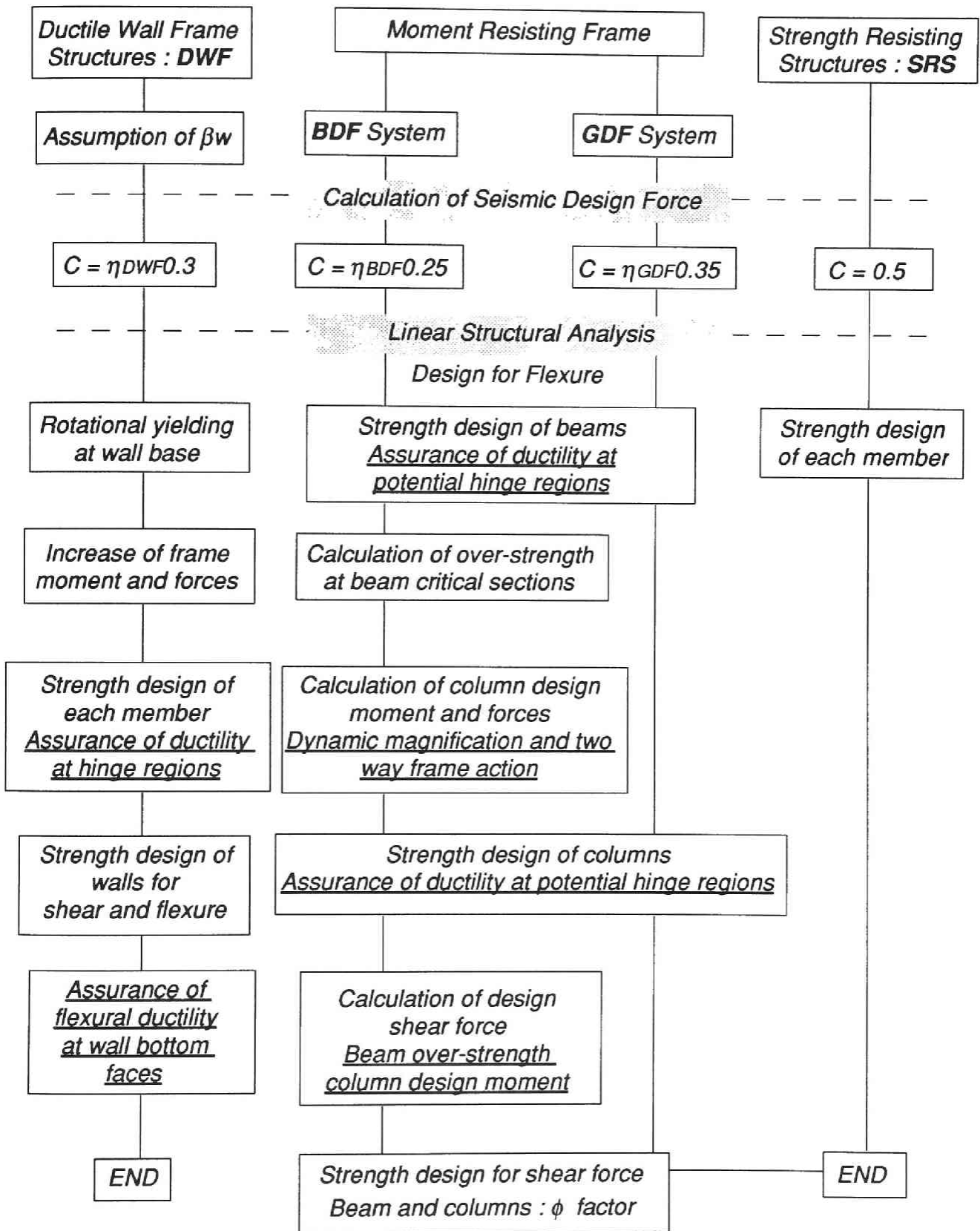


Fig.8.1 Design flow

Table 8.1 Material strength for reinforcing steel

Classification of Strength	Grade 30 Steel Grade 35 Steel	Grade 40 Steel	Prestressing Steel
Reliable Strength	σ_y	σ_y	σ_{py}
Average Strength	$1.10\sigma_y$	$1.10\sigma_y$	$1.15\sigma_{py}$
Over-strength	$1.30\sigma_y$	$1.25\sigma_y$	$1.18\sigma_{py}$

Numerical numbers of the steel grade indicates the specified yield strength in kgf/mm^2

σ_y : Specified yield strength of ordinary reinforcing steel

σ_{py} : Specified yield strength (0.2% off-set) of prestressing steel

significant reduction of load carrying capacity: the elastic deformation of the non-hinge region may be ignored. The hinge length is assumed to be 1.5 times the total depth of a beam or column section. The hinge length is defined for determining the length to be confined by transverse reinforcement. Besides that, it may be needed when a non-linear inelastic analysis is carried out.

8.2.2 Material strength used in structural design

Reliable strength, average strength and over-strength of sections or members are used in the design procedure. The contribution of slab reinforcements to negative moment resistance is taken into account in the calculation of beam flexural over-strengths at the plastic hinges. The material strengths for reinforcement specified in Table 8.1 are used in the calculation of reliable, average and over-strength of sections or members. For concrete, a specified design strength, which inherently incorporates an adequate margin, is used in strength calculation.

Table 8.2 Base shear coefficient for prestressed concrete structures

Structural System	BDF	GDF	DWF	SRS
C	$0.25\eta_{BDF}$	$0.35\eta_{GDF}$	$0.30\eta_{DWF}$	0.50

Table 8.3 Magnification factors

Constituent beams	BDF system η_{BDF}	GDF system η_{GDF}	DWF system η_{DWF}
Reinforced concrete	1.0	1.0	1.0
Prestressed concrete	1.2	1.1	1.05
Partially prestressed concrete	1.1	1.05	1.02

8.2.3 Seismic design load

The standard base shear coefficients for ordinary reinforced concrete buildings are assumed as below. In *GDF* system, the larger base shear coefficient than that for other ductile systems is specified to avoid an interstory drift angle greater than 0.01 radian at the critical story where a column sidesway mechanism might develop. These values are tentatively proposed with consideration of continuance from the current seismic design provisions.

- a) 0.25 : Beam-sidesway Ductile Frame Structures (BDF System)
- b) 0.35 : General Ductile Frame Structures (GDF System)
- c) 0.30 : Ductile Wall Frame Structures (DWF System)
- d) 0.50 : Strength Resisting Structures (SRS System)

On the basis of the dynamic response analyses [8.6, 8.7] and engineering judgements, the standard base shear coefficients for prestressed concrete building structures are given in Table 8.2 and 8.3. For example, the base shear coefficient for the *GDF* system with fully prestressed concrete beams is 20 % higher than that for an ordinary reinforced concrete *GDF* system.

In the current New Zealand design code [8.3], structural material factor M for ductile prestressed concrete moment resisting frame is 25 % higher than that for a ductile reinforced concrete moment resisting frame to allow for larger responses of prestressed concrete structures than reinforced concrete. This results in a 25 % higher total horizontal seismic design force.

For strength resisting concrete structures (*SRS* System), the base shear coefficient of 0.50 is given regardless of a type of the beams, because the primary concern is the strength and no ductile behavior is expected.

Design seismic story shear force at k -th story, Q_k , is given by Eq.1. This is the same as the current code provisions.

$$Q_k = C_k \cdot W_k \quad (8.1)$$

$$C_k = Z \cdot R_t \cdot A_k \cdot F_e \cdot F_s \cdot C \quad (8.2)$$

$$A_k = 1 + 2T \left(\frac{1}{\sqrt{\alpha_k}} - \alpha_k \right) / (1 + 3T) \quad (8.3)$$

$$\alpha_k = W_k / W \quad (8.4)$$

where Q_k : design seismic story shear force at k -th story
 W : total weight of the building
 W_k : weight of the building above k -th story

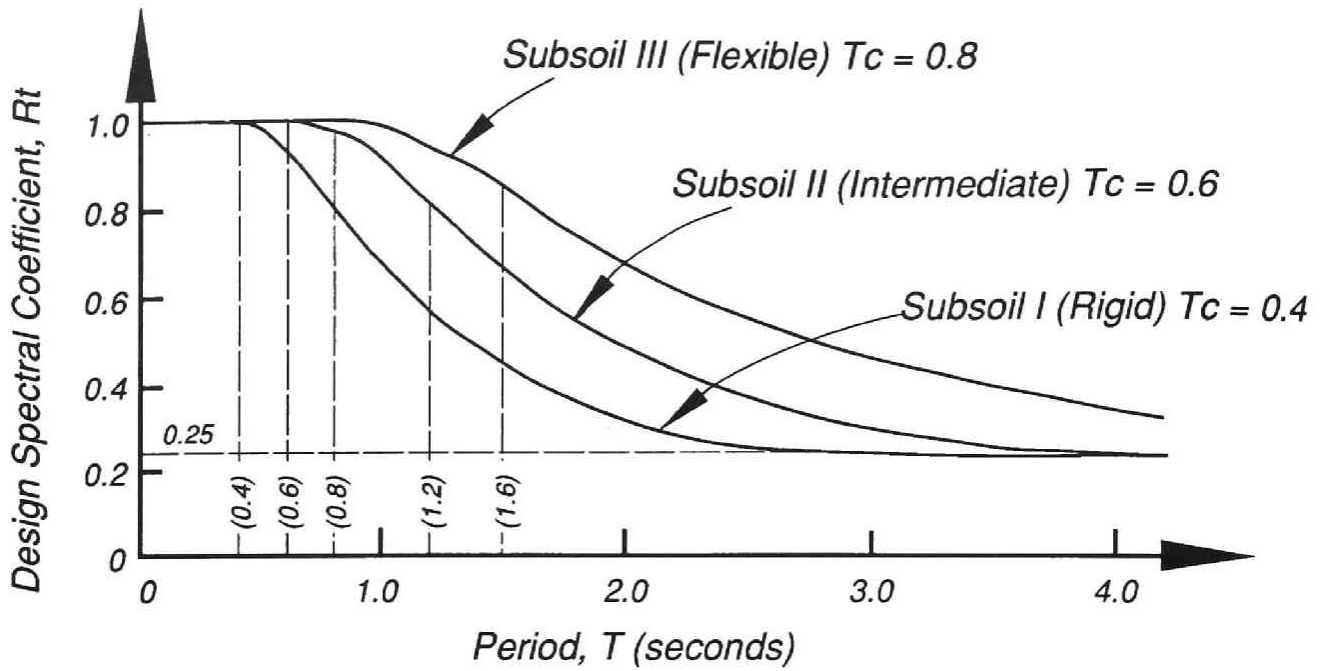
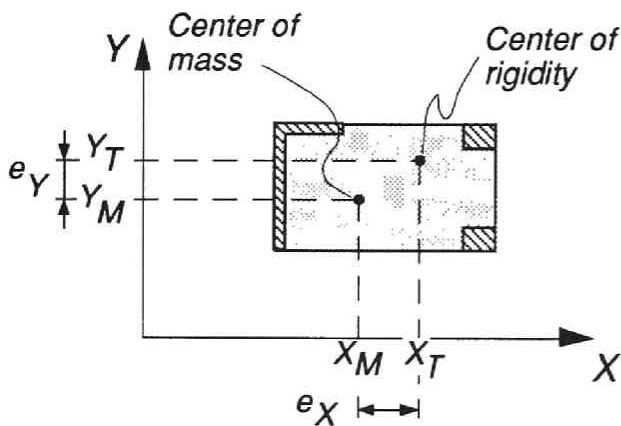


Fig.8.2 Design spectral coefficient, R_t



$$e_x = [X_M - X_T] \quad e_y = [Y_M - Y_T]$$

$$R_{ex} = \frac{e_x}{\sqrt{K_T / K_{hx}}} \quad R_{ey} = \frac{e_y}{\sqrt{K_T / K_{hy}}}$$

$$K_{hx} = \sum_i J_{xi} \quad K_{hy} = \sum_i J_{yi}$$

$$K_t = \sum_i J_{xi} \cdot y_i^2 + \sum_i J_{yi} \cdot x_i^2$$

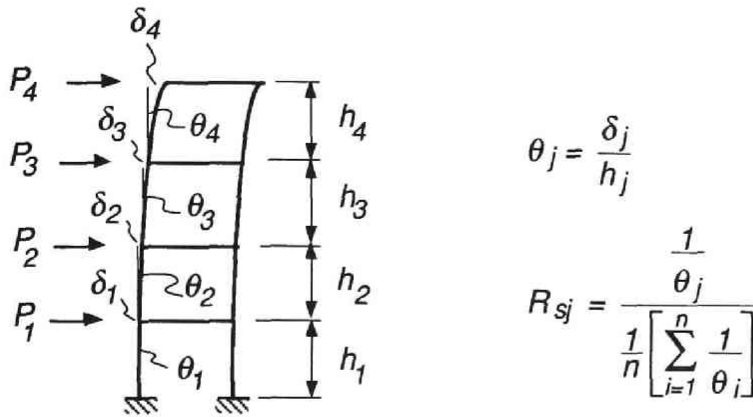
Note:

J_{xi}, J_{yi} : Lateral stiffnesses of vertical structural element i in X and Y directions, respectively.

X_i, Y_i : Coordinates of i -th element measured from the center of torsion.

R_{ex}, R_{ey} : Eccentricity ratios in X and Y directions, respectively.

Fig.8.3 Eccentricity ratio, R_e



Note:

θ_j : Interstory drift of j-th story under seismic design load of the first phase design load.

δ_j : Interstory displacement. h_j : story height.

R_{sj} : stiffness ratio. n : Number of stories.

Fig.8.4 Stiffness ratio, R_s

Table 8.4 Coefficient F_e and F_s with regard to the eccentricity ratio R_e and stiffness ratio R_s

R_e	F_e	R_s	F_s
≤ 0.15	1.0	≥ 0.60	1.0
0.15~0.30	Linear interpolation	0.30~0.60	Linear interpolation
≥ 0.30	1.5	≤ 0.30	1.5

- Z : seismic hazard zoning coefficient, $0.7 \leq Z \leq 1.0$
 T : fundamental period of vibration of the building in second
 R_t : design spectral coefficient which depends on the subsoil profile and the period of vibration of the building, and $R_t \geq 0.25$ (see Fig.8.2)
 A_k : lateral shear distribution factor at k-th story
 F_e : coefficient of structural eccentricity at k-th story, $1.0 \leq F_e \leq 1.5$ (see Fig.8.3 and Table 8.4)
 F_s : lateral stiffness coefficient at k-th story, $1.0 \leq F_s \leq 1.5$ (see Fig.8.4 and Table 8.5)
 C : base shear coefficient given by Table 8.2

8.2.4 Structural analysis

Linear elastic analysis for the specified static seismic design story shear force given by Eq.1 can be applied to evaluate the maximum effects. In the frame analysis, an adequate relative stiffness for each member shall be assumed. If necessary the effect of flexural cracking is considered. Moment re-distribution can be considered. However, the amount should be limited to slightly smaller than that for ordinary reinforced concrete structures, because rotational capacity of prestressed concrete beams is considered to be smaller than that for ordinary reinforced concrete.

Ultimate strength design method is useful because no iteration is needed for providing reinforcement with the members of a building.

8.2.5 Design of members

In seismic design, the most unfavorable load combinations should be considered. The loads to be considered have secondary stresses due to prestressing force (U), dead load (D), live load (L) and specified seismic design load (E) given by Eq.1.

a) Beams

Design for flexure

Reliable flexural strength of a beam section shall be equal to or greater than the design moment as given by Eq.6 for all structural systems.

The potential beam hinge regions shall behave in ductile manner without significant reduction of strength up to the required rotation angle of 0.02 rad. Therefore, an adequate amount of transverse reinforcement should be provided in potential plastic hinge regions to avoid the buckling of compression reinforcement and the premature crushing of concrete under reversed cyclic earthquake loading.

$${}_B M_R \geq {}_B U_M + {}_B D_M + {}_B L_M + {}_B E_M \quad (8.5)$$

where ${}_B M_R$: Reliable flexural strength of beam section
 ${}_B U_M$: Related beam moment due to prestressing
 ${}_B D_M$: Related beam moment due to dead load
 ${}_B L_M$: Related beam moment due to live load
 ${}_B E_M$: Related beam moment due to specified earthquake load

Design for shear

In the shear design of beams, following equations shall be satisfied.

Beams without hinges:

$${}_B Q_R \geq {}_B U_Q + {}_B D_Q + {}_B L_Q + {}_B E_Q \quad (8.6)$$

Beams with hinges:

For hinge region

$$\phi_B \cdot {}_B Q_R \geq ({}_B M_O + {}_B M'_O) / L_B + {}_B U_Q + {}_B D_Q + {}_B L_Q \quad (8.7)$$

For non-hinge region

$${}_B Q_R \geq ({}_B M_O + {}_B M'_O) / L_B + {}_B U_Q + {}_B D_Q + {}_B L_Q \quad (8.8)$$

where ${}_B Q_R$: Reliable shear strength of beams
 ${}_B U_Q$: Related beam shear due to prestressing
 ${}_B D_Q$: Related beam shear due to dead load
 ${}_B L_Q$: Related beam shear due to live load
 ${}_B E_Q$: Related beam shear due to specified earthquake load
 ϕ_B : Shear strength reduction factor for hinge regions of beams to assure the required hinge rotation indirectly : tentatively $\phi_B = 0.9$
 ${}_B M_O, {}_B M'_O$: Flexural overstrengths of plastic hinges at either of beam ends
 L_B : Clear span length of beams

b) Columns

Design for flexure

In a building to be designed as *BDF* system, reliable flexural strength of column section shall be equal to or greater than the design moment as given by Eqs.10 and 11.

The potential hinge regions in columns shall behave in a ductile manner without significant reduction in load carrying capacity up to the required rotation angle of 0.02 rad. Thus, an adequate amount of confining reinforcement should be provided in potential plastic hinge regions to avoid the buckling of compression reinforcement and the premature crushing of concrete under reversed cyclic earthquake loading.

For hinge region:

$${}_cM_R \geq {}_cU_M + {}_cD_M + {}_cL_M + {}_cE_M \quad (8.9)$$

For non-hinge region:

$${}_cM_R \geq \beta \cdot \lambda \cdot {}_cM_O \quad (8.10)$$

Dynamic response analyses on multi-mass shear systems were conducted to observe how large deformation was concentrated to weakest stories when a column sidesway mechanism formed. The systems were consist of eight masses. Each mass weighed 120 tons. Based on the weight of the masses design shear force imposed on each layer was calculated. The elastic stiffness of the systems were calculated so that the interstory drift angle of each layer in linear elastic range attained 1/300 radian when subjected to the design shear force based on the base shear coefficient of $C_0 = 0.25$. The yield capacities of the systems were calculated based on the different base shear coefficient but the elastic stiffness of the layer is the same. A_i distribution was used as a shear force distribution over the height of the systems.

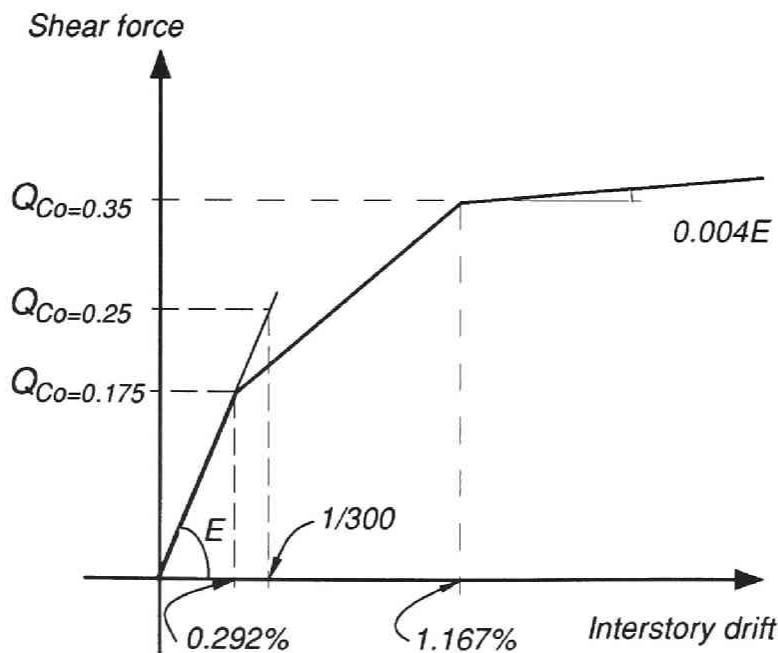


Fig.8.5 Shear force - interstory drift envelope model

The envelop curve model for shear force - interstory drift of each layer in the case of the base shear coefficient of $C_0 = 0.35$ is shown in Fig.8.5 as an example. As shown in this figure the elastic portion was a segment which connected the origin and the coordinate $(1/300, Q_{C_0=0.25})$.

El Centro NS 1940 earthquake wave record was used. To investigate behaviors of the frames during a severe earthquake the digitalized earthquake record was amplified so that the maximum velocity of the earthquake record was 50cm/s.

Fig.8.6 shows the maximum interstory drifts of the systems analyzed. The results include the responses of:

- (1) the linear elastic system,
- (2) the systems which were designed using base shear coefficients of 0.25, 0.35 and 0.45.
- (3) the systems designed basically using base shear coefficients of 0.45 and 0.35, but the story shear capacity of the second (Case 1), the fourth (Case 2) or the sixth (Case 3) layer was provided from the base shear coefficient of 0.25. Therefore, an interstory drift displacement was expected to concentrate into the weakest layer. If the shear capacity based on $C_0 = 0.25$ is assumed to be required, the layers other than the weakest layer had reserved strength. The ratios of the provided strength to the required strength were 1.8 ($=0.45/0.25$) and 1.4 ($=0.35/0.25$), respectively.

As expected, the interstory drift concentrated into the weakest story. Table 8.5 summarizes the analytical results of the maximum interstory drift angles in 10^{-2} radian. The column of the weakest story of each system was surrounded by double lines and included the corresponding ductility ratio.

The maximum interstory drift of the systems decreases as the design base shear coefficient increases even though some stories yielded. From the analytical results it can be concluded that larger base shear coefficient can lead to a smaller interstory drift angle even though interstory drifts of some stories should exceed the yield displacement.

However, in the system of $C_0 = 0.25$ the maximum response was 1.53% in the top story, while in the system of $C_0 = 0.45$ it was 1.12%, which was 27% smaller than the former system. The shear capacity of the latter system was 80% larger than the former. Therefore, to increase shear capacities of the layers are not so effective for reducing the maximum response.

The ratios of the maximum response of the C25-C45 systems (designed based on $C_0 = 0.45$, but there is a weakest story whose shear strength from $C_0 = 0.25$) to that

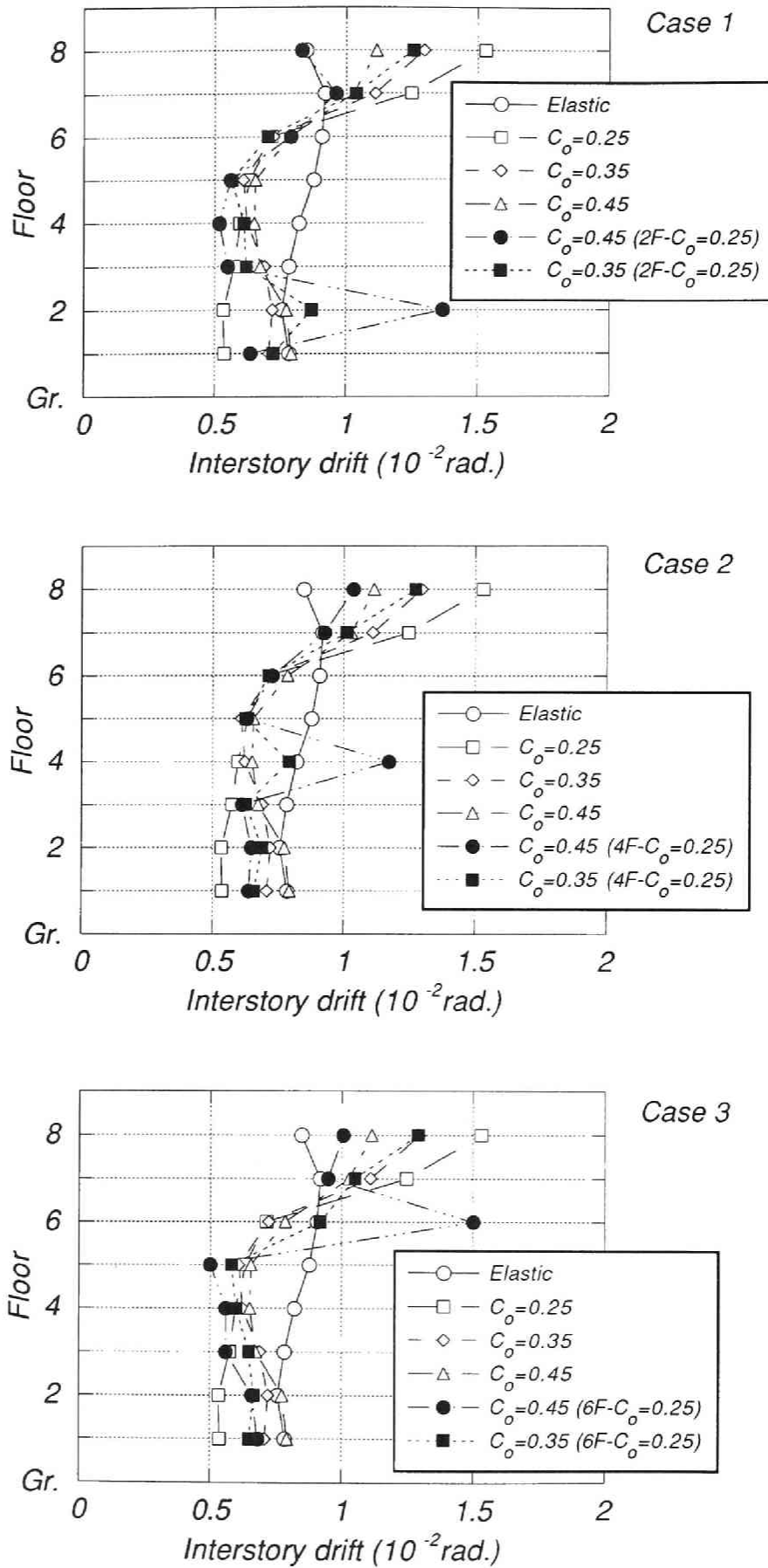


Fig.8.6 Analytical results of maximum interstory drift angle

Table 8.5 Maximum interstory drift angle

(10⁻² radian)

Floor	Elastic Response	Co=0.25	Co=0.35	Co=0.45	Co=0.45 (2F-C25)	Co=0.35 (2F-C25)	Co=0.45 (4F-C25)	Co=0.35 (4F-C25)	Co=0.45 (6F-C25)	Co=0.35 (6F-C25)
8	0.849	1.532	1.298	1.116	0.832	1.256	1.037	1.274	1.007	1.292
7	0.920	1.248	1.112	1.030	0.963	1.038	0.928	1.013	0.950	1.052
6	0.909	0.716	0.724	0.787	0.791	0.703	0.729	0.716	1.502 (1.81)	0.920 (1.109)
5	0.879	0.636	0.611	0.657	0.561	0.567	0.632	0.626	0.501	0.583
4	0.822	0.598	0.625	0.653	0.519	0.612	1.175 (1.41)	0.794 (0.956)	0.561	0.600
3	0.784	0.576	0.692	0.675	0.551	0.622	0.615	0.628	0.561	0.650
2	0.758	0.535	0.722	0.775	1.370 (1.65)	0.872 (1.05)	0.649	0.691	0.661	0.667
1	0.786	0.538	0.709	0.794	0.638	0.725	0.639	0.660	0.683	0.650

of C25-C35 (designed based on $C_0 = 0.35$, but there is a weakest story whose shear strength from $C_0 = 0.25$) systems ranged from 1.48 and 1.63. In the former systems the weakest stories yielded and the ductility ratios were 1.65, 1.41 and 1.81. In the latter systems the ductility ratios were 1.05, 0.96 and 1.11. These results indicate that both upper and lower limits of story shear strength should be required to control the interstory drift if a column sidesway mechanism should form.

In a building to be designed as a *GDF* system, Eq.8.11 shall be satisfied. Eq.8.11 gives not only the minimum required flexural strength of column sections but also the maximum allowable flexural strength of column sections. Eq.8.11 is intended to give the building the smooth distribution of lateral story shear strength along the building height. In *GDF* system, a column sidesway mechanism might be formed. This can result in the damage concentrating into the weakest story. To avoid such an unfavorable response, both upper and lower limits of story shear strength need to be introduced as shown in the above analyses. The maximum allowable value of γ is tentatively 0.30 on the basis of the dynamic response analyses on several types of buildings in which column sidesway mechanism was predicted [8.5].

$${}_cU_M + {}_cD_M + {}_cL_M + (1 + \gamma) {}_cE_M \geq {}_cM_R \geq {}_cU_M + {}_cD_M + {}_cL_M + {}_cE_M \quad (8.11)$$

where ${}_cM_R$: Reliable flexural strength of column section
 ${}_cU_M$: Related column moment due to prestressing
 ${}_cD_M$: Related column moment due to dead load
 ${}_cL_M$: Related column moment due to live load
 ${}_cE_M$: Related column moment due to earthquake load
 ${}_cM_O$: Column moment induced by the beams framing into the beam-column joint. The beam bending moments are assumed to reach the flexural over-strength and the moments induced by the beams are transferred into the columns following the distribution ratio of the results of the elastic linear frame analysis.

- β : Coefficient for two way frame action [8.4]
- λ : Dynamic magnification factor [8.4]
- γ : Coefficient to limit the distribution of story shear strength along building height (a tentative value is 0.3)

To assure the required ductility of columns (0.02 rad. in a member rotation angle) an adequate volume and arrangement of transverse reinforcement should be provided in the potential plastic hinge regions considering the design axial load.

Design for shear

In shear design of columns in a building to be designed as BDF system, the following equations shall be satisfied.

Columns without hinges:

$${}_cQ_R \geq \beta \cdot \lambda \cdot {}_cQ_U \quad (8.12)$$

Columns with hinges:

For hinge regions

$$\phi_c \cdot {}_cQ_R \geq ({}_cM_O + {}_cM'_O) / L_C \quad (8.13)$$

For non-hinge regions

$${}_cQ_R \geq ({}_cM_O + {}_cM'_O) / L_C \quad (8.14)$$

In shear design of columns in a building to be designed as GDF systems, the following equations shall be satisfied.

For hinge regions

$$\phi_c \cdot {}_cQ_R \geq ({}_cM_O + {}_cM'_O) / L_C \quad (8.15)$$

For non-hinge regions

$${}_cQ_R \geq ({}_cM_O + {}_cM'_O) / L_C \quad (8.16)$$

For the SRS system, the following equation shall be satisfied.

$$Q_R \geq {}_cU_Q + {}_cD_Q + {}_cL_Q + {}_cE_Q \quad (8.17)$$

where ${}_c Q_R$: Reliable shear strength of columns
 ${}_c Q_U$: Shear forces induced in columns by adjacent beam end moments through beam-to-column joints, where moments of resistance at beam ends should be assumed to reach flexural over-strengths
 ${}_c U_Q$: Related shear force due to prestressing
 ${}_c D_Q$: Related shear force due to dead load
 ${}_c L_Q$: Related shear force due to live load
 ${}_c E_Q$: Related shear force due to earthquake load
 ${}_c M_O, {}_c M'_O$: Flexural over strengths of plastic hinges at column top and bottom sections
 ϕ_c : Shear strength reduction factor for hinge regions of columns which assures the required hinge rotation indirectly ; tentatively = 0.85
 L_C : Clear height of columns

Design axial load

Design axial loads for columns are obtained from a linear frame analysis described in section 8.2.4, except for the *BDF* system.

In a structural design of *BDF* system, design axial loads of columns are basically evaluated on the basis of beam flexural over-strengths. The flexural over-strength is assumed to be developed at each potential plastic hinge region of the beams. However the full development of beam over-strength at every potential plastic hinge region in a high-rise building does not occur due to higher mode vibrations. Therefore, some reduction in design column axial load can be considered. The flexural strengths at critical column sections are likely to be overestimated when the design axial load greater than the actual axial force responses is estimated. Thus, the reduction factor R_v in New Zealand Code [8.2] can be used.

When two way frame action has to be considered, 50 % of axial load induced by perpendicular adjacent beams through beam-column joints shall be added to the design column axial load.

8.2.6 Design of the beam-column joint

Premature shear failure of beam-column joints and excessive slippage of beam longitudinal bars from beam-column joints shall be avoided. Therefore, the careful detailing of tendon anchorages and the adequate development length and anchorage details of beam longitudinal reinforcement shall be considered in addition to the assurance of enough shear strength of beam-column joint.

To resist bursting, horizontal splitting and spalling forces induced by the prestressing

tendon anchorages, an adequate volume and arrangement of reinforcements shall be provided in the anchorage zone.

8.2.7 Design Requirements for Walls in DWF System

In a building to be designed as a *DWF* system, the development of a collapse mechanism must be associated with the flexural yielding at the wall base or the rotational yielding of wall foundations. The rotational yielding means that the overturning moment at the wall foundations reaches the maximum moment of resistance of the wall foundations. The flexural yielding moment and corresponding shear at the end sections of the adjacent foundation beams must be considered. Soil pressure or pile resistances and the gravity load at the wall foundations should be also considered in addition to the flexural strength of the wall itself in the calculation of the maximum rotational resistance of the wall foundations.

The resultant lateral shear resistance of the walls at the first story is assumed to range between 30 % and 70 % of the specified seismic shear force at the first story. When the overturning moment at the wall foundation computed by a linear frame analysis exceeds the rotational yielding moment of the wall foundations, an additional lateral shear strength shall be allocated to the boundary frames. However, the walls shall not yield at the first story when the whole frame is subjected to the seismic design load resulting from the base shear coefficient of 0.2.

The observations of past earthquake damages have indicated non-ductile shear failure of the boundary beams in wall frame structures or coupling beams in coupled shear wall structures due to insufficient web reinforcement. Therefore, for the shear design of boundary beams or coupling beams, the following equation is applied to assure their ductile behavior.

For hinge regions

$$\phi_{w1} \cdot Q_R \geq ({}_B M_O + {}_B M'_O) / L_B + {}_B U_Q + {}_B D_Q + {}_B L_Q \quad (8.19)$$

For non-hinge regions

$$\phi_{w2} \cdot Q_R \geq ({}_B M_O + {}_B M'_O) / L_B + {}_B U_Q + {}_B D_Q + {}_B L_Q \quad (8.20)$$

where ϕ_{w1}, ϕ_{w2} : Shear strength reduction factors for boundary or coupling beams to assure the required member ductility indirectly; tentatively $\phi_{w1} = 0.8$, $\phi_{w2} = 0.9$.

8.3 Design example of prestressed concrete buildings

In this section, the required strength of a frame in order to force hinges into only the beams is parametrically demonstrated for a one-bay, four-story model frame.

Parameters investigated are;

(1) span length (10, 15, 20 and 25 m)

(2) live load which uniformly distributes on each floor (0.5, 1.0, 1.5 and 2.0 times 5.88 kPa) (a span length perpendicular to the plane of the frames considered is assumed to be 6m)

(3) tensile stress, σ_{ct} , induced at the bottom fiber of the mid-span beam section under service load condition when assuming that the beams are simply supported.

$$(a) \quad \sigma_{ct} = 0 \quad (8.21a)$$

$$(b) \quad \sigma_{ct} = f_t = 0.07f'_c \quad (8.21b)$$

$$(c) \quad \sigma_{ct} = f_{tb} = \frac{5}{3}f_t \quad (8.21c)$$

where, f_t : tensile strength of concrete

f_{tb} : modulus of rupture of concrete

The uniformly distributed dead load is assumed to be 5.55 kPa.

8.3.1 General description of model frame

The one-bay, four-story model frame used in this section is illustrated in Fig.8.5. The beams with a rectangular cross section of 400 mm wide by 1200 mm deep are post-tensioned. The square columns reinforced by ordinary strength non-prestressed steel are 600x600 mm. The compressive strength of concrete, f'_c , is 39 MPa and the elastic modulus is 3.13×10^5 MPa. A span length perpendicular to the plane of the frame considered is assumed to be 6 m. The story height of each layer was 4 m. The magnitude of live load and span length were chosen as parameters.

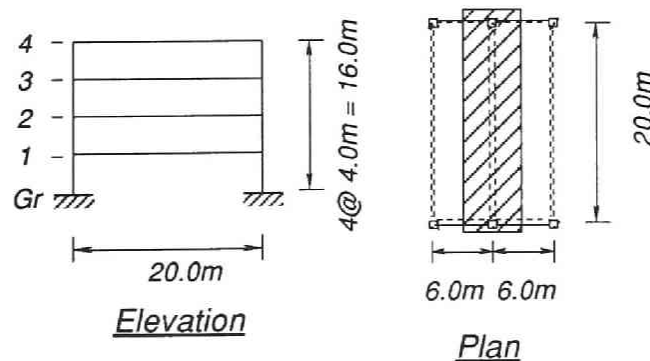


Fig.8.7 Model frame investigated

8.3.2 Design of prestressed concrete beams

Assuming that the beams are simply supported at their ends, bending moment at the mid-span section is given by the following formula.

$$M_o = \frac{(w_d + w_l) \cdot S^2}{8} \quad (8.22)$$

A prestressing force is generally introduced to reduce or to cancel the tensile stress in beam sections under service load. The magnitude of prestressing force is usually determined from how much tensile stress is permitted under the condition. Prestressing force introduced into the beam can be expressed by using the bending moment M_o and tensile stress permitted to occur at the bottom fiber of the section if no cracking occurs.

$$P = \frac{M_o - \sigma_{ct} \cdot Z_b}{\frac{Z_b}{A} + e_p} \quad (8.23)$$

where, w_d : dead load per unit area
 w_l : live load per unit area
 S : span length of the beam
 Z_b : elastic modulus of section of the beam
 A : sectional area of the beam
 e_p : distance of the centroid of the prestressing steel measured from the centroidal axis of the section

The sectional area of the prestressing steel A_p required to introduce this amount of prestressing force is given by

$$A_p = \frac{P}{\alpha \cdot \eta \cdot f_y} \quad (8.24)$$

where, α : allowable prestress introduced into the prestressing steel as a ratio to yield strength, η : ratio of the effective prestress to the prestress just after prestressing and f_y : yield stress of prestressing steel (f_y is assumed to be 1569 MPa). 0.85 and 0.8 are usually admitted as approximate values for α and η , respectively.

The minimum amount of bonded reinforcement should be provided by the following equation according to the current Japanese design code for prestressed reinforced concrete (and partially prestressed concrete) structures [8.14].

$$p_t = \frac{a_t}{bd} \geq \left(0.4 - 2.0 \frac{\sigma_g}{f_c'} \right) \cdot \frac{1}{100} \quad (8.25)$$

where, a_t and d : sectional area and effective depth of ordinary non-prestressed reinforcement, b : width of the section, σ_g : average effective prestress over the section and f_c' : compressive strength of concrete. a_t should not be less than the total sectional area of 2-D13 (2.53 cm^2).

Table 8.6 Prestressing force, sectional area of prestressing steel and ordinary non-prestressed steel

Frame	Prestressing force (kN)	Total sectional area of prestressing steel (mm ²)	Total sectional area of ordinary reinforcement (mm ²)
M-B(a)	5254	4940	253
M-B(b)	4900	4640	253
M-B(c)	4663	4340	253

Frame	Prestressing force (kN)	Total sectional area of prestressing steel (mm ²)	Total sectional area of ordinary reinforcement (mm ²)
M-S10(a)	1412	1380	1150
M-S10(b)	1050	990	1430
M-S10(c)	821	790	1430
M-S15(a)	3029	2860	253
M-S15(b)	2675	2570	253
M-S15(c)	2438	2270	253
M-S25(a)	8086	7600	253
M-S25(b)	7731	7210	253
M-S25(c)	7495	7010	253

Frame	Prestressing force (kN)	Total sectional area of prestressing steel (mm ²)	Total sectional area of ordinary reinforcement (mm ²)
M-L05(a)	3896	3650	253
M-L05(b)	3541	3360	253
M-L05(c)	3305	3160	253
M-L15(a)	6612	6240	253
M-L15(b)	6257	5900	253
M-L15(c)	6021	5680	253
M-L20(a)	7973	7520	253
M-L20(b)	7615	7180	253
M-L20(c)	7379	6960	253

Table 8.6 shows the prestressing force introduced into each beam, sectional area of prestressing steel and ordinary non-prestressed steel for each combination of the parameters. The suffix of the model name corresponds to the magnitude of tensile stress assumed at the bottom fiber of the section indicated in Eqs.8.1(a) to (c).

8.3.3 Calculation of secondary stress by prestressing

Fig.8.6 illustrates the tendon profile of the beam. The tendon force P and the member stiffness EI are assumed to be constant along the span. The secondary stress was calculated according to the following assumptions:

1. The ends of the beam are held against vertical displacement and rotation, but longitudinal deformation is not restrained, fixed-end moments are calculated.
2. The building structure has all been constructed and then the floor beams are post-tensioned at once, release moments and lateral forces due to prestressing are applied as external loads to the beam-column joints at each floor level. The release moments are as large as the fixed-end moments but opposite sign. The calculated results are based on the assumption that the frame remains uncracked.
3. The resultant stresses in the members are calculated using the stiffness matrix of the frame assembled on the basis of the elastic stiffness of the materials. Creep and shrinkage of concrete, and relaxation of prestressing steel are not considered.

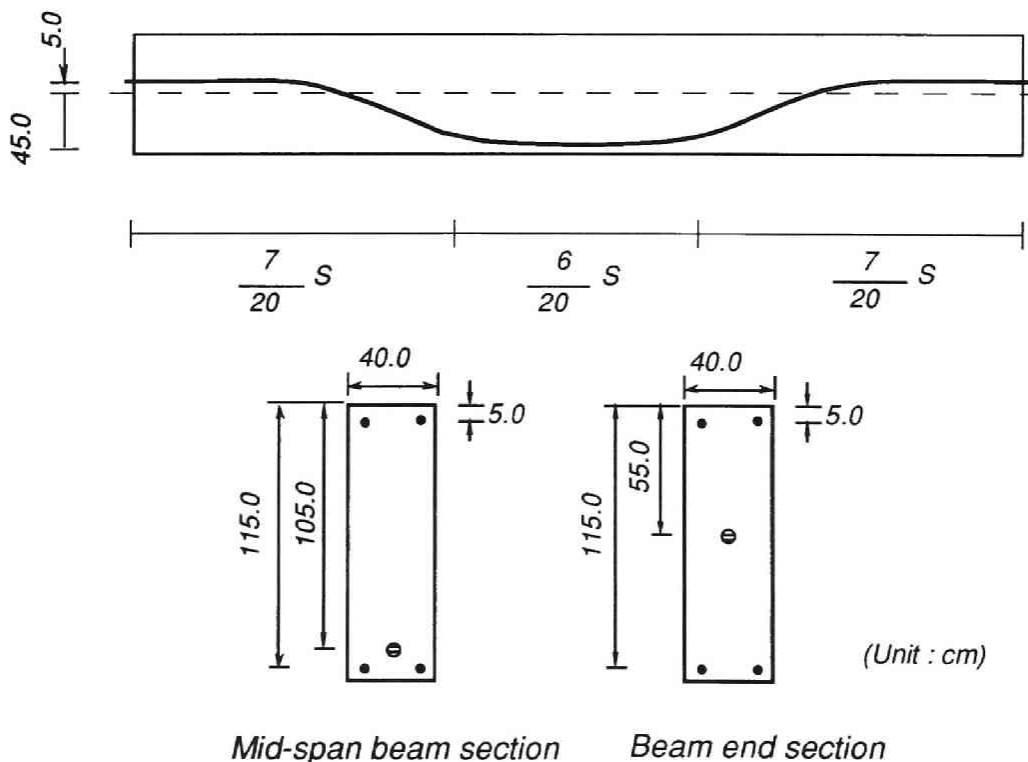


Fig.8.8 Tendon profile of beam

8.3.4 Design for seismic actions

The design seismic load in this study is based on the uniformly distributed vertical load on the floor. Only 1/3 of the live load was included because full live load is not likely to exist during an earthquake. The gravity load for calculating the seismic design lateral load at each floor level, W_i , is given by

$$W_i = \left(w_d + \frac{1}{3} w_l \right) \cdot 6 \cdot S \quad (8.26)$$

The base shear coefficient C_o was 0.2. Both the seismic hazard zoning coefficient Z and design spectral coefficient R_i were unity. The A_i distribution factor of lateral shear forces over the height was used. When calculating the design moment of each member, the effective member stiffnesses are assumed to be based on 50% of the area and moment of inertia of the gross section of the beams and 80% for the columns.

The combination of design actions considered was;

$$G + P + U + 1.5K \quad (8.27)$$

where, G and P denote the service dead and live load, respectively. U indicates the secondary stress due to prestressing force. K denotes the seismic design load due to the lateral shear force to each floor.

8.3.5 Calculation of beam flexural strength

The flexural strength of the beam sections was calculated using the equivalent rectangular stress block specified in ACI 318-89. The yield strength of prestressing steel was a nominal value ($f_y = 1569$ MPa). Overstrength which might develop in the beam plastic hinge regions was not calculated on the basis of overstrength of the constitutive materials, but considered to be 120% of the nominal flexural strength of the beam section. The overstrength was considered to be resisted by the upper and lower column critical sections joining to the beam following moment distribution ratio of the columns based on the results of the linear analysis which considers stiffness degradation of the members due to cracking. The moment distributed to the columns are required in order to avoid column hinging. Higher mode effect and two-way frame actions are not incorporated.

8.3.6 Calculation results

The ratio of the moment resistance required in order to avoid column hinging, to the design moment determined from the combination of design actions, M_{nyd} / M_{scd} , is plotted against the tensile stress permitted at the bottom of the beam section under

service load condition in Fig.8.7. When M_{nyd} / M_{scd} was less than unity, the design moment of the beam was determined from the earthquake load and M_{nyd} / M_{scd} was unity.

The maximum value of M_{nyd} / M_{scd} was 3.22. For reinforced concrete structures, the design moment of the beams are usually determined by the earthquake actions. Therefore, to prevent the columns from forming plastic hinges, the column design moment should be approximately 25% larger than that transferred from the beams unless higher mode effect and two-way frame actions are considered. For prestressed concrete buildings, as shown in Fig.8.7, a large strength is needed to cause the beam hinging mechanism.

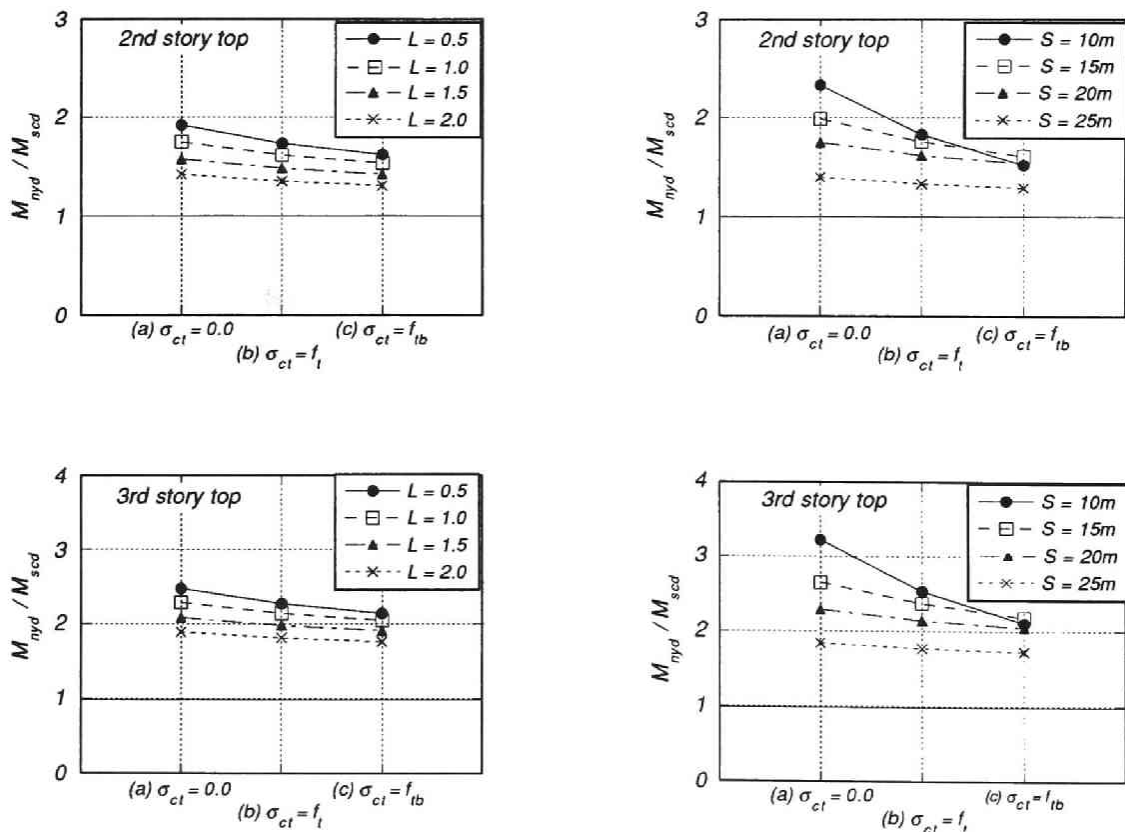


Fig.8.9(a) Calculated M_{nyd} / M_{scd}

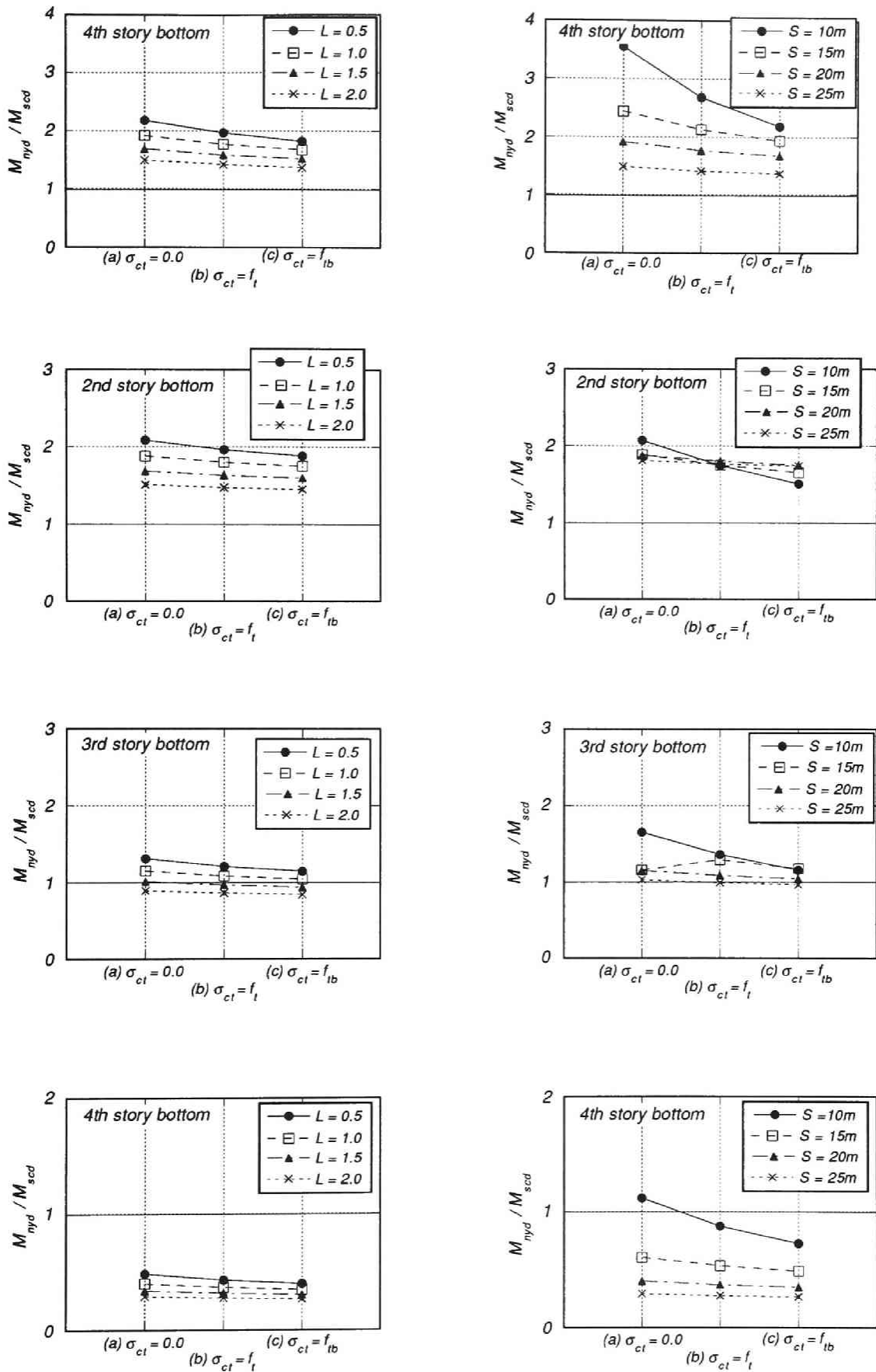


Fig.8.9(b) Calculated M_{nyd} / M_{scd}

8.4 Ductility of high strength reinforced concrete columns with high strength transverse reinforcement

8.4.1 Introduction

As shown in the preceding chapter, realizing beam hinging mechanism for prestressed concrete building structures is difficult especially for gravity-load-dominated building frames. Therefore, column hinging mechanism should be accepted for low-rise prestressed concrete buildings if ductility of plastic hinge region of columns is limited and the damage does not concentrate in the weakest story. Beam hinging mechanism is preferred because of the difficulty of ensuring ductility in the columns with high axial loads. Beams, which are theoretically free from axial load, have a high ductility capacity. Besides that, in prestressed concrete buildings higher compressive strength concrete is usually used than in reinforced concrete buildings. High strength concrete is more brittle than ordinary strength concrete with a sudden reduction of stress after the compressive strength is reached.

Lateral confining of concrete is often used to: (1) increase the strength of core concrete and (2) improve the ductility. However, past research has pointed out that the effect of lateral confining steel on columns of higher strength concrete is less than on those of ordinary strength concrete due to the smaller lateral strains of higher strength concrete. Volumetric expansion of high strength concrete is not as significant as that in ordinary strength concrete.

Muguruma et al. tested eight square reinforced concrete columns subjected to combined flexure and constant axial loads of 0.254 to $0.629 f'_c \cdot A_g$, and the test results were reported in the reference [8.8]. f'_c is the compressive strength of concrete and A_g is the gross sectional area of the column. The concrete compressive strengths were 85.7 MPa and 115.8 MPa. The confining reinforcement had yield strengths of 328 MPa and 792 MPa. The results of these column tests are summarized as follows: the test specimens, which had high strength confining reinforcement, achieved an interstorey drift of at least 0.06 rad. without significant strength reduction even under the axial load of $0.629 f'_c \cdot A_g$. High yield strength confining reinforcement improved the flexural ductility of the columns, although the confining reinforcement was less effective for columns of higher-strength concrete. On the basis of the test results the stress-strain models on confined concrete proposed by Muguruma et al. [8.9], and Kent and Park [8.10] were modified and the theoretical moment-curvature curves calculated using the models enabled the experimental curves to be well predicted.

In this section the flexural strength and ductility of columns with moderate or high axial compression loads are investigated. The ductility requirement for column plastic hinge regions has not yet been established. In this research work it will be shown that the ductility of high strength reinforced concrete columns can be improved more by

high strength lateral confining steel than by ordinary strength confining steel.

In addition, the stress-strain curve model proposed by Muguruma et al. [8.9] is re-modified to get a better prediction.

8.4.2 Column test units and test procedures

Four reinforced concrete column units with 200 mm square cross section were constructed. The axial loads applied to the columns were $P_c = 0.343 f'_c \cdot A_g$ for CL-3 and CH-3 and $P_c = 0.473 f'_c \cdot A_g$ for CL-4 and CH-4, where f'_c and A_g denotes the compressive strength of concrete and the gross area of columns, respectively. The longitudinal reinforcing steel for each column consisted of twelve 13 mm diameter deformed bars with a yield strength of 403 MPa. The transverse reinforcement of CL-3 and CL-4 was 6mm diameter hoops from a deformed bar with a yield strength of 408 MPa. For CH-3 and CH-4 the transverse reinforcements of 6mm diameter deformed bar hoops had a yield strength of 873 MPa (at the 0.2% offset strain). The mechanical properties of the steel are summarized in Table 8.6. The bar ends of the hoops were flash butt welded in order to develop their full efficiency. The cross sections and the dimensions of the columns, and the arrangement of longitudinal and transverse reinforcement in the columns, which were identical to those of the columns tested in the previous project, are shown in Fig.8.8. The loading setup is shown in Fig.8.9.

Table 8.7 Mechanical properties of steel

		D13	D6	
Yeild stress	(MPa)	403	408	873*
Yield strain	(%)	0.193	0.206	0.620
Modulus of elasticity	(MPa)	209000	202000	206000
Tensile strength	(MPa)	574	582	1021

Note : *0.2% offset yield stress

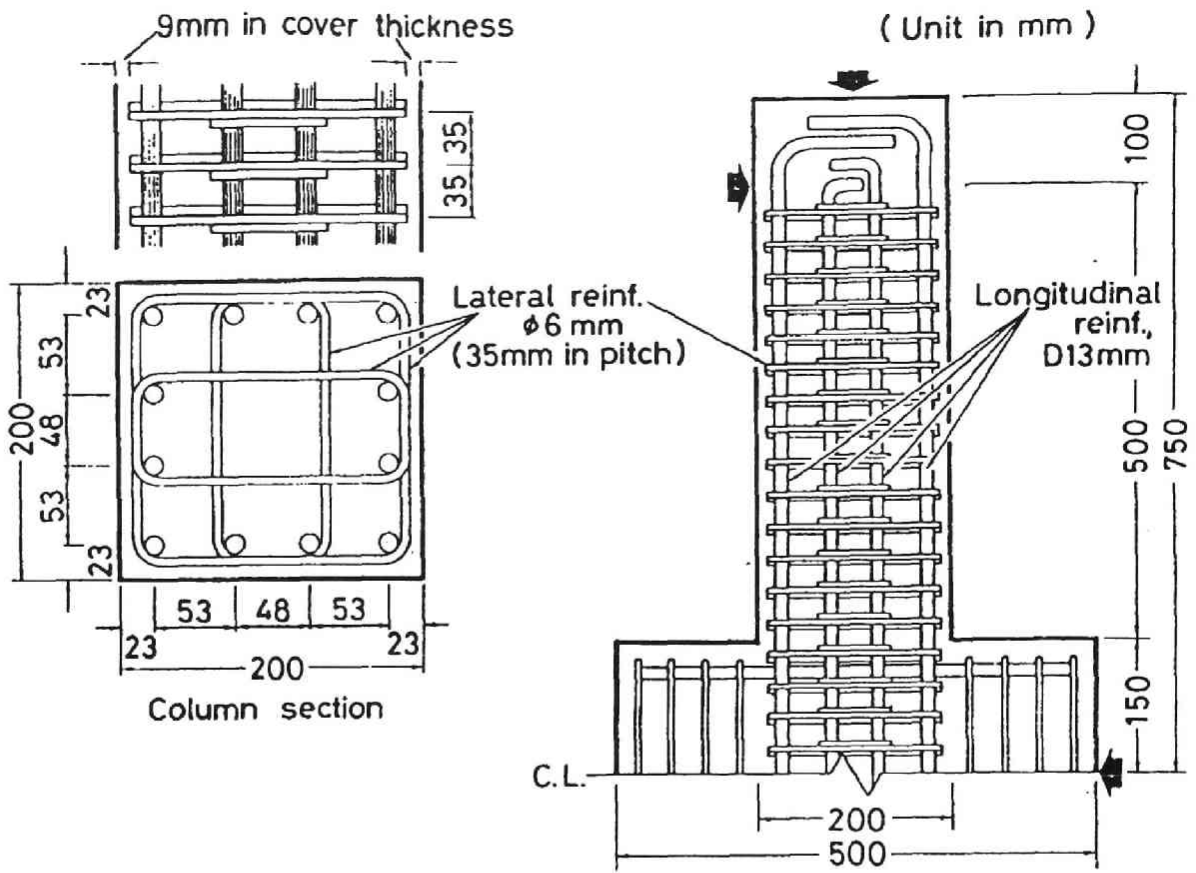


Fig.8.10 Test specimens

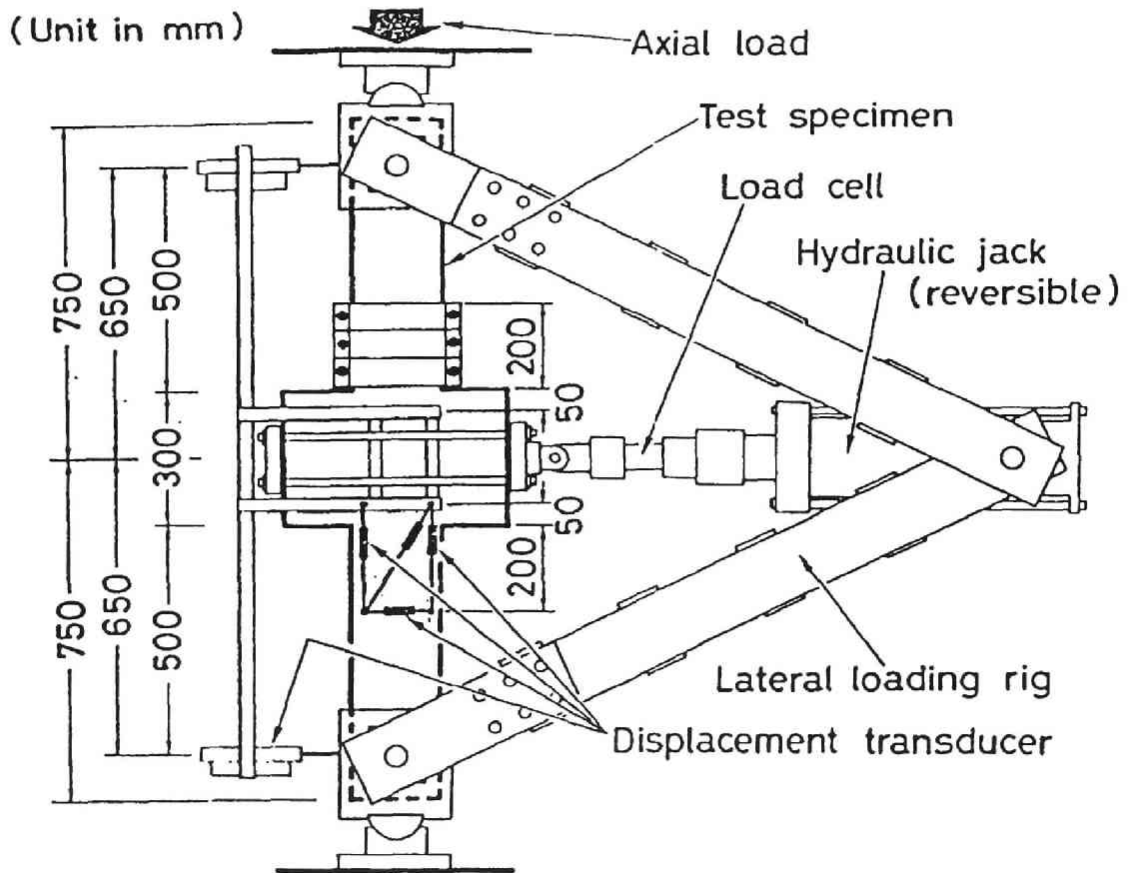


Fig.8.11 Loading setup and measuring devices

The mix design for the silica fume high strength concrete was :

15 mm aggregate (absolutely dry)	1018 kg/m ³
Sand (absolutely dry)	646 kg/m ³
High-early-strength Portland Cement	538 kg/m ³
Silica Fume	108 kg/m ³
Superplasticiser	13 kg/m ³
Water	133 Litre/m ³

Water/(Cement + Silica Fume) ratio = 0.18

The average slump was 134 mm. The compressive cylinder strength had reached $f'_c = 130$ MPa at the stage of testing the columns, that is, at the age of 73 days. The mechanical properties of concrete are summarized in Table 8.7. All columns were cast vertically, compacted using vibrators, and were damp cured in the laboratory.

Table 8.8 Mechanical properties of concrete

Compressive strength f'_c (MPa)	130
Strain at peak stress ϵ_c (%)	0.328
Modulus of elasticity E_c (MPa)	43900
Secant modulus at $1/3 f'_c$ (MPa)	43700

The volumetric ratio of confining reinforcement to confined core measured center-to-center was 4.93 % for all specimens. For CL-3 and CL-4, the area of confining reinforcement placed in the column was 85 % and 72 %, respectively, of that calculated according to Eq.6-24 and Eq.6-25 in the section 6.5.4.3 of NZS 3101:1982 [8.2] using the measured material strengths ($f'_c = 130$ MPa and $f_{yh} = 408$ MPa) and assuming that the capacity reduction factor $\phi = 1$. For CH-3 and CH-4, the area of confining reinforcement was 182 % and 155 %, respectively, of that calculated according to the above equations using the measured material strengths ($f'_c = 130$ MPa and $f_{yh} = 873$ MPa) and assuming $\phi = 1$. ACI 318-89 [8.11] requires 91 to 43 % of the area of confining reinforcement placed in the columns.

The critical plastic hinge regions of the columns were expected to be the regions above and below the central stub. However, as indicated in the previous test [8.8], the plastic hinge rotation concentrated mainly either above or below the stub. This prevented proper evaluation of ductility. In these additional tests, the possible critical regions

above the central stub were confined using steel plates on four sides of the column. The plates were firmly tied to each other. As tightened, the plates provided the critical region with biaxial confining pressure. Little rotation was observed in the regions above the central stub during the tests. In the regions below the central stub, which were not confined by steel plates, the maximum rotations measured in positive and negative loadings were almost the same.

Reversed cyclic horizontal load was statically applied to the stub by a hydraulic actuator. For CL-3 and CH-3 which had lower applied axial loads, the first loading cycle consisting of two cycles was followed by a series of deflection controlled cycles in the inelastic range, also comprising two full cycles to each of the displacements of the first loading cycle multiplied by ± 2 , ± 3 , ± 4 , ± 5 and two more cycles comprising one full cycle to ± 6 and ± 7 times the displacements of the first loading cycle. The first loading cycle displacements of the columns were found when the strain reading in the longitudinal tension reinforcement exceeded the yield strain which was obtained from material test. For CL-4 and CH-4 which had higher applied axial load, the first loading cycle up to the interstorey drift of $\pm 1/200$ was followed by a series of deflection controlled cycles comprising two full cycles to interstorey drifts of $\pm 1\%$, $\pm 2\%$, $\pm 3\%$, $\pm 4\%$, and sometimes higher.

8.4.3 Test results

Strength

Figure 8.10 shows the moment measured at the critical section versus interstorey drift during the tests. The moment displayed includes the $P - \Delta$ effect.

The ideal theoretical flexural strength M_i of the columns calculated using the ACI 318-89 equivalent rectangular stress block with $\beta_1 = a/c = 0.65$ based on the measured material strengths was 134.5 kNm for CL-3 and CH-3, and 131.5 kNm for CL-4 and CH-4. $\beta_1 = 0.65$ implies that a triangular compressive stress block of concrete is assumed. This is based on the characteristics of high strength concrete: linear ascending portion up to the peak stress followed by sudden and large reduction of stress. The strength reduction factor ϕ was assumed to be unity. These values and the flexural strength M_e obtained from the test results are shown in Table 8.8. For the columns subjected to lower axial loads the ACI method gave a good approximation. The worst discrepancy was of the order of 4 %. However, for the columns under high axial load the experimental results exceeded the flexural strength obtained by the ACI method by 9.4 % on average.

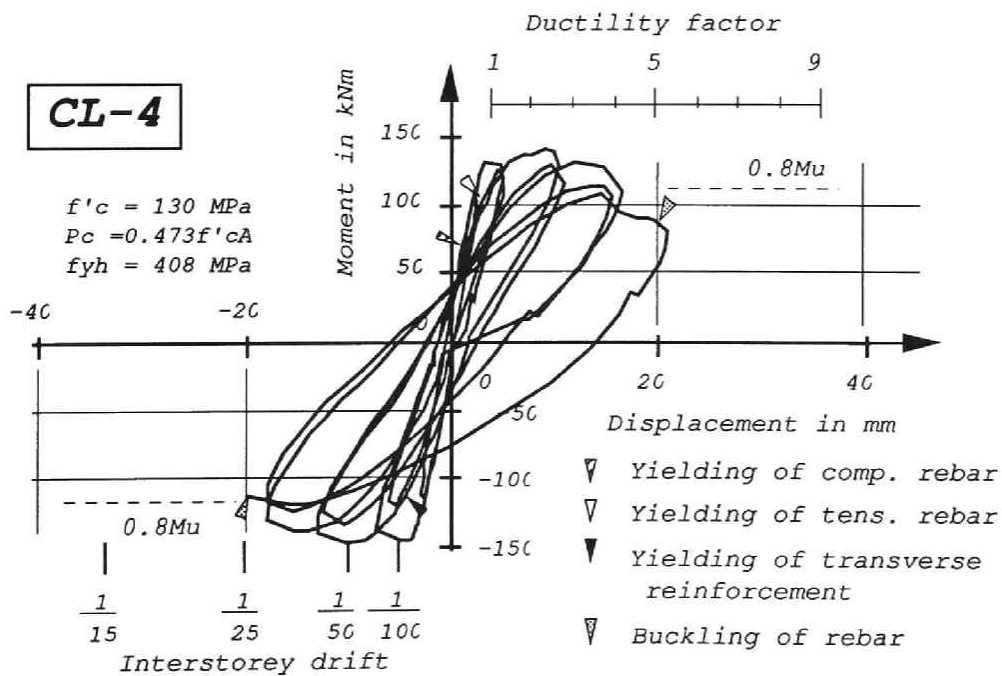
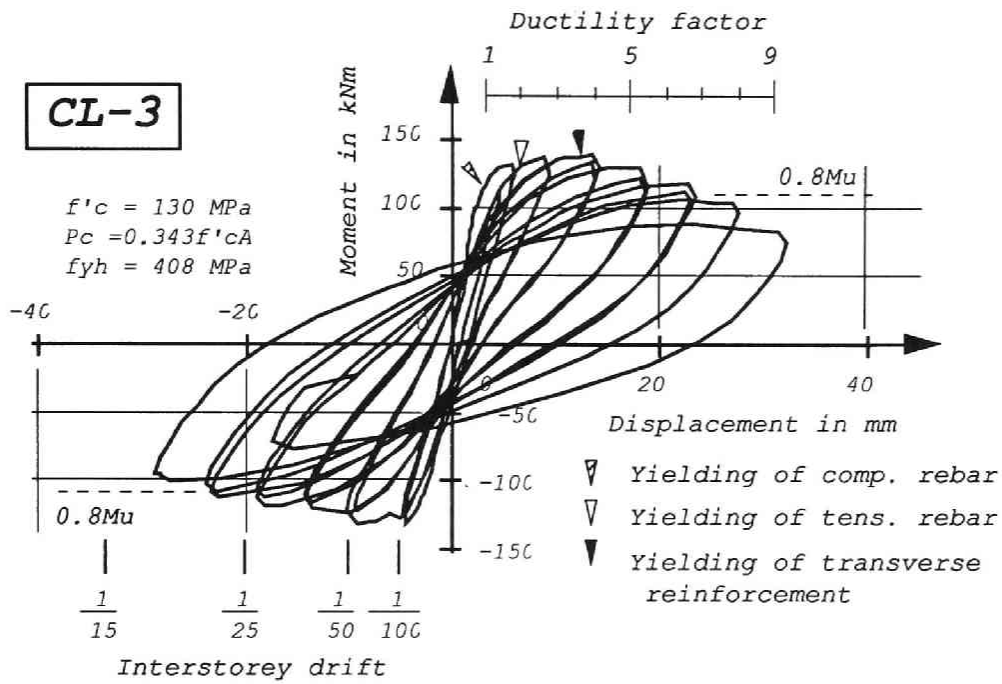


Fig.8.12(a) Moment - displacement curves

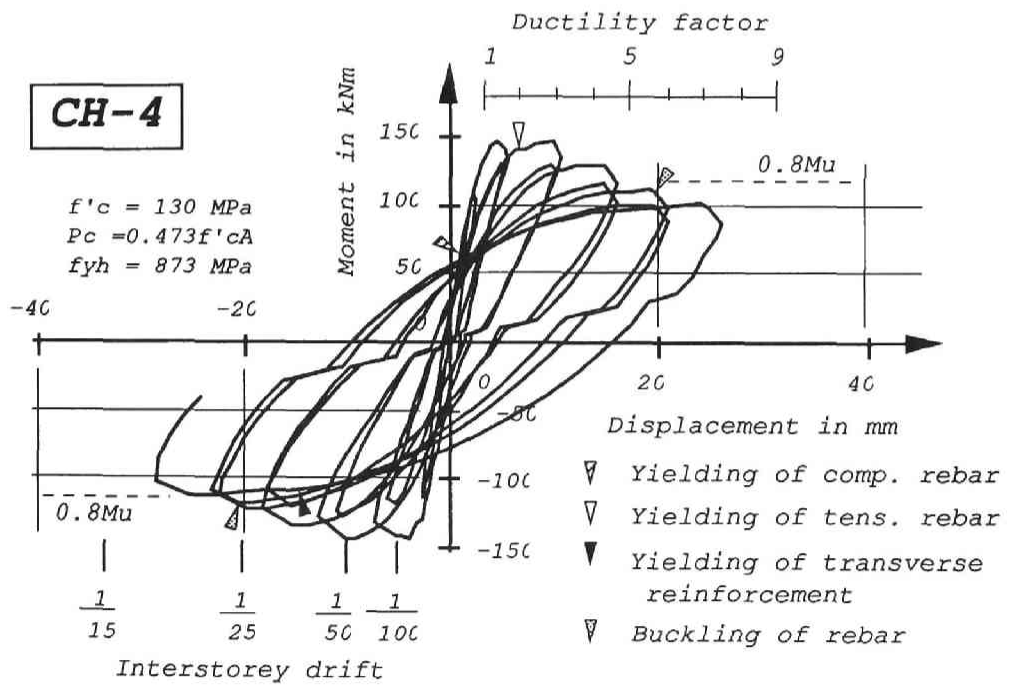
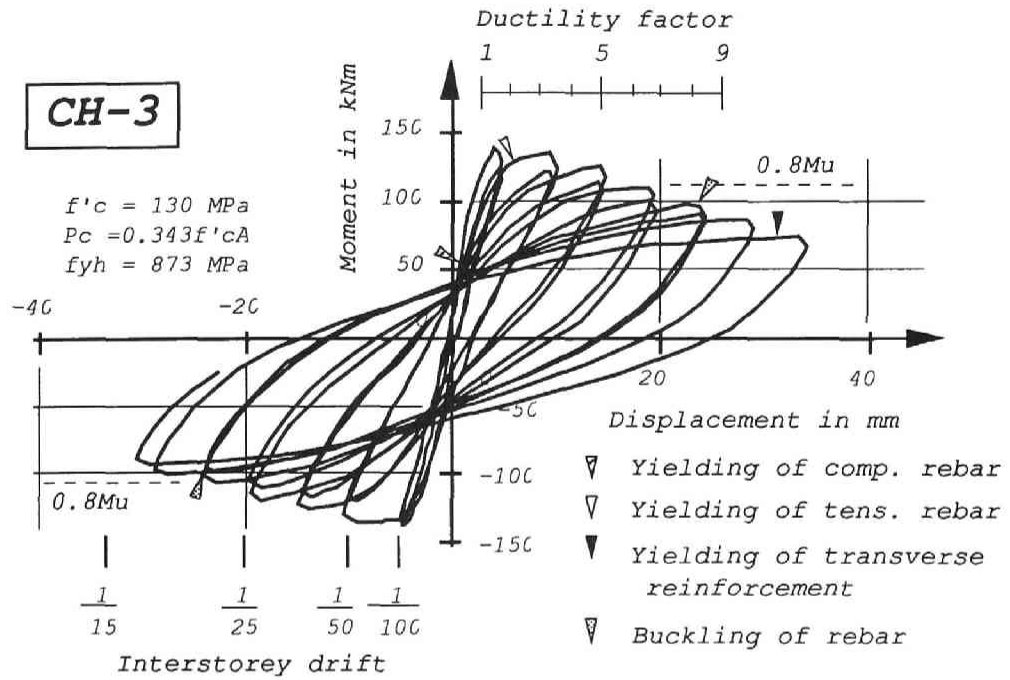


Fig.8.12(b) Moment - displacement curves

Table 8.9 Comparison of maximum experimentally measured flexural strengths and maximum calculated flexural strengths using ACI methods

Specimens	Experimental Results (kNm)		ACI Methods (kNm)	
	Positive	Negative	Positive	Negative
CL-3	138.9	-132.4	134.5 (0.97)	-134.5 (1.02)
CH-3	139.8	-136.4	134.5 (0.96)	-134.5 (0.99)
CL-4	141.5	-147.2	131.5 (0.93)	-131.5 (0.89)
CH-4	148.9	-139.0	131.5 (0.88)	-131.5 (0.95)

Note : Values in the parentheses indicate the ratio of the flexural strengths obtained theoretically to those obtained from the test results.

As pointed out in Ref. [8.10], “it appears that, for under-reinforced concrete beams, the present ACI 318 methods can be used without change, at least for concrete strengths up to 83 MPa, and for members subjected to combined axial compression and bending, important differences may occur.” Compared with the test results, the ideal strength calculated using the ACI methods is considered to give acceptable lower bounds for the columns with low axial loads less than $0.343 f'_c \cdot A_g$. However, most of the concrete shell outside the transverse reinforcement was observed to spall off just before or when the columns showed the peak measured flexural strengths, while the ACI methods are based on a gross sectional area. If they were based on a core dimension, they would have a much smaller strength. Therefore, it appears that the methods give a rather conservative strength for columns under high axial load.

The design of transverse reinforcement described in ACI 318 is based on the requirement that the final strength must be at least equal to the pre-spalled strength. In the column tests, spalling of the cover concrete commenced just before the peak of the first loading run into the inelastic range. The load carrying capacity of the columns kept increasing after the spalling until the peak flexural strength was reached. From the strength viewpoint, the present ACI equation for transverse reinforcement ratio can be used for high-strength concrete columns as well.

The shear distortion calculated based on the readings of the linear displacement transducers attached to the potential plastic hinge region shown in Fig.8.9 was so small that it was observed during the tests that flexure dominated the behaviour of the columns.

Ductility

In Fig. 8.10 the displacement ductility factors μ are shown. The displacement ductility factor μ is defined as $\mu = \Delta / \Delta_y$, where Δ is a displacement and Δ_y is a yield displacement of the equivalent elasto-plastic system with the same energy absorption as the moment - interstorey drift relationship obtained from the test results as shown in Fig.8.11. The available ductility was defined as the displacement ductility of the post-peak displacement when the load carrying capacity had reduced to 80 % of the peak load.

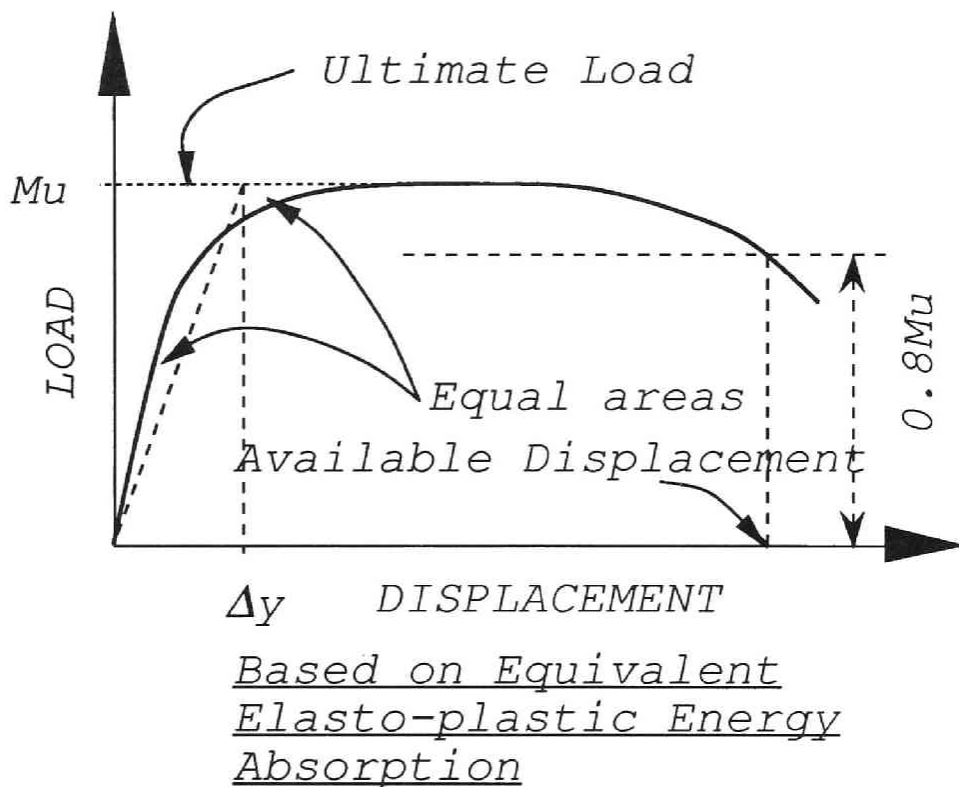


Fig.8.13 Definition of yield displacement

Compared with CH-3 of high yield strength confining reinforcement, the test results of CL-3 of low strength confining reinforcement indicated the similar hysteresis loops and the available ductilities were almost the same. This shows that under low axial load on the column, the yield strength of confining reinforcement did not contribute effectively to improve the available ductility, because the amount of confining reinforcement was supposed to be much more than enough.

Some of the transverse reinforcement fractured at the flash butt welding position during the tests of CL-3 and CH-3. For CL-3 two of them were found fractured just after the last loading run. A hoop just below the central stub of CH-3 was found fractured in the second loading run to the displacement ductility factor of 8.3. The transverse reinforcement of CL-4 and CH-4 did not fracture. In the material test of the transverse reinforcement some of test pieces fractured at the flash butt welding position while most of them developed their full strength and fractured somewhere else than the welding. It appears to be difficult to rely too much on flash butt welding.

For the specimens subjected to a higher axial load of $0.473 f'_c \cdot A_g$, the yield strength of the confining reinforcement gave a more important contribution to the improvement of ductility. The available ductilities were $\mu=+3.86$ and $\mu=-4.55$ for CL-4 and $\mu=+4.27$ and $\mu=-5.5$ for CH-4. In addition, the reduction in the load carrying capacity in the post-peak region of CH-4 was more gradual than that of CL-4. The first yielding of confining reinforcement was observed on the first loading run to the interstorey drift of $-1/50$ for CL-4 and on the second loading run to $-1/25$ for CH-4.

The critical factor of determining the available ductility is considered to be buckling of longitudinal reinforcement. For all specimens the buckling of longitudinal reinforcement was observed in the loading run following the loop where the load carrying capacity reduced to about 80 % of the peak load. In the tests of CL-3 and CL-4 with low yield strength transverse reinforcement, the buckling seemed to cause a sudden large drop of load carrying capacity. High yield strength confining reinforcement used in CL-4 prevented more effectively the buckling of longitudinal reinforcement than low yield strength confining reinforcement in CL-3 as shown in Fig.8.10.

8.4.4 Modification of previously proposed stress-strain model of confined concrete

In the paper written by Muguruma et al. [8.8], the stress-strain models on confined concrete proposed by Muguruma et al. [8.9], and Kent and Park [8.10] were so modified as to give theoretical moment-curvature curves closer to those obtained from the test results of the columns of high strength concrete. The theoretical moment-curvature curves calculated on the basis of the modified stress-strain curves and the measured material strength enabled the experimental curves to be well predicted.

However, there are still three problems left to be resolved; (1) The experimental flexural strength of the columns exceeded the predicted theoretical values. (2) The inclination of the theoretical moment-curvature curves in the large ductility were still steeper than that of the experimental curves after the modification of the stress-strain curve of concrete proposed by Muguruma et al. (3) The comparison in the reference [8.8] was conducted between the theoretical results of monotonic loading and the

envelope curves of the experimental results under reversed cyclic loading.

The analytical method used is as follows; The column cross-section was assumed as a series of parallel strips which are perpendicular to the depth of the section. The distribution of flexural strains was assumed to be linear through the depth of the section. Analysis proceeded by increasing the curvature at the critical section in a series of small steps. The position of the neutral axis was obtained by iteration until equilibrium of the internal forces was achieved.

Flexural Strength

Table 8.9 shows the theoretical flexural strength based on the measured material strengths. The theoretical flexural strengths obtained from the monotonic analysis were 88 to 103 % of the experimental values. Park et al. pointed out three reasons in their paper [8.10] why the experimental moments exceeded the theoretical moments as follows; (1) In the inelastic range, the actual stress-strain curve for the steel under cyclic loading lies above the monotonic curve, which is usually assumed in calculation of moment capacities, and results in higher steel stresses for a given strain. (2) The stress-strain model for confined concrete may not be absolutely accurate. (3) The extra confinement caused by the presence of the stiff central stub at high displacement ductility factors would mean that the critical section would tend to shift away from the region of influence of the stub. If the critical section is taken at 50 % of neutral axis depth from the stub face, the theoretical moment capacity would be closer to the experimental value.

Table 8.10 Maximum flexural strengths theoretically predicted

Specimens	Theoretical Results (kNm)			
	Monotonic Loading		Cyclic Loading	
	Positive	Negative	Positive	Negative
CL-3	135.8 (0.98)	-135.8 (1.03)	135.8 (0.98)	-135.8 (1.03)
CH-3	135.8 (0.97)	-135.8 (1.00)	135.1 (0.97)	-136.8 (1.00)
CL-4	131.4 (0.93)	-131.4 (0.89)	140.8 (1.00)	-138.5 (0.94)
CH-4	131.4 (0.88)	-131.4 (0.95)	133.3 (0.90)	-140.6 (1.01)

Note : Values in the parentheses indicate the ratio of the flexural strengths obtained theoretically to those obtained from the test results.

As for the first reason, Table 8.10 also shows the theoretical flexural strength obtained from the analysis of cyclic loading based on the stress-strain curve model proposed by Yokoo et al [8.13]. The analysis was proceeded following the hysteresis of curvature which was calculated the reading of the linear displacement transducers attached in the potential plastic hinge region of the column. The theoretical values increased to 90 to 103 % of the experimental values. However, for the columns under high axial load the difference between them were still larger than acceptable. The increment of compressive strength of confined concrete appeared to contribute less significantly to the flexural strength than the increment of steel stress. Therefore the large change in the flexural strength by the second reason can not be expected.

In the reference [8.8], the critical section appeared to shift away from the stub face based on the close observation of the appearance as well as in the tests reported in this paper. This seemed to be more remarkable in the columns subjected to high axial load than in those under low axial load. However, the third reason did not affect the peak-load because it was obtained at a rather small displacement although the load in the post-peak region at larger displacement was made larger. The theoretical values increased to 152.5 kNm for CL-3 and CH-3, 153.4 kNm for CL-4 and 154.3 kNm for CH-4. Thus, the ratio of the flexural strength obtained theoretically to those obtained from the test results also increased to 1.04 to 1.15.

Friction at the pin supports at the top and bottom of the column would give an additional strength especially to the columns subjected to higher axial load. However, this was not included quantitatively in the calculation.

Ductility

Figure 8.12 shows the moment-curvature curves calculated using the original Muguruma et al. model on confined concrete [8.9], the modified Muguruma et al. model with $\alpha=1.2$ [8.8] and the experimental results. The reduction in strength of the theoretical moment-curvature curves in the large ductility were still larger than that of the experimental curves after the modification. To account for this, the modified stress-strain curve was re-modified as shown in Fig.8.13 as the curve O-A-C-I. A descending branch of the skeleton curve after peak stress does not fall below the stress of $0.5 \sigma_{cm}$ and the stress is kept to $0.5 \sigma_{cm}$, while in the previous modification the descending branch was assumed to reach zero stress. The calculated results are also shown in Fig.8.12 as the re-modified model. In the large curvature region, the reduction in strength became more gradual than the results of the modified model. However, this region was beyond the available ductility and the re-modification seems not to be of great importance.

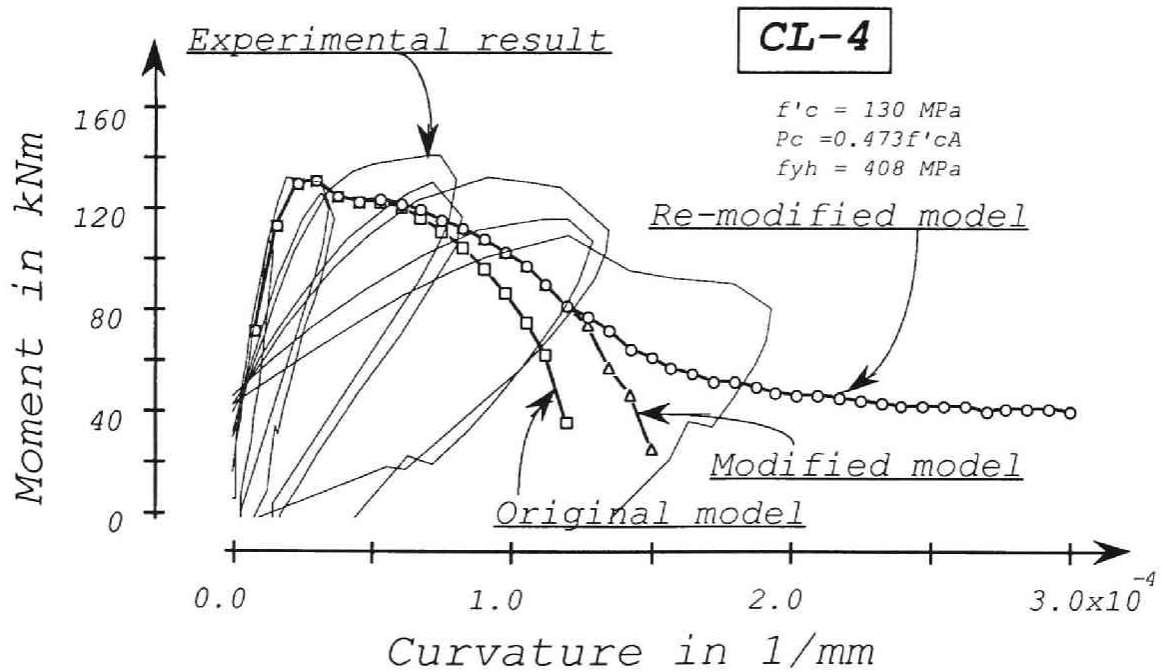
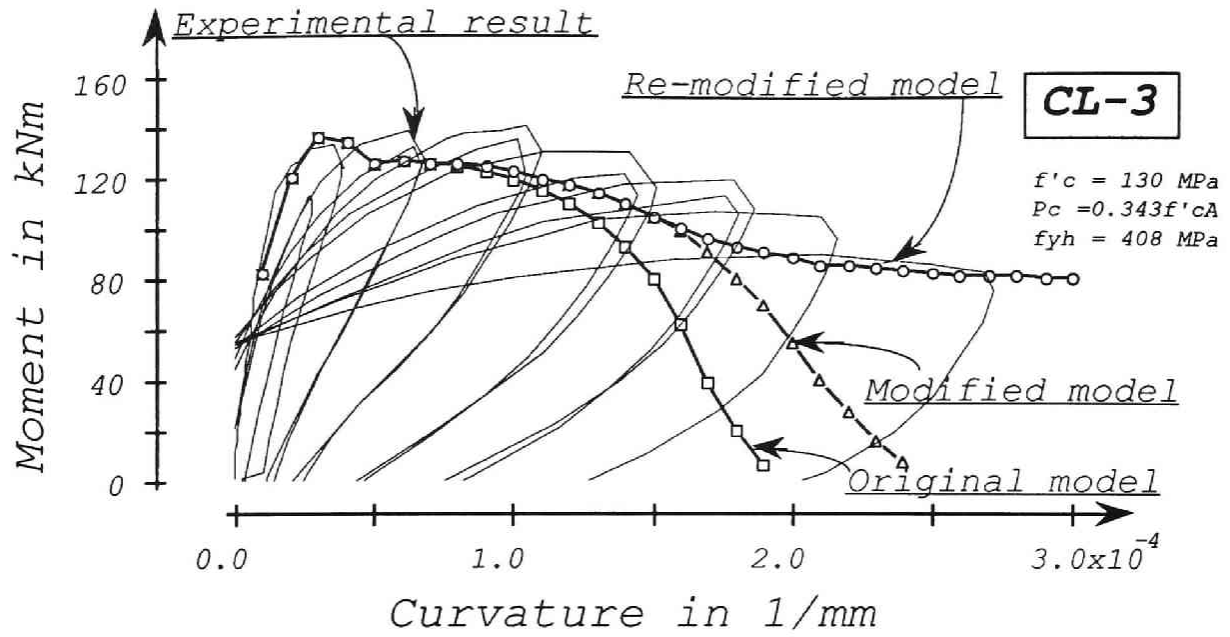


Fig.8.14(a) Comparison of moment - curvature curves experimentally measured and theoretically predicted

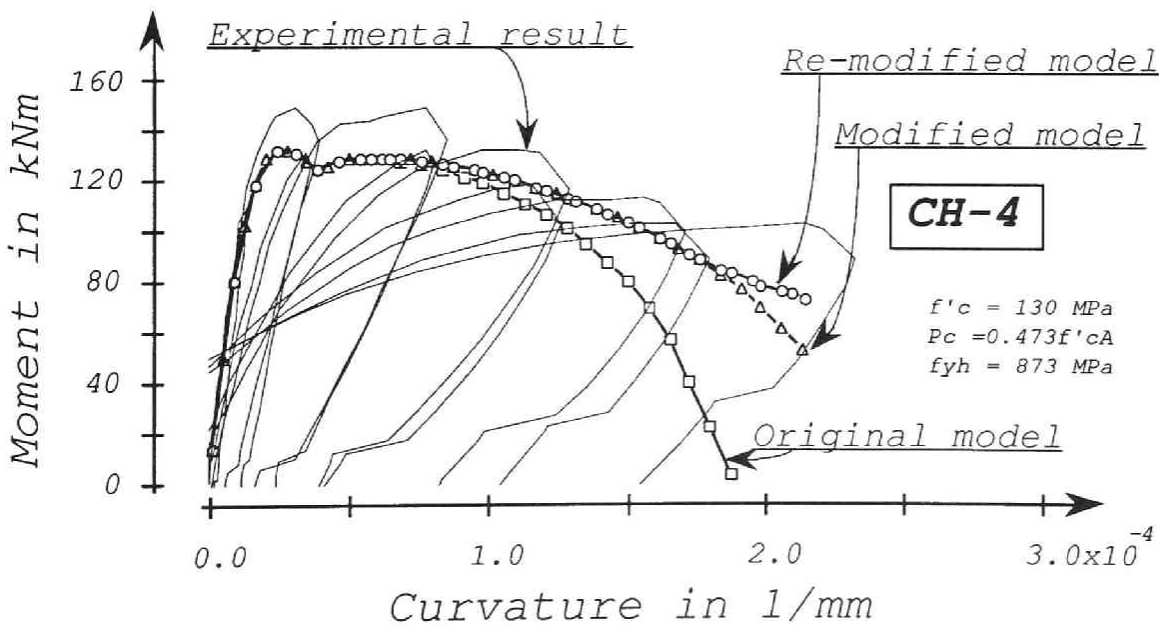
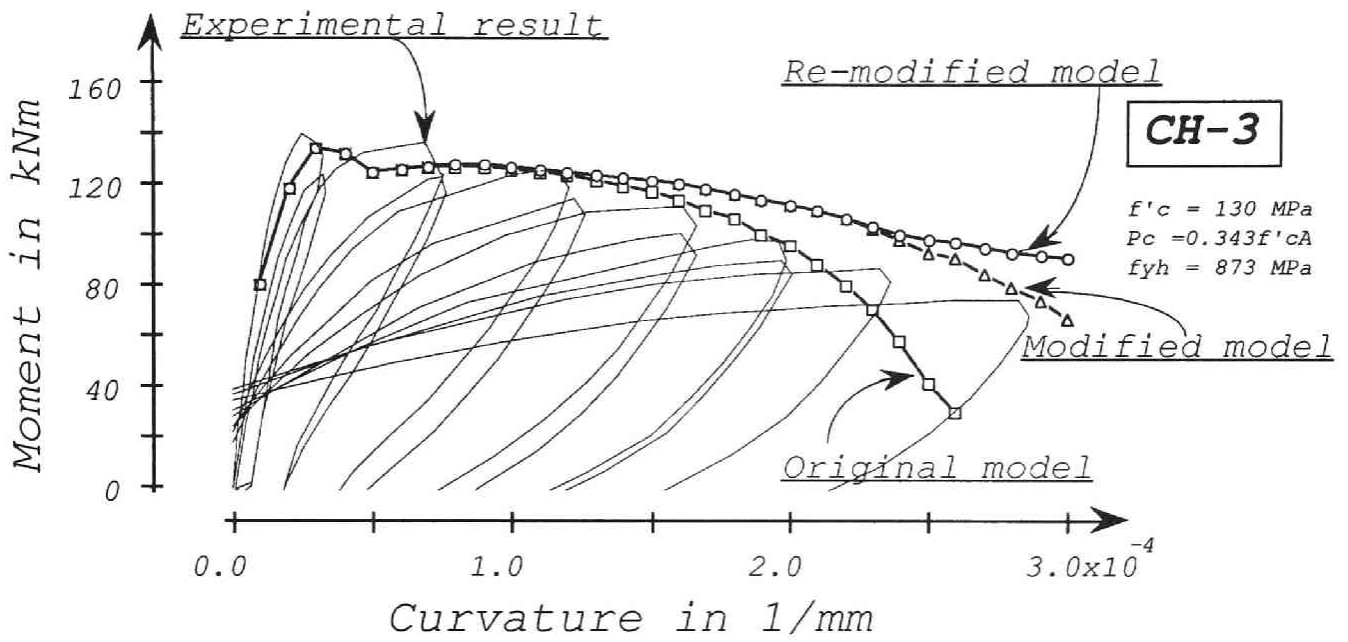


Fig.8.14(b) Comparison of moment - curvature curves experimentally measured and theoretically predicted

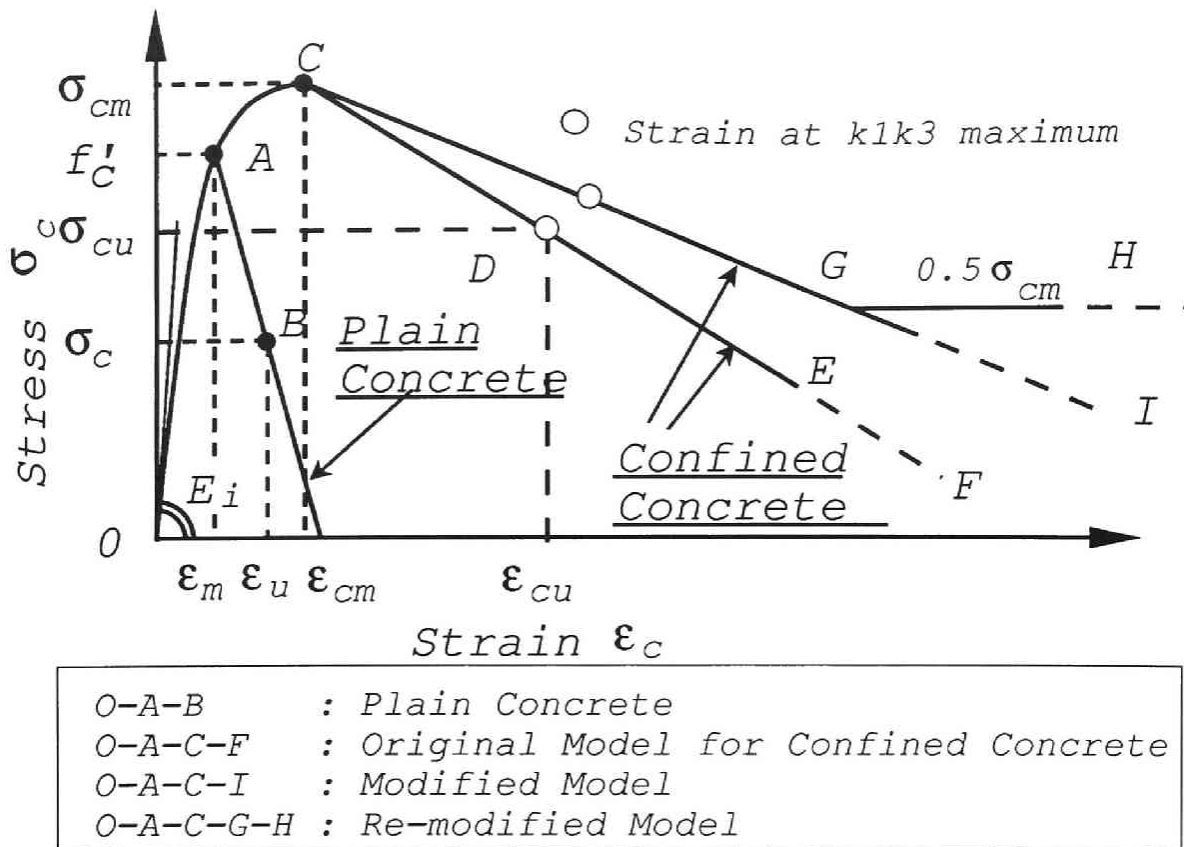


Fig.8.15 Stress - strain model on confined concrete

For CL-3, CL-4 and CH-4, the theoretical moments were much smaller than those of the experimental results while for CH-3 the theoretical moments were slightly larger than those of the experimental results. The problem is considered to be in the evaluation of spalling strain of cover concrete. The cover concrete of the columns was appeared to have some strength until the larger strain than assumed in the analysis. The spalling of concrete itself was so uncertain that a different result could be obtained even if two identical columns were tested under exactly the same condition.

Cyclic Loading

The influence of cyclic loading in the analysis is expressed in Fig.8.14. The figure contains three moment-curvature curves of CH-4 obtained theoretically; (A) the moment-curvature curve under monotonic loading calculated using the modified Muguruma et al. model proposed in the previous paper [8.8], (B) the moment-curvature curve under cyclic loading using the same model used in (A), and (C) the moment-curvature curve under cyclic loading using the re-modified model assuming that a descending branch of the skeleton curve after peak stress does not fall below the

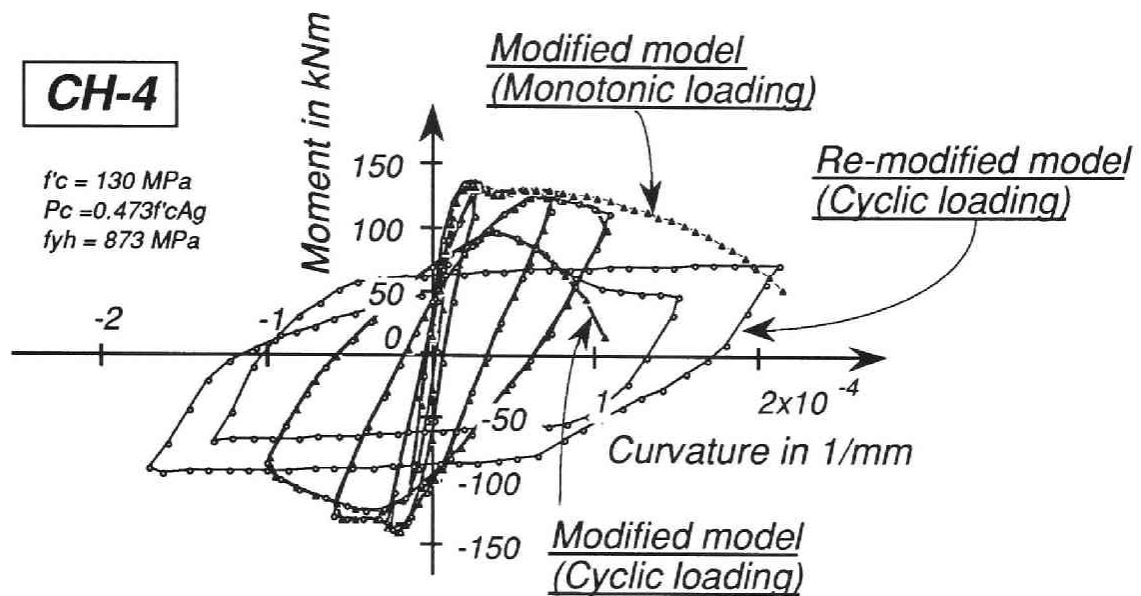


Fig.8.16 Comparison of analytical results under monotonic and cyclic loading

stress of $0.5 \sigma_{cm}$. As shown in Fig.8.14, the reduction in strength under cyclic loading (Curve (B) or (C)) is much larger than that of monotonic loading (Curve (A)) in the post-peak region. For the column subjected to high axial load of $0.473 f'_c \cdot A_g$, the theoretical moment-curvature curve of cyclic loading (B) dropped suddenly at a smaller curvature than that of monotonic loading, and the large reduction in strength resulted in instability in analysis. This is because the resultant compressive force in core concrete was not able to become large enough to sustain such a high axial load. The stress distribution in the column section in the analysis of reversed cyclic loading is different from that in the analysis of monotonic loading even if they are obtained at the same curvature because stresses in concrete under cyclic loading are smaller than those under monotonic loading at the same strains.

Fig.8.15 shows the stress distributions along the column section of CH-4 calculated theoretically. All the curves were obtained at the same curvature of $0.00003 / \text{mm}$. The peak-stress part shifted away from the extreme compression fiber to the extreme tension fiber of the section as the loading was advanced. That means the neutral axis depth increased. However large the neutral axis depth became, there was a limit that the resultant compressive force in concrete was not able to become large any longer. As the limit was being approached, the moment capacity dropped suddenly and this

reduction in strength led to instability and termination in analysis. In the post-peak region and under high axial load, the difference between the models is of greater importance. Besides, high strength concrete loses its strength suddenly in the post-peak region even if the concrete is well confined. The whole moment-curvature curve, even in the large ductility region, can be pursued by using the re-modified model as shown in the curve (C) in Fig.8.15, while in case the modified model was used the analysis terminated in the third cycle during the loading. In fact, core concrete is considered to have some strength up to a much larger strain than assumed in the original stress-strain model when it is well confined.

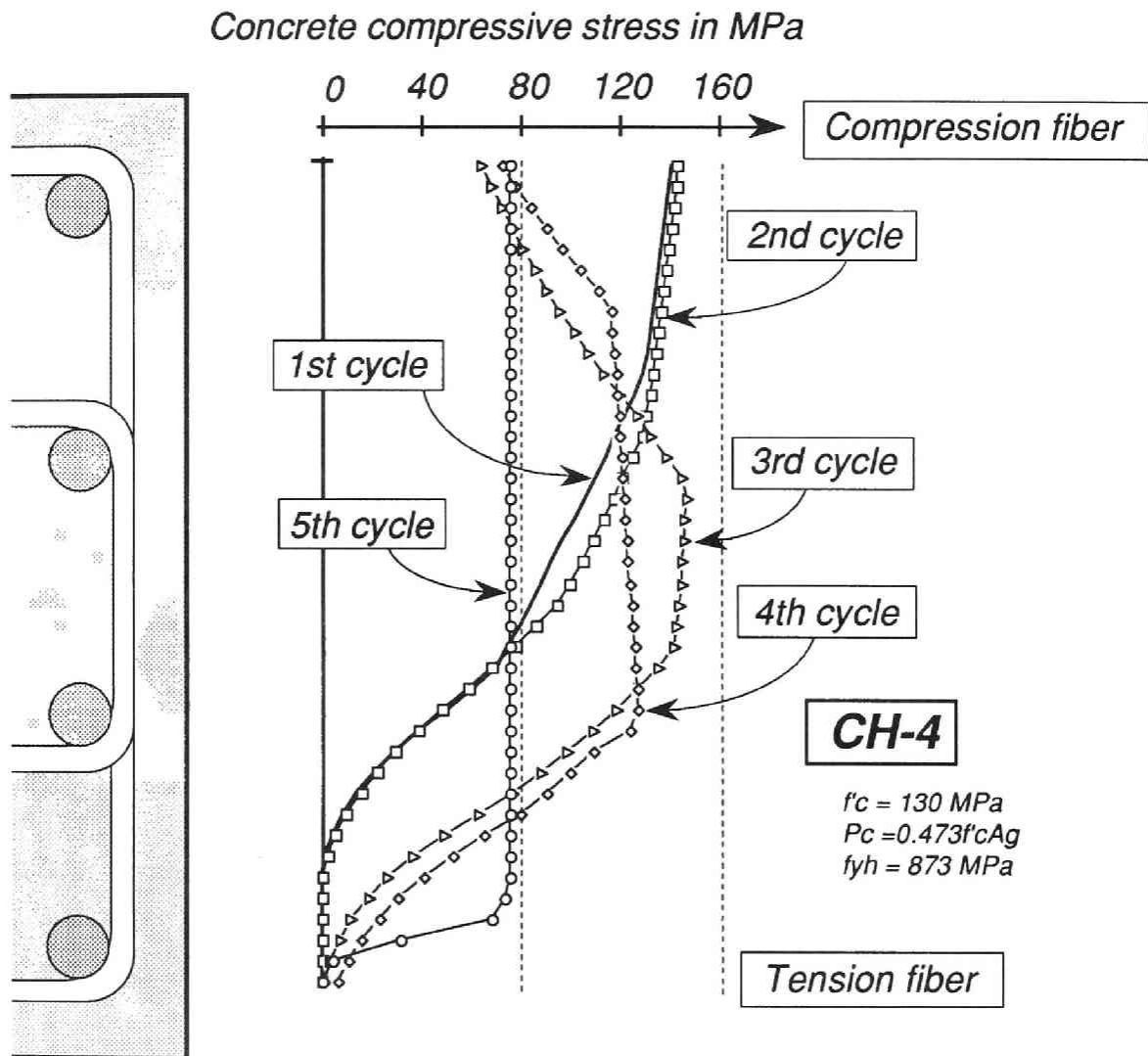


Fig.8.17 Distribution of concrete stress

8.5 Seismic design of building frames of limited ductility

The idea employed in the design proposal by AIJ committee that column sidesway mechanism could be permitted but design earthquake load should be increased is not innovative because NZS 3101:1982 has the provisions for structures of limited ductility. The provisions of NZS 3101:1982 may suggest a fundamental idea of seismic design method for prestressed concrete buildings.

Due to the configuration of structural components or functional requirements some building structures may have strengths which are greater than needed for full ductility. This type of structures need only limited ductility. Structures of limited ductility are defined as structures in which the system as a whole or the primary lateral load resisting components are not considered to be capable of sustaining the inelastic displacements that are expected in fully ductile structures, without significant loss of strength or reduction in energy dissipating capacity. As described in the commentary (NZS 3101:1982 Part 2 Commentary) typical building structures in which the application of the design procedure might be appropriate are:

- (a) Frame structures in which the geometrical limitations of Section 6 (in NZS 3101:1982) cannot be met.
- (b) Low framed structures in which beams are unavoidably over-reinforced, because of gravity load or to meet minimum reinforcement requirements.
- (c) Structures which, in accordance with generally understood conditions compatible with ductile design, are irrational, such as deep membered frames arising from the random penetration of walls.
- (d) Long squat wall structures, such as occur as fire or party walls between adjacent residential units, and which possess a great excess of strength over requirements for lateral load resistance. The provisions for structures of limited ductility would also be applicable to frames lying parallel to such walls, where such frames are not treated as secondary elements in accordance with 3.5.14 in NZS 3101:1982.

Prestressed concrete building structures may be included in the category (b) because prestressing steel is provided to reduce gravity load effects and it gives more strength needed for lateral load resistance. Moment resisting frames of limited ductility are assigned a structural type factor of $S = 2.0$. This structural type factor may be compared with the value of $S = 0.8$ assigned to ductile frames. That is, moment resisting frames of limited ductility are designed for seismic forces which are $2.0/0.8=2.5$ times the seismic design force used for the design of ductile moment resisting frames. The ratio of design seismic load of frames of limited ductility to that of ductile frames is very large in the New Zealand codes compared with the AIJ's proposal: for reinforced concrete frames the ratio of design seismic load of *BDF* buildings to that of *GDF* buildings is $0.35/0.25=1.4$, although the distribution of story shear strength along the height of the buildings should be as specified.

The provisions are applied to only relatively low structures: frames of limited ductility have a maximum height of four stories or 18m, or if roof and wall mass are less than $150\text{kg}/\text{m}^2$ of floor area a maximum height of five stories or 22.5m, while in the AIJ's proposal, there is no limitation of height of buildings to be designed as *GDF* buildings. Prestressed concrete tall buildings are quite attractive.

Required flexural strengths are also different between the two design procedures. Beams and columns outside the end regions should have flexural strengths, M_i , indicated in Eq.8.28.

$$\phi M_i \geq M_e + \left(\frac{3}{S} - 1\right) M_{eq} \quad (8.28)$$

where, ϕ : strength reduction factor ($\phi = 0.9 \sim 0.7$ depending on the axial compression load and transverse reinforcement provided.)

M_i : ideal flexural strength

M_e : moment resulting from loading combination U , involving earthquake loads

M_{eq} : moment associated with E

By substituting $S = 2.0$ into Eq.8.28, the following equation is obtained.

$$\phi M_i \geq M_g + 1.5M_{eq} \quad (8.29)$$

where, M_g : moment associated with G

$$= M_e - M_{eq}$$

G : factored gravity load - (dead load and/or live load) specified in NZS 4203 or other appropriate loadings code

In the regions of potential flexural hinging for beams and columns, required flexural strengths are given in the following equation.

$$\phi M_i \geq M_g + M_{eq} \quad (8.30)$$

In the AIJ's proposal for beams of *GDF* buildings, required flexural strengths are

$${}_B M_R \geq {}_B U_M + {}_B D_M + {}_B L_M + {}_B E_M \quad (8.31)$$

All the notations regarding the equations are given in Section 8.2.
for columns

$${}_C U_M + {}_C D_M + {}_C L_M + (1 + \gamma)_C E_M \geq {}_C M_R \geq {}_C U_M + {}_C D_M + {}_C L_M + {}_C E_M \quad (8.32)$$

Capacity reduction factor for flexural strength is not incorporated in the equations of the AIJ's proposal.

Shear strengths to be provided are given by the following equation.

$$\phi V_i \geq V_g + 2V_{eq} \quad (8.33)$$

where, V_i : ideal shear strength

V_g : shear associated with G described above

V_{eq} : shear associated with E

On the other hand in the AIJ's proposal shear strengths regarding hinge occurrence. Beams without hinges:

$${}_B Q_R \geq {}_B U_Q + {}_B D_Q + {}_B L_Q + {}_B E_Q \quad (8.34)$$

Beams with hinges:

For hinge regions

$$\phi {}_{B \cdot B} Q_R \geq ({}_B M_O + {}_B M'_O) / L_B + {}_B U_Q + {}_B D_Q + {}_B L_Q \quad (8.35)$$

For non-hinge regions

$${}_B Q_R \geq ({}_B M_O + {}_B M'_O) / L_B + {}_B U_Q + {}_B D_Q + {}_B L_Q \quad (8.36)$$

For hinge regions of columns of *GDF* buildings:

$$\phi {}_{c \cdot c} Q_R \geq ({}_c M_O + {}_c M'_O) / L_C \quad (8.37)$$

For non-hinge regions

$${}_c Q_R \geq ({}_c M_O + {}_c M'_O) / L_C \quad (8.38)$$

As shown above, shear strengths provided by the AIJ's proposal are based on the flexural overstrengths of end regions of the columns. It is stated in NZS 3101:1982 that a suitable margin over required flexural strengths as derived from the structural type factor used for flexural design in end regions. Due to larger seismic design load a margin as much as V_{eq} would be regarded enough although a capacity reduction factor is not taken into account.

8.6 Conclusions

- (1) A new seismic design procedure for prestressed concrete building structures proposed by AIJ task-committee was introduced. In the design procedure a column sidesway mechanism is permitted as one type of failure mechanisms. In order to avoid damage concentration into the weakest story, even if soft story forms, the lateral seismic design force should be increased and the smooth distribution of story shear strength be assured.
- (2) It has been stated that to secure beam hinging mechanism is difficult in prestressed concrete building structures because prestressing steel, which is usually high strength steel is provided to mainly reduce gravity load effect and the member sections have much larger strength than required by seismic lateral design force. Some design examples were demonstrated to show how difficult it is to realize beam hinging mechanism in prestressed concrete buildings. The ratio of the moment resistance required in order to avoid column hinging to the design moment determined from the combination of design actions, M_{nyd} / M_{scd} , reached 3.22 at most. For reinforced concrete structures the design moments of the beams are usually determined by earthquake actions. Therefore, to prevent the columns from forming plastic hinges the column design moment should be approximately 25% larger than that transferred from the beams unless higher mode effect and two-way frame actions are considered. For prestressed concrete buildings a large moment resistance is needed to realize beam hinging mechanism.
- (3) The flexural strength and ductility of columns with moderate or high axial compression loads were investigated by carrying out reversed cyclic loading tests on high strength reinforced concrete columns. The test results indicated that adequate ductility was obtained even for such high strength concrete columns by using high strength transverse reinforcement. The secured ductility would be enough even when soft story should form in one of the layers of a building. In addition, the flexural strengths of the test units subjected to the moderate axial load were well predicted by the ACI 318-89 methods with an equivalent rectangular stress block. However, for the columns under high axial load the flexural strengths obtained by the experiment exceeded the predicted values. Comparison between the experimental and theoretical results of moment-curvature curves indicated that the modified stress-strain model proposed by the authors should be re-modified so as to enable the moment-curvature curves to be well predicted, especially for columns subjected to reversed cyclic lateral loading with high axial compressive load.

[References]

- 8.1 Park, R. and Paulay, T. 1974. Reinforced Concrete Structures, John Wiley & Sons
- 8.2 Standard Association of New Zealand, 1982. Code of Practice for Design of Concrete Structures, NZS3101:1982
- 8.3 Standard Association of New Zealand, 1984. Code of practice for General Structural Design and Design Loadings for Buildings, NZS 4203:1984
- 8.4 Architectural Institute of Japan, 1990. Design Guidelines for Earthquake Resistant Reinforced Concrete Buildings Based on the Ultimate Strength Concept
- 8.5 Architectural Institute of Japan, 1990. Ultimate Strength and Deformation Capacity of Buildings in Seismic Design (1990).
- 8.6 Thompson, K. J. and Park, R. 1980. Seismic Response of Partially Prestressed Concrete, Journal of the Structural Division, ST8, ASCE, August 1980, pp.1755-1775
- 8.7 Okamoto, S. 1986. Fundamental Study on Earthquake Resisting Behaviors of Prestressed Concrete Frame Structures, Chapter 6, Doctoral Thesis of Kyoto University, 1986, pp.250-281
- 8.8 H. Muguruma and F. Watanabe, "Ductility Improvement of High Strength Concrete Column with Lateral Reinforcement", High Strength Concrete, Second International Symposium, ACI SP-121, 1990, pp.47-60.
- 8.9 H. Muguruma, F. Watanabe, T. Iwashimizu and R. Mitsueda, "Ductility Improvement of High-Strength Concrete by Lateral Confinement", Transactions of Japan Concrete Institute, Vol.5, pp.403-410, 1983.
- 8.10 R. Park, M.J.N. Priestley and W.D. Gill, "Ductility of Square-Confined Concrete Columns", Proceedings of ASCE, Vol.18, ST4, pp.929-950, April, 1982.
- 8.11 "Building Code Requirements for Reinforced Concrete (ACI 318-89) and Commentary - ACI 318R-89", American Concrete Institute, 1989.
- 8.12 "High Strength Concrete Seminar Course Manual", American Concrete Institute, SCM-15(87), 1987.
- 8.13 Y.Yokoo, T.Nakamura, T.Komiyama and Y.Kawada, "Non-Stationary Hysteretic Uniaxial Stress-Strain Relations of a Wide-Flange Steel", Transactions of Architectural Institute of Japan, No.259, September 1977, pp.53-66.
- 8.14 Architectural Institute of Japan, 1987. The Standard for Structural Design and Construction of Prestressed Concrete Structures.

REVERSED CYCLIC LOADING TESTS ON PRECAST PRESTRESSED CONCRETE BEAM-EXTERNAL COLUMN JOINT ASSEMBLIES

9.1 Background

Construction of prestressed concrete buildings requires more work than conventional reinforced concrete buildings. Such work consists of prestressing and grouting. This is troublesome and one of the reasons why prestressed concrete buildings have not become popular in spite of their performance under service load conditions. One of the solutions is use of unbonded tendons. This will be discussed later in the appendix. Another option is to adopt a precast prestressed concrete system, in which members are produced at a factory and transferred to a construction site, in some case members may be made at a construction site and assembled by post-tensioning. Generally in precast reinforced concrete systems, reinforcement is required to be connected between members to be joined in order to make their performance equivalent to a monolithic reinforced concrete building. However, this operation is very complicated although some methods have been proposed. Assembling members by post-tensioning is an easy way to obtain an equivalent monolithic building.

Under service load condition a precast prestressed concrete building shows good performance: a higher cracking moment than a ordinary precast reinforced concrete building and practically no slip deformation at the connections. Even after small earthquake motions it can maintain the original stiffness approximately as large as the elastic stiffness.

On the other hand, under large and medium earthquake motions it has been presumed that precast prestressed concrete buildings tend to be less ductile and tend to exhibit a less stable inelastic response than cast-in-place buildings. This is primarily because the inelastic strains are concentrated into the connections and the load-displacement hysteresis loops are narrower than cast-in-place reinforced concrete buildings. However, due to the limited data available, the seismic performance of precast prestressed concrete buildings has not yet been clarified.

On the basis of the conclusions of the preceding chapters the following two findings can be listed.

1. Yielding of prestressing steel and inelastic strains of compressed concrete in a prestressed concrete member lead to fatter hysteresis loops.
2. In a beam-column joint assemblage a suitable amount of prestressing force is beneficial for maintaining stiffness as the assemblage and preventing the beam-column joint core from failing in shear.

Thus, the author has made a suggestion to improve the seismic performance of beam-column subassemblages. (see Fig.9.1.)

1. The energy absorbing capability can be improved by locating prestressing tendons near the extreme fibers of the section to make them yield earlier. Also a larger ratio of introduced prestress to yield strength in a prestressing tendon may be used.
2. Shear behavior of the joint and slip deformation at the connection can be improved by having prestressing tendons at the center of the member section. They must remain within the elastic range. Thus, the ratio of introduced prestress to yield strength of the prestressing steel is kept small but the introduced prestress should be large enough to maintain the stiffness of overall assemblages.

A similar idea can be found in NZS 3101:1982 [9.1]:

"13.5.5.2 Except as provided by 13.5.5.3 the beam prestressing tendons which pass through joint cores shall be placed at the face of the columns so that at least one tendon is centred at not more than 150 mm from the beam top and at least one at not more than 150 mm from the beam bottom."

"C13.5.5.2 Such an arrangement of tendons results in more ductile plastic hinge behaviour of beams under inelastic cyclic loading than when the tendons are all concentrated at mid-depth in the beam. However, in addition to top and bottom tendons, it is desirable to have at least one tendon located within the middle third of beam depth to help carry the joint core shear force."

The reversed cyclic loading tests described in this chapter has been carried out in order to confirm the above ideas.

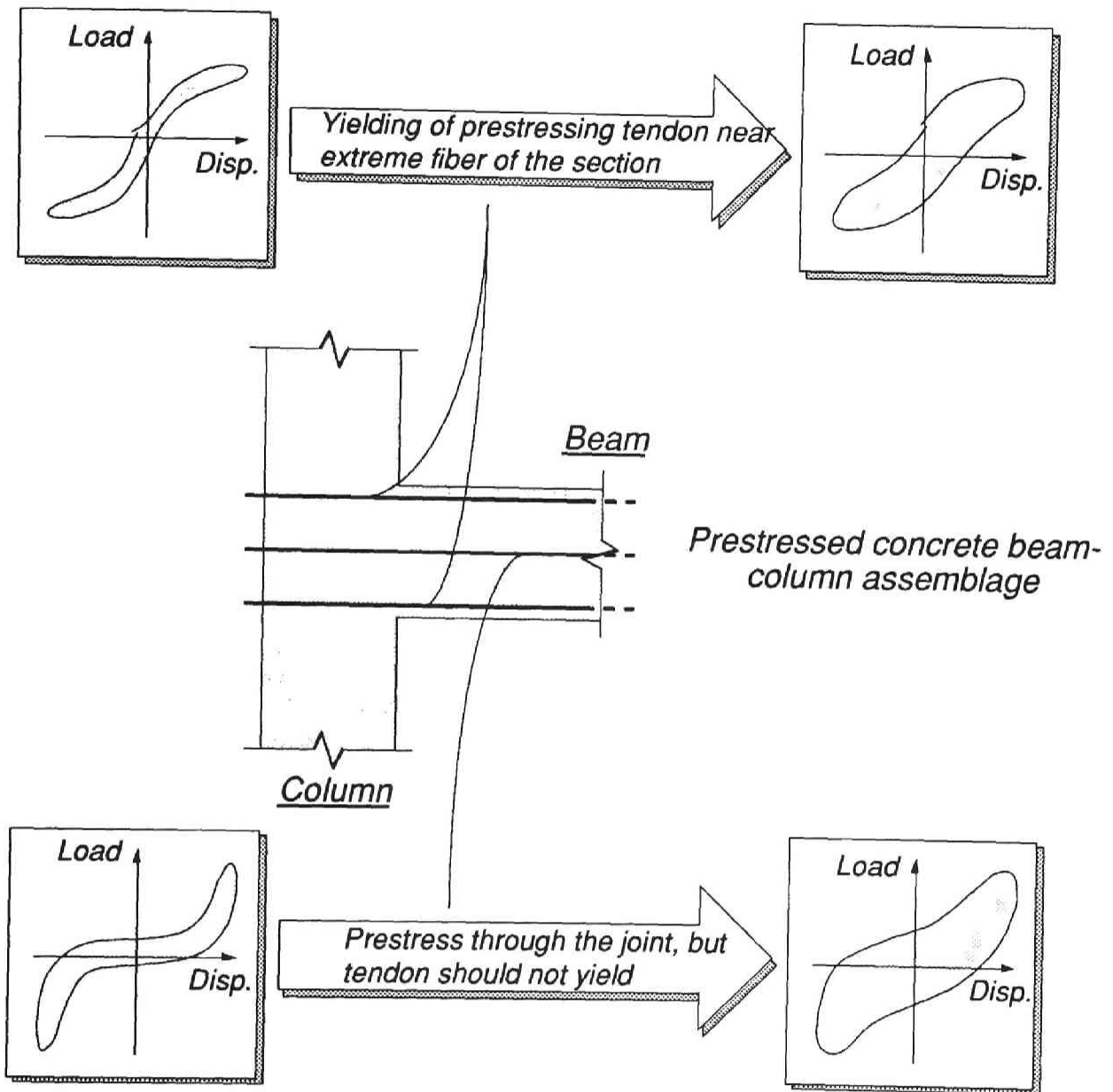


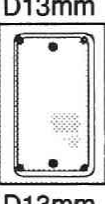
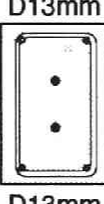
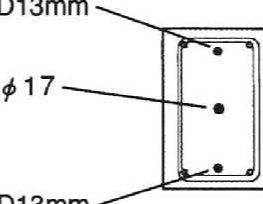
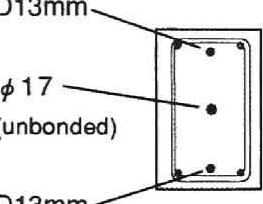
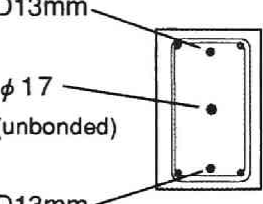
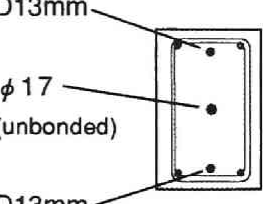
Fig.9.1 Procedure for improving seismic performance of precast prestressed concrete beam-column assemblages

9.2 Test program

9.2.1 Description of test units

Six precast prestressed concrete beam-external column joint assemblages were constructed. Those beams had total prestressing forces of 0.099, 0.095, 0.16, 0.131, 0.159 and 0.126 $f'_c \cdot A_g$. f'_c and A_g denote concrete compressive strength and gross sectional area of beam, respectively. Prestressing forces introduced to each prestressing tendon are given in Table 9.1. The Standard for Structural Design and Construction of Prestressed Concrete Structures published by the Architectural Institute of Japan (hereafter referred to as the AIJ Standard) [9.2] requires post-tensioning stress of at least 20 kg/cm^2 (1.96 MPa). In the case of the beam section in this test series the effective prestressing force should be greater than 117.7 kN. All test units satisfied the requirement.

Table 9.1 Specifications of test units

Specimen	PCX-1	PCX-2	PCX-3	PCX-4	PCX-5	PCX-6
Beam cross section						
Effective prestress of each prestressing tendon, P_e (kN)	89.59 (1.49)	86.85 (1.45)	88.95 (1.48)	89.25 (1.49)	88.85 (1.48)	79.44 (1.32)
(P_e / A_g) (MPa)	[0.049]	[0.0468]	[0.0489]	[0.0481]	[0.0489]	[0.0428]
$[P_e / A_g \cdot f'_c]$			114.6 (1.91)	57.63 (0.961)	108.71 (1.81)	49.90 (0.832)
A_g : gross area of beam section	89.49 (1.49)	89.1 (1.49)	[0.063]	[0.0311]	[0.060]	[0.027]
f'_c : compressive strength of concrete	[0.049]	[0.048]	86.5 (1.44)	89.69 (1.49)	87.92 (1.47)	87.72 (1.46)
			[0.0476]	[0.0484]	[0.0483]	[0.0473]
Total effective prestressing force, P_{et} (kN)	179.1 (2.98)	176.0 (2.933)	290.1 (4.83)	238.03 (3.97)	294.11 (4.90)	233.51 (3.89)
	[0.099]	[0.095]	[0.16]	[0.131]	[0.159]	[0.126]

The beam cross sections of the test units are shown in Table 9.1. PCX-1 and PCX-2 were the test units for investigating the effect of the location of prestressing steel bar in the beam section. The distances of prestressing tendons from the centroidal axis of the beams in PCX-1 and PCX-2 were 110 mm and 35 mm, respectively.

PCX-3 and PCX-4 had three tendons in the beam section. The prestressing force introduced into the prestressing tendon located at the centroid of the beam section was 114.6 kN for PCX-3 and 59.1 kN for PCX-4. In the case of PCX-3 it was almost as large as that required by the AIJ Standard. For PCX-4 it was half of the AIJ Standard requirement. Since those test units had the same prestressing tendons, the ratio of the introduced prestress to the nominal 0.2%-offset yield stress which was defined as a prestress index is 0.42 for PCX-3 and 0.21 for PCX-4.

PCX-5 and PCX-6 corresponded to PCX-3 and PCX-4, respectively excepting that PCX-5 and PCX-6 had an ungrouted tendon at the centroid of the beam section.

The precast beams were rested on the temporary supports until non-shrinkage mortar at the connections hardened, the ducts were grouted, the grout mortar reached enough strength to sustain the prestress and the prestress was introduced. The 15 mm-thick connections were filled with non-shrinkage mortar, whose compressive strength was 50.7 MPa at the time of testing. The stress-strain curve of the mortar was shown in Fig.9.2. This was done 33 days after casting 30.3 MPa concrete, that is, 19 days after casting 30.9 MPa concrete. The beams were post-tensioned to the columns and the ducts were grouted one week later. These operations were summarized in Table 9.2. The W/C of the grout mortar was 35%.

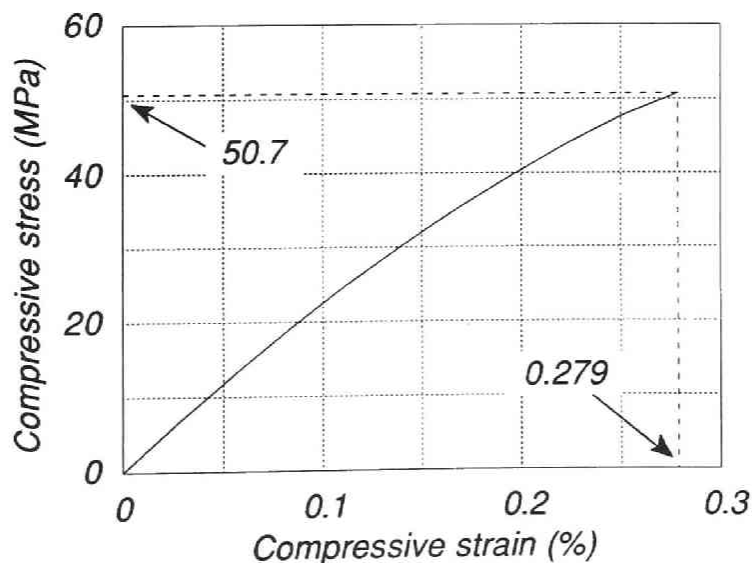


Fig.9.2 Stress-strain relationship of grout mortar for the connection

Table 9.2 Age of the test units

	PCX-1, PCX-3 and PCX-5 (days)	PCX-2, PCX-4 and PCX-6 (days)
Concrete casting	0	0
Non-shrinkage mortar cast in the connection	33	19
Post-tensioning and grouting	39	25
Tests	77	63

The longitudinal steel content was such that for each unit the flexural strength of the column section was greater than that of the beam section. Plastic hinging was expected to occur in the beams at the column faces. The mechanical properties of steel reinforcement are summarized in Table 9.3.

Prestressing tendons used in the test units were SBPR 95/120 whose nominal yield strength and tensile strength were 95 kg/cm^2 and 120 kg/cm^2 , respectively. The mechanical properties of prestressing steel bar are summarized in Table 9.4.

Table 9.3 Mechanical properties of steel reinforcement

	Yield strength (MPa)	Yield strain (%)	Modulus of elasticity (10^5 MPa)
D10 Beam non-prestressed longitudinal rebar	339.2	0.192	1.766
D19 Column longitudinal rebar	376.5	0.186	2.027
ϕ 9 Joint shear reinforcement	292.1	0.152	1.927

The centroidal tendon of PCX-3 was prestressed greater than that of PCX-4 and it was predicted to yield during cyclic loading while that of PCX-4 was expected to remain elastic. PCX-5 and PCX-6 were made because their ungrouted tendons were expected to remain elastic and not to lose prestress even at large ductilities.

Table 9.4 Mechanical properties of prestressing steel

	0.2% offset Yield stress (MPa)	Tensile strength (MPa)	Modulus of elasticity (10^5 MPa)
ϕ 17mm (SBPR95/120)	1166	1215	1.99
D13 mm (SBPD130/145)	1448	1400	2.02

Fig.9.3 shows overall dimensions of the six units tested. The dimensions were identical to the test units described in Chapter 4. The test units had a total column height of 1.9m and a total beam length of 1.85m measured from the column face. The column cross section was a 300mm square. The beam had a 200x300mm rectangular cross section.

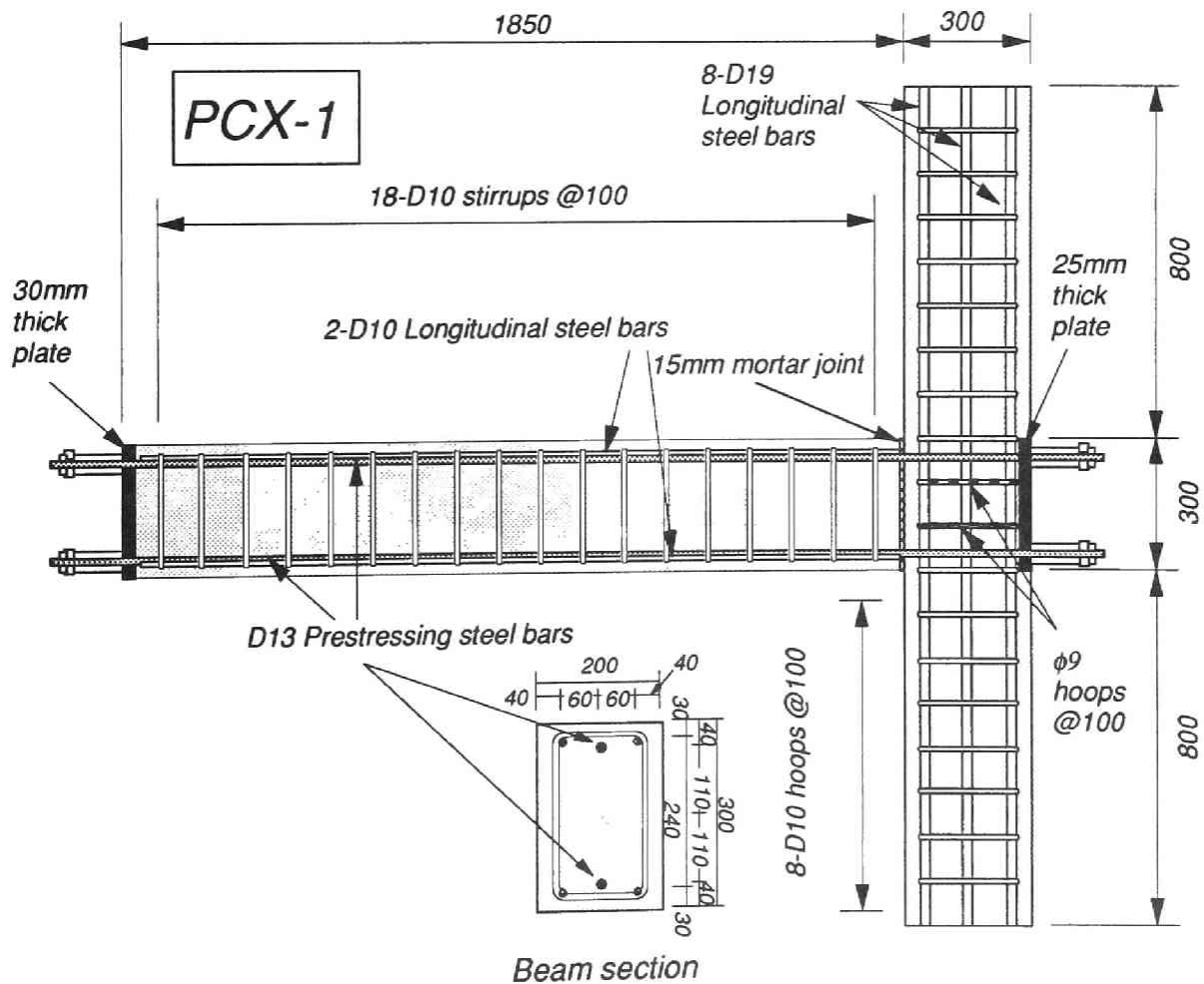


Fig.9.3(a) Test unit (PCX-1)

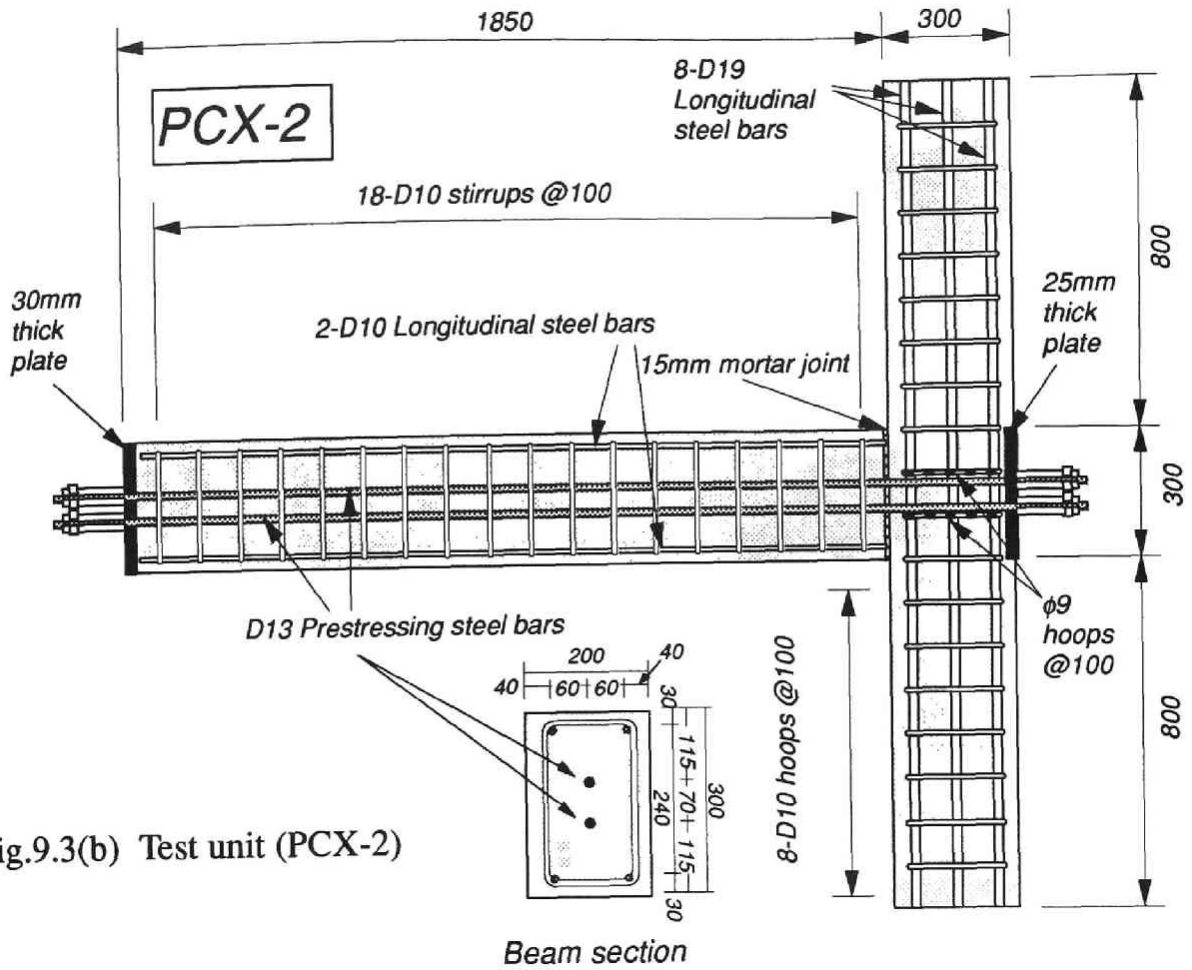


Fig.9.3(b) Test unit (PCX-2)

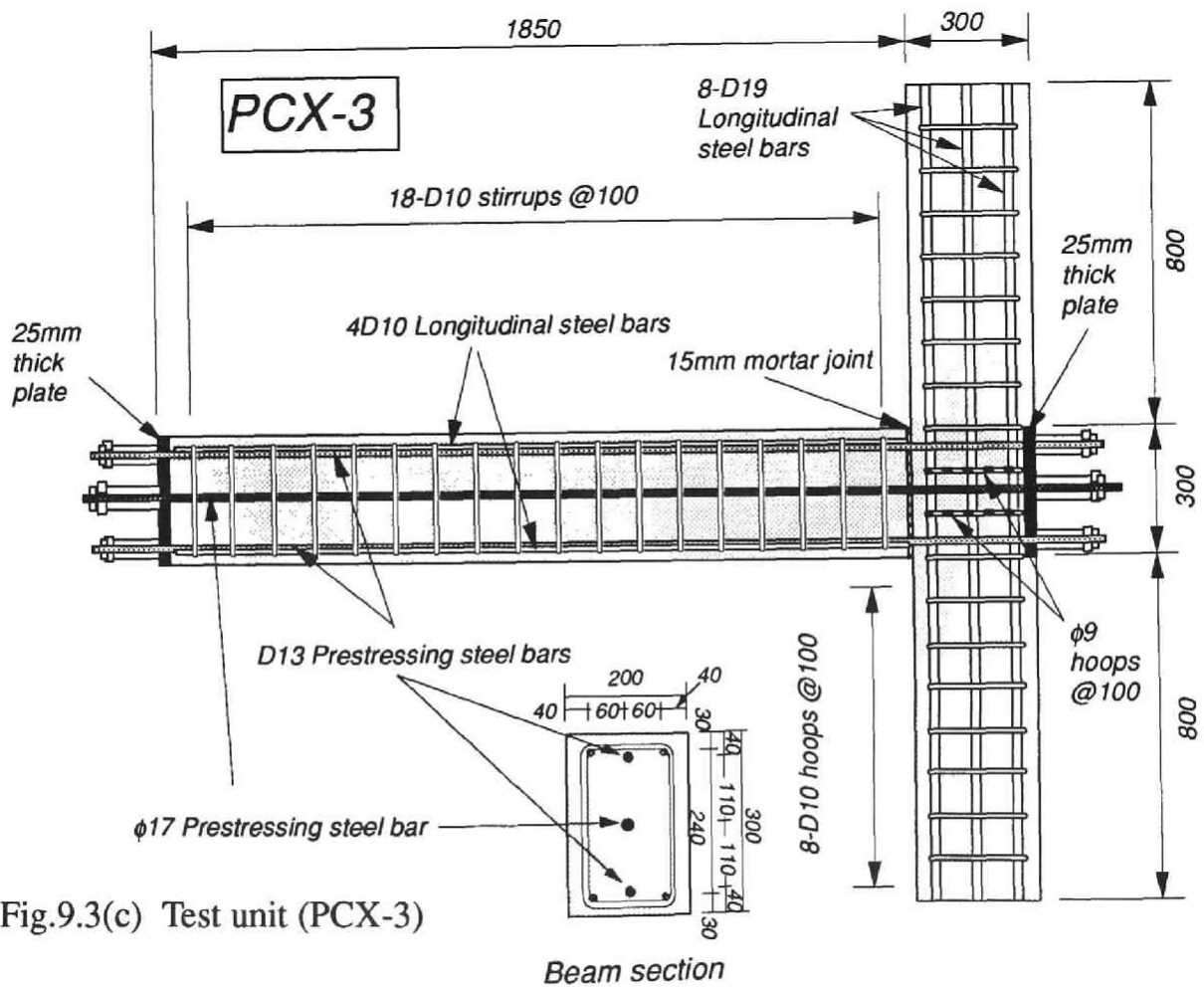


Fig.9.3(c) Test unit (PCX-3)

The mix design for the concrete used for the test units was:

25mm aggregate	...	986 kg/m ³
Sand	...	803 kg/m ³
Portland cement	...	350 kg/m ³
Water	...	175 liter/m ³
Superplasticizer	...	0.875 kg/m ³
Water / Cement ratio = 50%		

The compressive cylinder strength had reached $f'_c=30.3$ MPa for PCX-1, PCX-3 and PCX-5 at the stage of testing, that is, at the age of 77 days. For PCX-2, PCX-4 and PCX-6 it had reached $f'_c=30.9$ MPa at the age of 63 days. The mechanical properties of concrete and the non-shrinkage mortar are summarized in Table 9.5. The stress-strain curves obtained from compressive tests on concrete cylinders were illustrated in Fig.9.4. All units were cast vertically, compacted using vibrators, and were damp cured in the laboratory.

Table 9.5 Mechanical properties of concrete and grout mortar

Concrete	Compressive strength (MPa)	Strain at peak stress (%)	Initial modulus of elasticity (10 ⁴ MPa)
PCX-1, PCX-3 and PCX-5	30.3	0.233	2.29
PCX-2, PCX-4 and PCX-6	30.9	0.233	2.27
Non-shrinkage mortar	50.7	0.279	2.35

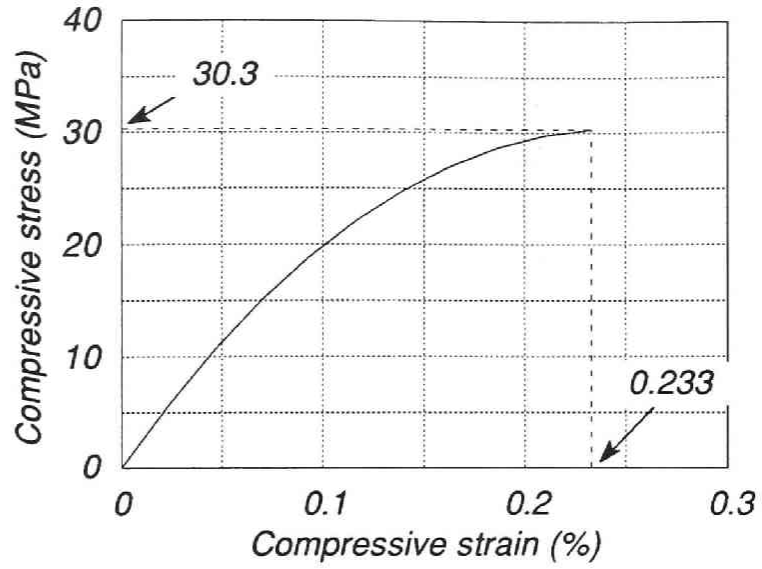


Fig.9.4(a) Stress-strain relationship of concrete for the test units PCX-1, PCX-3 and PCX-5

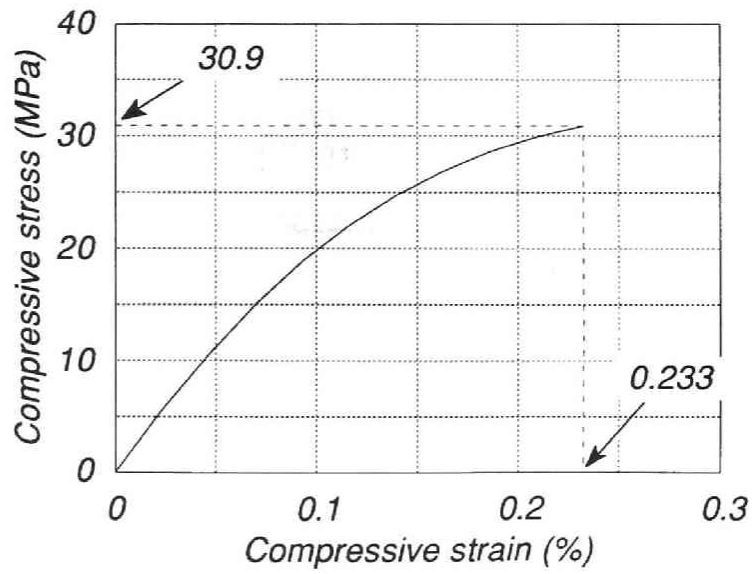


Fig.9.4(b) Stress-strain relationship of concrete for the test units PCX-2, PCX-4 and PCX-6

9.2.2 Joint induced shear force

Figure 9.5 shows the beam internal forces and the column shear force acting on the joint core when the ideal flexural strength of the beam develops. The maximum horizontal shear force, V_{jh} , occurs in the middle region of beam depth just below the neutral axis position of the beam section. V_{jh} is given by the following equation.

$$V_{jh} = P_1 + P_2 - V_{col} \quad (9.1)$$

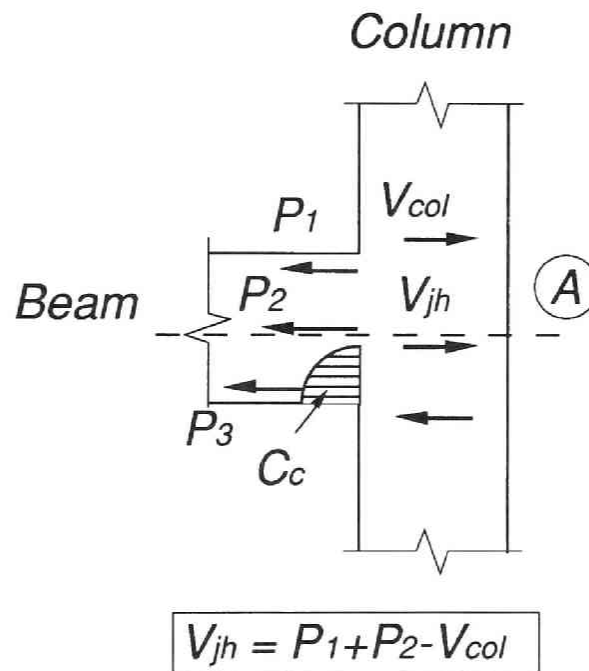


Fig.9.5 Beam internal forces and column shear acting on the joint

P_1 , P_2 , P_3 and V_{col} denote tensile force developed in prestressing steel bars and column shear force. Table 9.6 summarizes the neutral axis depth, the beam internal forces, the ideal flexural strength calculated using the ACI 318-89 [9.3] equivalent rectangular stress block as well as V_{jh} for each test unit.

9.2.3 Theoretical shear strength of joint cores

Table 9.7 summarizes the requirement for the maximum induced joint shear specified in NZS 3101:1982 [9.1], joint shear strengths according to ACI 318-89 [9.3] and to the AIJ Guidelines [9.4].

Table 9.6 Ideal flexural strength of the beams, theoretical internal forces in beams at flexural strength and maximum shear forces

Unit	n (mm)	C _c (kN)	P ₁ (kN)	P ₂ (kN)	P ₃ (kN)	M _{cal} (kNm)	V _{col} (kN)	V _{jh} (kN)
PCX-1	58.4	249.7	68.7	-	181.0	43.8	29.2	151.8
PCX-2	72.6	314.8	133.8	-	181.0	39.4	26.3	154.7
PCX-3	98.8	422.6	48.6	193.1	181.0	60.6	40.4	333.7
PCX-4	90.3	386.1	51.0	154.1	181.0	57.7	38.5	296.6
PCX-5	85.9	367.2	53.0	133.2	181.0	56.1	37.4	276.8
PCX-6	70.5	306.0	50.4	74.6	181.0	51.3	34.2	221.3

Note:

- n : Neutral axis depth
- C_c : Resultant compressive force in concrete
- C_s : Compression force in non-prestressed compression rebar
- P_s : Tensile force in prestressing steel bar
- T_s : Tensile force in non-prestressed tensile rebar
- M_{cal} : Theoretical maximum moment calculated using the equivalent stress block specified in ACI318-89
- V_{col} : Shear force in column
- V_{jh} : Theoretical maximum applied horizontal shear force

Table 9.7 Maximum input joint shear force and joint shear strengths

Unit	V _{NZS} (kN)	V _{ACI} (kN)	V _{AIJ} (kN)
PCX-1	743.1	495.4	313.6
PCX-2	750.4	500.3	319.8
PCX-3	743.1	495.4	313.6
PCX-4	750.4	500.3	319.8
PCX-5	743.1	495.4	313.6
PCX-6	750.4	500.3	319.8

Note:

$$V_{NZS} : 1.50 \sqrt{f'_c} \cdot A_j \text{ (NZS 3101:1982)}$$

$$V_{ACI} : 1.00 \sqrt{f'_c} \cdot A_j \text{ (ACI 318-89)}$$

$$V_{AIJ} : 0.18 \cdot f'_c \cdot A_j \text{ (AIJ Guideline)}$$

where f'_c : compressive strength of concrete (MPa) and A_j : specified cross-sectional area of the joint (mm²)

9.2.4 Details of steel in beam-column joint

The transverse steel in each joint core consisted of two rectangular column hoops which were placed around the longitudinal column bars between the top and bottom layers of longitudinal beam steel. The average spacing between the tie centers was 100mm. The two ties were formed from 9mm diameter round bar with a yield strength of 292 MPa.

9.2.5 Loading

The unit was rotated by 90 degree and set in the loading rig as shown in Fig.9.6. A horizontal load was applied at the end of the beam representing shear induced by seismic loading. The ends of the column were held on the same horizontal line between the pin and roller supports during the test and the applied beam load induced reactive shears at the ends of the column. By reversing the direction of the horizontal beam load, the effect of earthquake loading was simulated.

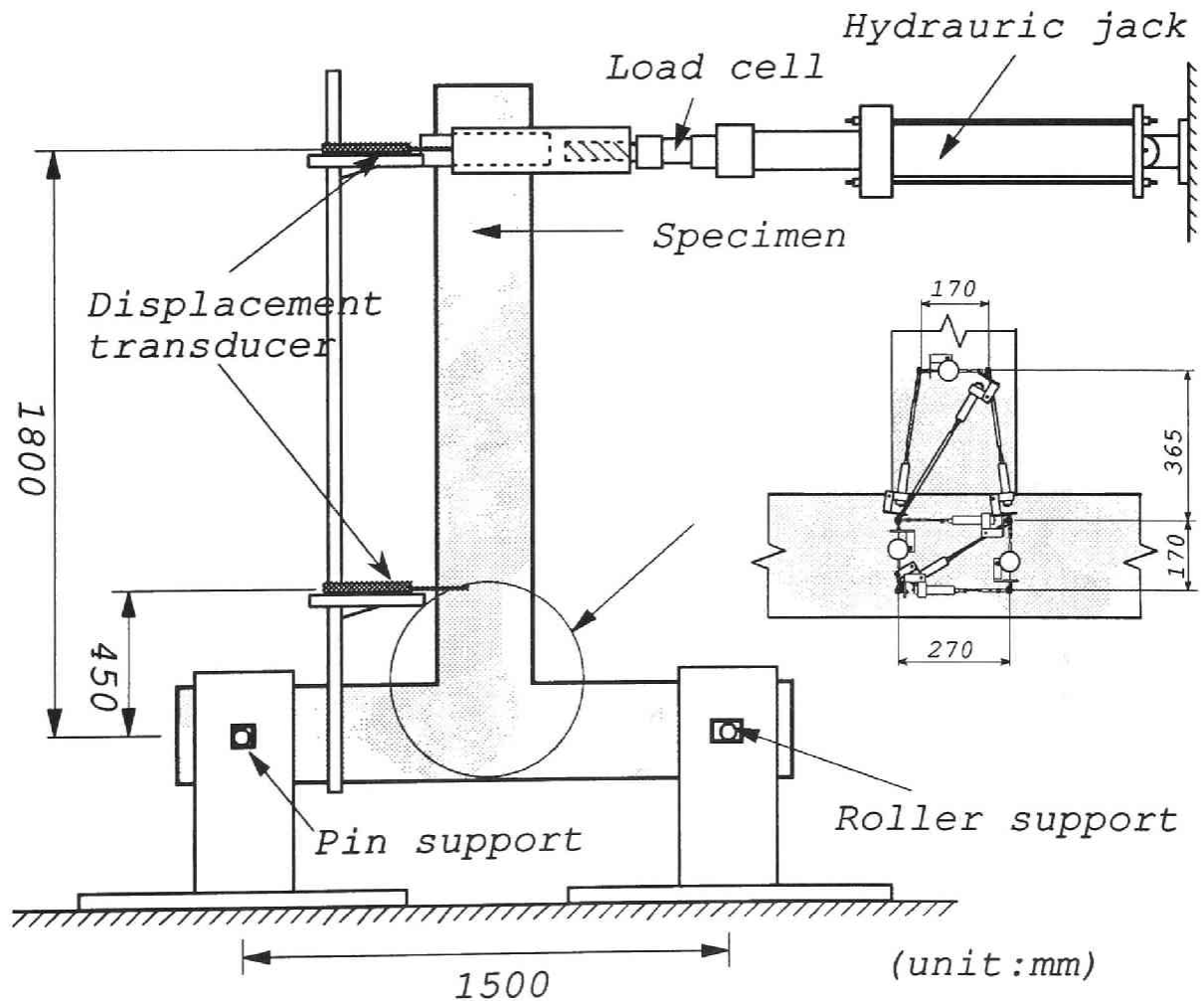


Fig.9.6 Loading setup and measuring devices

The first loading cycle was up to the beam rotation angle of $1/200$, and this was followed by a series of deflection controlled cycles in the inelastic range comprising two full cycles to each of the beam rotation angles of $\pm 1/100$, $\pm 1/50$, $\pm 1/33$, $\pm 1/25$ and $\pm 1/20$ rad. This loading sequence was unlike the test series in the preceding chapters was adopted because it was expected that definite yielding was not observed.

9.2.6 Measurements

The beam end deflection was measured by a linear displacement transducer which was attached to the pole fixed to the mid-height of the column as shown in Fig.9.6. The deflection consisted of the deformation of the beam, joint and column of half-height. It did not include the column deformation between the pin support and the place to which the measuring pole was fixed. No visible crack could be found in this part of the column and the deformation of this part was considered to be small enough to be disregarded. Curvature and shear deformation of the beam in the potential plastic hinge region and shear distortion of the joint core were measured and calculated from the readings of the linear displacement transducers attached to the units as shown in Fig.9.6 by the calculation method described in Chapter 4.3.

Strain gauges were attached to the joint transverse reinforcement on both sides of the column.

9.3 Test results

9.3.1 General behaviour of test units

Figure 9.7 (a)-(f) show the horizontal deflection at the end of the beam plotted against the corresponding load of the beam for each unit. All test units were able to be loaded to a beam rotation angle of $1/20$ rad. with little reduction in stiffness and strength. They indicated the load - displacement hysteresis loops with small residual displacement at zero load, which is typical for post-tensioned precast concrete subassemblages. Fig.9.8 (a)-(f) show the test units after testing.

9.3.2 Location of Prestressing tendons (PCX-1 vs. PCX-2)

Little difference between the load - displacement curves of PCX-1 and PCX-2 was observed. Since prestressing tendons were located near the extreme fibers of the section in PCX-1 and the tendon stress was larger than that of PCX-2, the maximum load resistance of PCX-1 was 13 % larger than that of PCX-2. Tendon stress will be discussed later in this Chapter.

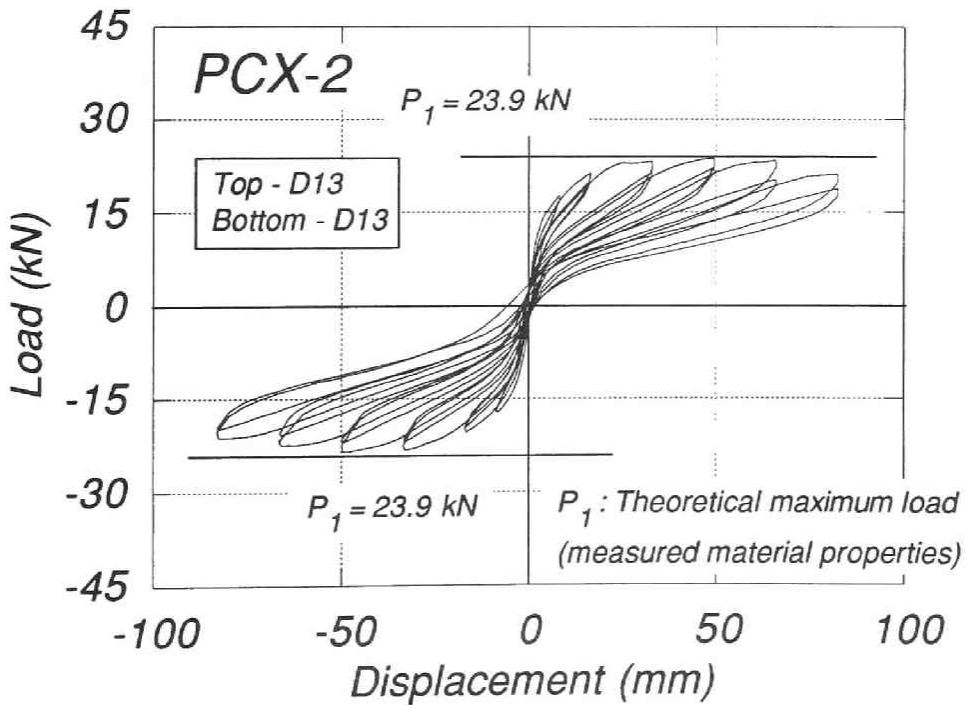
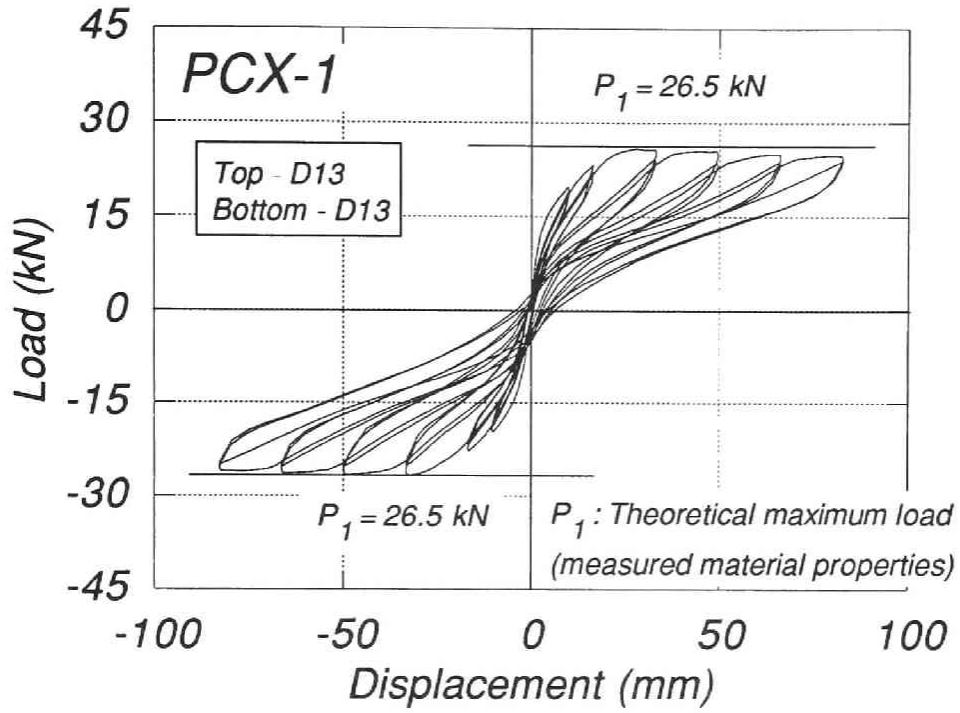


Fig.9.7(a) Horizontal load - deflection relationships at the beam ends

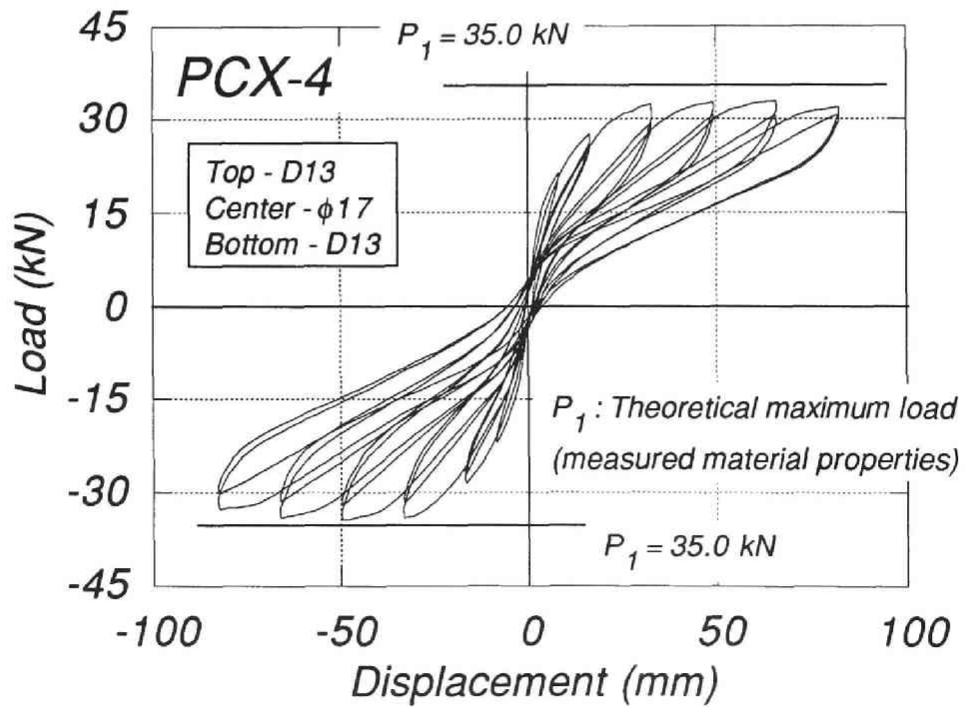
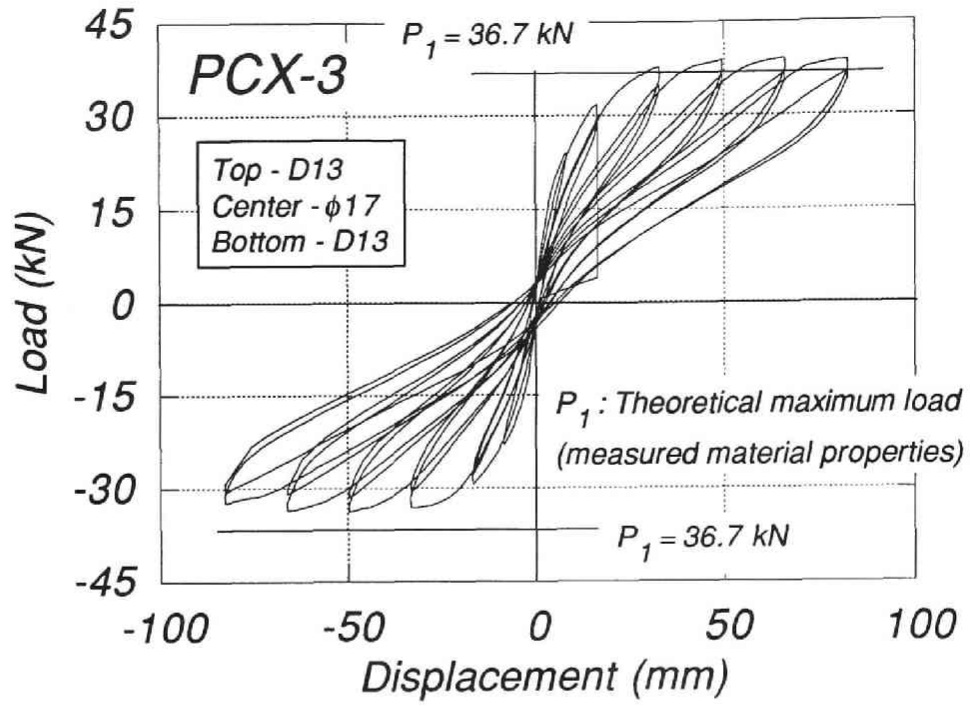


Fig.9.7(b) Horizontal load - deflection relationships at the beam ends

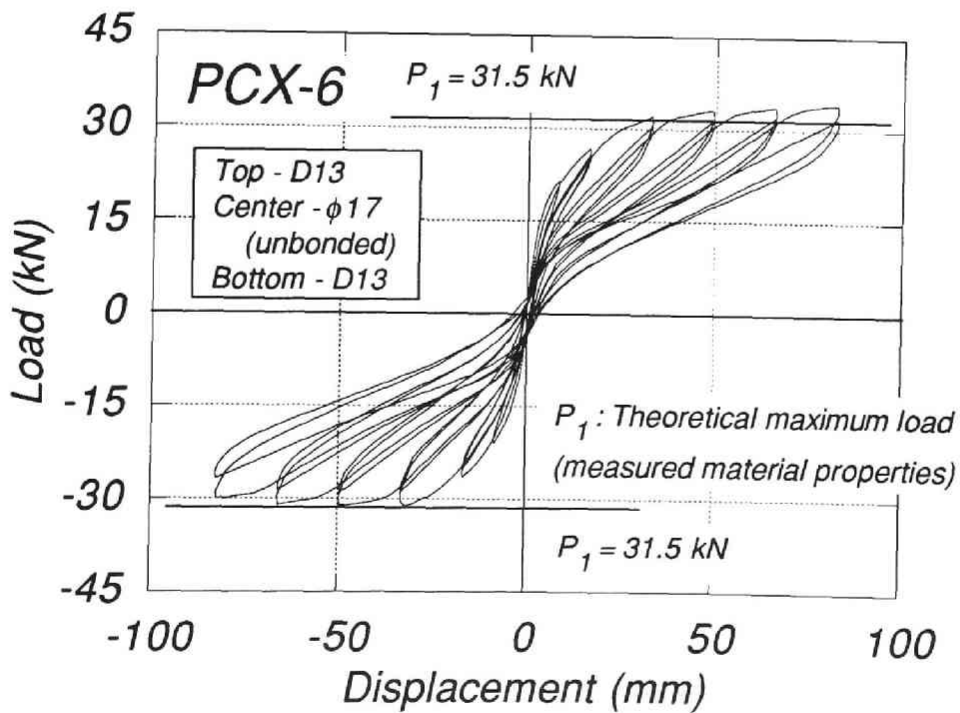
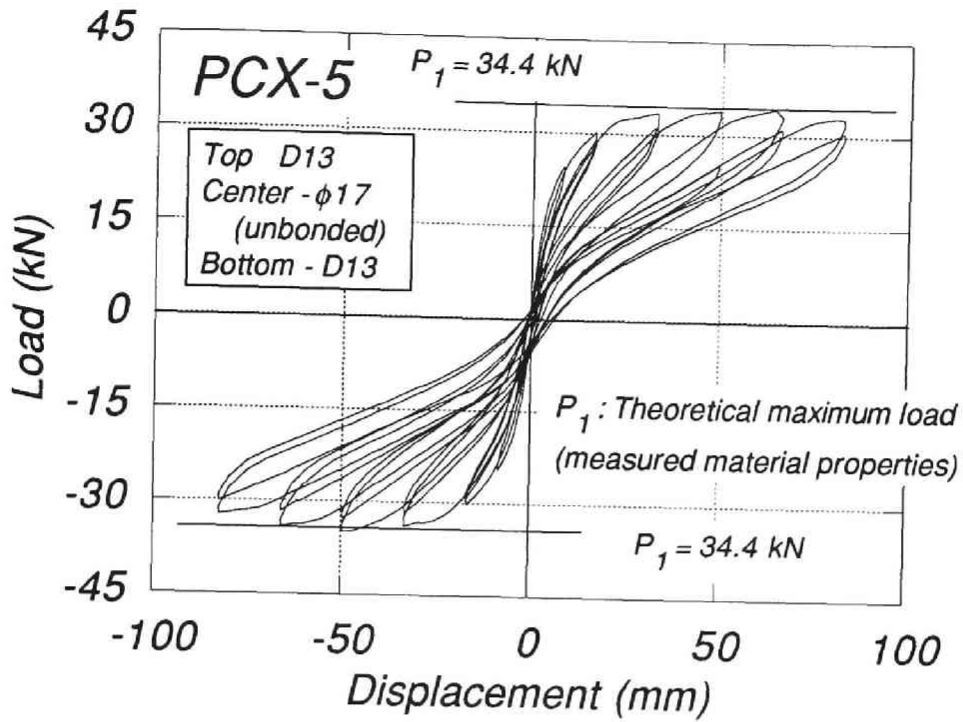


Fig.9.7(c) Horizontal load - deflection relationships at the beam ends

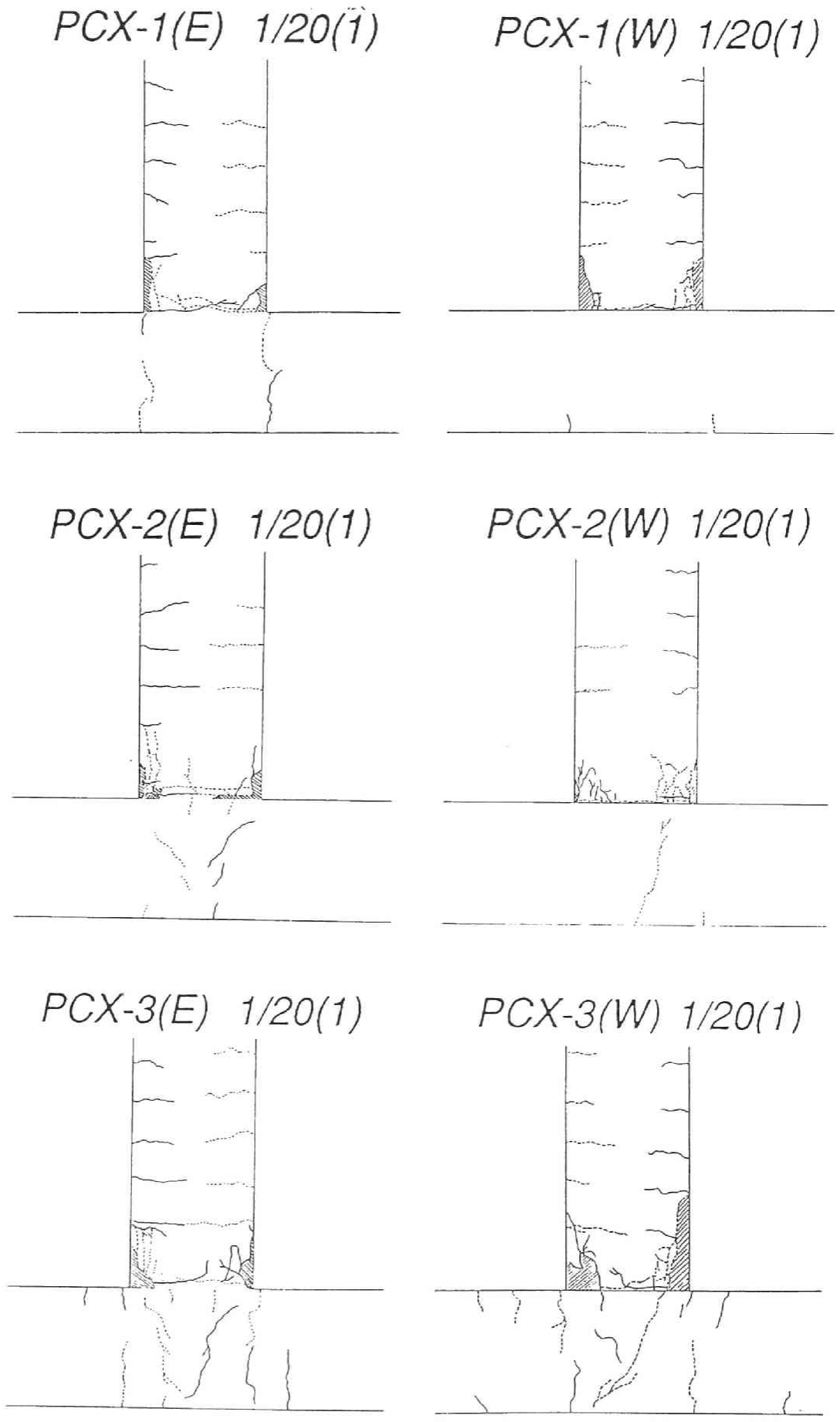


Fig.9.8(a) Test units after testing

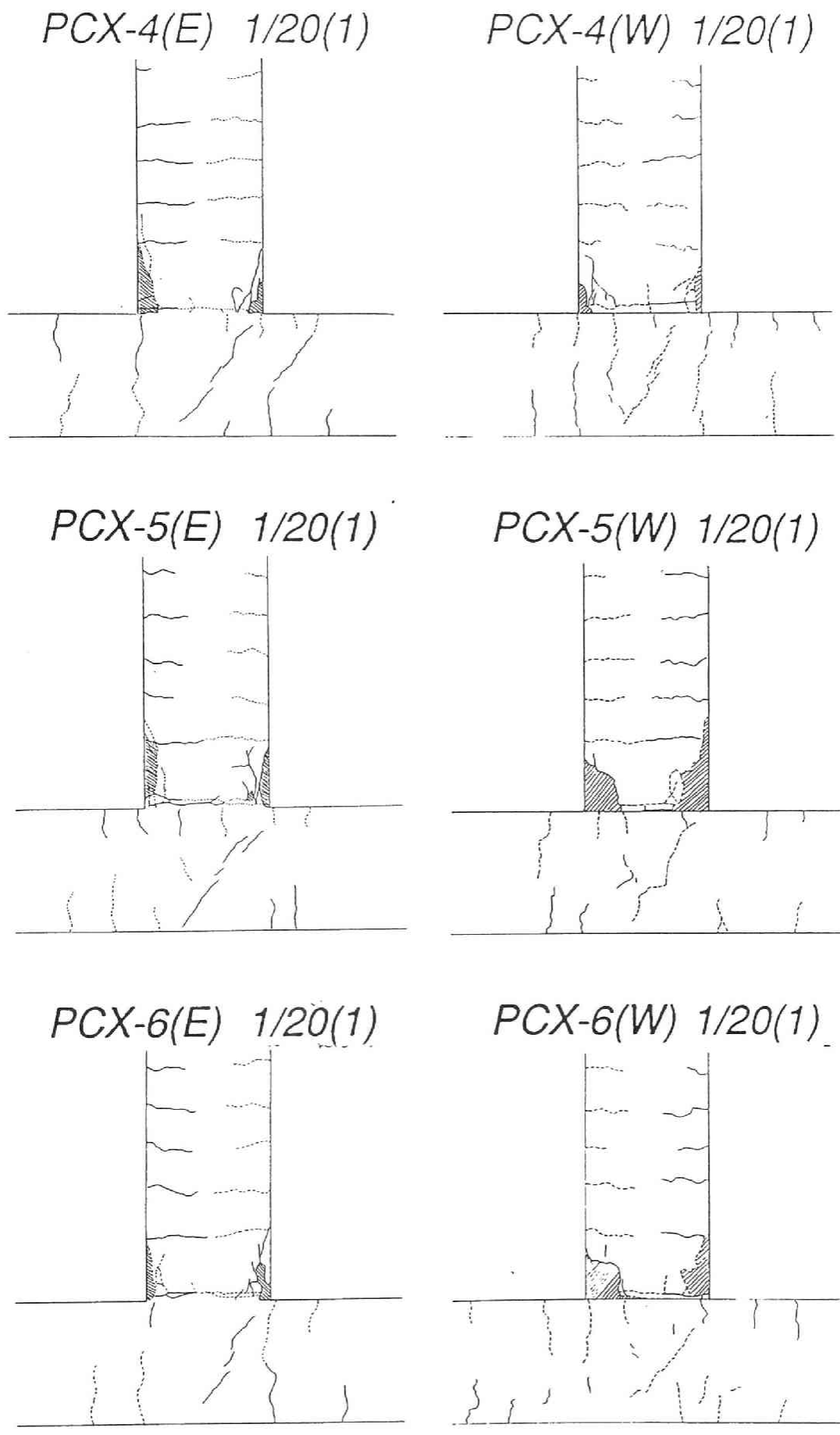


Fig.9.8(b) Test units after testing

9.3.3 Prestress introduced into the prestressing tendon at the center of the section

(PCX-3 vs. PCX-4)

Fatter hysteresis loops were expected in PCX-4 than in PCX-3 because the prestressing tendon at the center of the beam section of PCX-4 was expected to yield and lose its prestress. However, little difference between the load - displacement curves between the above test units was observed. This is mainly because of the bond deterioration between the concrete and the prestressing steel bar. This will be discussed further in the next section. The maximum load capacity of PCX-3 is 14 % larger than that of PCX-4. This is because a higher tensile stress was sustained by the tendon located at the center of the beam section.

9.3.4 Grouted and ungrouted tendons

(PCX-3 vs PCX-5 and PCX-4 vs PCX-6)

The maximum load capacities of PCX-5 and PCX-6, whose centroidal tendon was ungrouted were a little smaller than those of PCX-3 and PCX-4. Table 9.8 summarizes the maximum load capacity of each test unit experimentally and theoretically obtained. The theoretically obtained values are based on the ACI 318-89 methods. The tensile stress assumed for the ungrouted tendon was obtained using Eq.18.4 in Chapter 18 of ACI 318-89 code provisions.

$$f_{ps} = f_{se} + 67.8 + \frac{f'_c}{100\rho_p} \quad (9.1)$$

where, f_{ps} : stress in prestressed reinforcement at nominal strength, MPa

f_{se} : effective stress in prestressed reinforcement (after allowance for all prestress losses), MPa

f'_c : compressive strength of concrete

ρ_p : ratio of prestressed reinforcement = $\rho_p = \frac{A_{ps}}{bd_p}$

A_{ps} : area of prestressed reinforcement in tension zone, mm^2

b : width of compression face of member, mm

d_p : distance from extreme compression fiber to centroid of nonprestressed tension reinforcement, mm

The grouted tendons were assumed to have the same strain that the concrete at the same location. Concrete strain was obtained on the basis of the assumption that plain sections remain plain after bending. The load capacities theoretically obtained agreed well with the experimentally obtained values. However, the maximum measured

Table 9.8 Maximum load capacities experimentally and theoretically obtained

Specimen	PCX-1	PCX-2	PCX-3	PCX-4	PCX-5	PCX-6
Maximum load capacity (kN) (Experiment)	26.6	23.6	39.1	34.4	34.9	34.2
Maximum load capacity (kN) (ACI 318-89)	26.5 (1.00)	23.9 (0.99)	36.7 (1.07)	35.0 (0.98)	34.0 (1.03)	31.1 (1.10)

tensile force in the ungrouted tendon was 165.7 kN for PCX-5 and 118.7 kN for PCX-6. They were much larger than those obtained by Eq.9.1: 133.2 kN for PCX-5 and 74.6 kN for PCX-6. When the maximum moment capacity was attained, the tendon force was 147.1 kN for PCX-5 and 118.7 kN for PCX-6. The large difference in the tensile force in the ungrouted tendon did not result in a large difference in the load capacity because the ungrouted tendon was located at the center of the section and did not have significant influence on the load capacity.

9.3.5 Tensile stress of tendon

Figure 9.9 shows the fluctuation of the tensile forces in the prestressing steel bars measured by load-cells at both ends of the tendons. However, only the tensile forces measured at the anchorage ends on the column are shown in the figures. Because of the bond stress between concrete and the bar, they did not represent the tensile forces developed in the prestressing steel bars at the beam critical section. However, they are assumed to give a good estimation of the maximum tensile forces because the bond deterioration between concrete and the prestressing steel bars is likely to occur during the early stage of inelastic load excursion.

The maximum tensile forces measured in the tendons located at the center of the beam section were 180.1 kN for PCX-3 and 120.0 kN for PCX-4. They were well below the yield strength of 275.8 kN. According to the objectives of this test series, the prestressing tendon at the mid-height of the beam section of PCX-3 was expected to yield and the post-tensioning force connecting the beam and the column was expected to deteriorate. However, the ratio of the introduced prestress to the yield strength of the tendon was so small and bond between concrete and prestressing steel bar deteriorated so easily that the tendon stress of PCX-3 did not reach the yield stress that was predicted by the preliminary section analyses.

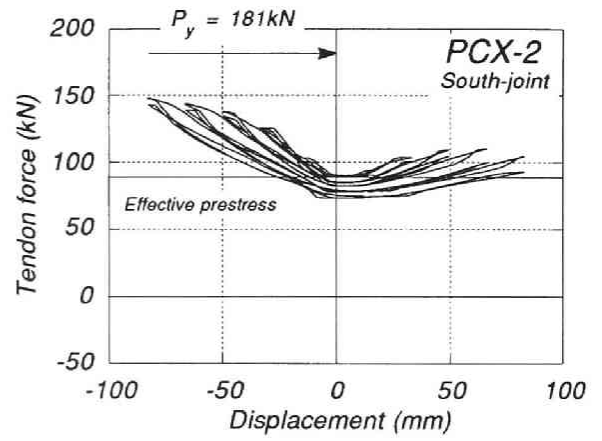
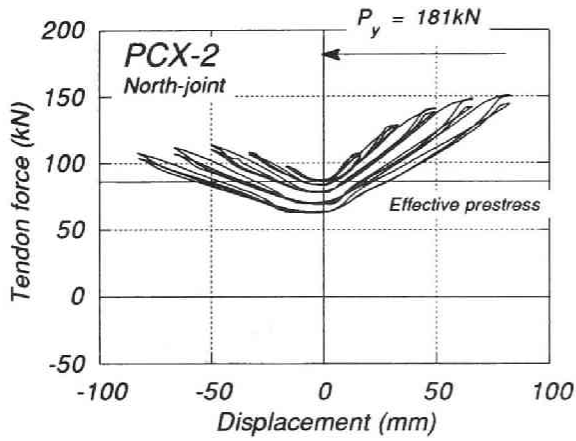
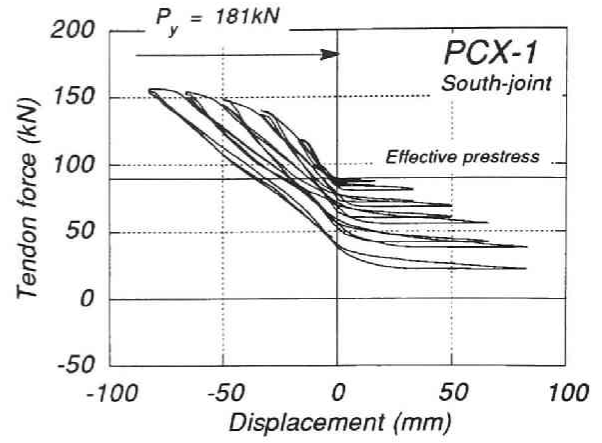
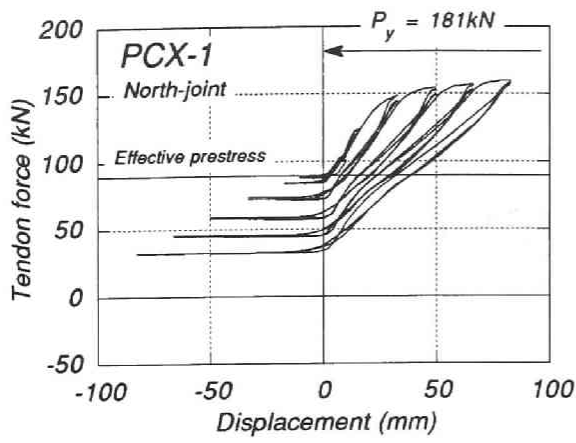


Fig.9.9(a) Tendon force measured at the column side - deflection at the beam ends relationships

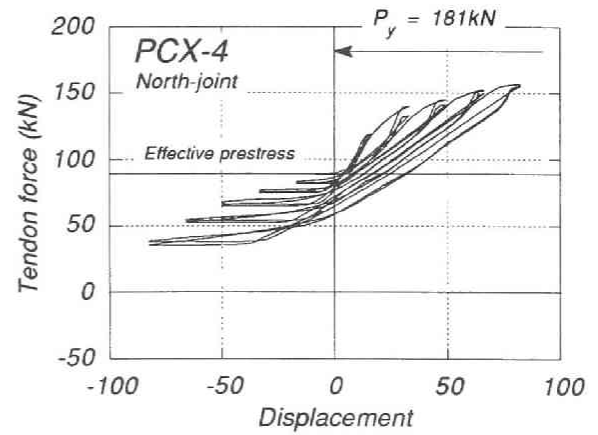
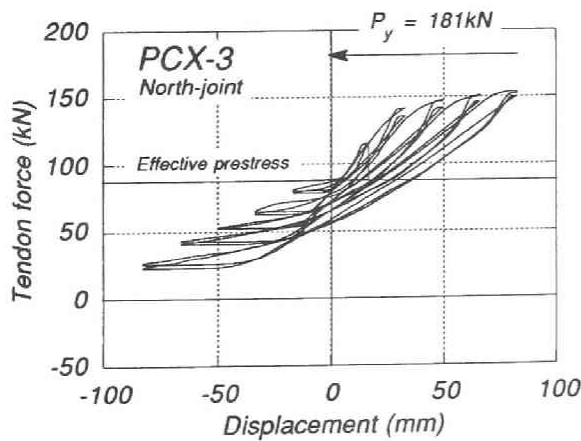
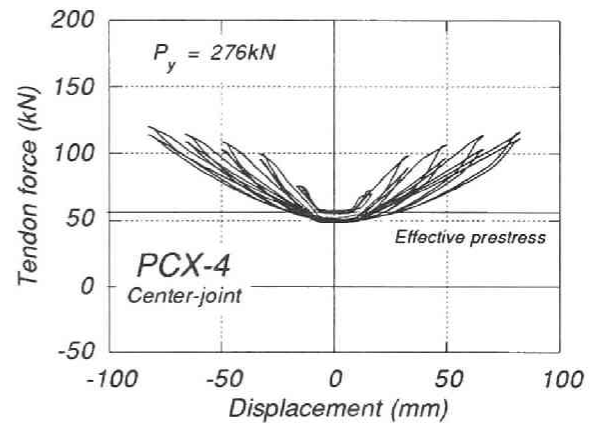
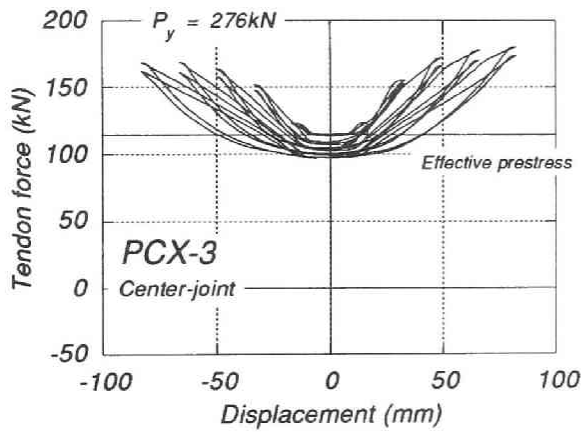
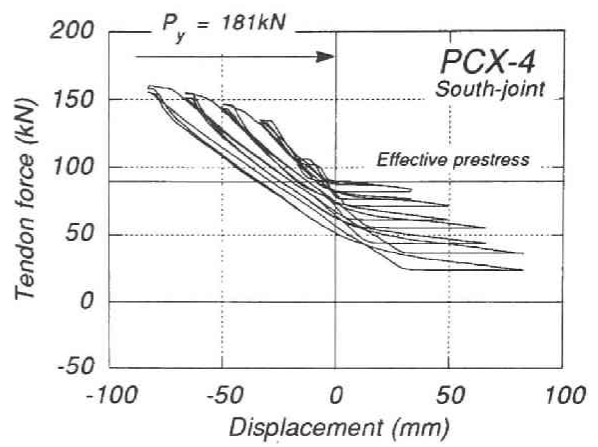
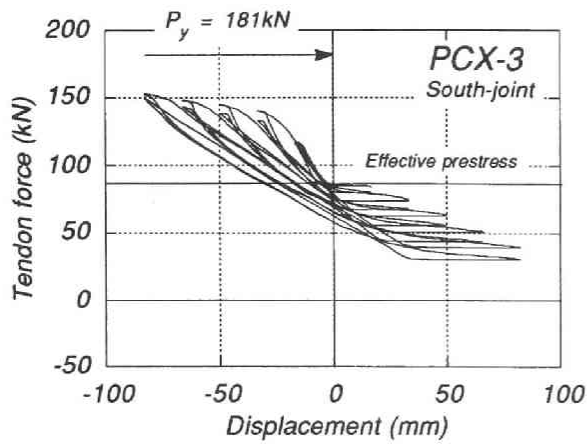


Fig.9.9(b) Tendon force measured at the column side - deflection at the beam ends relationships

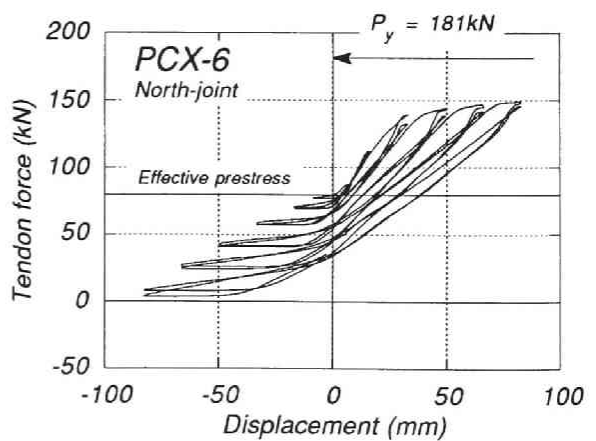
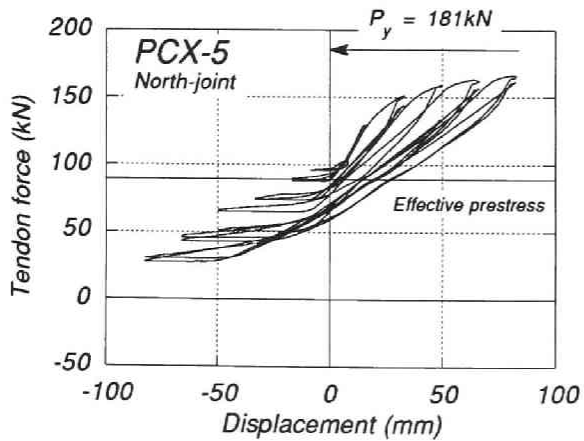
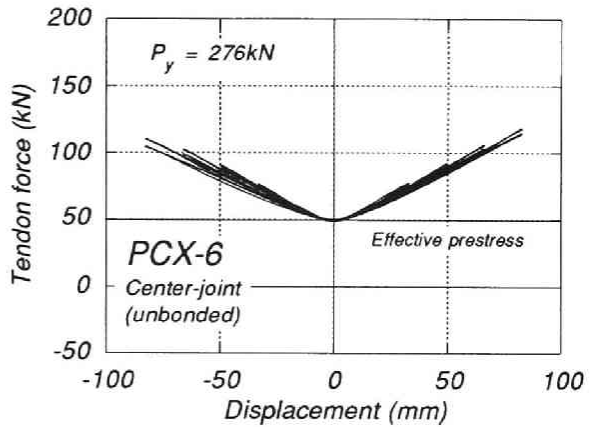
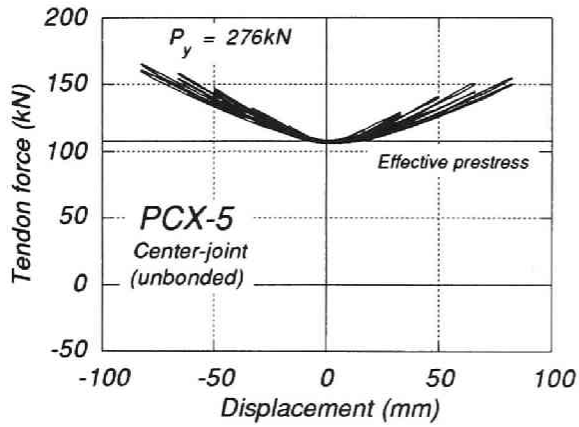
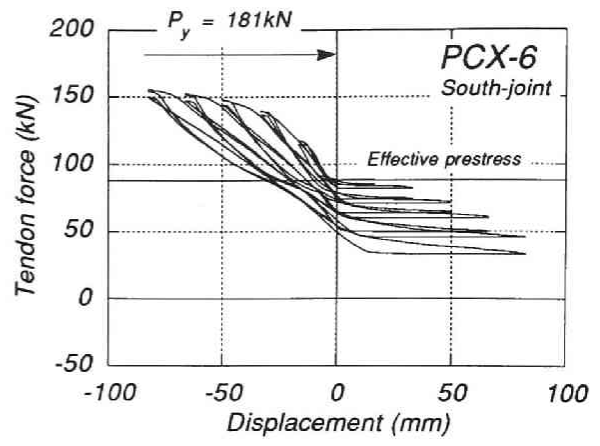
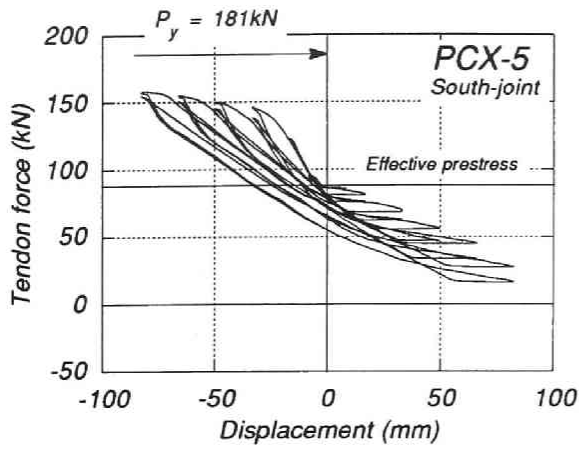


Fig.9.9(c) Tendon force measured at the column side - deflection at the beam ends relationships

The tendons provided near the extreme fibers of the beam section were also predicted by the preliminary section analyses to reach the yield stress. However, as far as the tendon stresses measured at the load-cells were concerned, they did not reach the yield stress. This is because of bond deterioration between concrete and the prestressing steel bars in the preliminary section analyses assumed no slip between the concrete and the prestressing steel was assumed.

9.4 Conclusions

On the basis of the test results described in Chapter 9 the following conclusions are derived.

1. In order to improve the seismic performance of precast prestressed concrete buildings two attempts have been made in this study:
 - (a) The energy absorbing capability can be improved by forcing prestressing tendons located near the extreme fibers of the member section to yield. This can be realized by larger ratio of introduced prestress to yield strength of a prestressing steel tendon.
 - (b) Shear behavior of the joint and slip deformation at the connection can be improved by placing prestressing tendons at the center of the member section. They must remain within the elastic range. Thus, the ratio of introduced prestress to yield strength of the prestressing steel is kept small but the introduced prestress should be large enough to maintain stiffness of overall assemblages.
2. Because of poor bond between the concrete and prestressing steel, stresses in the prestressing tendons did not reach the yield stress at the critical section of the beam. Thus, the performance which was expected was not confirmed.
3. An ungrouted tendon at the center of the beam section was used to keep post-tensioning force large enough to maintain uniformity of the whole assemblage. However, because of the same reason above the effect on the seismic performance of the test units was not observed.
4. If a prestressing strand with better bond characteristics had been used, a different result might have been obtained.

[References]

- 9.1 Code of Practice for the Design of Concrete Structures NZS 3101 Part 1 : 1982, and Commentary NZS 3101 Part 2 : 1982, Standard Association of New Zealand.
- 9.2 Standard for Structural Design and Construction of Prestressed Concrete

Structures, Architectural Institute of Japan, 1988.

- 9.3 Building Code Requirements for Reinforced Concrete (ACI318-89) and Commentary (ACI318R-89), 1989.
- 9.4 Design Guideline for Earthquake Resistant Reinforced Concrete Buildings Based on Ultimate Strength Concept, Architectural Institute of Japan, 1988.

Chapter 10

MAJOR CONCLUSIONS AND RECOMMENDATIONS FOR FUTURE RESEARCH

10.1 Major conclusions

Concluding remarks regarding the results from the study undertaken have generally been given at the end of each chapter. They are summarized again as follows:

Chapter 2

The current seismic design procedure for prestressed concrete buildings in Japan was summarized. The design procedure is complicated because of the options which a designer may choose.

The following aspect of the design of prestressed concrete buildings were described and compared with those for reinforced concrete buildings:

in NZS 4203:1984, the structural material factor M for prestressed concrete is 25% larger than that for reinforced concrete. However, this does not necessarily lead to 25% greater design seismic load. As shown in the section on the comparison of the seismic design loads, the design seismic load required for a prestressed concrete building may be smaller than that for an equivalent reinforced concrete building because of the longer period of vibration of the prestressed concrete building.

Chapter 3

1. Moment - curvature relationships of prestressed, partially prestressed and reinforced concrete beam sections were compared in terms of yield curvature, ultimate available curvature and ductility ratio as well as a whole shape of the curves.
2. The analytical procedure for obtaining moment - curvature relationships of prestressed, partially prestressed and reinforced concrete sections based on stress - strain relationships of constitutive materials was described.

Chapter 4

The following conclusions were derived from the test results reported in Chapter 4.3 on the prestressed concrete beam-column subassemblages with various locations of prestressing steel bars.

1. It has been pointed out by past research that reinforced concrete members are superior to prestressed concrete with respect to energy dissipation and deformability. However, this conclusion was obtained from the tests on prestressed concrete beams. In the case of a beam-column subassemblage, its behaviour may be largely dominated by the performance of the jointing part. Thus, hysteresis loops of a prestressed concrete beam-column subassemblage might be better than those of a reinforced concrete because prestress introduced into the beam can improve the shear behaviour of the beam-column joint core. This was confirmed by the cyclic loading tests on prestressed concrete beam-column subassemblages.
2. Larger prestress has more beneficial effect on the shear behaviour of a beam-column joint core unless it is excessive. However, it also results in crushing and spalling of the unconfined cover concrete and buckling of non-prestressed compression reinforcement of the beam in the earlier stage of the loading. Besides, larger prestress results in larger compressive strain of concrete and it may lead to the deterioration of the concrete due to reversed cyclic loading.

The following conclusions were derived from the test results reported in Chapter 4.4 on the prestressed and reinforced concrete beam - column joint assemblies which had the same dimensions, moment capacities of the beams and anchorage detailing of beam longitudinal reinforcement.

1. The hysteresis loops obtained from the test results of the reinforced concrete test unit indicated reduction in capacity and pinching due to bond deterioration of beam longitudinal reinforcement followed by pulling out of reinforcement. Conversely, the prestressed concrete test units showed much better hysteresis loops even in the large ductilities. However, larger prestressing force resulted in spalling and crushing of cover concrete and buckling of beam longitudinal reinforcement.
2. Until the ductility factor of 2 (beam rotation angle of approximately $1/30$), the equivalent viscous damping for all test units were almost the same. Past research has pointed out that there is less energy dissipation of prestressed concrete than reinforced concrete members. However, including beam - column joints the experimental results revealed this is disputable when prestressing force is not excessive. As the loading cycles progressed, the equivalent viscous damping in RCB-1 decreased to less than that of the ductility factor of 2 while in the

prestressed concrete test units the equivalent viscous damping increased proportionally with the ductility factor.

3. Small amount of prestressing force caused a much smaller shear distortion angle and a much stiffer joint core than in the reinforced concrete joint. However, a prestressing force larger than $0.12 f'_c A_g$ resulted in a small shear distortion angle and stiff joint core as the prestressed concrete unit with a prestressing force of $0.06 f'_c A_g$.
4. In order to predict the seismic response of reinforced concrete frames as closely as possible, the shear behaviour of beam - column joints needs to be idealized and incorporated in the analysis. Besides, it is necessary to consider bond deterioration of beam longitudinal reinforcement in the idealization of the behaviour of beam plastic hinge regions. However, the assumption of rigid beam - column joint core can be justified in the prestressed concrete beam - column joint assemblies. Moment - curvature hysteresis loops in beam plastic hinge regions can be idealized based on the analyses assuming that plane sections before bending remain plane after bending. Thus, from the view point above, the past research which indicated larger responses of prestressed concrete frame structures than those of reinforced concrete should be re-examined.
5. The ratio of the total tensile force in the prestressed concrete units to that in the reinforced concrete test units measured at a ductility factor of 3 was almost as large as the ratio of moment capacity carried by non-prestressed reinforcing steel to the total moment capacity resisted by non-prestressed and prestressed reinforcement.
6. To consider the beneficial effect of prestressing force on beam - column joint cores, their shear strength V_{ju} should be increased as the prestress level increases based on the assumption of NZS 3101:1982 [4.8] that part of shear force is attributed to the effective prestressing force.

Anchorage placed in beam - column joint core are common practice in Japan while the prestressing steel in the test units were anchored to the anchorage plate on the outer side of the column. NZS 3101:1982 [4.8] prohibited anchorages kept in beam - column joint cores. More research on this matter should be carried out.

Chapter 5

On the basis of the above analytical study, the following conclusions are reached with regard to the idealization of prestressed, partially prestressed and reinforced concrete moment - curvature relationships:

1. By modifying the idealization suggested by Thompson and Park [5.1], the idealization of prestressed, partially prestressed and reinforced concrete moment - curvature relationships was proposed by the author on the basis of the experimental work and the analytical work. The idealization curves can be applied from fully prestressed concrete to reinforced concrete members.
2. The idealization was compared with the experimental results described in Chapter 4. It turned out that the moment - curvature curves obtained experimentally can be well predicted by the idealization. However, all the test units consisted of partially prestressed concrete beams. The idealization should undergo many trials because only a few experimental results of partially prestressed concrete beam - column joint assemblages available were used to calibrate it.
3. Some examples of idealized moment - curvature characteristics for fully prestressed, partially prestressed and reinforced concrete sections under reversed cyclic loading were given for some ranges of the parameters (α, β) .

Chapter 6

From the dynamic response analyses, the following conclusions are reached with regard to dynamic response of prestressed, partially prestressed and reinforced concrete single-degree-of-freedom systems:

1. The idealized curves proposed in Chapter 5 were used as the load-displacement idealization. Response spectra of the idealized curves to earthquake excitations for various ranges of yield capacity, period of vibration, and so on were calculated to investigate the fundamental characteristics of the idealization. However, these calculations were conducted in order to examine the characteristics of the idealization curves because the idealized curves are not considered to express directly the load-deflection relationships of a structure or a layer of a building itself : they were derived based on the moment-curvature curves obtained experimentally. The response of a building is largely affected by the load-deflection response of reinforced concrete constituent elements such as columns and walls. A comparison between the idealizations for a prestressed concrete and a reinforced concrete system which will be described in the later part of this section should be referred to as the extreme case of these systems.
2. Comparison of displacement responses between prestressed, partially prestressed and reinforced concrete systems showed that the average ratios of the maximum displacement responses of the prestressed concrete systems to those of the corresponding reinforced concrete systems ranged between 0.98 and 1.39 with the maximum value of 3.23. For partially prestressed concrete systems those ranged 0.98 and 1.15 with the maximum value of 2.06. Generally, the ratios are

larger in the period shorter than approximately 0.5 seconds.

3. Responses of prestressed concrete systems were compared with those of corresponding reinforced concrete systems whose load - displacement hysteretic behaviour was controlled by slip of longitudinal beam bars, that is, indicated pinched hysteresis loops. The average values of the ratios of the maximum displacement response of the prestressed concrete systems to that of the reinforced concrete systems with pinched hysteresis loops ranged between 1.09 and 1.14. They are slightly smaller than those in the comparison between the prestressed and the reinforced concrete systems. The average values for the partially prestressed concrete are approximately unity.
4. Substitute damping was introduced and calibrated from the basis of the results of the time-history analyses in order to predict dynamic responses of prestressed, partially prestressed and reinforced concrete systems. The substitute damping was proved to give a good approximation of responses of those systems.
5. Some examples using the substitute damping revealed that increasing the strength of some types of structures may increase the maximum displacement.

Chapter 7

From the dynamic response analyses on reinforced and prestressed concrete model frames, the following conclusions have been reached with regard to dynamic response of prestressed, partially prestressed and reinforced concrete building frames:

1. Two dimensional dynamic analyses on the prestressed, partially prestressed and reinforced concrete building frames were carried out. Three typical earthquake wave records were used as their maximum velocities were amplified to 50cm/s. Four-, eight- and sixteen-story model frames were designed according to the AII Guidelines and the current seismic design method for prestressed concrete building structures. The frames were intended to fail with a beam-sidesway mechanism.
2. Comparison of the responses of the above model frames revealed that the responses of the prestressed concrete buildings were not always the largest. The interstory drift responses depended on the characteristics of the earthquake waves, too. Past research has pointed out larger response of prestressed concrete frames than that of reinforced concrete frames. Seismic design load for prestressed concrete frames specified in NZS 4203 : 1984 should be 25% larger than that for equivalent reinforced concrete frames. However, a difference large enough to give a motivation to assign a larger seismic design load for prestressed concrete frames was not observed.

3. Comparison of the responses between the two-dimensional frame analyses and the analyses using a multi-mass shear system revealed that the ratio of the responses of the prestressed and partially prestressed concrete frames to those of the reinforced concrete frames were overestimated in the analyses of multi-mass shear systems compared with two-dimensional frame analyses. Story shear force - interstory drift responses using these analytical methods indicated that assignment of prestressed concrete type hysteresis loops to each layer of a prestressed concrete frame which consists of prestressed concrete beams and reinforced concrete columns is not suitable. Two-dimensional frame analysis should be conducted on prestressed concrete building frames.
4. Considering the test results on the beam-column joint assemblies described in Chapter 4, the current seismic design concept that prestressed concrete frames should be designed against larger seismic design load than reinforced concrete frames, as specified in NZS 4203:1984, needs reconsideration.

Chapter 8

1. A new seismic design procedure for prestressed concrete building structures proposed by AIJ task-committee was introduced. In the design procedure a column sidesway mechanism is permitted as one type of failure mechanisms. In order to avoid damage concentration into the weakest story, even if soft story forms, the lateral seismic design force should be increased and the smooth distribution of story shear strength be assured.
2. It has been stated that to secure beam hinging mechanism is difficult in prestressed concrete building structures because prestressing steel, which is usually high strength steel is provided to mainly reduce gravity load effect and the member sections have much larger strength than required by seismic lateral design force. Some design examples were demonstrated to show how difficult it is to realize beam hinging mechanism in prestressed concrete buildings. The ratio of the moment resistance required in order to avoid column hinging to the design moment determined from the combination of design actions, M_{nyd} / M_{scd} , reached 3.22 at most. For reinforced concrete structures the design moments of the beams are usually determined by earthquake actions. Therefore, to prevent the columns from forming plastic hinges the column design moment should be approximately 25% larger than that transferred from the beams unless higher mode effect and two-way frame actions are considered. For prestressed concrete buildings a large moment resistance is needed to realize beam hinging mechanism.
3. The flexural strength and ductility of columns with moderate or high axial compression loads were investigated by carrying out reversed cyclic loading tests on high strength reinforced concrete columns. The test results indicated that adequate ductility was obtained even for such high strength concrete columns by

using high strength transverse reinforcement. The secured ductility would be enough even when soft story should form in one of the layers of a building. In addition, the flexural strengths of the test units subjected to the moderate axial load were well predicted by the ACI 318-89 methods with an equivalent rectangular stress block. However, for the columns under high axial load the flexural strengths obtained by the experiment exceeded the predicted values. Comparison between the experimental and theoretical results of moment-curvature curves indicated that the modified stress-strain model proposed by the authors should be re-modified so as to enable the moment-curvature curves to be well predicted, especially for columns subjected to reversed cyclic lateral loading with high axial compressive load.

Chapter 9

On the basis of the test results described in Chapter 9 the following conclusions are derived.

1. In order to improve the seismic performance of precast prestressed concrete buildings two attempts have been made in this study:
 - (a) The energy absorbing capability can be improved by forcing prestressing tendons located near the extreme fibers of the member section to yield. This can be realized by larger ratio of introduced prestress to yield strength of a prestressing steel tendon.
 - (b) Shear behavior of the joint and slip deformation at the connection can be improved by placing prestressing tendons at the center of the member section. They must remain within the elastic range. Thus, the ratio of introduced prestress to yield strength of the prestressing steel is kept small but the introduced prestress should be large enough to maintain stiffness of overall assemblages.
2. Because of poor bond between the concrete and prestressing steel, stresses in the prestressing tendons did not reach the yield stress at the critical section of the beam. Thus, the performance which was expected was not confirmed.
3. An ungrouted tendon at the center of the beam section was used to keep post-tensioning force large enough to maintain uniformity of the whole assemblage. However, because of the same reason above the effect on the seismic performance of the test units was not observed.
4. If a prestressing strand with better bond characteristics had been used, a different result might have been obtained.

10.2 Recent trends of seismic design of prestressed concrete building structures

There are two trends in seismic design of prestressed concrete building structures. The first is toward development of rational and suitable seismic design of prestressed concrete building structures and the second is toward uniform design procedure of concrete building structures. These should be discussed in respect of two points: obtaining design stresses, and proportioning member sections and providing reinforcing steel.

Structural design is usually carried out as follows.

- (1) Design stresses in the constituent members are obtained when external loads are imposed on the building structure.
- (2) On the basis of the design stresses the member sections are proportioned and reinforcing steel are provided.
- (3) In the case of ultimate strength design procedure the above two items are enough to accomplish the structural design. However, it is often required to confirm that the building structure has enough structural resistance at a specified interstory drift angle.

As for the item (1), seismic design load to be applied statically to building structures is a main concern: is larger seismic design load for prestressed concrete building structures really needed? Besides that, interstory drift of each layer should be within a certain limit. In the current seismic design provisions in Japan, although it is complicated because of several options in the procedure, prestressed concrete buildings are so designed as to have larger lateral load resistance than reinforced concrete buildings. This is originally incorporated mainly due to less ductile behaviour of prestressed concrete members. Since several research on dynamic response of prestressed concrete structures another reason has been added: to reduce dynamic response to as much as reinforced concrete structures larger seismic design load is needed. The limitation of interstory drift angle is the same as reinforced concrete structures. This must be considered because prestressed concrete buildings are generally more flexible than reinforced concrete buildings: less number of columns and larger span beams. A too flexible building frame is harmful to non-structural members and P- Δ effect should be considered. In Chapter 7, when a sixteen-story model frame was designed, the limitation of interstory drift angle of 1/200 was difficult to be met. Unless structural walls are incorporated, a tall prestressed concrete building cannot be realized. A building structure in which lateral force resistance is provided by the combined contribution of frames and structural walls is usually referred to as a dual system or a hybrid structure. Ductile frames can provide a significant amount of energy dissipation interacting with walls, while good story drift control during an earthquake can be achieved as a result of the large stiffness of walls. The development of column hinges can readily be avoided. This may be an answer to design a tall

prestressed building.

The effect of increasing the design seismic load on reduction of dynamic response is not clear nor significant. Dynamic response is very dependent on the characteristics of earthquake waves used in the analyses. As a uniform seismic design procedure the AIJ proposal realizes that seismic design procedure accommodates not only prestressed concrete buildings but also partially prestressed and reinforced concrete buildings. However, the results of dynamic response analyses in the previous chapters imply that it is not necessary to have a larger design seismic load for prestressed concrete building structures than reinforced concrete structures.

The second item, proportioning members and providing reinforcing steel, is recently discussed as uniform design code provisions are proposed in some literature. It has been stated that unification of the design methods of prestressed and reinforced concrete structures is of great importance for development of concrete structures. Recently ACI 318 committee proposed a partial unification of the design requirements of prestressed and reinforced concrete members [8.10]. Since in the U.S.A. prestressed concrete structural members are not allowed to be used in high-seismicity areas, static design seismic load for prestressed concrete structures is not specified in the current design or loadings codes. The proposal of ACI 318 committee is just for proportioning members according to the known design stresses. The proposed method applies to beams and columns, reinforced and/or prestressed. The key concept is the definition of the strength reduction factor ϕ in terms of the maximum steel tensile strain at nominal strength. This strain also defines permissible moment redistribution.

Naaman presented in his paper [8.11] a set of unified recommendations related to the reinforcement in reinforced, prestressed and partially prestressed concrete flexural and compression members.

As stated above unification is divided into two phases: design seismic load for concrete structures which accommodate not only reinforced concrete but also prestressed concrete and member design procedure whichever members should contain prestressing steel or not.

10.3 Recommendations for future research

Several additional problems encountered during the research work conducted for this thesis could not be investigated in detail due to lack of time. The following research topics are suggested to establish a better and more rational seismic design procedure for prestressed concrete building structures.

1. Is a larger seismic design load for prestressed concrete buildings than for conventional reinforced concrete buildings really needed? From the analytical results on single-degree-of-freedom systems described in Chapter 6 a larger seismic design

load appears to be justified. However, at the same time, increasing design seismic load was found to not reduce the responses. Besides that, on the basis of the dynamic response analyses on prestressed and reinforced concrete building structures the difference between the responses of the two systems were not as significant as that of the former analyses. However, the responses were much more dependent on earthquake waves than the systems, and only a limited number of model frames were analyzed. Thus, more research in this field is needed.

2. As shown in Chapter 8 it is difficult to design prestressed concrete buildings which fail in beam-sidesway mechanism. It was confirmed in the same chapter by loading tests on the columns that considerable ductility could be secured even in high strength concrete columns if an adequate amount of transverse reinforcement was provided. Thus, for low buildings a soft story mechanism can be accepted if a larger seismic design load is specified. However, since for tall buildings higher mode effects is more significant, a dual system in which lateral load resistance is provided by the combined contribution of frames and structural walls may be an option for the design of tall prestressed concrete buildings. Further investigation is expected.

3. Concerning to the above topic, to place the upper limit to column flexural capacities as well as the lower limit proposed by AIJ committee has not been investigated in detail. In this thesis no examination was not conducted. More practical analyses like two-dimensional frame analyses should be conducted in order to confirm the effect of this design procedure.

4. In Chapter 4 it was pointed out that seismic performance of prestressed concrete beam-column joint assemblages were not always inferior to that of reinforced concrete ones. However, how much prestress is the most effective to improve seismic performance has not clarified yet. This should be quantified for successful use of prestressing not only under service load condition but also under seismic loading.

謝辞

本論文は、筆者の過去約5年間の研究成果をまとめたものであります。この間、多くの先生方、同僚の皆様より暖かい御指導、御鞭撻をいただきました。

京都大学防災研究所教授六車熙先生には、私が研究生活に入りました当初より、研究者のあるべき姿を教えてくださいとともに、本論文全体にわたる御指導、御教示を賜りました。ここに深甚なる感謝の意を表します。

京都大学助教授渡辺史夫先生には、日常より直接御指導を賜りました。渡辺先生には、研究環境の整備にも御理解をいただきました。

本論文を英語で執筆するにあたりましては、Dr. G. A. MacRaeより多大な協力を得ました。本論文のすべての英語を丁寧にチェックしていただきました。ここに深く感謝いたします。

本論文を審査していただきました京都大学教授森田司郎先生および京都大学防災研究所教授藤原悌三先生からは有意義な御意見、厳しい御指摘をいただきました。

本論文の4章および9章は、西崎隆氏、大平真および小田雄生の各氏の修士論文執筆のために行なわれた実験を基礎にしてまとめたものであります。また、骨組の地震応答解析には、太田義弘氏の多大なる協力を得ました。ここに、各氏に感謝の意を評します。

実験実施などに御協力いただいた岩本敏憲技官、および、実験作業などに助言をいただいた小松勇二郎技官には、厚くお礼を申し上げます。

また、本論文を英語にて執筆するきっかけを与えてくれましたのは、1990年にNew ZealandのCanterbury大学で過ごしました9ヵ月間でありました。この期間におけます様々な国からの留学生との交流は、大変有意義なものであります。また、同大学のR. Park教授およびT. Paulay教授には私の稚拙な英語に対しても辛抱強く、御指導、御示唆をいただきました。

最後に、私事で恐縮ではありますが、私が、勉学・研究に専念できる環境を与えてくれました両親、そして妻・房子に心より感謝いたします。

1993年9月1日

西山峰広

Appendices

1. M. Nishiyama, H. Muguruma and F. Watanabe, "Hysteretic Restoring Force Characteristics of Unbonded Prestressed Concrete Framed Structure under Earthquake Load," Proc.of Pacific Concrete Conference, Auckland, New Zealand 8-11 Nov. 1988, pp.101-112.
2. H. Muguruma, F. Watanabe and M. Nishiyama, "Behaviour of Unbonded Prestressed Concrete Beam in Rigid Frame," Transactions of the Japan Concrete Institute 1986, pp.259-266.

HYSTERETIC RESTORING FORCE CHARACTERISTICS OF UNBONDED PRESTRESSED
CONCRETE FRAMED STRUCTURE UNDER EARTHQUAKE LOAD

M Nishiyama, H Muguruma and F Watanabe

Kyoto University, Japan

SUMMARY

An analytical method, by which hysteretic restoring force characteristics of unbonded prestressed concrete framed structure can be statically pursued on the basis of material properties, is presented. The bond-slip relationship between concrete and prestressing tendon is taken into account, and thus the method covers unbonded members and bonded members. For verifying the propriety of the analytical method, the experiment is carried out on a portal frame with an unbonded prestressed concrete beam of 4.2 m in length and reinforced concrete columns of 1 m in height. High intensity reversed cyclic lateral loading is applied. The experimental results show a good agreement with the analytical ones in terms of load-deflection relation and the fluctuation of the tendon stress at anchorage end.

INTRODUCTION

In seismic area, the application of unbonded prestressed concrete to primarily earthquake resistant members is prohibited due to several reasons, i.e., safety of tendon anchorage assembly against cyclic earthquake load, uncertainties with regard to the fluctuation of tendon stress, little available data on hysteretic restoring force characteristics and complexity in analysis, etc. However, unbonded prestressed concrete members can be very useful to develop the further demand for prestressed concrete structure, because of economical advantage of unbonded tendon, that is, no need for grouting at the construction site, and of practically perfect protection against corrosion comparing with the grouting which is likely to be imperfect. In addition, the past researches reported that small amount of additional nonprestressed reinforcement can improve the restoring force characteristics and the flexural ductility [1,4].

In this study, an analytical method, by which hysteretic restoring force characteristics of unbonded prestressed concrete member and framed structure can be statically pursued on the basis of material properties, is presented. In this method, a structural member is divided into several blocks along member axis and each block is further subdivided into layers, which reflect mechanical properties of the materials. The stiffness matrix of the member is derived from these segments based on the assumptions that stresses and strains are constant in a segment and the cross section of the member remains plane after loading. The bond-slip relationship between concrete and prestressing tendon is taken into account, and thus, this method covers unbonded members and bonded members.

For verifying the propriety of the analytical method, the experiment is carried out on a portal frame with an unbonded prestressed concrete beam of 4.2m in length and reinforced concrete columns of 1m in height. High-intensity reversed cyclic lateral loading is statically applied. The experimental

results are compared with analytical results in terms of lateral load - deflection relation and the fluctuation of tendon stress at the anchorage end.

GENERAL DESCRIPTION OF ANALYTICAL METHOD

For the purpose of numerical calculation, a structural member is divided into several blocks in the direction of longitudinal member axis and each block is further subdivided into layers. This method is called "Layer Element Method" and it has been developed by many researchers. In this study, the followings are assumed;

- 1) Stress and strain are constant in a layer element.
- 2) The cross section of the member remains plane after loading, i.e., the longitudinal strain in concrete and the nonprestressed reinforcement is proportional to the distance from the neutral axis.
- 3) Shear deformation is not taken into consider. Although shear deformation is undoubtedly important in case of column, here the bending and axial force are assumed to dominate the deformation of the member.
- 4) The linear bond-slip relation between concrete and prestressing tendon is assumed.
- 5) Assumed stress-strain relation of concrete and reinforcement are proposed by Kent and Park [2], and Park, Kent and Sampson [5].

Bond Stress and Slip between reinforcement and Concrete

Increment of bond stress between (j-1)-th block and j-th block ($\Delta\tau_j$) is calculated by the following equation.

$$\Delta\tau_j = \frac{2 (\Delta_s P_{j-1} - \Delta_s P_j)}{\phi_s (l_{j-1} + l_j)} \quad (1)$$

where, $\Delta_s P_j$ = force increment of reinforcement in j-th block, ϕ_s = nominal surface area of a bar of unit length, and l_j = length of j-th block. $\Delta\tau_j$ is also expressed by bond-slip relationship ($\Delta\tau_j - \Delta S_j$), as follows,

$$\Delta\tau_j = K_j \cdot \Delta S_j \quad (2)$$

where, K_j = tangential modulus of bond-slip relation. In this study, K_j is assumed to be constant during loading.

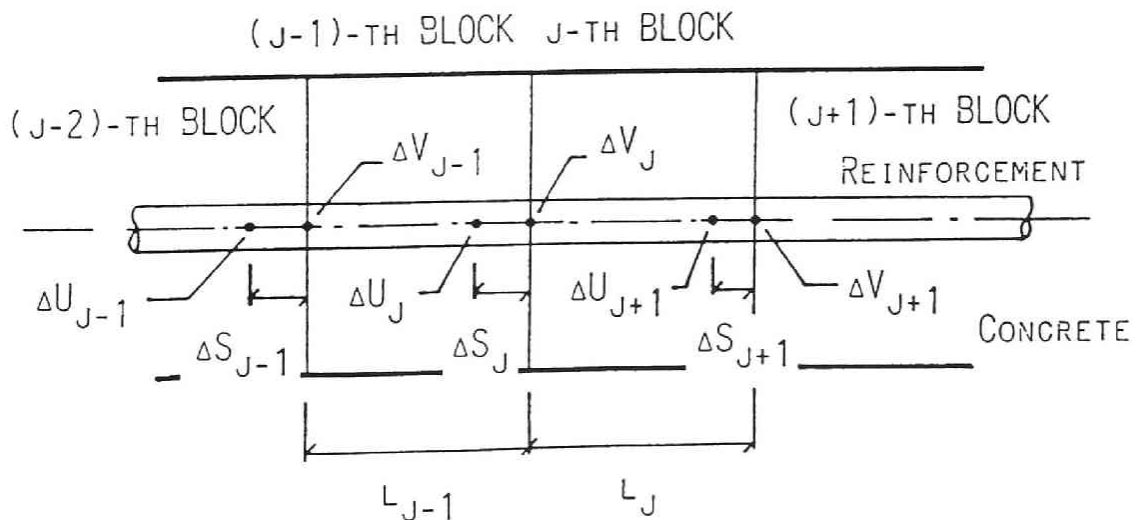


Figure 1 Compatibility of displacements in the member

The System of Linear Equations of Increments of Slip

The method used here was proposed by Kosaka et al. [3]. Dividing the member in the longitudinal direction into block elements $i = 1, 2, \dots, j, \dots$ of length l_j , as shown in Fig.1, the longitudinal strain increment of reinforcement $\Delta_s \epsilon_j$, the concrete strain increment $\Delta_c \epsilon_j$ and the increment of slip in unit length $\Delta_b \epsilon_j$ are calculated by compatibility of displacements as follows,

$$\Delta_s \epsilon_j = (\Delta u_{j+1} - \Delta u_j) / l_j \quad (3)$$

$$\Delta_c \epsilon_j = (\Delta v_{j+1} - \Delta v_j) / l_j \quad (4)$$

$$\Delta_b \epsilon_j = (\Delta S_{j+1} - \Delta S_j) / l_j = (\Delta v_{j+1} - \Delta v_j) / l_j - (\Delta u_{j+1} - \Delta u_j) / l_j \quad (5)$$

where, S_j = slip between concrete and reinforcement, u_j and v_j = displacements of reinforcement and concrete. Therefore,

$$\begin{aligned} \Delta_s \epsilon_j &= \Delta_c \epsilon_j - \Delta_b \epsilon_j \\ &= \Delta_c \epsilon_j - (\Delta S_{j+1} - \Delta S_j) / l_j \end{aligned} \quad (6)$$

From the equilibrium of forces, we get the relations between the stress of reinforcement and slip as below,

at the end 1 of member, as shown in Fig.2;

$$-E_{s1} \cdot \Delta_c \epsilon_1 = \left(\frac{E_{s1}}{l_1} + \frac{pK_1}{A_s} \right) \Delta_p S_1 - \frac{E_{s1}}{l_1} \Delta S_2 \quad (7)$$

between the ends;

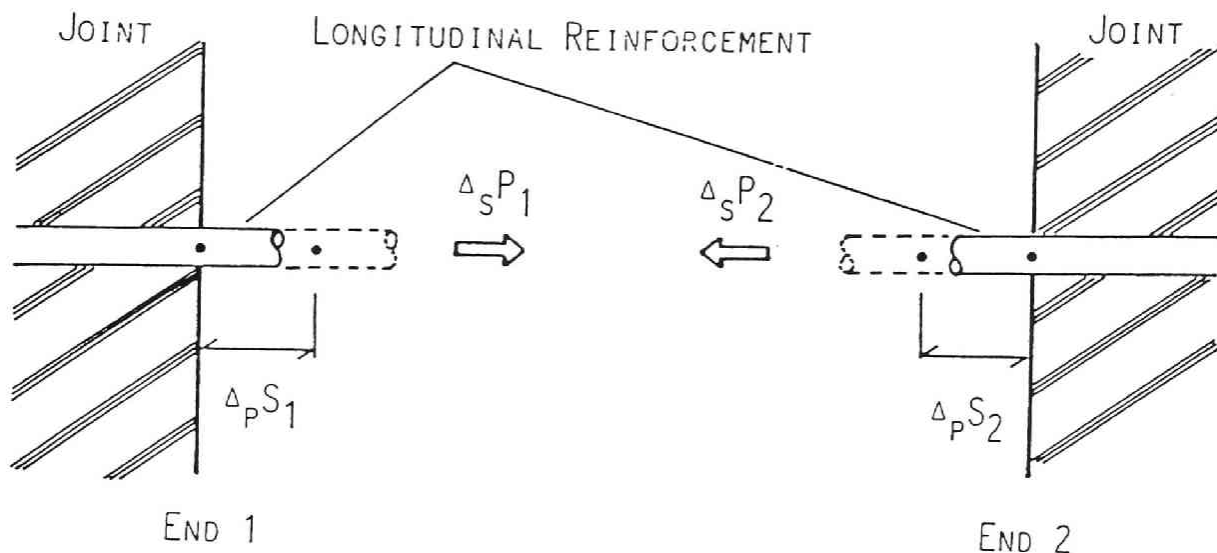
$$\begin{aligned} E_{sj-1} \cdot \Delta_c \epsilon_{j-1} - E_{sj} \cdot \Delta_c \epsilon_j &= -\frac{E_{sj-1}}{l_{j-1}} \Delta S_{j-1} \\ &+ \left\{ \frac{E_{sj-1}}{l_{j-1}} + \frac{E_{sj}}{l_j} + \frac{K_j \phi_s (l_{j-1} + l_j)}{2 A_s} \right\} \Delta S_j - \frac{E_{sj}}{l_j} \Delta S_{j+1} \end{aligned} \quad (8)$$

at the end 2 of member, as shown in Fig.2;

$$E_{sn} \cdot \Delta_c \epsilon_n = -\frac{E_{sn}}{l_n} \Delta S_n + \left(\frac{E_{sn}}{l_n} + \frac{pK_2}{A_s} \right) \Delta_p S_2 \quad (9)$$

where, E_{sj} and A_s = tangential modulus and cross sectional area of reinforcement, $pK_1 = -\Delta_s P_1 / \Delta_p S_1$, $pK_2 = \Delta_s P_2 / \Delta_p S_2$, $\Delta_s P_1$ and $\Delta_s P_2$ = force increment of the reinforcement, $\Delta_p S_1$ and $\Delta_p S_2$ = slip increment of reinforcement at the ends of the member. Although pK_1 and pK_2 should be determined by some calculation, in this study because of simplification it is assumed that they are constant and large enough to restrain the tendon from coming out from the joint. This could be justified because prestressing tendon was anchored almost perfectly on the steel plate.

These equations (7-9) represent the system of linear equations of ΔS_j . Increments of slip (ΔS_j) can be determined by given $\Delta_c \epsilon_j$ (strain increment of concrete element located at the reinforcement level).



$${}^P K_1 = -\Delta_S P_1 / \Delta_P S_1$$

$${}^P K_2 = -\Delta_S P_2 / \Delta_P S_2$$

Figure 2 Force and slip increment of reinforcement at the ends of the member

Substituting the calculated values of S_j into Eq.5, we get $\Delta_b \epsilon_j$. Stress increment of reinforcement $\Delta_s \sigma_j$ are calculated by

$$\begin{aligned} \Delta_s \sigma_j &= E_{sj} \Delta_s \epsilon_j \\ &= E_{sj} \Delta_c \epsilon_j - E_{sj} \Delta_b \epsilon_j \end{aligned} \quad (10)$$

Derivation of the Stiffness Matrix of the Cross Section

The cross section of the member is subdivided in the z-direction into layers $i = 1, 2, \dots, m$ of cross-sectional areas A_{ij} and centroidal coordinates Z_{ij} . Centroidal coordinates of longitudinal steel reinforcement in j-th block is denoted as sZ_{ij} , ($i = 1, 2, \dots, n$). The longitudinal nominal strain increment of concrete at any point of the cross section is

$$\Delta_c \epsilon_{ij} = \Delta \epsilon_{0j} - Z_{ij} \Delta \phi_j \quad (11)$$

in which, ϵ_{0j} = normal strain at the member axis, ϕ_j = curvature of j-th block.

Bending moment ΔM_j^c and normal force ΔN_j^c in concrete are expressed by the following equations.

$$\Delta M_j^c = - \sum_{i=1}^m Z_{ij} A_{ij} \Delta_c \sigma_{ij} + \sum_{i=1}^m c E_{ij} I_{ij} \Delta \phi_j \quad (12)$$

$$\Delta N_j^c = \sum_{i=1}^m A_{ij} \Delta_c \sigma_{ij} \quad (13)$$

where, A_{ij} = area of concrete in i-th layer of j-th element, and $\Delta_c \sigma_{ij}$ = normal stress in concrete in the longitudinal direction in i-th layer of j-th block element. I_{ij} = moment of inertia of i-th layer about centroidal axis of its layer.

The similar expressions for reinforcements can be obtained as follows.

$$\Delta M_j^s = - \sum_{i=1}^n s_{ij} A_{ij} Z_{ij} \Delta \sigma_{ij} \quad (14)$$

$$\Delta N_j^s = \sum_{i=1}^n s_{ij} A_{ij} \Delta \sigma_{ij} \quad (15)$$

On the other hand, normal stresses in concrete and reinforcement are expressed by the following equations.

$$\Delta \sigma_{c\,ij} = c E_{ij} \Delta \epsilon_{ij} = c E_{ij} (\Delta \epsilon_{0j} - Z_{ij} \Delta \phi_j) \quad (16)$$

$$\Delta \sigma_{s\,ij} = s E_{ij} \Delta \epsilon_{ij} = s E_{ij} (\Delta \epsilon_{c\,ij} - \Delta_b \epsilon_{ij}) \quad (17)$$

cE_{ij} , sE_{ij} = tangent modulus of concrete and longitudinal steel.
Substituting Eqs.16 and 17 into Eqs.12-15, this yields,

$$\Delta M_j^c = \left\{ \sum_{i=1}^m (-Z_{ij} A_{ij} c E_{ij}) \right\} \Delta \epsilon_{0j} + \left\{ \sum_{i=1}^m c E_{ij} (A_{ij} Z_{ij}^2 + I_{ij}) \right\} \Delta \phi_j \quad (18)$$

$$\Delta N_j^c = \left\{ \sum_{i=1}^m c E_{ij} A_{ij} \right\} \Delta \epsilon_{0j} + \left\{ \sum_{i=1}^m (-c E_{ij} A_{ij} Z_{ij}) \right\} \Delta \phi_j \quad (19)$$

$$\Delta M_j^s = \left\{ \sum_{i=1}^n (-Z_{ij} s_{ij} A_{ij} s E_{ij}) \right\} \Delta \epsilon_{0j} + \left\{ \sum_{i=1}^n s E_{ij} s_{ij} A_{ij} Z_{ij}^2 \right\} \Delta \phi_j \quad (20)$$

$$\Delta N_j^s = \left\{ \sum_{i=1}^n s_{ij} A_{ij} s E_{ij} \right\} \Delta \epsilon_{0j} + \left\{ \sum_{i=1}^n (-s E_{ij} s_{ij} A_{ij} Z_{ij}) \right\} \Delta \phi_j \quad (21)$$

The total forces ΔN_j and ΔM_j in the cross section are obtained by summing up the contributions of concrete and steel. This yields

$$\Delta N_j = \Delta N_j^c + \Delta N_j^s = \alpha_j \Delta \epsilon_{0j} + \beta_j \Delta \phi_j \quad (22)$$

$$\Delta M_j = \Delta M_j^c + \Delta M_j^s = \beta_j \Delta \epsilon_{0j} + \gamma_j \Delta \phi_j \quad (23)$$

$$\alpha_j = \left\{ \sum_{i=1}^m c_{ij} E_{ij} A_{ij} \right\} + \left\{ \sum_{i=1}^n s_{ij} A_{ij} s_{ij} E_{ij} \right\} \quad (24)$$

$$\beta_j = \left\{ \sum_{i=1}^m (-c_{ij} E_{ij} A_{ij} Z_{ij}) \right\} + \left\{ \sum_{i=1}^n (-s_{ij} E_{ij} s_{ij} A_{ij} Z_{ij}) \right\} \quad (25)$$

$$\gamma_j = \left\{ \sum_{i=1}^m c_{ij} E_{ij} (A_{ij} Z_{ij}^2 + I_{ij}) \right\} + \left\{ \sum_{i=1}^n s_{ij} E_{ij} s_{ij} A_{ij} Z_{ij}^2 \right\} \quad (26)$$

Eqs.23 and 24 represents the force-deformation relations for a cross section of the beam. When Eqs.23 and 24 are rewritten in the matrix form, this provides

$$\begin{Bmatrix} \Delta N_j \\ \Delta M_j \end{Bmatrix} = \begin{bmatrix} \alpha_j & \beta_j \\ \beta_j & \gamma_j \end{bmatrix} \begin{Bmatrix} \Delta \epsilon_{0j} \\ \Delta \phi_j \end{Bmatrix} \quad (27)$$

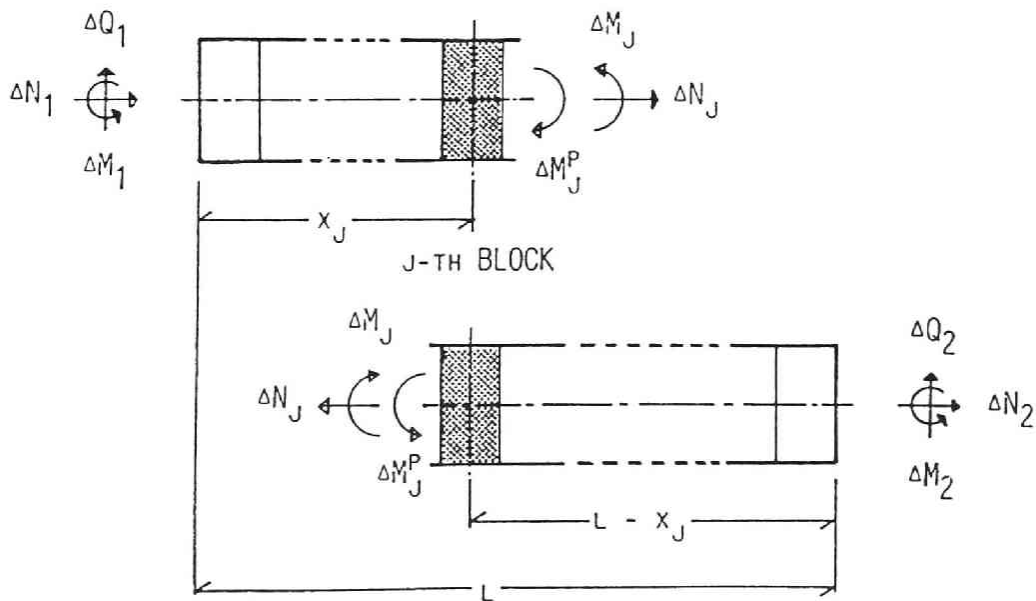
Consideration of Prestress

From the equilibrium of forces shown in Fig.3, the increments of axial force and bending moment in j-th block, ΔN_j and ΔM_j are obtained as follows.

$$\Delta N_j = \Delta N_2 = -\Delta N_1 \quad (28)$$

$$\Delta M_j = \Delta Q_2(1-x_j) + \Delta M_2 + \Delta M_j^P = -\Delta M_1 + x_j \Delta Q_1 + \Delta M_j^P \quad (29)$$

where, ΔN_1 , ΔQ_1 and ΔM_1 = axial force, shear force and moment at the end 1 of the member, and ΔM_j^P = moment induced by the prestress transfer, given by $\Delta N_p \cdot e_j$, where ΔN_p = effective prestressing force, e_j = eccentricity of



ΔM_j^P IS AVAILABLE DURING PRESTRESSING

Figure 3 Equilibrium of forces of the member

tendon measured from the centroidal axis of the section. That is, prestress, which is divided into some loading steps, is assumed to be applied to each block as external loads ΔN_p and ΔM_j^p . During prestressing, tendons are not considered as reinforcements but prestressing force is just replaced by the external loads ΔN_p and ΔM_j^p . After prestress transfer, they are assumed to behave like nonprestressing reinforcements with yield strength of $\sigma_y - \sigma_p$ in tension and $-\sigma_y - \sigma_p$ in compression, where σ_y = nominal yield stress of prestressing tendon and σ_p = effective prestress.

Derivation of the Stiffness Matrices of the Member and the Structure

The stiffness matrices of the member and the structure were constituted by the procedure presented by Kosaka et al. [3] and Tani et al. [6]. The effect of prestress is included in the terms due to bond-slip and nonlinearity of material properties.

Computational Algorithm

The computational algorithm in each loading step may proceed as follows;

1. For all elements, assume that $\Delta \epsilon_{oj}$ and $\Delta \phi_j$ are the same as in the previous step.
2. Set up the bond stiffness equation in which the bond stiffness and the tangential modulus of reinforcement are assumed to be the same as in the previous step.
3. Solve the equation above to get the slip between concrete and reinforcement in each block.
4. Set up the stiffness matrix of each block and transfer it into the flexibility matrix.
5. Combine the flexibility matrices of the sections so that the member flexibility matrices can be obtained.
6. Transfer the member flexibility matrices into the stiffness ones and constitute the stiffness matrix of the structure.
7. Solve the equation above under some support conditions and get the unknown displacements and forces.
8. Calculate $\Delta \epsilon_{oj}$ and $\Delta \phi_j$ again by using the displacement and force increments obtained above.
9. Compare the assumed values and calculated values of $\Delta \epsilon_{oj}$ and $\Delta \phi_j$, and return to step 1 if the difference between them is larger than one percentage of the assumed values. If not, go next.
10. Calculate the stresses and tangential modulus of concrete and reinforcement according to the strains obtained by using $\Delta \epsilon_{oj}$ and $\Delta \phi_j$. If the tangential modulus in this step differs from the assumed value, unequivocal stress is calculated and released in the next step.

EXPERIMENT OF UNBONDED PRESTRESSED CONCRETE PORTAL FRAME

For verifying the propriety of the analytical method above, the experiment was carried out on two portal frames with an unbonded prestressed concrete beam 4.2 m long and reinforced concrete columns 1 m high, shown in Fig.4. These two frames were so designed as to have the same lateral load resistance. The mechanical properties of concrete and reinforcement are listed in Table 1 and 2. Specified 0.2% offset yield strength and tensile strength of prestressing tendon are 1078 MPa and 1225 MPa, respectively. The moment capacity of the column is about 1.5 times that of the beam, so that the plastic hinges are intended to be located in beam ends and column bases. One frame, 'FR35', was consisted of the beam where the eccentricity of prestressing tendon is 35 mm (D/6:D indicates the whole depth) and the other, 'FR60', has the prestressing tendon whose eccentricity is 60 mm (D/3.5). Effective prestresses are 107.8 kN for FR35 and 63.7 kN for FR60.

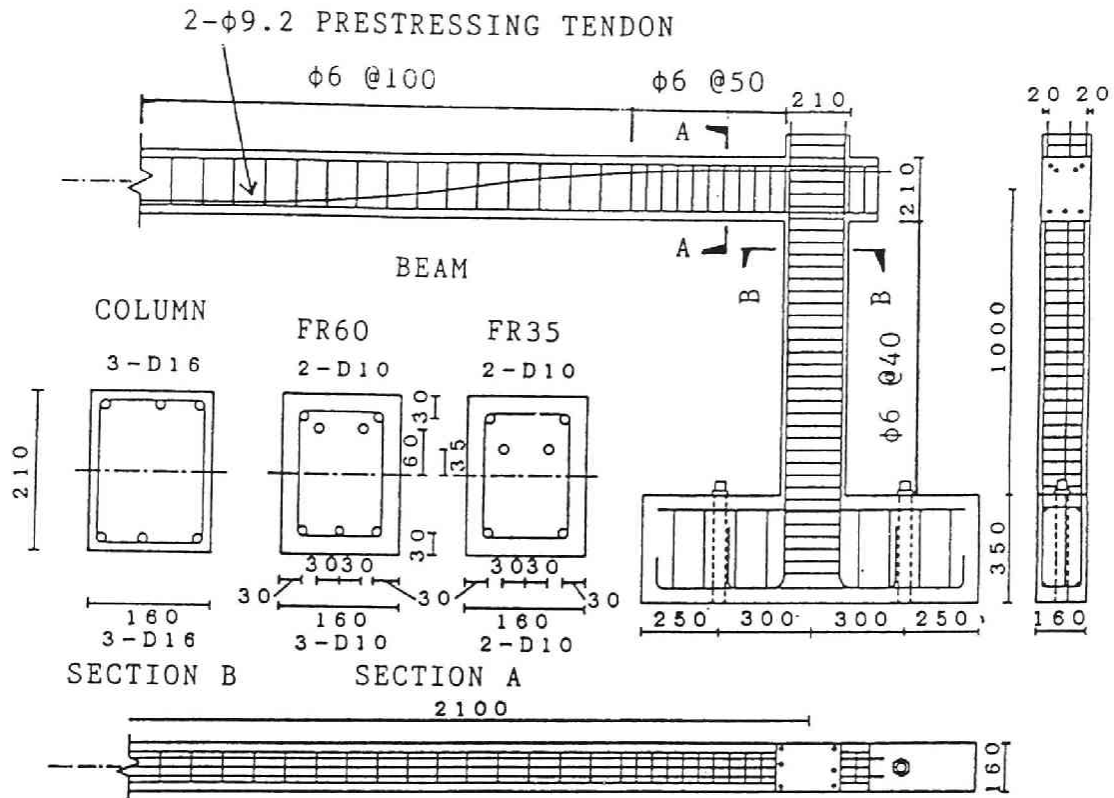


Figure 4 Dimensions and reinforcing details of specimen

Table 1 Mechanical properties of concrete

Specimen	FR35	FR60
Compressive Strength f_c' in MPa	36.9	36.8
Strain at f_c' in %	0.244	0.218
Tensile Strength f_t in MPa	3.4	3.3

Table 2 Mechanical properties of reinforcements

Reinforcement	D10	D16	$\phi 8$
Yield Strength f_y in MPa	350.8	348.3	395.9
Yield Strain ϵ_y in %	0.205	0.180	0.224
Modulus of Elasticity in 10^5 MPa	1.72	1.92	1.78

Prestress was transferred to the beam while one column base is supported by pin and the other is supported by roller. Therefore, the columns were free from the moments, shears and axial forces produced by prestressing. After prestress transfer, the frame was fixed to the floor. This procedure was followed in the calculation, but the friction of tendon during prestress transfer is ignored.

Fig.5 shows loading set-up. Reversed cyclic horizontal load was statically applied to the mid-span of the beam by hydraulic jack. Besides the horizontal load, the vertical load was also applied at the mid-span of the beam, so that the bending moments at the beam ends and the mid-span due to the prestressing were offset at the beginning of the test. This vertical load was kept constant during the test.

The frames were subjected to several slow load reversals simulating very severe earthquake loading. The "first yield" displacement of the frames were found when all the tension reinforcements in expected hinging regions had

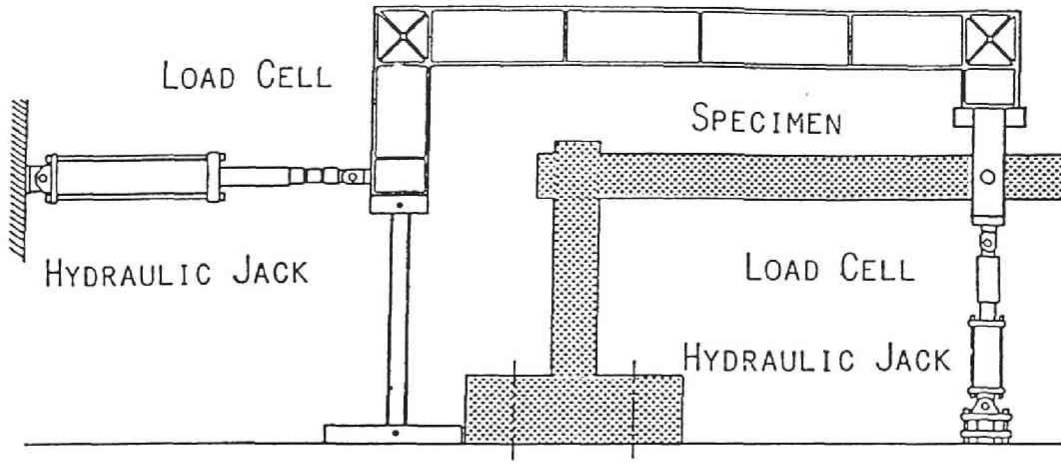


Figure 5 Loading set-up

yielded. The first loading cycle consisting of ten cycles was followed by a series of deflection controlled cycles in the inelastic range, also comprising ten full cycles to each of the displacement ductility factors of ± 2 , ± 3 , ± 4 , and sometimes higher, as illustrated in Fig.6.

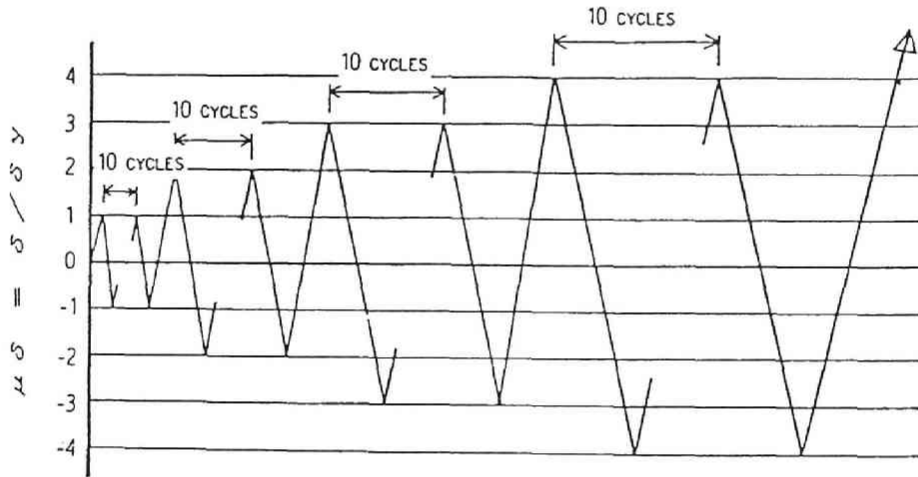


Figure 6 Imposed loading history on the specimen

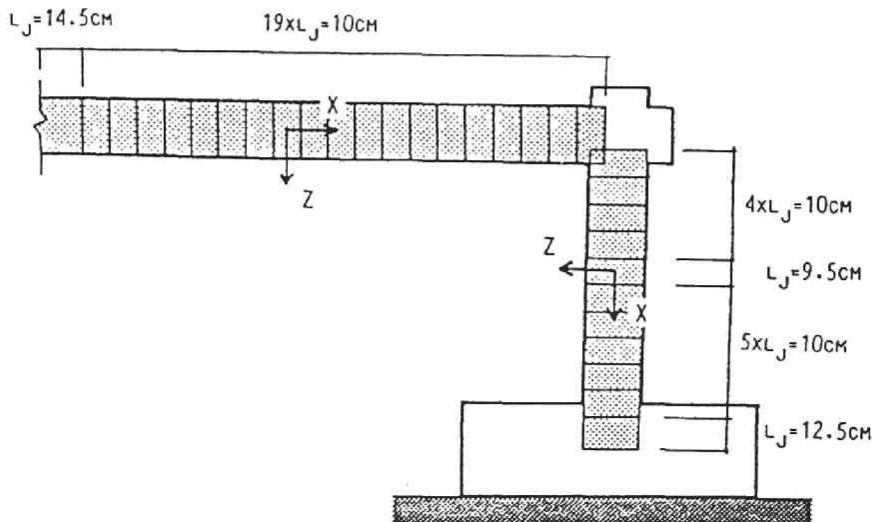


Figure 7 Divided block elements of the member used in the calculation

In the calculation bond stiffness assumed for prestressing tendon is $9.8 \times 10^3 \text{ N/mm}^3$. This is about 1/1000 used for nonprestressed deformed bar. Fig.7 shows layer elements assumed in the calculation.

EXPERIMENTAL RESULTS AND COMPARISON WITH THE ANALYTICAL RESULTS

Figs.8 and 9 show the first cycle in each series of deflection cycles of the measured horizontal load versus horizontal deflection at the midspan of the

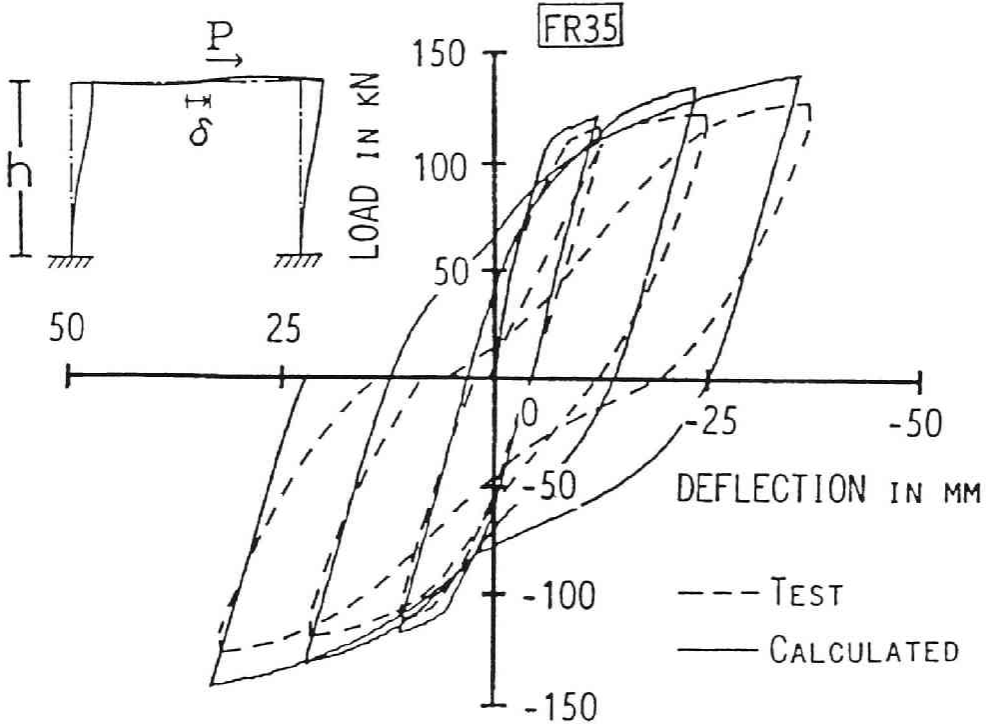


Figure 8 Load - deflection relation in FR35

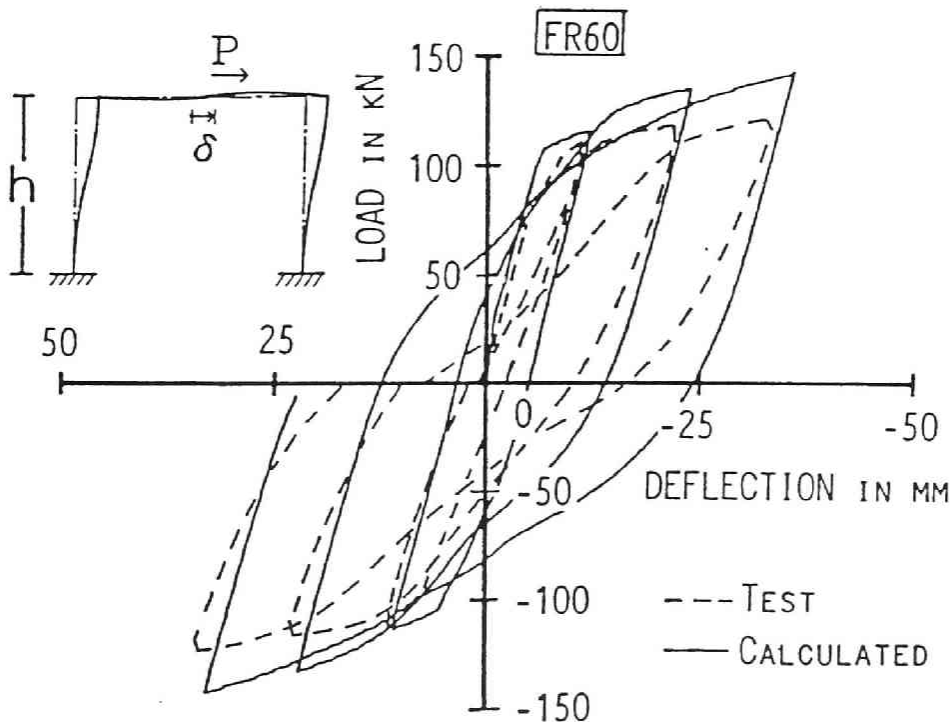


Figure 9 Load - deflection relation in FR60

beam. These figures also show the calculated load - deflection curves. The deterioration due to load cycles in concrete and bond is not considered in this calculation, so that each loading cycle comprises only one full cycle. When the experimental results are compared with analytical results, fairly good agreement can be observed.

However, the larger the deformation became, the larger difference could be observed. It is mainly because the shear deformation was not taken into consider in the calculation. The shear deformation, especially in the column, dominates the whole deformation of the frame in the loading cycles to high ductility values, and some pinching of the load-deflection loops was noticeable in the experiment. Just before the failure, where the ductility

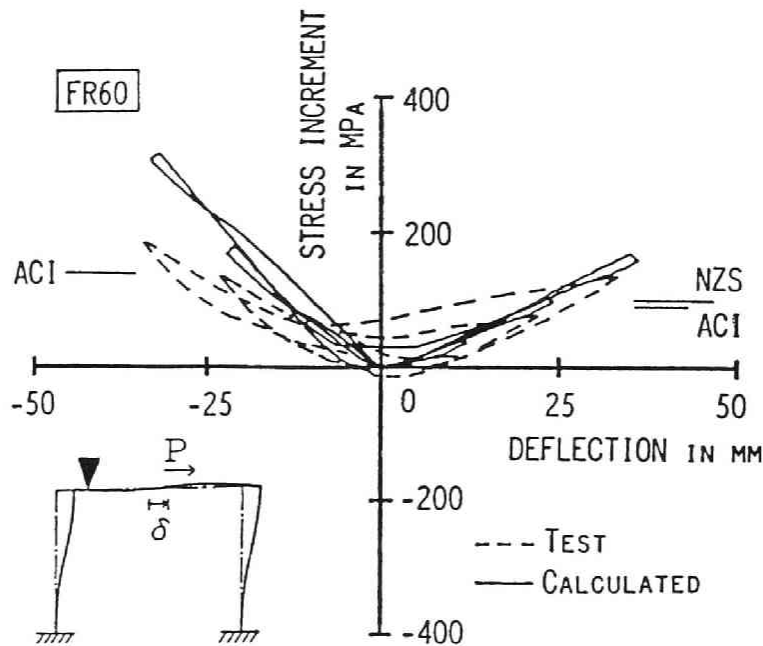


Figure 10 Increment of tendon stress - deflection relation in FR60

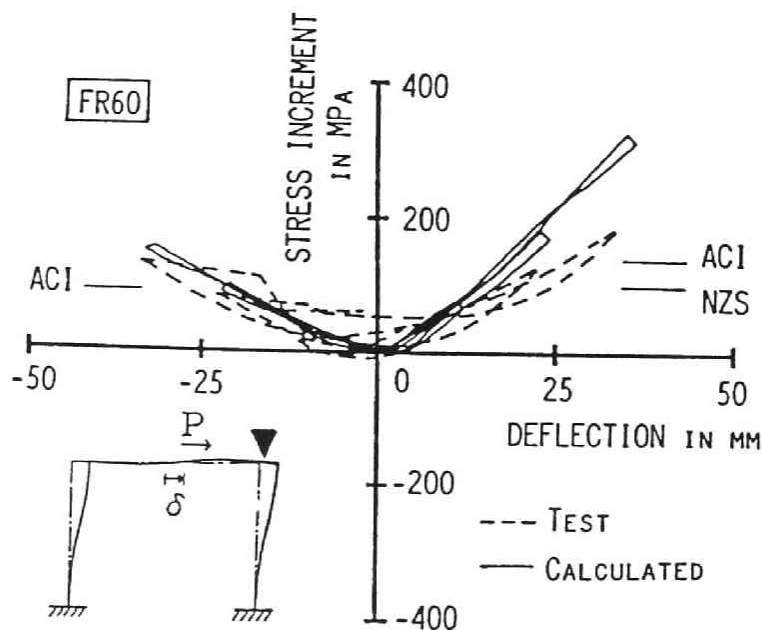


Figure 11 Increment of tendon stress - deflection relation in FR60

factor is almost +4, the shear deformation of the column base occupies a large portion of the whole deformation, while the deformation of the beam remains small. Therefore, the frame moves like a rigid body connected to the foundation at the column base.

In Figs.10 and 11, the first cycle in each series of deflection cycles of the measured tendon force increments versus horizontal deflections at the midspan of the beam are shown. The calculated results are also shown in the same figures. As described before, the shear deformation at the column bases results in imposing not so large rotation on the beam ends even in the inelastic range. Therefore, the calculated results are larger than the experimental results. In addition, in the calculation, the tendon force increment continues to increase almost linearly with the deflection of the frame because the rotations at the beam ends have a linear relationship with the lateral deflection of the frame.

The maximum tendon force increment measured in the test was up to 196 N/mm². From analytical and experimental results on the portal frame, the tendon force measured at the anchorage ends is not so large. It may be not necessary to consider any risk of tendon fracture even in the inelastic range. The tendon force increment measured in the test showed good agreement with the predicted value obtained from ACI and NZS.

CONCLUSIONS

The analytical method, by which hysteretic restoring force characteristics of unbonded prestressed concrete framed structure can be statically pursued on the basis of material properties, was presented. The analytical results were compared with the experimental results of unbonded prestressed concrete portal frame in terms of lateral load versus deflection and increment of tendon stress versus deflection relation. Fairly good agreement can be observed. However, the larger difference could be found in the loading cycles to high ductility values because the shear deformation became dominant. Therefore the method has to be so improved as to take inelastic shear deformation into consider.

The analytical and experimental results showed that the tendon force was not so large because the rotation of the beam ends was not so large while the large inelastic deformation was imposed on the frame. Therefore, it may be not necessary to consider any risk of tendon fracture and the unbonded tendon will be successfully used in a primarily earthquake resistant members.

REFERENCES

- [1] Du, Gongchen and Tao, Xuekang 1985 Ultimate Stress of Unbonded Tendons in Partially Prestressed Concrete Beams PCI Journal/Nov.-Dec. 72-91
- [2] Kent, D.C. and Park, R. 1971 Flexural Members with Confined Concrete Proc. of ASCE, Vol.97, ST7, July. 1969-1990
- [3] Kosaka, Y., Tanigawa, Y. and Yamada, K. 1983 Inelastic Analysis of Reinforced Concrete Based on Endochronic Theory - Part 1 Procedure of analysis - Transaction of the AIJ No.326, April, 78-90 (in Japanese)
- [4] Muguruma, H., Watanabe, F. and Shimizu, Y. 1982 Improving the Flexural Ductility of Post-tensioned Unbonded Beam by Using Laterally Confined Concrete Proc. of JCI 4th Conference 361-364 (in Japanese)
- [5] Park, R., Kent, D.C. and Sampson, R.A. 1972 Reinforced Concrete Members with Cyclic Loading Proc. of ASCE, ST7, July 1341-1360
- [6] Tani, S., Nomura, S., Nagasaka, T. and Hiramatsu, A. 1977 Restoring Force Characteristics of Reinforced Concrete Aseismic Elements (Part 4) - Pursuit of Restoring Force Characteristics by Means of a Static Elastic-Plastic Analytical Method - Transaction of the AIJ No.262, Dec. 61-72

(III-5-A)

BEHAVIOUR OF UNBONDED PRESTRESSED CONCRETE BEAM
IN RIGID FRAME

Hiroshi MUGURUMA*, Fumio WATANABE* and Minehiro NISHIYAMA*

ABSTRACT

Many experimental and analytical studies on unbonded prestressed concrete beams have been carried out, but most of them are on the behaviour of simply-supported beams or cantilever-type beams.

In this paper, reversed cyclic lateral flexural shear loading tests on unbonded prestressed concrete end-restrained beams for simulating flexural deformation hysteretic behaviours of them in earthquake resistant framed structure are reported. Test results were discussed in terms of the capacity, the fluctuation of tendon stress and the hysteretic restoring force characteristics. Test results revealed that the capacity of unbonded prestressed concrete beams was about 7% smaller than that of bonded beams and the increment of tendon stress measured at the anchorage end of bonded prestressed concrete beams was larger than that of unbonded prestressed concrete beams. Furthermore, little difference on hysteretic restoring force characteristics between unbonded and bonded beams was recognized.

1. INTRODUCTION

The remarkable progress of unbonded prestressed concrete has considerably expanded the range of application of prestressed concrete because of the easiness of field work and the economy with unnecessary of grouting. In applying unbonded prestressed concrete beam to a constituent member in earthquake resistant framed structure, it is important to investigate the fluctuation of tendon stress and the hysteretic restoring force characteristic. According to the earlier researches, smaller tensile stress increment due to applied load and less energy dissipation to earthquake motion are pointed out as the disadvantages in comparison with the bonded beams. However, most of the researches on unbonded beams are the experimental studies on simply supported beams and cantilever type beams and still comparatively little experimental data on the behaviour of unbonded beams in rigid frame are available.

In this paper, reversed cyclic lateral flexural shear loading tests carried out on unbonded prestressed concrete end-restrained beams for simulating flexural deformation hysteretic behaviours of them in earthquake

* Department of Architecture, Faculty of Engineering, Kyoto University

resistant framed structure are reported. Besides, the same test mentioned above carried out on bonded beams is also reported. The parameters considered in this study are (1) bonded beam or unbonded beam, (2) tendon profile (straight or concordant with moment diagram) and (3) location of tendon at critical section. Test results are discussed in terms of the capacity, the fluctuation of tendon stress and the hysteretic restoring force characteristics.

2. TEST SPECIMENS

Fig.1 and Table 1 show the details and specifications of test specimens used in this study. The specimens consisted of unbonded prestressed concrete beam with 3 m in length and 16x21 cm² in cross sectional dimension and heavily reinforced column stubs at both ends of the beam. In the beam section, 4-D10 mm supplementary reinforcements were arranged for preventing concentrated crack formation and $\phi 6$ mm rectangular web reinforcements were placed in a pitch of 15 cm through the whole length of the beam.

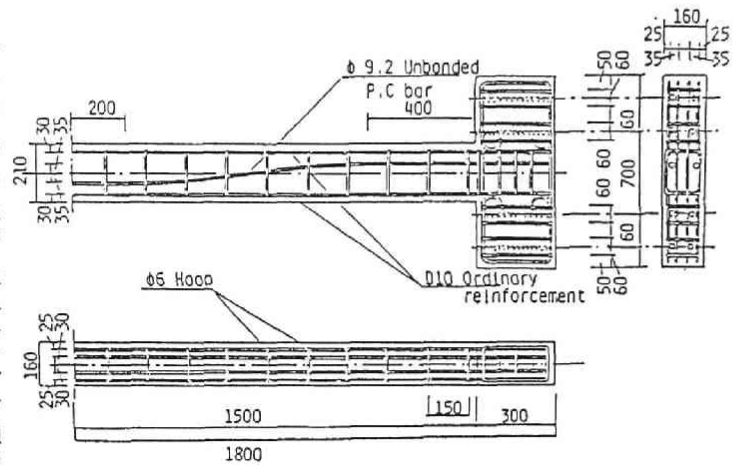


Fig.1 Specimen

Mechanical properties of ordinary reinforcement and prestressing steel bar are summarized in Table 2. Properties of concrete at the age of testing are listed in Table 3. Prestressing force for each beam was introduced so that the tension stress in the extreme fiber of concrete due to prestressing was less than the allowable tension stress ($0.07f_c'$, where f_c' is a compressive strength of concrete) before the live load was applied. In case of the beams having draped tendon profile, the live loads applied to the mid-span under the end-restrained condition. On the other hand, beams having straight tendon the live loads were applied in simply supported condition.

Table 1 Specifications of Specimens

Specimen	U3SCR	U35SR U35SM	U6OCR	U6OSR U6OSM	B35CR	B35SR	B6OCR	B6OSR
Prestressing tendon	2- $\phi 9.2$ SBPR 110/125				2-D9.2 SBPD 110/125			
Eccentricity (mm) (e/D)	35 (1/6)		60 (1/3.5)		35 (1/6)		60 (1/3.5)	
Prestressing tendon index	qpt	0.17	0.17	0.14	0.14	0.21	0.21	0.18
	qpc	0.34	0.33	0.53	0.51	0.41	0.41	0.64
Concrete	C1	C2	C1	C2	C3	C3	C3	C3
Effective prestressing force (ton)	10.44	12.34	10.57	11.94	11.58	11.63	11.61	11.33
σ_{pe}/σ_{py}	0.59	0.72	0.60	0.69	0.67	0.67	0.67	0.67
P_e/bDF_c	0.07	0.08	0.07	0.08	0.10	0.10	0.10	0.10
Concentrated load at midspan	1.00	0.51	1.70	0.90	0.96	0.50	1.70	0.84

- e :eccentricity of tendon
- D :total depth of beam section b :breadth of beam section
- σ_{pe} :stress of prestressing tendon at prestressing
- σ_{py} :yield stress of prestressing tendon
- P_e :prestressing force
- F_c :compressive strength of concrete
- qpt = $A_p \sigma_{py} / (b d_p F_c)$
- qpc = $A_p \sigma_{py} / [b(D-d_p)F_c]$
- A_p :area of prestressing tendon
- d_p :effective depth of prestressing tendon

3. TEST PROCEDURES AND MEASUREMENTS

For applying reversed cyclic transversal load as simulated earthquake load, one end column stub was fixed to a rigid steel frame column, while the other end column stub was moved up- and downward without stub rotation. Thus, the beam was subjected to an antisymmetric flexure with constant shear force over the whole length of the beam. In addition, the constant load as the live weight was applied by servo-actuator. Fig.2 shows the schematic figure of loading procedure. Flexural moment applied to the beam was measured at both ends of the beam by load-cells. Each end of these load-cells had an universal joint so that only the axial load applied to the load-cells was measured. Flexural moment was obtained by both upper and lower load-cells. Shear force was calculated by using these measured flexural moments at both ends of the beam.

Table 2 Mechanical properties of reinforcements

	D10	φ6	φ9.2 tendon
Yield stress (kgf/cm ²)	3830	3570	13300*
Yield strain (%)	0.204	-	-
Elastic modulus (x10 kgf/cm ²)	1.88	1.93	2.02

* 0.2% offset yield stress

Table 3 Mechanical properties of concrete

Concrete	C1	C2	C3
Compressive strength f_c' (kgf/cm ²)	403	467	372
Tensile strength (kgf/cm ²)	33.3	42.9	30.3
Initial tangent modulus (x10 kgf/cm ²)	3.99	3.03	2.32
Strain at f_c' (%)	0.18	0.24	0.23

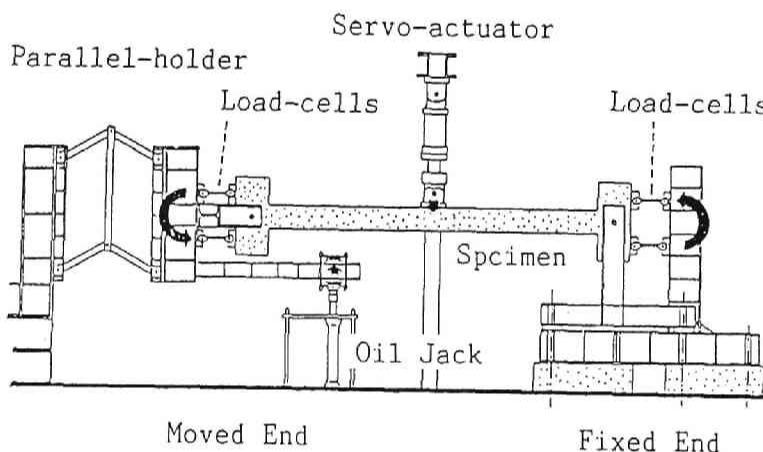


Fig.2 Loading set up

During cyclic loading, the displacement at the loading stub was measured by displacement transducer. Also, top and bottom fiber strain distributions within the length of 30 cm from both beam end sections were measured by displacement transducers in gauge length of 10 cm. From the fiber strain measurements, the average flexural curvature distributions were calculated. However, flexural curvature will be left for another paper because of the limitation of space. In addition, tensile force increments of prestressing steel bars due to the load application were obtained by load-cells inserted at the anchorage ends.

4. TEST RESULTS AND DISCUSSIONS

All the specimens failed in flexure with crush of concrete and buckling of ordinary reinforcements in compression zone at both beam end sections. These failures gradually occurred without sudden fall of load capacity.

In Fig.3a and 3b, measured flexural moment at beam end section - the beam rotation angle relationships of U60CR are illustrated. And in Fig.3c, shear force defined as the sum of flexural moments divided by the beam length at both beam end sections is shown against the beam rotation angle. Because of the prestressing force, excessive recovery of deformation can be seen in these figures.

4.1 SHEAR FORCE CAPACITY

In Fig.4, maximum shear force in each specimen is plotted against its compressive strength of concrete. Generally, the capacity of unbonded beams is smaller than that of bonded beams because the tensile strain of the prestressing steel bars in unbonded beams is uniform over whole length of them. However, little data on the ratio of the capacity of unbonded beams to that of bonded beams, especially in rigid frame, are available. In this study, according to this experimental study, capacity of unbonded beams is about 7% smaller on an average than that in bonded beams.

In Fig.5a and 5b, shear force capacities obtained from test are compared with the calculated values with particular reference to the effect of a strain compatibility factor F . From these figures, the most fitted F values for unbonded and bonded beams are 0.1-0.2 and 0.65-1.0, respectively. F value for unbonded beams in this paper agrees with the value suggested for simple supported beams by the authurs(1). Therefore, F value can be used for the design of unbonded prestressed concrete beams in rigid frame under reversed cyclic loading. It should be noted that F values for

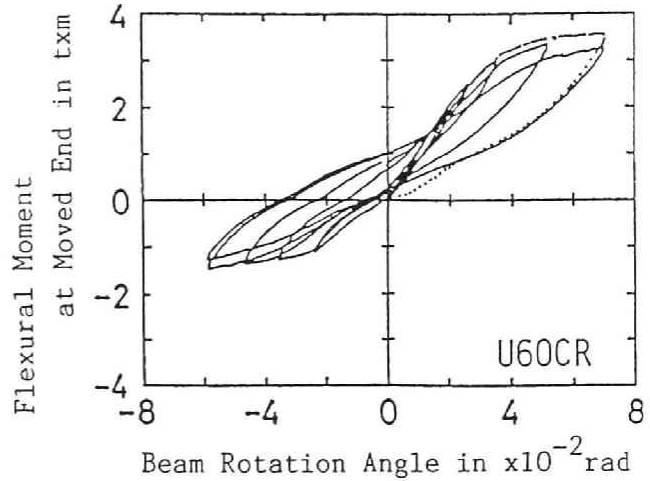


Fig.3a Flexural moment at moved end

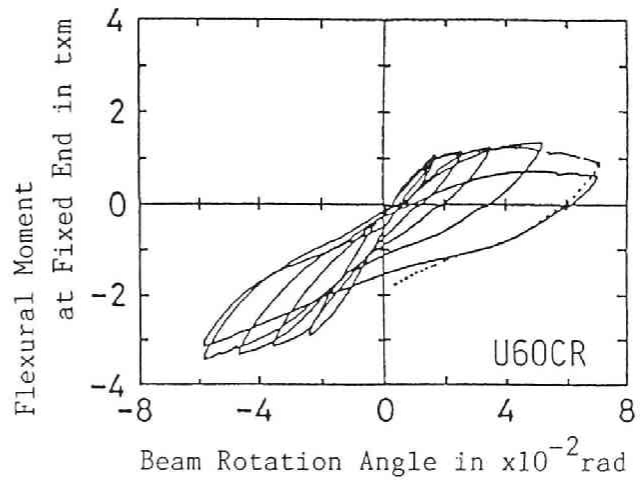


Fig.3b Flexural moment at fixed end

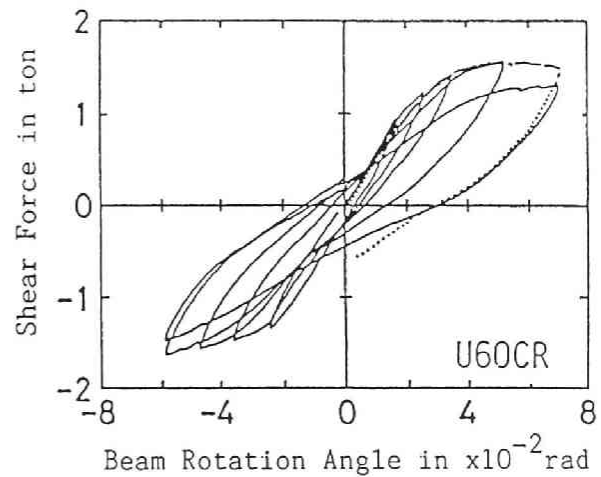


Fig.3c Shear force

bonded beams scattered in the range of 0.65-1.0 with the specimens. This may be because bond stress between concrete and prestressing bar deteriorated easily under reversed cyclic loading and the degree of the bond deterioration depended on the loading history and so on. And also, little difference in calculated capacity in the range of $F = 0.3-1.0$ may be one of the reasons.

Concerning to the tendon profile, there was little difference in the load carrying capacities of bonded beams having straight or draped tendon, because the moment capacity at the critical section having same sectional area of tendon is only affected by the eccentricity of tendon. However, in case of unbonded beams the beam having draped tendon showed about 17% larger capacity due to the existence of friction between tendon and surrounding concrete at the bent-up and -down corners. Further details will be discussed later.

According to the eccentricity of prestressing steel bar, little effect in shear force capacities could be recognized. However, there was a large difference in the moment capacities at beam ends. When the beam end section was subjected to positive moment, the moment capacity was smaller and the crush of concrete at the top fiber occurred in relatively earlier stage in loading with the buckling of ordinary reinforcements than that when subjected to negative moment. These tendencies were notable in case of the section having large tendon eccentricity.

4.2 FLUCTUATION OF TENDON STRESS

Fig.6a and 6b show the fluctuation of tendon stress in

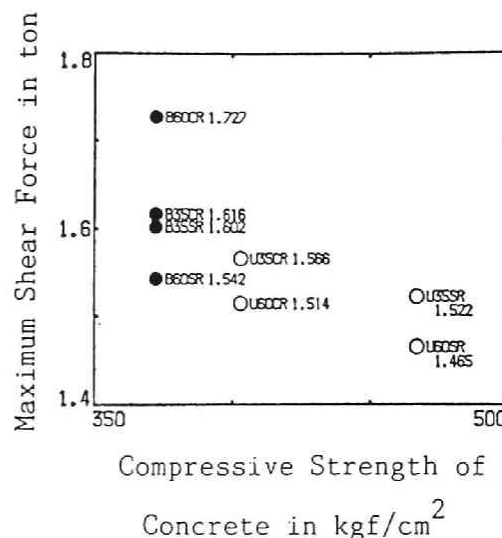


Fig.4 Shear force capacity

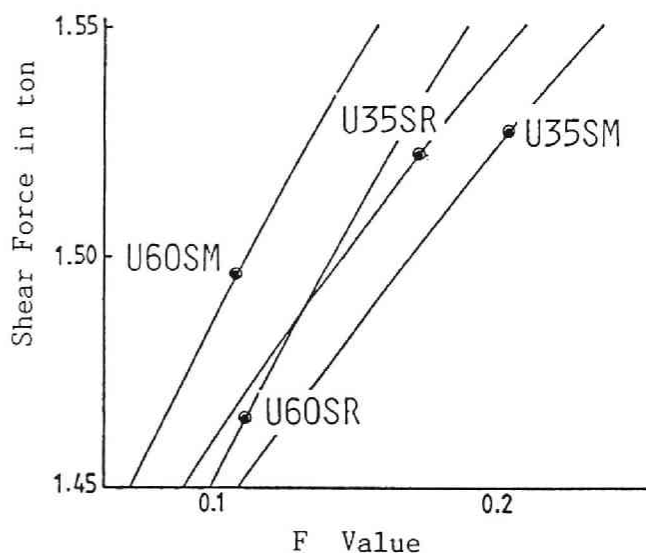


Fig.5a F value for unbonded beams

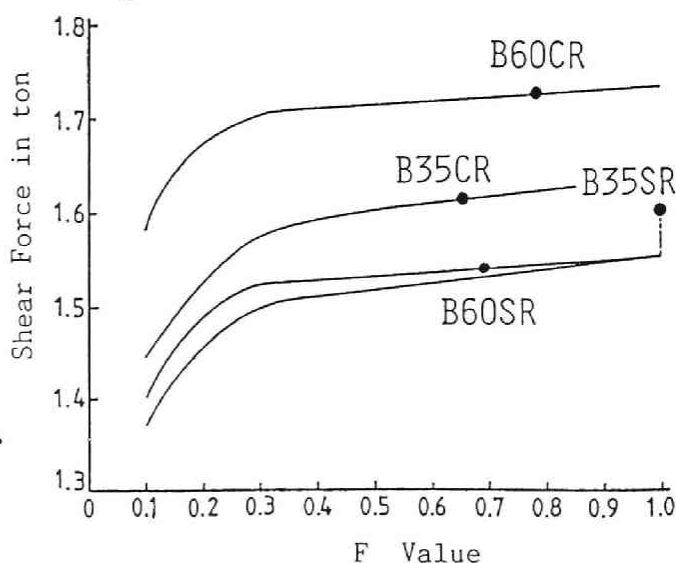


Fig.5b F value for bonded beams

U60CR measured at the anchorage end of the beam against the beam rotation angle. Fig.7 shows the increment of tendon stress in B60CR. Up to the present it has been thought that the fluctuation of tendon stress at the anchorage end of the unbonded beam is larger than that of bonded beam and there may be some fear of the fracture of the unbonded prestressing steel bar under reversed cyclic loading. However, in this test, the increment of tendon stress at the anchorage part of the bonded beam B60CR was 1.5 times larger than that of the unbonded beam U60CR. The reason is that under high intensity reversed cyclic loading the expected bond action between concrete and prestressing bar in the column stub deteriorated easily and most of the increment of tendon stress at the critical section was transferred to the anchorage end. Therefore, in so far as this test is concerned, the bonded beam has a larger possibility of low-cycle fatigue failure at the anchorage end than the unbonded beam.

It is recognized that the tendon profile did not affect the increment of tendon stress at the anchorage part in bonded beams, but in unbonded beams having draped tendon there was a large difference between the fluctuations of tendon stresses at the both beam ends (see Fig.6a and 6b). As shown in the figures, tendon stress increments were almost proportional to the beam rotation angle at the beam end section subjected to negative moment. But at the other end of the beam subjected to positive moment, smaller tendon stress increments and larger hysteresis were observed. Then, in Fig.8a and 8b, the difference of tendon stress increments at the anchorage part

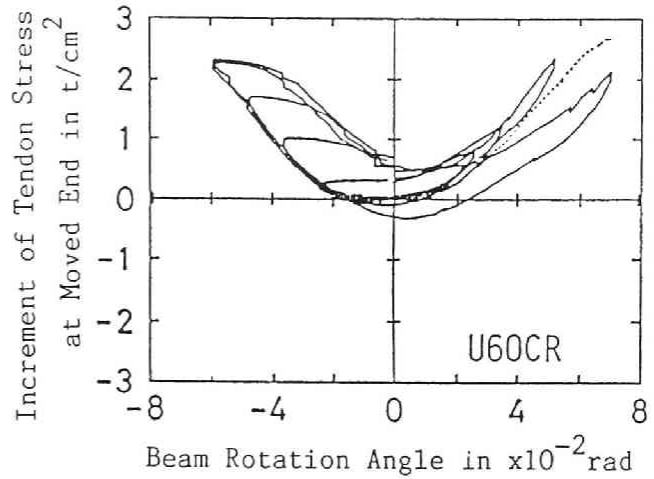


Fig.6a Fluctuation of tendon stress at moved end

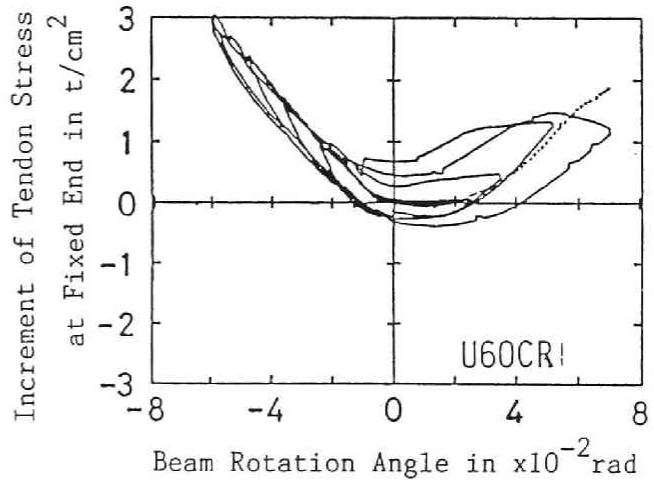


Fig.6b Fluctuation of tendon stress at fixed end

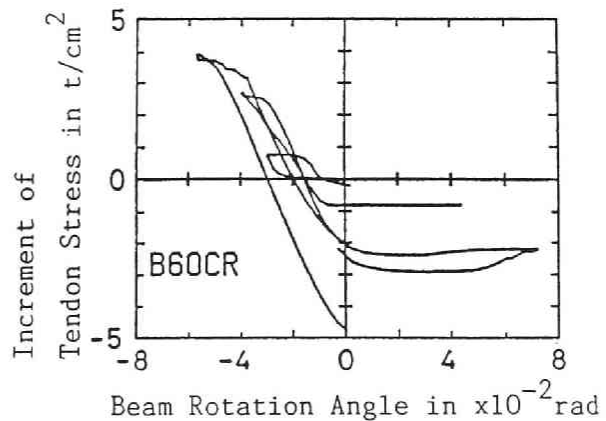


Fig.7 Fluctuation of tendon stress

between moved end and fixed end of the beam U60CR and U60SR are shown against the beam rotation angle. It is noted from these figures that constant frictions were existent between prestressing bar and its surrounding concrete no matter how large was the deformation of the beam and these frictions became 1/3 of tendon stress increment at the maximum. Furthermore, these constant frictions may be mainly due to the change in angle of unbonded prestressing steel bar.

4.3 HYSTERETIC RESTORING FORCE CHARACTERISTIC

Fig.9 shows equivalent damping factor against the displacement divided by δy . From this figure, there was little difference in the ability of energy dissipation between bonded and unbonded beams.

Fig.10a and 10b show the non-dimensional hysteretic loops of the bonded beam B60CR and the unbonded beam U60CR at deflection amplitude of δy (displacement when the ordinary reinforcement yielded initially) cycle and 2.0 δy cycle, respectively. From these figures, there was little difference in hysteretic loop between the unbonded beam and the bonded beam.

According to the location of prestressing bar, equivalent damping factors of the specimens having small eccentricity of tendon (U35CR, U35SR, B35CR and B35SR) are slightly larger than that of the specimens having large eccentricity of tendon (U60CR, U60SR, B60CR and B60SR). The reason is that concrete at the top fiber of the beam end subjected to positive moment tended to be damaged and the moment capacity reduction occurred under reversed cyclic loading in the specimens having large eccentricity of tendon than in the specimens having small eccentricity.

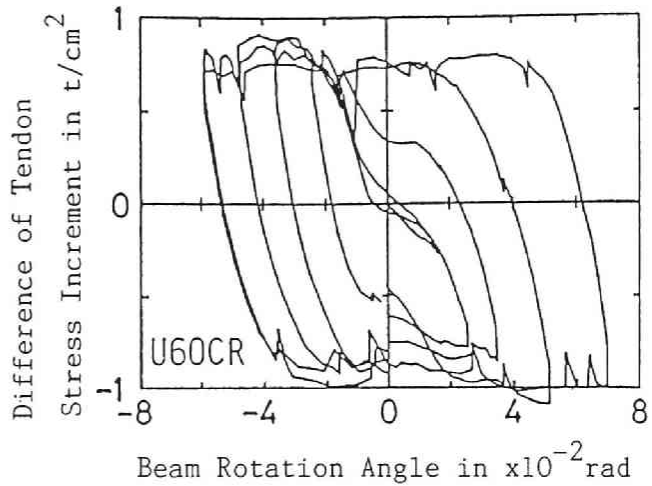


Fig.8a Difference of tendon stress

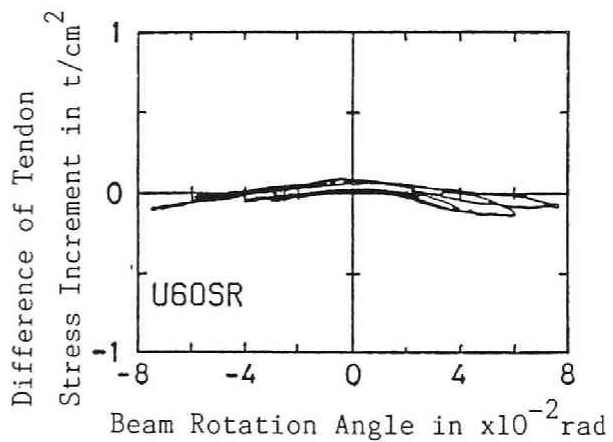


Fig.8b Difference of tendon stress

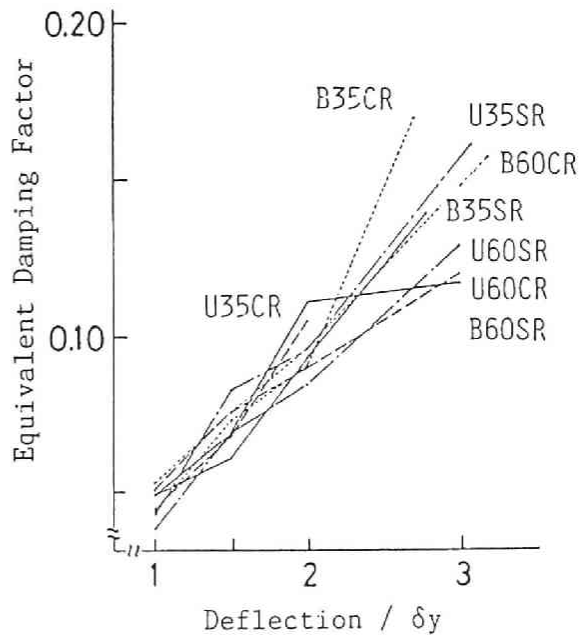


Fig.9 Equivalent damping factor

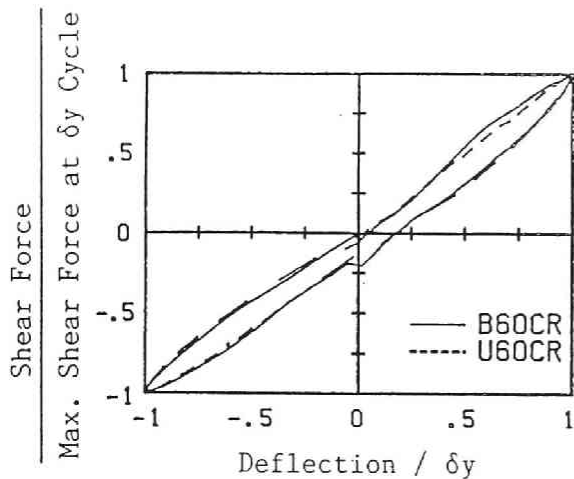


Fig.10a Non-dimensional hysteretic loop at δy

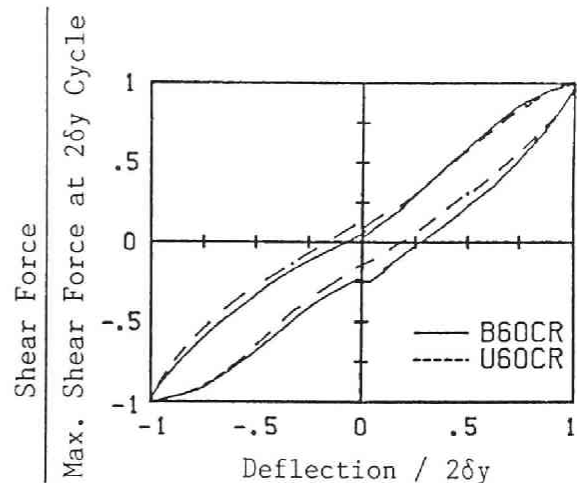


Fig.10b Non-dimensional hysteretic loop at $2\delta y$

5. CONCLUSION

The following conclusions can be derived from the test results.

- (1) The shear force capacity of unbonded prestressed concrete beams was 7% smaller than that of bonded beams under reversed cyclic lateral flexural shear loading test.
- (2) A strain compatibility factor F can be used for evaluating the capacity of unbonded prestressed concrete beams. The most suitable F value for unbonded beams was in the range of 0.1-0.2. F value obtained from the test was almost the same value obtained from the test carried on the simple supported beams.
- (3) The fluctuation of tendon stress at the anchorage end of bonded prestressed concrete beams was larger than that of unbonded beams because of the deterioration of bond in the column stub under reversed cyclic loading. Therefore, the bonded beams has a larger possibility of low-cycle fatigue failure at the anchorage end than the unbonded beams.
- (4) Constant friction was existent between unbonded prestressing tendon and its surrounding concrete no matter how large was the deformation of the beam because of the change in angle of prestressing tendon.
- (5) There was little difference in hysteretic restoring force characteristic between bonded beams and unbonded beams.

REFERENCE

- (1) Muguruma, H. et al., "The Ultimate Moment Capacity of Unbonded Prestressed Concrete members", J. of Prestressed Concrete, Japan Prestressed Concrete Engineering Association, Vol.26, No.1, Jan.1984, pp.10-16 (in Japanese)

